Final Programme and
Proceedings

WPP
127

ESA/NATO 1997 Workshop on

Microwave Tubes for Space, Military and Commercial Applications

7 - 10 April 1997
ESTEC, Noordwijk, The Netherlands

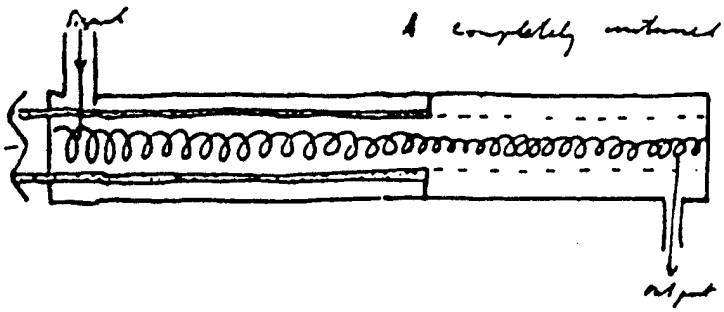

DISTRIBUTION STATEMENT A
Approved for public release
Distribution Unlimited

DTIC QUALITY INSPECTED

esa ESTEC

REPORT DOCUMENTATION PAGE

Form Approved OMB No. 0704-0188

Public reporting burden for this collection of information is estimated to average 1 hour per response, including the time for reviewing instructions, searching existing data sources, gathering and maintaining the data needed, and completing and reviewing the collection of information. Send comments regarding this burden estimate or any other aspect of this collection of information, including suggestions for reducing this burden to Washington Headquarters Services, Directorate for Information Operations and Reports, 1215 Jefferson Davis Highway, Suite 1204, Arlington, VA 22202-4302, and to the Office of Management and Budget, Paperwork Reduction Project (0704-0188), Washington, DC 20503.

1. AGENCY USE ONLY (Leave blank)	2. REPORT DATE	3. REPORT TYPE AND DATES COVERED
	14 April 1997	Conference Proceedings

4. TITLE AND SUBTITLE

ESA/NATO 1997 Workshop on Microwave Tubes for Space, Military, and Commercial Applications

5. FUNDING NUMBERS

F6170897W0075

6. AUTHOR(S)

Conference Committee

7. PERFORMING ORGANIZATION NAME(S) AND ADDRESS(ES)

European Space Agency ESTEC
Postbus 299
Noordwijk 2200 AG
Netherlands

8. PERFORMING ORGANIZATION REPORT NUMBER

N/A

9. SPONSORING/MONITORING AGENCY NAME(S) AND ADDRESS(ES)

EOARD
PSC 802 BOX 14
FPO 09499-0200

10. SPONSORING/MONITORING AGENCY REPORT NUMBER

CSP 97-1016

11. SUPPLEMENTARY NOTES

12a. DISTRIBUTION/AVAILABILITY STATEMENT

Approved for public release; distribution is unlimited.

12b. DISTRIBUTION CODE

A

13. ABSTRACT (Maximum 200 words)

The Final Proceedings for Microwave Tubes for Space, Military and Commercial Applications, 7 April 1997 - 11 April 1997

The Topics covered include: Microwave Tube Technology and Design.
TWT applications: military, space, commercial
TWT technologies: manufacturing, materials, thermal management, high voltage, new technologies.
TWT Design/CAD, Reliability
Power Conditioners & Controllers

14. SUBJECT TERMS

High Power Microwaves, High Power Generation, Space Science

15. NUMBER OF PAGES

392

16. PRICE CODE

N/A

17. SECURITY CLASSIFICATION OF REPORT	18. SECURITY CLASSIFICATION OF THIS PAGE	19, SECURITY CLASSIFICATION OF ABSTRACT	20. LIMITATION OF ABSTRACT
UNCLASSIFIED	UNCLASSIFIED	UNCLASSIFIED	UL

Final Programme and
Proceedings

ESA/NATO 1997 Workshop on

Microwave Tubes for Space, Military and Commercial Applications

7 - 10 April 1997
ESTEC, Noordwijk, The Netherlands

DISTRIBUTION STATEMENT A
Approved for public release
Distribution Unlimited

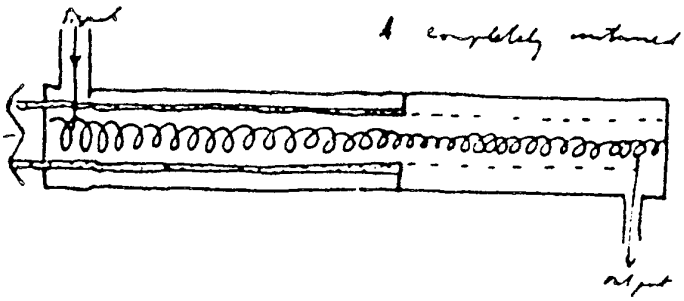

19970703 020

esa ESTEC

NATO RSG19

European Space Research and Technology Centre
Keplerlaan 1, Noordwijk, The Netherlands

European Space Agency
8-10, Rue Mario Nikis, 75738 Paris Cedex 15, France

Disclaimer

The ESA Workshop Preliminary Proceedings (WPP) series are informal documents intended to promulgate quickly the results of a workshop to participants and others. As such they are working documents, and have not been edited nor compiled in the normal ESA format for proceedings.

The opinions expressed and the conclusions reached do not necessarily reflect the policy of the Agency. Some of the key-papers and recommendations may be published later in the ESA SP-xxxx series.

The Steering Committee

F. Emma	ESA/ESTEC, Technical Directorate
G. Gatti	ESA/ESTEC, Technical Directorate
R. van Heijster	TNO-FEL, Chairman NATO RSG-19
J.M. Schouten	Directorate of Materials Royal Netherlands Navy

Workshop Organizer

F. Emma
ESA/ESTEC
P.O. Box 299
2200 AG Noordwijk
The Netherlands

Tel.: +31 71 565 5002
E-mail: femma@xrsun0.estec.esa.nl

Workshop Secretariat

ESTEC Conference Bureau
P.O. Box 299
2200 AG Noordwijk
The Netherlands

Tel.: +31 71 565 5005
Fax: +31 71 565 5658
E-mail: confburo@estec.esa.nl

Acknowledgements :

We wish to thank the "United States Air Force European Office of Aerospace Research and Development" for their contribution to the success of this workshop

Final Programme

Monday 7 April 1997

10:00 Start registration

13:00 Welcome

13:10 Opening Address

13:20 Invited Speaker: " Status and Perspectives of R&D activity on Non Traditional Microwave Tubes in Russia."
Savvin V. (Moscow State Un. Faculty of Physiscs, Russia)

Session 1 **TWTAs Status and Capabilities**
Chairman: Mr. G. Fleury (Thomson Tubes Electroniques Velizy, France)

13:50 Power Booster Travelling Wave Tubes
Ward, K.D.; Duffield, M.J.; Wise, A.R. (EEV, Great Britain)

14:10 Travelling Wave Tube Amplifier: State-of-the-Art and Future Trends
Hübner, K.-H. (ANT Bosch Telecom, Germany)

14:30 Present and Future Trends in High Power Generation
Van Heijster, R.M.E.M.; Schouten, J.M.** (* TNO - FEL, The Netherlands; **Directorate of Materials, Royal Netherlands Navy, The Netherlands)*

14:50 Ka-Band 15W to 80W Space TWT Series
Kurahashi, M.; Hamada, S.; Kubo, H. (NEC Corporation, Japan)

15:10 The Commercial Space TWTA Market Review and Trends
Heider, S. (ANT Bosch Telecom, Germany)

15:30 Coffee Break

Session 2 **MPMs**
Chairman: Mr. G. Gatti (ESA/ESTEC, NL)

16:00 Microwave Power Module for Space Application
Sironi, L.; Ceruti, L.; Gambarara, M.; Nebuloni, L.; Trivulzio, A; Vigano, D. (FIAR S.p.A. Space Division, Italy)

16:20 60% Efficient C-Band TWT for the Microwave Power Module
Whaley, D.; Armstrong, C.M.; Gannon, B.; Groshart, G.; Hurt, E.; Hutchins, J.; Roscoe, M. (Northrop Grumman Corporation, USA)

16:40 MPM Technology - The Miniaturized Transmitter Solution
Smith, C.R.; Armstrong, C.; Duthie, J.; Pierce, G.; Sievers, M. (Northrop Grumman Corporation, USA)

17:00 Microwave Power Modules: Technology for the Future
Ninnis, T.; Schoemehl, T.; Pelster, W.; Ballagh, Ph.C.; Watkins, R.; Taylor, J.; Lednum, G.; McKay, J. (Litton Industries, USA)

17:20 Dual Linearized TWTA with Integrated Channel Amplifier - A First Step Towards the MPM
Jaumann, G. (ANT Bosch Telecom, Germany)

Session 3 Power Conditioners
Chairman: Mr. P. Perol (ESA/ESTEC, NL)

17:40 Degradation of Power Supplies Due to Transients
Hyle, R.A. (US Air Force / Rome Laboratory, USA)

18:00 Breadboarding of a Novel EPC for TWT Based on Diode-Capacitor Voltage Multipliers
Olsson, D.H.L.; Marti, J.M. (ESA ESTEC, The Netherlands)

18:20 EPC and TWTA for Telecomunication Satellites
Delporte, P.; Fayt, P.; Gak, M.; Pequet, E. (Alcatel-ETCA, Belgium)

18:40 Cocktail party in the Noordwijk Space Expo

Tuesday 8 April 1997

Session 4 TWTAs Applications
Chairman: Mr. J.M. Schouten (Directorate of Materials-Royal Netherlands Navy, NL)

09:00 30GHz 150W High Gain Helix Traveling Wave Tube
Tonegawa, S.; Machida, T.; Matsuoka, J.; Fukui, H.; (NEC Corporation, Japan)

09:20 FIAR Space TWTAs for DBS Applications
Orsenigo, G.; Ceruti, L. (FIAR S.p.A. Space Division, Italy)

09:40 Ku Band 90 to 125 W Radiation Cooled TWT
Yoshida, M.; Katakami, K.; Mori, M. (NEC Corporation, Japan)

10:00 New Generation of Highly Efficient Ka-Band TWTs 15 to 140 W
Bosch, E.; Andre, F.; Christ, R. (Thomson Tubes Electroniques, France)

10:20 New Generation of Radiation and Conduction Cooled High Power 220-W Ku-Band TWTs
Pelletier, A.; Pasdeloup, R.*; Bosch, E.**; Alex, M.** (*Thomson Tubes Electroniques, France; **AERG, Germany)*

10:40 Coffee Break

Session 5 Other Vacuum Tubes
Chairman: Mr. C. Lin (ESA/ESTEC, NL)

11:00 Compact Millimeter Wave TWTs
Armstrong, C.M.; Gallagher, D.A.; Groshart, G. (Northrop Grumman Corporation, USA)

11:20 High Power Super-Reltron Experiments
Cross, A.W.; He, W.*; Phelps, A.D.R.*; Ronald, K.*; Spark, S.N.** (*Univ. of Strathclyde, Great Britain; **DRA Malvern, Great Britain)*

11:40 Litton High-Power Folded-Waveguide Ka-Band TWTs
Theiss, A.J. (Litton Industries, United States of America)

12:00 Progress in 94 GHz TWT Development
Malzahn, P.; Lipper, G. (AERG, Germany)

12:20 High Power Millimetre Waves from Extended Interaction Klystrons
Steer, B.; Nilsen, Chr. (Communications & Power Industries Canada Inc., Canada)

12:40 Magnetron Frequency Twinning
Carter, R.G.; Ball, E.M.**; Brady, M.B.** (*Lancaster University, Great Britain; **EEV Ltd., Great Britain)*

13:00 Lunch Break

Session 6 **TWTAs Technologies & Reliability**
Chairman: Dr. G. Kornfeld (AERG-ULM, Germany)

14:30 Vacuum Insulator Flashover, Mechanisms, Diagnostics and Design Implications
Wetzer, J.M (Eindhoven University of Technology, The Netherlands)

14:50 Overview of NASA LeRC Cathode Technology Development Program
Dayton, J.; Wintucky, E.G.; Krainsky,I. (NASA Lewis Research Center, USA)

15:10 The Measured Angular Distribution of Elastically Scattered Electrons and Computations of their Effect on Collector Performance
Dayton, J.; Krainsky, I.; Vaden, K.R. (NASA Lewis Research Center, USA)

15:30 The Effect of Tolerances on TWT Performance
Dayton, J.; Kory, C.L. (NASA Lewis Research Center, USA)

15:50 Coffee Break

16:10 Life Test Performance of Impregnared Cathode for High Reliable Satellite TWTs
Chiba, A.; Akiyama, Y. (NEC Corporation, Japan)

16:30 The Secret to Achieving Microwave Tube Reliability
Jones, E.J. (US Air Force / Rome Laboratory, USA)

16:50 Achieving Microwave Tube Reliability Using an Advanced Computer Software Tool
Ciskowski, E. (US Air Force / Rome Laboratory, USA)

17:10 A Modeling and Simulation Approach for Assessing Helix TWT Interaction Circuit Thermal Behavior
Rocci, P.J. (US Air Force / Rome Laboratory, USA)

17:30 RF Design for Low Cost
Ryan, J.P. (US Air Force / Rome Laboratory, USA)

17:50 Military Specifications and Standards Reform
Gorniak, M. (US Air Force / Rome Laboratory, USA)

18:10 End of the day

Wednesday 9 April 1997

Session 7 **RSG-19 Day**
Chairman: Mr. R.M.E.M. van Heijster (TNO-FEL, NL)

09:00 Opening and Introduction
van Heijster, R.M.E.M. (TNO-FEL, NL)

09:15 Reliability Enhancement for Microwave Tubes and High Voltage Power Supplies
Rocci, P. (USAF-Rome Laboratory, USA)

09:40 Generic System Description
Philips, G. (TMD, USA)

10:05 The Operational Envelop Concept
van Heijster, R.M.E.M. (TNO-FEL, NL)

10:30 Environment
Kreager, G.; Gilmour, A.S. (NWSC Crane, USA)

10:55 Coffee break

11:15 Input Signal Conditioner
van Heijster, R.M.E.M. (TNO-FEL, NL)

11:40 Power Conditioner
Al Biddings (CPI, USA)

12:05 Controller
Stegeman, A.P. (Hollandse Signaal Apparaten, NL)

12:30 Lunch break

14:00 Power Amplifiers Appliations and Reliability
Schouten, J.M. (Directorate of Materials-Royal Netherlands Navy, NL)

14:25 Cooling
Kreager, G.; Gilmour, A.S. (NWSC Crane, USA)

14:50 Reliability and Measurements Tools
Ryan, J. (USAF Rome Lab., USA)

15:15 Shelflife Study of Missile TWTs - Results and Conclusions
Vetter, H.;Peters, A. (AERG, Germany)

15:35 Coffee Break

15:55 Testing
Fly, E. (TASC, USA)

16:15 System Examples
Schouten, J.M. (Directorate of Materials-Royal Netherlands Navy, NL)

16:40 RSG19 Accomplishments
van Heijster, R.M.E.M. (TNO-FEL, NL)

17:05 MiDAS Microwave Device Analysis System
van Huut, J. (Naval Electronics and Optics Establishments, NL)

17:25 NATO Handbook on: Microwave & Millimetre Wave Tubes
Jones, E. (USAF Rome Lab, USA)

20:00 Workshop Dinner

Thursday 10 April 1997

Session 8 **TWT Design/CAD**
Chairman: Mr. E.J. Jones (US Air Force/Rome Laboratory, USA)

09:00 The MMACE Framework: An Integrated Environment for Power Tube Design and Analysis
Hantman, B.; Abrams, R.**; Labelle, J.*; Siarkiewicz, K.*** (*Raytheon Company, USA; **Naval Research Lab (NRL), USA; ***US Air Force / Rome Laboratory, USA)*

09:20 Equivalent Circuit Modelling of Helix Slow-Wave Structures
Carter, R.G.; Wang, P. (Lancaster University, Great Britain)

09:40 A Three-Dimensional Finite-Element Simulator for the Design of High Effiency TWTs Multistage Depressed Collectors
*Coco, S.***; D'Agostino, S.**; Emma, F.*(*ESA/ESTEC, The Netherlands; **University of Rome "La Sapienza", Italy; ***University of Catania, Italy)*

10:00 A New Criterion for the Comparison of TWT and Linearized TWT and for the Optimization of Linearizers used in Transmission Systems
Sombrin, J. (C.N.E.S., France)

10:20 Optimizing Efficiency in a Coupled-Cavity TWT with a Simulated Annealing Algorithm
Wilson, J.D. (NASA Lewis Research Center, United States of America)

10:40 Coffee Break

11:00 High Efficiency Linear TWT
Nunn, R (AERG Ulm, Germany)

11:20 Efficiency Improvements in KU-Band Space Helix Traveling Wave Tubes
Benton, R.T.; Burdette, J.T.*; Davis, J.A.*; Feicht, J.R.*; Komm, D.S.*; Menninger, W.L.*; Robbins, N.R.*; Thorington, C.B.*; Zhai, X.*; Adler, E.A.*; Force, D.A.**; Heinen, V.O.**; Vaden, K.R.**; Wilson, J.D.**; Dayton, J.R.** (*Hughes Telecommunications and Space Company, USA; **NASA Lewis Research Center, USA)*

11:40 L Band TWT for Worldstar
Heumüller, P.; Hördler, M.; Schmelzer, M.; Fischer, G. (AERG Ulm, Germany)

12:00 Introduction to an Accurate Cold-Test Model of Helical Slow-Wave Structures
Kory, C.L.; Dayton, J. (NASA Lewis Research Center, USA)

12:20 Workshop Closure

Non-Traditional Microwave Tubes Based on Electron Beam Cyclotron and Synchronous Waves Using. Status and Perspectives. (Russian Experience)

V. Vanke, V. Savvin
Faculty of Physics, Moscow State University
Moscow 119899, Russia

#1. The purpose of this report is to inform briefly on the non-traditional microwave tubes based on using of cyclotron and synchronous waves. This advantageous type of interaction was successfully studied and applied to modern systems of radiolocation and communication in Russia in two past decades.

#2. Most high-quality microwave systems in Russia use electron-beam devices for both the last stage of the transmitter and the first stage of the receiver with everything in between solid state.

It can be explained by a wide complex of various rigid requirements imposed to the powerful microwave output amplifiers and low-noise input preamplifiers which are opposed rather often.

For the input preamplifier it is important that the linearity should be combined with stability to high-power pulse impact, small level of impact leakage especially of short high-power pulses, reliable protection of subsequent cascades of the receiver and fast recovery time. At the same time, a low noise figure should be provided in combination with a wide dynamic range and high values of the gain.

For the output amplifier the linearity especially of phase characteristics must be combined with a high level of power, a broad frequency range and operation with high efficiency.

#3. When applying the conventional longitudinal grouping of electrons in bunches there appear some principle problems connected with the non-linear character of Coulomb forces which usually play a decisive role in formation of dense electron bunches.

To a considerable extent, these problems can be rather eliminated, if we apply a transverse grouping of the electron beam drifting in a longitudinal magnetic field. It should be pointed out that in this case, in contrast to gyrotrons, relativistic effects are not used and the interaction remains linear.

#4. In the case of transverse modulation of the electron beam drifting in the longitudinal constant magnetic field, four kinds of waves can be excited: two cyclotron waves and two synchronous waves. In each case the beam assumes the shape of a uniformly charged spatial helix having no space charge bunches.

In contrast to space charge waves, phase velocities of cyclotron waves are dependent on the cyclotron frequency, which is determined by the external magnet system only. Phase velocities of synchronous waves are equal to the longitudinal velocity of the electron beam. All the four transverse waves are circularly polarized.

Stability of phase velocities of transverse waves and their circular polarization provide high selectivity of interaction with the fields of electrodynamic structures. It should again be pointed out that the absence of space charge bunches insures the linearity of the energy exchange processes.

#5. Now, a few words about the history of the appearance and development of the concept of the transverse grouping in electron beams. The first fundamental work on interaction of the electron beam with the resonant transverse field was published in 1949 by C.I.Cuccia in the USA.

Ten years later, nearly simultaneously in the USA and Russia there appeared publications on parametric and, later, electrostatic amplifiers using a fast cyclotron wave of the electron beam. Record values of the amplifier noise temperature, those of the order of 60-200 K, were achieved quite soon. This success was so impressive that it led to a great number of concrete proposals for design of new devices. Subsequent experiments, however, gave poor results. Perhaps, as a consequence, all research on transverse waves in the USA was stopped almost completely

The main reason was the theory available at that time, which did not allow extended application of transverse waves.. Today, the existing three-dimensional models of the electron beam and accumulated design experience give us confidence to confirm the possibility of developing a new class of microwave devices with unique sets of parameters.

With your permission I would omit computational details and dwell on those physical ideas and their possible applications that appear today to be most advantageous.

#6. The simplest device which interacts selectively with a fast cyclotron wave of the electron beam is a resonator with a transverse field (the Cuccia coupler). At the cyclotron resonance, the electron beam excited on a fast cyclotron wave

rotates around the system's axis and has no spatial distortions. In contrast to klystrons, such a resonator operates at large transit angles and is capable of transmitting practically all signal power into the fast cyclotron wave of the electron beam and extract the noise power of this wave back into the external circuit. Two resonators connected in series interact with the electron beam quite efficiently and the attenuation during signal transmission through such a system can be very low (of the order of 0.5 dB and less).

#7. At high levels of the input signal the electron beam could be trapped by the input resonator and the resonators turn out to be disconnected. Thus, there appears a possibility to design a good protective device which could be placed between the antenna and the input amplifier of the receiver (for example, in radars). In case of the beam trapping, the matching conditions of the input resonator are sharply violated. The VSWR is increased up to a few tens of units and the main part of power is reflected from the input of such a device.

In this figure you can see protective devices designed recently in Russia for the frequencies of 9 and 35 GHz. Principal advantages of such protective devices on cyclotron waves are a low level of losses, short recovery time and deep protection (including suppression of an leakage power peak). The output signal peak (the leakage of high-power pulse impact) cannot generally be greater than 0.1-1 mW and is therefore quite harmless for subsequent cascades of the receiver.

#8. If an additional microwave resonator with a quadrupole electric field is placed between the input and output resonators and is fed from the external pump generator with a frequency about the double cyclotron frequency, we shall have a parametric amplifier which retains all the protective functions of the previous device. Besides, here the input resonator efficiently removes noises of the fast cyclotron wave of the electron beam.

At the late 50-s - early 60-s such amplifiers were designed and constructed both in the USA and in Russia.

You can see experimental results obtained at Moscow University - noises of the fast cyclotron wave are reduced 33 times. The minimum noise temperature of the amplifier is 45 K. Those were quite good results for that time.

#9. Instead of a microwave pump resonator, it is possible to use an electrostatic quadruple helix forming a spatially twisted electrostatic quadrupole field. The electrons moving along such a system 'feel' the time-variable electric field,

and the amplitudes of the electron beam cyclotron waves will be increased if the resonance condition at the double cyclotron frequency is fulfilled.

Amplification of a fast cyclotron wave in such a system is achieved due to active coupling with a slow cyclotron wave that does not interact with the input resonator field. A high value of the magnetic field at the cathode surface and subsequent reduction of this value provide a low noise level of cyclotron waves in the electron beam at the entrance into the interaction region.

You can see a general view of a variant of the electrostatic amplifier which is manufactured today only in Russia. In total about several thousand devices have been sold. The input amplifier of this type is unique, it provides a low level of intrinsic noises, wide dynamic range, stability to overloads, low impact leakage, efficient self-protection and short recovery time after overloads.

#10. The operation principle of the CWESA amplifier makes it possible to provide a reliable protection of subsequent receiver cascades, in particular, against the leakage power peak that occurs usually in conventional protective devices at the transmitter pulse front. This is not the case for CWESA, since the leakage spikes are related to the risetime of the pulse, and decreasing pulsewidth and risetime does not increase the energy in the leakage spike. The output signal peak in CWESA cannot, in principle, be greater than 0.1-1 mW and is therefore quite harmless.

There is some positive experience of applying such amplifiers in radars operating with pulses of 3 ns duration only.

#11. A tuneable CWESA can be designed if traveling-wave structures are used as couplers. In this case a high degree of selectivity in energy exchange with the fast cyclotron wave of the electron beam is preserved.

Operational band of such couplers is narrow (of the order of 1 percent or smaller), however, it can be tuned within a wide range by changing the magnetic field strength and the beam potential.

Such traveling-wave couplers have been tested and the experimental results are in a good agreement with the existing theory. A tuneable protective device based on this principle in combination with a low-noise FET amplifier may prove to be promising for many applications in modern microwave technologies.

#12. Now, I would like to dwell on another interesting possibility of design new type of TWT - Circularly Polarized TWT using synchronous transverse wave of electron beam.

Let us consider a filamentary electron beam propagating along the axis of slow-wave structure with a circularly polarized wave. The transverse electric field of the wave combined with the longitudinal constant magnetic field (the Lorenz force) will move the electron from the axis into the region of the decelerating longitudinal electric field of the wave. Each electron injected along the axis at the velocity equal to the phase velocity of this wave will be equally and monotonously decelerated by the longitudinal field of this wave.

It should be pointed out that this is the case for each electron regardless of the time of its entrance into the wave field. Thus, a filamentary electron beam remains mono-energetic after such an interaction and can be recuperated very efficiently.

In the figure below you can see a variant of the slow- wave system in the shape of a spatially twisted binary comb, which allows us to create different phase velocities of circularly polarized waves with the right and left polarizations.

#13. However, for practical design of high power device a more improved beam model ought to be used. Therefore during last years, our efforts were concentrated on the development of advanced theory of this interaction.

New improved 3-D beam model was developed allowing adequate description of interaction of finite-diameter electron beam with circularly polarized traveling wave and the influence of beam space-charge field. Special computer codes for CP TWT design were developed.

You can see the results of computer simulation and optimization of such CP TWT. The electron efficiency can reach 40% level. The efficiency with recuperation is up to 80% and the frequency band is of the order of 30%. It is very important that the non-linearity of the phase frequency characteristics in non-linear high-efficiency regimes turns out here to be several orders smaller than in ordinary TWT. This is a direct consequence of the new type of spatial grouping of the electron beam, which is not accompanied by formation of electron bunches.

#14. Double-cascade CP TWT with good values of the parameters is also feasible.

#15. In these figures you can directly see the computer display when the processes in CP TWT are simulated. The displayed data are: the initial values of the parameters, current results of calculation of the gain, the electron efficiency and the efficiency with the beam recuperation.

At the bottom of the screen we can see the spectrum of longitudinal velocities of the electron beam.

In the right-hand part of the screen the interaction channel and the positions of the elementary beams inside this channel are shown. The rotating arrow indicates the direction of the transverse electric field of the traveling circularly polarized wave along the interaction region.

The upper figure refers to the linear region and the bottom figure - to the region of the maximum values of gain and efficiency.

In the linear region the shape of the electron beam cross-section remains round, and the beam itself is shifted into the maximum of the decelerating longitudinal electric field of the circularly polarized wave.

In the non-linear region the beam has lost its initial shape and is drifting gradually from the decelerating phase into the accelerating one.

#16. The basic experiment was performed in Russia at the time when no adequate theory was available to describe the electron beam of a finite cross-section and there were no possibilities for optimization of the device. Nonetheless, serviceability of such CP TWT was demonstrated at the constant output power of about 2 kW. The experimental results obtained at that time were used later to verify the constructed three-dimensional theory and they were found to be in a good agreement.

The second optimized experiment was designed recently but its technological realization had to be suspended because of general financial problems in Russia.

Nevertheless, in our opinion the powerful variants of CP TWT can possess unique parameters and are advantageous for many technological applications.

#17. The developing ideas of Wireless Power Transmission and Space Power Satellites initiated the problem of back conversion of microwave energy into the energy of direct current using simple, reliable and powerful devices.

We studied CWC (Cyclotron Wave Converter) for this purpose both theoretically and by experiment. The CWC principle is rather simple: microwave energy is introduced into a fast cyclotron wave of the electron beam, than is converted into the energy of longitudinal motion in the region of the reverse magnetic field and then during recuperation in the collector decelerating field it is released at the outside load of the collector.

Such device is advantageous because it can have a high efficiency at a high power level, stability to overloads in high-frequency and low-frequency circuits, and a high output direct voltage.

At Moscow University the CWC was tested for the power level of 100 W at the efficiency of 74%.

A good experimental device was developed jointly by MSU and Toriy Corp. At continuous input power of 10 kW the efficiency was as high as 83%.

At present, the work is also under way to design new type of CWC with Istok Corp.

#18. One more promising idea should be outlined. It involves combined (longitudinal-transverse) interaction to broaden the operating band of powerful klystrons.

At the first stage an ordinary klystron grouper forms electron bunches. Then they are injected into the region of reverse magnetic field biased with respect to its axis. At the region output a large part of the longitudinal energy of the electron beam can be converted into its rotational energy. Besides, if the cyclotron resonance condition is fulfilled, all the bunches would happen to be on one straight line rotating as a whole around the Z axis. In the resonator with the transverse field this energy can be almost completely extracted from the electron beam. The transverse field of the resonator gap is uniform and the spreading of bunches in the longitudinal direction is not important, while continuous interaction provides 10-15 times more efficient load of the resonator by the electron beam. Thus, at high efficiency (70-80%) the interaction band of the order of 8-10% and even more can be provided.

#19. In conclusion we should again point out the principal advantages of devices based on interaction with cyclotron and synchronous waves of the electron beam:

* The absence of non-linearity connected with formation of space charged bunches. Relativistic (non-linear) dependence of the electron mass on the electron energy is not used here.

* Stability and circular polarization of phase velocities of transverse waves make it possible to provide a high level of selectivity in energy exchange with external electromagnetic fields.

* Levels of microwave power in the electron beam can significantly exceed the initial energy of the injected electron beam.

These factors, which seem to be quite simple, allow us to overcome a number of limitations which restrict today the development of microwave vacuum electronics.

#20. As a result of application of these new principles of electron beam grouping, various devices with unique parameters can be created.

In this table you can see that one group of devices is already manufactured commercially, another group is under industrial tests or just passed these tests, the third group is under laboratory tests, and finally, there is a great number of interesting designs based on reliable experimental data.

#21. Finally, it should be emphasized in conclusion that this report was not intended to discuss all the known and possible types of transverse interaction. The discussion included only those types which are, as the authors believe, most promising.

Motivation

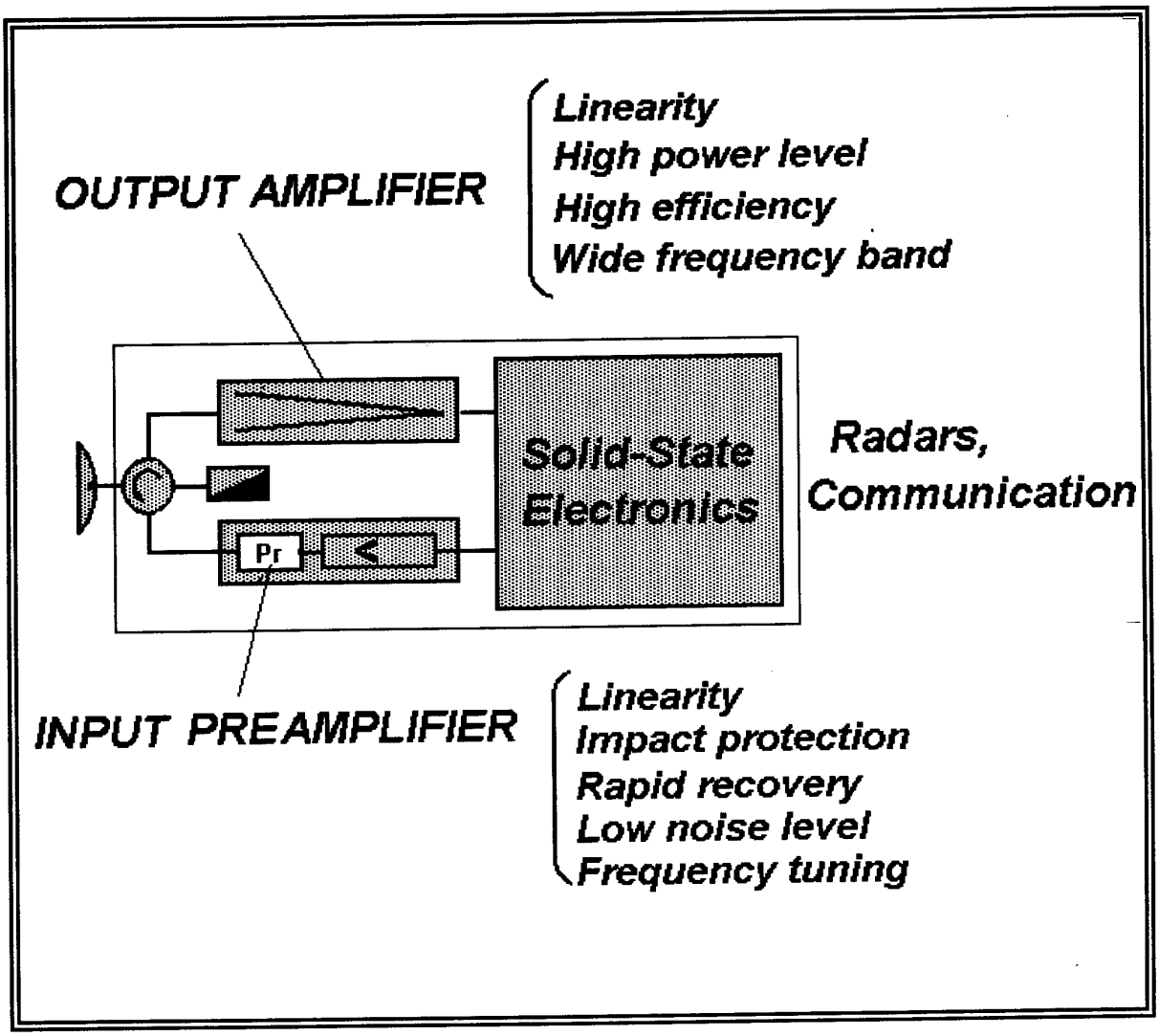

- High level of requirements to input and output amplifiers of radar, communication and navigation systems today.

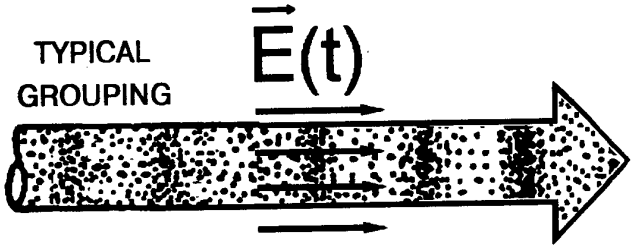

Klystron,
TWT,
BWO, etc.

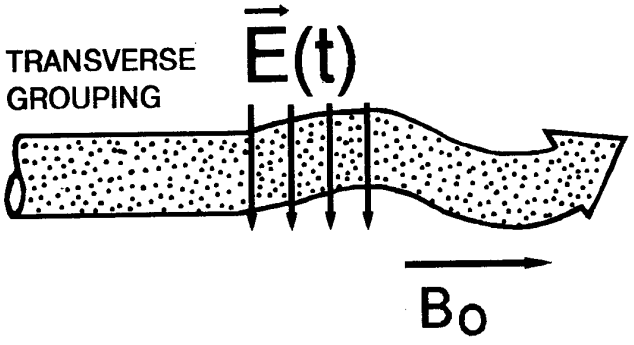

CWP, CWPA,
CWESA,
CWESA- filter,
CP TWT,
CWC, etc.

* **Beam twisting instead of electron bunching.**

* **Space charge forces do not take part in microwave interaction directly.**

* **Relativistic effects are not used.**

TRANSVERSE WAVES (CYCLOTRON AND SYNCHRONOUS)

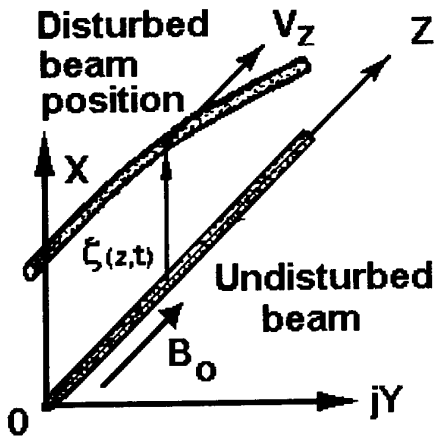

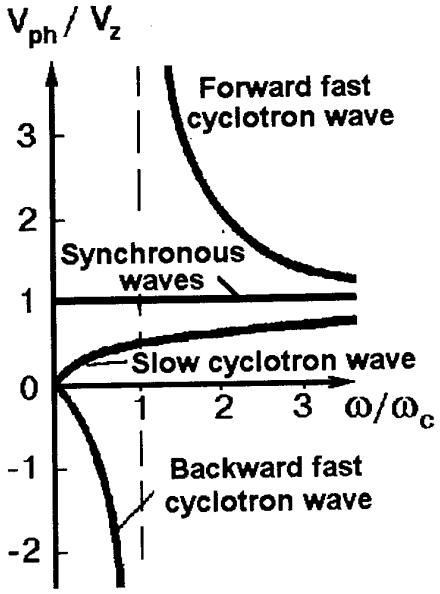

CW $\rightarrow V_{ph\pm} = V_z / (1 \mp \omega_c / \omega)$

SW $\rightarrow V_{ph\pm} \equiv V_z$

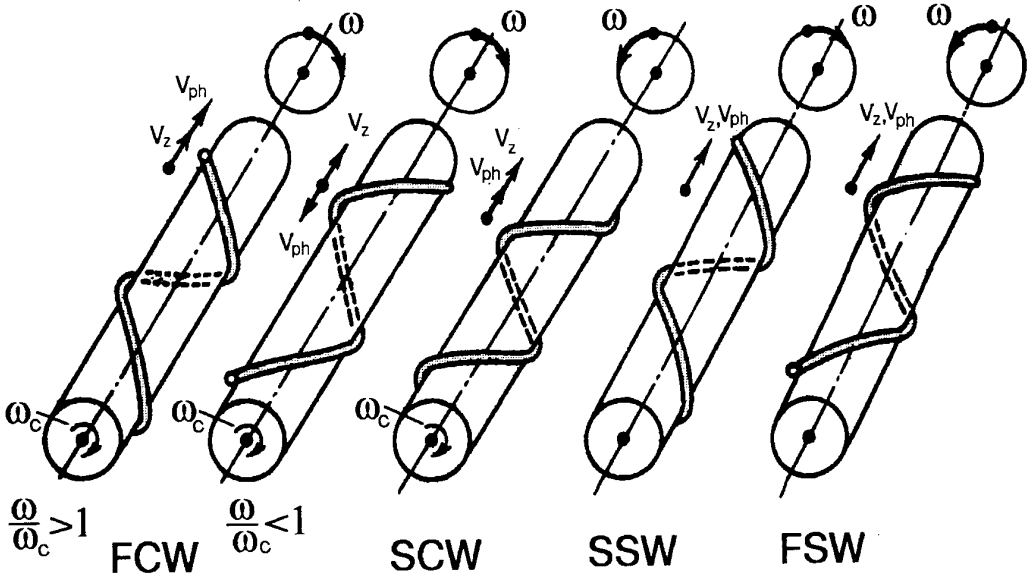

Fast Cyclotron Wave Couplers

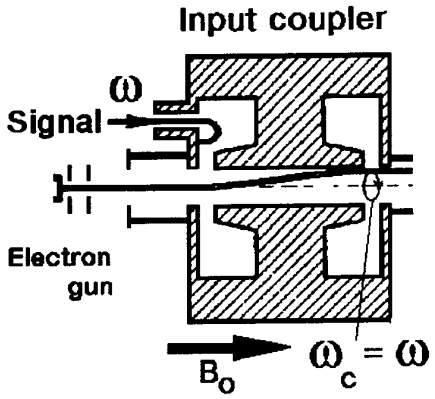

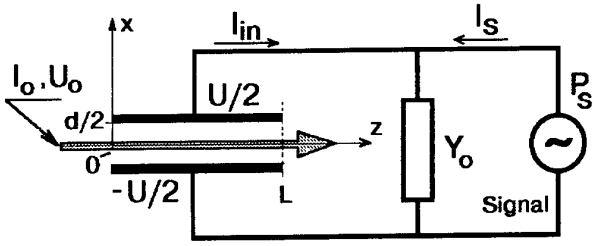

$$\theta_L = \beta_c L >> 1$$

$$Y_\Sigma = Y_o + Y_e,\ Y_e = G_e + jB_e.$$

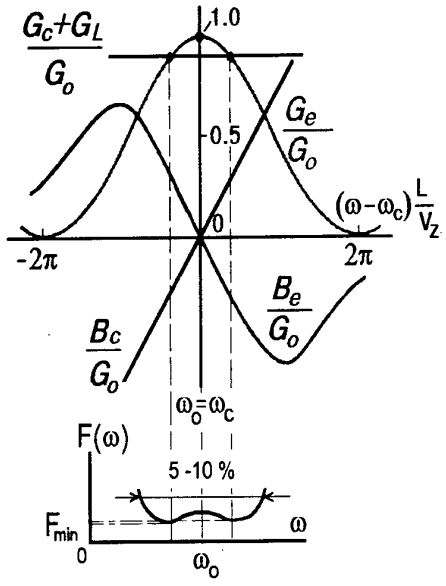

Bandwidth up to 10%

$$P_{1+}(L) = \left|1 - \frac{2G_e}{Y_\Sigma}\right|^2 P_{1+}(0) + \frac{4G_L G_e}{|Y_\Sigma|^2} P_s,$$

$Y_e = Y_o^* \rightarrow P_{1+}(L) = P_s$

Beam "cooling".

Low losses at signal propagation < 0.5 dB

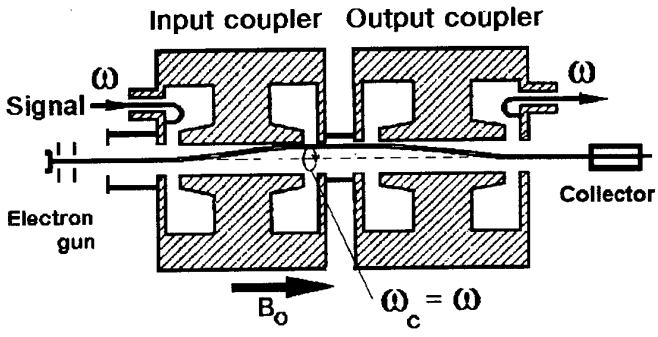

CYCLOTRON WAVE PROTECTIVE DEVICES (CWP)

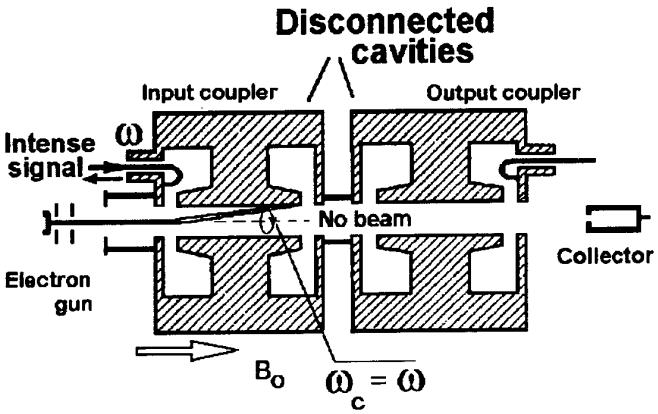

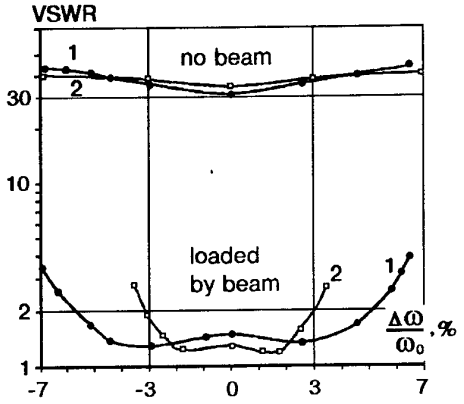

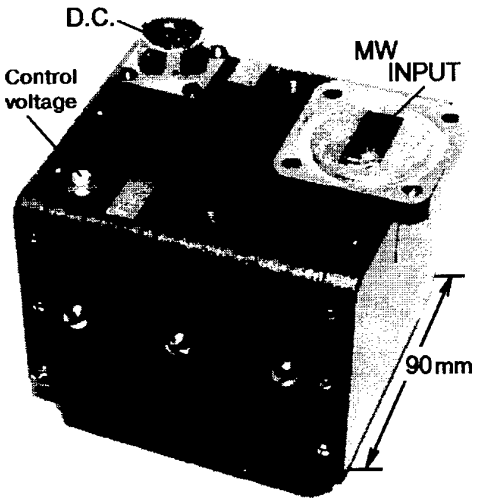

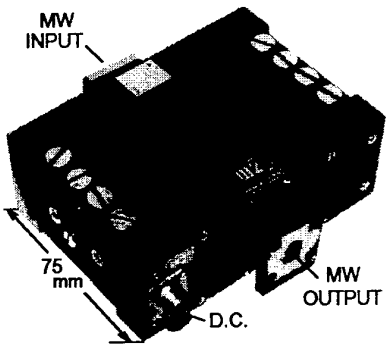

CW Protectors developed by ISTOK Corp. at 9 and 35 GHz

Efficient protection from microwave impact (>100 kW)
Short restoration time (<10 ns)

CYCLOTRON WAVE ELECTROSTATIC AMPLIFIER (CWESA)

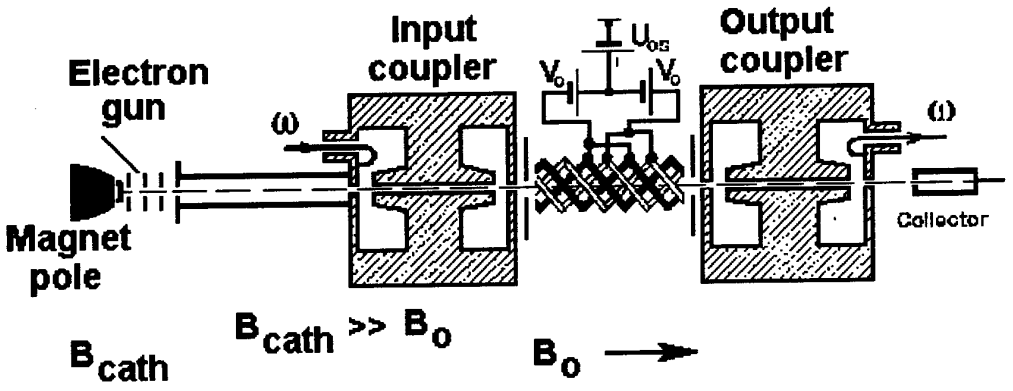

Super-high protection against microwave impact - up to 500 kW in pulse

High isolation (small leakage of large and narrow pulse impact) >100 dB

Rapid recovery time 1-10 ns

Low noise level - 50-100 K

Gain linearity, third order interception point >18dBm

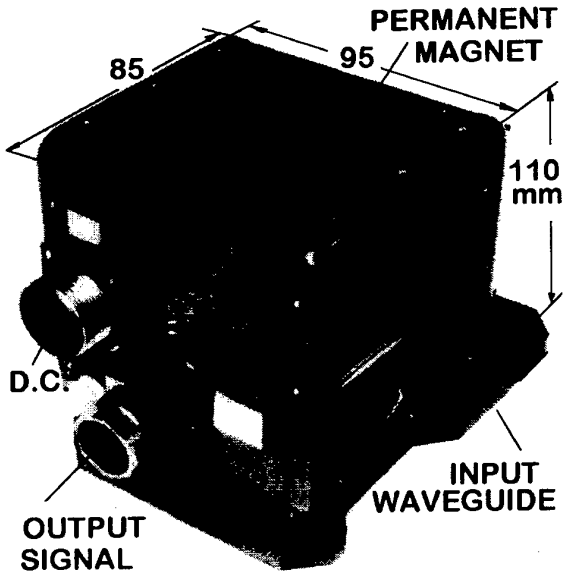

CWESA (ISTOK Corp.)

Applications:
Receiver-protector in high-quality pulse doppler radars and communication systems

Several thousand CWESA manufactured only in Russia

CWESA PROTECTION ABILITY

CWESA are primarly reflective and tolerant of high power impact.

Protection against short pulse microwave impact up to 100-500 kW.

Leakage spikes are related to pulse risetime and don't exceed 0.1mW.

Rapid recovery <10-20 ns.

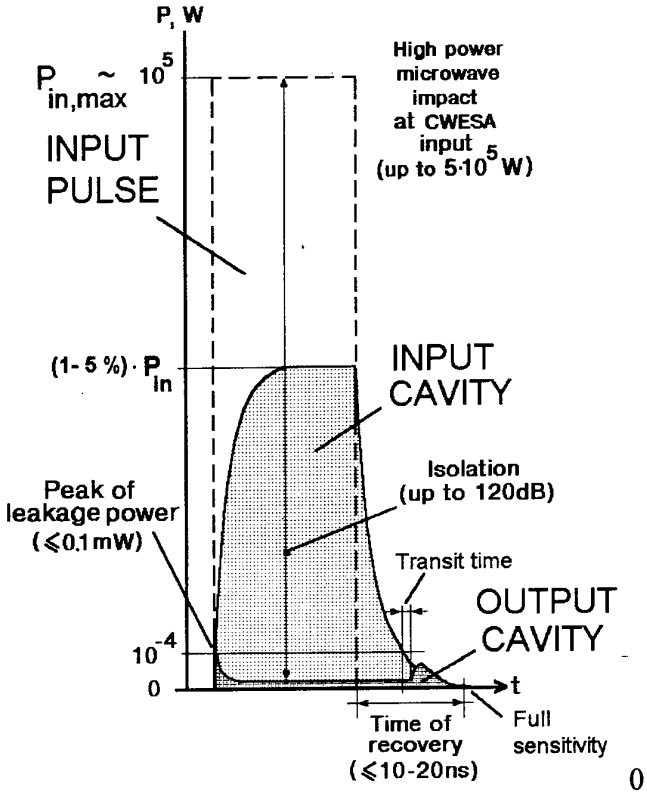

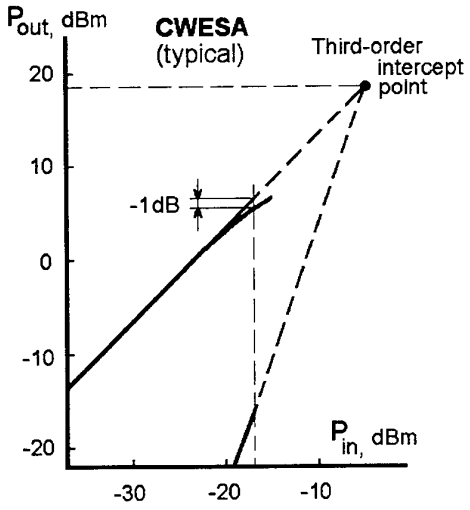

CWESA Linearity

Typical level of third-order intercept point is about 18 dBm

Circularly Polarized TWT (CP TWT)

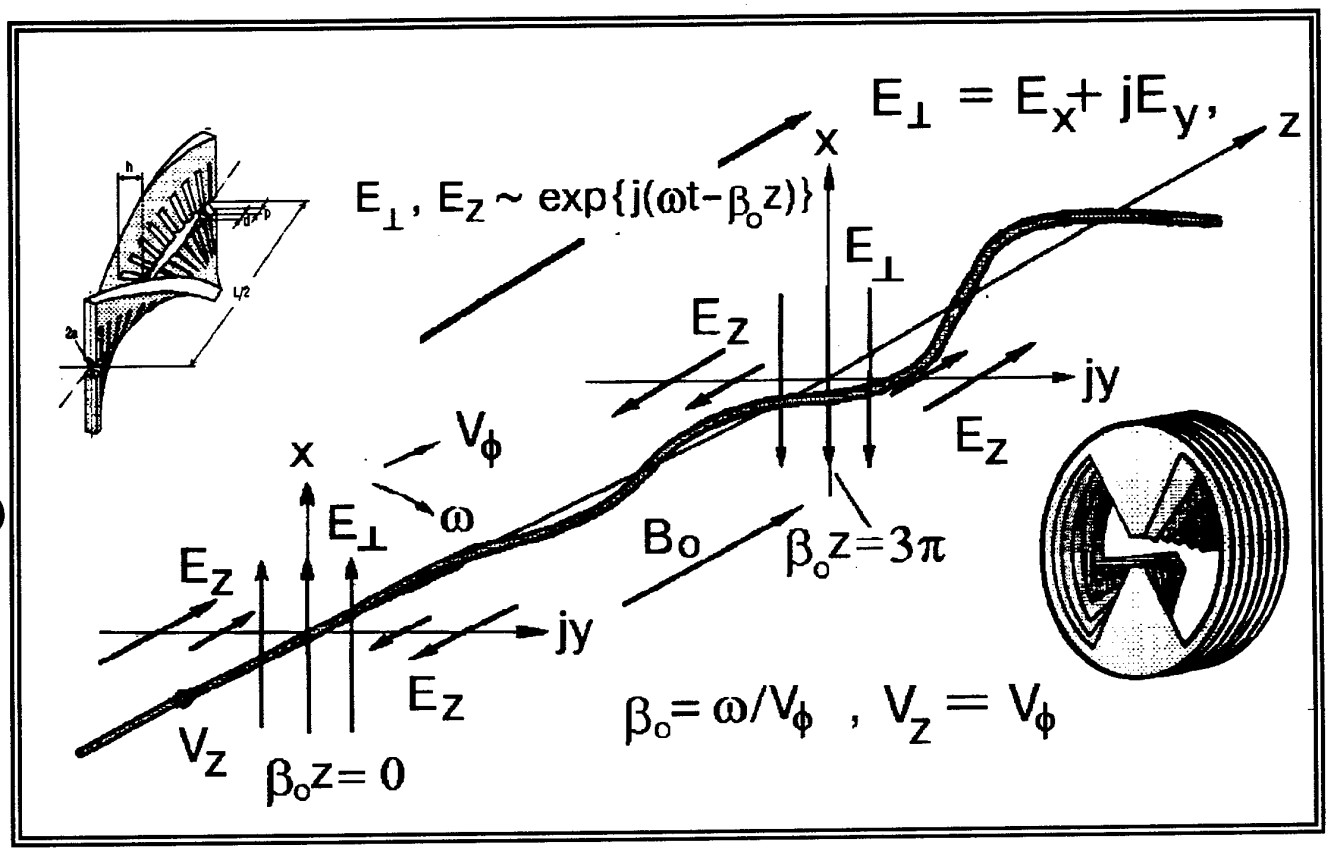

Each electron injected (at any moment of time) along Z axis will be decelerated ***equally and monotonously*** *by the electric field E_Z of the circularly polarized wave.*

The filamentary beam will be ***monoenergetic*** *at the end of interaction.*

Beam twisting is instead of electron bunching.

3D Computer Simulation of CP TWT

Efficiency :

40% (into load),
75-80% (with recuperation)

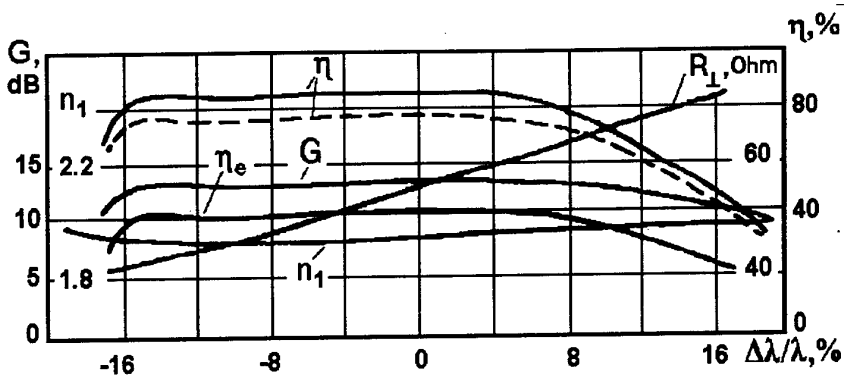

Bandwidth : up to 25-30%

λ=11cm, I_o=4.3A, I_o=94kV, P_{in}=10kW, B_o=0.15Tl, R_o=1mm
L_{str}=96cm

Extreme linearity in operation regimes of maximum efficiency

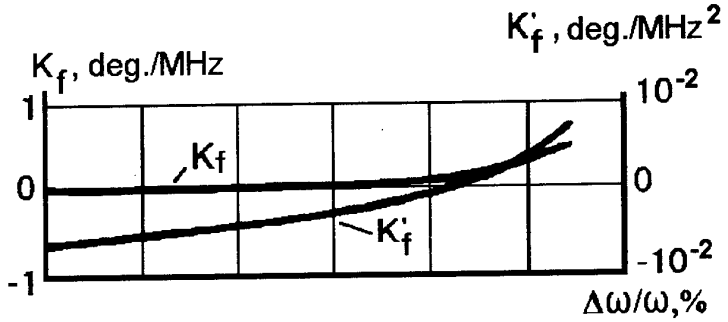

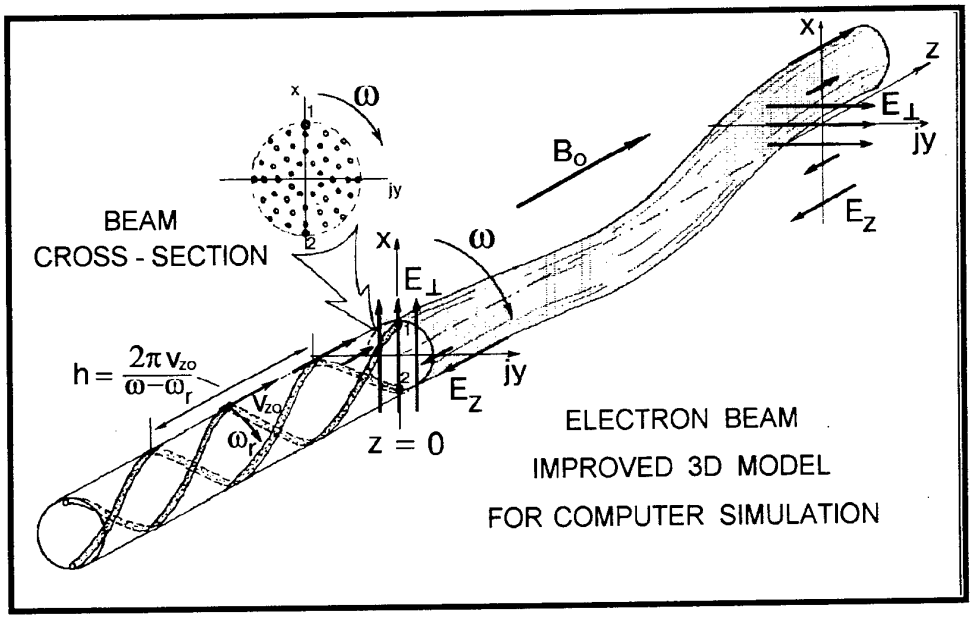

CIRCULARLY POLARIZED TWT *(preliminary experiment)*

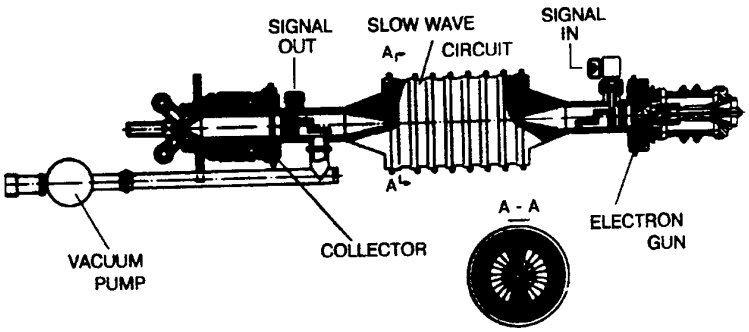

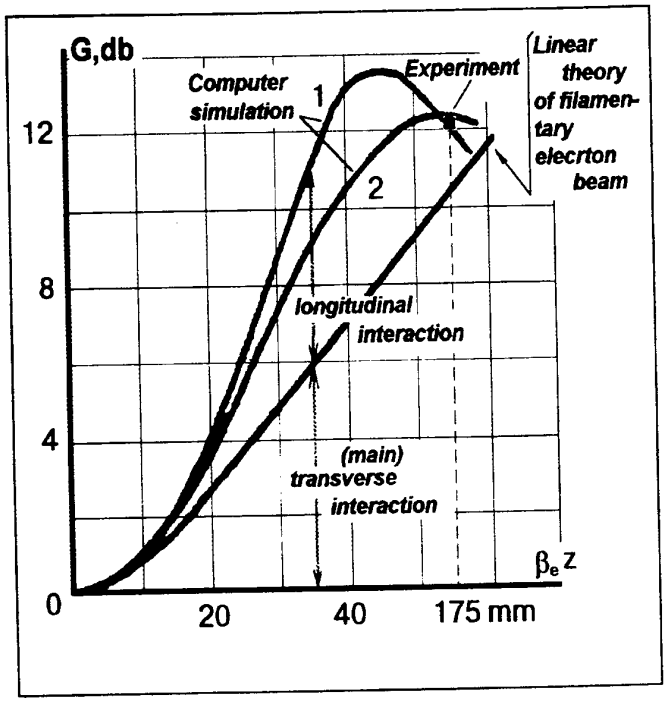

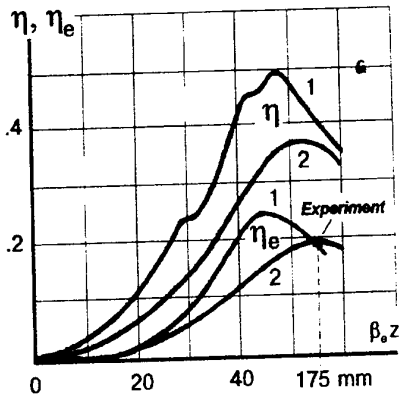

1 – $\left\langle (\delta v_z / v_z)^2 \right\rangle_{z=0} = 0,$

2 – $\left\langle (\delta v_z / v_z)^2 \right\rangle_{z=0} = 5\%.$

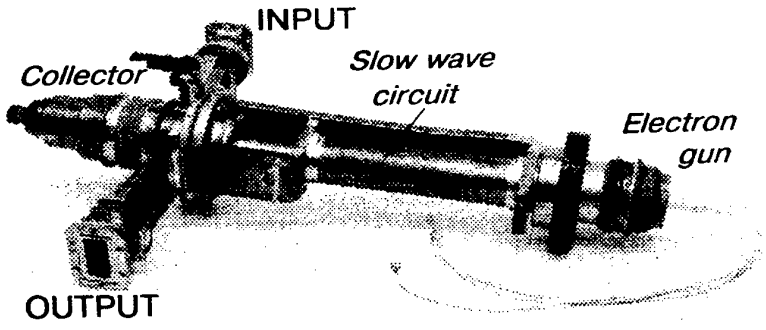

CYCLOTRON WAVE CONVERTER

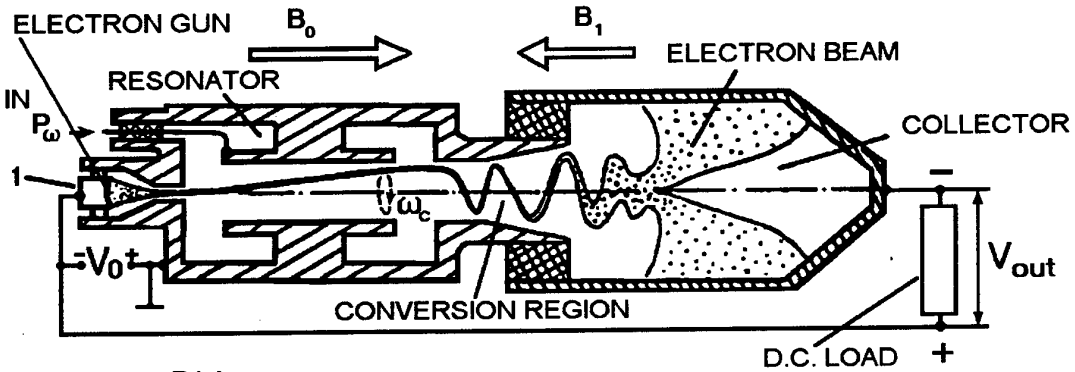

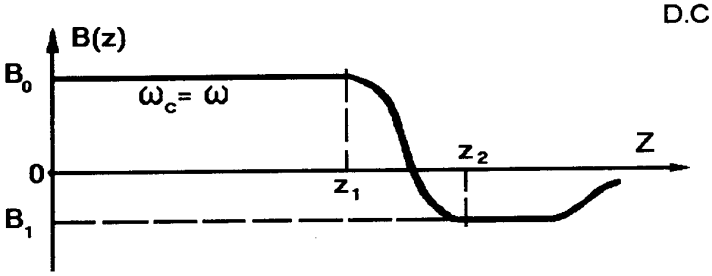

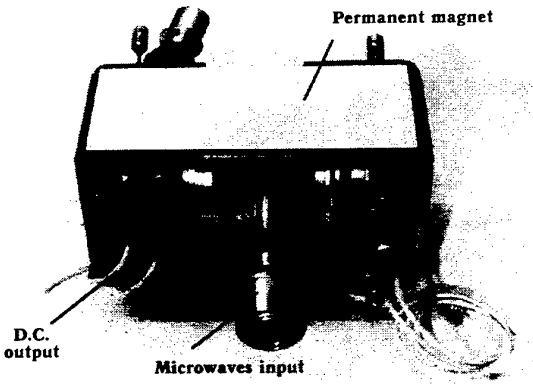

- High level of self-protection against microwaves and dc overloads.

- High output power level (up to 50-100kW) and high output voltage range (10-100 kV).
- Efficiency of conversion of microwave into d.c. up to 80-90%.

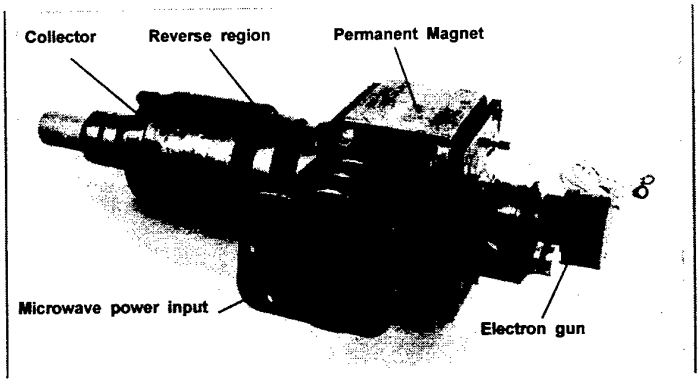

Cyclotron Wave Converter #17
(Experimental Device, TORIY Corp.),

Efficiency from 60-70% up to 83% has been achieved.

KLYSTRON WITH COMBINED INTERACTION

(longitudinal - transverse)

$$G_1 \cong \frac{2I_0}{(1.3 \div 1.5)U_0},$$

$$G_0 = \frac{I_0}{8U_0} \cdot \frac{L^2}{d^2},$$

$$\frac{L^2}{d^2} \approx 50 \div 100,$$

$$\frac{G_0}{G_1} \approx 10 \div 15.$$

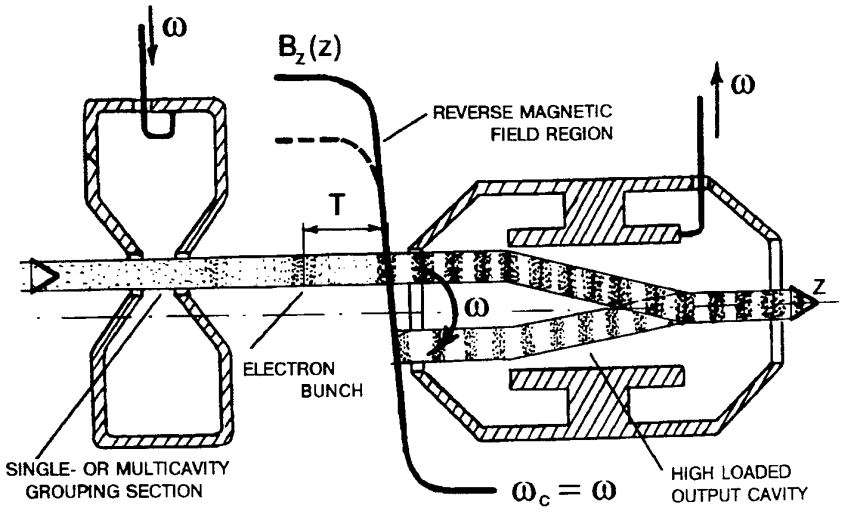

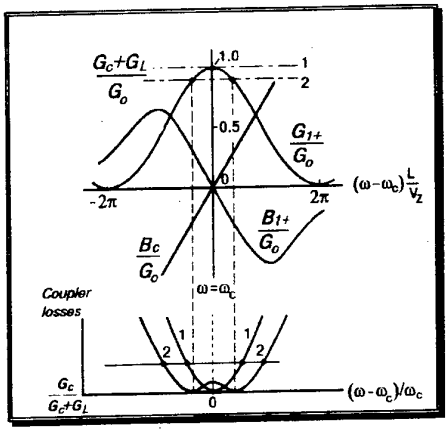

- **Extended bandwidth** (up to 8-10%),
- High efficiency (up to 75-80%),
- Various power levels (up to 50-100kW).

ESA/NATO Workshop on Microwave Tubes for Space, Military and Commercial Applications

7 - 10 April 1997

SESSION 1
TWTAs Status and Capabilities

Chairman: G. Fleury, Thomson Tubes Electroniques Velizy, France

POWER-BOOSTER TRAVELLING WAVE TUBES

K.D. Ward, M.J. Duffield, A.R. Wise
EEV Ltd, Witham, UK.

ABSTRACT

A key feature of some modern TWT transmitters and amplifiers, including the microwave power module, is the use of a high gain, high power (typically 1 Watt) solid state driver amplifier and a low gain (typically 25dB) TWT. The smaller size and weight of the low gain TWT enables the transmitter to be small and lightweight compared with traditional TWT amplifiers, and the overall noise figure to be reduced.

Development of these transmitters has been largely based around a low gain mini TWT, capable of producing typically 100W saturated RF output power. However, the concept of using a low gain TWT with a high power driver amplifier can also be used with higher power TWTs. The development of such low gain high power TWTs is reported.

A range of power-booster TWTs operating in the frequency range 6 - 18 GHz, and with saturation output powers from 100W to 500W is described. These tubes have been designed using advanced CAD, including 3D-PIC modelling which is capable of accurately predicting TWT output power, gain and other parameters over a wide frequency range. The use of modern CAD for TWT design is discussed and the accuracy of the predicted performance showed by comparison with TWT test results.

INTRODUCTION

Probably the most significant development in travelling wave tube amplifiers (TWTAs) in recent times has been the microwave power module (MPM). The MPM work was initially funded by ARPA/Tri-Services in the USA for 1D phased array applications. Essential features of these MPMs are, a redistribution of gain from the TWT to the solid state driver amplifier, making use of the higher output power available from modern microwave FET amplifiers, the use of a TWT with a low electron beam voltage (typically 4kV) to achieve a relatively high gain per unit length, and close integration of the TWT, Solid State driver amplifier (SSA), and the PSU.

All of the initial MPM work used TWTs which were low gain variants of the mini TWT, with an operating band of 6 - 18 GHz and band edge power of typically 80W, and saturation gain of typically 25dB. The low gain TWT was called a "power-booster tube".

However, the essential features of the MPM apply equally well with higher output power-booster TWTs. For those applications which require more output power than can be achieved using a single mini power-booster tube, a high output power-booster TWT can be used to avoid having to combine the outputs of two or more tubes. As will be described below, higher output power can be realised in power-booster TWTs which are only slightly increased in size and weight compared with the mini power-booster.

We describe the development of a range of power-booster TWTs which operate in the I/J frequency band and which are capable of producing between 100W and 500W output power. Variants of these TWTs are available for use in ECM, communications and radar applications. These tubes have been developed using numerical CAD tools. This paper also includes a discussion of the use of modern CAD tools to accelerate the development process and achieve better optimised designs.

POWER-BOOSTER TWT

The small signal gain per unit length of a TWT is given by the equation:

$$G_L = BCN$$

Where B is the increasing wave parameter, which depends on the relation of electron beam to circuit velocities, C is the Pierce gain parameter, and $N=\beta_e/2\pi$, is the number of waves per unit length. β_e is the slow space charge wave propagation constant. In order to make a tube physically short, the gain should be kept to a practical minimum and the beam voltage should be as low as is possible in order to maximize β_e.

There is a lower limit on gain which is determined by two factors, the available drive power from SSAs, and the requirement to keep the overall gain above approximately 25dB in order to maintain device efficiency. The power that is economically available from SSAs (6 - 18GHz) is around 30dBm.

The practical limit is determined by magnetics. As β_e, and the electron beam perveance increases, so the required strength of magnetic confinement field also increases. Modern PPM designs use high energy product SmCo magnets. In practice, a beam micro-perveance (μP) of typically 0.6 is a good design value. The mini TWT operates at a beam voltage of 4kV, and a beam current of 150mA; μP=0.59. Older TWTs which operated with a beam voltage of around 9kV, were used in EW, ground based satcom, and radar applications. These tubes provided more output power than the mini TWT, typically 200W in I/J band. However the μP was approximately 0.25. The principal advantage of increased μP is reduced volume and weight. The volume and weight of a 0.6 μP, 200W I/J band TWT is typically only 30% that of a similar but 0.25 μP TWT.

In order to realise high output power in a compact package, a range of low gain "power-booster" tubes, each operating

TABLE 1: *Power-Booster TWT Characteristics*						
Type No.	Freq' Range (GHz)	Nominal Output Power (W)	Beam Voltage (kV)	Beam Current (mA)	μP	Overall TWT Length (mm)
N10122	6 - 18	100	4.15	150	0.56	165
N10123	6 - 18	150	5.3	230	0.60	180
N10121	6 - 18	220	6.2	260	0.55	190
N10117	11 - 17	400	7.3	320	0.51	180

with a beam μP of approximately 0.55, and with a band-edge saturation drive power of +25dBm, have been developed. The operating characteristics of these tubes are given in table 1. Three of the tubes are CW broad band types, one is a J band pulsed helix TWT. Each TWT comprises a convergent electron gun, two helix sections, PPM focusing, and a either a single or dual stage depressed collector.

A conventional Pierce type electron gun with separate focus electrode and anode is used in each type. One of the tubes, type N10117, is designed for pulsed operation and incorporates an intercepting grid switch. M-type cathodes are used with current loading up to 4A/cm^2. The gun/PPM designs were derived using a conventional particle trajectory gun code. A beam stiffness factor, λ_p/L, of 3 was used, and the designs were compensated for operation over a wide temperature range (-55 to +200 °C).

The helix slow wave structures were designed using TLM (Ref. 1). Overall gain was adjusted for the +25dBm saturation drive, and the distribution of gain between the two sections was chosen so that the gain in the output section was sufficient for maximum output power efficiency. Broad band types incorporate a slow wave circuits with dispersion correction to reduce the level of second harmonic output power, better than -4dBc (6 - 18 GHz).

Single and dual stage collector versions of the tubes are available. The overall band centre efficiency with a single stage collector is typically 31%, and 39% with a dual stage collector. The band-edge efficiency of the broad band tubes is typically 22%/28%.

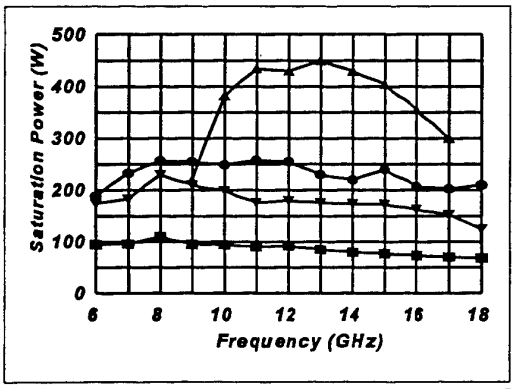

Figure 1: *Saturation Output Power;* ■ *N10122,* ▼ *N10123,* ● *N10121,* ▲ *N10117.*

TWT PERFORMANCE

The saturation output powers for these tubes are shown in figure 1. Applications which require high output power but where space and mass restrictions apply, may benefit from the use of a high power booster; as can be seen a 200W power-booster tube is only 25 mm longer than a 100W mini power-booster. The weight of the 200W power-booster is 0.8kg, compared with 0.5kg for the 100W TWT.

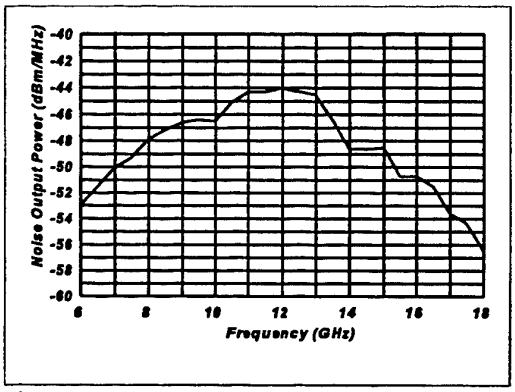

Figure 2: *Undriven noise output power for type N10123.*

The maximum noise power is typically -45 dBm/MHZ, the noise output power from the 150W tube, type N10123, is shown in figure 2. Assuming the driver amplifier noise figure and gain are 10dB and 20dB respectively, the combined SSA and N10123 TWT noise figure is 11dB, compared with 22 dB for a conventional gain TWT SSA.

These tubes have been designed for use in severe military environments. Some applications require operation over an extended temperature range. Tubes can be fitted with either a conventional PPM stack for applications where the stack temperature does not exceed 160°C, or with a temperature compensated stack which allows the stack temperature to exceed 200°C.

COMPUTER AIDED DESIGN

The speed and capacity of modern computers and the availability of numerical programs which model underlying physical interactions to determine the response

of large scale systems, can now provide the opportunity to compute the performance of microwave tubes with a high degree of accuracy. The advantage of this approach is that approximations about device physics and geometries can be avoided and therefore a more accurate prediction of performance is potentially realisable. More information, and therefore insight, about the device can also be obtained. The disadvantage is the computer resource required to run accurate models. Even with the fastest workstation currently available, the computational time for PIC codes to determine the saturation output power over the bandwidth of a TWT will take several days. However, this is still significantly less time than it takes to build and test a tube, and costs a fraction of the amount it costs to build a tube.

Numerical CAD has been developed and used at EEV over several years. Codes for modelling electromagnetics, electrostatics, magnetostatics, particle codes, and thermal and mechanical codes are routinely used for product design and optimisation. TWT specific design codes have been developed for modelling the RF characteristics of slow wave structures, and for carrying out TWT PIC calculations (ref 2). The development of these codes has been supported by the Defence Research Agency in the UK. The use of CAD for designing helix slow wave structures, and collectors is described in this section. TLM (ref 1) is used to determine the phase velocity and interaction impedance of helix slow wave structures. This information is used to calculate TWT performance using a parametric code which can be run within a few seconds to obtain a first cut design. A new 3D PIC code is used to accurately determine the microwave performance of TWTs.

TLM

In TLM (Transmission Line Modelling), the electromagnetic field is represented as signals on a dense three dimensional network of transmission lines (ref 1). The networks are analysed in the time domain, by initially placing pulses on certain transmission lines and then tracking the pulses as they are scattered throughout the network.

For analysis of helix slow wave structures, a length of the structure is modelled, using a cylindrical polar coordinate system, and boundary conditions are applied to each end, to logically identify the end planes of a periodic structure. Resonant loops are effectively modelled. The response at certain points in the structure is Fourier transformed to obtain the resonant frequency, and hence the phase velocity. A series of different lengths of the structure can be modelled in this way to obtain the frequency-dispersion characteristic.

TLM can also be used to determine the spatial field distribution at the loop resonant frequencies, by convolution of the time domain response at all points on the TLM network with the resonant frequency. This field distribution can be used to determine the Pierce interaction impedance.

The accuracy of the phase velocity determined in this way is typically ±0.5%. The interaction impedance is estimated to be accurate to ±20%. Since TWT gain is proportional to the cube root of the interaction impedance, this degree of accuracy is adequate for most purposes.

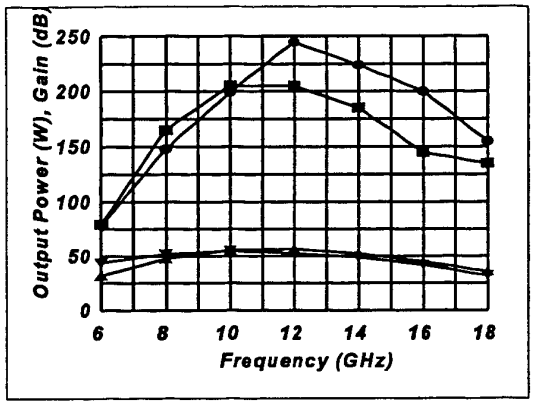

Figure 3: *A comparison of the predicted and measured saturation output power and small signal gain for an experimental TWT. The predicted values were obtained using a 1-D large signal model with circuit parameters derived using TLM.* ■ *predicted power,* ● *measured power,* ▲ *predicted gain,* ▼ *measured gain.*

PIC

Particle-in-cell (PIC) modelling uses a finite element net to represent electromagnetic fields. Electrons are represented by super-particles, each of which corresponds to many electrons, which move within the net as they are subject to electromagnetic field forces and space charge forces. The development of the PIC modelling of helix TWTs has been carried out by AEA Technology in the UK, work supported by the DRA. A 2D axi-symmetric model has been previously reported (ref 2). More recently, a 3D PIC codes

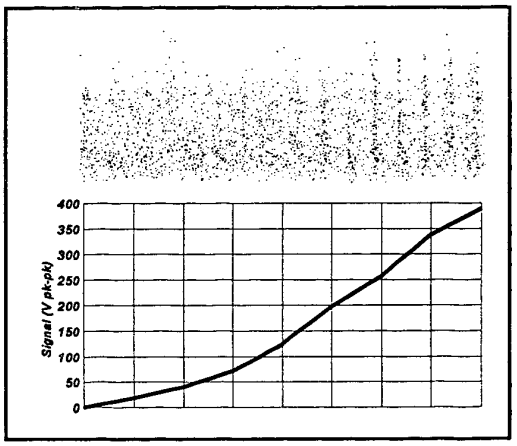

Figure 4: *Example of the PIC beam in the output section of a TWT, and the growth of the RF voltage.*

have been developed (ref 3), including a 3D code adapted for modelling helix TWTs. This code is now routinely used at EEV to validate designs before they are built. A brief description of the performance of this code is given herein, a full description will be published later.

The adaptation of the 3D PIC code for modelling helix TWTs uses specialized pre- and post-processors for the definition and analysis of helix TWTs. Unlike established PIC codes for microwave modelling which use orthogonal elements, this code incorporates body-fitted finite elements to facilitate the accurate modelling of the slow wave structure geometry.

An example problem is illustrated in figure 4, which shows the PIC beam in the output section of a TWT which is operating at saturation output power. The growth in the amplitude of the RF signal is also shown. In this calculation, approximately 160,000 super particles were used. As can be seen by inspecting figure 4, bunching of the beam is increasingly evident towards the output of the section (RHS) where the signal is strongest.

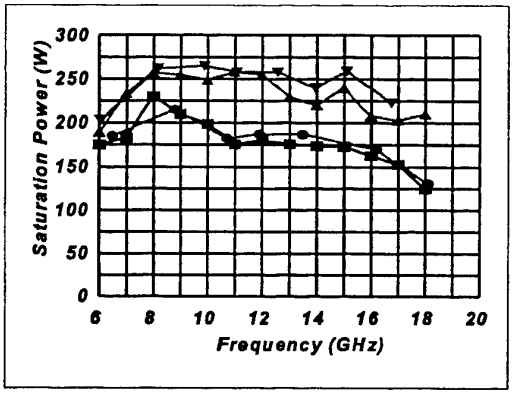

Figure 5: *Measured and PIC predicted saturation power N10123;* ■ *measured,* ● *PIC, N10121;* ▲ *measured,* ▼ *PIC.*

The accuracy of the code is illustrated in figure 5 where the saturation output power as a function of frequency is compared with the PIC prediction for types N10123 and N10121. The agreement across the frequency band is very good, the discrepancy between predicted and measured performance is similar to the tube-tube variation.

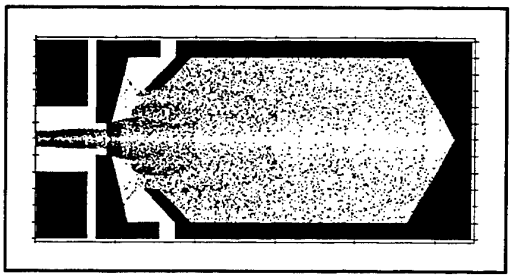

Figure 6: *Example of PIC collector model.*

PIC codes are also used for predicting the performance of TWT collectors. The advantage of PIC is that it can accurately predict the performance for the case of an RF modulated beam. Many other codes are only able to model unmodulated beams. An example of a PIC model of a dual stage collector model is shown in figure 6. The accuracy of the method is shown in figure 7, where the PIC results are compared with the measured performance of an

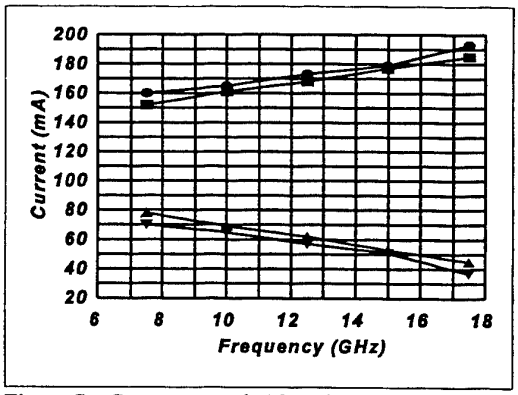

Figure 7: *Comparison of PIC and measured collector current for a TWT with a dual stage depressed collector. Stage 1:* ■ *Measured,* ● *PIC; stage 2:* ▲ *measured,* ▼ *PIC.*

experimental TWT which incorporates a dual stage depressed collector. The agreement between the two sets of results is approximately 5%.

SUMMARY

A family of low gain power-booster TWTs has been described. High output power from a small packaged is achieved by virtue of the low gain, and by use of an increased perveance electron gun. The TWTs are available for use in a range of applications, communications, EW and radar. All the tubes are designed for use in rugged environments. For those applications where operation at high temperature is required, temperature compensation can be provided.

The use of advanced CAD has been used in the development of these TWTs. The use of TLM and PIC analysis provides the opportunity to accurately model and optimise TWT performance.

ACKNOWLEDGEMENTS

The authors gratefully acknowledge the support of the UK Defence Research Agency, Malvern for supporting the development of CAD tools described herein.

REFERENCES

1. K.D. Ward, J. Wlodarczyk, *"Transmission Line Modelling of Helix Slow Wave Structures"*, IEDM Technical Digest 1993, pp 157-160. pub. IEEE 1993.

2. N.J. Brealey, J.W. Eastwood, K.D. Ward, M.J. Duffield, R.H. Boyle, *"Computer Modelling of TWTs"*, Proc. Space TWTAs 1994 Workshop, ESA WPP-072, May 1994.

3. J.W. Eastwood, W. Arter, N.J. Brealey, R.W. Hockney, *"Body-fitted PIC software for electromagnetic problems: the time domain code PIC3D"*, Proc. 3rd Int. Conf. on Computation in Electromagnetics, April 1996, pub. IEE.

TRAVELLING WAVE TUBE AMPLIFIER STATE-OF-THE-ART AND FUTURE TRENDS

K-H. Hübner

Bosch Telecom
Space Communications Systems
71522 Backnang, Germany

Abstract

Since the application of Travelling Wave Tube Amplifiers (TWTA) in space systems started, some trends in their evolution could be seen, which also influenced strongly the design of the Electronic Power Conditioner (EPC). An increase in RF output power (up to 260 W), higher frequency ranges (up to 60 GHz) and more complex and powerful satellite systems called for higher power handling capability, higher supply voltages for the tubes and in parallel less weight and higher efficiency (= 56 %) are required. The TWTAs which cope with these requirements are state of the art and improve the overall satellite system capability.

This paper describes a TWTA consisting of two TWTs (Travelling Wave Tube) and an EPC with advanced technology, which is the basic design of a high reliable new family, and a TWT with the latest design. Some information about this TWTA performance will be presented. The last part gives a view on the possibilities of TWT and EPC in the near future.

Introduction

For more than 25 years Bosch Telecom has been involved in a lot of communication satellite programmes as far as the TWTA and EPC equipment are concerned. All delivered TWTAs are highly successful. During these years a lot of experience has been gained in electrical, mechanical and technological design. This knowledge together with new devices were the basis for the basic design of a new EPC generation. This new generation covers a RF output power range from about 35 W to 260 W. The very high power is used in direct broadcast satellites (DBS) for high definition TV (HDTV) and is achieved by paralleling two 130 W high power TWTs which are supplied from one single EPC. This Ku-Band TWTs can be a conduction or radiation cooled version.

Description of TWTA

The **TWTA** is made up of two components: a travelling wave tube (TWT) and a power supply or electronic power conditioner (EPC). This is the final stage power amplifier in the transponder of a communication satellite. It is a key component because of its high RF output power, efficiency, weight, life, reliability and RF performance. While the major RF parameters are determined by the tube, the power supply forms the interface to the satellite power and command lines.

A **TWT** is an electronic device in which an electron beam travelling in a vacuum interacts with a weak radio frequency (RF) signal. This signal will be amplified by a factor of about 60 dB in the output signal by converting the kinetic energy of the electron beam into RF electric energy. The tube can be subdivided in three major parts: gun, focussing and delay line system and collector.

The **EPC** converts the low unregulated or regulated DC voltage from the spacecraft bus to extremely well regulated high voltages for the TWT. It also processes the telecommand and telemetry signals coming from and going to the spacecraft bus system. Therefore the EPC is subdivided in three sections: power converting, high voltage generation and telemetry and telecomand interface with internal protection circuits.
Both equipments are interconnected by a high voltage cable and individually packaged to provide utmost flexibility for integration into the satellite structure; Figure 1.

The EPC

The design of the EPC is mostly dependent on three principle interfaces: spacecraft/EPC, TWT/EPC and communication system/EPC. Stable operation, high efficiency, low weight and high reliability must also be considered in the design of the EPC which has to provide the following functions:

- A highly efficient generation of the high voltages required to operate the TWT from the variable or constant spacecraft bus voltage
- Provision of telemetry signals
- Matching of telecomand signals
- Protection of TWT and EPC in case of malfunction
- Provision of operational sequence for the special TWT switch on requirements
- Isolation of RF amplification from noise inputs from the spacecraft bus (radiated and conducted susceptibility)
- Isolation from noise generated by the TWTA (radiated and conducted emissions)

For better understanding of the function and internal processes of the EPC, it has been divided into functional blocks. The blocks are depicted in Figure 2.

The variable spacecraft bus voltage is fed to a preregulator which converts it into a constant output voltage. This constant voltage is directly applied to the filament converter producing an AC voltage with square waveform for the TWT heater. The power converter is also supplied by this voltage and generates a special square output voltage waveform. The initial switch on of the EPC is followed by a preheating period of a few minutes after the power converter starts. The output voltage of this converter is transformed and rectified in the high voltage section to produce the TWT supply voltages.

Due to the high RF performance sensitivity, the helix voltage is additionally regulated for current (load) variations and ageing. One of the important requirements of the TWTA is to have a constant RF output power during its lifetime. Therefore the cathode current of the TWT must be kept constant as a function of the anode voltage.

The TWT

The TWT is the component of the TWTA which mainly influences the RF performance, efficiency and lifetime. The basic design of a TWT consists of

- metal ceramic technology
- dispenser type cathode
- round wire helix held in place by beryllia rods
- multistage bucket collector

The functional description of the TWT is illustrated by the block diagram in Figure 3 which shows the three main TWT parts.

The **electron gun** is a Pierce type gun which includes the cathode, the heater and two electrodes. The heater has the task of heating up the cathode in order to enable the emission of electron beams. The cathode temperature is a very sensitive parameter for the lifetime of the TWT and should therefore kept constant for the entire mission time. The two electrodes have different functions: one is to accelerate electrons and generate and control the beam current (anode), the other is a beam forming electrode (wehnelt) to improve beam efficiency.

The **delay line system** (helix) consists of the RF delay line and the focusing system. The RF circuit consists of two helix sections which are separated to provide RF isolation between input and output. The system is held in place by three beryllia rods. The electron beam is focused by a ppm stack with SmCo5 magnets.

The **collector system** plays an important role in improving the overall efficiency of the TWT because the DC beam power, which is coupled with the RF signal through the slow wave structure, is collected at the collector. The multistage bucket collector selects and collects electrons whose velocity differs according to the coupling effect of the slow wave. The more collector stages the higher the TWT efficiency. The collector stages are isolated by ceramic segments and are cooled by conduction or radiation.

Dual TWTA (state of the art)

A new type of TWTA which is shown in Figure 4 was developed, qualified and delivered in several flight programmes. This new type of a dual EPC supplies two radiation cooled TWTs which are built accordance to the state of the art tube technology. The dual TWTA can be operated as two independent TWTAs or as one TWTA with both TWTs combined [5]. The test findings in Table 1 show the very advanced technology of both components.

The dual EPC can operate with a constant spacecraft bus voltage between 70 V and 100 V and can drive two TWTs with RF output power of up to 140 W each. The basic electrical concept is a space proven well known design, which has been qualified several times. The improvements are achieved by using new devices and technologies, e.g. ASIC, MOSFET, SMD parts, simple mechanical design and coated high voltage section. The used radiation cooled TWTs have a high efficiency of more than 63 %. This is achieved by an improvement of the helix taper and the collector stages.

Trends and Technology of TWTA

Substantial improvements have been made in recently designed TWT and EPC making the TWTA more efficient and linear, with lower weight and improved reliability. The following trends can be identified in the history of the evolution of Bosch Telecom TWTA (Table 2):

- The output power has increased from less than 10 W to a current maximum of about 260 W for the first DBS satellites like german TV-Sat or french TDF. Despite of the great improvements in the receiving equipment this high RF power is needed due to the new HDTV technique which is coming up.
- Due to the lack of transmission channels new frequency bands were used. They are now used throughout the C-Band (4 GHz), Ku-Band (11/12 GHz) and Ka-Band (20/23 GHz) for mainly commercial application besides some other frequencies like X-Band (7/8 GHz) for military and environmental application.
- The evolution in the cathode technology changing to mixed metal type cathodes has increased the design life time from less than 7 years to now more than 15 years.
- Application of new technologies and materials and the more powerful computer aided design tools have increased the efficiency of the TWTA from about less than 25 % to nearly 62 % while the weight per watt has continuously decreased (Table 3).

Trends and Technology of TWT

The TWTA performance has been improved by continuously applying newest technology [1, 2, 3]. No part of the TWT has remained unchanged during its evolution:

Gun:

The trend to higher output power and higher frequencies requires higher beam current on the one hand and smaller beam diameter on the other hand. The evolution of the cathode started with oxide cathodes via standard tungsten matrix wolfram cathodes and has resulted in the mixed metal (MM) cathode or metal coated (M) cathode used nowadays. This cathode operates even with less temperature so that the heater power can be reduced which leads to a high overall efficiency.

Delay Line System:

Focussing and power handling capability were improved by applying new magnet materials, new vacuum envelope processing (integrated pole piece structure) and decreasing heat resistance from the delay line to the

housing by new rods material and shrink fitting technique, as well as new computer programmes to predict performances.

Collector:
To handle the higher power and improve efficiency, the number of collectors were increased and new technology (ceramic metal construction, no potting, new shape) introduced. With the high power TWTs the radiation cooled collector was introduced.

Trends and Technology of EPC
In the same manner as the tube was improved, the EPC was also improved step by step within the major design areas [4].

High Voltage Technology and Generation:
High voltage generation changed from parallel to serial voltage generation and the maximum voltage increased from 3 kV to 8 kV. For higher frequencies (up to 60 GHz) the maximum voltage will be increased to about 20 kV. The high voltage technology changed from potted (foam) design to an unpotted and open design which is not useable for operation in critical pressure. For critical pressure operation a coated high voltage design at a special printed circuit board (PCB) is used. Up to 260 W RF output power a single high voltage transformer concept is verified. All high voltages are supplied to the TWT simultaneously. The size and volume of the high voltage section is mainly determined by the maximum generated voltage and the mechanical and thermal layout.

Power Conversion:
The power conversion is done in a power chain which consists of a combination of a DC/DC converter (mostly a PWM regulator) and a push-pull converter. For low and medium power only one power chain is sufficient. For high power application two and more chains are necessary, also due to the special application of the supply voltages of the TWT. With the increase of the DC power demand the regulator topology changed from a simple buck converter to a boost converter or a modified topology. Also the spacecraft bus voltage changed from variable voltage (26 V to 43 V) for low and medium power to constant voltage (50 V/70 V or 100 V) for medium and high power up to 260 W. For very low power (RF < 10 W) the switching frequency is increased up to 500 kHz to reduce size and weight. Increase of the switching frequency for the high voltage generation seams at the moment possible due to the recovery time of the current qualified high voltage diodes.

Electrical and Mechanical Layout:
Due to the increase of TWTA mission time additional regulation loops are necessary such as constant cathode current regulation, and anode voltage change over life by telecommand. Secondary power supply for channel amplifier or linearizer are nowadays also part of the EPC. Due to weight reduction electrical and mechanical piece parts are used such as MOSFET transistors, CMOS ICs, surface mounted devices (SMD), multilayer printed circuit boards (PCB), power switching hybrids, special low power hybrids as ASICs and low weight structure material such as aluminia or magnesia. With the reduction of size and volume and the increase of power which is now achieved, it is evident that the thermal flux will be the major limitation criterion in the future.

Future Trends and Performance Demand

In the next 3-4 years additional improvement of the TWT efficiency up to 70 % and weight reduction of about 100 g will be achieved [1]. In the EPC a higher integration will be done which leads to an additional mass reduction of about 400 g for single TWTAs and about 300g for Ku-Band dual TWTAs. The efficiency of the EPC will be around 94 % for unregulated and about 96 % for regulated spacecraft bus voltages. With these values a single Ku-Band 140 W TWTA will have a weight of less than 2000 g and an overall efficiency of about 62 %. A Dual Ku-Band 2 x 140 W TWTA will have a weight of less than 4100 g and an efficiency of about 64 %. Due to such improvements, TWTAs will be again used for C-Band applications. Therefore it is possible to have a C-Band 60 W TWTA with an overall efficiency of more than 60 % and weight figure of less than 1600 g. Table 4 shows typical state of the art and future Ku-Band TWTA performance data.

For multimedia application new frequency ranges will come up. In the Ka-Band (20 GHz) TWTAs with output power up to 150 W for the down link will be required. For inter satellite links V-Band (60 Ghz) TWTAs with about 20 W output power are foreseen. This new TWTA families require TWTs with new delayline systems (e.g. combe structure) with high voltages up to 20 kV. Therefore the high voltage design of the EPC has to be redesigned and qualified up to this high voltage values.

A new TWTA configuration will arise, the so called MPM (Microwave Power Modul). A MPM is like a small transponder which consists of a TWTA with a short TWT of about 30 dB gain, a linearizer and a channel amplifier in one housing. With a MPM an optimization of the overall efficiency, weight, RF performance, mounting area and cost can be done. Such MPMs can be used in all frequency ranges. To achieve a low overall volume new technologies must be used such as MMIC, ASIC, hybrid and short TWT (STWT) with very high efficiency. Some of this new parts like MMIC, STWT have to be qualified for space application.
BOSCH Telecom has done the first step in this MPM direction and has qualified and delivered for a flight programme an "integrated Dual Linearized Channelized TWTA". This DLCT is a MPM which includes one EPC with two TWTs, two channel amplifiers and two linearizers. Both MIC components are qualified and in the standard flight programme at BOSCH Telecom [6].

Conclusion

TWTA with high efficiency, low weight and less volume are possible with new technologies and electrical design. This allows to increase significantly the satellites channel capacity and the overall performance of satellites. The future satellite market requires high equipment integration, long life time (> 15 years), high reliability, short delivery time and low prices. **BOSCH Telecom has developed a TWTA generation with the utmost advanced technology for providing state of the art performance**. The EPC design includes the possibility to make step by step improvements in the next 5 years as predicted above maintaining the flight qualification. Table 4 provides some typical performance data and the prediction for the next future.

References

[1] E. Bosch, P. Heumüller: "Achievements and New Development Trends of Satellite Communication TWTs", ECSC-2, October '91, Liège.

[2] Dr. G. Palz: "Advanced Space TWTAs for Communications Direct Broadcast and Earth Remote Sensing", 14th AIAA, March '92, Washington.

[3] J. F. Auboin: "Second Generation DBS Satellite TWTs", 14th AIAA, March '92, Washington.

[4] K.-H. Hübner: "An Advanced Electronic Power Conditioner for 12 GHz, 100 W to 150 W Travelling Wave Tube Amplifiers", 12 th AIAA, March '88, Arlington.

[5] K-H. Hübner: " A Dual Tube Ku-Band TWTA for Advanced DBS Application", 16th AIAA, February '96, Washington

[6] G. Jaumann: "Dual Linearized TWTA with integrated Channel Amplifier", ESA/NATO 1997 Workshop on Microwave tubes for Space, Military and Commercial Application, April '97, ESTEC Noordwijk

Table 1: Dual TWTA Test Findings

Weight	TWTA	4200 g	
	EPC	2200 g	
Efficiency	TWTA	62 %	
	EPC	95 %	
High voltage		6500 V	
Frequencyrange		12.2 to 12.75 GHz	
RF Output Power		2x 125 W	
DC Input Power		403 W	
(w/o secondary power supply)			
Secondary Power Supply		2x ± 8 V, 2x 5 W	
Temperature Range		-25°C bis +65°C	
Vibration		20 grms	
Telecommand		TWT A o/a B	ON
		secondary power supply A o/u B	ON/OFF
		TWTA A and B	OFF
Operation Modus		TWT A and B parallel operation	
		TWT A and B independent channel and operation modus (e.g. CW, TDMA)	

Table 2: TWTA Evolution in Flight Programmes

Programme	Launch Date	Frequency [GHz]	RF Output Power [W]	Weight [g]	Efficiency [%]
Synonym (TWT)	1963	2.3	2.5	-	-
Synphonie	1974	4	13	1670	-
TDRSS 1-6	1983	14	30	3350	30
FEP	1986	20	25	3300	30
TV-SAT	1988	12	260	12000	38
DFS	1989	11/12	20	2750	33
DFS	1989	20	20	3000	30
Telecom II	1991	12	55	3400	47
Intelsat VII	1992	11/12	50	3200	45
HISPASAT	1992	12	55	3200	49
HISPASAT	1992	12	110	3400	52
ASIASAT	1995	12	115	2550	56
Telecom II/F4	1996	12	55	2400	56
State of the art					
Pioneer 2	1997	12	2x 125	4500	62
Hotbird 4	1998	12	135	2500	59
Sirius	1998	12	55	2300	57
Future	2000	12	2x 160	3900	64
Future	2000	12	230	2800	62
Future	2000	12	60	1600	61
Future	2000	20	2x 120	3900	55

Table 3: Weight per Watt Evolution of TWTA

Programme	Frequency band	Weight per RF Output Power [g/W]	Input Voltage	RF Output Power [W]
Synphonie	C	130	variable	13
DFS	Ka	150	variable	20
DFS	Ku	150	variable	20
Telecom II	Ku	62	variable	55
HISPASAT	Ku	58	variable	50
Telecom II/F4	Ku	44	variable	55
State of the art	Ku	42	variable	55
Future	Ku	27	variable	60
TV-SAT	Ku	46	constant	260
HISPASAT	Ku	31	variable	110
ASIASAT	Ku	22	constant	115
State of the art				
single	Ku	18,5	variable	135
dual	Ku	18	constant	2x 125
Future				
single	Ku	12	constant	230
dual	Ku	12	constant	2x 160
dual	Ka	16	constant	2x 120

Table 4: Performance Data for High Power Ku-Band TWTA

		State of the art		up to 2000		> 2000 Future	
		single	dual *	single	dual *	single	dual *
Efficiency							
	TWTA	60 %	62 %	63 %	64 %	65 %	67 %
	EPC	93 %	95 %	94 %	95 %	94 %	96 %
	TWT	65 %	65 %	67 %	67 %	70%	70 %
Weight							
	TWTA	2400 g	4200 g	2300 g	3900 g	1900 g	3600 g
	EPC	1600 g	2200 g	1300 g	1900 g	1000 g	1800g
	TWT	800 g	2x 1000g	1000 g	2x 1000g	900 g	2x 900 g

* radiation cooled TWT

Figure 1: TWTA Block Diagram

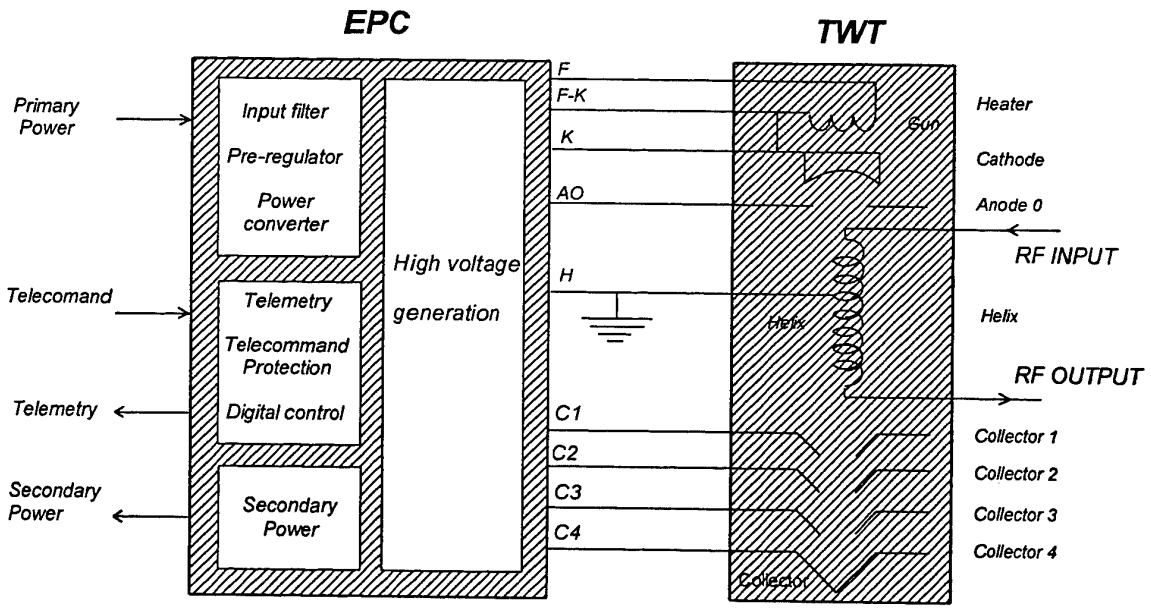

Figure 2: Dual EPC Block Diagram

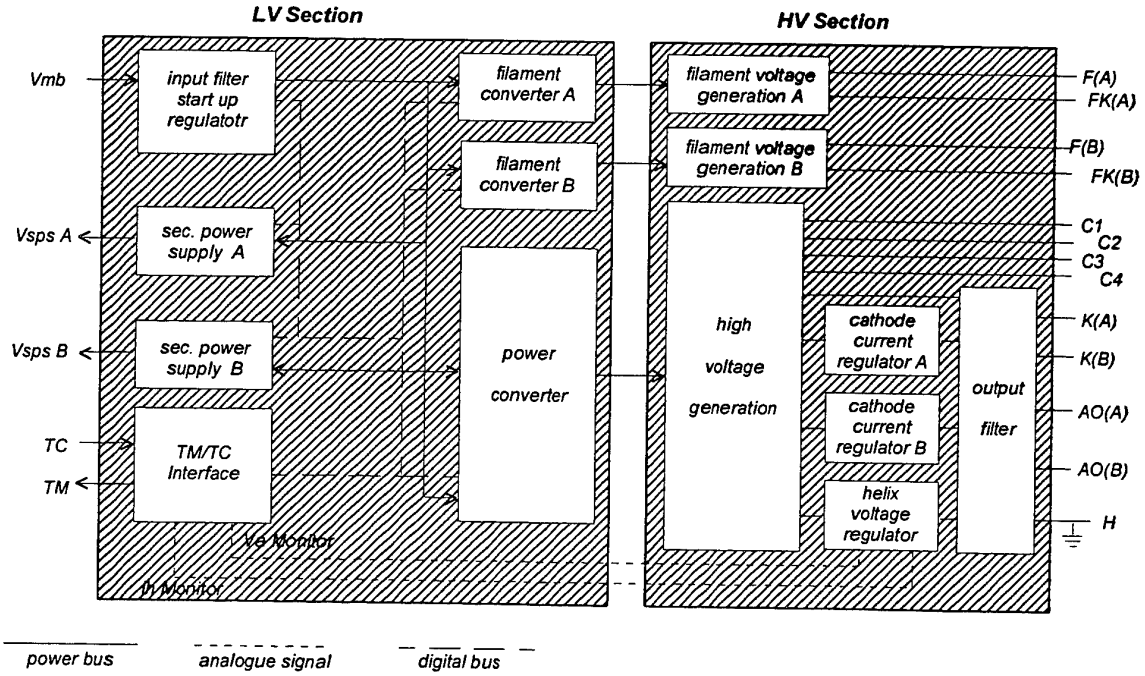

Figure 3: Block Diagram of the TWT

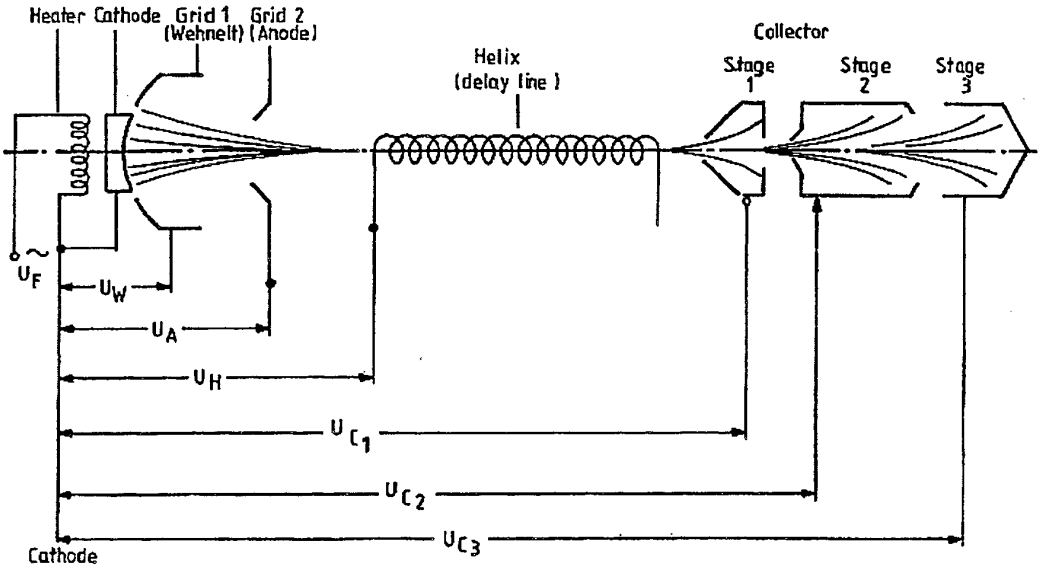

Figure 4: Dual TWTA Ku-Band 2x 113W

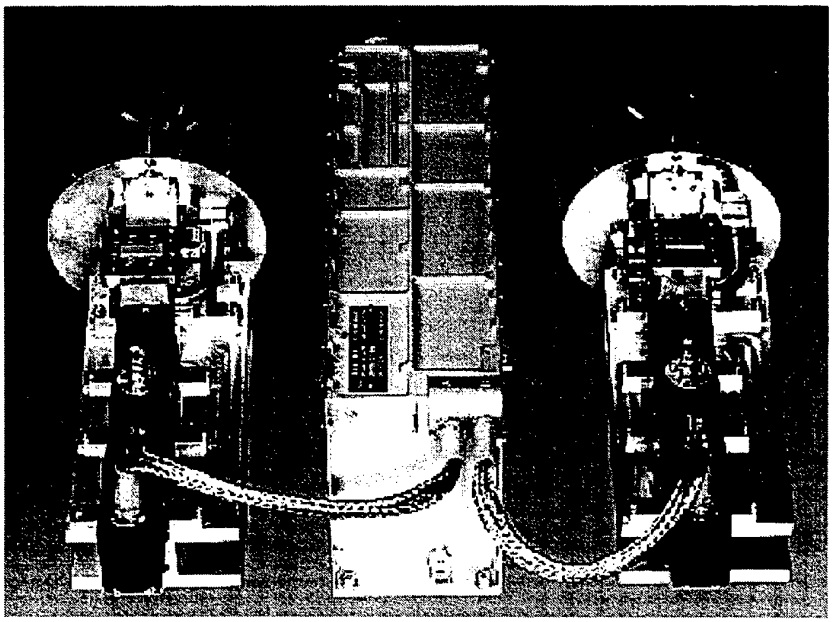

PRESENT AND FUTURE TRENDS IN HIGH POWER GENERATION.

Rob M.E.M. van Heijster
Physics and Electronics Laboratory TNO
P.O. Box 96864
2509 JG The Hague
The Netherlands (1)

Jan M. Schouten
Ministry of Defense, Directorate of Materials
P.O. Box 20702
2500 ES The Hague
The Netherlands (2)

1. SUMMARY

Modern warfare requires high levels of microwave power for various applications. Semiconductors are only suitable for low and medium power levels, for high power generation microwave tubes are still the most effective solution.

The feasibility of high power levels is mainly dependent on technology. The topics are given below:

- Tube type
- Tube design
  - Electron beam
  - Efficiency & cooling
  - Operating voltage.
- Energy storage

The reliability requirements are strongly related to the modes of operation.

Tube designs, production techniques and maintenance greatly determine tube reliability. Good power supply design can strongly increase tube reliability and hence system reliability. New power supply topologies also necessitate protection systems for the tube to run under high power conditions.

---

(1) Rob van Heijster is program manager at TNO Physics and Electronic Laboratory (TNO-FEL). He is a member of RSG-19 on "Micro- and millimeter wave tubes".

(2) Jan Schouten is EMC co-ordinator at the Ministry of defense, Directorate of Materials. He is also a member of RSG-19.

The procurement costs, the limited lifetime of the tube and the necessary maintenance are the main cost-drivers. Tube design and efficient maintenance procedures will increase the lifetime of the tube. The build-in test equipment of the power supply will reduce maintenance costs.

New cathodes and higher efficiencies will allow for higher output power. Reliability and lifetime will be increased by new technologies and "smart" power supplies, the latter also being responsible for decreasing maintenance costs.

2. ABBREVIATIONS

The abbreviations used throughout the text are explained in this section.

BIST	Build-in Self Test	MPM	Microwave Power Module
CFA	Cross Field Amplifier, a tube type family.	MTBF	Mean Time Between Failure
CW	Continuous Wave	MTTF	Mean Time To Failure
EC	European Community	MTTR	Mean Time To Repair
EMI	Electro Magnetic Interference	OE	Operational Envelop
EOL	End Of Live	OP	Operation Point
EW	Electronic Warfare	RSG	Research Study Group
FEA	Finite Element Analysis	TNO	Netherlands Organization for applied scientific research
HV	High Voltage	TNO-FEL	TNO Physics and Electronics Laboratory
HVPS	High Voltage Power Supply	TWT	Traveling Wave Tube, a tube type.

3. INTRODUCTION

Modern warfare requires high levels of microwave power for various applications. Semiconductors are only suitable for low and medium power levels, for high power generation microwave tubes are the most effective solution. The paper will give an overview of present and future trends in high power microwave systems, based on electron beam tubes.

Modern warfare requires high levels of microwave power, often in combination with wide bandwidth and high duty cycles. For many years, the generation of high power levels was the domain of microwave tubes, such as: Magnetrons, Klystrons, CFA's and TWTs.

In the past years, the reliability of the microwave tubes and the related power supplies proved to be limited. High maintenance cost and the vulnerability to single point failures accelerated the design of solid state replacements in the 70's. The design of new tube technology and HVPSs (High Voltage Power Supply) ceased.

The development of high power solid state amplifiers in D, E and F band amplifiers started. The designers made use of medium power amplifiers, called books, the power of which was combined. This made the solid state amplifier very reliable and user friendly.

The design of solid state microwave amplifiers had to rely on:

- The development of the combiner.

  The design of combiners, specially the Wilkinson combiner proved to be very successful. The bandwidth, combining losses and power handling were well predictable and the production method well within the present technology.

- The availability of transistors.

  The development of high frequency high power transistors slowed down. The expected 200 to 400 W transistor was only met in the D-band. For the other bands the power stopped at 150 W (E/F band) to 5 W (J-band). The large quantities of transistors required in the high power amplifiers brought the price of the amplifiers out of the range of many users.

The interest in the use of microwave tubes returned. System designers took full advantage of:

- The development and studies in scandate cathodes;
- The use of dedicated cathode-types in specific tubes;
- Improved brazing technology and tube processing;
- Increased understanding of the operational use by the manufacturer;
- The fine tuning of the HVPS, the protection circuits and R.F. circuits to the tube.

Within NATO, RSG-19 is assigned to develop a new standard for the reliability of high power microwave tubes. The work of this RSG has led to the writing of the handbook which encompasses all RSG-19 achievements. This handbook is discussed more in detail in another paper of this workshop. MIL-HNDBK-217 has been updated based on RSG-19work also.

For the assessment of the various reliability aspects of tubes and their HVPS the concept of the OE (Operational Envelop) is a useful tool. It also helps to adept the feasibility of tube and HVPS concepts.

This paper will first address the concept of the OE. Feasibility, reliability and cost-effectiveness are the three aspects that will be covered next.

4. OPERATIONAL ENVELOP

To model all various aspects of tube reliability, RSG-19 introduced the "operational envelop" concept. Three definitions will clarify this concept:

- Operation point (OP):

  Any combination of voltages and currents (temperatures, shock, vibration etc. may also be included) that is applied to the tube or is present on the HVPS.

- Valid operation point:

  Any OP that the tube or HVPS can handle for prolonged time (the specified lifetime).

  Valid OPs are often subject to time constraints, their validity is restricted to a given pulse width and/or duty cycle.
- Operational envelop :

  The boundary of the set of all valid OPs.

As long as the tube is operated within the OE, the stress factors are within the limits and the (well designed) tube will exhibit a good reliability. A more comprehensive description of the operational envelop concept is given in another paper presented at this workshop.

5. FEASIBILITY

The feasibility of high power levels is mainly dependent on technology. The topics are given below:

- *Tube type*

  The requirements for coherency, stability and bandwidth mainly determine the most suitable tube type and hence the maximum obtainable peak power.
- *Tube design*

  New tube designs and production techniques allow for higher power levels. Three aspects require our special attention:
  - *Electron beam*

    The electron beam converts DC power to RF power. The ability to generate and focus high energy electron beams is of major influence on the power level that can be achieved. We will focus on modern cathode design and cathode materials to investigate how the beam current can be increased.
  - *Efficiency & cooling*

    Increasing system efficiency allows for more output power at the same level of dissipated heat. Better cooling implies a higher level of allowable dissipation and hence output power.
  - *Operating voltage.*

    Higher operating voltages increase output power, however they also increase the electron velocity and hence require a major change in tube design. This limits the operating voltage in being a tool to increase output power.
- *Energy storage*

  High peak power levels require large energy storage and cause, due to fast switching, high levels of Electro Magnetic Interference (EMI). Modern techniques to store and control energy, under both operational and error conditions, will be addressed.

The system specification is the technical translation of the operational requirement. This specification dictates the class of tube and the technology to be used in the tube. In this paragraph the tube type, design, power supply and interface will be discussed.

5.1 Tube type

The tube class is driven by:

1 Frequency and bandwidth;

This determines the use of a TWT, klystron or magnetron etc.. For a wide frequency band, up to 2 octaves, a TWT will be the best choice. For a limited bandwidth but tunable over a 4 to 5 % bandwidth, a klystron is a good choice. A magnetron will be the best alternative for up to 3 % bandwidth.

2 Power output;

For the power output and the related duty cycle a TWT and klystron is capable of delivering medium peak powers (200 kW) with duty cycles up to 20%. The use of a magnetron will give high peak powers (1 MW) but low duty cycles up to 1%.

3 Stability;

Stability in a tube depends strongly on the power supply of the system. For stable, good AM and PM noise figures <-100dBc/Hz the TWT and klystron is the best choice. For a magnetron special measures have to be taken in a coherent system, -60 dBc/Hz can be accomplished.

4 Reliability;

The reliability of the three tube classes mentioned above depends on the stress that is applied to the tube. This will be discussed further in paragraph 6.

An overview is given in table 1.

	TWT	Klystron	Magnetron
Freq. tuning	External source	External source	Fixed/ tuned
Bandwidth	Octave(s)	Tunable w.r.	Tunable s.r.
Peak power	Medium	Medium	High
Duty cycle	Up to CW	Up to CW	1% max.
Coherency	Excellent	Excellent	Poor
AM/PM noise in dBc/Hz	<-100	<-110	<-60
Stability	Depending on external source	Depending on external source	0.2%
Reliability	20.000 hrs	20.000 hrs	3.000 hrs

Table 1, Overview tube types

w.r. = wide range, > 3 %.

s.r. = small range, < 3 %.

5.2 Tube design

The system application plays a major role in the design of a high power tube. It dictates the materials and the constructions to be applied to the tube. Each application has its own specific design restrains. The role of the system application is also addressed in another paper of this workshop.

A search radar will be operational during a long period of time. A tracking and illumination radar will be used during a short period of time only. EW systems are active over short periods and are in a Standby mode for a long period. This is also the case with fire control and illumination radars whose reliability must be very high upon activation. Systems that are in standby for long periods, often exhibit arcing. Due to the long standby hours, ions may be collected around the cathode and the evaporation of barium oxide out of the cathode may pollute the ceramics and grid structure. Applying the HV (High Voltage) to the tube an arc may be induced by those effects. Failure will cause extreme danger to the platform on which the radar and/or EW is mounted.

In communication systems the operational use is different from the earlier mentioned systems. The tube is in the operational mode for long periods of time. The ions produced are collected by the beam and the evaporation of barium oxide is less due to the beam cooling of the cathode surface and the equal temperature over the gun parts. During the design of the cathode special measures on, cathode material, oxide, B or M type cathode, grid and thermal stress and stability have to be taken.

The platform that carries the system will dictate the mechanical stress applied to the tube. Land-based systems do not show high shock and vibration levels. Missile applications show high levels of shock, vibration and acceleration during the start. Fighter airplanes will shock and vibrate over a long period of time. Tubes on board ships will see low frequency vibrations over long periods of time. The three described situations all require special attention to the construction of the different parts in a tube. Restrictions apply to design also. In missile and fighter applications the weight of the tube and its power supply will be limited while for land-based and shipborne applications the weight is less stringent. This implicates that the tube designer has to be aware of the platform on which the tube will be used. Finite Element Analysis (FEA) proves a valuable instrument here. It allows the tube designer to predict the mechanical strength of his design and to simulate the impact of various stimulation's.

The second part of this paragraph will focus on future strategies and techniques to cope with the above-mentioned problems.

5.2.1 Strategy

Future trends will focus on an increasing use of computer aided design. Libraries of tube parts (e.g. cathodes, RF-structures etc.) will be built up. A new tube will be designed by using the library-parts. More attention will be paid to the tube parts during their design, since they can be used in many tube designs. This will result in thorough FEA and thereby good mechanical strength, in good electric figures, in high reliability and in as simple as possible manufacturing. The manufacturer can easy adapt a given tube design to specific user requirements.

The users will tend to apply standard tube types and HVPS. The manufacturers can produce larger quantities of these standard products at lower costs. This allows for the application of many tubes, mini-tubes or MPMs (Microwave Power Module) in a high power amplifier to increase output power.

5.2.2 Cathode

Tube development will benefit from improved cathode design. Higher current densities and longer lifetimes are required. The development of coatings for the cathode, to lower the work function, are under investigation. Scandate proves to be very successful. Research is still required as the understanding of the physics is still not fully understood. A new development is the Field Emission Cathode Array (see fig. 1). High current densities can be reached in a medium vacuum environment. Figures of 40 to 400 A per square centimeter are attainable in a vacuum of 1.10-6 torr. Heaters are not required for this type of cathodes. TaSi2 is a basic material for this type of cathodes. The limitation is the short life of the cathode. This is due to the relative fast deterioration of the tips in the TaSi2 array. Further research using other materials and alloys are proceeding.

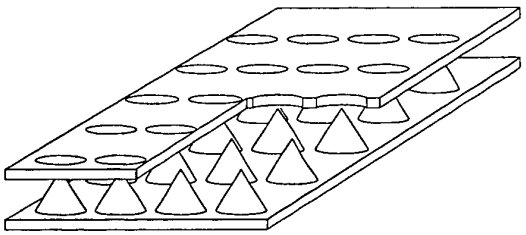

Fig. 1, Field Emission Cathode Array.

5.2.3 Cooling

The cooling of the tube has a major effect on the power handling of the tube. By efficient cooling of the R.F. structure, the power handling can be improved by at least 3 db. There are three distinctive groups of R.F. structure: Helix, Coupled Cavity and Ring Bar. In the coupled cavity and ring bar tubes the cooling of the structure is limited by the surface area of the structure. In the helix tube the heat transfer from the structure is limited by the heat resistance of the isolation material between the helix and the body. In general Beryllium Oxide or Aluminium Oxide is used. The use of diamond rods is under investigation, which promises a reduction of the heat resistance by a factor of 4. FEA proves a valuable instrument here. It allows the tube designer to predict the thermal behavior of his design and to simulate the impact of various thermal stimuli.

5.2.4 Focusing

Higher efficiency and improved focusing will reduce the energy absorbed in the RF-structure of the tube. Stronger and more reliable magnets, such as Samarium Cobalt magnets, are key elements. Due to the reduced thermal load of the RF-structure, the tube output power can be increased.

5.2.5 Structure

The use of special plastic mandrills for manufacturing the RF-structures are investigated. This technology make use of a mandrill on which material, such as copper, is electroformed thereby creating the RF-structure. The mandrill is etched out of the structure and the RF-structure remains. Due to the limited amount of brazing high accuracy and high yield can be reached by this technique. It will also reduce the RF-losses in the structure and improve the R.F. efficiency.

5.2.6 Microwave Power Module

Hybrid technology combines the best of two worlds, the high power of the microwave vacuum tube and the gain of the solid state amplifier. To increase power (gain) of a tube higher electron velocities are required. This implies an increase of the operating voltage of the tube. There are a number of disadvantages. Higher voltages will add extra difficulties to the design and reliability of the power supply and increase the complexity of the design and production of the tube. In solid state higher gains are available. By combining the gain of the solid state amplifier and the power output of the tube a cost effective solution can be found. The low gain of the tube will reduce the high voltages of the tube. When the HVPS is added to the combination of tube and solid state amplifier the MPM is obtained. The MPM has the advantage of no external HV connection and no complex wiring, only three connections have to be made: input, output and power (e.g. 28 or 270 Vdc).

So far this approach has been seen in medium power amplifiers of 200 W and frequencies up to 18 GHz. The AM/PM noise performance of the MPM is only fair due to the poor stabilization of the HVPS. The high power per cubic centimeter rating results in stringent cooling requirements. It can be foreseen that a further development to higher power levels is achievable. Future developments will focus on improvement of AM/PM noise performance and cooling.

MPMs are perfectly suited for active phased array applications, where each antenna element (or set of antenna elements) requires its power amplifier. A comparison between vacuum devices and solid state devices with respect to power generation is given in figure 2.

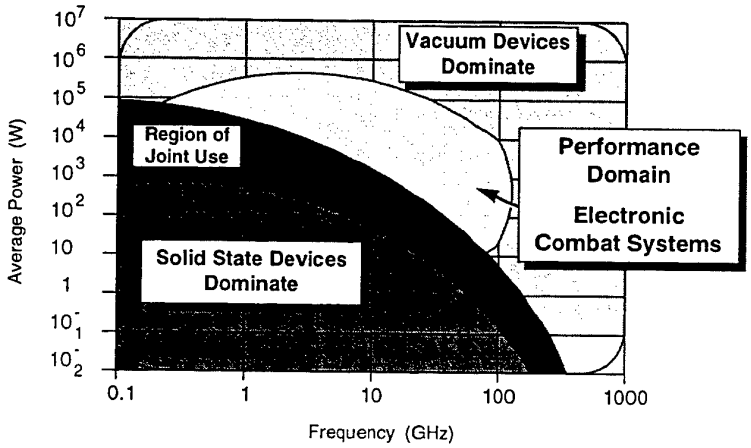

Fig. 2 Application area for Solid state and Vacuum devices.

The increased power of the MPM can be used either to decrease the number of units or to increase output power, depending on system requirements. Both MPM and solid state amplifier require extensive cooling systems.

5.2.7 Mini tube

A way of increasing the system power output is the use of multiple mini tubes. The voltage required with mini-tubes is reasonably low, about 4 kV. By combining the power in a Wilkinson combiner or Rothman lens and using multiple power supplies, a reliable high power amplifier will be designed.

5.2.8 Dual mode tube

The development of dual mode tubes started in the 80's. The difficulties with the design of the vacuum envelope and gun slowed it down. New interest, specially for the designs from the former eastern block countries, can be seen in this type of tubes.

5.2.9 Klystron

The limited instantaneous bandwidth has been a disadvantage of klystrons. New developments in the E.C. have been started on the design of inter active klystrons. This design will give the klystron a bandwidth comparable to that of a TWT.

5.2.10 Magnetron

One of the life shortening effects in the magnetron is the wear-out of the cathode and the secondary emission of the cathode stem area. The improvements of the cathode material follow the trends shown for TWT and klystron. The effect of secondary emission can greatly be reduced by adding an appropriate coating to the cathode stem and by decreasing the stem temperature.

5.3 Power supply

The feasibility of a microwave power generator is not limited by the voltage and current ratings of today's HVPS. More important however is the protection and control of the power supply. The power supply should be kept within its OE under all conditions. The OE of the HVPS should include that of the tube, so the power supply can never be damaged by any operation condition of the tube. Both control and protection greatly enlarge the HVPS OE.

Present HVPS developments benefit from resonant switching converter topologies, that have among others the following advantages:

- Low EMI.

  Due to the sinusoidal current EMI is reduced;
- Low stored energy.

  The resonant converter allows for higher switching frequencies which, in combination with low EMI, leads to simple output filters with a low amount of stored energy;
- Tight control.

  The high operating frequency and simple filtering allow for high control bandwidth and tight converter control;

The low converter EMI allows for fast acting control and protection circuits without the disadvantage of erroneous operation. Semiconductor protection devices are available that can react in nanoseconds and can handle several hundreds of amperes. They can make the HVPS virtually insensitive to the most extreme tube OP: the HV-arc.

The sinusoidal converter current reduces the electrical stress on the converter semiconductors which on the one hand increases reliability and on the other hand allows for an increased power handling. Also the switching losses are reduced resulting in a higher efficiency and, consequently, smaller heatsinks.

The high frequencies allow for small capacitors, transformers and, due to the sinusoidal current, simple filtering.

Future trends will bring small and efficient power supplies. The main design effort will be on protection and control. The OE will be widened by adequate protection. The control electronics will be programmed to exactly monitor the OP and keep it within the OE unconditionally.

5.4 Interface

The power supply has two major tasks in relation with the tube, it should deliver enough power and it should keep the tube unconditionally within the tube OE.

Tight control of the OE will gradually allow for higher output power without over-stressing the sensitive parts of the tube. Tube design will be influenced by this trend, and gradually go towards tubes that allow for very high powers in return for a very narrow OE.

The OE will become more and more important in the future. It enlarges the possibilities of power tubes at the expense of increased risk to destroy tube or HVPS in case the OE is not properly maintained.

5.5 Energy storage

The energy, necessary to generate high power microwave levels, is drawn from the HVPS. The energy, supplied by power inverters, is temporarily stored in capacitors. In case of tube, the stored energy is uncontrollably released into the tube, which can be destroyed eventually. There are several techniques to avoid this energy release:

- Application of a crowbar.
- Limitation of energy storage.
- Application of HV switches.

These techniques are discussed more in detail below.

5.5.1 Crowbar

A crowbar is the conventional solution to avoid excessive energy release. It provides a low impedance pad for the energy source, thereby diverting the energy off the tube. Crowbars however show several drawbacks:

- Their reliability is limited due to sensitivity to wear;
- Their ability to "fire" is often not unconditional;
- Their reaction time is fair, a part of the stored energy is still released in the tube before the crowbar fires;
- The operation principle implies high currents compared to the operating current;
- The operation principle implies high current rise-times, the resulting EMI may easily cause damage to HVPS electronics.

5.5.2 Limited energy storage

The energy storage is limited to the maximum rating for the tube. This state of the art technique requires electronic circuits to compensate the effect of limited energy storage. Modern semiconductor technology provides high bandwidth components with sufficient voltage and current rating to enable these control circuits. The compensation electronics guarantee operation within the OE.

5.5.3 HV switch

HV-switches between energy storage and tube can block the energy release. Certain tube types (CFAs) require the switch also to switch the tube on and off. The conventional switches have drawbacks about equal to the already mentioned crowbar. To avoid these drawbacks, the HV-switch is often replaced by a low voltage, high current switch combined with a pulse transformer.

Future developments will bring the stacked transistor topologies. This emerging technology enables fast reacting reliable switches that can handle high voltages and high current levels. Today these switches still are bulky, in the near future they will be available in the same size as conventional switches. Stacked transistor topologies also enable control of rise- and fall-times, thereby reducing the amount of EMI. Moreover, operation within the OE, both under operating and error conditions, can be guaranteed by adequate control of the stacked transistor system.

6. RELIABILITY

The reliability requirements are strongly related to the modes of operation. The paper will address various aspects, including Mean Time Between Failure (MTBF) and the certainty that a tube will run upon switch-on.

Tube designs, production techniques and maintenance greatly determine tube reliability. Good power supply design can strongly increase tube reliability and hence system reliability. New power supply topologies also include the necessary protection systems for the tube to run under high power conditions.

This chapter will focus on reliability of power tubes and HVPS. The system reliability is not only determined by the sole reliability of the tube and HVPS but also by the tube-HVPS interaction. The concept of the OE is a useful tool to describe the various reliability aspects.

6.1 Tube

The TWT is taken as example, since it has all functions in physically separated areas:

- Electron generation in the cathode;
- Beam control in the grid;
- Beam focusing & acceleration;
- RF is generated/amplified in the RF structure;
- Electron collection in the collector.

Other tube types have some or all of these elements. The CFA family generally lacks beam control and focusing, electron collection is done by the RF structure. The klystron has the same outline as a TWT, however the RF structure is distinctive and they often lack a beam control grid.

In relation to general tubes, the MTBF of high power tubes is more related to:

1 Cathode stress.

High output power requires high current densities in the electron beam and thus at the cathode surface. This asks for new cathode (micro-) structures and materials. It can be necessary to operate the cathode at elevated temperatures. The latter will decrease cathode life and increase the out-gassing process.

2 Electrical stress.

High power tubes generally run under high voltages. This makes the tube sensitive to flash-overs due to gas in the vacuum envelope or contamination of the ceramics. Eventually this will lead to the inability of the tube to withstand the HV.

3 Thermal stress of the helix.

Due to imperfections in beam focusing a part of the electron beam is intercepted by the RF structure. The high speed of the electrons causes high heat dissipation in the RF structure.

4 Thermal stress of the collector(s).

All energy supplied to the tube is either converted to RF-energy or to heat. Almost all heat is, under normal conditions, dissipated in the collector. Overheating may cause the collector to melt or to evaporate metal (copper) which will form conductive layers on isolating ceramics. Collector cooling therefore is an crucial factor in tube reliability.

5 Vacuum.

Due to (thermal) stress in the brazing and/or hot spots anywhere in the tube, micro-leaks can develop, thereby causing loss of vacuum. High surface temperatures of parts inside the vacuum envelop can cause out-gassing, thereby destroying the vacuum. Also the evaporation of barium out of the cathode can have this effect.

Under certain circumstances, a "quick-start" is applied to the tube. The OE is "widened" to include the OPs with high inrush currents which can be done with special cathode and heater design. Special grids can keep the tube from operating thereby allowing for a fast switch-on of the HV.

The certainty that a tube will run upon a "quick-start" can be checked by the BIST (Build-in Self Test) of the HVPS. The heater can be tested upon resistance, where the quality of the vacuum can be proved with a static HV test. Tubes, equipped with an ion pump, can maintain their vacuum and allow for an easy check of the quality of the vacuum.

Tube technology nowadays moves to a "narrowing" of the OE in favor of an increased reliability. Better knowledge of thermal cathode behavior can result in an OE that, under strict control of the OP locus, will allow for quick-start.

6.2 HVPS

HVPS reliability is, of course, subject to general reliability aspects that apply for all electronic devices. Due to its high power and voltage handling some specific aspects are noteworthy:

1 Electrical stress.

Semiconductors are used as close as possible to their maximum ratings, which requires adequate derating to meet the reliability specifications. The sinusoidal currents of resonant converters lack high dV/dt and dI/dt which reduces the electrical stresses.

2 Thermal stress.

Most of the components are operated close to their maximum operating temperature, once more requiring derating. Resonant converters, running with sinusoidal currents however exhibit greatly reduced switching losses that allow for reduced operating temperatures and enhanced reliability.

3 Switching

The high voltage levels implicate high levels of stored energy in parasitic capacitance's. This energy is released upon switching and can destroy semiconductors. Resonant converter topologies can reduce rise-times, thereby reducing the current through the parasitic capacitors. This also can compensate certain parasitic capacitance's.

4 EMI

The high pulsed output power causes high levels of EMI, which can destroy other parts of the HVPS. Once again rise-time reduction can reduce EMI.

BIST equipment does not increase reliability in statistical terms. A failure cannot be avoided by BIST. The certainty that both tube and HVPS will run upon switch-on however can greatly be increased by proper BIST procedures. This reliability aspect is especially important for missile systems, fire control and EW systems, since they are (only) switched on when life-threatening situation occurs.

6.3 Tube-HVPS control.

Tubes and HVPS strongly interact. As far as reliability is concerned, malfunction of either one can destroy the other. The increase of reliability depends on the HVPS that has to fulfill four requirements:

- It has to keep the tube within the tube OE;
- It has to keep itself within the HVPS OE;
- It has to be able to withstand all the tube's possible operating points, including arcing (=short circuit of the HVPS!). The HVPS OE itself should be wide enough to enclose all the tube's operating points;
- It has to be fail-safe: never should the tube be put in an invalid OP due to power supply failure.

The above-mentioned requirements can be met by new power supply technology. The power supply control has, apart from regular HVPS functions, four major tasks in tube & HVPS control:

- Monitor the OP of the tube;
- Compare the OP with the internally stored OE;
- Take corrective actions to keep the OP within the OE;
- Shut-down the power supply in case the OP is near the edge of the OE. At shut-down, the OP should remain within the OE.

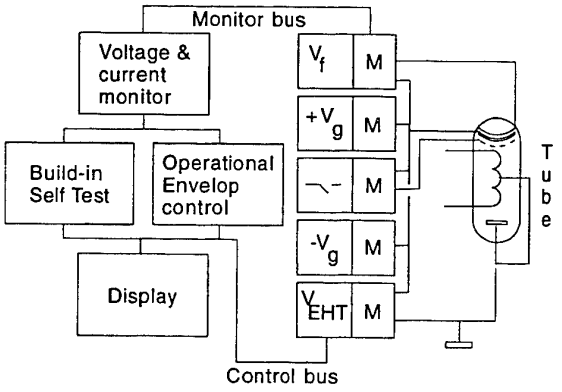

Fig. 3, Power supply with full OE control and BIST.

Given the above mentioned guide-lines concerning reliability of tube, HVPS and their interaction, a power supply was designed at FEL-TNO in the Netherlands. This power supply has extensive control electronics to guard the OE and BIST to check the power supply and the TWT. It has a display panel indicating which part of the TWT or HVPS is malfunctioning. The prototype still meets all reliability requirements after a more than four year test period. The lay-out of the HVPS is given in fig. 3.

6.4 Mini-tube

At a first glance, the choice between a "mini" and a "normal" tube has no impact on reliability. The mini-tube however works with lower electron speeds and hence lower voltages. This factor enables a significant increase in reliability of both tube and HVPS.

The major drawback of the mini is its relatively low peak output power. The mini is easier to produce, especially in series production, which allows for a lower price and a strict quality program. The mini has the potential to run at a significant lower dollar per watt rating than its bigger opponent. Even with the extra costs of combiners, large amounts of power can be generated cost-effectively by using a sufficient number of minis.

The mini will be the future solution in many RF power generators.

6.5 Microwave power module

The consists of a solid-state pre-amplifier, a (mini) TWT and a HVPS, all combined in one housing, see fig. 4.

The MPM further increases the reliability that is obtained by the use of mini-tubes:

- The gain is obtained by the solid state amplifier so the gain requirement for the tube is minimal. The tube designer can concentrate on reliability instead of on gain.
- The MPM runs at lower voltage than the mini tube.
- The tube and the HVPS can be perfectly matched with respect to their OE.
- Maintenance personnel does not have to handle HV-parts, which both increases reliability and safety.

The MPM has, as already stated, a lower power rating than the mini. For the same reasons however, their dollar to watt rating can be reasonable. The main application for MPM is the phased array antenna that benefits from the multiple amplifier concept and from the power combination that is done "in free space".

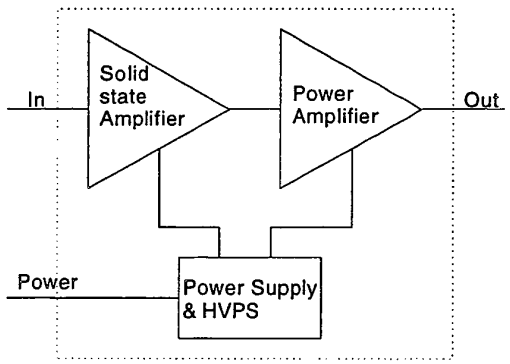

Fig. 4, The Microwave Power Module.

7. COST-EFFECTIVENESS

The procurement costs, the limited lifetime of the tube and the necessary maintenance are the main cost-drivers. Tubes also require maintenance when they are non-operating or in storage.

Production technology is in an on-going process of decreasing production costs, however tubes are labour-intensive to produce which strongly limits the effect of production technology on tube procurement costs.

Tube design and efficient maintenance procedures will increase the lifetime of the tube. The build-in test equipment of the power supply will reduce maintenance costs.

The maintenance cost of a system is not only the cost of repair and periodic maintenance, but also the cost of the logistic system.
The repair of the microwave tube is complicated and can in general only be done by the manufacturer at high expenses. The microwave tube has to be returned to the tube manufacturer for analysis and repair. This causes long turn-around times, meaning extra investments in spares tubes.
Repair of the defective HVPS may be performed by the maintenance organization of the system owner or may be contracted to the system manufacturer, requiring spare HVPSs due to long turn around times.

Maintenance personnel can only perform a limited fault analysis. A key factor is the limited time available for repair. A system has to be operational within the specified MTTR, often less than 1 hour. The maintenance engineer however has to determine whether tube or HVPS is defect. Effective HVPS BIST however can give a quick, good and well specified analysis of the fault.

Periodic maintenance can greatly be reduced by BIST. As long as tube and HVPS are operated within the OE, there is no objection to use the tube as a test load for the HVPS and/or the HVPS as a test device for the tube. This however requires auto-calibrating facilities, fail-safe BIST and fail-safe OE control. Human interference, if necessary, then is limited to maintenance that requires specific equipment.

Periodic maintenance can also be reduced by training of the maintenance engineer in fault diagnostics on microwave tubes and HVPS. The basic principles on microwave tube theory and tube maintenance has to be part of his education.

Tubes do change their OE over lifetime. Maintenance engineers often report increased lifetime due to slightly changed voltage settings. When aging is included in the OE programmed in the HVPS, this can increase tube lifetime. The operation within the OE itself also increases lifetime.

Failure data comprise a great amount of information regarding reliability and MTTF. With data, obtained from BIST, maintenance engineers (following a well defined procedure) and factory repair engineers, an in-depth analysis of the failures can be made. Here the use of HV and STANDBY hours is of major importance and a real MTBF can be calculated. Special circumstances such as land-based and ship- or airborne, type of system fire control, illumination, search radar or jammer, have to be taken into account. The results of the analysis have to be available to the system user, tube manufacturer and/or the system designer. Depending on the results of the analysis operational procedures, system modifications or tube modifications have to be discussed.

8. CONCLUSIVE REMARKS

New cathodes and higher efficiencies will allow for higher output power. Reliability and lifetime will be increased by new technologies and "smart" power supplies, the latter also being responsible for decreasing maintenance costs.

After a decreasing interest in the use of high power vacuum tubes in the 70's and 80's, new developments started in the field of cathode technology, efficiency, power supplies and tube-HVPS interfaces. This brought the tube back into the newly developed systems as a reliable microwave power source.

The combining of power, as is common practice for high power solid state amplifiers, showed its benefits at the introduction of the mini tube. The marriage of the low power solid state amplifier and the mini tube resulted in the MPM, a versatile and easy to use power amplifier.

The development of new tube technologies will depend on the performance requirements of systems. The active phased array antenna act as a technology push into the development of MPMs. The need for small lightweight systems, for example used in Unmanned Aireal Vehicles, also pushes the needs for MPMs.

The OE will be increasingly important for tube and HVPS design and development. Future developments will benefit from tight OE control. Close corporation between the designers of tube, HVPS and system is necessary to formulate the OE.

New technologies as scandate cathodes will allow for higher output power. Tube designers will take advantage from OE control to further increase output power.

Effective BIST will reduce maintenance costs.

The power amplifier of the future will consist of a number of (cheap) standard tubes, in most cases mini tubes or MPMs. The system will be virtually maintenance free, indicating the defective tube or HVPS part in case of a failure. The latter results in repair by replacement.

Ka-BAND 15W to 80W SPACE TWT SERIES

M. Kurahasi, H. Kubo and S. Hamada

NEC Corporation
Microwave Tube Division
1753, Shimonumabe, Nakahara-ku, Kawasaki, Kanagawa, Japan

ABSTRACT

The demand for a Ka-band transponder, for application to satellite-based high data rate communications systems and inter-satellite communication systems, is rapidly increasing. In fact, many specific Ka-band satellite systems are already proposed. One of the key technical challenges in these Ka-band transponders is middle to high power, high efficiency TWTs.

NEC continues challenging to increase the efficiency and reduce the weight based on long experience in Ka-band TWTs. To be available for the latest demand, NEC has developed new variety of TWTs, Ka-band 40W and 60W TWTs, which are characterized by high efficiency of 57% over frequency range 21GHz to 23GHz and light weight of 690g.

1. INTRODUCTION

Since the utilization of Ka-band for the satellite communications was proposed in the early 1970's in Japan, many satellites were launched. The first satellite using Ka-band transponder is the Japanese experimental communication satellite (CS) which was launched in 1977. In this satellite, 20GHz 4.5W space TWTs model LD4098 were used. At present , state of the art TWT model LD7849 which produces 40 to 60W over the 21 to 23GHz frequency band will be used for the latest Japanese satellite. The features of NEC's Ka-band space TWT's which have developed during more than 20 years are shown in Table 1.

In this paper, the latest lineup of NEC's Ka-band TWTs is introduced and the technical trend of these TWTs is described.

2. TWT DESIGN

2.1 Efficiency Improvement

The performance of NEC's Ka-band TWTs has been improved remarkably. Especially overall efficiency was increased from 23% to 57% as shown in Table 1. NEC has achieved several technique to improve the overall efficiency so far. The first technique is to reduce the circuit losses. In that technique NEC employs mainly two method. One is to use wedge shaped BeO support rods in order to reduce dielectric loading. Figure 1 shows a cross-sectional view of the latest helix circuit structure. Another is to employ a gold plated helix tape for the output section to reduce RF loss.

Table 1 Features of NEC's Ka-band space TWTs

Model No.	Program	Launched Q'ty	Output Power (W)	Efficiency (%)	Weight (grams)	Feature	Development Complete
LD4098	CS	1	4.5	23	780	Oxide cathode Single-stage collector	1975
ECL-1481	CS-2	12	5	25	640	Advanced version of LD4098	1980
ECL-1602	CS-3	30	10	30	850	M-type cathode 2-stage collector Velocity tapered helix	1984
LD4620	ETS-6	3	10	33	640	Advanced version of ECL-1602	1988
LD7811	COMETS	(2)	35	40	850	3-stage collector	1992
LD7812	N-STAR ROCSAT	14 (2)	15-30	51	540	3-stage collector Magnesium alloy baseplate	1992
LD7814	ADEOS-1 ADEOS-2	2 (2)	25	38	1,000	2-stage collector	1992
LD7816	COMETS	(2)	230	55	5,000	Coupled cavity type 4-stage collector Radiation cooled	1993
LD7837	Future program	—	60-80	57	720	4-stage collector Magnesium alloy baseplate	(1997)
LD7849	Future program	—	40-60	57	690	4-stage collector	(1997)
	Total	70					

The second technique is to select an optimum beam perveance. The optimum microperveance is generally selected in the range from 0.05 to 0.12 in accordance with the output power. The third technique is to optimize the helix pitch profile and to find a well-matched attenuator loss pattern. These technique are essential for the suppression of backward wave oscillation (BWO) and for good linearity. Final technique is to improve collector efficiency. NEC adopts a four-stage collector not only for the Ku-band TWTs but also Ka-band TWTs. The optimum shape and position of the four electrodes are determined by means of computer simulation. For example, electron trajectories of Ka-band, 60W TWT model LD7849 is shown in Figure 2.

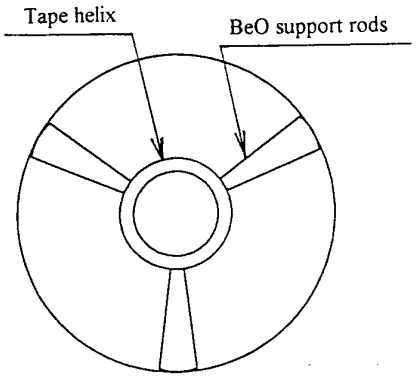

Figure 1 Circuit design

As a summary of this section, the beam efficiency of NEC space TWT over the frequency range from 2.5 GHz to 44 GHz is shown in Figure 3. As for the Ka-band TWT, beam efficiency of 17% and overall efficiency of 57% are obtained at present.

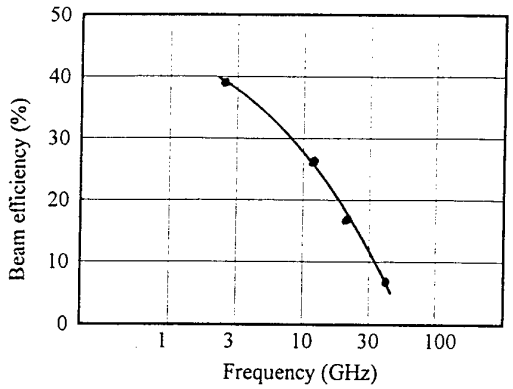

Figure 3 Beam efficiency versus frequency

2.2 Weight Reduction

In order to reduce the TWT weight, NEC employs magnesium alloy as the material of the baseplate in satellite program base. N-STAR is the first satellite program that magnesium alloy was used. Magnesium alloy is specially treated to prevent corrosion.

2.3 Life Prediction

The life time of the TWT depends on the cathode life time, then the cathode life time depends on the cathode current density and cathode operating temperature. From this point of view, NEC is conducting life test using 195 pieces M-type cathode test tubes. A total accumulated time of the life test is more than 5.3 million hours. Based on the result of this evaluation test, cathode loading of the Ka-band TWTs with output power range from 15W to 80W is selected between 0.6 and 1.2 A/m m^2 and operating temperature is set for 910 to 930 °CB. Consequently estimated life time, on the condition that the cathode current density is 1.2 A/c m^2 and the operating temperature is 930 °CB, is about 320,000

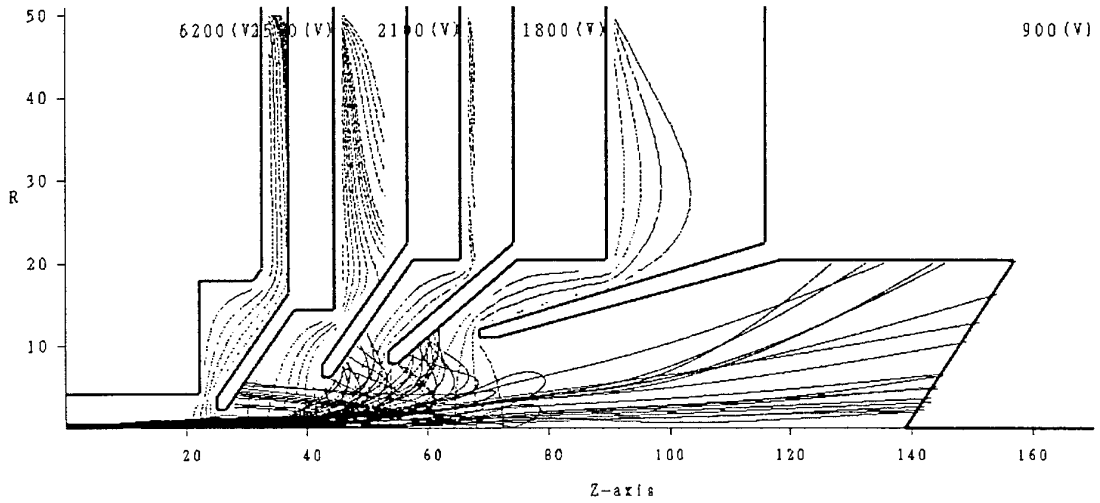

Figure 2 Computed electron trajectory traces for multistage depressed collector

hours. Therefore the typical life time of the Ka-band TWTs is predicted about 31 years with anode voltage compensation.

The expected line of the cathode current versus operating time is shown in Figure 4.

3. MAJOR PERFORMANCES

In this section, major performances of three power level TWTs, LD7812, LD7849 and LD7837 are presented. Table 2 shows a major performances of three type TWTs. These TWTs cover power level from 15W to 80W with high efficiency and light weight.

Appearance of these TWTs are shown in Photograph 1 to photograph 3. Figure 5 shows an outline drawing of Ka-band 40 to 60W TWT, model LD7849.

The input/output transfer curve, C/3IM & NPR characteristics, and phase shift & AM/PM conversion of the Ku-band 40 to 60W TWT model LD7849 are shown in Figure 6 to Figure 8.

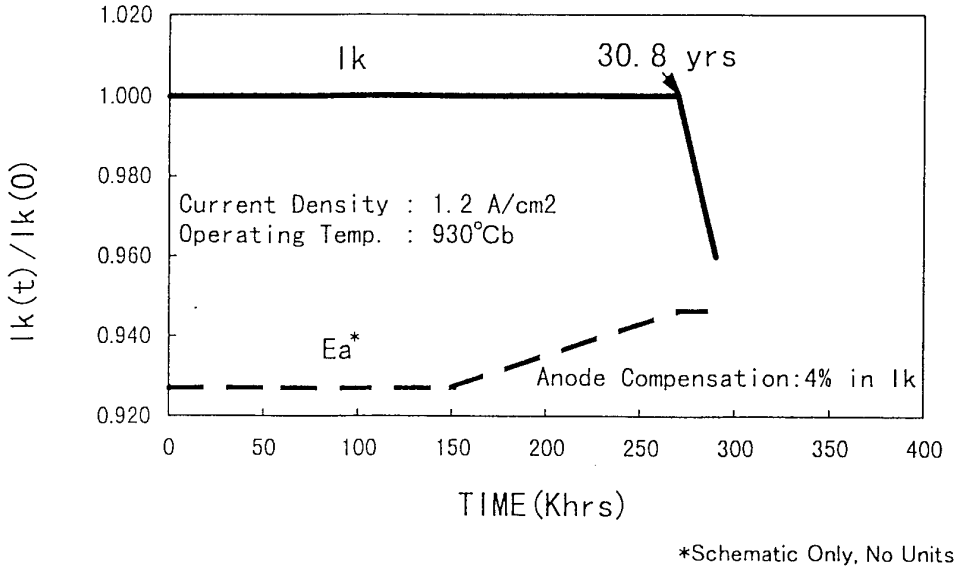

Figure 4 Cathode life time of Ka-band TWT

Table 2 Major performances of LD7812, LD7849 and LD7837

parameter		Unit	LD7812	LD7849	LD7837
Power range		W	15 - 30	40 - 60	60 - 80
Frequency		GHz	20	21	23
Helix voltage		Vdc	5590	6200	6900
Anode voltage		Vdc	6670	4200	5080
Cathode current		mAdc	32.0	51.0	67.0
RF output power		W	31.4	55.0	81.5
DC input power		W	61.8	97.0	142.7
Overall efficiency		%	50.8	56.7	57.1
Gain	saturation	dB	45.0	54.6	53.4
	small signal	dB	49.0	61.0	64.6
Phase shift		deg	43	43	40
Mass		gram	540	690	720
Dimension (LxWxH)		mm	272x67x47	298x64x51	298x62x53

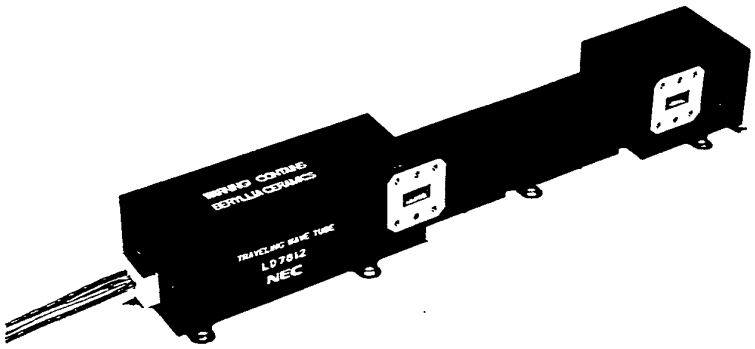

Photograph 1 Ka-band 15 - 30W TWT LD7812

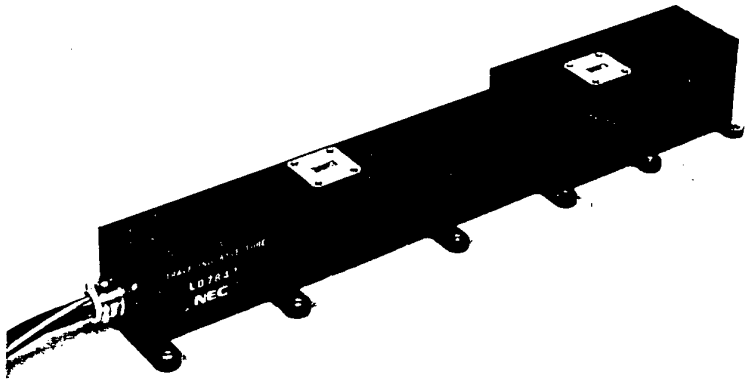

Photograph 2 Ka-band 40 - 60W TWT LD7849

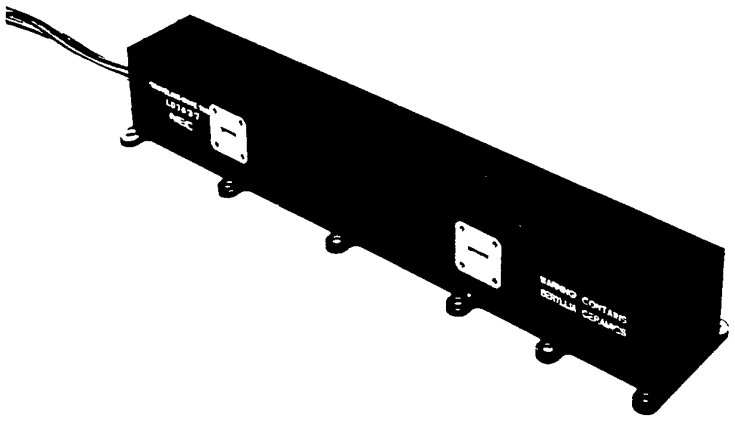

Photograph 3 Ka-band 60 - 80W TWT LD7837

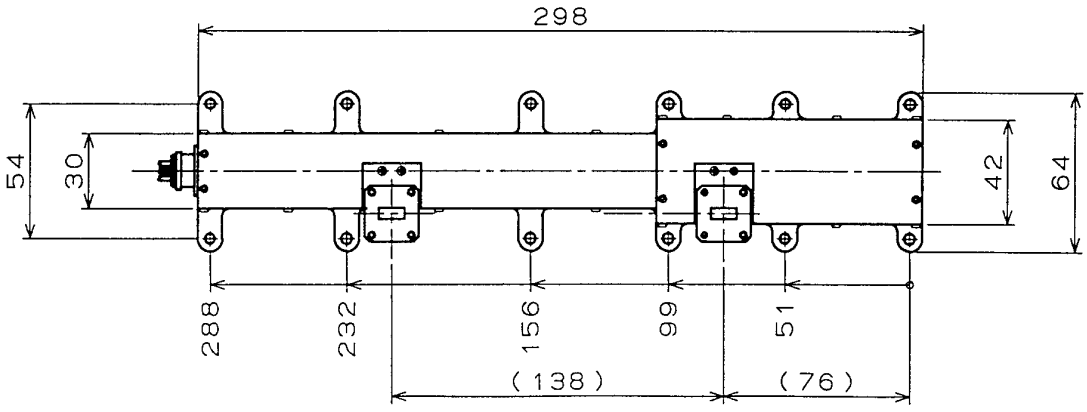

Figure 5 Outline drawing of Ka-band 40 - 60W TWT, model LD7849

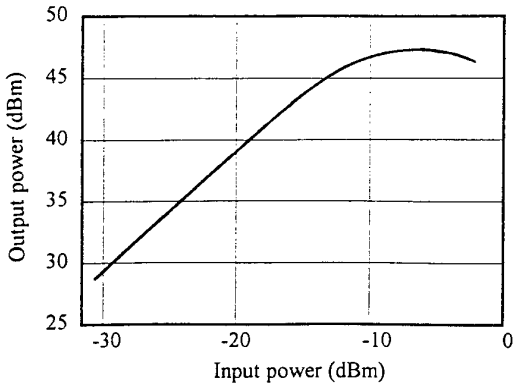

Figure 6 Input / output transfer curve of the LD7849 TWT

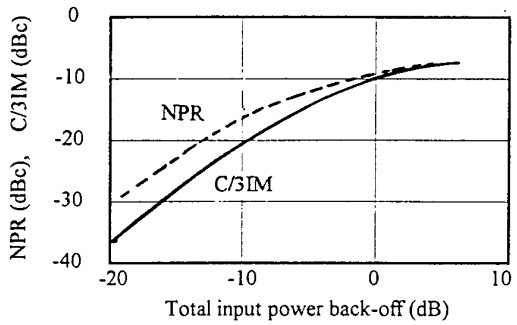

Figure 7 C/3IM and NPR characteristics of the LD7849 TWT

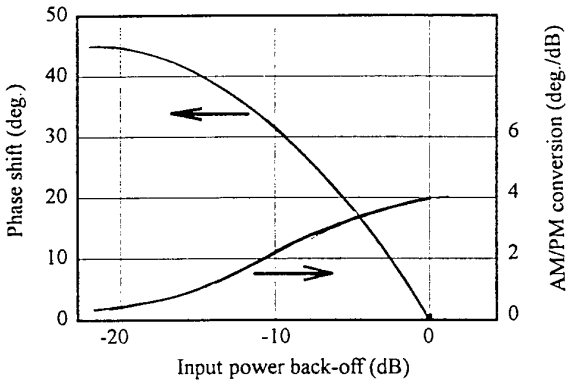

Figure 8 Phase shift and AM/PM conversion of the LD7849 TWT

4. CONCLUSION

The design and major performances of Ka-band 15W to 80W TWTs are presented. The latest design establishes high power output up to 80W, high efficiency of 57% and light weight of about 700g.

NEC's high performance Ka-band TWTs are available and suitable for the Ka-band satellite systems.

ACKNOWLEDGEMENTS

The authors wish to express their gratitude to Dr. T. Kageyama of NEC Microwave Tube Division for his valuable directions.

REFERENCES

1. T.Kageyama, S. Hamada, H. Hashimoto and K. Tsutaki, "REVIEW OF NEC's Ka-BAND MICROWAVE TUBES FOR SPACE AND GROUND APPLICATIONS", Proceedings of the 2nd Ka Band Utilization Conference, 1996, pp.299-306

Ka-Band 15W to 80W Space TWT Series

Authors: M. Kurashi; S. Hamada; H. Kubo (NEC Cooperation, Japan)

Paper not available

BOSCH
TELECOM

THE COMMERCIAL SPACE TWTA MARKET- REVIEW AND TRENDS

S. Heider
Bosch Telecom
Gerberstr. 33, 71522 Backnang, Germany

INTRODUCTION:

This paper will touch several aspects relating to TWTAs. It will show development of following topics, during the past, touching the situation in our times and give a forecast to the near term future:

1. the world market for TWTAs
2. the technical development of TWTAs
3. the prices and schedule for commercial TWTAs

1. THE WORLD MARKET OF TWTAs

Since "Early Bird" TWTAs are used for the amplification and transmission of RF-signals from the satellite to the ground. The first TWTAs that has been used for this application were operating in C-Band with an output power below 20 W. Due to the rapidly emerging use of satellites for telecommunication applications, the C-Band was heavily loaded and the Ku-Band came into place. In our days Ku-Band TWTAs up to 250W are state of the art. Because the Ku- Band is not capable to cover all predicted needs for bandwidth, mainly in the field of multimedia applications, the systems designers are now looking into Ka- Band transmission.
During the second part of the 80ths it was assumed that SSPAs would replace the TWTAs. The reason for this was mainly the lower mass and volume of the SSPAs. Due to the continuos development of the TWTAs that can reach now up to 60% efficiency compared to maximum 40 % for SSPAs, this trend was converted and we can observe an even higher market share for the TWTAs. Also the demand for higher output power, that cannot be efficiently fulfilled by SSPAs, led to an increased use of TWTAs.
Figure 1 shows the estimated TWTA world market starting in 1972 up to the year 2000. This market raised constantly up to 1995 with a small slope and exploded starting 1996. The main reason for the strong increase of the market is the raising customer demand for direct broadcast services in Europe, US and the Asian Pacific Region. We assume that the top of the demand in C- and Ku- Band for this application is reached in 1998, followed by a remarkable decrease. This decrease may be compensated by new applications for Multimedia Systems, where mainly high power Ka- Band TWTAs will be used.

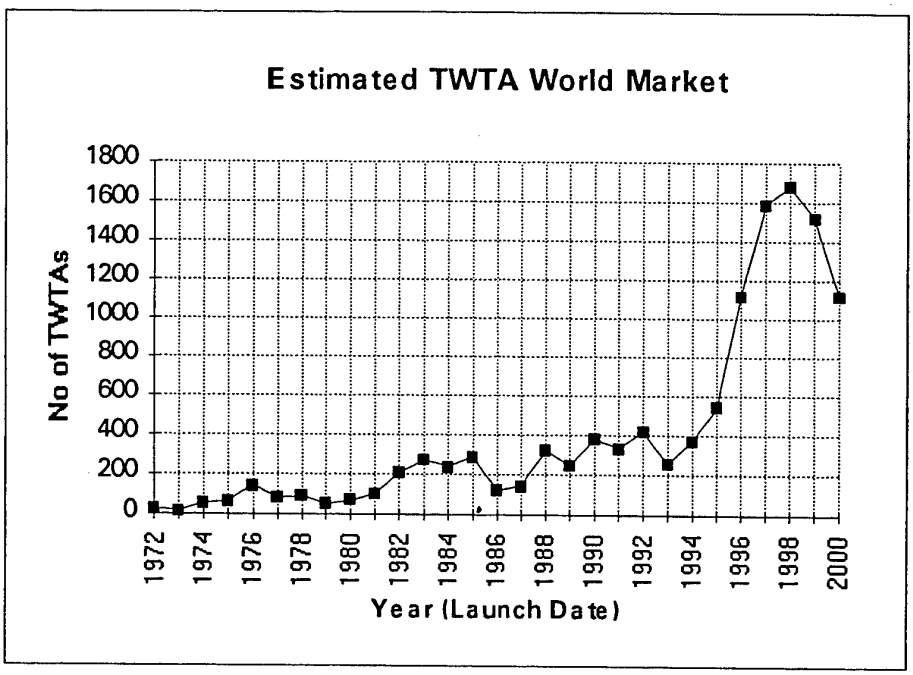

Figure 1

2) TECHNICAL DEVELOPMENT OF TWTAs

Three main issues are relevant for space TWTAs:

- maximum output power
- mass in relation to output power
- efficiency

Figure 2 shows the development of the mass to output power coefficient versus time and the maximum output power of the TWTAs. We can clearly see, how output power is rising during time, starting with 30 W on TDRSS satellites, having an exceptional peak with 260 W output power on the TV-SAT/TDF satellites in 1988 and using between 100 W up to 2*125 W in our days. The trend is going to high power amplifiers up to 240 W in the year 2000. It has to be stated that the trend to high power TWTAs was seen very early by the Europeans. Nevertheless it took more than 10 years until this development was used by a bigger customer base.

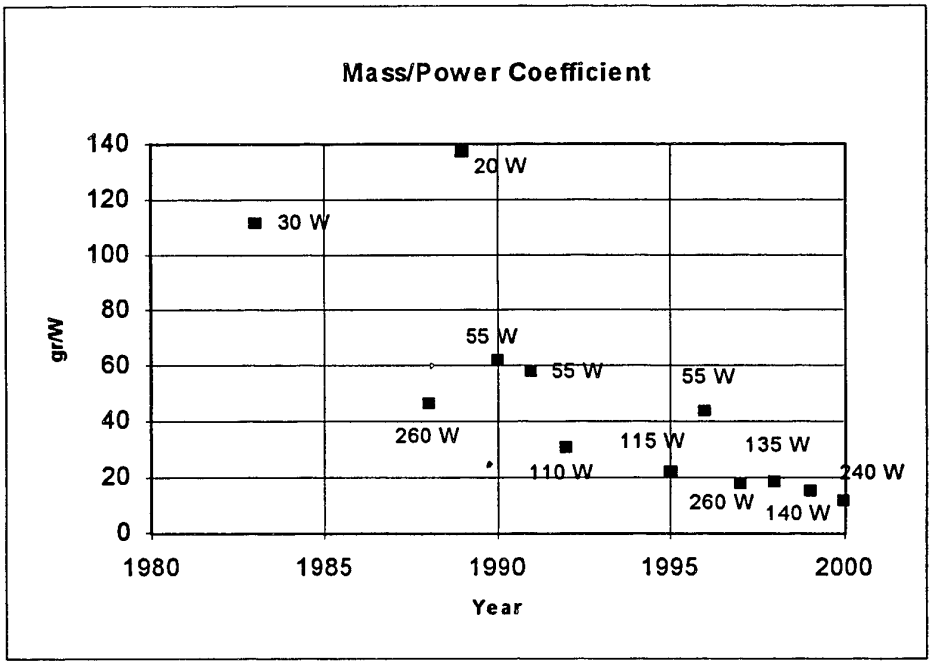

Figure 2

Starting with approximately 120 gr/W to 140 gr/W in the 80th, the TWTA technology evolved rapidly up to a mass to power coefficient of 20 gr/W in our days. We even can expect 12 gr/W in the year 2000. This is caused by steady improvement of technology, both in TWT and EPC. The TWT development was mainly focused on efficiency improvement, the EPC development on efficiency and mass improvement. Due to the fact that the EPC efficiency up to 95% is more or less saturated, the EPC development focuses mainly on further massreduction. This is done by higher integration of the electrical circuits (SMD-technology, Multilayer PCBs, ASICs...), new topologies (resonance converters, higher switching frequencies....) and new technologies (use of better materials....).

Figure 3 shows the efficiency improvement of TWTAs during time. Starting with approximately 30% in the early 80th we can reach 60% today with the trend to efficiencies above 65 % in the year 2000. This is caused by improvements both on EPC and TWT. In the 80th the EPC efficiency was in the order of 80% with TWT efficiencies of around 35%. The state of the art average values today are about 94% for the EPC and 65% for the TWT. We see no further big improvement on EPC side, but expect an improvement of efficiency up to 75% in the year 2000 for TWTs.

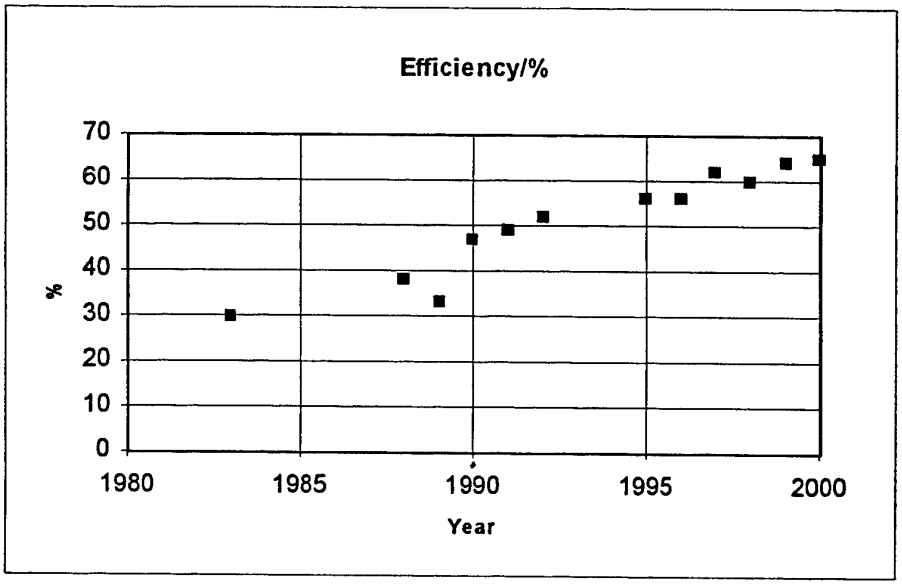

Figure 3

3) TWTA PRICES AND SCHEDULE

At the begin of satellite communications the TWTAs has been manufactured and tested more or less on a single unit basis. Due to the fact that each mission in the early days had its specific requirements every program required its own development program. This led to delivery schedules above 3 years for a flight set of TWTAs. The TWTA price reflected this enormous effort. When satellite communication became common, the requirements for the different programs got more and more similar, leading to shorter development times for the TWTAs and also leading to lower prices. In our times the TWTA requirements are determined more or less independently of specific programs. That means that the payload manufacturer has only to determine the actual output power and bandwidth and can order the needed TWTAs in advance of the actual program start. In case that the specific program is not awarded he can change these two parameters later to serve an other program.

To further reduce schedule and price many primes/payload manufacturers have secured their needs by so called Long Term Agreements (LTAs). In these LTAs the contractor garantees to the subcontractor to buy a certain number of TWTAs within a certain time frame and for a defined price. Having this commitment the unit manufacturer is able to procure parts, to manufacture PCBs and to preassemble the TWT and EPC up to a certain stage in advance to the order. After issue of the order the manufacturer only has to finish the assembly, integrate, test and deliver the TWTAs.

Figure 4 shows the development of the TWTA schedule from 1980 up to the year 2000. In 1980 the delivery of TWTAs was completed approximately 2 years after the order, in our days we deliver within 8 months and the goal for next year will be in the order of 6 months. This enables the satellite prime contractor to deliver a satellite in less than 18 months.

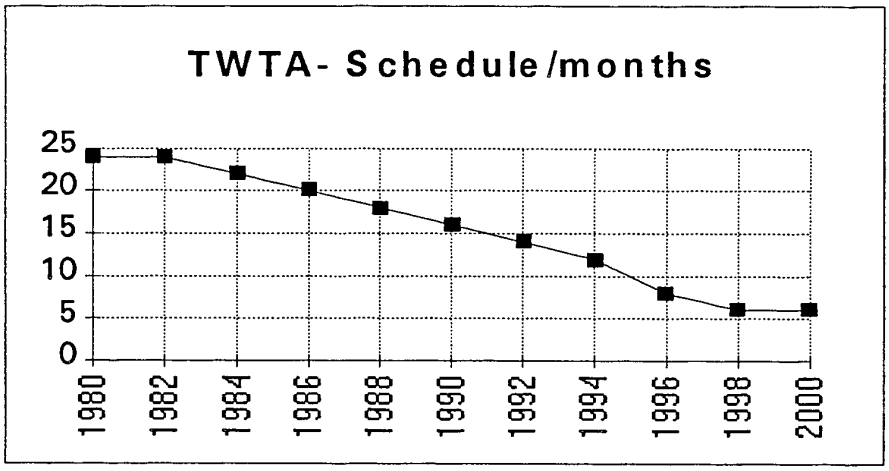

Figure 4

Figure 5 shows the development of the TWTA prices starting 1980. We can see a more or less linear decrease from 280 % in 1980 up to 100 % today.

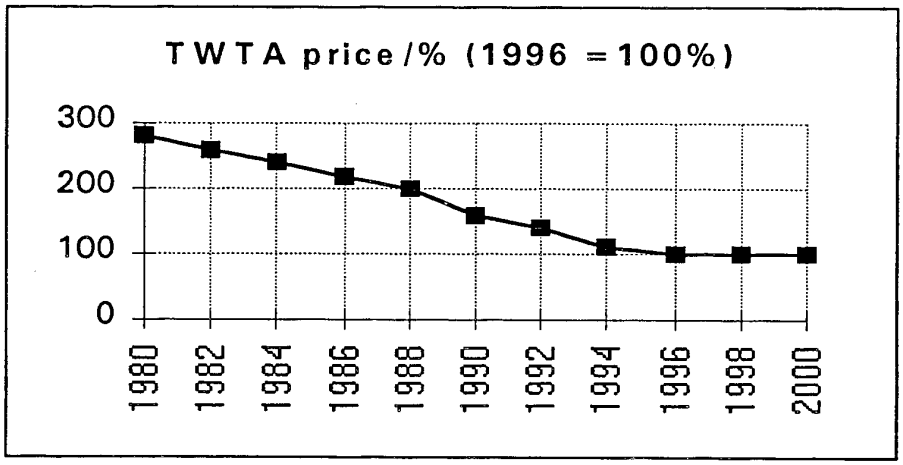

Figure 5

The main reasons for this price and cost decrease are as follows:

- Development time and effort could be reduced due to the standardisation of the product
- Parts cost could be reduced due to buying higher number of parts and holding them on stock
- Manufacturing cost could be reduced by manufacturing larger number of TWTAs in a certain time frame (Bosch Telecom manufactures more than 80 TWTAs per month) and by more automatization in the manufacturing process
- Test time and effort has been reduced due to the higher credibility of the product.

SUMMARY

In conjunction with other means, such as price and schedule reduction, efficiency improvement, and mass reduction of TWTAs, being the core equipment of the communication

satellite, leads to lower overall channel price in orbit and therefore improves the competitiveness of satellite communications compared to other communication means. Therefore the TWTA was in the past and will be in future the first choice for high power satellite application.

SESSION 2
MPMs

Chairman: G. Gatti (ESA/ESTEC, NL)

MICROWAVE POWER MODULE
for
SPACE APPLICATION

L. Sironi, L. Ceruti, M Gambarara, L. Nebuloni, A. Trivulzio, D. Viganò

FIAR S.p.A. Space Division, Milan - Italy
A Finmeccanica Company

ABSTRACT

The Microwave Power Module (MPM) concept has been developed for the military market; attention has been focused to similar devices to be developed for ground terminals and space-borne applications.
This paper presents the MPM for space applications currently under development at FIAR in co-operation with AERG, DASA and Ylinen Electronics as subcontractors.
The MPM work is performed in the frame of a ESTEC R&D contract. The basic contract calls for the design and development of state-of-the-art building blocks to be used in a MPM. In particular, EPC (Electric Power Conditioner), STWT (Short TWT) and SSDU (Solid State Drive Unit) for a 150 W RF/Ku-band and a 40 W RF/Ka-band are under development.
Moreover, ASI (Italian Space Agency) is supporting, through ESTEC, additional tasks in order to validate the MPM concept for space applications; these activities will be finalised with the manufacturing and testing of a complete 150 W RF/Ku-band MPM to demonstrate full performances and to qualify the critical parts.
Information given in this paper are relevant to the present status of the development and future planned activities.

KEYWORDS: MPM, TWTA, EPC, STWT, SSDU, Channel Amplifier, Lineariser, Solid State, Telecommunication Satellites, High Voltage.

INTRODUCTION

The MPM is a revolutionary device that links advantages of solid-state and Vacuum-Electronics Technologies for RF Power Amplification.
Developed for the military market (Refs 1-4) it has focused attention to application of similar devices to space-borne applications (Ref. 5). The MPM combines a wide-band MMIC driver, a highly efficient miniaturised vacuum power boost (also called STWT) and an integrated power conditioning in a compact light-weight package and leverages the advantages of each while minimising their disadvantages.
The peculiar performances and limitations imposed by space applications (e.g. in-orbit lifetime, electrical, mechanical and thermal interfaces) do not allow a simple straightforward approach and need accurate trade-offs in close co-operation with payload and/or spacecraft manufacturers, in order to design a MPM for the next generation of on-board power amplifiers with significant improvements in terms of:

- mass
- payload integration
- cost

with respect to a standard approach.

POWER AMPLIFIERS REQUIREMENTS

A Market Survey has been performed in order to identify:

- present and future trend in required RF output power and operational bands

- potential MPM applications
- acceptability of MPM interface constraints.

In particular, the following main requirements have been identified:

- 60 to 120 (150) W in C-band
- 60 to 250-300 W in Ku-band
- 40 to 120 W in Ka-band
- increased demand of TWTs with radiating collectors.

TWTs are commercially available up to about 80 W in C-band, 140-150 W in Ku-band and 60 W in Ka-band; single and dual TWTAs have been developed to meet market requirements. However, developments are in progress and reliable high power TWTs will be available by mid '98 for above 200 W in Ku-band, 120 W in C- and Ka-bands; these values will be increased in the coming years being technological improvements continuously applied.
MPMs can be interested provided that they can bring significant advantages compared with conventional TWTA. In particular, designs for conduction and radiation cooling must be available and a careful trade-off in terms of mass and efficiency has to be done: assumed values for the trade-off have been 3,500 $/Wdc for efficiency and 40,000 $/kg for mass.
In addition, thermal interfaces constraints have to be taken into account.

MPM CONFIGURATION

If we consider the MPM as replacement of the TWTA it easily appears that to compensate the lower gain of the STWT a solid state driver has to be added. This solution penalise cost and efficiency: no efficiency advantage from the STWT and efficiency penalisation from the solid state driver.
A different conclusion can be reached if we consider the overall transmit chain of a payload for telecommunication applications. As shown in Figure 1, the complete chain is composed of a channel amplifier with remotely settable gain adjustment, an Amplitude/Phase lineariser (optional) remotely adjustable to the specific operating band, a TWT with a typical gain of 50÷55 dB and a very high efficient EPC providing all required voltages and protections needed by proper TWT and channel amplifier operation.

In remote sensing applications, the transmit chain is composed by the TWTA alone, being the other equipment specific to each instrument.

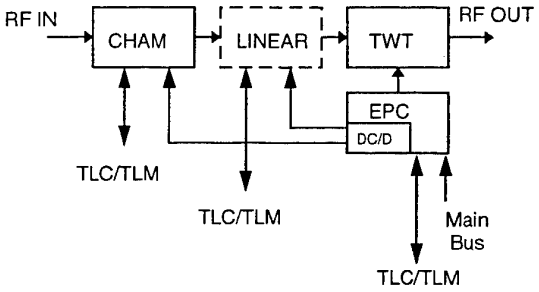

Figure 1: Typical transmit chain for telecommunication payloads.

Several solutions are under consideration in order to simplify it and/or to improve performances i.e.:

- replacement of TWT with a LTWT (Linearised TWT)
- solid state parts and EPC packaged together plus TWT or STWT
- everything packaged in a single box.

Table 1 summarises the trade off to define the best MPM configuration for telecommunications payload; Figure 2 shows the MPM concept: all units composing the transmit chain packaged together in a compact, lightweight box.

	TWT+ RF+EPC	TWT+ EPC/RF	STWT+ EPC/RF	MPM
N° of box	3	2	2	1
Mass (g)	2210	2080	1880	1700
Eff. (%)	59.9	60.36	60.1	60.1

Table 1: MPM trade off.

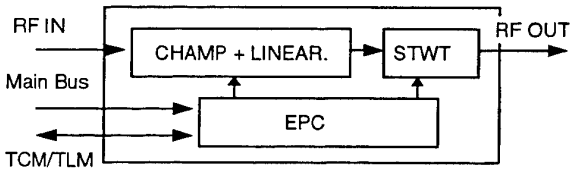

Figure 2: MPM configuration for telecommunication payloads.

The advantages of this solution with respect to

classic transmission chain are here below summarised:

- lower mass
- single TLC/TLM interface
- lower HW cost
- simplified P/L integration
- lower procurement cost
- reduction of EMC problems at P/L level
- single end to end specification.

On the other hand, only two drawbacks are envisaged:

- Thermal constraints to platform
- STWT mechanical interface to be adapted to specific MPM design.

In summary, in order to demonstrate the validity of MPM concept, the following tasks must be reached:

- no limitation in power handling (thermal criticality must be removed)
- no penalisation with respect to classic TWTA overall efficiency
- availability of conduction and radiation cooling versions
- mass and cost advantages when compared with classic transmit chain
- critical pressure resistance design
- possibility to procure and integrate STWTs from different suppliers

THERMAL ASPECTS

The continuous increase in RF power from TWTAs, increase in payload complexity and increase in mission lifetime are rising the requirements for power dissipation and worsening the thermal conditions at which the units will be exposed at end of life.
Today spacecrafts employ panels with embedded or surface heatpipes allowing a heat flux in the range 1.5÷2.5 W/cm^2, enough to dissipate the higher heat flux of STWT with respect to TWT, but there is a limit on the total dissipated power that a spacecraft thermal control can manage. Radiation cooling TWTA improves the thermal balance of the spacecraft and allows either to embark an higher number of transponders or the same number with higher power.
Current TWTA design is compatible with dual thermally controlled areas, one for the EPC and the other one for the TWT, allowing a large dissipation adjusting the two areas at different baseplate temperatures. The integration of TWT with other electronics in a single box could bring the MPM to two conditions:

- components derating out of limits, if TWT baseplate temperatures are applied
- thermal inefficiency of the system, if the baseplate temperatures are limited to electronics requirements.

From a thermal point of view, the worst case is represented by a 150 W RF conduction cooling MPM. Several ideas on how to thermally decouple the STWT from the electronics and related baseplate thermal profiles have been analysed. At the end, a preliminary thermal analysis has been performed considering a 150 W RF conduction cooling MPM (no radiation effect considered) whose thermal profile along the baseplate is as per Figure 3. Worst case dissipation values and zero drive dissipation conditions have also been taken into account.

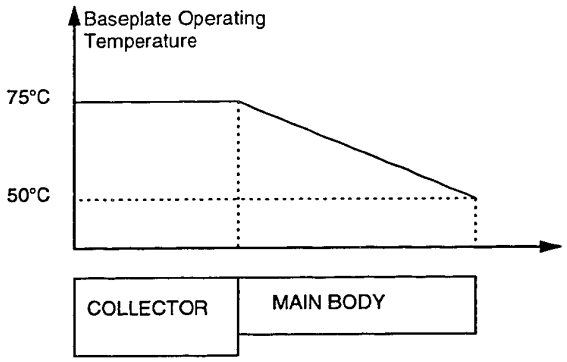

Figure 3: MPM temperature profile.

A thermal interface filler of 2000 W/K-m^2 type has been envisaged. More efficient fillers will provide margin for the collector temperatures. From the analysis, no criticality on electronics components have been evidenced, but at spacecraft level a reduction on thermal efficiency is envisaged.
In fact, with respect to current TWTA design 18% more panel area is required to allocate MPM units with the temperature profile of Figure 3, making the MPM thermal rejection more similar to the values assumed for SSPA payloads.
The increase of the total mounting area is reduced to 9% provided that the temperature at the main body side can be increased of 5°.

A ΔT of 15°C between collectors and main body minimum temperature is considered a value requirement not penalising the thermal system.
To avoid to develop a very attractive idea but for real-estate limited programmes, particular efforts are in progress to optimise the MPM layout in order to allow maximum baseplate operational temperature to +60 °C (+65 °C goal) maintaining ESA derating rules.
Higher operational temperatures are under discussion with customers in a "management risk approach" looking to revised component derating rules, all thermal design margin, etc.

MPM BASELINE SELECTION

MPMs in Ku and Ka frequency ranges have been selected as the most attractive in terms of potential number of units requested from the satellite market in the next years.
The Ku-Band TWTA market is expected to be divided into two categories of equipment:

- 60 ÷ 150 W RF conduction cooled type
- 100 ÷ 250 (300) W RF radiation cooled type.

Therefore the MPM design must be compatible with both conduction and radiation cooling approaches but, from a thermal control point of view, the conduction cooling type is the most challenging.
In order to validate the MPM concept, a 150 W RF conduction cooling MPM has been selected to be designed and developed. Considering the continuous increment in TWT efficiency and the potential thermal improvements in the MPM packaging over the production life cycle, this concept should be able to provide up to 170÷180 W RF in three years time.

The Ka-Band TWTA market, up to now limited to experimental systems, come from the new multimedia service spacecrafts planned to be deployed in the coming years. The expected RF power requirement is in the 40 to 120 W range with the largest near term market within 40÷60 W.
A 40 W RF output power has been selected to be developed at breadboard level in the frame of the contract in order to validate the MPM concept also for low power applications; 80 W STWT is being developed in the frame of another ESTEC contract.
A set of design specifications for the two selected baseline has been established.
A 150 W Ku-Band EM model with 50 V Main Bus interface will be manufactured to validate the concept.

MPM DEVELOPMENT STATUS

From a functional point of view, the MPM can be divided into two blocks: the RF chain and the EPC section.

a) RF section.
In order to demonstrate the validity of the MPM concept within the funding constraints, the MPM design is not incorporating the Channel Amplifier functions.
For both Ku- and Ka-band, the established baseline includes a wide band RF chain with a total gain of 55 dB whose block diagram is provided in Figure 4.

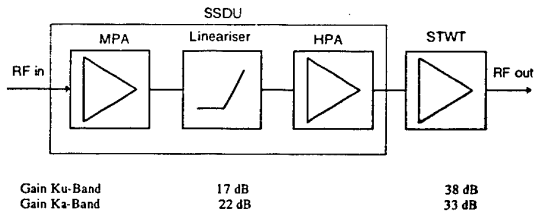

Figure 4: RF section Block diagram.

The selected STWTs, developed by AERG, have the following efficiency and estimated mass:

Operating Band	Efficiency (%)	Mass (g)
Ku-Band	> 64	540
Ka-Band	> 58	557

The SSDU (Solid State Driver Unit) is a MMIC device composed of a Medium Power Amplifier (MPA), an amplitude and phase Lineariser and a High Power Amplifier (HPA) able to deliver 19 dBm at 1 dB compression (Ku and Ka-Band).
The lineariser is developed by Ylinen Electronics while the rest of the SSDU is from DASA. The MMICs will be procured from UMS foundry.
The expected intermodulation and NPR performances of the RF chain are provided in Figures 5 and 6.

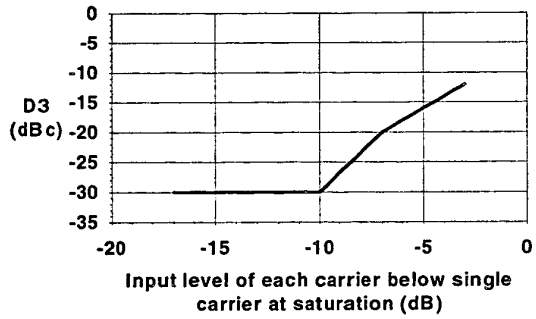

Figure 5: Ku and Ka-Band MPM Intermodulation Products

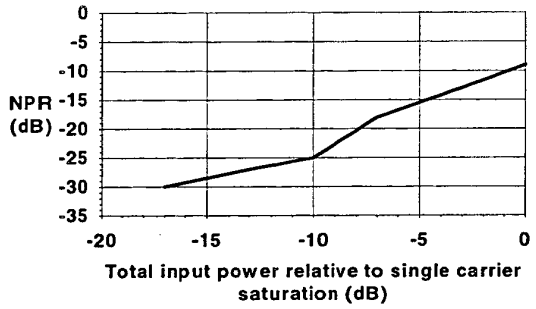

Figure 6: Ku and Ka-Band MPM NPR.

b) EPC Section.

The EPC block diagram is provided in Fig. 7. It consists of an input pre-regulator, a HV module, an auxiliary converter to drive the filament supplier and the SSDU and a Control and Monitoring block. The power components are assembled in dedicated power modules.

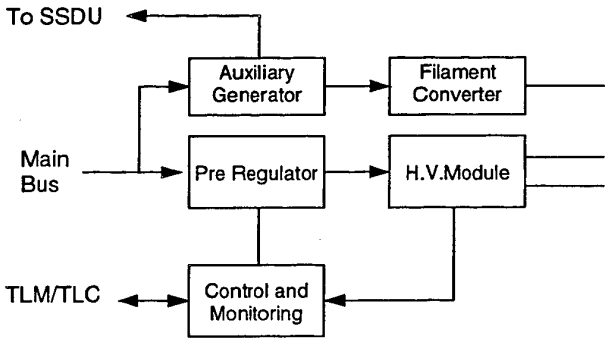

Figure 7: EPC Section Block Diagram

The pre-regulator is a Buck PWM converter designed to interface 50, 70 and 100 V fully regulated Main Bus; operation with gross regulated Main Bus is also under consideration.

The HV block features potted design for critical pressure operation free and a new topology for high efficiency and low mass. Input power converter is a Push-Pull type for 50 and 70 V MB versions while a Bridge configuration has been selected for the 100 V version.

The Control and Monitoring functions take care of proper operation and monitoring of MPM.
An 8000 gates ASIC is used; automatic restart function (ARU) is standard.
The overall efficiency of the EPC section is greater than 95%.

c) MPM Packaging

The complete MPM is packaged in a compact, single box 55 mm wide, 360 mm long and 120 mm high (conduction cooling version, excluding mounting feet). Overall mass is expected to be below 1700 g (1930 g for the radiation cooling version). External interfaces are:

- RF output waveguide
- RF input SMA coaxial connector on top
- Connector for Power and TLM/TLC functions on top of the unit

Room is reserved to interconnect specific customer's interface modules (e.g. serial I/F) as well as for the Channel Amplifier functions, also if not presently implemented.
The layouts of conduction and radiation cooling versions are respectively provided in Figure 8 and 9.

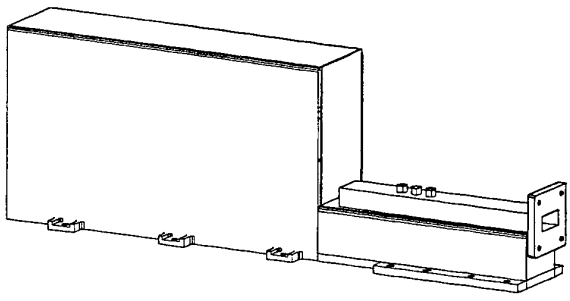

Figure 8: MPM Layout (conduction cooling version)

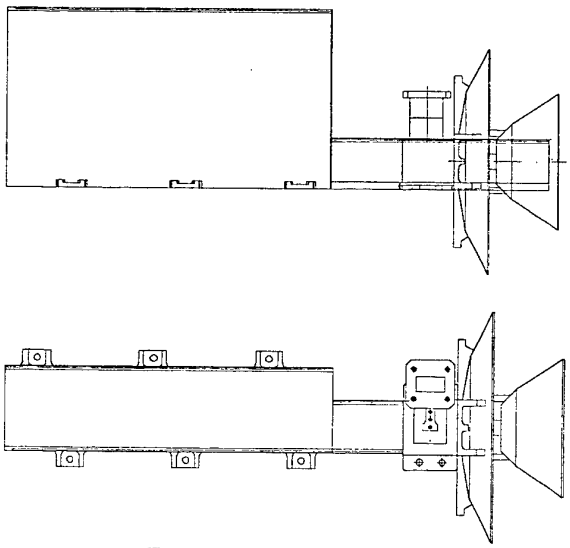

Figure 9: MPM Layout (radiation cooling version)

MAIN TECHNICAL PERFORMANCES

Main MPM performances are here below summarised. The performance are relevant to MPMs including Channel Amplifier functions.

PARAMETER	Ku-Band	Ka-Band
Operating Frequency (GHz)	10.7-12.75	18.55-20.2
Instantaneous BW (MHz)	500	500
RF Output Power (W)	150	40
RF Gain (dB)	90±20	90±20
Noise Figure (dB)	10÷20	10÷20
Phase Shift (°)	15	15
AM/PM Conversion (°/dB)	4	4
AM/PM Transfer (°/dB)	5	5
Total Harm. Power (dBc)	-15	-15
Discrete spurious (dBc) 0.01 to 70 KHz 70 to 1000 KHz 1000 to 10000 KHz	 -60 lin. to -75 -75	 -60 lin. to -75 -75
Efficiency (%)	> 60.5	> 53.5
MB Input Voltages (V)	50, 70 or 100 V reg.	
Telecommand	MPM On/Off ARU On/Off Champ Setting	
Telemonitoring	MPM On/Off status ARU Status ARU En./Dis. Helix Current Anode Voltage Main Bus Current Champ TLM	
Mass (g)	< 1700 (cond. cooling)	

CONCLUSIONS

From the market survey there is a general consensus that the MPM may change the way how to implement the transponders.
The critical factor of thermal interface with the spacecrafts has been investigated and a solution that avoid penalization of thermal efficiency has been identified.
The MPM concept and the main characteristics of the MPM under development at FIAR have been presented, conduction and radiation cooling versions will be possible. The detailed design of the MPM unit and relevant functional blocks is running with complete manufacturing and test activity to be completed by the end of the year.
To validate the MPM concept, an EM of a 150 W RF/Ku-band conduction cooling version will be manufactured and tested by mid '98.

ACKNOWLEDGEMENTS

The authors wish to thank:

- our industrial Partners AERG, DASA and Ylinen Electronics for the fruitful co-operation
- the spacecraft manufacturers met during the market survey for the useful support in the understanding of the interface problems with the platforms and for encouraging us in pursuing the MPM development
- the ESTEC Technical Officers.

References

1: R. H. Abram, Jr, and R.K. Parker: "Introduction to the MPM: what is and where it might fit", 1993 MTT-S.

2: L. Cosby: "MPM Applications: a forecast of near- and long-term applications", 1993 MTT-S.

3: J. A. Christensen et. al.: "MPM technology development and industry prospective", 1993 MTT-S.

4: R. H. Abrams, Jr: "The Microwave Power Module: a "supercomponent" for space applications". Proceeding ESA 1994 Space TWTA Workshop.

5: R. A. Nunn et al.: "High power C- and Ku-band amplifiers in hybrid solid-state/vacuum technology". Proceeding ESA 1994 Space TWTA Workshop.

60% EFFICIENT MINIATURE C-BAND TWT FOR THE MICROWAVE POWER MODULE

D. R. Whaley, C. M. Armstrong, B. Gannon, G. Groshart,
E. Hurt, J. Hutchins, M. Roscoe

Northrop Grumman Corporation
Electronic Systems Integration Division
600 Hicks Rd., M/S H6402
Rolling Meadows, IL 60008 USA

ABSTRACT

Recent advances in the Northrop Grumman High Efficiency C-Band TWT development program have resulted in the development of a miniature C-Band TWT operating at 32% circuit efficiency and 61% total efficiency at an output power in excess of 170W. When inserted into the Northrop Grumman Microwave Power Module this TWT results in a module DC/RF conversion efficiency of 51%. This high efficiency power amplifier is particularly well suited for space applications where small size, light weight and low thermal dissipation is required. A second parallel development program for TWTs operating at lower perveance and higher power has also been pursued and has resulted in nearly identical performance of 32% circuit efficiency and 63% total efficiency at power levels in excess of 240W.

INTRODUCTION

Northrop Grumman Corporation's ongoing development of microwave power modules (MPMs) provides microwave power at various power levels, frequencies, and bandwidths for a variety of applications including communications, radar, and ECM. The MPM combines an integrated power conditioner (IPC), solid state amplifier (SSA), and traveling wave tube (TWT) within a single module resulting in a small, lightweight package for efficient DC/RF energy conversion. The family of Northrop Grumman MPMs include a Low-Band MPM (2-6GHz), C-Band MPM (4-6GHz), Ultra-Band MPM (4.5-18GHz under development), High-Band MPM (6-18GHz), and MMPM (18-40GHz under development). This unique combination of both solid state and vacuum electronic technologies results in significant reduction in size and weight over conventional transmitters as well as increasing overall efficiency, decreasing thermal dissipation and prime power requirements, and reducing noise.

The MPM subcomponent which most limits the overall MPM efficiency is the TWT which serves as the module power booster. Over the past two years, Northrop Grumman has concentrated on increasing the efficiency of the TWT for the C-Band MPM while maintaining its miniature size and light weight. Several advances have been realized in methodology, modeling, and testing which have substantially improved TWT and MPM performance. The resulting TWTs are the smallest and lightest of their kind operating at such efficiency and power levels.

GENERAL DESIGN

A photograph of the C-Band MPM is shown in Fig. 1 and a table of general MPM specifications is shown in Table. 1. The components shown include the high voltage IPC, SSA, modulator, TWT, and high power output connector. This multipaction-free high power connector designed for 200W at 3GHz has a safety margin of 6dB. A photograph of a C-Band TWT with a low power output connector is shown in Fig. 2 before module insertion and shows the electron gun, pole piece-magnet structure, RF vacuum windows, and collector. The length and weight of the TWT is 18.5cm (7.3in) and 0.2kg (0.44lb) respectively. TWT fabrication uses high temperature precision brazed metal

Work supported in part by the Naval Research Laboratory under contract No. N00014-94-C-2242.

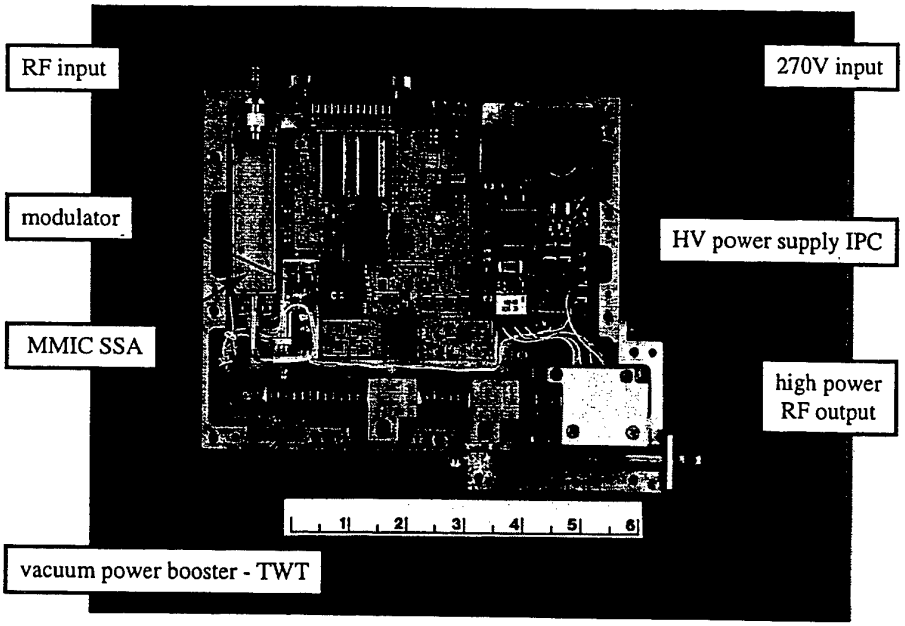

Figure 1. C-Band Microwave Power Module with High Power Output Connector.

High Efficiency C-Band MPM	
parameter	value
frequency range (-1dB)	3.7 - 5.3GHz
RF power @ f_c	170W
CW module efficiency @ f_c	51%
small signal gain	68
saturated gain	53dB
duty factor	0% - 100%
max harmonic power @ f_c	-11dBc
sat harmonic power @ f_c	-17dBc
supply voltage	270VDC
supply current at P_{RFmax}	1.3A
heater voltage	12.6V
heater current	0.4AA
MPM length	19.8cm (7.8in)
MPM width	15.2cm (6.0in)
MPM height	2.5cm (1.0in)
MPM weight	< 1.2kg

Table 1. General Characteristics of the High Efficiency C-Band MPM.

and ceramic parts. Major sub-assemblies as well as the helix sever joint are connected together via laser welded flanges. The electron gun is of Pierce type using a focus electrode designed to provide beam cutoff at approximately 1kV. The low perveance design, at 0.51μP produces a 0.13A beam at 4.0kV using an M-type dispenser cathode with a current density of 1.2A/cm^2. The gun assembly incorporates an adjustable gun housing which allows change of the relative anode-cathode spacing and therefore of gun perveance. This permits empirical perveance correction required due to build tolerance and assures tube-to-tube reproducibility. The interaction circuit consists of 2 helix sections supported in a barrel assembly by three BeO rods. The rod ends are sputtered with graphite which serve as attenuators of the RF wave near the sever. The collector is a graphite four-stage depressed collector required for high total efficiency under saturated conditions and low thermal dissipation under low drive conditions.

MODELING ADVANCES

The TWT performance has been increased substantially during the C-Band Efficiency Enhancement Program. Advances include accurate modeling and optimization of the TWT PPM stack magnetic field and beam entrance conditions, enhanced accuracy of design codes, new hybrid circuit design methodology for high efficiency interaction including harmonic power growth, and development of a real-time automated system for collector optimization.

Much care has been taken to properly model and optimize the PPM stack magnetic field structure to allow simulation and optimization of the entrance conditions of the electron beam as it passes from the field-immersed cathode surface to well into the PPM stack. A method has been developed to rapidly compute the actual vector potential fields generated by the PPM stack magnets which are required to produce an arbitrary user-defined PPM stack profile. In this way rapid and accurate magnetic profile optimizations can be performed which result in highly laminar electron beams. An example of a beam immersed in an optimized PPM stack magnetic field is shown in Fig. 3.

A highly laminar beam has several advantages. Such a beam has good transmission characteristics and requires essentially no empirical optimization of the magnetic field during tests. This is the case

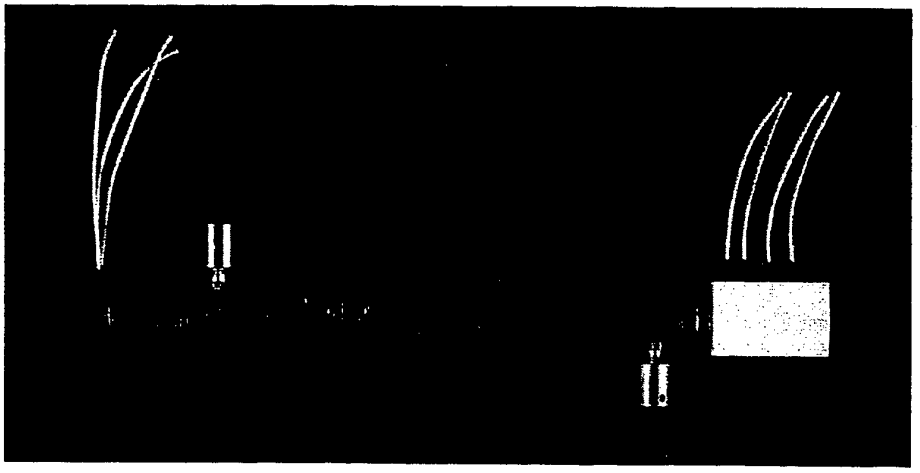

Figure 2. Photograph of C-Band Traveling Wave Tube.

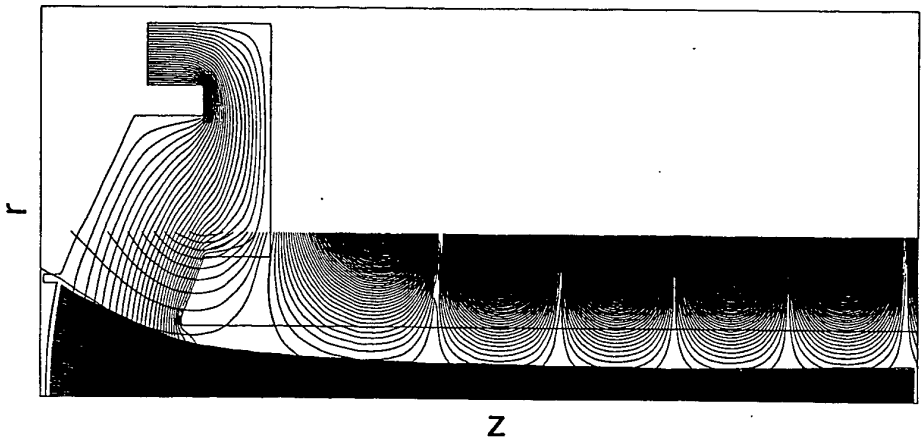

Figure 3. Electron Gun Simulation of First Five Cells of PPM Stack Using Optimized Magnetic Field Profiling.

for these C-Band TWTs which exhibit 100% transmission (<0.1mA helix current) at turn-on with no tuning of the original field required. No shimming magnets are placed on the TWT as seen in Fig. 1. When the collector lenses are then biased, the backstreaming helix current also remains low, typically less than 1%. This increased beam laminarity allows for an increased fill factor and therefore higher beam/circuit coupling without sacrificing the good helix current characteristics of the device. The fact that the TWT requires no shims decreases test time considerably, favors fundamental over harmonic power growth, and does not introduce azimuthal field asymmetries which in itself induces scalloping. The method for calculation of vector potential fields in the gun region is also applied to the collector region to determine the optimum refocusing cell field profile for maximum collector efficiency.

The RF interaction circuit has also been optimized for high fundamental circuit efficiency. The design is a compromise between high gain, high fundamental current generation, low harmonic power generation, and proper phasing of the circuit phase velocity and beam velocity in the large signal region of the output circuit. The methodology developed to determine the proper circuit profile for high fundamental efficiency has now been used on the two C-Band programs totaling 6 TWT builds. All of these TWTs have performed at over 30% circuit efficiency.

In order to achieve high total TWT efficiencies, the kinetic energy in the spent beam of the TWT must be efficiently recovered in the collector. The four stage collector used has been optimized geometrically to maximize the current collected on the highly efficient back stages. The collection efficiency also depends on the bias voltages of each of the stages and final optimization of these voltages for efficiency must be performed empirically. Since the total TWT efficiency is a function of many measured parameters, most of which are changing during the optimization procedure, an automated optimization system has been developed which yields real-time calculation of the total efficiency of the TWT as a function of the four collector bias voltages and corresponding currents. Not only has the optimization time for the TWT been reduced to ~15 minutes, one can be sure to have completely optimized the collector voltages for maximum efficiency. Sensitivity to variation in collector voltages supplied by the IPC of the MPM can be also easily determined. This optimization system is now used on all TWTs developed at Northrop Grumman.

EXPERIMENTAL RESULTS

Performance data of the C-Band TWT and MPM is shown in Figs. 4-5. Figures 4(a) and (b) show the efficiency and fundamental power output of the optimized C-Band TWT showing 61% efficiency centerband at a power of 170W. The bandwidth at 1dB power points is approximately 1.6GHz. With this TWT inserted into the C-Band MPM gives the results of Fig. 5. Here the 94% efficient IPC allows for a maximum total MPM DC/RF conversion efficiency of 51%.

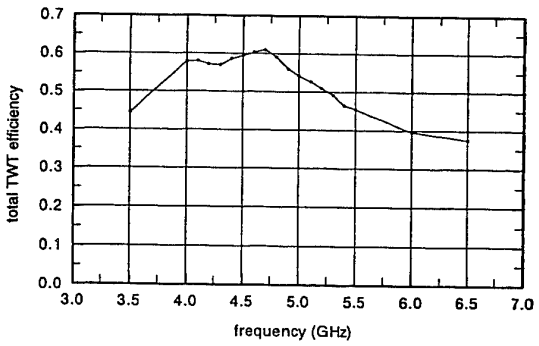

Figure 4(a). C-Band TWT total efficiency variation with frequency.

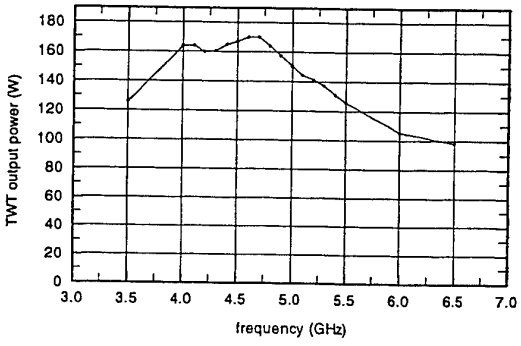

Figure 4(b). C-Band TWT output power variation with frequency.

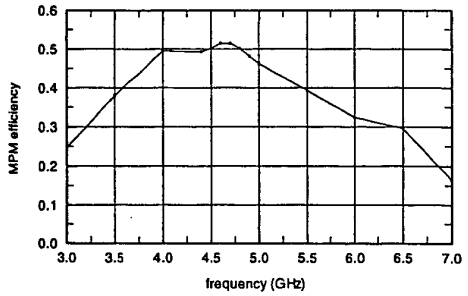

Figure 5. C-Band MPM total efficiency variation with frequency.

The prime power requirements for the TWT are shown in Fig. 6 as well as the dissipated power as a function of drive power. For a saturated output power of 170W, the prime power increases from 125W in the small signal regime to ~275W at saturation. Due to the four stage collector, the dissipated power remains approximately constant over the entire drive curve, the current being collected on the highly efficient back stages under small signal conditions and on the lower voltage front stages under full drive conditions. This low thermal dissipation, independent of drive, reduces MPM cooling requirements and increases reliability regardless of the chosen operating point.

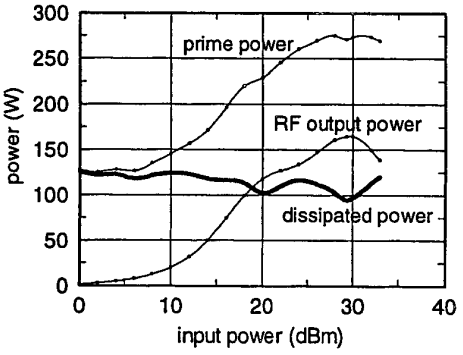

Figure 6. TWT prime power, RF power, and dissipated power vs. input drive.

The drive curve for fundamental and harmonic power is shown in Fig. 7. This figure shows evidence of the good electron bunching and harmonic control of these high efficiency circuits. The minimum harmonic separation over the drive curve is 11dB and over 20dB separation is seen at saturated drive. The good electron phase bunching manifests itself in the n=2 drive curve where the electron bunch is seen to fall in and out of phase with the second harmonic circuit wave as the electron bunch is progressively slowed by the fundamental interaction as saturation is approached with increasing input drive.

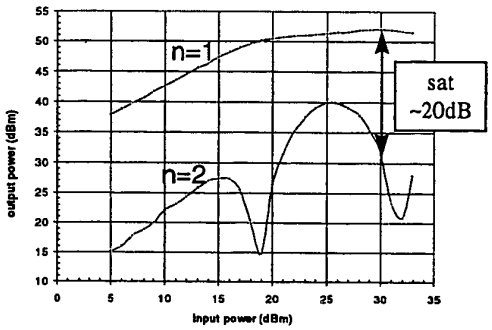

Figure 7. Fundamental and second harmonic drive curve of C-Band TWT.

One remark that should be made is that after testing and optimizing the total TWT efficiency at many points in the drive curves for several tubes in each of the two programs, it is found that maximum total TWT efficiency with this design always corresponds to maximum circuit efficiency. No conditions were found in which one can optimize the collector at a backed off point in the drive curve and with the increased collector efficiency achievable, exceed the total efficiency achieved when the TWT is optimized at saturation.

The experimental results for the High Power C-Band TWT, developed as a parallel effort to the High Efficiency C-Band TWT, is shown in Fig. 8(a)-(b). An efficiency of over 63% is shown at a corresponding power of 245W. Due to the high power of this device, the TWT was operated at 10% duty factor. General operating parameters of both TWTs are summarized in Table 2.

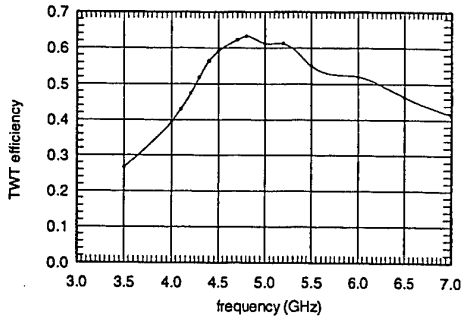

Figure 8(a). High Power C-Band TWT efficiency variation with frequency.

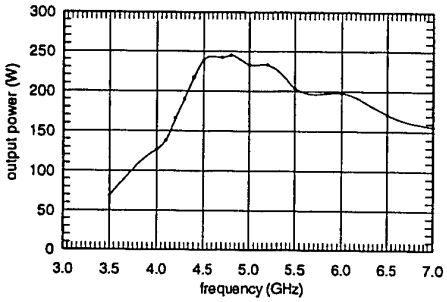

Figure 8(b). High Power C-Band TWT output power variation with frequency.

CONCLUSIONS

The development and results of a high efficiency C-Band TWT and MPM have been presented. The TWTs are lightweight and highly miniaturized. The performance presented in this paper is a result of improvements in beam quality through magnetic modeling, new circuit design methodology, and development of a real-time automated collector optimization system. Two different programs have resulted in TWTs operating at over 30% circuit efficiency and over 60% total efficiency, both TWTs having a length of 18.5cm and weighing less than 200g. The resulting MPM incorporating the 170W TWT operates at over 50% DC/RF conversion efficiency with a total weight and volume of only 1.2kg and 770cm^3 respectively. These highly efficient miniature TWTs and the MPMs incorporating them are particularly suited for space applications where lightweight power amplifiers of small size and low thermal dissipation are required.

High Efficiency C-Band TWT		High Power C-Band TWT	
parameter	value	parameter	value
frequency range (-1dB)	3.7 - 5.3GHz	frequency range (-1dB)	4.3 - 5.5GHz
RF power @ f_c	170W	RF power @ f_c	245W
circuit efficiency @ f_c	32%	circuit efficiency @ f_c	32%
total TWT efficiency @ f_c	61%	total TWT efficiency @ f_c	63%
collector efficiency	73%	collector efficiency	74%
small signal gain	33dB	small signal gain	27dB
saturated gain	23dB	saturated gain	19dB
duty factor	0 - 100%	duty factor	0 - 10%
max harmonic power @ f_c	-11dBc	max harmonic power @ f_c	-13dBc
sat harmonic power @ f_c	-17dBc	sat harmonic power @ f_c	-20dBc
noise power density (beam off)	<-172dBm/Hz	noise power density (beam off)	*
cathode voltage	4000V	cathode voltage	5000V
cathode current	0.131A	cathode current	0.152A
heater voltage	12.6V	heater voltage	12.6V
heater current	0.4A	heater current	0.4A
collector type	4-stage graphite	collector type	4-stage graphite
TWT length	18.5cm (7.3in)	TWT length	18.5cm (7.3in)
TWT width	1.6cm (0.64in)	TWT width	1.6cm (0.64in)
TWT height	1.6cm (0.64in)	TWT height	1.6cm (0.64in)
TWT weight	< 0.2kg	TWT weight	< 0.2kg

*not measured

Table 2. General Characteristics of the High Efficiency C-Band TWT and the High Power C-Band TWT.

MPM TECHNOLOGY - THE MINIATURIZED TRANSMITTER SOLUTION

C. Smith, Dr. C. Armstrong, J. Duthie, Dr. G. Pierce, M. Sievers
Northrop Grumman Corporation
Electronics & Systems Integration Division
Electronic Systems

ABSTRACT

A supercomponent family, known as Microwave Power Modules (MPMs), has been in development since 1991. MPMs combine the desirable attributes of vacuum electronics and solid-state technology to achieve a high power, high efficiency, miniaturized amplifier applicable to various commercial, military and space transmitters, including communication, radar, and electronic countermeasure (ECM) applications.

INTRODUCTION

Power modules are highly miniaturized and fully integrated amplifiers (transmitters) operating in the microwave and millimeter wave frequency bands. Three traditionally dissimilar components—a traveling wave tube (TWT), power supply, and solid-state amplifier (SSA)—are integrated into one package to form the power module "supercomponent." Depending on design requirements, Northrop Grumman power modules deliver nominally 100 to 200 watts of continuous wave (CW) radio frequency (RF) output power with greater than 50 dB gain over bandwidths reaching 1.5 octaves. Various MPMs have demonstrated unsurpassed efficiencies and previously unattainable noise performance for the required gain and output power levels.

When compared to fielded military electronic systems, MPMs are one-tenth the volume and one-sixth the weight with 2.5 times the RF output power and 5 times the efficiency. Reliability is estimated to be 3.6 times better than traditional hardware as a result of fewer components, lower typical operating temperatures, and interconnection technologies. Monolithic microwave integrated circuit (MMIC) and application specific integrated circuit (ASIC) devices have been incorporated within the power modules to support the next generation high performance electronics requirements (reliability, acquisition and life cycle cost, and area/volume).

A family of power modules (table 1) is being developed at Northrop Grumman from 2 to 40 GHz. This family of power modules can be used to support narrow- and broad-band transmitter requirements.

POWER CONDITIONER DESIGN

Figure 1 is the block diagram of the Ultra-band MPM power conditioning and control circuitry. The MPM power conditioners have achieved a high voltage conversion efficiency of 90 to 94%. In the case of the 6 to 18 GHz MPM, a power supply packaging density of 90 W/in^3 with 350 W and 4 kV within a 0.272 in height was accomplished. The significance of this can be recognized by comparing existing airborne power conversion systems for TWTs which typically have power densities of 10 to 15 W/in^3. Techniques to achieve high overall power density include: hybrid construction, ASIC technology, high energy density magnetics, high energy and high voltage capacitors, and innovative circuitry development.

Functional blocks of the power supplies are implemented as hybrid circuits as indicated in figure 2. The high voltage power supply (HVPS) consisting of the Boost Converter, Resonant Inverter, High

Table 1. Northrop Grumman MPM performance specifications

	Freq. (Hz)	Nominal Power (W)	Sat. Gain (dB)	Small-Signal Gain (db)	Noise Figure (dB)	Efficiency (%)	Prime Power (V)	Input Power (W)	Size (in)			Volume (in^3)	Weight (lb)
									L	W	H		
Low-Band MPM	2-6	100	55	62	10	30	270	350	9.9	6.4	1.2	76.0	3.1
									9.8	5.3	1.2	62.3	2.9
C-Band MPM	4-6	170	55	62	10	50	270	350	7.5	6.0	1.0	45.0	2.5
									8.3	5.3	1.0	44.0	2.2
Radar MPM	7-11	125	55	65	10	35	270	350	6.0	2.0	1.0	12	0.6
Ultra-Band MPM	4.5-18	125	55	62	13	30	270	650	8.3	6.5	1.0	54.0	3.2
									8.3	5.3	1.0	44.0	2.2
High-Band MPM	6-18	100	65	71	13	30	270	350	7.9	5.8	0.8	36.7	2.8
									8.3	4.5	1.0	37.4	2.2
High-Band MPM (Array)	6-18	100	65	71	13	30	270	350	6.0	4.0	0.32	7.7	1.2
DMPM	5-17.5	200	55	62	12	30	300 VDC 2 kV	300	9.5	2.1	0.78	15.6	0.45
MMPM	18-40	100	50	56	13	30	270	350	8.0	3.5	0.8	22.4	1.2

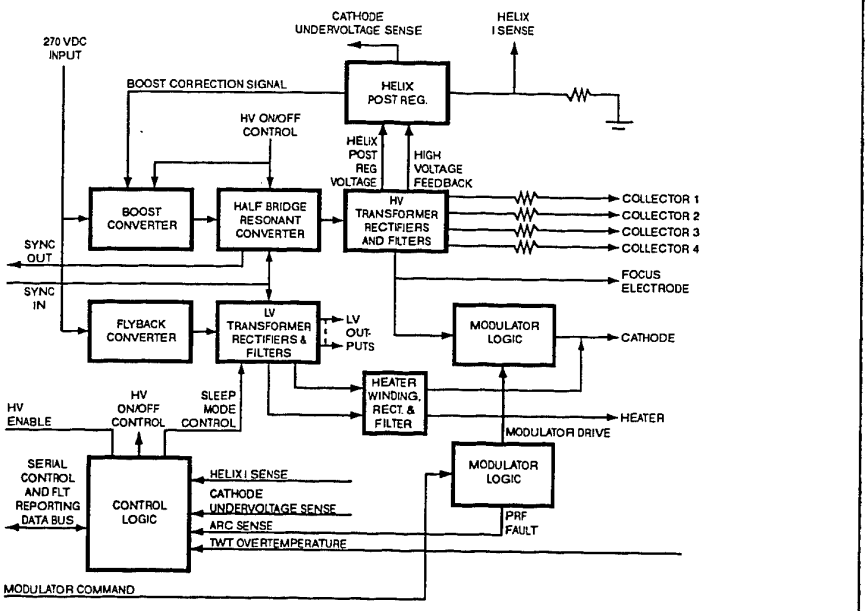

Figure 1. MPM power conditioner block diagram

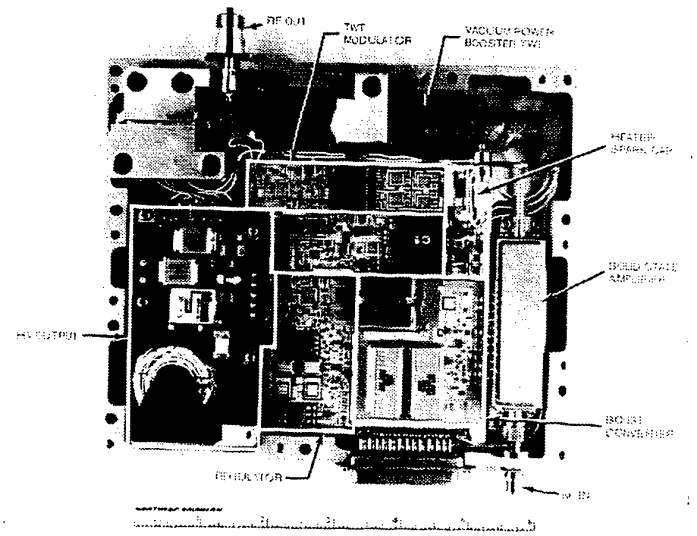

Figure 2. C-Band MPM functional blocks

Voltage Transformer, and High Voltage Output subassemblies provides up to 650 W of conditioned power to the TWT booster cathode (-4500 V) and collectors (ranging from 300 to 2500 V with respect to cathode). The multi-output housekeeping power supply (20 W) furnishes control power to the TWT heater (isolated at cathode high voltage potential), SSA, modulator control logic, and power supply logic. The TWT modulator consists of two parts: a low voltage modulator control logic section and the high voltage switch section which is at cathode potential.

Prime power for the MPMs conforms to MIL-STD-704E. This prime power is applied to the Boost Converter and housekeeping power supplies. The housekeeping power supply is a 300 kHz flyback switching power supply and provides all internal required ancillary voltages. The Boost Converter is part of the HVPS chain. The Boost Converter's

function is to minimize the impact of input voltage transients and to provide an adaptable nominal 350 VDC bus as the input to the Resonant Inverter. The Resonant Inverter applies fixed pulse width modulated 200 kHz drive voltage to the primary of the high voltage transformer. This transformer has several secondary windings whose outputs are rectified and stacked to form the various collector and cathode operating potentials required by the booster TWT. The cathode to ground potential is monitored by the frequency compensated, precision high voltage divider network. Precise cathode regulation is achieved via a wide-band linear helix post regulator circuit. The resistive portion of this divider is thick film construction. A sample of the cathode voltage from the the divider network is used to regulate the cathode voltage to the required precision (+0.5%). The housekeeping, Boost Converter, and Resonant Inverter utilize conventional pulse width modulation circuitry in die form and operate with the synchronized switching frequencies. Current mode control is used in both the Boost Converter and Resonant Inverter regulation loops.

The modulator controls the TWT beam and utilizes a proprietary cathode pulse modulation technique. Slew times for modulator transitions are 10 to 15 nsec. This is achieved with high speed, high voltage metal oxide semiconductor field effect transistors (MOSFETs). Total transition time from the transistor transistor logic (TTL) signal at the MPM input to completion of the modulator voltage transition is 30 nsec. Minimum pulse width is DC. The maximum modulator CW switching frequency is 330 kHz and burst operation up to 5 MHz has been demonstrated.

Control and precision features are included for both power supply and booster TWT operation and protection. These include: a TWT heater warm-up timer, cathode undervoltage, helix overcurrent, inverter overcurrent and temperature limits. The MPM power supply and booster TWT are protected from arc damage by a combination of helix current sense shutdown, circuit impedances, and surge limiting components.

VACUUM POWER BOOSTER (VPB) TWT DESIGN

Recent work at Northrop Grumman has concentrated on the development of highly miniaturized, high efficiency, VPB TWTs for a family of power modules covering the 2 to 40 GHz frequency range. VPB TWTs successfully developed at Northrop Grumman under Tri-Service (Ref. 1) and DARPA (Ref. 2) sponsorship include High-band (6 to 18 GHz) and Low-band (2 to 6 GHz) 100 W TWTs operating at over 40% efficiency, and the NRL (Ref. 3) sponsored ultra-high efficiency (60%) high power narrow-band 170 W and 240 W C-Band TWTs. In addition, work is actively underway extending power booster performance in peak power, bandwidth and frequency under the kilowatt X-Ku, Ultra-band and Millimeter Wave Power Module (MMPM) development programs, respectively.

The Northrop Grumman VPB family is based on a common modular design approach to ensure flexible manufacturing at reduced cost. Assembly and construction of the VPB requires half the number of pieces and assembly steps of conventional tubes. Component design for the VPB TWT is identical with all Northrop Grumman power boosters. The general tube fabrication is high temperature precision brazed metal and ceramic parts. Major subassemblies, as well as the sever joint, are connected together by laser welded flanges.

The gun design is a basic electrostatic converged beam Pierce gun with a low cost focus electrode for beam control. A moderately high beam perveance ranging from around 0.5 to 1, depending on the tube, is chosen to minimize the circuit length and reduce the cathode voltage. An M-type cathode operating at a low loading of just a few A/cm^2 is employed for long life operation. The focus electrode is designed to provide beam cutoff with about 1300 V of negative bias. Mechanical design of the gun uses a single cylindrical header ceramic with metalized through holes into which metal pins are brazed for connection to the cathode, heater and focus electrode. Metalized rings are provided on the face of the header to braze mounting rings for the cathode and focus electrode.

The cathode heater assembly has a concentric sleeve support structure to provide high thermal impedance along with good mechanical stability over a broad temperature range. Only 5 W of filament power is required to bring the tube to operating temperature in less than 30 seconds.

An important feature of the gun assembly design is the adjustable gun housing which provides at least ± 10 mils movement of the cathode assembly with respect to the anode. The metal disk attaching the gun housing to the anode assembly is designed to flex under a force in excess of 40 lb. This makes the structure stable under normal tube handling, but movable with appropriate fixturing while being tested. This feature allows the perveance of the gun to be adjusted during test for optimum beam current.

The interaction circuit employs two helix sections supported by BeO rods. A short input circuit is separated from the output circuit by a sever with a graphite attenuator on the support rods on either side of the sever. This provides better than 80 dB of isolation from the input to the output and the ability to

absorb high RF power from an external mismatch, thus protecting the SSA. Broadband performance with low harmonic power is obtained by nearly flat (slightly negative) circuit velocity dispersion provided by metalized vanes on the sides of the support rods. A strong broad-band circuit efficiency of around 20% is obtained by employing a velocity step in the output circuit. For narrow-band applications, vane loading is not required for dispersion control, while an optimized dual velocity step circuit is employed for a circuit efficiency in excess of 30%. The TWT uses coaxial RF vacuum windows to couple to the circuit. The input and output window design depends on the tube frequency and power requirements. The window configurations range from modified SMA for the low power (100 W) microwave tubes to TNC output on the high power tubes and 3.5 mm (input)/waveguide (output) for the millimeter wave tube. The input and output match on all tubes is excellent being better than 10 dB across most of the band.

An integral pole piece (IPP) and helix barrel design make the pole piece inside diameter (ID) the outer conductor for the helix circuit. The body ID is precision honed to accept the helix and support rod assembly. This hubless pole piece design is magnetically efficient and provides a high degree of on-axis magnetic field uniformity.

A low cost, well established manufacturing method of "hot stuffing" is used to assemble the helix and rods in the IPP barrel to establish an interference fit of the circuit. Such a structure provides excellent thermal transfer and mechanical ruggedness.

A high field periodic permanent magnet (PPM) stack using 20 x 10^6 GOe energy product samarium cobalt 2:17 magnet material is employed on all VPB TWTs to reduce the transverse cross section of the vacuum envelope. This material was selected as a trade-off between high energy product and low magnetic field variation with temperature.

An important finding of the C-Band MPM TWT development program is the requirement for ultra-laminar electron beam flow for high circuit and collector efficiency. As demonstrated on the C-Band TWT, laminar beam flow requires careful profiling of the magnet stack entrance field. The optimum magnetic field entrance profile is obtained by performing electron gun simulations including the realistic stack magnetic field. Electron ray trajectory calculations are performed using the Hermannsfeldt electron optics code, while the stack field profile is obtained using the Maxwell magnetostatic simulation code. Upon determination of the optimum magnetic entrance profile, the stack entrance magnets are then individually charged to the desired level.

All Northrop Grumman VPBs employ a four-stage depressed collector with a short collector refocussing section for high beam energy recovery. The collector electrical design was established based on the methods obtained at NASA/Lewis. This approach uses the spent beam data from the large signal code as input for the electron ray trajectory calculations in the collector. Dissipated power is then calculated for each collector lens. Total collector energy recovery is then optimized by varying the individual lens shape and position. The novel Northrop Grumman collector design uses a one piece beryllia ceramic shell made in a rectangular shape and metalized on the ID. The collector stage lenses are made from graphite to suppress secondary electron emission and metalized on the outside diameter for brazing. This design provides for very high thermal conductivity to the module cooling blocks while minimizing the overall height.

SSA DESIGN

The SSA serves as a front-end amplifier for the TWT in the MPM. The primary function of the SSA is to provide the required small signal gain of approximately 25 dB, typically half the MPM overall gain, with the desired RF drive level required by the TWT to achieve rated output power. The SSA also serves the function to compensate for the small signal gain variation of the TWT over frequency yielding a relatively flat gain response over 2 to 3 octaves of bandwidth. One of the many benefits of an MPM based amplifier approach compared to conventional traveling wave tube amplifiers (TWTAs) is improved noise figure. Typical noise figures of less than 10 dB, as compared to the TWTA alone of 30 dB, are achieved. Figure 3 shows a typical block diagram of a SSA. All SSAs include MMIC amplifier gain stages and voltage variable attenuators (VVAs), with some containing control functions such as: phase shifters and amplitude modulation.

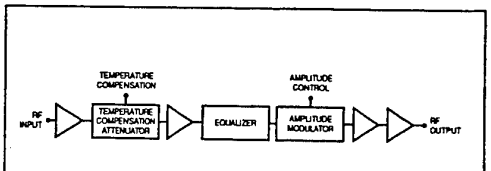

Figure 3. Typical block diagram of a SSA for MPM applications

Because of the stringent size and cost constraints imposed by many MPM programs, the use of anything but MMIC technology is precluded. If this amplifier were to be designed using discrete components, the size of the SSA would easily be 2 to 3 times larger with only half the functionality. In addition to the size reduction benefit, added performance improvements in the area 5 to 10 times reliability enhancements due to the reduced parts

count and 2 to 3 times reduction in overall cost is achievable. Also because of the lower number of components required in the assembly, cost of the MMIC based amplifier will typically be 50% lower than an amplifier using conventional technology.

PACKAGING AND MANUFACTURING

The major emphasis of all MPMs being developed at Northrop Grumman is commonality. This is the only way to achieve economies of scale. The design requirements for the various applications of MPMs have been identified in the ECM, radar, and communications arenas. From the overlapping design requirements, performance specifications for a standard product line have been established. Other MPMs are certainly perceived and will be derivatives of the standard line. For example, a radar application at 9.8 GHz with 500 MHz bandwidth, may require 125 watts RF output power. The standard 100 W, 6 to 18 GHz MPM design would undergo minor modifications to meet the higher power for the narrow bandwidth. Other performance parameters can be optimized such as noise figure and linearity response for the narrow bandwidth required.

Design flexibility, automation and utilization of known processing techniques are essential in achieving a low cost product. Since the initial proving of the MPM cost concept feasibility which started in 1991, Northrop Grumman MPMs have gone through three design iterations all focused on improving manufacturability, flexibility, and commonality (figures 4 to 6). Automating and minimizing the required processing types have been the major objectives. These efforts have dramatically reduced recurring cost and production cycle. An example of this is the evolution of the low voltage portion of the Integrated Power Conditioner (IPC). Since the initial conception of the 6 to 18 GHz MPM, over 100 discrete components have been replaced on the housekeeping subassembly (figure 2) with one ASIC and four resistor networks. This ASIC insertion which is common to all Northrop Grumman MPMs, reduces assembly time and parts cost by more than $150. Libraries of ASIC and MMIC component building blocks have been created and are used for power modules as well as production hardware designs at Northrop Grumman. ASIC and MMIC insertions have resulted in typical reliability improvements of 5 to 10 times, reduction in power consumption of 1.5 to 2.5 times, reduction in parts count of 10 to 20 times, reduction in circuit area of 3 to 10 times, and a reduction in cost of 2 to 5 times over conventional hardware. All of these attributes contribute to lower acquisition and life cycle cost.

Depending on application, two thermal management techniques are employed. For phased array applications where multiple MPMs directly feed an antenna array, forced convection is utilized to maximize the benefits of MPM technology. The most significant challenge in the 6 to 18 GHz module development (6 x 4 x 0.32 in) was meeting the overall maximum thickness of 0.32 in. This required technology advancements in the booster TWT, IPC, and thermal management areas. Meeting this maximum allows the MPMs to mate directly with the antenna, eliminating cabling and combining losses which are often 50% of the RF output power. The limitation of this benefit is restricted to 18 GHz. Feasibility of this concept was demonstrated in a 1 x 3 array in September 1994 (figure 4).

Most applications for power modules are envisioned to be conduction cooled. In this situation, the power module mounts directly to a coldplate or heat exchanger. This configuration was not intended to be stacked as in phase array applications. Therefore, several cost drivers associated with meeting the 6 to 18 GHz phased array thickness requirement of 0.32 in have been eliminated. The power dissipated within the module is conducted through the substrates and spread via an aluminum housing to the cold plate. The typical effective heat transfer coefficient required is 180-220 BTU/hr.-ft^2-F, which is dependent on power output, mounting locations, hardware size, surface finish, etc. Conduction-cooled modules are thicker as a result of approximately 0.2 in aluminum being required in the base of the housing for heatspreading. A gel di-electric is used, eliminating the concerns associated with liquid dielectrics. The subassemblies are fabricated from multilayer thick film alumina substrates. Double-sided layouts have been created to fully utilize the package height which is set by the TWT and IPC magnetics.

CONCLUSION

Several Northrop Grumman MPMs have demonstrated unsurpassed efficiencies and previously unattainable noise performance for the required gain and output power levels. Northrop Grumman MPMs have displayed significant technological advances in the areas of power conditioners, modulators, TWTs, and packaging. Specific achievements include:

- Integration of traditionally dissimilar hardware into one-tenth the volume and one-sixth the weight of conventional hardware while delivering 2.5 times the RF output power and increasing the efficiency by a factor of five.
- High voltage power conversion of up to 94%.
- Power supply packaging density up to 90 W/in^3.
- 350 W, 4 kV, multiple output high voltage transformer within 0.272 in height.
- Miniaturized TWT modulator capable of slewing 1200 V in 10 nsec.
- 6 to 18 GHz booster TWT delivering 100 W (nominal) RF output power, with 30% effi-

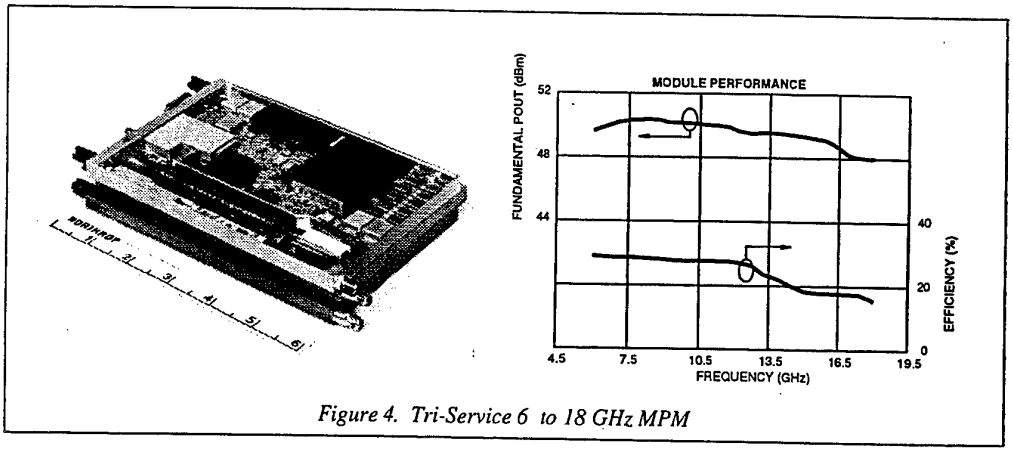

Figure 4. Tri-Service 6 to 18 GHz MPM

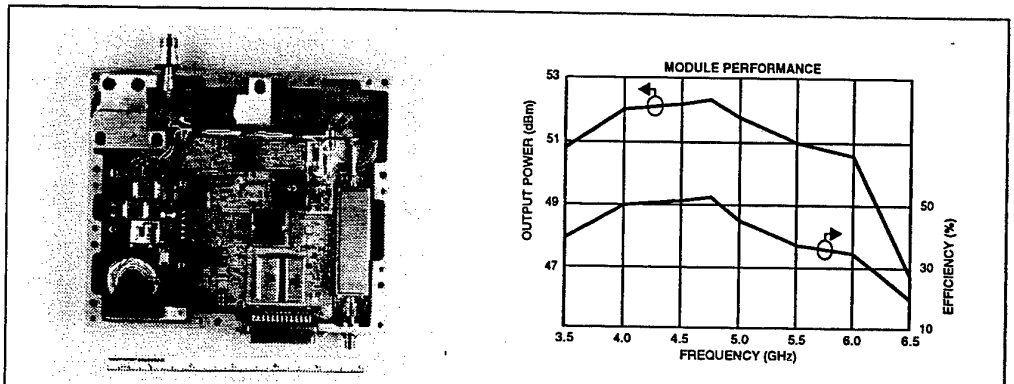

Figure 5. C-Band MPM

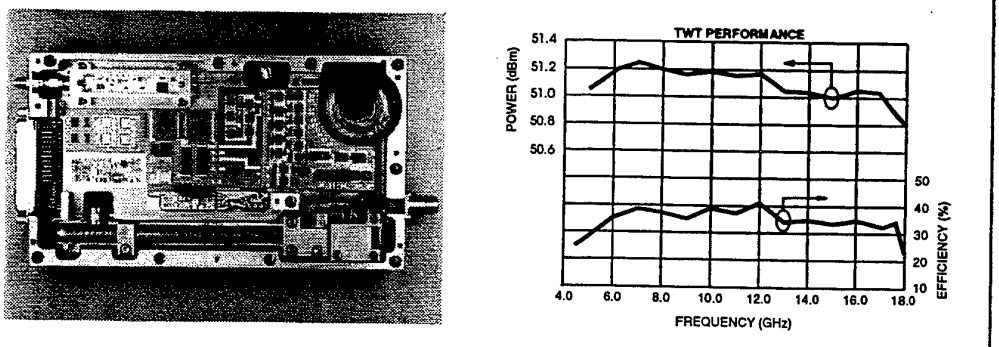

Figure 6. Ultra-Band (brassboard) MPM

ciency within an envelope 5.5 in long and 0.288 in high.

- C-Band booster TWT delivering 170 W RF output power with delivery >61% efficiency.
- Single braze, high efficiency, four-stage collector.
- Integral gain equalization and temperature compensation (SSA).

ACKNOWLEDGEMENTS

The work discussed in this paper was completed through contract, Technology Reinvestment Program and Northrop Grumman Research and Development efforts. Special thanks to Naval Research Laboratory (NRL), Wright Laboratory, and the Defense Advanced Research Project Agency (DARPA) for their support and direction.

REFERENCES

1. Contract #F33615-91-C-1815, Tri-Service MPM.
2. Agreement F33615-94-2-1524, Low-band MPM and Millimeter Wave Power Module with WL/ARPA.
3. Contract N00014-94-C-2242, C-Band MPM with NRL.

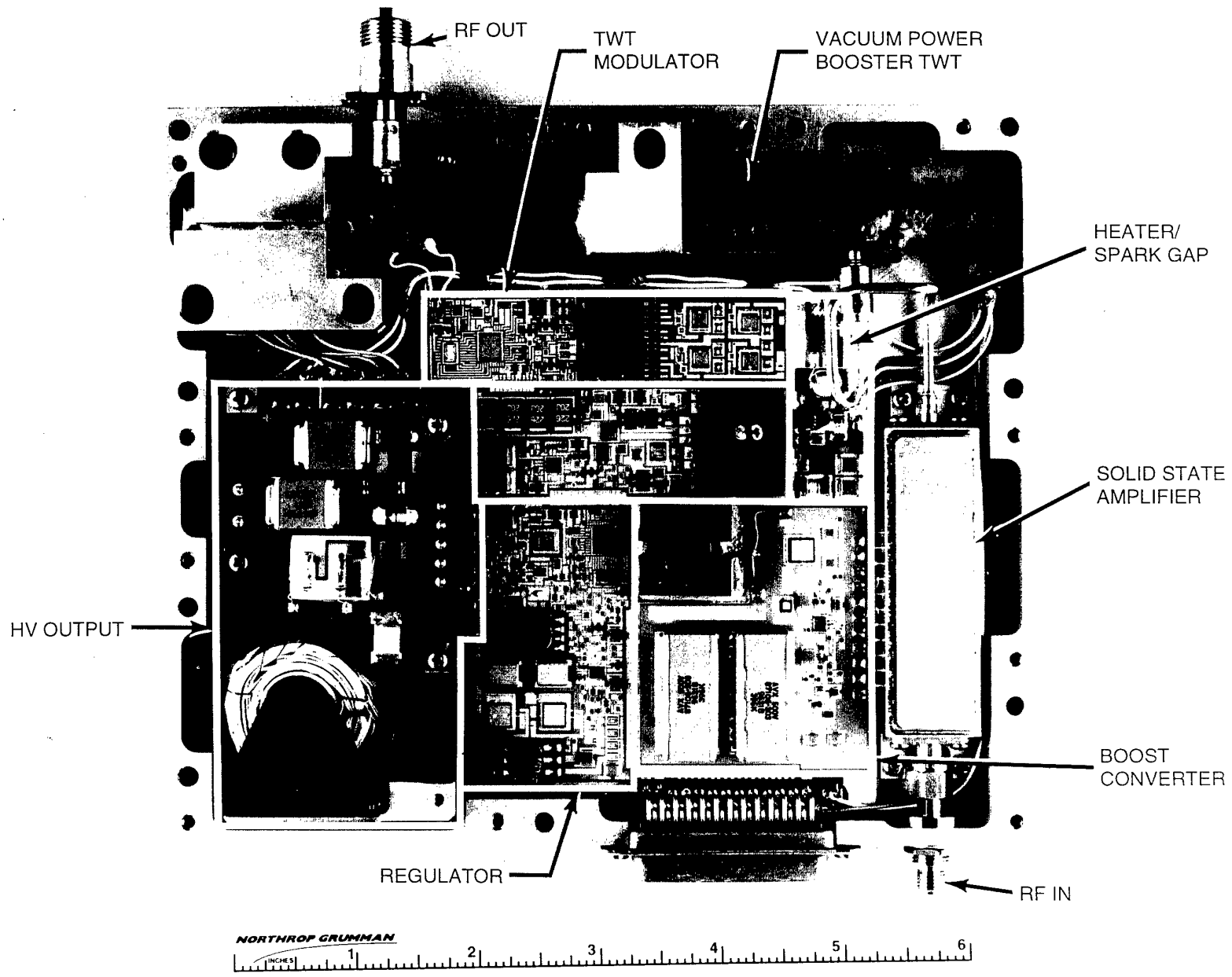
RF OUT
TWT MODULATOR
VACUUM POWER BOOSTER TWT
HEATER/ SPARK GAP
SOLID STATE AMPLIFIER
HV OUTPUT
BOOST CONVERTER
REGULATOR
RF IN
NORTHROP GRUMMAN
INCHES
1
2
3
4
5
6

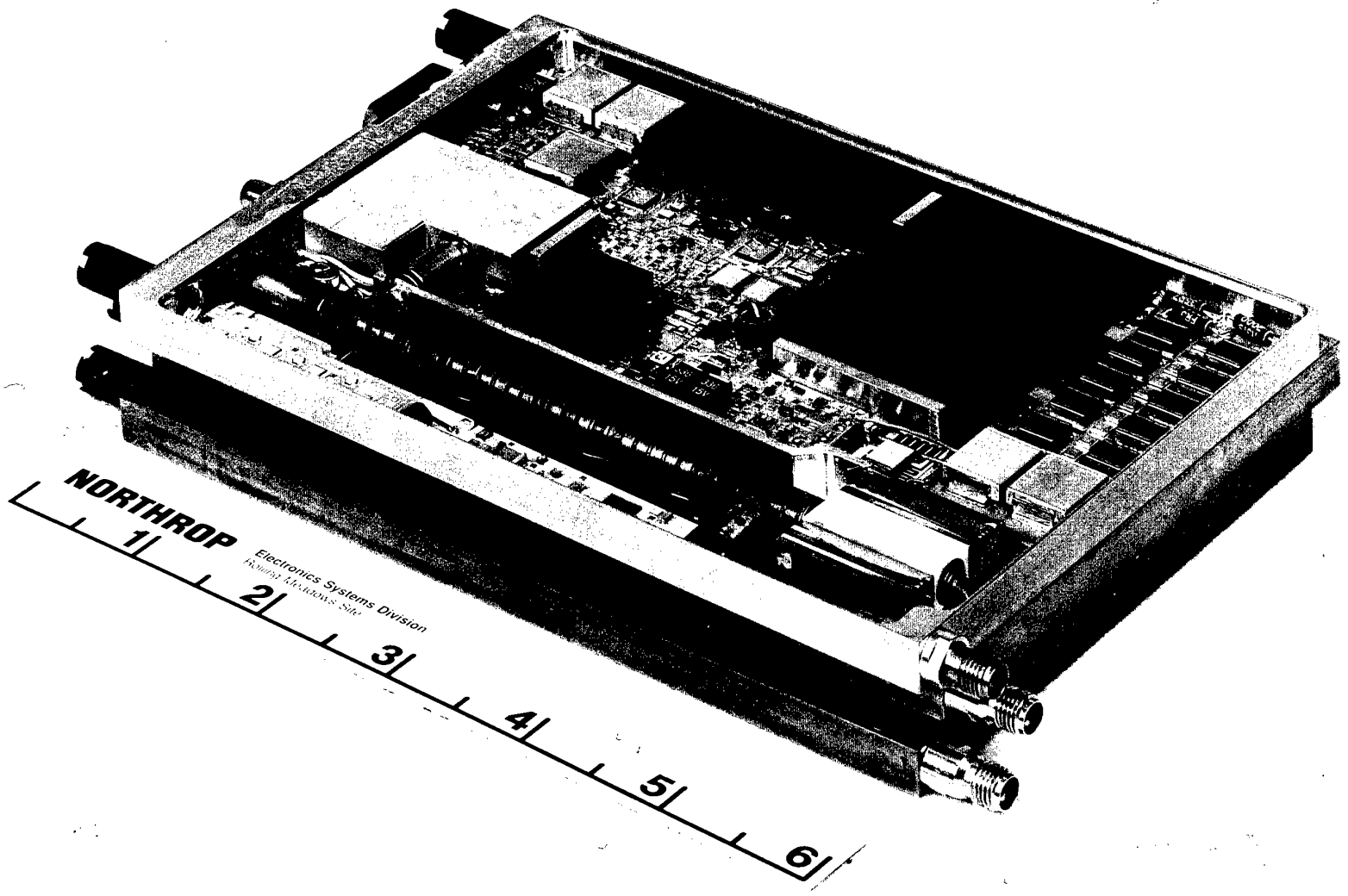
NORTHROP
Electronics Systems Division
Rolling Meadows Site
1
2
3
4
5
6

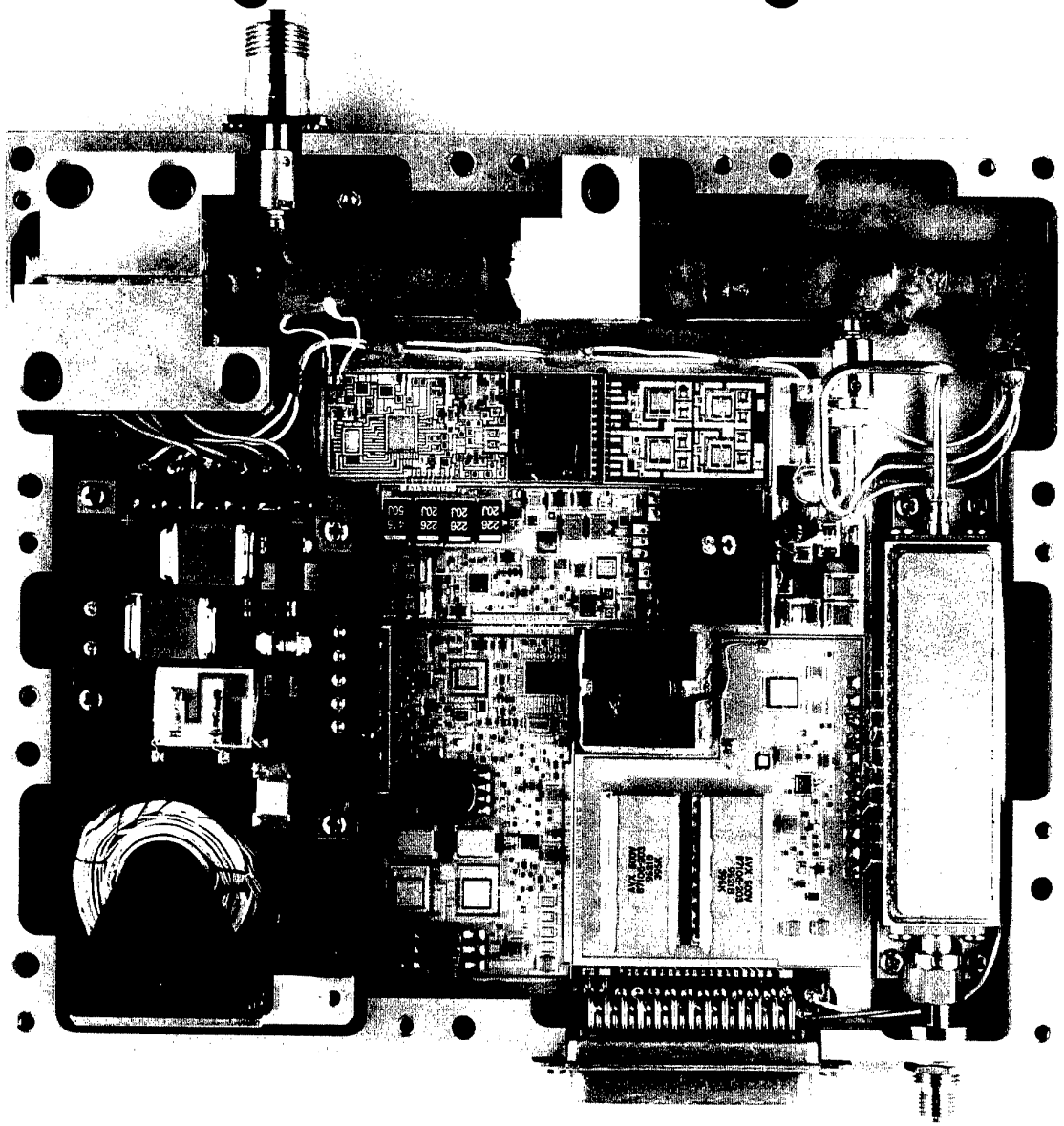

NORTHROP GRUMMAN

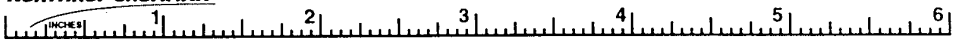

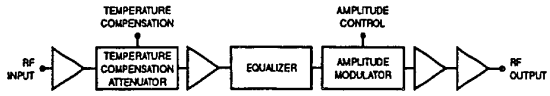
TEMPERATURE COMPENSATION
AMPLITUDE CONTROL
RF INPUT
TEMPERATURE COMPENSATION ATTENUATOR
EQUALIZER
AMPLITUDE MODULATOR
RF OUTPUT

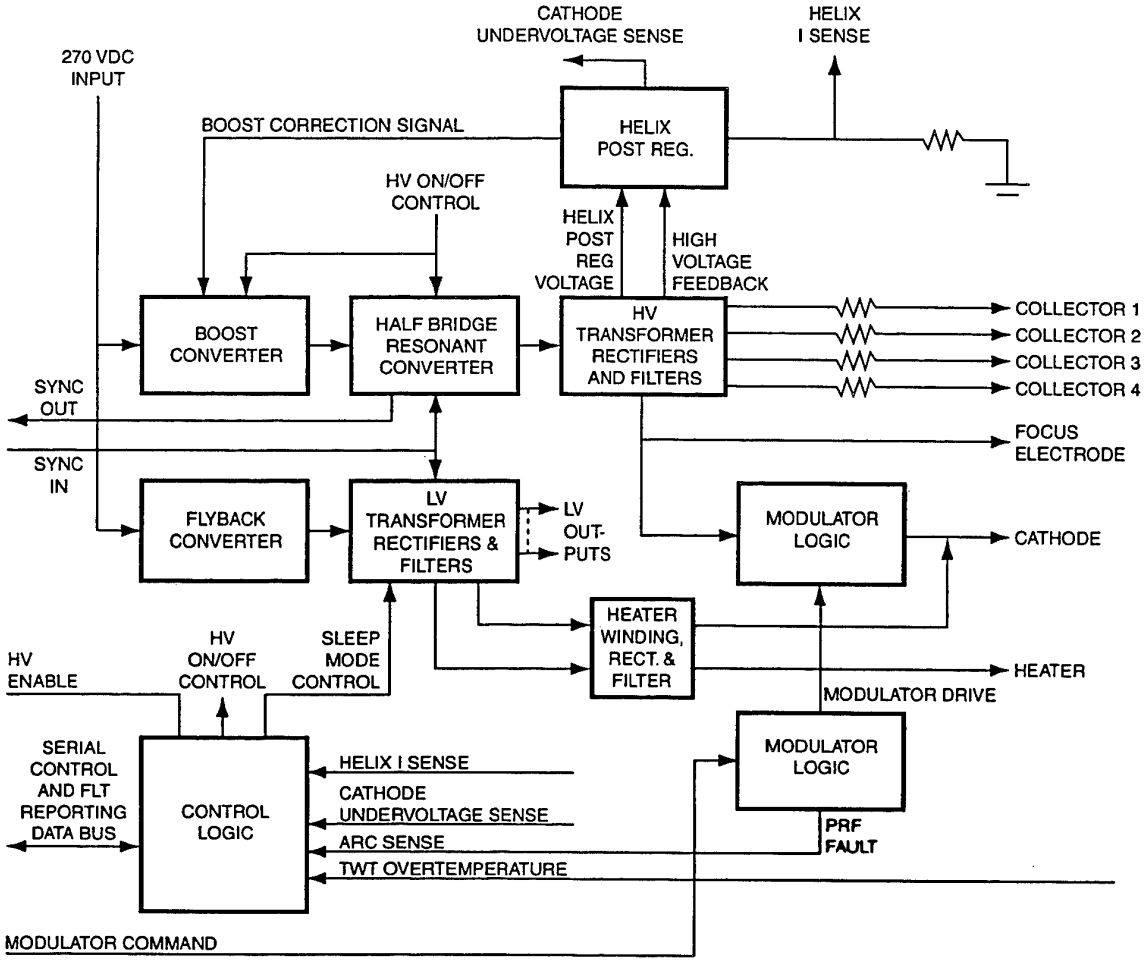
CATHODE
UNDERVOLTAGE SENSE
HELIX
I SENSE
270 VDC
INPUT
BOOST CORRECTION SIGNAL
HELIX
POST REG.
HV ON/OFF
CONTROL
HELIX
POST
REG
VOLTAGE
HIGH
VOLTAGE
FEEDBACK
BOOST
CONVERTER
HALF BRIDGE
RESONANT
CONVERTER
HV
TRANSFORMER
RECTIFIERS
AND FILTERS
COLLECTOR 1
COLLECTOR 2
COLLECTOR 3
COLLECTOR 4
SYNC
OUT
SYNC
IN
FOCUS
ELECTRODE
FLYBACK
CONVERTER
LV
TRANSFORMER
RECTIFIERS &
FILTERS
LV
OUT-
PUTS
MODULATOR
LOGIC
CATHODE
HEATER
WINDING,
RECT. &
FILTER
HEATER
HV
ENABLE
HV
ON/OFF
CONTROL
SLEEP
MODE
CONTROL
MODULATOR DRIVE
SERIAL
CONTROL
AND FLT
REPORTING
DATA BUS
CONTROL
LOGIC
HELIX I SENSE
CATHODE
UNDERVOLTAGE SENSE
ARC SENSE
TWT OVERTEMPERATURE
MODULATOR
LOGIC
PRF
FAULT
MODULATOR COMMAND

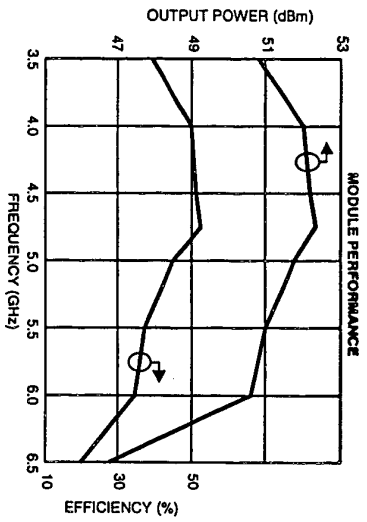
OUTPUT POWER (dBm)
47
49
51
53
3.5
4.0
4.5
5.0
5.5
6.0
6.5
FREQUENCY (GHz)
MODULE PERFORMANCE
10
30
50
EFFICIENCY (%)

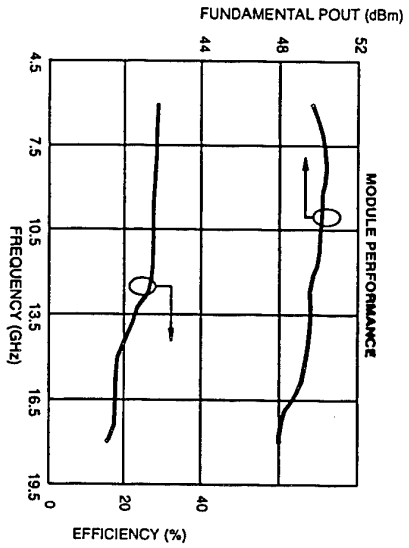
FUNDAMENTAL POUT (dBm)
44
48
52
4.5
7.5
10.5
13.5
16.5
19.5
FREQUENCY (GHz)
MODULE PERFORMANCE
0
20
40
EFFICIENCY (%)

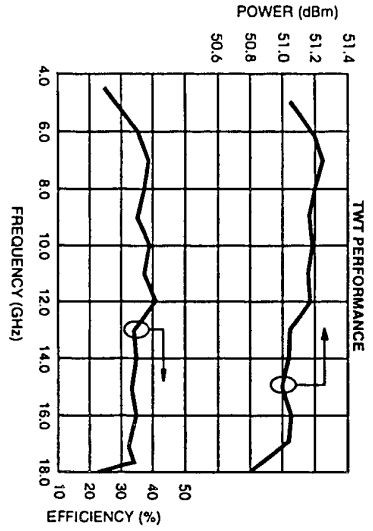
POWER (dBm)
50.6
50.8
51.0
51.2
51.4
4.0
6.0
8.0
10.0
12.0
14.0
16.0
18.0
FREQUENCY (GHz)
10
20
30
40
50
EFFICIENCY (%)
TWT PERFORMANCE

MICROWAVE POWER MODULES: Technology for the Future

T. Ninnis, T. Schoemehl, W. Pelster, R. Watkins,
J. Taylor, G. Lednum, J. McKay, and P. Ballagh
Litton Systems, Inc., Electron Devices Division
San Carlos, CA, USA

ABSTRACT

This paper summarizes the capability of a family of Microwave Power Modules (MPMs) developed by Litton Systems, Inc., Electron Devices Division. The MPM is a complete microwave amplifier which includes a helix TWT, otherwise known as a vacuum power booster (VPB), a solid-state driver amplifier (SSA), and a high density electronic power conditioner (EPC). All three components are housed in a small, compact, lightweight package. Both military and industrial versions are available. MPMs have been developed to operate from 2 GHz to over 45 GHz. The primary sub-bands are 2 to 6 GHz, 6 to 18 GHz, and 18 to 40 GHz. Narrow band MPMs include C, X, Ku, Ka, and Q-bands. RF performance is up to 150 watts CW output power, noise figures of less than 10 dB, and up to 40% efficiency. The Electron Devices Division manufactures both the VPB and the EPC.

INTRODUCTION

The most significant recent advancement in high power microwave amplifiers has been the introduction of the Microwave Power Module (MPM). The MPM is a supercomponent comprising a vacuum power booster (VPB), a solid-state driver amplifier (SSA), and an electronic power conditioner (EPC). Compared to traditional TWT amplifiers, the MPM is significantly smaller, lighter, more efficient, and has a greater signal-to-noise ratio. MPMs are available in various physical configurations and frequencies, providing 40 to 150 watts of CW output power. Such amplifiers are required by the electronic countermeasures (ECM) market, where MPMs have generated tremendous interest.

Litton Systems Inc., Electron Devices Division offers a full range of Microwave Power Modules for Military and Commercial Applications. MPMs have found use in a variety of military applications, including unmanned aerial vehicles (UAVs), military satellite communications, radar illuminators, weather radars, phased array systems, and towed decoys. Commercial applications include satellite communications, high power RF sources for laboratory use, and rapid prototyping of microwave amplifiers for various applications. Figure 1 is a photograph of Litton's current military and commercial modules. Figure 2 is the RF performance from this family of MPMs.

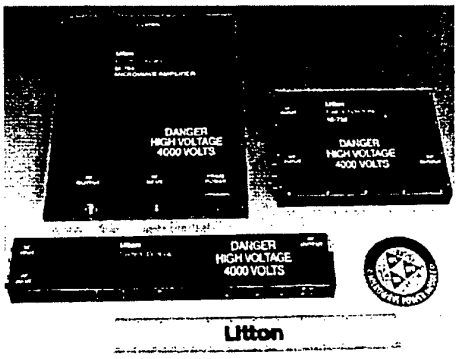

Figure 1: Litton MPMs

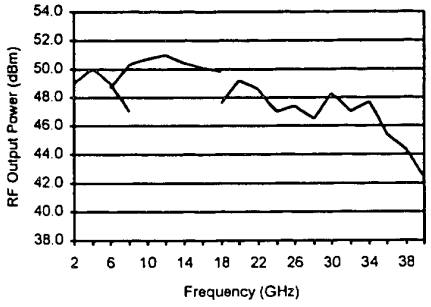

Figure 2: MPM RF Output Power

Litton has designed the MPM to be modular. Users will require a variety of mechanical formats to meet future systems needs--one size will not fit all. The use of modularity allows the components within the MPM to be reconfigured to a variety of form factors. Figure 3 is a block diagram of a typical MPM. Table 1 is a summary of Litton's MPMs.

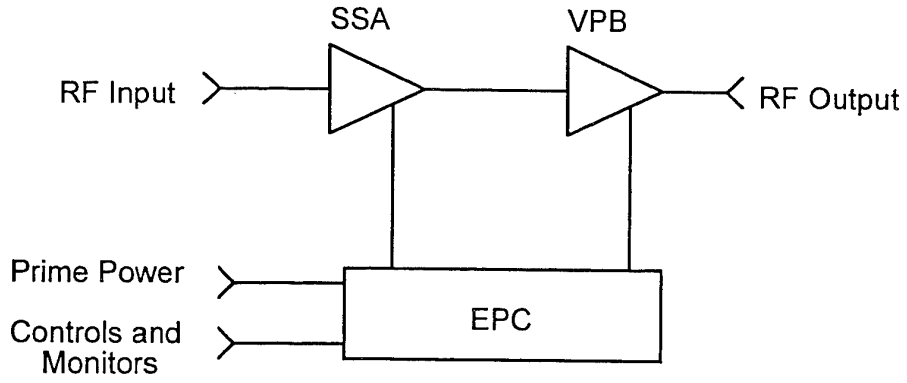

Figure 3: MPM Block Diagram

Part Number	Frequency (GHz)	P_{OUT} (dBm)	Efficiency (%)	Volume (in^3)
M 768-00	C-Band	52	40	54
M 762-00	18 - 40	44 -48	20 - 30	35
M 761-AB	X-Band	52	35	49
M 761-02	6 - 18	49 - 51	20 - 35	49
M 762-01	K_A-Band	47	20	35
M 760-00	2 - 8	48 - 51	20 - 35	54
M 773-00	Q-Band	47	25	42
M 764-00	K_U-Band	47	20	191
M 764-AC	2 - 8	48 - 51	20 - 35	247
M 764-01	6 - 18	49 - 51	20 - 35	191
M 764-AE	18 - 40	44 - 48	20 - 30	231

Table 1: Litton Microwave Power Modules

The performance of the module is fully dependent upon electrical performance characteristics of the major components: the vacuum power booster, the solid state amplifier, and the power conditioner. The vacuum power booster provides the high power RF output with the gain split equally between the VPB & SSA. The SSA receives the RF input, amplifies it up to approximately 1 watt to provide the RF drive to the VPB. The EPC accepts the input voltage, provides the required voltages to the SSA and VPB, monitors the condition of the modules, and provides module protection and controls. Figure 4 is a photograph of Litton MPMs with the covers removed.

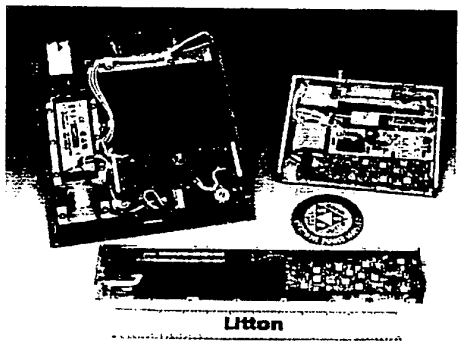

Figure 4: Photograph of Litton MPMs

VACUUM POWER BOOSTERS

Litton's Electron Devices Division is a recognized industry leader in the design and production of a variety of CW and pulse helix TWTs for ECM, radar, and communication applications. The VPB has its origin with the mini-TWT. The mini-TWT is typically a high gain device with RF output power up to 100 watts CW. Figure 5 is a photograph of a number of Litton VPBs. Table 2 is a summary of these VPBs:

Part Number	Frequency (GHz)	P_{OUT} (dBm)	Cathode Voltage (E_K)	Number of Collectors
L 5978	6 - 18	44 - 47	3000	2
L 5983	6 - 18	42 - 48	3900	1
L 5987	C-Band	52	4000	4
L 5988	18 - 40	44 - 49	6500	3
L 5990	X-Band	52	4100	1
L 6002	6 - 18	49 - 51	3850	1
L 6012	6 - 18	49 - 51	3850	3
L 6015	K_A-Band	47	6500	3
L 6017	2 - 8	48 - 51	2800	4
L 6024	Q-Band	47	7200	3

Table 2: Litton Vacuum Power Boosters

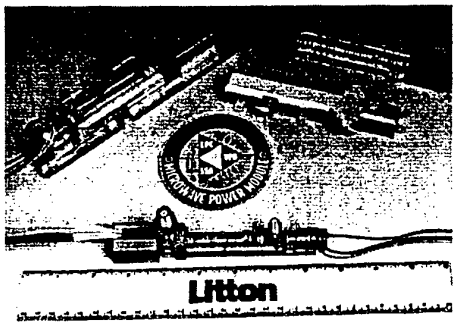

Figure 5: Photograph of Litton VPBs

All VPBs utilize high-temperature precision-brazed metal and ceramic parts. Each VPB contains an electron gun, RF circuit slow-wave structure, and most use a multi-stage collector. The electron gun is a generic assembly used on many of Litton's Mini-TWTs. The helix design is typically comprised of a three-rod APBN and tungsten wire assembly. For broad-band applications, dispersion rails are added to tailor the helix phase velocity, optimize second harmonic separation, and provide precise phase and gain tracking. The mechanical design of the collector consists of a ceramic sleeve (BeO or alumina 300) with specially treated copper electrodes brazed to the inside diameter with "pin" feed-throughs. The ceramic sleeve furnishes the vacuum envelope mechanical support for the electrodes, electrical isolation, and heat conduction. The electrodes are coated to reduce secondary emissions.

ELECTRONIC POWER CONDITIONERS

With the demand for smaller, lighter-weight power supplies, Litton has continually increased the switching frequency, employed advanced packaging techniques, and developed improved inverter topologies and circuit techniques for TWT power supplies. Development of miniaturized high voltage power supplies for MPM programs has been underway at Litton for over three years.

A block diagram of the power conditioner is shown in Figure 6. The input power comes into the module via the 15 pin dc connector. The power is routed to the inverter PC board where it powers both the auxiliary supply and the main inverter. The auxiliary supply creates the SSA voltages, the internal housekeeping voltage, the heater voltage for the VPB and the modulator bias-on and bias-off voltages. The power is also routed to the main inverter which converts it to a high frequency AC voltage that drives the high-voltage transformer. The output of the high-voltage transformer drives a multiplier and high-voltage filter circuit which provides the VPB with the cathode and collector voltages.

All Litton EPCs can support up to four collectors, with a pulse frequency modulation up to 100 KHz and pulse widths 100 nsec, or greater. Table 3 is a summary of Litton's EPCs. Figure 7 is a photograph of these EPCs.

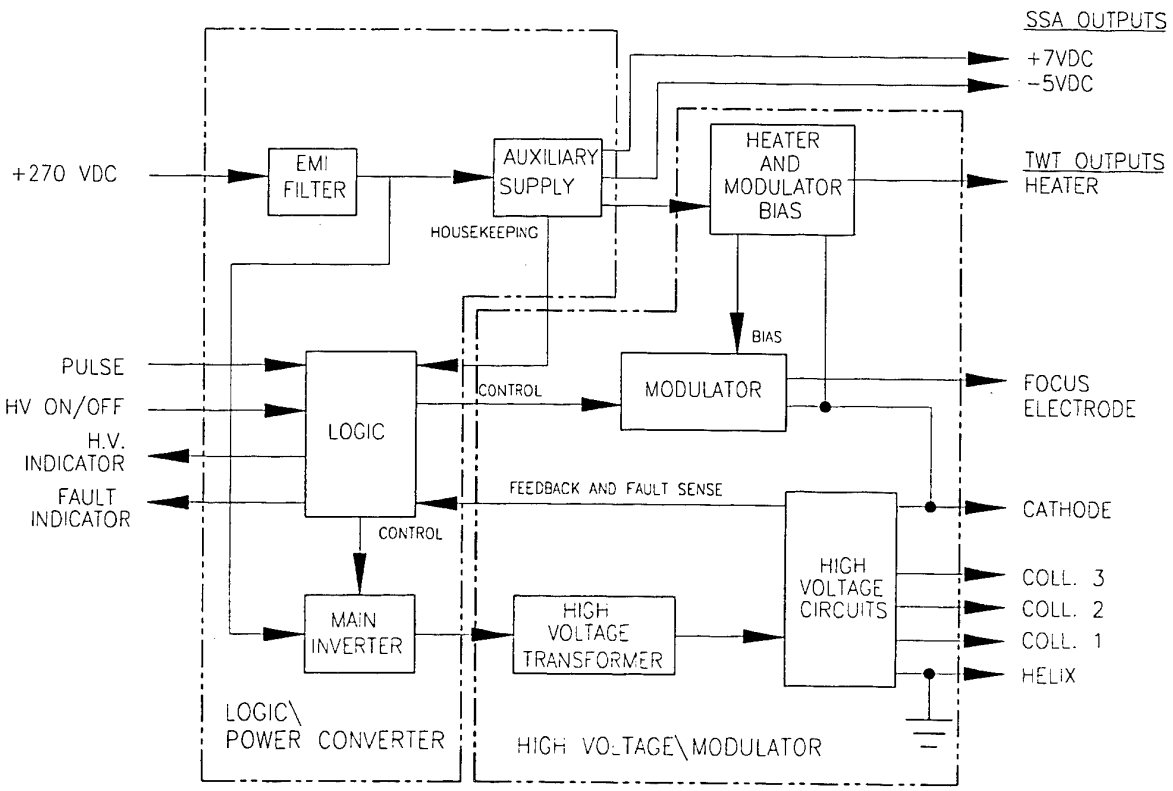

Figure 6: EPC Block Diagram

Part Number	Input Voltage	Output Voltage	P_{OUT} (Watts)
M 758-00	270 VDC	4,000	300
M 758-01	270 VDC	3,000	310
M 759-00	270 VDC	6,500	270
M 780-00	28 VDC	7,500	300
M 764-00	115 VAC	4,000	300
M 764-01	115 VAC	3,000	270
M 764-02	115 VAC	6,500	270

Table 3: Litton's Electronic Power Conditioners

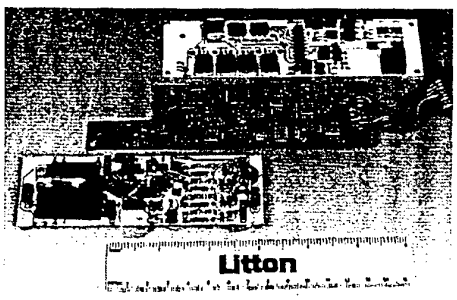

Figure 7: Photograph of Litton EPCs

MPM MODULARITY

Litton has concentrated on two (2) primary form factors for military applications: MPMs in C, S, and Ka bands are typically 14.0" (360 mm) x 4.0" (100 mm) x 1.2" (30 mm); MPMs in I/J bands are typically 7.5" (190 mm) x 6.3" (160 mm) x 1" (25 mm); commercial MPMs are typically 10.0" (254 mm) x 10.0" (254 mm) x 2.0" (51 mm).

To accommodate additional form factors, Litton has used a design approach in the EPC that contains three main sub-assemblies instead of a single printed circuit board. These sub-assemblies are the high voltage assembly, logic assembly, and low voltage/inverter assembly. As a result, these assemblies can be oriented in a variety of ways. Figure 8 and 9 are examples of the primary form factors discussed above. Figure 10 is Litton's commercial MPM.

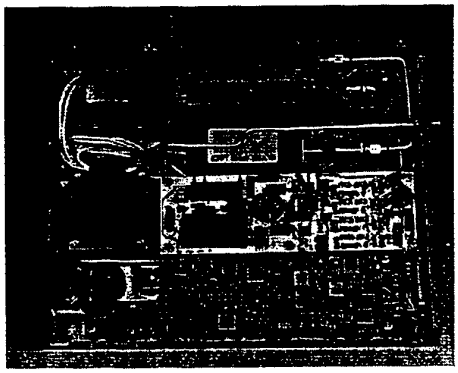

Figure 8: Litton's I/J Band MPM

Figure 9: Litton's S/C and KA Band MPM

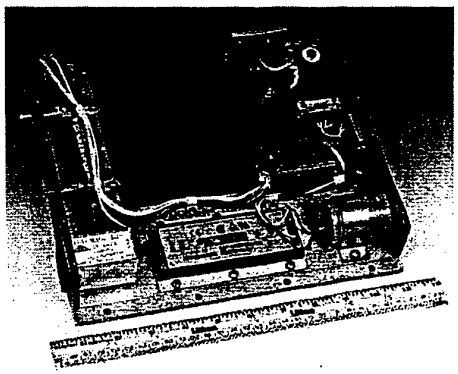

Figure 10: Litton's Commercial MPM

This concept of modularity extends to the VPB as well. Litton has developed multi-stage depressed collectors that contain up to four (4) stages, a common adjustable perveance gun, and a variety of gain distributions between the SSA and VPB.

Multi-stage collectors have been developed and demonstrated for MPMs covering all the bands. Four stage collectors are currently being utilized in the 2 to 8 frequency band, single, dual, and triple stage collectors in the 6 to 18 frequency band, and triple stage collectors in the 18 to 40 frequency band. The choice of which collector format to use is based on the required efficiency.

Another factor for consideration is the gain split between the SSA and VPB. Initially, MPMs were developed with a 50/50 gain split between these two components. As a result, one watt SSAs were required to saturate the VPB. As MPMs have evolved, it has become apparent that this gain split is not necessarily a requirement--just an option. The use of lower power SSAs can be a cost effective alternative to the original concept. The cost of a 250 mW (24.0 dBm) SSA is approximately one-third the cost of a 1 W (30 dBm) SSA. The corresponding cost increase to add additional gain into the VPB is trivial; however, there may be a nominal impact to module noise figure.

FUTURE DEVELOPMENTS

Litton has developed MPM power supplies, VPBs, and advanced pulse ECM TWTs. With these recent development efforts, a pulsed MPM for ECM and radar applications is now readily achievable. For

ECM, the MPM will operate over the I/J-Band at 1kW and up to a 7% duty cycle. For radar, the MPM will operate in X-band at 1.5kW and up to a 7% duty cycle.

CONCLUSION

The Microwave Power Module blends the best of solid state and vacuum electronics. It has high RF output power, a low noise figure, is small and extremely lightweight. In comparison to traditional TWTAs, there is a greater than 5:1 reduction in size and weight. The MPM has the potential to become the standard high-power amplifier for ECM, radar, communication, and other commercial applications. Litton's position as a supplier of both the VPB and EPC is a tremendous advantage for MPM customers; having a single source for these critical components eliminates the integration difficulties which arise when using components from different suppliers. The full line of microwave power modules, in military and commercial formats, make Litton the ideal source for all MPM requirements.

DUAL LINEARIZED TWTA WITH INTEGRATED CHANNEL AMPLIFIER.
A FIRST STEP TOWARDS THE MPM

G. Jaumann
BOSCH Telecom
Gerberstr. 33 71522 Backnang, Germany

Abstract

The paper presents a Dual Microwave Power Modul (MPM) - assembly consisting of an electronic power conditioner (EPC), two independent linearized channel amplifiers (LCAMPs), and two travelling wave tubes (TWTs). The LCAMPs are assembled together with the EPC in one housing; the TWTs may be connected with the LCAMPs either directly or via a switching network.

The different equipments are described briefly, some test results from the qualification test are shown and discussed.

1. Introduction

To accommodate the need of satellite manufacturers for more usable channels with higher output power, higher efficiency, lower size, and lower mass BOSCH developed from the well known and highly successful AT-EPC a new version capable of supplying two TWTs, each up to 125 Watts of RF Output power. The EPC allows nearly total freedom for the satellite user, e.g. operation of either TWT alone, of both independently, or of both with the RF power combined.
Apart from a significant reduction in mass and improved efficiency this EPC minimizes the differential phase shift of the TWTs by supplying them with the same helix voltage, therewith allowing easy power combining.
As a next step of integration the CAMPs and Linearizers (individual for each TWT) were build and attached to the EPC housing in a way to minimize the overall size and mass without sacrifying the freedom of operation.
The overall assembly consisting now of 1 EPC, 2 CAMPs, 2 Linearizers, and 2 TWTs, is named furtheron „DLCT" (Double-Linearized-CAMP-TWTA).
A qualification unit was built and qualification tested; the FM production for 30 DLCTs is running. The overall block diagram of the DLCT is shown in fig. 1.

2. Technical Description

2.1 The EPC

The basic function of the EPC is to convert the main bus voltage to very stable supply voltages for the TWT (or TWTs). In addition the EPC provides supply voltages for the CAMP(s) and the Linearizer(s).
The main functional blocks as shown in fig. 1 are described briefly below.

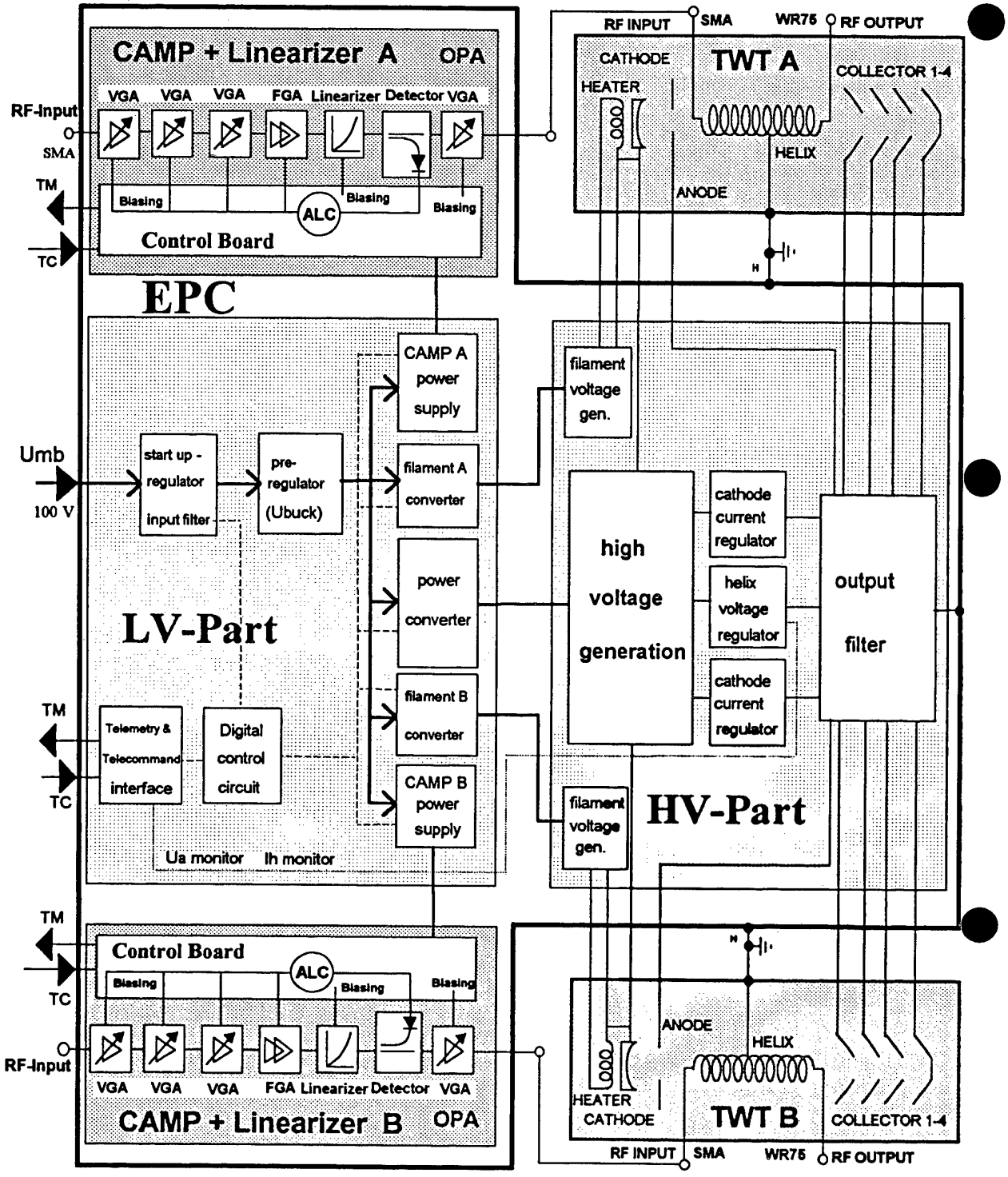

Fig. 1 Block Diagram of the DLCT

The main bus voltage (U_{mb}) is fed to a preregulator which converts it into a constant output voltage (U_{buck}). This preregulator is one of the key components of the EPC affecting several DC- and RF parameters of the TWTA. The main requirements for the regulator are very high efficiency, low conducted susceptibility, high loop stability and low undershoots at pulsed loads. All these requirements are best met with a **buck regulator.**

An **input filter** is inserted in the input to suppress voltage ripples from the main bus and switching noise from the EPC.

A **startup regulator** generates the supply voltages for the internal electronic and is automatically switched off as soon as the auxiliary converter operates.

The U_{buck} is directly applied to the **filament converters**, producing AC voltages with square waveform for the TWT **filament voltage generation**.
The filament converters are soft-started to avoid surge currents when the tube filament is cold.

The supply voltages for the channel amplifiers are generated by the **secondary power supply voltage generator** with an internal overpower protection circuit.

The **power converter** is also supplied from U_{buck} and generates a square wave output voltage. The main features of the power converter are high efficiency, avoidance of high-voltage transformer ringing, avoidance of short-circuit currents in the switching transistors, and soft recovery for the high voltage diodes. All these features are achieved using a push-pull converter to generate a special square voltage waveform including a definite gap time.

An important part of the power chain is the **high voltage generation**. The method used to generate high voltage and to apply it to the TWT is an important influencing factor on TWT behaviour. With the **output filter** design the tubes can be switched on by applying all high voltages simultaneously without an excessive spike on the helix current in the TWTs.

The output voltage of the power converter is transformed by one high voltage transformer and rectified by stacked doubler stages for collector, helix and anode voltages. The stability of the collector voltages is only determined by the preregulator output voltage. In addition, the helix and anode voltage are regulated by the **helix regulator** and the **cathode current regulator** to ensure a stable RF behaviour of the TWT in all operating conditions during the life of the satellite. Each TWT has its own independent cathode current regulator to account for individual TWT ageing.

All internal processes of the EPC are managed by the **digital control circuit**. This functional block is integrated in an Application Specific Integrated Circuit (ASIC) and has the following tasks:

- → generation of the clock frequency
- → generation of filament, power converter and CAMP supply drive signals
- → controlling of the switch-on sequence of the high voltages
- → processing of the telecommand signals
- → generation of telemetry status signals
- → protection of the EPC including automatic restart unit (ARU)

The optimized and mature design of the EPC results in a typical efficiency of 95% with both TWTs operating and about 94% in single-TWT operation, averaged now over more than 200 FM units.

2.2 The CAMP and Linearizer

The overall assembly of two CAMPs and two Linearizers consists of two identical and independent DC- and RF-parts, build into one housing, and sharing one DC connector. The block diagram is contained within fig. 1.

The **Control Board** contains driving circuits for the RF modules, telemetry/telecommand interfaces, and other electronic control circuits, e.g. for temperature compensation, gain/output power level setting, and circuits to enable or disable the linearizer.

Each RF part is subdivided into 7 modules (all in MIC technology); four **variable gain amplifier** modules, a **fixed gain amplifier** module, a **linearizer bridge** module and a **power detector** module:

Three **variable gain amplifier** modules and the **fixed gain amplifier** module at the input amplify the nominal input power to the level required for proper operation of the linearizer bridge. In fixed gain mode (FGM) the gain setting range is 31 dB in 1 dB steps.

The **linearizer bridge** is a predistortion network in a transmission type configuration. The RF input signal is predistorted in such a way that the application of the predistorted signal at the input of a TWT results in a less distorted output signal. The linearizer may be enabled or disabled by telecommand. In disabled mode the RF input signal is passed through the linearizer undistorted.

The **detector module** provides the ALC circuit with the detected RF-signal in order to regulate the output power level to the level selected by telecommand. Setting range is 15 dB in 0.5 dB steps.

The output **variable gain amplifier** module provides an additional telecommandable power setting range of 7.5 dB in 0.5 dB steps to allow easy adjustment of the CAMP output power to the actual TWT input power without change of the operating point of the linearizer.

Isolators are inserted at the input, in front of the linearizer bridge, and at the output in order to ensure good return loss.
All in all, the CAMPs provide about 63 dB of gain with a typical input power range between -58 and -27 dBm and a very low DC power consumption in the order of 2.5 Watts per chain. Nominal output power is +5 dBm.

2.3 The TWT

The design of the EPC allows the use of radiation or conduction cooled TWTs of all providers. For the actual program the TTE-TWT TH3787G of the successful 3787 family is used.
The main features of the TWT are:

- → M type cathode
- → Gun with ion barrier and control anode for RF power 95 - 140 W
- → Delay line of copper-plated tungsten ribbon, supported by boron nitride rods, double taper helix pitch profile
- → Collector with 4 stages, copper electrodes, either for conduction- or radiation cooled housings

These TWTs are build in high quantities with a typical efficiency around 64% over a 500 MHz bandwidth.

3 DLCT Performance

3.1 Test Levels

The assembly of EPC, two LCAMPs, and two TWTs was subjected to a qualification test in the frame of a commercial project. The test consisted of a thermal test, vibration test, thermal vacuum test, and EMC test. The test levels were as follows:

Temperatures:	-10 °C to + 70 °C	(operating)
	-30 °C	(cold start)
Vibration:	13 g sine vibration	
	20 g random vibration	

3.2 Test results

There were 4 different configurations of the DLCT for the test. They are highlighted below:

1.) LCAMP A connected to TWT A and LCAMP B connected to TWT B (standard)

2.) LCAMP A connected to TWT B and LCAMP B connected to TWT A (cross-strapped)

3.) LCAMP A connected to TWT A and TWT B, LCAMP B switched OFF (combined)

4.) LCAMP B connected to TWT A and TWT B, LCAMP A switched OFF (combined)

As each linearizer is tuned to a dedicated TWT it was expected to find some performance degradations for configurations 2-4. However, the tests showed only minor impacts. (see fig. 2 and 3).

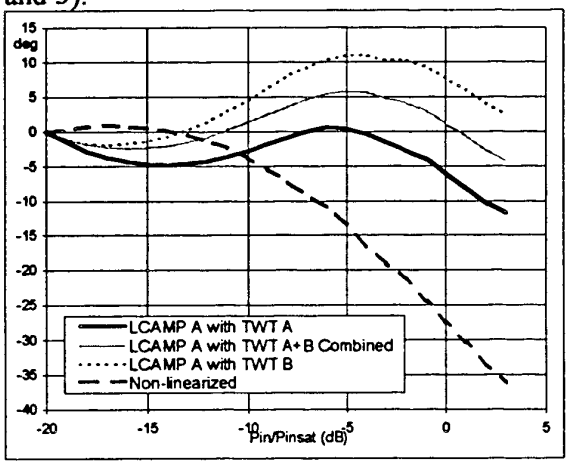

Fig. 2 Phase shift for different configurations

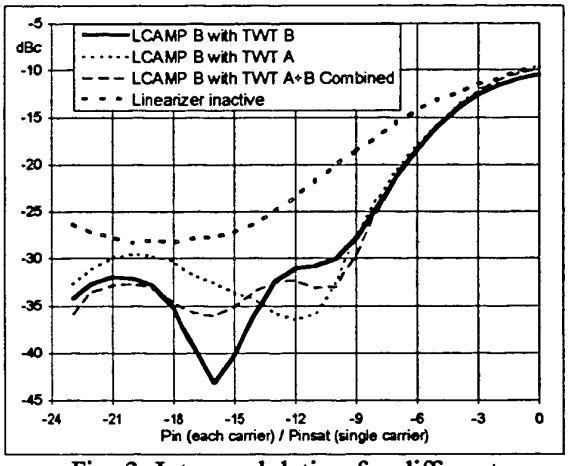

Fig. 3 Intermodulation for different configurations

To account for the individual gain of each TWT and the attenuation of the switching network between LCAMPs and TWTs dedicated attenuators are inserted between LCAMPs and TWTs. This measure ensures that the linearizer is properly aligned to the TWT. If the TWT gain changes with time this alignment is no longer maintained. The impact on the performance by misalignment was measured and found to be minor. (See fig. 4 and 5)

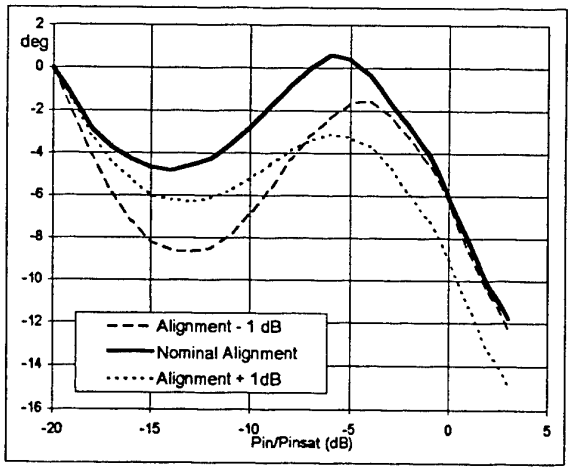

Fig. 4 Phase shift for different alignment (± 1 dB) between LCAMP and TWT

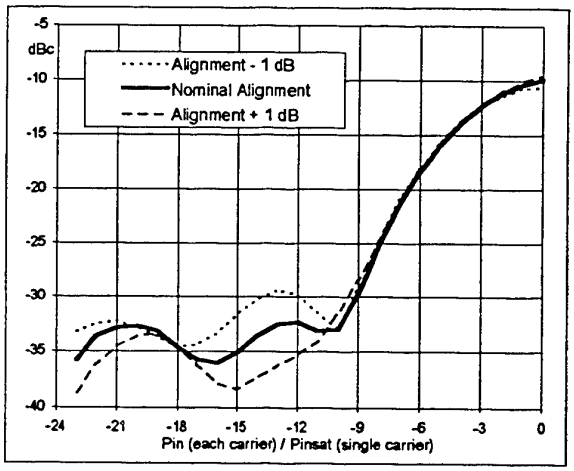

Fig. 5 Intermodulation for different alignment (± 1 dB) between LCAMP and TWT

The change of the AM/AM characteristic and the DC power consumption vs. drive in linearized - and non-linearized mode is shown in fig. 6 and 7.

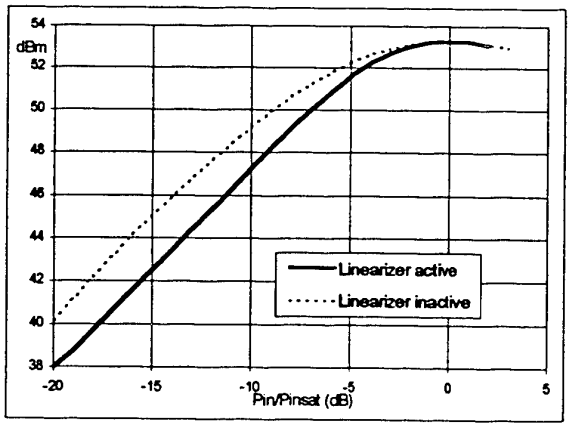

Fig. 6 AM-AM Transfer Characteristic with Linearizer active and inactive

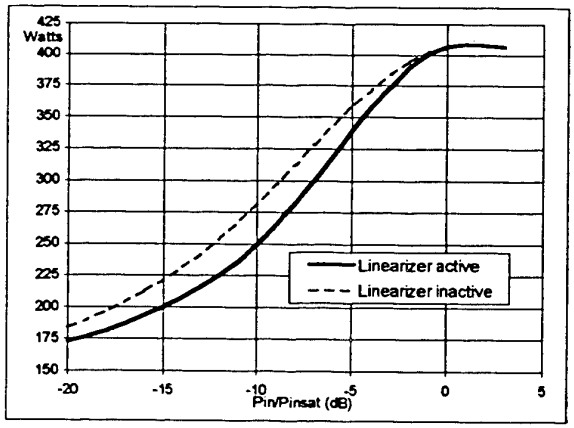

Fig. 7 DC Power Consumption with Linearizer active and inactive

The most important test results are summarized hereafter:

RF Output Power:	more than 2*113 W or 220 W combined better than 0.03 dB/10 K temperature stability
Frequency range:	11.7 - 12.2 GHz
Small Signal Gain:	81 - 115 dB, 31 dB adjustment range by TC better than 0.20 dB/10 K temperature stability (FGM)
Intermodulation (linearized)	$Pin_{(each\ carrier)}/Pinref_{(single\ carrier)}$= -3 dB: -12 dBc $Pin_{(each\ carrier)}/Pinref_{(single\ carrier)}$= -10 dB: -28 dBc $Pin_{(each\ carrier)}/Pinref_{(single\ carrier)}$= -17 dB: -31 dBc
Phase shift (linearized)	typ. 10 degpp
DC Power Consumption	less than 406 W (both TWTs and LCAMPs ON)
Overall Mass (w/o external networks)	between 4500 and 5300 g depending on TWT design (radiation or conduction cooled)
Size of the EPC+DLCAMP	296 mm * 99 mm * 125 mm

Table 1. Performance Summary

4. Conclusion and Outlook

With the presented design BOSCH managed to set a new milestone for a size- and mass optimized MPM-assembly already in flight production. Depending on the TWT type chosen (radiation or conduction cooled) an overall mass between 4500 and 5300 g with an overall efficiency above 60% is achievable. The MPM allows either independent operation of two channels or operation in combined mode for higher output power.
The near future will see the implementation of MMICs in the CAMPs to reduce size and mass again. At the same time the EPC will be optimized in size and mass to maintain the leading position of BOSCH.

SESSION 3
Power Conditioners

Chairman: P. Perol (ESA/ESTEC, NL)

DEGRADATION OF POWER SUPPLIES DUE TO TRANSIENTS

Richard A. Hyle Jr.
Rome Laboratory
525 Brooks Road
Rome NY, USA 13441-4505

ABSTRACT

Degradation of power supplies has been a major concern of system designers for years. Within military systems, the power supplies have been determined to be a significant failure contributor. The operating conditions that high voltage power supplies must survive need to be clearly defined. Shorted outputs, voltage transients, in-rush current, in-rush voltage, cycling times, temperature fluctuations, intense vibration and shock, and other environmental factors induce failures in the power supply. Power supplies are currently undergoing a dramatic change due to the insertion of new technologies (i.e. microelectronics, planar magnetics, solder-free interconnects, etc.), size, weight, parasitic constraints and power requirements. In order to produce reliable power supplies one needs to know what failure modes/mechanisms and what protection schemes impact their performance and availability. Once this determination has been made, system designers can design for reliability and incorporate appropriate protection schemes and other sound design practices (i.e. derating, thermal management, etc.).

This paper will identify the transients, along with their sources that impact power supplies and the protection schemes utilized to enhance their survivability. Basically, there are three transient suppression techniques: (1) redirect the transient, (2) shut down the power supply, and (3) attenuate the transient. A detail discussion of these techniques will be presented in this paper. During this discussion, design/decision guidelines will be provided with lessons learned, in addition to design "do's or don'ts" information which can improve system performance. The paper provides valuable information with which designers and planners can make educated choices in the development of power supplies to improve their reliability, availability and support costs.

1. INTRODUCTION

An electrical transient is defined as the condition which exists while a circuit is seeking equilibrium following the upset of a steady state condition, the result of stored energy being quickly released into a circuit. This could be brought about as a result of an unpredictable voltage and current level phenomenal (lightning) to predictable levels (switching of well defined inductive loads).

In a matter of several microseconds, this applied voltage/current can break down semiconductor devices. Damage is usually originated by a large reverse voltage across the PN junction causing avalanche conditions to occur at a small area of the junction due to high electrical field concentrations. A device may survive an avalanche condition as long as the current is restricted. If the current is excessive, the device is heated beyond its coefficient of resistivity and becomes negative, permitting greater currents to flow. This causes the device to experience a secondary failure mechanism characterized by current instabilities which lead to high concentrated currents. These high currents propagate failures due to the melting of the semiconductors and creating low resistance paths. This tends to cause arcing to other semiconductors or passive devices (thermal melting of lead wires and circuit traces, dielectric breakdown, etc.) leading to a catastrophic failure of the power supply.

2. TRANSIENT SOURCES

Transients can evolve internally or from an external source. The predominant internal source of transients is due to the switching actions of high rates of voltage or current displacement at the power supply inputs and from the release of energy stored in the circuit capacitance and inductance. Transients caused by the releasing of stored energy in inductors into power supply circuits occur when the current is switched off (design or fault), this is one of the prevailing failure modes.

Prior to energizing a power supply, the input and output filter capacitors are fully discharged. Once energized, very high currents (in-rush currents) will flow in an attempt to charge the input capacitors. Concurrently, the regulator will sense the output voltage and, since the output voltage is low, drive the pass transistor on, allowing the high currents to flow through the transistor to charge the output capacitor. Several fatalistic events can take place under these transient conditions. The rectifier

diodes may become overheated and the pass transistor will be subjected to intense currents at a time when the voltage drop across it is at a peak, creating extreme power dissipation and junction temperatures. These conditions can contribute to transistor failure or degradation. In addition, any inductor in series with this large current pulse will amass a tremendous amount of energy. When the transistor finally turns off, this energy will dissipate across the output capacitor and load in the form of a high overshoot voltage with considerably destructive effects.

External sources of transients include electro-static discharges (ESD), electro-magnetic pulses (EMP), power line transients and lightning. It is unlikely that one can protect power supplies to survive direct lighting strikes due to the concentration of current (~200k amps) demonstrated. Literature from the Institute of Electrical and Electronic Engineers (IEEE) has suggested that a circuit design approach to withstand peak voltages to 5kV and peak current to 50A (Ref. 1) will protect against 95% of the transients induced by coupling from lightning.

3. TRANSIENT SUPPRESSION TECHNIQUES

Three common techniques for suppressing transients are: (1.) redirect the transient, (2) shut down the power supply, and (3) attenuate the transient. Transients can be diverted with crowbars and clamps. Shut down procedures are commonly the results of a monitor/control device or a response of a fusing device. Resistors, filters and thermistors are used to attenuate transients.

Crowbars are equipped with devices that are "switched" from a very high impedance to a very low impedance at a given voltage threshold. Crowbars are occasionally referred to as active transient protection due to this switching action. When switched to the low impedance state, the voltage across the circuit to be protected drops to a very low level and the current flow is shunted to ground. Since the resulting voltage across the circuit is so low, the circuit becomes non-functional, a major disadvantage of crowbars. Another disadvantage of a crowbar is the current which flows after the device begins to conduct can be very high, commonly known as follow-on current. This current will not damage the crowbar device since the dissipated power is so low, but it can cause damage to other components through which the transient current is flowing. To stop the follow-on current, the voltage must be lowered below the holding current, thus resetting the crowbar.

Voltage clamps are supplied with devices which have nonlinear voltage-current. Benefit of a voltage clamp is that the operating voltage is sustained across the protected device, allowing normal circuit functions to continue. Clamps are connected in parallel with the protected device and are sometimes referred to as passive transient protection. A disadvantage of a clamp is that during the clamping period, the clamp will dissipate a considerable amount of power if current levels become excessive. Clamping efficiency depends on the source impedance of the transient since the clamp forms a voltage divider network with the source impedance. If the source impedance is very small, clamping techniques will not be effective.

To shut off a power supply one only needs to eliminate the base drive from the drive transistors or by a fusing mechanism for handling an over-current condition. Over-current protection is intended to protect the power supply from the effects of shorted outputs by shutting it down. Shorted outputs can be created by a conducting crowbar device, load failing short, transmission line shorting or through careless maintenance practices. Short circuits cause high current levels to flow which will not be detectable by an overvoltage sensor. Over-current conditions are sensed by currents sensing transformers or voltage divider networks. The output of these devices is fed to voltage comparators with a reference voltage as the other input. Excessive current provides an output signal that will trip the comparator. The comparator outputs a signal which can be used to shut down the supply. Fuses and circuit breakers can be used to shut a power supply down; a disadvantage of these devices is the slow response time and the human interaction.

Filters are used to attenuate transients. Since most transients are high frequency in nature, a low pass filter is generally effective. Disadvantages include self-induced resonance with other active components in the circuit and high in-rush currents during turn-on. Resistors, thermistors and inductors can be used to limit the in-rush current, but they reduce the efficiency of the power supply under normal operating conditions.

Table 1 and 2 present device attribute characteristics and transient device comparisons.

1	NO LEAKAGE CURRENT (STANDBY POWER CONSUMPTION)
2	HIGH SURGE ENERGY ABSORPTION CAPABILITIES
3	NO CHARACTERISTIC CHANGE/DRIFT WITH TIME
4	INSTANT RESPONSE
5	NO FOLLOW-ON CURRENT
6	INEXPENSIVE AND RELIABLE
7	A CLAMP RATIO EQUAL TO ONE

ATTRIBUTE CHARACTERISTICS FOR TRANSIENT SUPPRESSORS

TABLE 1

DEVICE	CLAMPING RATIO	RESPONSE TIME	LEAKAGE CURRENT	ALLOWABLE CURRENTS	VOLTAGE RANGES	SIZE
Zenor (TSD)	1-1.5	10^{-12} s	Med	50A (1ms) 600A (200ns)	5-400V	Small
Thyristor (SCR)	~0	10^{-9}-10^{-6} s	Low	2000A(1ms)	5-800V	Med
Metal Oxide Varistor	1.25-2	10^{-9}-10^{-6} s	Med	6500A(1ms)	5-1200V	Med
Spark Gap or Gas Tube	~0	10^{-6}-10^{-5} s	Very Low	10000A(1ms)	90-20kV	Large
Surgector	~0	10^{-12}-10^{-9} s	Low	200A (20μs)	30-270V	Med
Thermistor	NA	10^{0} s	NA	-	-	Small
Fuse-Circuit Brkr	0	10^{-3}-10^{0} s	NA	-	-	Med
Ideal	1	10^{-12} s	Very Low	Very High	Low-High	Small

TRANSIENT DEVICE ANALOGY

TABLE 2

4. PROTECTION SCHEMES

In order for power supplies to survive transient effects one must design protection schemes into them. These schemes will enhance the life expectancy of the power supply and improve their availability. Designers place protection devices between all potential sources of transients and the devices to be protected. Placing these protection devices as close to the transients as possible, helps avoid transients induced by parasitic impedance's of the transmission lines. Some kinds of protection schemes and design guidelines are (1) current limiting on all outputs, (2) High temperature shutdown, (3) low line voltage shutdown, (4) output overvoltage crowbar, (5) reverse voltage protection, (6) line surge limiting and regulator soft start, (7) fusing on AC line and individual regulators and (8) remote

sensing with open sense circuit protection.

Table 3 and 4 presents sample design considerations for severe and benign environmental applications with corresponding solutions.

Design Considerations	Solutions/Recommendations
Transient Effects	
• In-rush current	Apply resistor-triac technique, thermistor technique
• High-voltage spikes	Apply metal oxide varistor (MOV) transient voltage suppressor
• Short circuits	Apply constant current and current feedback protection
• Switching voltage transients	Apply snubber circuits
Effects of AC Ripple Current	Consider use of electrolytic tantalum capacitors
Corrosion Due to Leakage	Avoid wet slug tantalum capacitors and use plating and protective finishes
Aluminum Electrolytic Capacitors	Epoxy end-seals minimize external contamination
Temperature Stability	Use low temperature coefficient capacitors (mica or ceramic)
Packaging Techniques	Enhance heat transfer, control electromagnetic interference, decrease parasitic capacitance
Saturation	Use antisaturation diodes (Baker Clamps) in conjunction with a switching transistor
Potentiometers	Replace with precision fixed resistor
Short Mounting Leads	Derate the operating voltage below 50% to prevent hot spots
Static Discharge Damage	Use antistatic grounds for manufacturing and maintenance
Field Effect Transistor (FET) versus Bipolar Device	FET's increase switching speeds but reduce drive capability
Junction Temperatures	Do not exceed 125°C
Mechanical Stresses	Use of vibration isolators/shock mountings, parts spaced to prevent contact during shock & vibration
Solder Joint Process	95% (goal) of solder joints should be made via automated process
Cooling	Conductive cooling to a heat exchanger is preferred

DESIGN CHECKLIST (SEVERE ENVIRONMENTS)

TABLE 3

Design Considerations	Solutions/Recommendations
Part Quality	Vendor selects best commercial practice parts Vendor selects screened industrial grade parts
Unit Quality	Vendor burns-in all units at higher temperatures
Part Derating	Vendor has in-house standards
Electrical Parameters	Vendor values exceed needs at temperature extremes
Failure Analysis	Vendor has failure tracking program
Protection Circuits	Vendor has built-in voltage and current sensors
Fault Flags	Vendor has built-in failure indicators
Reliability Experience	Successful operation in similar environments

DESIGN CHECKLIST (BENIGN ENVIRONMENTS)

TABLE 4

5. CONCLUSION

Power supplies have always been identified as a predominant failure cause in systems. There is a strong need to collect data on failures of these supplies so that designers can better understand the failure modes/mechanisms so that they can correct the problems in new design approaches. To facilitate collection of data, metering (diagnostics, TSMD, BIT, ATE, etc) provisions must be included in the design. Metering of all the output voltages and currents, power output in watts and model and serial number is just not enough. What part failed, why it failed and what environmental (temperature, shock, humidity, etc) stresses caused it to fail all need to be available. This type of data is needed so vendor's can make sound engineering decisions in their part selection/control. This information is needed to design reliable power supplies to withstand those stresses experienced in most applications. With the continued advances in electronics technology and synergistic exploitation of advances in material science, power supply reliability figures-of-merit can be significantly improved when enhanced design rules and data collection procedures are implemented. New technologies such as ASICs, PEMs, Planar Magnetics, Silicon Carbide, Co-fired Ceramics, modularity, etc. must be addressed in assuring performance and reliability.

6. REFERENCES

1. Richard D. Winters, "Power Supply Voltage Transient Analysis and Protection," General Semiconductor Industries, Inc., Powercon III Proceedings; 1976.

2. David A. Followell, "Power Supply Fault Tolerant Reliability Study," McDonnell Aircraft Company, RL-T-91-39; 1991.

3. David Nicholls & Seymour Morris " Reliability Toolkit: Commercial Practices Edition," Reliability Analysis Center/Rome Laboratory, 1995

BREADBOARDING OF A NOVEL EPC FOR TWT BASED ON DIODE-CAPACITOR VOLTAGE MULTIPLIERS.

Jesús Maicas i Martí, Dan Olsson.
Power Conditioning Section, ESA, ESTEC.
Noordwijk, The Netherlands.

Abstract.

EPCs for TWTs are currently made with multiple winding high voltage transformers. This technique is efficient, but also heavy, complex and expensive.

In an attempt to improve mass and cost we have studied the feasibility of a new HV generation structure combining the classical diode-capacitors multipliers and the new techniques of high frequency soft switching. In this study we have built a Cockroft-Walton and a bridge multiplier. The development is done for powers in the 250 W DC range, corresponding to 170 W RF, but with the option of use it for smaller power with a smaller transformer. The main advantage we have seen, is a significant reduction in complexity, cost and weight, mainly due to the smaller size of the HV transformer. Current multi-layer transformers weight about 250 g, the size of the required transformer for the new HV converter is only 60 g. Meanwhile, the rest of the components, number and size of capacitors and diodes, are more or less comparable.

The bridge multiplier has reached efficiencies about 96%, with output impedance and output voltage ripple comparable to the *conventional* multi-layer transformer EPCs.

Introduction.

Current EPCs for TWTs based on multi-layer transformers give a typical figures of 1.4 kg and 94% efficiency for 80 W RF power.

We are going to explore the features and present the results of the breadboarding three different HV generation configurations based on diode-capacitor voltage multipliers. All three were provided with an input filter and a buck-type pre-regulator that acts as current limiter and stabilises the input voltage to 43 V. The same current drive push-pull zero current zero voltage is also shared by all configurations. It is feeded by an inductor and a tuning capacitor, each leg switch is composed by three mosfets IRFP 250 in parallel. The high voltage transformer has been designed 'ad hoc' for each type of multiplier. Three main configurations of multipliers have been tested, Cockroft-Walton, bridge and double-tripler.

A dynamic high voltage load, Eurofeedback CDY 500, has been used to simulate the TWT. It has four collector plus helix terminals.

The initial specifications for the output were:

- $V_{Helix} \approx 6.4$ kV.
- Four collectors.
- Voltage step between collectors ≈ 600 V.
- Input power of ≈250 W.

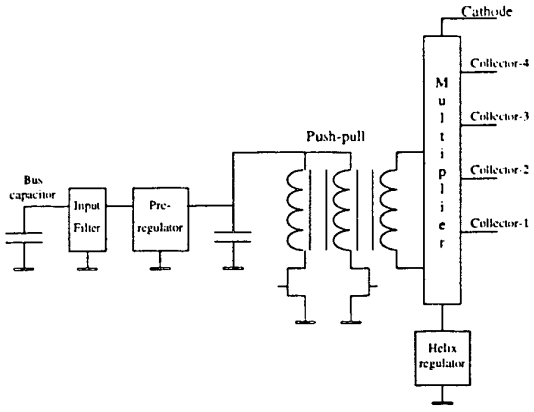

Figure 1. Block diagram of the converter.

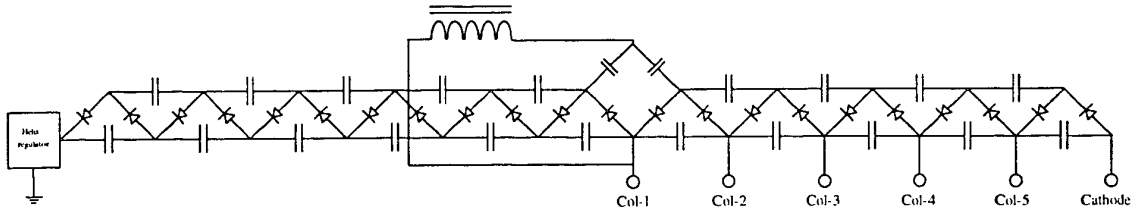

Figure 2. Cockroft-Walton multiplier.

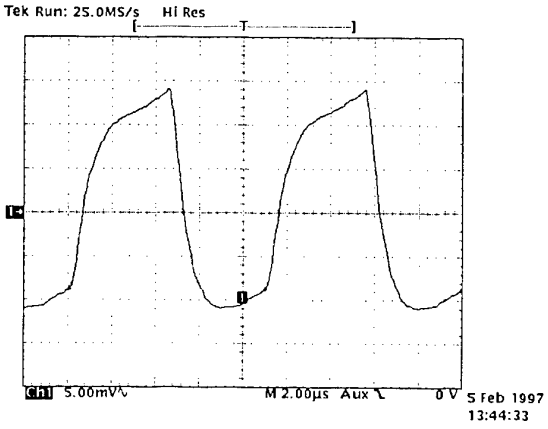

Figure 4. Ripple on Cathode (x1000).*

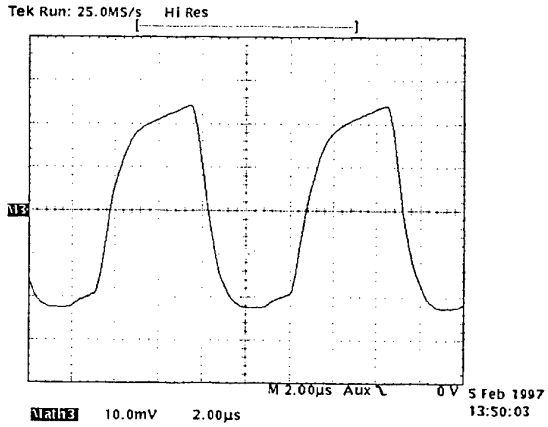

Figure 3. Ripple Cathode-Collector 1 (x1000).

Cockroft-Walton Multiplier.

A single stage of a diode-capacitor Cockroft-Walton multiplier rectifies an AC voltage, V, in such a way that the rectified output voltage doubles the peak value of the AC input voltage, $V_o = 2\ V_p$. If we add successive stages we get output voltages multiples of the initial stage, $V'_o = 2\ n\ V_p$. By spec we have fixed the output voltage of each stage of our multiplier to 600 V. Then that means a number of stages of 11. That will give room enough to the helix linear regulator. Then the output voltage of the transformer must be 300 V.

In fact in order to build a more efficient structure the multiplier has been built in two separated multipliers added side by side, one for the power part, from the collector 1 up to cathode and the other from collector 1 to helix (see Figure 2). The capacitors for the low power part are ceramic capacitors 10 nF 2000VCC TCK281S. And the ones for the power part are 100 nF 2000VCC TCK285S also ceramic type. All diodes are SDR3N.

Core	Prim.	Sec.	$L_{leakage}$
ETD-29	9T	62T	1.2 µH
ETD-34	9T	62T	1.8 µH

Table 1. Transformers used with Cockroft-Walton multiplier.

With such a configuration, it can be noted that the tuning of the push-pull stage is mainly done in secondary, the secondary equivalent capacity reflected in primary seen by the push-pull is smaller than the centre tap capacitor at the primary. That made it more difficult to change the tuning capacitance in order to reduce the working frequency looking for better efficiencies, as it was indicated by test results. Table 2 shows the best efficiency figures got with the basic Cockroft-Walton structure. Figure 4 & Figure 3 show the voltage ripple in cathode and collector 1 for the same configuration.

η**	Tuning freq.	I_{peak}	C_T	Core	L_{mag}	Mass***
92.51%	140 kHz	12 A	3.88 µF	ETD-29	30 µH	532 g
91.90%	141 kHz	9 A	.66 µF	ETD-34	39 µH	544 g

Table 2. Efficiency of Cockroft-Walton Multiplier.

Influence of the stages capacitance in the tuning.

Given the fact that the tuning is driven by the secondary capacitance, this one has been increased and efficiency measurements has been done in that process. It could be observed that efficiency increases with more capacitance and lower frequency. Table 3 has been obtained with the ETD 34 core, a similar one has been obtained for the ETD 29.

η**	Tuning freq.	I_{peak}	C_T	L_{mag}	Mass***	Stages Capacitance (nF)
94.28%	92 kHz	13 A	3.88 µF	64 µH	668 g	300-300-200-200-200
94.23%	100 kHz	13 A	3.88 µF	64 µH	636 g	200-200-200-200-200
94.02%	105 kHz		2 µF	39 µH	628 g	200-200-200-200-200
93.93%	107 kHz	11 A	2 µF	39 µH	612 g	200-200-200-200-100
93.80%	109 kHz		2 µF	39 µH	596 g	200-200-200-100-100
92.91%	115 kHz	12 A	2 µF	39 µH	580 g	200-200-100-100-100
92.60%	120 kHz		3.88 µF	39 µH	572 g	200-100-100-100-100

Table 3. Influence of the stages capacitance in tuning.

* Helix regulator shorted out.

** This is the efficiency at 250 W output power for the multiplier including push-pull and control compsumtion, it does not include the pre-regulator or the linear helix regulator.

*** This is the mass of all the components, it includes input filter, pre-regulator inductor and switch, centre tap capacitor, transformer, output and coupling capacitors, push-pull transistors, diodes, etc.

Configuration:	
Power multiplier:	Cockroft-Walton, 100 nF.
Helix Multiplier:	Cockroft-Walton, 10 nF.
Transformer:	ETD-29, L_{mag}≈30 µH, $L_{leakage}$≈1200 nH.
Centre tap capacitor:	3.88 µF.
Tuning:	Frequency: 140 kHz, I_{peak}=12 A,

Item	V (V)	I (mA)	P (W)
Cathode	6459		
Collector-5	5945	9.09	4.67
Collector-3	4876	14.90	23.59
Collector-2	4279	35.42	77.21
Collector-1	3622	45.08	127.89
Helix		1.00	6.48
	Total output power:		239.84

Overall efficiency: η= 92.51%

Ripple on Collector-1≈ 36.8 V_{pp}

Table 4. Efficiency measurement example.

Bridge multiplier.

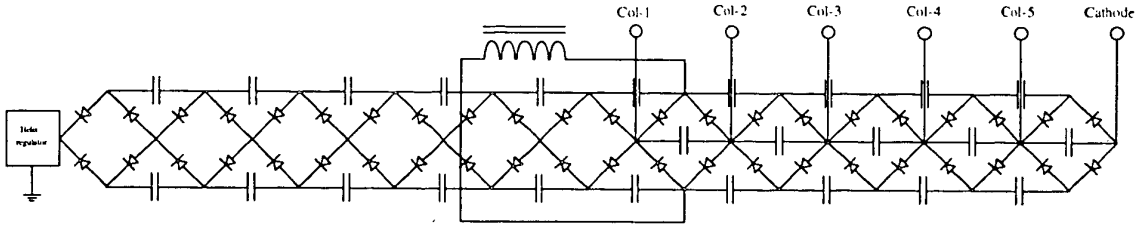

Figure 5. Bridge multiplier.

The single cell of a bridge multiplier, in fact a rectifier bridge, rectifies the AC voltage providing in its output a voltage equal to the peak value of the AC voltage. Coupling a pile of cells by means of side capacitors, we obtain an output voltage product of the number of cells by the single cell voltage. Then to obtain 600 V output voltage in each cell, the secondary voltage of the transformer should be equally 600 V.

Core	Prim.	Sec.	$L_{leakage}$
RM-12	8T	112T	750 nH
ETD-29	9T	126T	1.55 µH
ETD-29	6T	83T	800 nH
ETD-34	9T	126T	1 µH
ETD-44	9T	126T	1.2 µH

Table 5. Transformers used with bridge multiplier.

Same as Cockroft-Walton we use 11 stages to built the whole multiplier, and we feed it in the 6th stage, the capacitors used for the low power part are ceramic capacitors 10 nF 2000VCC TCK281S. For the power part has been used 100 nF 2000VCC TCK285S also ceramic type and 47 nF PS13S 1600V metallized polypropylene, that has lower losses than ceramic type. Also, two types of diodes has been used, SDR3N and BYV26E.

η**	Tuning freq.	I_{peak}	C_T	L_{mag}	Mass***
95.81%	82 kHz	10 A	3.88 µF	37.5 µH	602 g
95.22%	89 kHz	13 A	1.6 µF	37.5 µH	602 g

Table 6. Efficiency measurements for the Bridge configuration.

For the best efficiency measurement the configuration was: ETD-34, L_{mag}≈38µH, all capacitors in the power part 100 nF ceramic and C_T=3.88 µF.

It has been noticed that the ETD cores are easier to wind than RM due to isolation problems. We also tested the 47 nF PS13S 1600V metallized polypropylene capacitors without any effect in the efficiency, but with an increase of the mass. The two types of diodes has been tried, but no meaningful efficiency difference has been seen.

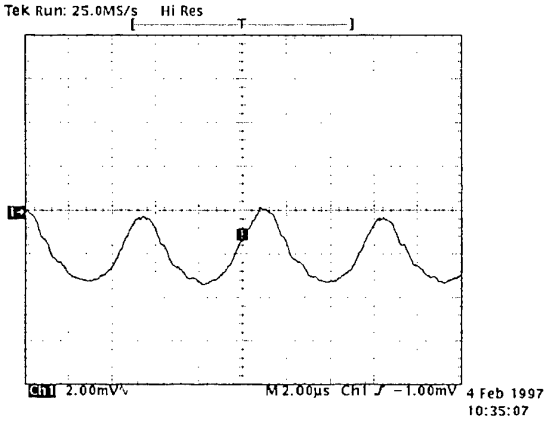

Figure 6. Ripple on Cathode (x1000).*

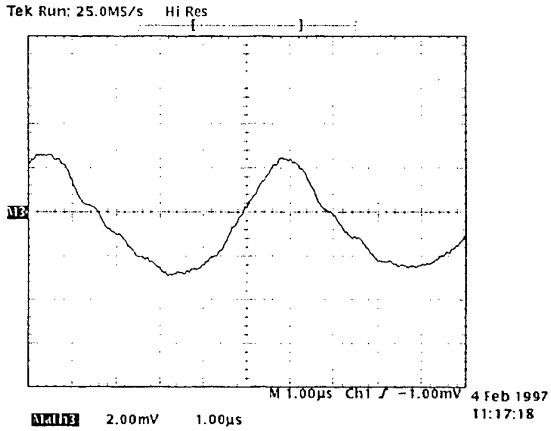

Figure 7. Ripple Cathode-Collector-1 (x1000).

The ripple for this configuration is much smaller than for the Cockroft-Walton (see Figure 6 & Figure 7) and the TDMA simulation indicates an output impedance for the collector-1 to cathode output of about

$$Z_o \approx \frac{\Delta V}{\Delta I} = \frac{40V}{60mA} \approx 666\Omega$$

Bridge multiplier for Power and Cockroft-Walton for Helix.

With the idea of reducing the number of diodes, and the associated cost, it has been tried a combination of bridge multiplier for the power part and Cockroft-Walton multiplier for the helix.

The efficiency is about the efficiency of the pure bridge multiplier, but the ripple increases and also TDMA simulation shows worse results.

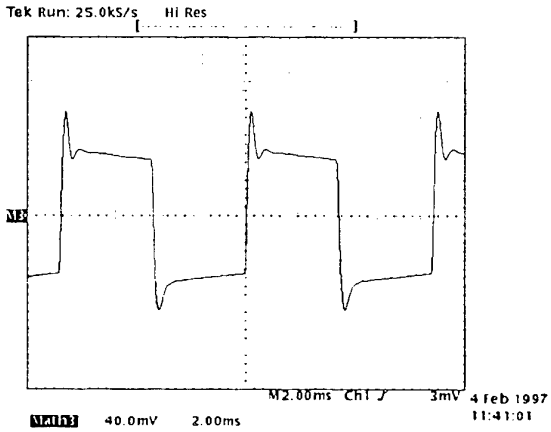

Figure 8. TDMA simulation without any pre-regulation (collector1 - cathode voltage x1000).

Double tripler multiplier.

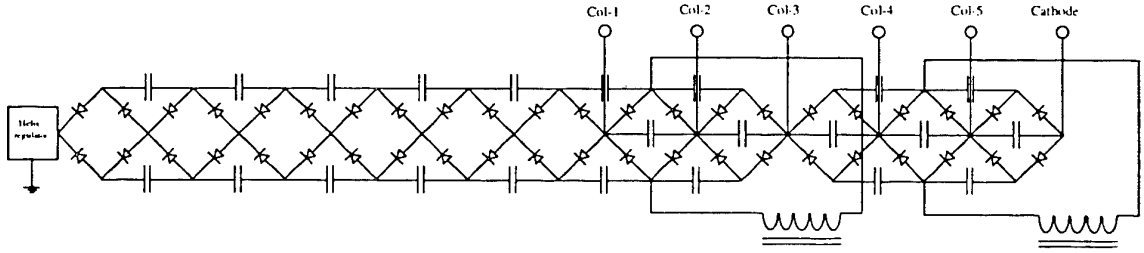

Figure 9. Double-Tripler Schematics.

This topology is something in between the conventional multi-layer transformer and the diode-capacitor multiplier. Two secondaries are needed to feed the two multipliers, but it is still possible to use a small transformer core. It is also possible to have different voltages between stages in the two triplers, having more degrees of freedom, and permitting to adjust the values of collector-1 and collector-2 to the desired values.

The components used are the same than for the previous configurations: ceramic capacitors 10 nF 2000VCC TCK281S for the helix multiplier and 100 nF 2000VCC TCK285S for the power part, the diodes were SDR3N.

Core	Prim.	Secondary windings	$L_{leakage}$
ETD-44	9T	126/126T, multi-layer.	800 nH
ETD-44	9T	126/126T, side by side.	1 µH

Table 7. Transformers built for the double tripler multiplier.

Two types of secondary windings configurations has been used in the transformer: multi-layer and side by side. Both structures presented some difficulties in the tuning, because this is slightly different for each secondary due to different secondary capacitance and load. In the multi-layer configuration it could be observed a certain shifting in the secondary currents, due to the different coupling of both secondaries. In the present stage of the study, work is still on-going on this configuration.

Conclusions.

A brief summary of the pros and cons of each configuration can give us a clearer picture of this study:

- Cockroft-Walton : It is the lighter and the cheaper because of the less number of components, but it is not the most efficient and has quite a lot of ripple.
- Bridge : It is a very simple structure with a very simple transformer that provides very little ripple and good TDMA results. A mass comparison between the high voltage side of a multi-layer conventional EPC and the proposed multiplier one give that numbers : 430 g. for transformer, rectifiers and output and tuning capacitors for the multi-layer structure and 240 g. for the same components of the multiplier configuration. That mass difference could be even greater if instead of using 2000 V capacitors, 1600 V ones are used or using a smaller capacitor value, 68 nF.
- Double tripler : This is a promising structure with more degrees of freedom than the pure multiplier, the first results show an efficiency about the same as the bridge one and also good results in output ripple. We believe that following the study on this structure we will get even better results than the bridge.

We have presented the present state of our study on the performances of high frequency diode-capacitor multipliers for EPCs, they are lighter, simpler and cheaper, and almost as efficient as the conventional multi-layer HV transformers.

The further developments planned are the study of an EPC for 100V bus without pre-regulator, to determine the power bus quality necessary to delete the pre-regulator function.

References:

1. Olsson, D. 1994, EPC Mass and Efficiency Improvement. Space TWTAs 1994 Workshop. ESA WPP-072
2. Ghislanzoni, L. & Weimberg, A.H. A new Zero Voltage and Zero Current Power Switching Technique. IEEE Transactions on Power Electronics. Vol. 7, No. 4. Oct. 1992, p.655-665
3. Martinelli, R.M. & Ahrens, A.F. 1978, Multiphase Capacitor-Diode Voltage Multiplier. PESC - 78

EPC and TWTA for telecommunication satellites

P. DELPORTE , P. FAYT , M. GAK , E. PEQUET

Alcatel ETCA s.a.
BP 4008
B-6000 Charleroi - Belgium

ABSTRACT

In the frame of an ESA contract, Alcatel ETCA has developed a new generation EPC for TWTA. The major design drivers of this development were low cost, low mass, small size, and high efficiency. The EPC is able to supply TWT's from different manufacturers in the power range 15 to 170 W_{RF} and its performances are particularly optimised for the power range 90 to 140 W_{RF}. The design and characteristics of the EPC will be described in this paper.

Two demonstration models were manufactured and tested. The performances measured on these models will be presented. In particular the **mass below 1.3 kg** for a **fully potted** version able to operate at critical pressure and the **efficiency exceeding 93%** for the 50V regulated bus version make the EPC very competitive for the commercial telecommunication satellites market.

Five EPC's will be manufactured for the formal ESTEC qualification. Three of them will be integrated with TWT's from different manufacturers. The qualification will be performed at EPC and at TWTA level. Besides of this a specific qualification is in progress to validate the new high voltage technologies used on the EPC, and is performed on five pieces of each high voltage module. The different qualification sequences will be explained.

1. INTRODUCTION

The development of high voltage EPC for TWT started in Alcatel Espace (Toulouse) during the eighties. The first application was for a 20W X-band TWTA used in the military telecommunication payload of Telecom II.

In order to rationalise its industrial product policy, Alcatel decided in 91 to concentrate the high voltage EPC activities into one single company: Alcatel ETCA. More than 20 flight models were manufactured for several programs (Telecom II, C-BERS and INSAT) for Ku-band and X-band TWT's up to 25 W_{RF}. Some are already in orbit, the other ones will be launched soon. This EPC was however limited in power (about 30 W_{RF}) and in voltage (up to 4.5 kV).

Today the satellites communication systems request higher power (up to 100-150 W_{RF}), as well as higher RF frequencies (Ku and Ka-bands). In order to respond to this new market, Alcatel ETCA has developed a new generation of EPC characterised by its high voltage and high power capability, up to respectively 6.7 kV and 170 W_{RF}.

2. FRAME OF DEVELOPMENT

The development of this EPC was performed in the frame of an ESTEC ASTP contract. It started with a study phase during which several electrical topologies were considered and a breadboard manufactured and tested (Ref. 1).

During the development phase the product was improved to reach the objectives of mass, cost and efficiency. Two demonstration models were manufactured and tested (see figure 1). In the meantime evaluations were performed to select the most appropriate high voltage technologies.

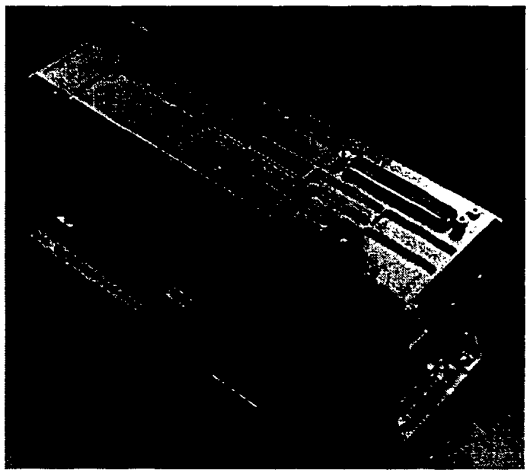

Figure 1: EPC demonstration model

The qualification **phase is now** in progress. It includes the qualification at EPC and TWTA level, as well as a **specific** qualification of the high voltages modules and is based on the ESA PSS requirements.

3. EPC DESCRIPTION

The selected topology is a buck type pre-regulator followed by a quasi resonant push-pull inverter. The block diagram is shown in figure 2 and indicates the separation between low voltage and high voltages modules. The different functional blocks are described in the following sections for the standard 50V regulated bus version. An adaptation of this version for the 26-42.5 V semi-regulated bus is also in development outside the frame of the ESTEC contract.

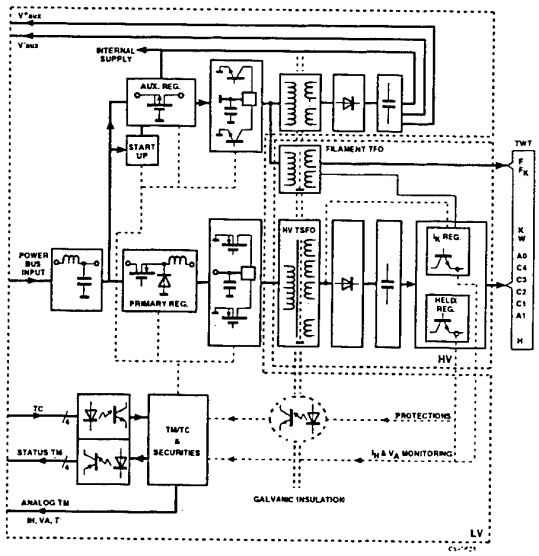

Figure 2: EPC block diagram

3.1. Input filter

The input filter is the interface between the power bus of the satellite and the EPC. It has the following tasks :

- Limit the current ripple generated by the EPC and injected to the power bus (switching spikes, TDMA...).
- Isolate the EPC from the bus noise and transients (susceptibility).
- Adapt the EPC to the power bus impedance.

3.2. Primary regulator

A Buck type primary regulator is used to isolate the high voltage convert from the bus variations (see figure 3). This topology has the also following advantages:

- Protection of the high voltage transformer at the primary side (decreasing of the electrical stress).
- High degree of collector 1 voltage adaptability for the same transformer.
- Optimisation of the high voltage transformer.
- Limitation of the bus current: at switch-on or in case of failure inside the EPC or TWT.

The primary regulation is based on the MC2 principle with two nested loops: a voltage loop, monitoring the primary regulator output voltage, controls a current loop that monitors the peak-current of the buck inductor.

The design is free of single point failure and includes the following protections:

- Output undervoltage detection.
- Input current limitation.

A 100 kHz switching frequency was selected. It allows to achieve simultaneously low mass and high efficiency.

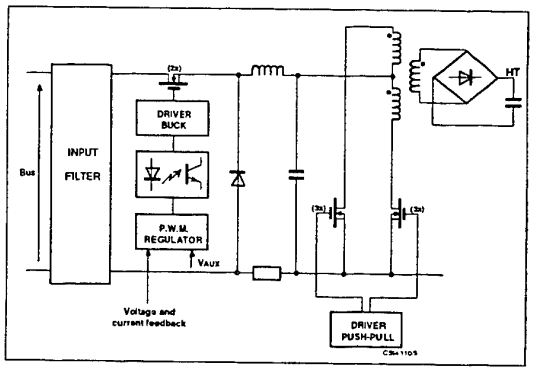

Figure 3: Primary regulator

3.3. Secondary power stage

The push-pull power stage drives the high voltage transformer in order to transfer the energy from the primary to the secondary stage. A full galvanic isolation is provided between the primary and the secondary sides.

In order to improve efficiency and reduce the output ripple, the switching mode is quasi resonant. The Zero voltage switching has been chosen in order to increase the efficiency. The Zero current switching increases the efficiency too and avoid the use of snubber.

The resonance frequency is 100 kHz and is adjusted with a tuning capacitor at the primary transformer centre tab (see figure 3). The choice of this frequency as well as the one of the buck pre-regulator is the result of a trade off between mass and efficiency. The same cost impact at satellite level was assumed for an increase of dissipated power of 1 W or for an increase of mass of 100 g.

3.4. EPC control and telemetry

All internal management is made by an ASIC circuit which use space qualified CMOS technology. The following tasks are realised by this circuit:

- Converters synchronisation.
- Telecommands processing.
- Sequencing the EPC switch on and switch off operations.
- Management of the protections.
- Management of the autorestart function.
- Clocks and timers generation (preheating, auto restart...).

Up to four telecommand lines and four status telemetries are available, all with optocoupler isolation. They can be configured according to specific platform requirements. Three analog telemetries can also be provided: helix current, anode 0 voltage and EPC temperature.

The following protections are implemented in the EPC standard design:

- High voltage protection : the EPC is completely protected face to any TWT output short circuit.

- Helix overcurrent protection. This protection can be disabled at connector level.
- Bus undervoltage protection.
- Input current : the MC2 regulator gives an inherent over current protection to 1.3 Imax during transient and 1.5 Imax in case of internal failure.
- Platform protection: no single failure may lead to short the power bus or stress the TM/TC platform circuits.
- Selectable autorestart mode.

3.5. Auxiliary supply

The auxiliary supply is switched off when the EPC is switched off allowing a very low power consumption in this mode. When the EPC is switched on, a start-up circuit provides the power to the control circuits during the rise time of the auxiliary supply.

The auxiliary supply includes one serial regulator followed by one single converter for the generation of the high voltage of the TWT filament and the low voltages for external equipment (such as channel amplifier or lineariser) and for EPC internal use. The TWT Anode 1 voltage, if any, is also generated from the auxiliary supply.

The main serial regulator is current protected and any internal failure of the auxiliary supply stops the EPC. A specific starting sequence is used in the auxiliary supply to limit the heater current when the filament is cold.

3.6. High voltage generation

This functionality is realised by the high voltage transformer, followed by the diodes rectifiers or the voltage doubler stages, then the high voltage capacitors and the helix and anode regulators (figure 4).

The high voltage generation has been designed in order to sustain the critical pressure. The key component on that matter is the transformer which has been qualified in 1989 and have only minor modification for this new generation EPC. The transformer has 8 secondary layers and can supply voltages up to 6.7 kV.

Between collector 1 and cathode six transformer layers with diodes bridges are used to give very low output impedance. Up to four collector outputs can be provided to the TWT, with flexibility of the connections to the transformer layers. Between collector 1 and helix, two transformer layers with multiplicator bridges are placed as the helix current flowing through them is very low.

Due to the resonant mode switching, the currents through the rectifiers are quasi sinusoidal. This produces very little recovery current allowing to use classical 1 kV diode. Furthermore the output noise has a small spectral bandwidth (no hard switching spikes) which reduces the TWT spurious output.

Series resistor are placed in collectors 4, 3, 2 and 1 and helix for arcing protection. The new generation EPC is able to sustain short TWT arcing up to ~1 msec without causing any Spurious Switch Off (SSO) or stress on the components. For longer arcs the EPC will enter in protection mode. If autorestart mode is selected, the EPC is restarted after few tens of milliseconds. If a second arc occurs within 3 minutes, the EPC is completely switched off.

3.7. Helix regulator

The stability of the helix to cathode voltage is a key factor to guarantee the RF performance of the TWT. The helix regulator is a feature of the EPC which provides this very high stability and also suppress the ripple generated by the high voltage converter and by the TDMA operation.

The helix regulator contains a serial regulator embedded with an ETCA patented "ripple suppression" circuit using active filters. The TDMA response is excellent (below 2 V_{pp} at 50 Hz) and the output ripple is below 60 mV_{pp}.

The reference section uses also a special design in order to achieve a good temperature stability together with a total insensitivity to load or auxiliary supply variation.

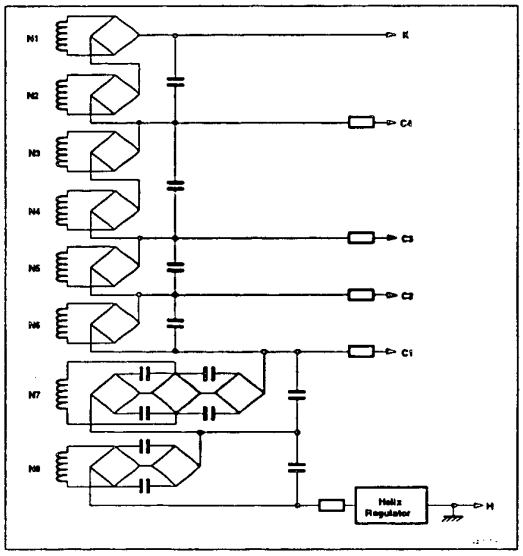

Figure 4: High voltage generation

3.8. Cathode current regulator

In order to compensate the degradation of the cathode characteristics over the life of the TWT, the EPC includes an anode Ø voltage regulator. This module contains a circuit monitoring the cathode current, a serial regulator at cathode voltage and a voltage translation circuit. Two circuits were designed, one for the low cathode to anode Ø voltages (e.g. TTE TWT's...), one for the high voltages (e.g. AERG TWT's...).

3.9. Technological design

The EPC is designed to operate at the critical pressure. The high voltage PCB's use an ETCA patented process to reduce the electrical field at the edges of the copper layers. They are fully potted with polyurethane resin. The casting of the high voltage transformers uses epoxy resins already used in the previous 20W design.

A simulation of the electric field of the critical high voltage components was performed using the ANSYS program. The field into the high voltage transformer was limited by design to 3.5 kV/mm. The implantation of components on PCB and the potting thickness takes into account the voltage differences between components and with the structure.

In manufacturing, the high voltage modules are tested against internal partial discharge on a test bench able to discriminate discharges as small as 0.1 pC.

Besides the high voltage technologies, the following ones are used in order to save mass ,size and cost:

- one gate array ASIC circuit developed by the Alcatel ETCA microelectronics division.
- one low cost power hybrid containing the pre-regulator and push-pull power transistor and their driver circuit. This hybrid is manufactured on the ESA qualified production facility of Alcatel ETCA.
- Surface mounting technology for active and passive components. They represent 90% of the low voltage component.
- Flex-rigid multilayer PCB.
- Radiation hardened components for ASIC, power transistors, linear integrated circuits.

3.10. Mechanical and thermal design

The overall EPC dimensions are 249.5 x 84 x 104.6 mm including fixation lugs (see figure 5).

The housing is made of an aluminium milled box in order to provide high rigidity and low weight. A central wall separates the low voltage and the high voltage sections: it provides EMC isolation, increases the box stiffness and gives a low thermal resistance path for the power hybrid and the high voltage transformer.

It includes a separate cavity for TWT cable interconnection. The TWT cable output angle is adaptable to 0°, 45° or 90° according to payload requirements.

The EPC is designed for an operational temperature range of -20 to +70 °C. This was verified by tests performed in thermal vacuum conditions on the demonstration model. Several thermocouples were placed inside the equipment. The measured temperatures have validated the results of the thermal analysis. The EPC was also successfully tested with a random vibration level of 25g.

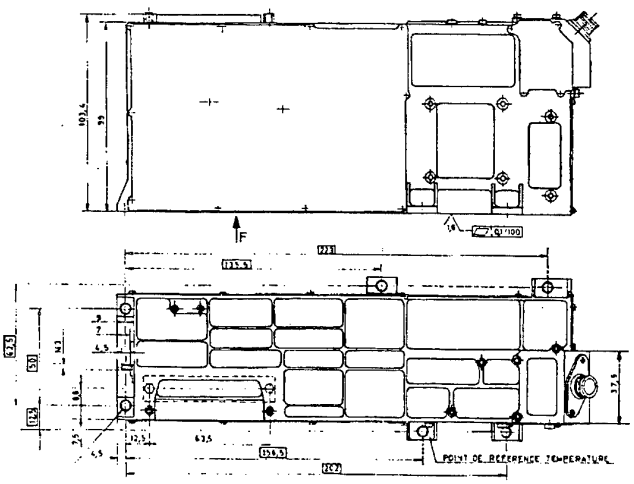

Figure 5: EPC dimensions

4. PERFORMANCES

The demonstrations models were tested on an Eurofeedback active load and then integrated with a TTE 115 W radiating collector TWT. The following table resumes the main measured performances. The mass is given for a completely potted model.

parameters	value	units
mass	1.275	kg
efficiency	93.2	%
V_{KH} ripple	< 50	mV_{pp}
V_{KH} ripple in TDMA	< 2	V_{pp}
V_{KH} temperature stability	< 2	V_{pp}
Bus current ripple (@ 100 kHz)	28	mA_{pp}

The figure 6 shows the spurious modulation measured on the TWT output.

One demonstration model is now in life test at 70 °C and has shown so far no degradation of performance.

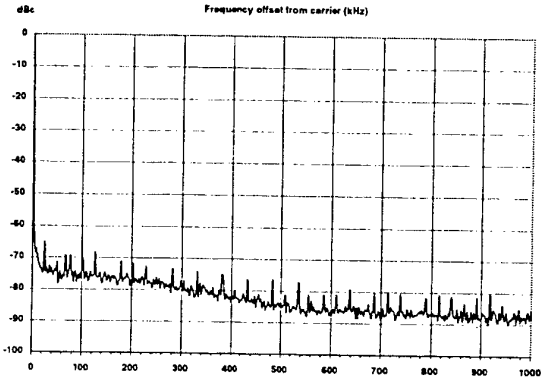

Figure 6: TWT spurious ripple

5. QUALIFICATION

The qualification of the EPC is performed in a two step process: first a technological qualification of the high voltages modules, then a qualification of the EPC product. They are based on the ESA PSS requirements.

5.1. Technological qualification

The aim of this technological qualification is to qualify the technologies and manufacturing processes used for the high voltage modules. The modules can be tested individually at a detail level not possible when integrated into an EPC.

The qualification sequence follows the **ESA PSS-02-303** (Ref. 2) with few adaptations of the testing method agreed with ESTEC and with extension of the temperature range.

Five pieces of each high voltage modules are manufactured and individually tested. Two sets are combined to form an EPC and are tested at EPC level, the 3 remaining sets are tested individually , except during the thermal vacuum test where they are combined to form an EPC and then dismounted for individual testing.

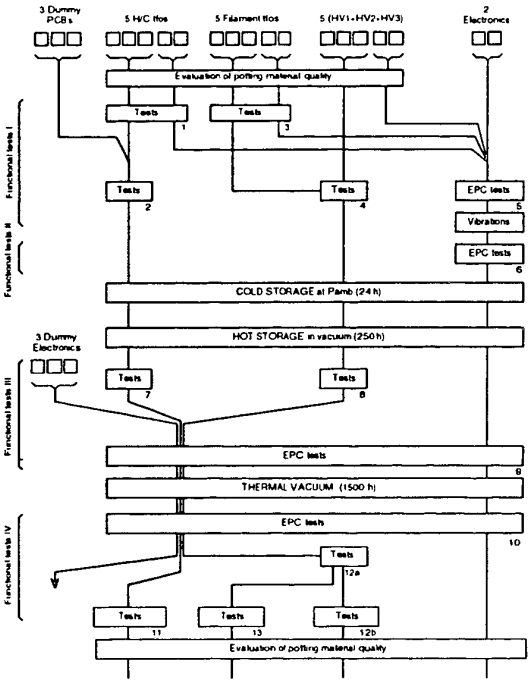

Figure 7: Technological qualification flow chart

The duration of the thermal vacuum test is 1500 h, with thermal cycling between -20 and +70°C and cold start at -30°C. The qualification flow chart is given in figure 7.

The technological qualification is in progress and is intended to be completed in the next months.

5.2. EPC qualification

The EPC qualification will be performed according to **ESA PSS-02-30** (Ref. 3), with also few amendments on tests methods and increase of temperature ranges (-20 to +70 °C) and vibration level (25 g_{rms}).

Five qualification model EPC's are in manufacturing and cover different configuration in term of power, TWT manufacturer and type.

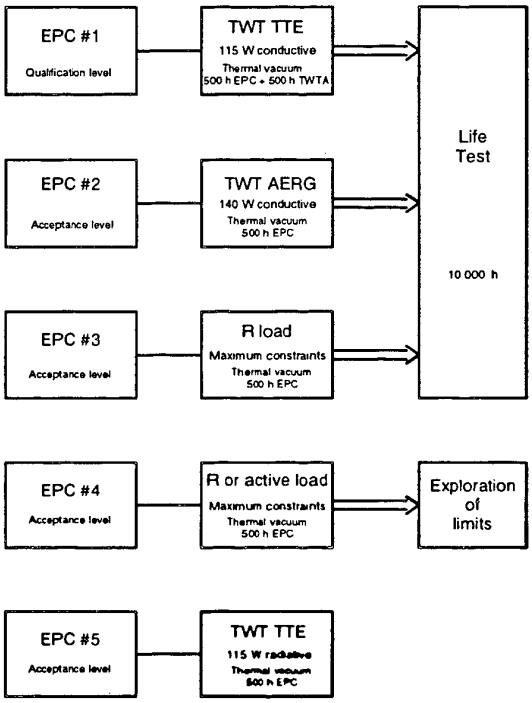

Figure 8: EPC/TWTA qualification flow chart

One EPC will be formally qualified. It will be integrated with a 115 W conductive collector TWT from TTE. The thermal vacuum test has a duration of 1000 h and will be split into two parts. During the first 500 h, only the EPC will be subject to thermal cycles in the vacuum chamber, the TWT used as a load remaining at ambient conditions. This allows to monitor the EPC/TWT interface and present a constant load to the EPC. Then the final connection with the tube will be realised to form a TWTA. This TWTA will follow the TWTA qualification sequence, including 500 h thermal cycling in vacuum.

Besides of this qualification model, the remaining four models will be screened at acceptance level according to ESA-PSS-02-30. This means they will be each subjected, among other tests, to critical pressure and to 500 h of vacuum thermal cycling.

One model will be integrated with a 140 W conductive collectors TWT from AERG. Two others will be designed for the maximum constraints (voltage, current) on the EPC. Since the constraints do not correspond to a an existing TWT, these EPC's will be tested on resistive or active loads. One of them will be used for an exploration of the

limits. The last TWT will be integrated with a 115 W radiating collectors TWT.

After their qualification or acceptance testing, three out of the five EPC's will be placed in life test during 10 000 h.

The activities on the 5 EPC's are summarised in figure 8. The EPC qualification is scheduled to be completed in the next months.

Alcatel ETCA has build a new workshop dedicated to EPC and TWTA. It is an integrated shop where most of the manufacturing and test activities are concentrated into one single location. The 5 qualification EPC's will be the pre-series models for this facility.

6. CONCLUSIONS

The new generation EPC developed by Alcatel ETCA is particularly well adapted to the commercial telecommunication satellite market and will be qualified in the next months.

Besides the technical characteristics, the cost and manufacturing aspects were always kept in mind during the development. The system cost at satellite level was the major driver for the design trade-off's.

The short delivery time requested by the satellite projects was also taken into account. The manufacturing flow charts were optimised and a new manufacturing shop dedicated to EPC's was set up. Automatic tests equipment's for EPC and TWTA are developed and a stock of components for flight models is already available.

With its new EPC, Alcatel ETCA will offer a very competitive product for commercial payloads. In the next months, the product range will also be progressively broadened, with versions for other bus voltages, for higher power TWT or MPM integrating the channel amplifier and lineariser.

REFERENCES

1. Desne, Fayt & Gak 1994, EPC new generation for telecommunication power TWT's, *Space TWTA 1994 Workshop proc.*

2. Requirements for High Voltage Transformers and Components used in EPC for ESA Space Systems, ESA PSS-02-303, draft issue 2, Aug.1992.

3. Requirements for the Procurement of TWTA for space applications, ESA PSS-02-30, draft issue 1, July 1992.

ACKNOWLEDGEMENTS

The authors wish to acknowledge ESTEC and in particular MM I. ARENS and P. PEROL for their support and invaluable contribution all along the development.

A special thank also for TTE and AERG for their help and advises as well as for supplying us the TWT's essential for our studies and tests.

SESSION 4
TWTAs Applications

Chairman: J.M. Schouten
(Directorate of Materials-Royal Netherlands Navy, NL)

30GHz 150W High Gain Helix Traveling Wave Tube

Satoshi TONEGAWA, Tetsuo MACHIDA,
Jyunichi MATSUOKA, Hajime FUKUI

Microwave Tube Division, NEC Corporation
1753,Shimonumabe,Nakahara-ku,Kawasaki,
Kanagawa,211 JAPAN
Tel. +81-44-435-1697 Fax +81-44-435-1923

ABSTRACT

To construct the Global Information Infrastructure (GII), Ka-band frequency range is utilized widely and Ka-band high power amplifier is required. For this purpose, NEC developed 150W high power Traveling Wave Tube (TWT) which operates Ka-band frequency range. This TWT is designed based on the NEC's reliable Computer Aided Design (CAD) system which can analyze electron gun, RF circuit, collector, beam focusing and impedance matching. Newly developed TWT achieved output power over 150W for the frequency range of 27.5GHz to 30GHz. The small signal gain of this TWT is more than 60dB and operating gain at 150W output power is 56dB. The intermodulation of this TWT is -28.8dBc at 20W total power and high linearity was demonstrated. The high linearity of this TWT enables the multi-signal communications such as 50 carriers frequency division multiplex (FDM) system at Ka-band frequency range. The proper surface finish of each electrode and suitable cleaning process were applied to the manufacturing of electron gun, RF circuit, collector and other TWT components. These technology achieved the electron gun of micro-discharge free and reliable operation of digital signal transmission. The cathode loading is about 2.7A/cm^2 and the expected life time of this TWT is more than 30,000 hours. The newly developed TWT is suitable for the Ka-band communication such as Local Multipoint Distribution Service (LMDS), Local Multipoint Communication Service (LMCS) and other advanced global satellite communication systems.

1. INTRODUCTION

In Japan, the Ministry of Posts and Telecommunications decided to utilize Ka-band frequency range as a domestic satellite communications in 1968. NEC has been developing various kinds of Ka-band high power microwave tubes since the beginning of 1970 (Ref.1). Recently, GII for 21 century started to be reconstructed and the utilization of Ka-band frequency range is spreading widely. In Japan, advanced satellite communication system such as N-star, Super-Bird and other satellite communication systems have been proposed and started to operate. In U.S.A, large scale Local Area Network (LAN) system such as LMDS and LMCS has already started to operate. These advanced communication systems require higher performance microwave tubes which operate Ka-band frequency range.

The use of Ka-band frequency range enables to achieve high speed and high capacity communications because of high frequency transmission. On the other hand, Ka-band frequency belongs to mm-wave range, so it is easily affected by the weather conditions such as rain and snow fall.

So, the TWT used for the power amplifier of LMDS, LMCS and other advanced satellite communication systems is required to achieve high power, high efficiency, high linearity for multi-signal operations, stability for the various environments and long life.

Followed by the above situations, the authors developed a 150W high power TWT which operates at the Ka-band frequency range as a key component of Ka-band High Power Amplifier (HPA). The newly developed TWT demonstrates the best performance in the world (Ref.2,3,4,5), featuring high power of 150W, high efficiency of 40.6%, high gain of 60.3dB, wide output frequency range from 27.5GHz to 30GHz and improved intermodulation of -28.8dBc at 20W operation.

2. TWT DESIGN

This TWT is designed based on the NEC's reliable CAD system. To achieve the output power over 150W, the suppression of backward

wave oscillation (BWO) and stable beam transmission are the most important design items. The design of helix pitch profile and electron gun was optimized by CAD. The optimized carbon coating attenuater enabled the high gain operation over 60dB at Ka-band frequency range. A two stage depress collector is employed to achieve the total efficiency of 40.6%. This efficiency is the best data of Ka-band grand terminal TWTs in the world (Ref. 2,3,5). The CAD considering the operating gain and phase compression achieved the high linearity of intermodulation such as -28.8dBc at total 20W operation. The detail of TWT design and features are described below.

2.1 Electron Gun

The electron gun is a pierce-type gun, employing a M-type cathode in order to operate at a comparatively low temperature to achieve the stable TWT operation and long life. The cathode loading is about 2.7 A/cm^2 and the cathode temperature is chosen to be 980 °C brightness. The expected life time of this TWT is more than 30,000 hours.
During the beam turn on procedure, to avoid high helix current is key technology for the stable operation of TWT. So anode modulation type is selected in stead of beam focusing electrode modulation type. Anode modulation type enabled the peak helix current of less than 3mA during the high voltage turn on procedure. At the same time, proper surface finish of each gun electrodes and suitable cleaning process were applied for the manufacturing of electron gun. These technologies achieved the electron gun of micro-discharge free and reliable operation for the digital signal transmission.

2.2 Slow-Wave Circuit

The structure of slow-wave circuit is helix type, which enables the TWT compact size and light weight. This slow-wave circuit consists of three sections to achieve high gain more than 60dB and suppress the backward wave oscillation. The helix is made of molybdenum and output section of the helix is plated with gold to reduce the RF transmission loss.
The helix support rod is made of Boron Nitride (APBN) because of high conductivity compared with other ceramics such as aluminum oxide (Al_2O_3) and beryllium oxide (BeO). Carbon film was coated on the surface of helix support rod to control the TWT gain and stabilize the TWT performances.
The velocity taper of helix was designed to optimize TWT performances by CAD. The optimization was carried out considering the interaction efficiency, TWT gain, linearity, the suppression of BWO, spent beam energy distribution and cooling of slow wave circuit. The input and output terminals are both UG-599/U standard waveguide. The impedance matching between helix circuit and waveguide section was also optimized by the three dimensional simulation code.

2.3 Beam Focusing Section

Focusing magnets made of samarium cobalt with low temperature coefficient are adopted to focus the electron beam. The optimization of electron beam trajectories was carried out considering the beam diameter, beam scalloping and thermal velocity distribution of electron beam. The average beam diameter is less than 0.5 mm and designed beam scalloping is 9.3%.
In case of Ka-band TWT, electron beam is easily affected by the inner gas of TWT. So, getter is installed to keep the inner vacuum pressure and achieve the stable beam transmission during the field operation for over 30,000 hours.

2.4 Collector

A two stage depressed collector is employed in order to minimize beam energy recovery loss. The shape and the location of each collector electrodes were optimized by CAD considering the beam trajectory with secondary electron emission from the collector electrodes. Finally, the consideration of secondary electron emission enabled the total efficiency over 40%. The high voltage of collector electrodes was held outside the vacuum to simplify the tube assembly process to TWT housing. The heat produced by electron beam at each collector electrodes is conducted to the base plate of TWT.

3. CHARACTERISTICS OF TWT

The newly developed TWT is shown in Photo. 1. The TWT has demonstrated excellent performance as shown in Table. 1. The output power is more than 150W over the frequency range of 27.5GHz to 30GHz. Total

efficiency of 40.6%, small signal gain of 60.3dB and gain at rated power of 56.2dB are achieved. Fig.1 shows the output power, helix current and collector current-1,2 as a function of drive power. TWT gain is almost constant up to the 100W operation and output power reaches over 150W by the drive power of -4dBm at 28.5GHz. The maximum helix current is less than 1mA at saturated power. Extremely low helix current is the feature of this TWT. Such a low helix current enables the high reliability operation over 30,000 hours operating time. Frequency responses of small signal and large signal operation are shown in Fig.2. The variation of saturated power and small signal gain is 0.27 dB and 1.27dB respectively over the frequency range of 27.5GHZ to 30GHz.

Fig.3 shows the 3rd-order intermodulation as a function of total output power. The values are less than -13 dBc at 50dBm operation, -28dBc at 43 dBm operation, respectively over the frequency range of 27.5GHz to 30GHz. This value is the best data of Ka-band helix traveling wave tube in the world. The high linearity of this TWT enables the multi-signal operation and it is suitable for LMDS, LMCS and other advanced satellite communications.

Table 1 Typical Performance of TWT

Heater voltage	6.3	V
Heater current	1.07	A
Anode voltage	10.0	KV
Anode current	0.001	mAdc
Helix voltage	12.5	KV
Helix current	0.29	mAdc
Collector-1 voltage	4.8	KVdc
Collector-1 current	45	mAdc
Collector-2 voltage	2.4	KVdc
Collector-2 current	75	mAdc
Cathode current	120	mAdc
Frequency	29	GHz
Saturated output power	165	W
Large signal gain	56.2	dB
Small signal gain	60.3	dB
Overall Efficiency	40.6	%
Power Consumption	406	W
IM3 at 20W output	-28.8	dBc
Cooling	Conduction	

4. QUALIFICATIONS

To evaluate the performance and reliability of this TWT, various kind of evaluation test such as operation life test, temperature test, altitude test and shock & vibration test were carried out. During the operation life test, stable output power and TWT performance were observed. The expected operation life of newly developed TWT is more than 30,000 hours.

At the temperature test , TWT operated stably under the condition of -30°C to +75 °C. As the non operation condition, TWT was left under the condition of -55°C to +100 °C, and no damage was observed.

At the altitude test, TWT operated stably at the altitude of 12,000 ft. As the non operation condition, TWT was left at the altitude of 50,000 ft. , and no damage was observed.

5. CONCLUSION

The design, performance and evaluation test result of Ka-band 150W helix TWT was presented. To achieve the new GII for 21 century, Ka-band frequency range is utilized widely. TWT presented this time is suitable for this purpose. The newly developed TWT can achieve the small size high power transmitters which operate Ka-band frequency range. This TWT is expected to be utilized widely for the expanding Ka-band communication fields such as LMDS, LMCS and other advanced satellite communications.

ACKNOWLEDGEMENTS

The authors would like to thank all persons concerned with this work especially for the members of NEC microwave tube division.

REFERENCES

1. T.Kageyama, S.Hamada, H.Hashimoto, and K.Tsutaki, Review of NEC's Ka-band microwave tubes for space and ground applications, Second Ka Band Utilization Conference, Florence, Italy, September 24-26, 1996

2. Varian Canada Microwave Products, Microwave Tube Catalog (1996), Ontario, Canada.

3. Thomson-CSF Tubes Electroniques, Microwave Tube Catalog (1996), Cedex, France.

4. NEC Microwave Tube Division, Microwave Tubes Selection Guide 6th Edition (1996)

5. T.Machida, S.Tonegawa, W.Suzuki 1996, The 30GHz 150W Helix Traveling wave Tube, Technical Report of the Institute of Electronics, Information and Communication Engineers (Japanese) ED96-129

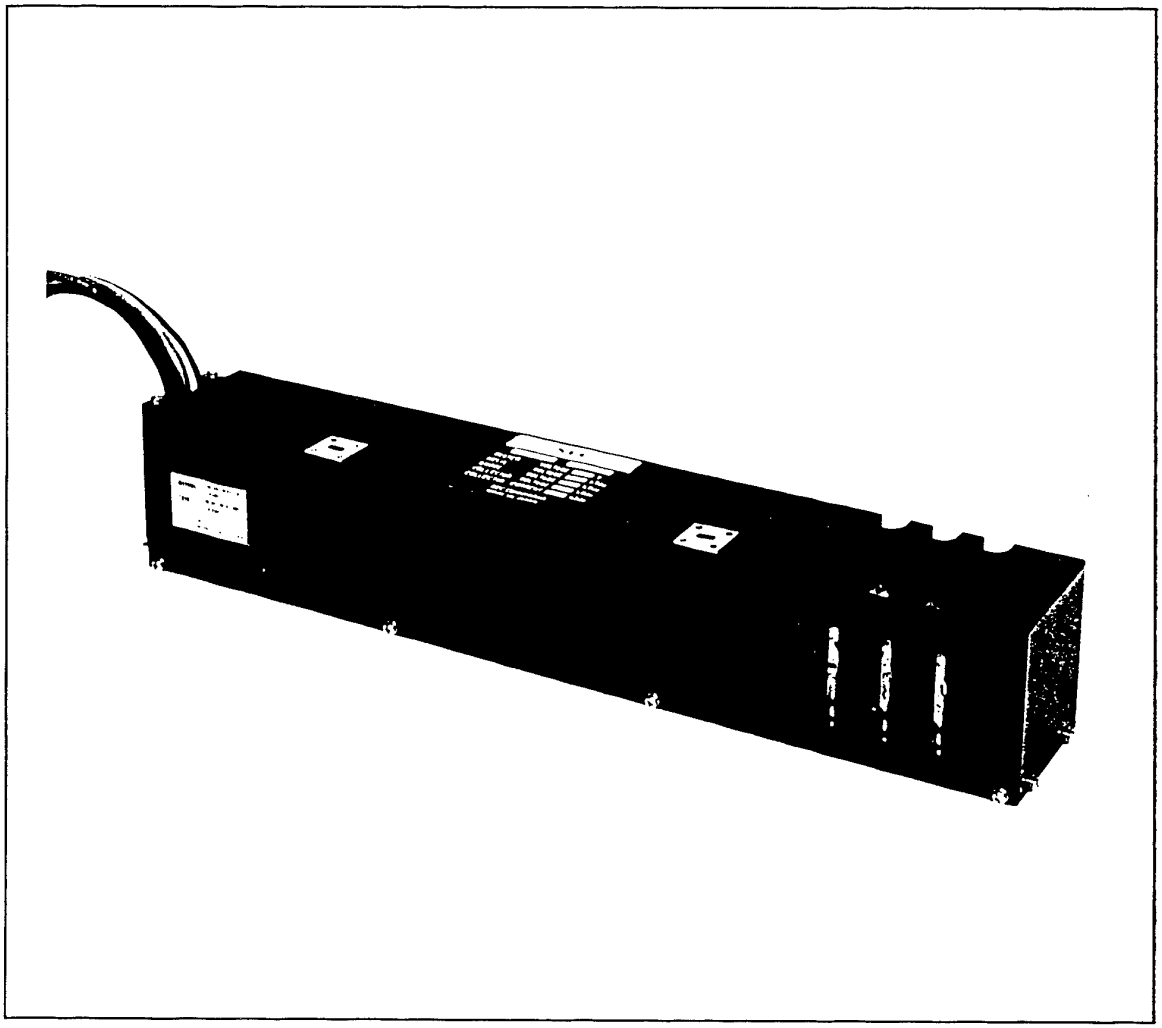

Photo 1 30GHz 150W high gain helix traveling wave tube

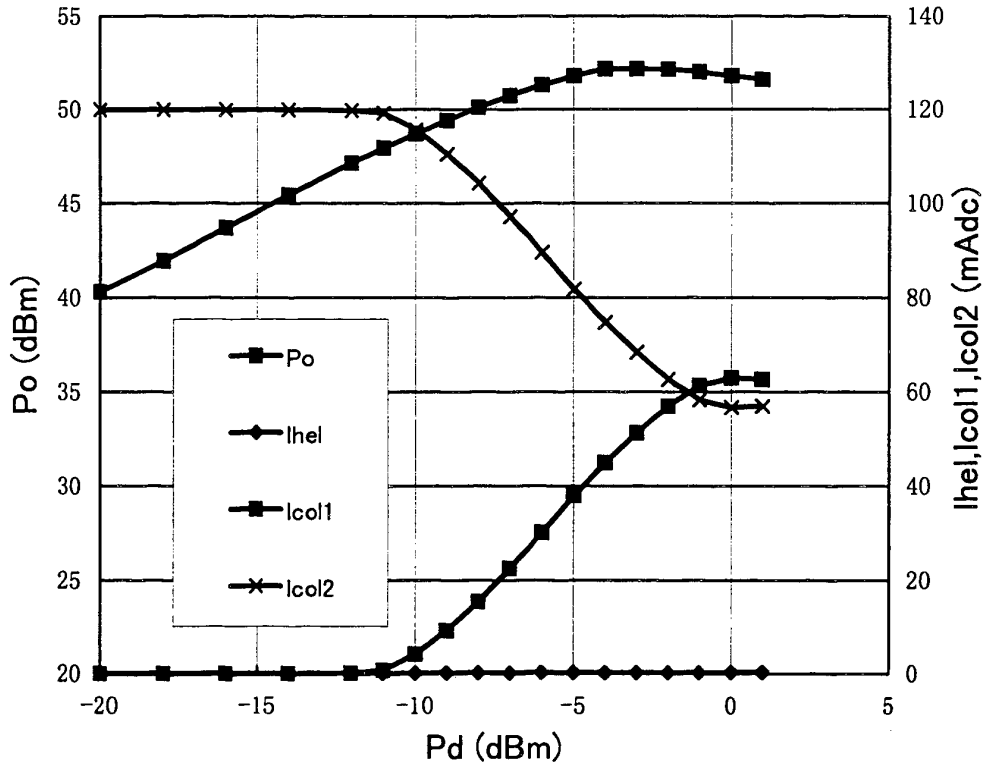

Figure1 Output power, helix current, collector current-1,2 vs. drive power

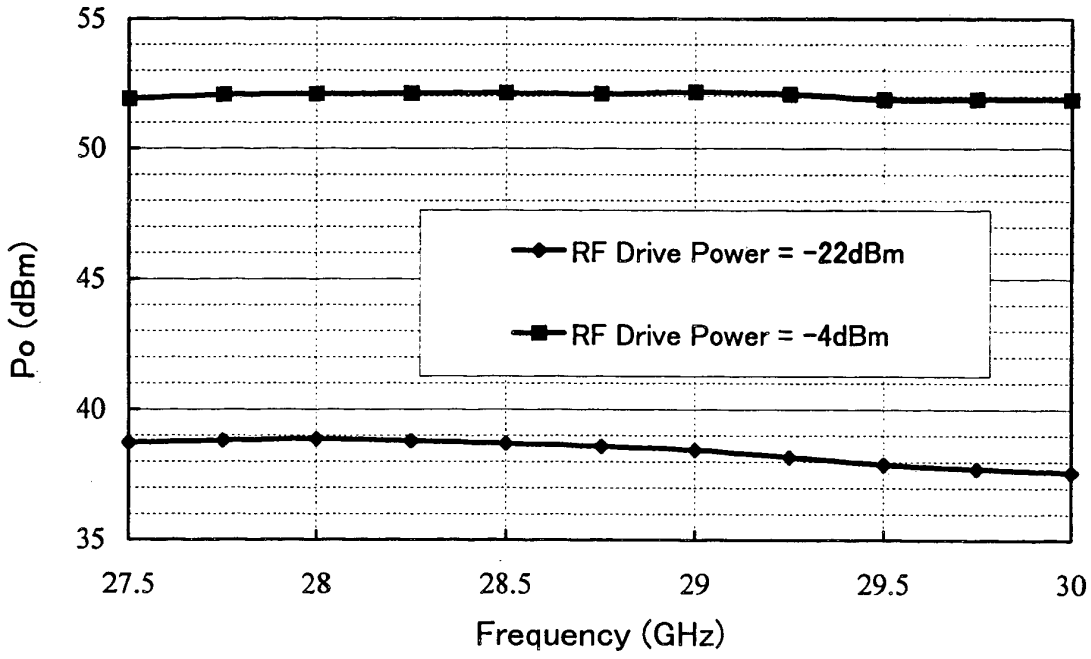

Figure 2 Output Power vs. frequency

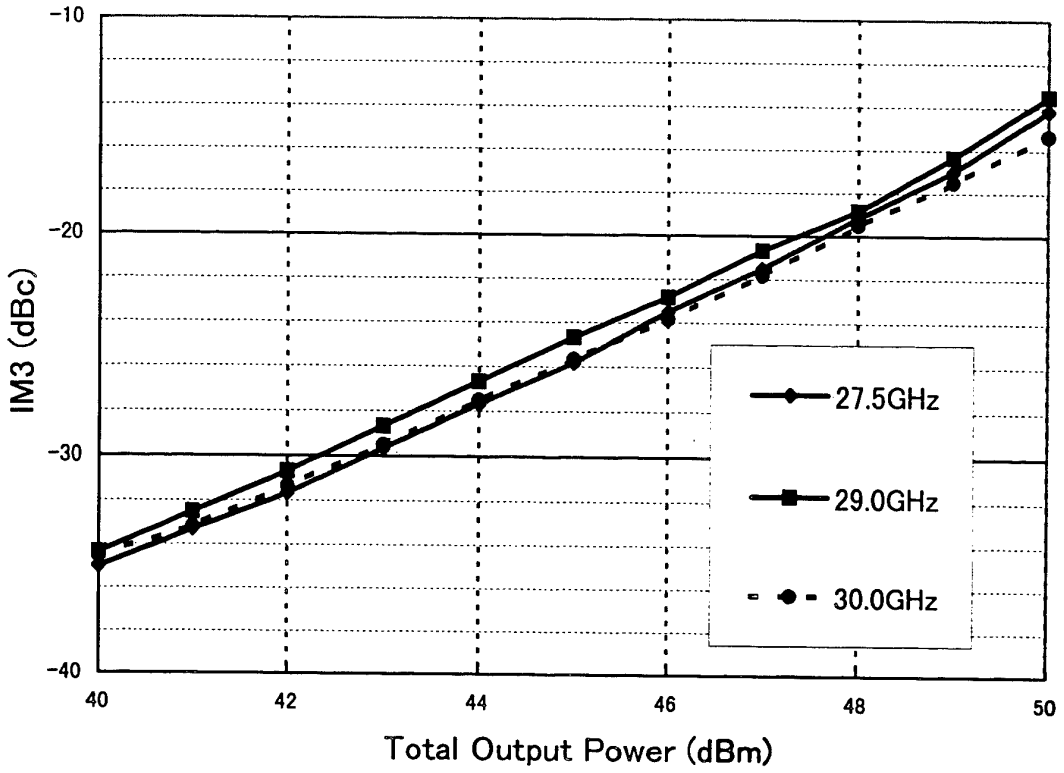

Figure 3 Intermodulation vs. output power

FIAR SPACE TWTAs FOR DBS APPLICATIONS

G. Orsenigo, L. Ceruti

FIAR S.p.A. Space Division, Milan - Italy
A Finmeccanica Company

ABSTRACT

The continuous effort devoted by FIAR to meet the performances dictated by the TWTA commercial market has led to qualify a new EPC design.

Currently, the FIAR EPC is able to supply TWTs delivering up to 135 W RF with overall good performances and, in particular, an efficiency of 92 % for an unregulated bus (up to 94 % for regulated buses) and a mass of 1.4 Kg for the vented solution (1.65 Kg for the potted one).
Competitive price and short delivery schedule are also main characteristics of this new EPC. One of this new EPC has been successfully qualified and integrated with AERG TWT for Hot Bird 4 payload.

This paper provides the main performances both at TWTA and EPC levels.
Moreover the paper summarizes the development activities and improvements areas that will be pursued in the near future, in order to achieve a new product able to meet the TWTA targets with EPC mass of 1.2 Kg and 95 % efficiency.

KEYWORDS: TWTA, EPC, TWT, Telecommunication Satellites.

INTRODUCTION

Since the beginning of space communications, in the early 1960's, TWTA has been a key element in high power and high frequencies satellites applications.

FIAR has been involved for 25 years as TWTA supplier in the frame of many significant space programmes for communications and scientific missions. The tremendous advance of the Telecom and DBS market in the last decade has led to a formidable increase in the space TWTAs demand. FIAR is devoting great efforts to gaining an important role in this increasingly more attractive and competitive market.

THE HISTORY

In 1993 FIAR started with the development of the "FEC" EPC, a new generation of EPCs, in the frame of an ESA ASTP 3/4 contract and internal funding (Ref. 1 and 2).
Aim of this activity was to have a unit with the following capabilities:

- Supply TWTs up to 135 W.
- Interface both regulated and unreg. buses.
- Competitive mass (1.4 Kg), efficiency and cost.

During the entire development phase FEC EPCs have been integrated with TWTs manufactured by various suppliers (listed in table 1).

AERG TL 12077	90 W Ku-Band
AERG TL 12112	110 W Ku-Band
AERG TL 14134F	135 W Ku-Band
AERG TL22033	35 W Ka-Band
TTE DAS/DEV-03	90 W Ku-Band
NEC LD 7833S	110 W Ku-Band

Table 1: TWTs successfully integrated with the new FIAR EPCs.

In 1995, the EPC design was furtherly improved in order to extend the capability to include the channel amplifier supply circuitry.
Moreover, an high voltage section potted was developed to allow the EPC to withstand the critical pressure condition (performance impacts on the weight of about 250 gr).

In parallel to this activity, a qualification programme has been performed on three complete EPC high voltage sections (assembled without the low voltage circuitry) following the sequence shown in figure 1.

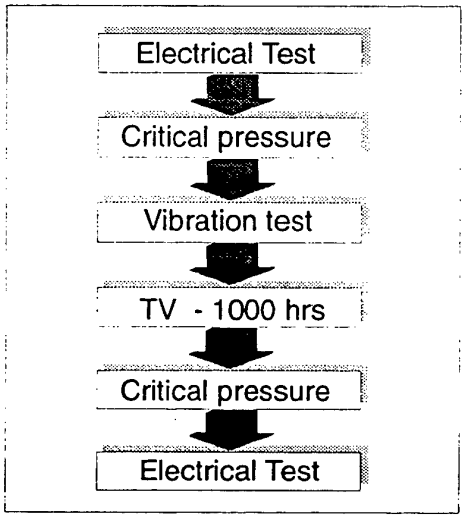

Figure 1: Qualification programme.

Operating time	**1000 hrs**
Output voltage	**6875 V**
Output power	**240 W**
Temp. Cycling	**-20 / +70 °C**
Cold start	**- 40 °C**
N° of cycles	**90**

Table 2: Operating conditions during the qualification of the HV sections.

In 1996, after the successfully completion of the qualification programme and the production of an Engineer Qualification model, FIAR delivered a flight unit fully qualified.

DESIGN DESCRIPTION

The unit design is briefly described. The structure, is composed of a baseplate, two lateral walls, one cover and one internal frame. The frame separates the high voltage section from the low voltage circuitry. The active power components have been allocated close to the baseplate for minimizing their junction temperatures.
In the low voltage section a single rigid-flex PCB has been used to reduce the internal wirings.

The lay-out has been furtherly optimized by using passive SMD components and two thick film hybrids that include almost all the EPC control circuitry.

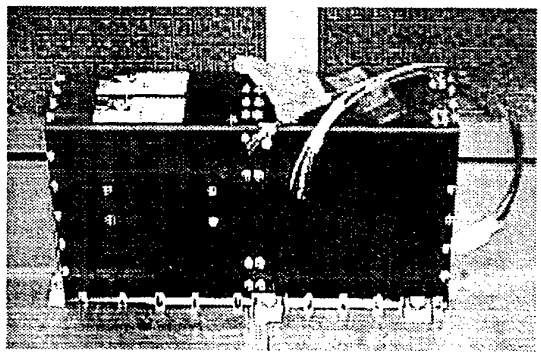

Figure 2: The FEC EPC manufactured for HB4; dimensions 284 x 77 x 122 mm.

From the electrical point of view the following blocks are mainly identified:

(a) The current limiter; it switches on the unit and protects the main bus from any overcurrent conditions due to output short circuits or internal malfunction.
The main features of this circuit are a high efficiency, negligible current overshoot and high noise immunity (EPC switch off after a persistence of 50 msec in limitation condition).

(b) The Input preregulator; it allows the EPC to be interfaced with both regulated and unregulated buses.

(c) The HV Converter, composed on the primary side of a push pull driving the HV transformer and, on the secondary side, of rectifiers, filters and output protections. It is able to supply output voltages up to 6.2 KV with an output power up to 240 W.

(d) The HV transformer; it generates the HV outputs with the exception of the anode. The HV outputs are filtered and connected to the TWT electrodes through a protection network

that limits the peak currents in case of short circuit conditions.

(e) The helix regulator; it regulates the helix voltage and reduces the cathode ripple working as active filter.

(f) The filament push pull, connected at the output of the input preregulator. It supplies, on the secondary side, the AC voltage needed by the TWT filament.

(g) Anode regulator; it regulates the anode voltage to maintain the RF output power constant over the life.

(h) The control circuitry; it controls and manages the unit operations: TLCs, TLMs, ARU, protections, timing.

The characteristics of the TWT TL 14134F, integrated and qualified with the FIAR EPC, are hereafter summarized:

- Metal ceramic technology, Mixed metal matrix cathode.
- Tapered helix held in place by ceramic rods shrink force fitting for higher output powers.
- Ppm-focussing with SmCo5 magnets.
- Integrated pole piece structure.
- Depressed three stages collectors.
- Mechanical structure in magnesium.

Telecommands	**TWTA ON/OFF (+ARU)**
Telemetries	**I Helix** **V Anode** **TWTA Status** **ARU Status**
MB voltage	**26 ÷ 43 V**
Sec. suppply outputs	**+7.6 ±0.375 V / 430 mA** **-7.6 ±0.375 V / 60 mA**
EPC I/Fs	**37 pins connector**
RF Input	**SMA female**
RF Output	**WR 75**

Table 3: TWTA electrical interfaces.

TYPICAL TWTA PERFORMANCES

The main performances measured during the test campaign are shown in table 4 and 5.
Figure 3 reports the RF spurious profile, well below the equipment specifications.

Operational life	**12 years**
Op. frequency	**10.7 ÷ 12.75 GHz**
NB channels	**33 / 36 / 46.5 MHz**
Power consumption	**243 W** **(@ VMB 43 V, 10.7 GHz)** **247 W** **(@ VMB 26 V, 10.7 GHz)**
RF Pout (EOL)	**> 134 W**
Overdrive	**17.5 dB**
Gain	**52.5 ÷ 58.5 dB**

Table 4: operating parameters.

Group Delay	**.22 nspp (@ 12.5 GHz)**
Group D. slope	**.01 ns/Mhz (@12.5 GHz)**
C/I3 (O/P IBO)	
3 dB	**-10.8 dBc (@12.75 GHz)**
10 dB	**-17.3 dBc (@12.75 GHz)**
17 dB	**-26.7 dBc (@12.75 GHz)**
Ph.Shift dB IBO	**(@12.75 Ghz) degrees**
0/3/6/9/12/15/20	**31/23/16.5/10/7,5/3/0**
AM/PM Coeff.	**3 °/dB (@ 12.75 GHz)**
AM/PM Transf.	**4.5 °/dB (@ 12.75 GHz)**
Spurious	
10÷40 KHz	**60 dBc**
40÷1 MHz	**linear decr. to 85 dBc**
1÷10 MHz	**-85 dBc**
DPout vs temp.	**< 0.1 dBpp**
Noise Figure	**33.5 dB**

Table 5: RF Performances.

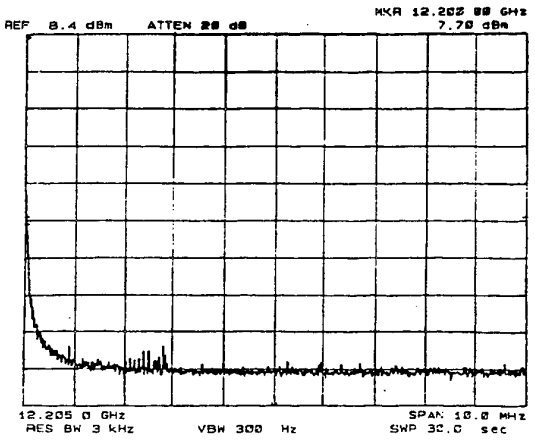

Figure 3: RF output spurious (vert. scale 10 dB/div.).

The TWTA mass budget is shown in figure 4.

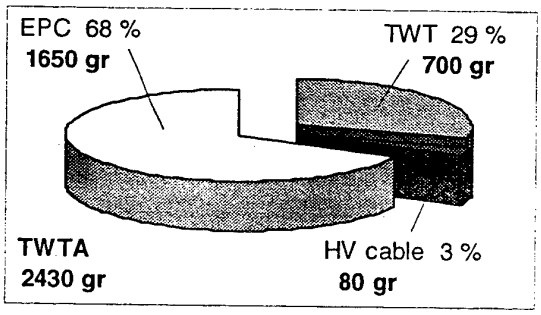

Figure 4: TWTA mass budget.

The unit has been submitted to the environmental test conditions listed in table 6.

Burn-in	**500 hrs**
Qual.Temp. range	
cold start	**-30 °C**
TWT op.	**-15 ÷ +85 °C**
TWT non op.	**-35 ÷ +90 °C**
EPC op.	**-20 ÷ +60 °C**
EPC non op.	**-35 ÷ +60 °C**
Qualif. Sine Vibr.	
5 ÷ 20 Hz	**11.0 mm (Zero-pk)**
20 ÷ 100 Hz	**± 20.0 g**
Qual. Rdm Vibr.	**Perp. 18 grms :**
10 ÷ 80 Hz	**+6 dB/octave**
80 ÷ 400 Hz	**0.5 g²/Hz**
400 ÷ 2000 Hz	**-6 dB/octave**
	Lat. 13 grms :
10 ÷ 80 Hz	**+4 dB/octave**
80 ÷ 1000 Hz	**0.1 g²/Hz**
1000 ÷ 2000 Hz	**-3 dB/octave**

Table 6: environmental conditions.

Telemetries
Sat. research
Pout stability
SS & SAT Gain
TWTA efficiency
AM/PM Coeff.
AM/PM Transfer
RF Spurious & Noise Figure
Intermodulation
Phase shift
Overdrive

Table 7: ATE TWTA test capability

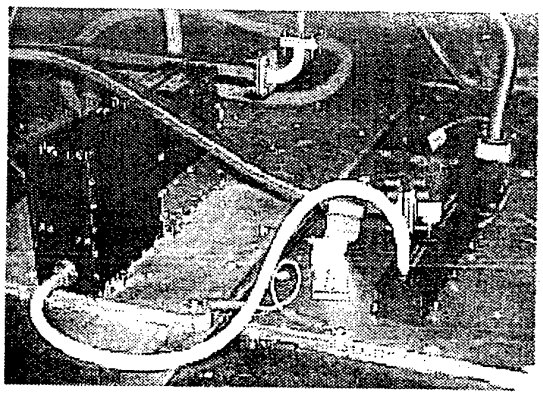

Figure 5: the HB4 TWTA (flight model) during the thermal vacuum test.

The TWTA electrical characterization is performed by means of an Automatic Test Equipment (ATE) to optimize the testing phase during the production of TWTAs in terms of repeatibility, cost and time schedule.
The software has been developed in Lab Windows/CVI environment.
The switch on/off procedures and the electrical tests, listed in table 7, are executed via PC; the results are acquired by the PC in standard Excel format. The test sequence and the test limits are easily re-configurable by the user and adapted to the unit under test.

FUTURE DEVELOPMENT

The FIAR efforts to continously improve the EPC/TWTA performances are presently concentrated in the design of a new EPC based on a revision, mainly focused on the technological aspects.

FIAR is developing a unit that presents a massive use of SMD devices, both for the low voltage and the high voltage sections. The logic functions are completely integrated in one ASIC while, for the power circuitry, the use of a power module is foreseen.
The mechanical structure will be made of magnesium. From the electrical point of view the input pre-regulator will be optimized considering the use of regulated buses up to 100 V.
All these improvements lead to an EPC mass reduced to 1200 gr for a version capable to withstand the critical pressure, with an efficiency of 95%, states of art values for this product.

CONCLUSIONS

The main characteristics of FIAR TWTAs have been presented in this paper.
The good results reached to date, togheter with the design improvements foreseen in the next two years, have created a sound base for successfull results on the commercial market.

ACKNOWLEDGEMENTS

The authors wish to thank AEG Elektronische Rohen GmbH, Thomson Tubes Electroniques and NEC Corporation for the supplying of the TWTs and for the fruitfull cooperation.

REFERENCES

1. M.Gambarara - L.Ceruti, "Lightweight EPC for (up to) 80 W 12 Ghz TWTAs", Proc. European Space Power Conference, Graz, Austria, ESA WPP-054. 1993

2. M.Gambarara - M. Cantamessa, "Qualification results of a lightweight EPC for medium/high power TWTAs", Fourth European Space Power Conference, Poitiers, France. 1995

Ku-BAND 90 TO 125 W RADIATION COOLED TWT

M. Yoshida, M .Mori and S. Hamada

Microwave Tube Division, NEC Corporation
1753, Shimonumabe, Nakahara-ku, Kawasaki, Kanagawa 211, Japan
Tel: +81-44-435-1698, Fax: +81-44-435-1923

ABSTRACT

A Ku-band 90 to 125W radiation cooled TWT which features a novel shaped collector radiator has been developed. Satellite system requirements for TWTs are reduction of heat dissipation to a satellite, light mass and reliability. In order to minimize the heat dissipation, the radiation cooled collector should be chosen and moreover its mass should not be high as compared with the conduction cooled TWTs. The newly developed TWT features light mass and high efficiency together with good other performance. The most significant feature concerning the radiator design is low thermal interference with adjacent TWTs. This results from the novel radiator shape which is different from those of other existing radiator types such as a dome type, a fin type, etc. The TWT vacuum envelope is identical to a 125W conduction cooled TWT which was already qualified. The collector cooling structure is only changed to the radiation type. The engineering model of this radiation cooled TWT was built and demonstrates the good performance which features high efficiency, good thermal performance and low mass.

1. INTRODUCTION

Demand for communication and direct-to-home broadcasting via satellites is growing more and more at present time and is expected to continue growing toward full multimedia communication era of 21 century. In order to realize it successfully, it is inevitable to provide economical system which is competitive in commercial market. According to this needs, an individual satellite is required to increase quantity of transponders and also raise these output power. However as the satellite has a limited electrical power generated at solar panels as well as a limited thermal dissipation capability, onboard TWTs have to be traded off regarding power consumption (or efficiency), thermal dissipation conducted to a satellite and mass. Under the circumstances, TWTs have been needed recently to be capable of higher output power, higher efficiency, low mass and radiation cooling which reduces thermal load to a satellite as compared with conduction cooling.

NEC has developed a Ku-band 90 to 125 W radiation cooled TWT featuring a novel shaped radiation collector with low mass to meet these requirements. In the following sections, the design, measured results, etc., of this TWT are described.

2. PAST ACHIEVEMENT IN NEC SPACE TWTs

2.1 Dome type radiation cooled TWT

NEC developed a Ku-band 135W radiation cooled TWT model LD4600 (shown in Figure 1) for BS-3a and b about 10 years ago, which were launched in 1990 and 1991 respectively. The LD4600 demonstrates very stable operation without any trouble as well as any SSO in orbit for about 6 years. Reliability of a dome type radiation cooled collector employed in the LD4600 has been proved from the in-orbit data together with qualification efforts conducted on ground before launch. At present the LD4600 is old-designed and loses advantage because its mass is 3kg, being heavy as compared with state of the art TWTs. However even now the dome type collector is advantageous for higher output power range more than 200W due to high reliability and low mass achieved by mass reduction efforts and low generated heat at the collector thanks to efficiency enhancement.

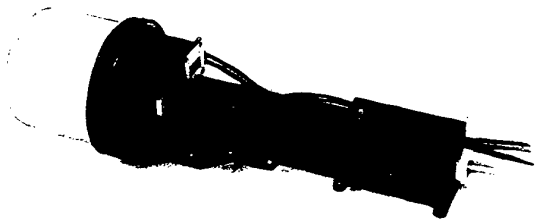

Figure 1. Photograph of LD4600

2.2 Efficiency improvement

Remarkable achievement for last several years is a great amount of efficiency enhancement. Strong market demand has pushed up the efficiency from about 50% of a decade ago to about 65% of recent years in Ku-band high power TWTs. NEC Ku-band 90 to 125 W conduction cooled TWT model LD7833 is capable of 64-66% efficiency and as a result thermal dissipation becomes considerably lower than that of the LD4600. This technology

improvement has come to facilitate to make low mass radiation cooled TWTs.

3. DESIGN APPROACH FOR A NEW RADIATION COOLED TWT

The significant points to be considered to create a new radiation cooled TWT are as follows;

- Reliability
- Mass
- Percentage of radiated heat in total heat dissipation generated in the TWT
- Thermal interference between adjacent TWT radiators each other and between the TWT radiator and a satellite panel seen from it
- Cost

First of all before considering above points, it is necessary to determine maximum operating temperature of the radiator, which affects the radiator size (or mass) and reliability on especially mechanical strength dependent on mass and material property dependent on temperature. The maximum temperature was selected to be 200℃ from material reliability point of view.

For an objective product of Ku-band 90-125W TWT, a fin type radiator is preferred rather than a dome type one because mass is lower than the latter within maintaining necessary reliability. Furthermore a novel shape of the radiator was created to reduce the thermal interference as described in section 5.

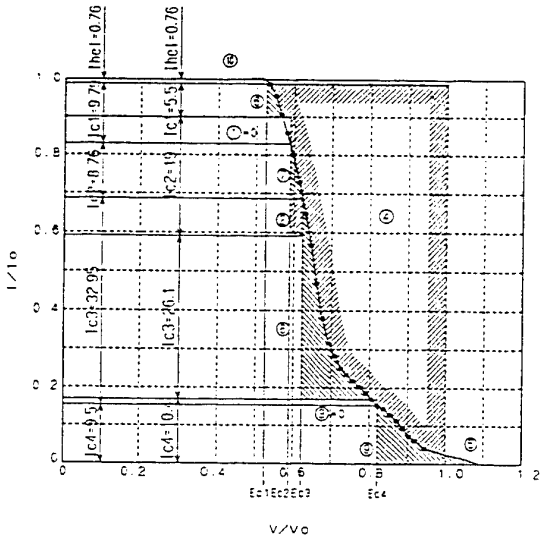

Figure 2. Spent beam energy distribution of Ku-band 90-125W conduction cooled TWT model LD7833.

4. CONDUCTION COOLED TWT AS A BASELINE

The Ku-band 90-125W radiation cooled TWT has same tube envelope as the conduction cooled TWT model LD7833. Both TWTs are different only in collector cooling configuration. This is effective for reduction of cost and delivery time.

The design feature and performance of the LD7833 are summarized in Table 1 and Table 2 respectively. This TWT features high efficiency and low mass. Figure 2 shows a spent beam energy distribution. Heat generated at each portion of the TWT is shown in Table 3 which is obtained from measured data of Figure 2 and estimated values based on analysis.

Table 1 Design feature of Ku-band 90-125W conduction cooled TWT model LD7833

TWT portion	Design features
Slow wave circuit	-Velocity taper pitch helix -Gold plated helix of output section -Shaped Beryllium oxide rods
Electron gun	-Ion barrier electrode -M type cathode for a long life operation -Low power consuming and vibration-proof cathode support structure -SSO free
Beam focusing	-PPM focusing -Samarium cobalt magnet with low temperature coefficient
Collecor	-4 stage collector -Molybdenum electrodes specially treated for secondary electron suppression -Conduction cooling
RF input and output	-Input: SMA femaile -Output: WR-75 waveguide
Housing	-Light weight, Magnesium alloy base-plate treated corrosion proof

Table 2 Performance of Ku-band 90-125W conduction cooled TWT model LD7833

Frequency range	10.8 to 12.8GHz
Output Power	90 to 125W
Input Drive Power	-3dBm
Gain	53dB
Efficiency	64-66%
Total Phase Shift	40deg.
AM-PM Conversion	4deg/dB
Mass	680g
Design Life	≧20years
Temperature Acceptance Qualification Cold Turn on Non-Operating	 -15℃ / +90℃ -20℃ / +95℃ -30℃ -40℃

Table 3 Loss analysis of Ku-band 90-125W conduction cooled TWT model LD7833.

Effect	Percent of Qdc	Watt
Output power	65.5	97.5
Heater power	1.6	2.4
Circuit losses	8.7	.13.0
Skin loss	4.9	7.3
Reflected power	0.7	1.0
Harmonic power	3.2	4.7
Helix interception	2.4	3.6
Primaries	1.7	2.5
Secondary+Backstreaming	0.7	1.1
Collector Losses	21.8	32.4
Primaries	14.4	21.4
Secondary+Backstreaming	7.4	11.0
DC power consumption Qdc	100	148.9

5. DESIGN OF THE NEW RADIATION COOLED COLLECTOR

A new radiator of the collector has a shape as shown in Figure 3. This radiator comprises a cylinder to include a tube collector envelope inside of itself, a small fin and a large fin to radiate heat toward mainly axial forward direction and a flat plate to connect together 3 portions mentioned above for mechanical rigidity and also increase radiator surface area. This flat plate also acts as a radiator fin to radiate heat toward mainly upper and lower directions and not to thermally interfere with adjacent TWTs on a satellite panel. Radiator surface is treated to has high emissivity more than 0.85 excluding back surface of both small and large fins.

Actual shape of the radiator was determined by thermal analysis to optimize thermal performance under constraint of radiator temperature range and mass reduction. Figure 3 is one of analyzed examples of radiator temperature distribution, which shows mesh partition for analysis and temperature distribution at saturated operating condition. As shown in this Figure, a heat spot at saturated operation is located between a small fin and a large fin. The heat spot at no drive condition is located at a little ahead of the small fin.

Thermal analysis was performed also in various operating and environmental conditions. Calculated collector temperature was shown in Table 4. The worst case is the case 2 including sun light. The highest temperature occurs at base of a small fin in case of no rf drive condition and is about 200℃. Temperature of same point at saturated condition is about 170℃.

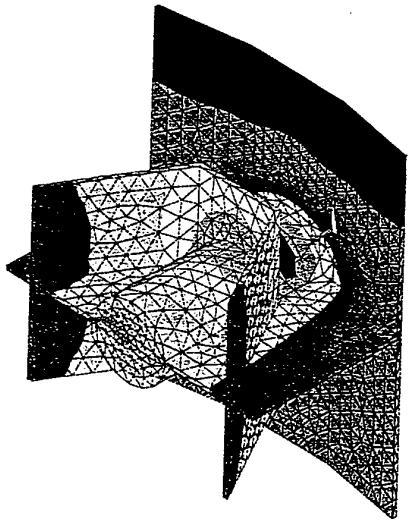

Figure 3. Collector radiator of Ku-band 90-125W TWT --- Analyzed temperature distribution at saturated operating condition

Table 4 Calculated collector radiator temperature of a Ku-band 90-125W TWT

Case / Condition		Case 1		Case 2		Case 3		Case 4		
-Baseplate temperature		80℃		80℃		80℃		-30℃		
-Collector environmental temp		-180℃		+75℃		-180℃		-180℃		
-Sun light		Exist		None		None		None		
-Operating condition		Sat.	No RF	Sat.	No RF	Sat.	No RF	Sat.	No RF	All off
Collector radiator temperature (℃)	-Base of small fin	125	164	151	185	105	147	73	122	-58
	-End of small fin	118	152	144	174	98	135	67	111	-58
	-Base of large fin	124	151	148	172	104	134	70	106	-57
	-End of large fin	115	138	138	158	95	121	59	91	-56

Heat generated at collector : 37W at Sat., 54W at NO RF

6. MEASURED RESULTS

An engineering model TWT was built and tested. Photograph of this TWT is shown in Figure 5. The collector radiator is made of aluminum and is put on a tube envelope of the LD7833. Mass is 880g , which is greatly lighter as compared with 3100g of the conventional dome type radiation cooled TWT model LD4600, and is only about 200g heavier than the conduction cooled TWT LD7833.

Measured temperature of the radiator is shown in Figure 5 as compared with calculated values in case of no drive operation and collector environmental temperature of -180℃. The maximum temperature is 130℃ at base of a small fin, which is a little under a calculated value. Therefore The worst case temperature is estimated to be under 200℃ which is a design criteria.

Breakdown of heat generated in the TWT is shown in Table 5. Heat radiated to space relative to total power dissipation is about 51% and 73% at saturated and no drive conditions respectively. Concerning heat conducted to a satellite mounting panel, that of saturated condition is higher than that of no drive condition. Therefore thermal load to satellite from the radiation cooled TWT is reduced to about a half of that from the conduction cooled TWT.

Thermal interference between adjacent TWTs on a satellite panel depends on a spacing between TWTs. In case of the dome type radiation cooled TWT LD4600, temperature rise due to thermal interference was 7℃ at the spacing of 250mm. The new fin type radiation cooled TWT which has been developed is designed to minimize the interference effect. Therefore the temperature rise due to interference is estimated to be not so high even if the spacing is as short as 150 mm.

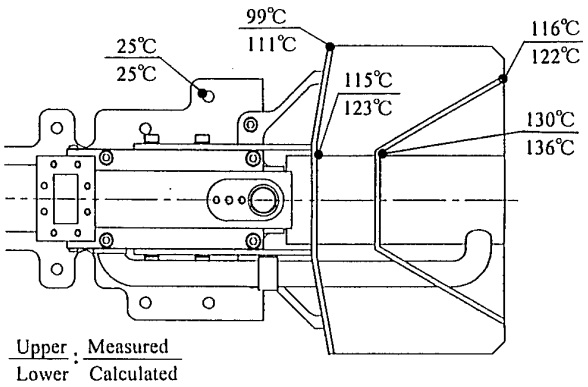

Figure 5. Radiator temperature at no drive condition of 125W output power operation

Table 5 Breakdown of heat generated in TWT

Parameter	Saturated (Note)		No drive	
	W	%	W	%
Total power dissipated in TWT	70.3	100	57.9	100
Heat generated at collector	46.3	65.9	54.3	93.8
Heat conducted to TWT body	10.2	-	11.9	-
Heat radiated to space	36.1	51.4	42.4	73.2
Heat conducted to satellite panel	34.2	48.6	15.5	26.8

Note. Output power 125W

7. CONCLUSION

A new shaped, low mass radiation cooled TWT has been developed to meet satellite system requirement of low mass, low thermal dissipation at TWT baseplate and low thermal interference with adjacent TWTs. The development is underway to perform qualification.

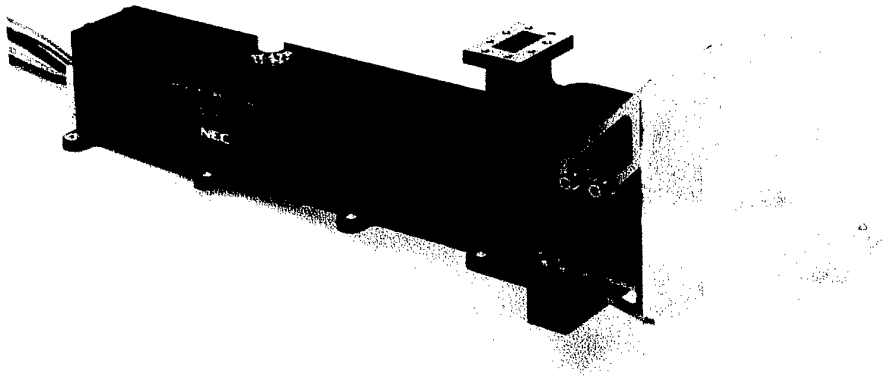

Figure 4. Photograph of Ku-band 90-125W radiation cooled TWT

NEW GENERATION OF HIGHLY EFFICIENT KA-BAND TWTs 15 to 140 W

E. Bosch, R. Christ, AERG, F. André, Velizy

AEG Elektronische Röhren GmbH
Ein Unternehmen der THOMSON TUBES ELECTRONIQUES

Abstract:

During the last two years a tremendous increase in the demand for Ka- Band TWTs (18 to 22 GHz) for Commercial Communication Satellites has been observed. In response to this situation both at AERG Ulm and TTE Vélizy parallel developments of a new highly efficient Ka- Band Space TWTs generation were started
The new tube generation is based on qualified TWT designs running in flight productions up to 60 W RF power. The developments cover the RF power range from 15 to 140 W.
The following results for the efficiency were obtained so far over a bandwidth of more than 500 MHz:

15 to 20 W:	50 %
40 to 60 W:	60 %
60 to 90 W:	62 %
90 to 130 W:	60 %

Compared to the previous state of the art, all nonlinear charateristics have been improved. For TWTs with an output power over 90 Watt, two cooling concepts are offered, the normal conduction cooling and the radiation cooling.

Introduction:

From experience with many delivered Ka - band programs for both AERG and Vélizy, and of course many TWT`s for C and Ku - band in conduction and radiation cooled version, the development of the Ka TWThave the best starting point.
The wellkown qualified TWT in Ulm, a 40 Watt TWT and in Vélizy a 65 Watt TWT are the baseline for the new development. Each main part of the tube has been in detail analysed and with the help of computer-software improved. For the great range of the output power, which is demanded from the market, the TWT development is devided in 4 classes. The power classes are up to 20 Watt, up to 60 Watt, up to 90 Watt and up to 130 Watt. Tubes from the same class have also the same technologie for the main tube parts.

General Tube Design

The main parts of the tube are the gun, the delay line, the collector and at least the housing with is adapted to the different principes of the TWT cooling, the conduction and radiation cooling. Also an dirckt influence to the housing is the mechanical interfaces, which is a common interface between both plants and of course,with respect to the requirements from the customer.(see Fig.1)

a.) The Gun

The important design change for the gun was only necessary for the high power tube. Coming from a beam voltage around 5.5 kV for the basic TWT ,the gun optics has to modify for the higher voltage up to 6.8 kV. For the higher voltages the focusing conditions for the

electronic beam are easier to achieve and the overall design criteria for the delay line fall in the theoretical optimum range. For the ceramic stack design as we used for all Ka and Ku band TWT`s, no change was necessary, because in respect to the high voltage isolation the

marign is many times better than required. For the lower classes the qualified gun can be used as it is. In both plants for Ka - band TWT´s a Mix Matrix cathode with 2.2 mm is used, and the design life criteria are proved in accelerated life tests for more than 20 years.

b.) Delay line

For the principle of the barrel technology there was no reason to find a better solution because it´s a prooven design for all kinds of TWT which are build in the previous programs.The most sensible part is the helix system. The helix and 3 shaped dielectric BeO rods are heat forced shrink fitted in the envelope. The geometrie of the rods is improved to give the lowest dielectrical loading for the RF-wave and also the best thermal path (low thermal resitance) between helix and envelope. An other great potential to improve the electrical efficiency and the useful HF - bandwidth is the geometrie and the taper of the helix. These parts are optimized with the help of the large signal program. By optimizing the helix sytem, the theoretical results shows very clearly, that several classes for the output power are necessary, specally for the focusing of the beam. So we have to reduce the magnetic periode of the system for the higher cathode current which is needed an output power of more than 100 Watt. With the reduced megnetic period the magnetic flux could be increased and the useful axial magnetic field. The first results of TWT, which are build in this way showed an improved focusing behaviour.
Overall the improvements are remarkable, the first bread board with an output power around 70 Watt showed an efficiency improvement of 5 % points.
The large signal program allowes by the help of an automactic iteration methode to optimize the helix for fix boundries. The calculated parameters are not only the beam efficiency and the nonlinear behaviour of the helix, an additional important point is to improve the electron velocity spectrum of the electrons over the drive situation of the TWT and the useful frequency bandwidth. Thuch an improved spectrum garanties for a high collector efficiency and for the whole tube and increased total efficiency.

c.) Collector

The overall efficiency and the behaviour of the whole tube, for example the back streaming electrons and the stability are main points which can directly improved by the collector. In other frequency ranges, Ku- and C - band the expierence showed a sigificant improvement in efficiency and focusing behaviour due to the change from the 3 or 3 stage plus spike collector to a real 4 stage collector. In the 4 stage collector the last stage has like the other stages a direct heath path via ceramic to the outer surface of the collector and therefore no limit for the voltage at the stage. Normally 600 Volts are used for the 4 th stage, but the voltage is adjustable so that the dissipated power, mainly in zerodrive, could reach very low value, without impassing thr rf performance. This qualified collector (in Ku- and C- band) is allready implemented in the lower output power class Ka-band production with an adapted iris and will be the baseline for the whole Ka - band family.

d.) Housing

The technologie of the housing was improved step by step through running developments and programs due to reduced mass and size. This standard housing process is the baseline for the new Ka- band generation. The main difference to other frequency ranges is that both, the in - and output, have a wavequide solution, which can be either WR 42 or WR 51

depending on customer preference. If there is a strong need for a coaxial input, this solution will also be available.
Since the developments are running parallel in both plants for several Ka-band TWTs, the machanical interface (baseplate footprints and wavequide orientation)have been standardised so that the TWTs are interchangeable. This common interface exists for conduction and radiation cooled TWT`s.

The typical mass for the Ka-band TWT up to 90 Watt will be around 720 g for conduction cooled and below 1100 g for 120 Watt and radiation cooled.

Radiation Cooling Princip

One of the major goals in improving TWT performance is the reduction of dissipated power in order to reduce the thermal loading od the satellite. Generally this approach will tend to development of TWT`s with higher efficiency. About a decade ago a different way has been started, using the direct heat transportation into space by radiation cooling of the TWT`s itself.
This second approach appears to be more attractiv, as in conjuction with increasing efficiency the self radiation design allows a significant higher output power of the TWTs together with increasing number of tubes on one satellite system. Obviously this has been a major step towards the demand of Direct Television for increasing the number of channels by an order of magnitude.
Dissipated power of the TWT is mainly generated in the collector by the missmatch between the electron velocity spectrum and the electrical potential distriubtion inside the collector. The collector voltages are adjusted to recover as much as posible of the electron energy. As a concequence radiation cooling of the collector will be usefull.
The first generation of self radiated TWTs have an electrostatic focused collector with a large surface Even with the large radiation surface the inner collector temperature appered to be arround 300 ^{0} C, not at least caused by the radiation interaction of the surrounding neighbour TWTs.
The new geration of radiation cooled TWTs have prooved their capability for Ku - band up to 150 Watt (new development up to 250 Watt) since the last 3 to 4 year and the first TWT are ready for launch. The radiation cooled collector is identical to that of standart conduction cooled TWTs, but useing a radiation structure out of light material, as Beryllium or Aluminium, connected to the collector envelope. The geomerty of the structure is chosen by different aspects:

- effictiveness of radiation coupling to space
- minimizing the distance between the TWTs without remarkable thermal interaction between the tubes.(see fig.3)

Two different concepts have been established statisfying the disired thermal requirements: the vane structure solution with high surface area and the cone structure solution with high radiation directly into space (90 %).(see fig.2)
Regarding the power class in Ku - band up to 150 Watt and in Ka - band up to 130 Watt and more, both concepts allow a collector temperature below 200 ^{0} C even under solar heating and for tube postioned as close as 5 - 6 inches. For the second approach high radiation directly into space was achieved by using selective coating applied on the specific cone geometry. the coupling between neighbours results in a temperature incresa of 2 ^{0} C, measured on the cone structure(see fig.4).
The collector temperature is also balance between radiation energy and the thermal backflow into the delay line system: achieving a maximum temperature of 200 ^{0} C for the considered 120 Watt Ka - band is aquivalent to a collector thermal radiation efficiency of 70 %, that will results in more than 50 % of the total dissipated power into space.

No impact on the collector efficiency and for the electrical performance could be observed at Ku - band, demonstrating the interchangeability of the radiation cooled and the standart concept
At the present development for radiation cooled concept in Ka - band the same results between conduction and radiation cooled design are expected.

Results:

To demonstrate the sucessful new Ka-band development the paper will show electrical results of all power classes up to 120 Watt from AERG and Vélizy (see. fig.5).

Conclusion:

Sigificant improvements in the electrical performances and RF power level have been obtained thanks to Ulm and Vélizy parallel development of a new generation of Ka - band TWTs. TWT designs are available today at RF power levels up to 130 Watt with an electrical efficiency of more than 60 % for a bandwidth of 500 MHz to 1 GHz within 18 to 20 Ghz.
Our capability to turn this development improvment into a commercial product has been proved up to 70 Watt in 20 Ghz programs. An average electrical efficiency around 60 % was measured in this programs, confirming the good development results.
The developments will continue up to RF power outputs of 140 Watt with improved efficiency and reduced mass.
These developments are also aimed at giving the maximum flexibility to our customers: conduction or radiation cooled TWT, WR 42 or WR 51 wavequides, coaxial or wavequide at the input and interchangeable TWTs between Ulm and Vélizy.
Moreover, the parallel development of a linearized short TWT will complete this new generation of highly efficient, high power TWTs in the Ka - band.

Fig.1: Conduction and Radiation Cooled Ka TWT (AERG and Vélizy)

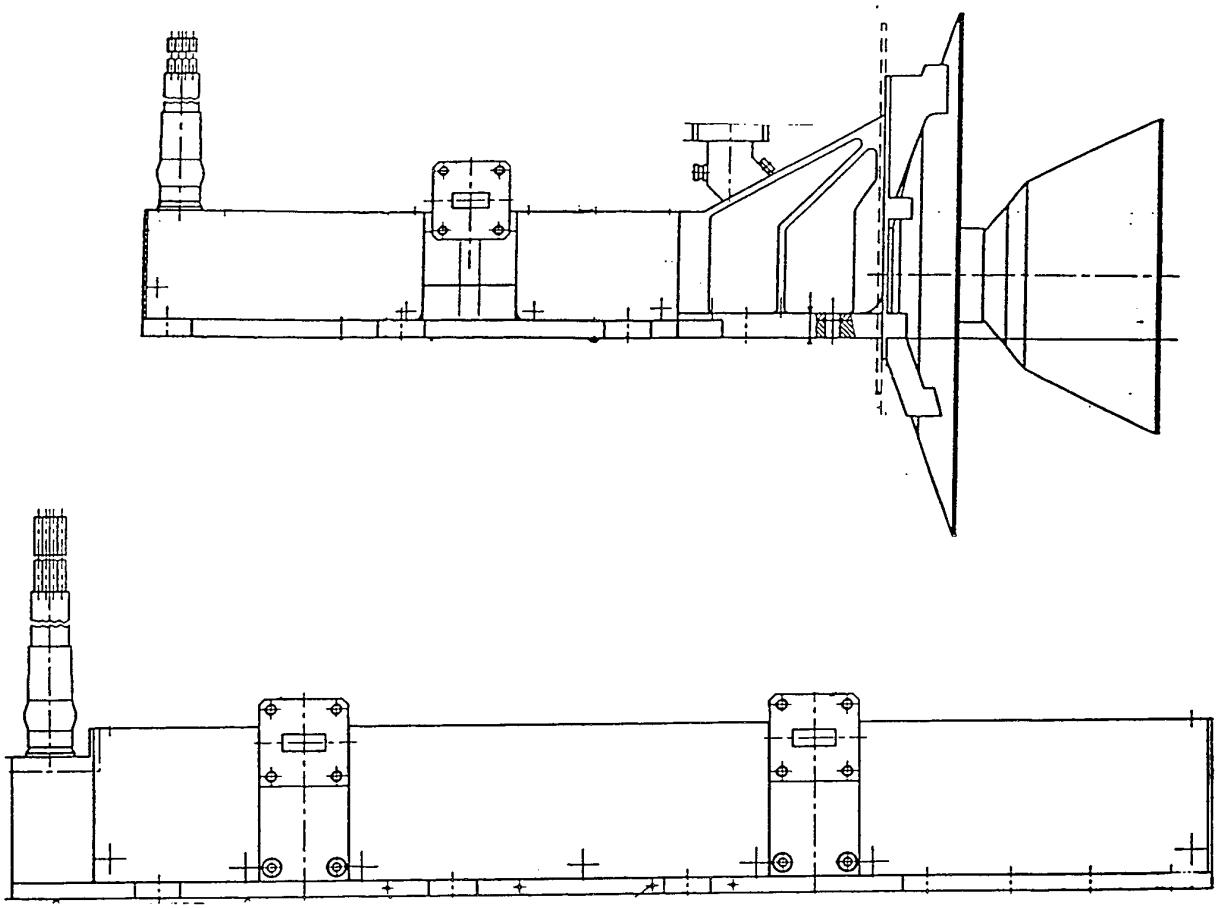

Fig.2: Concepts for Radiation Colled TWTs

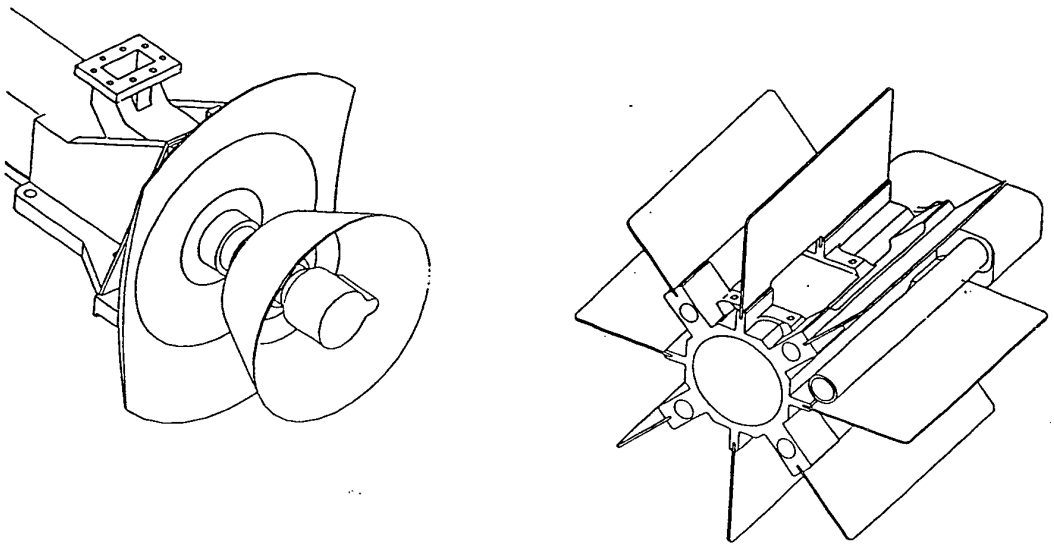

Fig.3: Calculation of Radiation Charateristics of Cone Collector

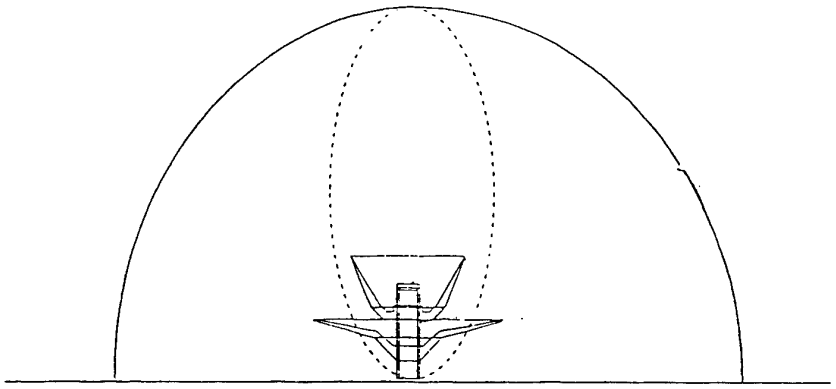

Fig.4: Coupling between next Nighbours TWTs

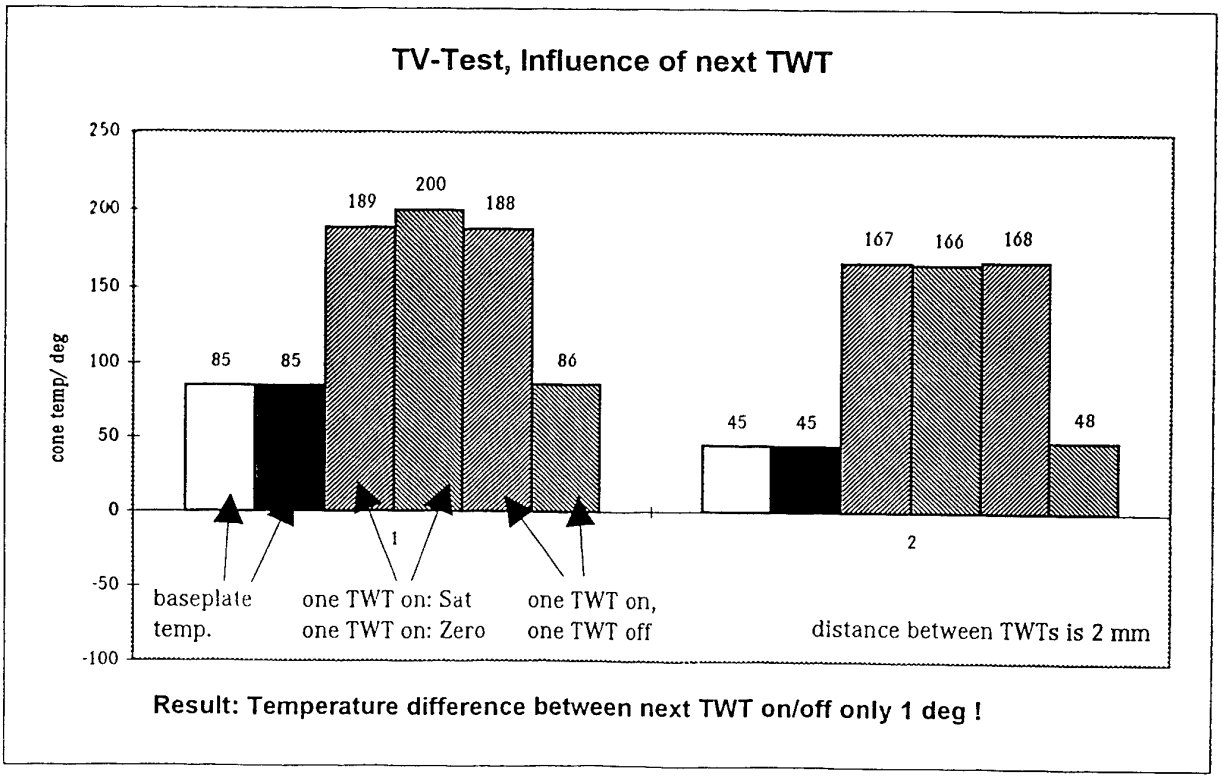

Result: Temperature difference between next TWT on/off only 1 deg !

Fig.5a : AERG Testresults Ka-band TWT from different Power Classes

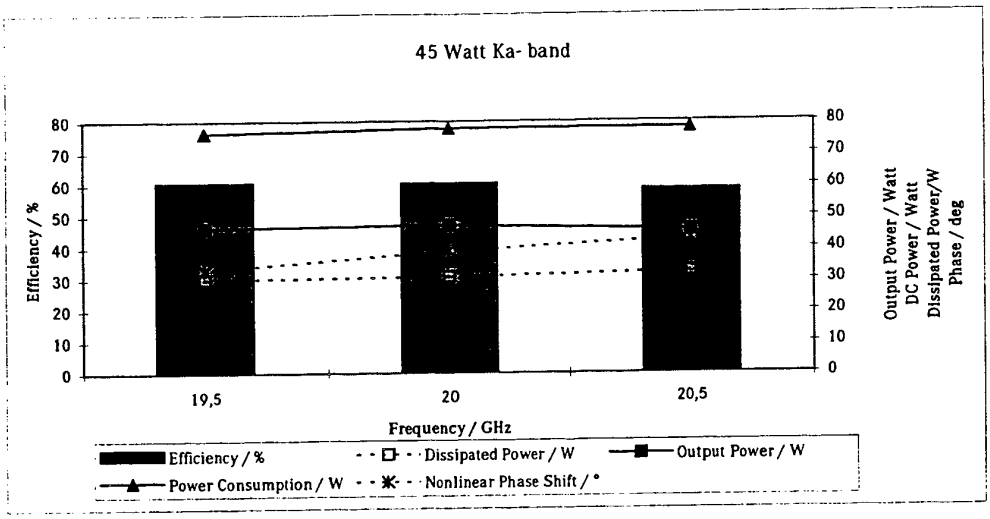

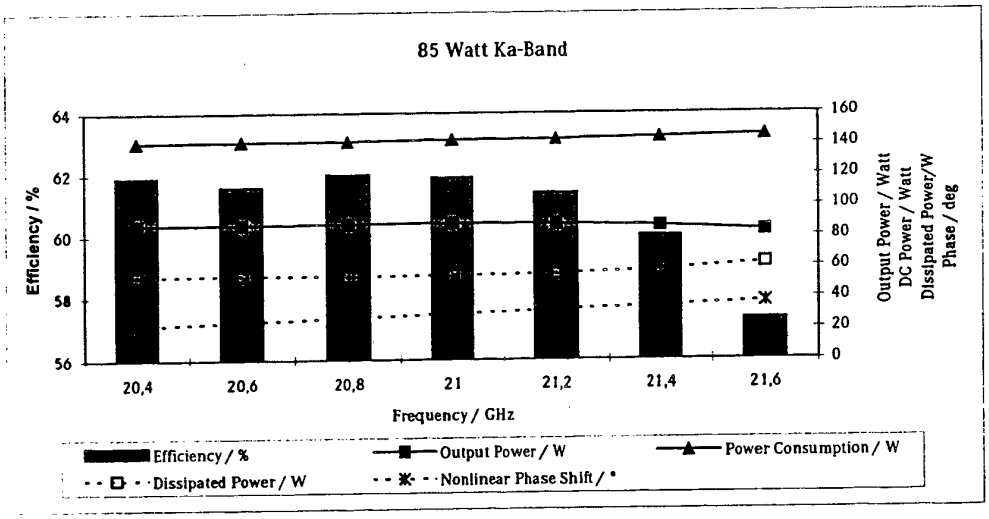

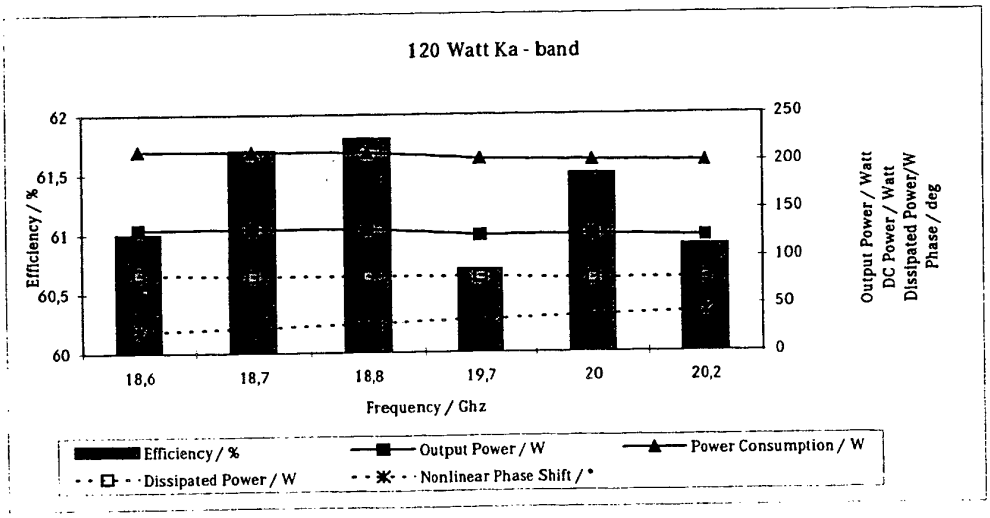

Fig.5b : Vélizy Testresults Ka-band TWT from different Power Classes

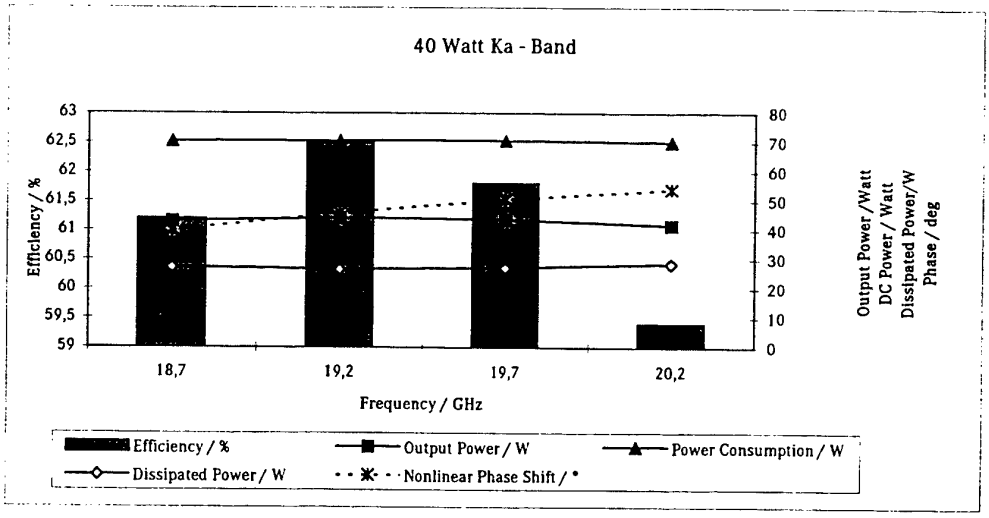

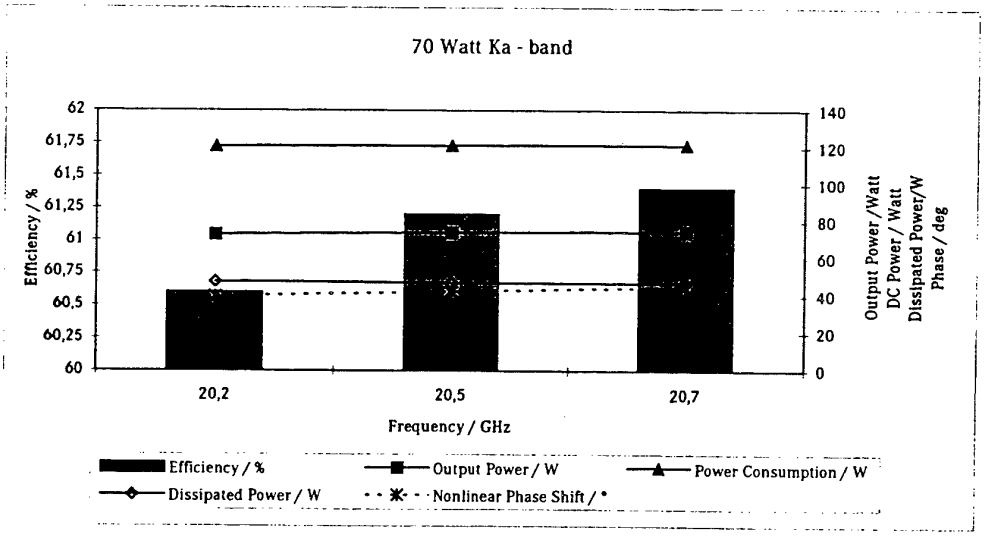

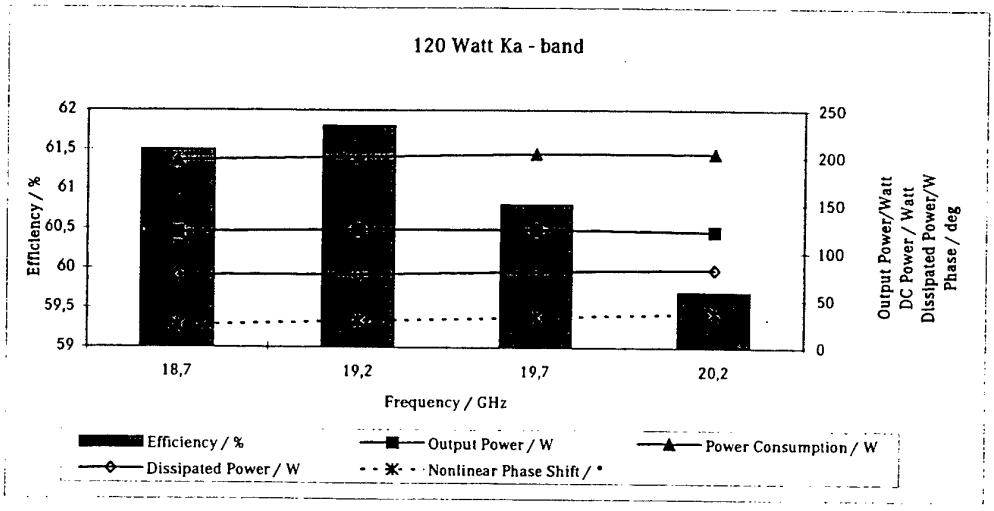

NEW GENERATION OF RADIATION & CONDUCTION COOLED HIGH POWER 220 W Ku BAND TWTs

A. Pelletier	**TTE Velizy**
E. Bosch	**AERG Ulm**
R. Pasdeloup	**TTE Velizy**
M. Alex	**AERG Ulm**

INTRODUCTION

A significant increase of DBS satellite market has been observed during the last 5 years, in the same time some applications ask for output powers exceeding 200 W. On recently built satellites this power was obtained by paralleling two 100 W TWTs.

This paper presents the results of new 200 W TWTs developed simultaneously in Velizy and Ulm and allowing to operate at this power level with a single TWT.

BASIC CHOICES

a) Operating point

The operating voltage has been chosen to be lower than 7000 V ; this value allows the work with the present proven generation of EPC. This choice leads to a typical cathode current of 120 mA that can be obtained with a 3 mm diameter cathode loaded with less than 2 A/cm2 of current density.

b) Technology

Both TWTs are using the same technology as the well proven 100 W class TWTs. These technologies are summarized on the table 1 for both designs.

TABLE 1 - 200 W TWTs - BASIC TECHNOLOGY

		TTE VELIZY	AERG ULM
GUN	Type Cathode Current density	Pierce "M" type < 2 A/cm2	Pierce "MM" type < 2 A/cm2
DELAY LINE	Type Material	Tapered helix Helix : W Support : BN	Tapered helix Helix : Mo Support : Be0
COLLECTOR	Type	Electrostatic 4-stage	Magnetic 4-stage
RADIATION	Type	Fins	Dish

ELECTRICAL PERFORMANCES

On table 2 is given a typical operating point for both TWTs when delivering more than 220 W.

This output power is obtained with classical amplitude and phase non linearities at saturation (typically 7 dB gain compression and 40° phase shift).

Although the overall efficiency is about 63 %, a classical performance for high power space TWTs, it must be noticed that this number is significantly lower than the 65 % demonstrated with both designs on commercial programs at 100 W level. A preliminary analysis shows that the increased operating beam perveance due to the limitation of helix voltage has an impact on the overall efficiency.

TABLE 2 - TYPICAL PERFORMANCE

	TTE VELIZY		AERG ULM	
Helix voltage (V)	6750		6665	
Cathode current (mA)	115		123	
	No drive	Saturation	No drive	Saturation
Helix current (mA)	0.29	2.17	0.19	1.70
Collector 1 current (mA)	2.7	37.8	0.34	53.9
Collector 2 current (mA)	2.2	44.9	0.51	36.2
Collector 3 current (mA)	13.7	16.9	4.76	15.8
Collector 4 current (mA)	96.0	13.4	117.7	15.9
Power consumption (W)	117.6	371.7	134.3*	358
Output power (W)	/	235.3	/	223
P diss (W)	117.6	136,5	134.3	135.2

THERMAL DESIGN

a) Collector cooling

In both TWTs two versions are available ; these two versions differ only by the collector cooling, the tube vacuum envelope remains identical in both configurations.

In the conductive cooled version all the remaining power is dissipated by conduction through the base-plate.

In the radiation cooled version the collector is equipped with a structure that directly radiates the power to space.

* Adjustable down to 100 W with collector voltage of stage 4

Both designs differ by this structure :

- AERG uses a cone structure allowing a directional radiation and a low sensitivity to thermal back loading (adjacent TWTs, sun power, satellite structure) (see figure 1).
- Velizy uses a vaned radiator with omnidirectional radiation, increasing the useful surface but, more sensitive to environmental conditions (see figure 2).

b) Typical radiation cooling operation

On tables 3 to 5 are given typical operational points for thermal points of view.

Two cases have been considered for the vaned radiator structure, the first corresponding to operation without environmental interaction, the second one taking into account thermal effects of neighbour. TWTs, sun illumination and satellite structure effects leading to an equivalent additional 30 W dissipated power on the collector.

TABLE 3 - TYPICAL SATELLITE OPERATION (cone radiator)

Base-plate temperature (°C)		TWT dissipated power (W)	Conducted power (W)	Radiated power (W)	Radiator temperature (°C)
20	No drive	133.6*	45.3	88.3	158
	Saturation	144.5	53.9	90.6	161
90	No drive	134.1*	30.1	104	176
	Saturation	144.2	38.2	106	179

TABLE 4 - TYPICAL SATELLITE OPERATION (vaned radiator) (free radiation)

Base-plate temperature (°C)		TWT dissipated power (W)	Conducted power (W)	Radiated power (W)	Radiator temperature (°C)
35	No drive	117.6	17.6	100	140.7
	Saturation	136.5	43.5	93	133.3
90	No drive	119.5	14.2	105.3	146.1
	Saturation	140	40.3	99.7	140.4

* Adjustable down to 100 W with collector voltage of stage 4

TABLE 5 - TYPICAL SATELLITE OPERATION (vaned radiator) (hot radiative environment)

Base-plate temperature (°C)		TWT dissipated power (W)	Conducted power (W)	Radiated power (W)	Radiator temperature (°C)
35	No drive	117.6	23.6	126.8	166
	Saturation	136.5	57.3	119.7	159.8
90	No drive	119.5	21.7	132.2	170.6
	Saturation	140	43.5	126.5	165.8

CONCLUSION

The new developed TWTs at more than 200 W output power is able to answer to the highest power required by customers to day without paralleling approach.

A present development is underway to standardize the mechanical interface to offer, to the payload manufacturers, a total compatibility of both designs.

By combining AERG ULM and TTE VELIZY respective experiences in the field of space TWTs it is expected to improve the electrical performances in the next future to be able to offer a typical efficiency exceeding 65 % as demonstrated at lower output power level.

FIGURE 1 - CONE TYPE RADIATIVE STRUCTURE

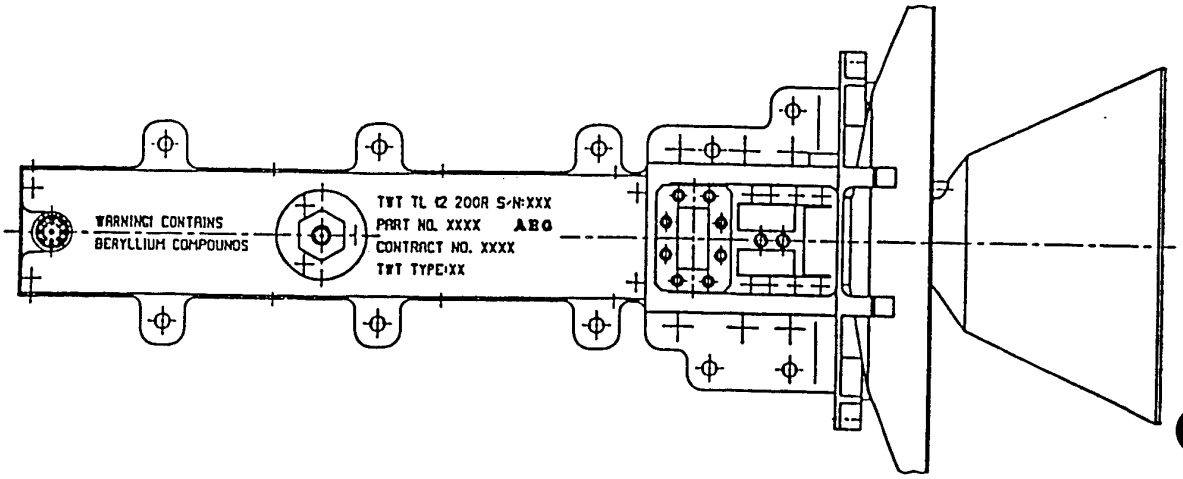

FIGURE 2 - VANED RADIATIVE STRUCTURE

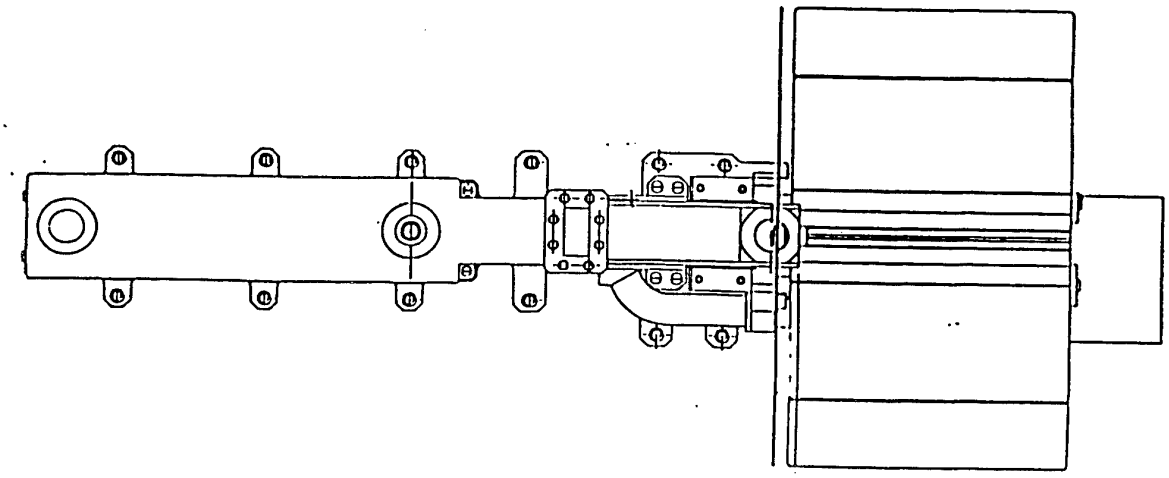

SESSION 5
Other Vacuum Tubes

Chairman: C. Lin (ESA/ESTEC, NL)

COMPACT MILLIMETER WAVE TWTs[1]

C. M. Armstrong, D. A. Gallagher, G. G. Groshart

Northrop Grumman Corporation
Electronic Systems & Integration Division
Electronic Systems
600 Hicks Rd., M/S H6402
Rolling Meadows, IL 60008 USA

ABSTRACT/INTRODUCTION

Northrop Grumman (NG) is developing reduced gain vacuum power booster Traveling Wave Tubes (TWTs) for a family of microwave and millimeter wave power modules covering the 1 to 100 GHz frequency range for radar, electronic countermeasure, and communication applications. In the millimeter wave region of the spectrum, two primary TWT development efforts are underway: a 100 W helix TWT covering the 18-40 GHz frequency band, and a W-Band folded waveguide TWT providing 100W from 90-100 GHz. The helix and folded wave guide millimeter wave booster TWTs build on past TWT development at 20-40 GHz and 40-55 GHz, respectively, with the miniaturization techniques recently developed for the 6-18 GHz and C-Band MPM TWTs applied for size reduction.

COMPACT HELIX TWT DEVELOPMENT AT 18-40 GHz

The development of the 18-40 GHz booster TWT is based on NG's state-of-the-art high power microwave devices, in particular the 6 to 18 GHz booster TWT for the MPM, the high efficiency booster TWT for the C-Band MPM and the 100 W, 20-40 GHz TWT. The circuit design of the 18-40 GHz MMPM TWT is based on the proven vane loading of the 6-18 GHz TWT. The miniaturization technology of the MPM is applied to the gun and collector. Samarium cobalt 2:17 magnetic material is used for the magnets to reduce the voltage and size requirements. Partially confined flow beam focusing, initially developed under the C-Band MPM program, is used to generate an ultra-laminar electron beam. Before discussing the 18-40 GHz TWT, a short description is given of the other TWTs.

<u>20 to 40 GHz TWT</u> In the late 1980's, before the origination of the MPM TWT concept, Northrop Grumman developed and delivered a transmitter system covering the 20 to 40 GHz frequency band. Excellent performance was obtained from the tube. The CW power exceeded 100 W from 20 to 39.5 GHz with small signal gain greater than 40 dB. The unequalized gain variation and fine grain were only 15 dB and 3 dB, respectively. An equalizer reduces the gain variation to less than 6 dB. The tube efficiency was greater than 20% over the full band. The gun operated at 12 kV and 0.167 A (0.127 microperveance). The design, however, incorporated neither graphite electrodes nor the miniaturization applied to the MPM booster TWT. Also, unlike the MPM, the circuit employed the more expensive brazed helix support structure with T-shaped notched rods. The present 18-40 GHz design is therefore quite unlike the earlier 20-40 GHz TWT, but rather incorporates the design features of the 6-18 GHz TWT and focusing of the C-Band TWT.

<u>6-18 GHz MPM Booster TWT</u> The booster TWT developed for the MPM is 5.5 inches long and less than 0.29 inches thick. The general tube fabrication consists of high-temperature precision-brazed metal and ceramic parts. The gun design is an electrostatically focused Pierce gun with focus electrode beam on/off control at about 1000 V. The cathode-heater assembly has a concentric sleeve support structure to provide high thermal impedance along with good mechanical stability over a broad temperature range. Only 5 watts of heater power are required to bring the cathode to operating temperature. The interaction circuit is severed (after a short input section) with graphite attenuation on the support rods on either side of the sever. This provides high isolation between input and output and also provides the ability to absorb high Radio Frequency (RF) power from an external mismatch. Broad band performance is obtained

[1]Work supported in part by DARPA TRP and monitored by Wright Laboratory under Contract No: F33615-94-2-1524.

by nearly flat circuit velocity dispersion provided by metalized vanes on the sides of the support rods. A unique four-stage depressed collector provides very high beam recovery efficiency. This collector design uses a one piece beryllia ceramic shell made in a rectangular shape and metalized on the inside diameter (ID). The collector stage lenses are made from graphite to suppress secondary electron emission and are metalized on the outside diameter (OD) for brazing to the ceramic shell. This design provides very high thermal conductivity to the cooling blocks attached to each side, while maintaining an overall height of less than 0.300 inches. When mated with a MMIC SSA, the tube demonstrated more than 100 W over most of the frequency band with more than 60 dB saturated gain. This performance was achieved with the beam current adjusted so that the maximum prime power input to the tube was less than 300 W.

High Efficiency C-Band TWT Northrop Grumman recently completed the successful development of a 50% efficient 125 W C Band MPM. A description of the C-Band TWT is presented elsewhere in the proceedings. A key technical milestone for the C Band MPM program was the development of the ultra-high efficiency vacuum power booster TWT. This tube provides in excess of 170 W with an overall efficiency of 61%. Realization of ultra-high efficiency in a miniature vacuum power booster TWT requires the careful design of the gun, interaction circuit and collector assemblies. An ultra-laminar reduced perveance electron beam is required for good circuit efficiency and high spent beam recovery in a multi-stage depressed collector. An optimized entrance taper to the PPM stack, obtained through full magnetics gun simulations, results in excellent beam focus with a shimless stack under both DC and rf drive conditions. A low body current of less than 6 mA is observed from small signal up to saturated drive. A dual velocity step circuit is employed for high circuit conversion efficiency (31%) and low harmonic content (<-11 dBc). The collector voltage splits for maximum overall efficiency are obtained using a unique collector optimization program on an automated TWT power supply test console.

18-40 GHz MMPM Booster TWT Development

Figure 1 shows a layout of the 18-40 GHz MMPM TWT including the electron gun, pole piece-magnet structure (with helix circuit and RF vacuum windows) and collector. The length of this tube is 6.7 inches. The tube is fabricated from high temperature precision brazed metal and ceramic parts. Major subassemblies as well as the helix sever joint are connected together via laser welded flanges. The collector was designed in the same manner as was the 6-18 GHz MPM TWT. It has four graphite stages for high efficiency and low secondary current.

The electron gun is a Pierce design with an M-type cathode for long life and a low cost focus electrode to provide beam cutoff at about 1000 V. A partially immersed flow beam with a beam voltage of 8 kV was chosen for good interaction efficiency and high gain per unit length. To obtain 100 W simulated output power, the current needs to be 0.135 A (0.188μP). Mechanical design of the gun uses a single cylindrical header ceramic with metalized through holes into which metal pins are brazed for connection to the cathode, heater, and focus electrode. Metalized rings are provided on the face of the header ceramic to braze mounting rings for the cathode and focus electrode. The cathode-heater assembly has a concentric sleeve support structure to provide high thermal impedance along with good mechanical stability over a broad temperature range. An important feature of this gun assembly design is the adjustable gun housing which provides at least ±10 milli-inches movement of the cathode assembly with respect to the anode. The metal disk attaching the gun housing to the anode assembly is designed to flex and allows the perveance of the gun to be adjusted during test for optimum TWT performance.

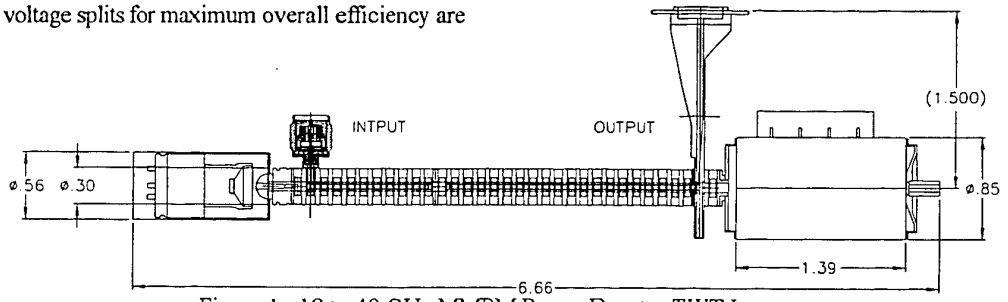

Figure 1. 18 to 40 GHz MMPM Power Booster TWT Layout

The interaction circuit consists of 2 helix sections supported in a barrel assembly by 3 BeO rods. A short input circuit is separated from the output circuit by a sever with graphite attenuation on the support rods on either side of the sever. This provides high isolation from the input to the output and the ability to absorb high RF power from an external mismatch. An integral pole piece (IPP) and helix barrel design make the pole piece ID the outer conductor for the helix circuit. The ID is precision honed to accept the helix and support rod assembly. A low-cost, well-established manufacturing method of "hot stuffing" is used to assemble the helix and rods in the IPP barrel to establish an interference fit of the circuit. Such a structure provides excellent thermal transfer and mechanical ruggedness. A plot of simulated circuit power at 40 GHz is shown in Figure 2, and indicates 100 W output power. At the low end of the band (18 GHz) the simulated output power is in excess of 100 W.

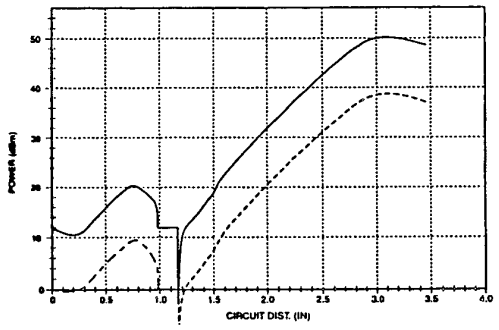

Figure 2. Large Signal Simulation Plot

The use of high energy product magnet material makes the overall diameter of the stack small. Samarium cobalt 2:17 magnet material with an energy product of about 20 x 10^6 GOe was selected as a compromise between size and field stability over a wide temperature range. The pole piece design is hubless and therefore is magnetically efficient and provides a high degree of on-axis magnetic field uniformity.

The RF input coaxial vacuum window uses beryllia ceramic. The male connector interface meets 2.5 mm standard interface dimensions with 50 Ω coaxial line sections on either side of the ceramic. HFSS electromagnetic simulations indicate better than 13 dB return loss at 45 GHz. The brazed window assembly is laser welded into the adaptor to complete the vacuum seal.

The output adapter is a waveguide that transitions from standard double ridged waveguide (WRD-180) to the helix. A stepped, double ridged waveguide impedance transformer is used to transition from WRD-180 to the lower impedance of the RF vacuum window. The alumina window, cut to the profile of a WRD-180 waveguide, is brazed into a coexpansive flange made of a tungsten-copper composite (Elkonite). The RF match to the helix is typically better than 2.0:1 over the 18 to 40 GHz band.

Figure 3 shows a photograph of a cold-test circuit, including input and output adaptors, as well as the helix and one of the three metallized support rods. Cold test results from this test circuit indicate that the match at both input and output are good. Phase velocity (c/v) measurements show that c/v is correct at the high end of the band and the dispersion is within 3% of the target design as shown in Figure 4.

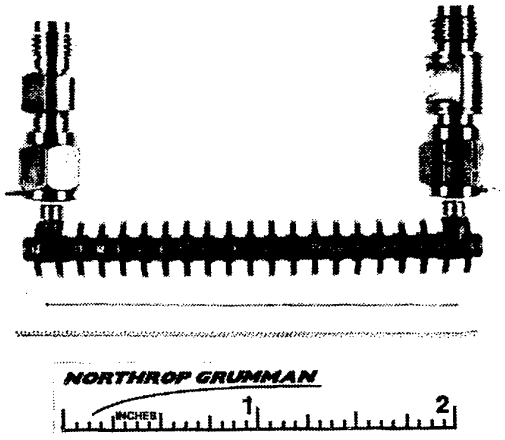

Figure 3. Photograph of Cold-Test Circuit

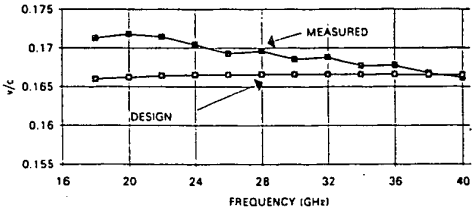

Figure 4. Measured and Design Delay Ratio

COMPACT MILLIMETER FOLDED WAVEGUIDE TWTs

The power and bandwidth requirements at W-Band require a folded waveguide interaction circuit, because of relatively high power not possible in helix TWTs above 40 GHz and because of relatively broad bandwidth not possible in coupled cavity TWTs and fast wave devices. By employing miniature MPM-style gun and collector designs, the combination of broadband 50-100 W coverage in W-band with reduced size and weight will enable the folded waveguide TWT to address a wide range of emerging system needs including: electronic counter measure (ECM), missile seeker, and driver amplifier for high power millimeter wave radar and electronic warfare (EW) systems. In addition, recent advances in millimeter wave P-Hemt solid state amplifiers (100 mW from 80-100 GHz) combined with miniature high voltage integrated power conditioner technology demonstrates the feasibility of developing a W-band power module.

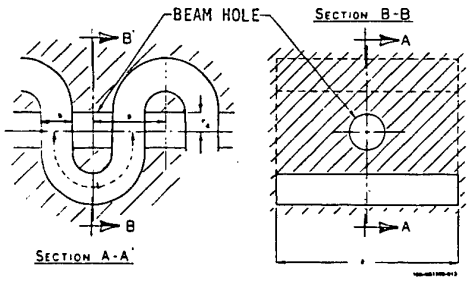

Figure 5. Cross-Sections of Folded Waveguide

The electrical design of the W-Band folded waveguide TWT is based on a previously developed 40-55 GHz folded waveguide TWT. This TWT looks like an ordinary helix TWT since the gun, PPM stack, and collector were designed in the same manner. The circuit, however, consists of a rectangular waveguide which bends back and forth, as shown in Figure 5, while the beam passes through a tiny hole running the length of the circuit. The principle of operation and the steps in fabricating the circuits,[1] and the design, fabrication, and test results at 40-55 GHz[2] are described in earlier publications. For the 40-55 GHz TWT, the beam voltage and current were 21.5 kV and 200 mA, respectively. The circuit incorporated a one-inch attenuator by making that part of the circuit from graphite. Figure 6 shows the power performance of three of these TWTs. For all three tubes, at least 50 W output power was obtained from 40 to about 52 GHz. At the frequency of maximum output power, tubes #4 and #5 performed at a duty cycle of 50 percent and 75 percent, producing an average output power of 90 W and 135 W, respectively. Figure 7 shows large signal gain across the frequency band for tube #5, demonstrating 25 to over 35 dB gain between 40 and 53 GHz.

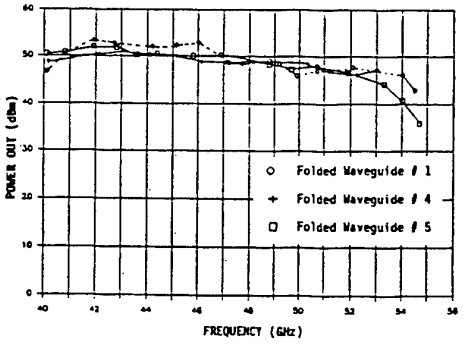

Figure 6. Measured Output Power from Three 40-55 GHz TWTs

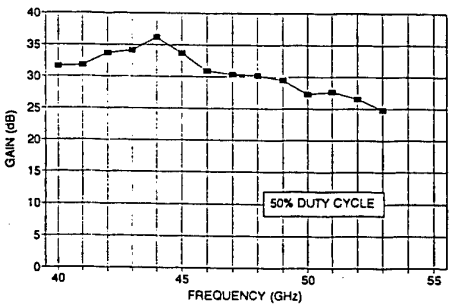

Figure 7. Large Signal Gain from 40-55 GHz TWT #5

For the 80 to 110 GHz frequency band, several preliminary scaled transitions and circuits (without either graphite attenuator or precision cutting of the beam-hole) were fabricated and cold-tested. The measured cutoff frequency was 88 GHz, and the return loss of the circuit was about 9 dB from 88 to over 110 GHz, except for a $\pi/2$ mode "stop band" at 101 GHz (caused by a super symmetry due to the misalignment beam). The insertion loss was about 7 dB for the circuit and about 3 dB for back-to-back transitions. Since the loss in the copper circuit calculates to be about 1 to 2 dB, that leaves 2 to 3 dB of additional loss, which must be due to leakage at the junctions between transition and circuit, which are held together mechanically.

The incorporation of a graphite attenuator and a precision beam-hole was accomplished by making the circuit from pellets that are predrilled undersized for the beam hole. Figure 8 shows a photograph of (starting at the bottom of the photograph) the unprocessed and processed pellets of copper for the circuit, of graphite for the attenuator, and of Elkonite for transition material, the brazed circuit blank, the circuit blank after cutting the flats, sputtering, and silver plating, and the final serpentine circuit (with precision cut beam hole) and the covers (the middle ones being made from Elkonite to match to the attenuator). All these steps were performed with nearly 100% yield. Unfortunately, the wire cutting of the serpentine caused the metalization to blister off the graphite. (This problem occurred only at the edges of the fingers at 45 GHz.) Numerous tests on mock metalized graphite sections and numerous variations in the processing of the material and the cutting of the material failed to solve or even reveal the cause of the problem.

However, recent advances in wire electron discharge machining have solve the circuit blistering problem. Figure 9 shows a photograph of both a blistered circuit and a recent sample resulting from the new process. The new circuit shows no blistering at all. Not even at 45 GHz, had such a perfect-looking circuit been made. The same can be said about the circuit after the cover plates were brazed onto it. Preliminary cold-testing, without brazing the input/output transitions to the circuit, indicate no problems in the match across the full 82 to 110 GHz frequency band. Also, the unwanted $\pi/2$-mode stop band that appeared mid-band in earlier circuits was absent as expected.

The electrical design for the remaining subassemblies were performed using the Northrop Grumman suite of design tools. Figure 10 shows the electrical gun design. The design beam voltage and current are 20 kV and 180 mA, respectively. The simulated perveance and beam size are correct, the laminarity is good, and the cathode is recessed to reduce edge emission. By incorporating the magnetic field of the periodic permanent magnetic (PPM) stack into the gun simulation and optimizing the peak fields at the entrance, the beam ripple and scalloping were made quite small as shown in the same figure. The collector design is in pro-

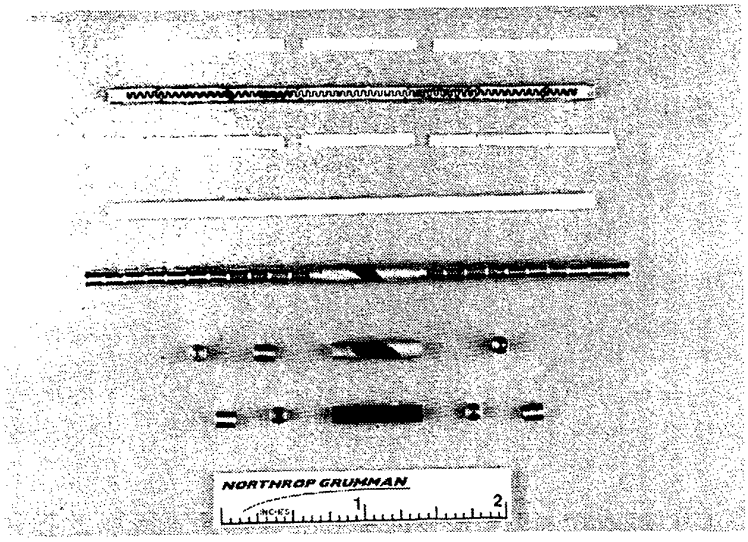

Figure 8. Photograph of W-Band Folded Waveguide Circuit Parts

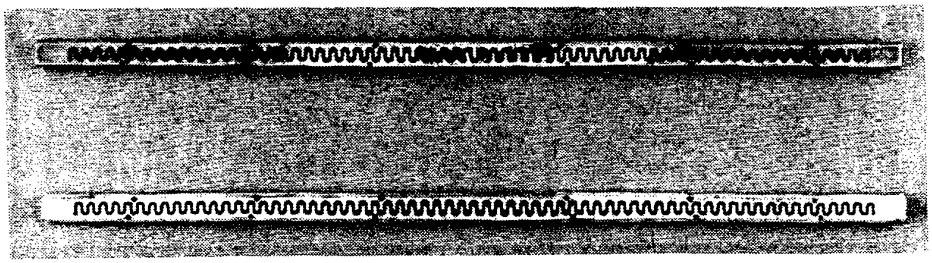

Figure 9. Photograph of Good and Bad W-Band Circuits

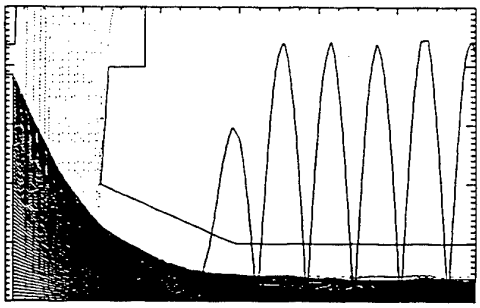

Figure 10. Herrmannsfeldt Simulation of Gun Design

cess, and also takes into account the magnetic field of the PPM stack. The window development is complete: the measured return loss is better than 20 dB from 88 to over 110 GHz.[3] Finally, the design of the waveguide transitions was modeled by the high frequency structure simulator (HFSS) code. The results show that the present design is good, but the insertion loss could be cut in half, without degradation of the return loss, by cutting the transition length in half.

The expected RF performance is shown in Figure 11. Over 100 W of power is simulated at "center" frequency, with a 3 dB bandwidth from 85 to 100 GHz, assuming 7 dBm of drive power (which can be expected from the solid state driver).

Planned work is to generate the mechanical design of all the subassemblies, following the miniaturization technologies of the MPM, assemble and test the subassemblies, including two more circuits with brazed input and output transitions, and assemble and test the first miniaturized W-Band folded waveguide TWT, which will be applicable as the vacuum power booster for a W-band power module. Figure 12 shows a preliminary design sketch of the miniaturized TWT, which has a total length under 10 inches.

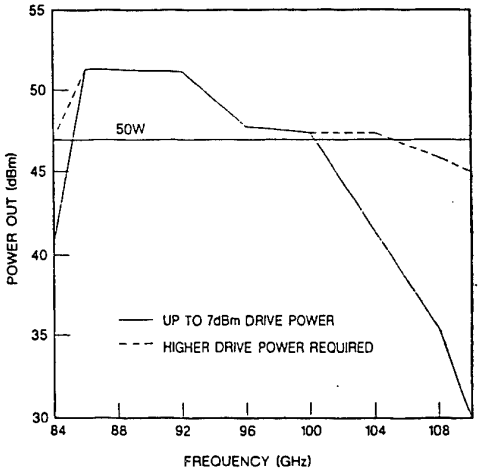

Figure 11. Simulated Output Power Across Frequency Band

CONCLUSIONS

Development of the compact millimeter wave TWTs covering the 18 to 40 GHz and the 90 to 100 GHz frequency bands is progressing and the TWTs should be in hot-test by the end of the year.

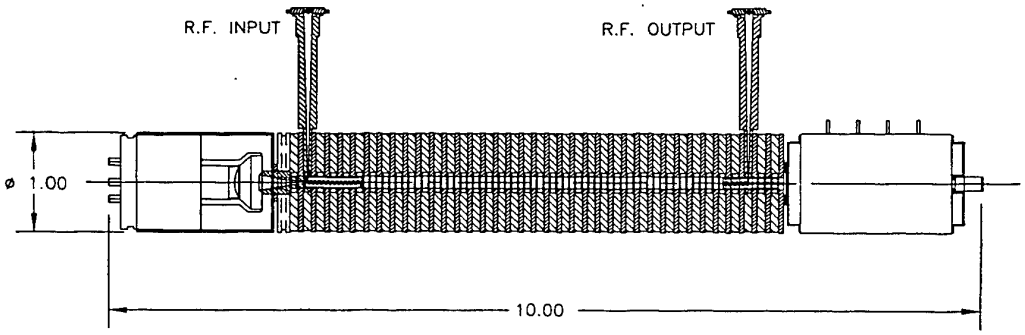

Figure 12. Preliminary Design Sketch of Miniaturized W-Band TWT

REFERENCES

1. G. Döhler, D. Gagne, D. Gallagher and R. Moats, "Serpentine Waveguide TWT," International Electron Devices Meeting, Technical Digest, 1987, pp. 485-488.

2. G. Döhler, D. Gallagher and J. Richards, "Millimeter Wave Folded Waveguide TWTs," Vacuum Electronics Annual Review Proceedings, Crystal City, Virginia, 1993, pp. V15-V20.

3. G. Döhler, D. Gallagher, J. Richards, and F. Scafuri, "High Harmonic High Power 95 GHz Peniotron," Vacuum Electronics Annual Review Proceedings, Crystal City, Virginia, 1993, pp. IV5-IV10.

HIGH POWER SUPER-RELTRON EXPERIMENTS

A.W. Cross, W. He, K. Ronald, A.D.R. Phelps and S.N. Spark*
Department of Physics and Applied Physics, University of Strathclyde, Glasgow G4 0NG, UK
**DRA Malvern, Worcester, WR14, 3PS, UK*

ABSTRACT

Experimental results are presented of a highly efficient, high power microwave source called a 'super-reltron'. The super-reltron relies for its operation upon the efficient relativistic klystron interaction mechanism. The novelty of this device lies in the combination of the formation of intense well-modulated electron bunches in conjunction with post acceleration of these bunches. The modulated electron beam is generated by periodic virtual cathode formation in a structure which consists of two pillbox cavities coupled to an intermediate cavity by magnetic coupled slots. Upon application of ~200kV across a velvet cathode and anode gap of the injector, beam current at a significant fraction of the space-charge limited current (~1kA) is injected into the modulating cavity. Beam injection is achieved by the presence of grids in the input and output of the modulating cavity which have the dual purpose of electrostatically focussing current from the cathode and reducing space charge effects in the beam. Reduction in space charge forces results in a decrease in the diameter of the beam due to the influence of the beam's own self-generated magnetic fields. It is the self-focussing of the beam which enables the super-reltron to operate with no external magnetic focussing field. Post acceleration by application of a further ~800kV between the modulating cavity and the grounded output cavities acts to reduce the relative electron energy spread while simultaneously increasing the beam kinetic energy available for the conversion into RF energy. Multi-cavity output sections are used to efficiently extract power without RF breakdown. By satisfying three fundamental requirements namely, 1) the formation of an intense, high current beam 2) the acceleration of electron bunches in this beam to high energies and 3) the existence of an efficient mode of particle-field interaction the super-reltron can produce high power (400MW), 400ns duration, 1.2GHz RF pulses with ~50% efficiency.

1. INTRODUCTION

The super-reltron HPM source was developed by Titan Advanced Innovative Technologies, Albuquerque, USA (Refs. 1-4) and is essentially a relativistic klystron with the unique feature of post accelerating to relativistic energies well-formed electron bunches created by a virtual cathode modulating mechanism. While the virtual cathode mechanism is quite efficient in modulating the beam, the emerging electron bunches invariably have a large energy spread. However relativistic acceleration after the modulating cavity causes all the electrons in the bunches to move at nearly the speed of light, thereby freezing the temporal bunch structure of the beam. This acts to reduce the relative kinetic energy spread of the electrons in the bunched beam. It also supplies much more beam kinetic energy which can be converted into RF energy. Multiple output cavities are used to efficiently extract the available microwave power without RF breakdown.

In the remaining sections of this paper, we discuss several aspects of the super-reltron tube and then summarise the results of our 1.2GHz experiments.

2. SOURCE COMPONENTS

The key elements of the super-reltron are (1) the velvet cathode and injector stack, (2) the modulation cavity, (3) the acceleration gap and (4) the output cavities (four output cavities embedded in WR770 waveguide) as shown in figure 1.

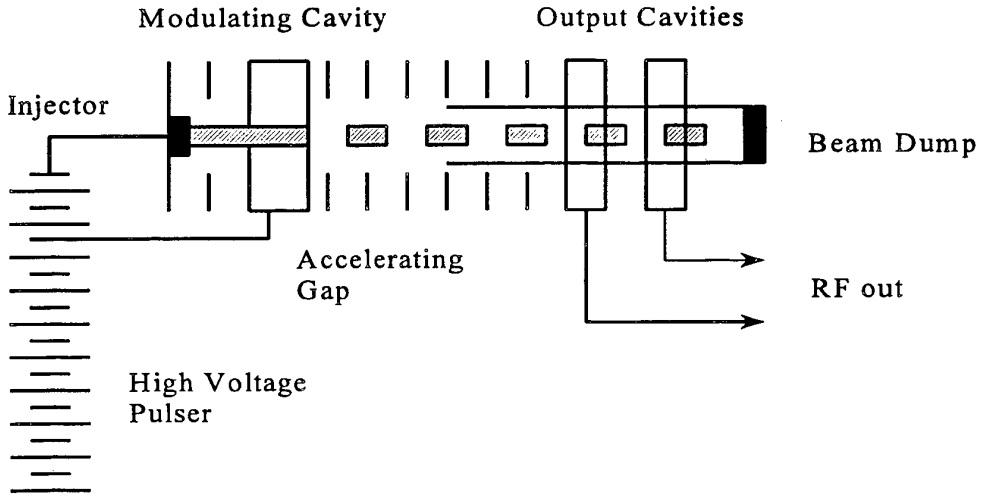

Figure 1. Schematic diagram of Super-reltron tube

(1) Injector. Upon application of a voltage pulse of <200kV across the cathode-anode gap of the injector, beam current at a significant fraction of the space-charge limited current is injected into the modulation cavity from a ~14cm diameter velvet cathode. Beam injection is achieved by the presence of grids in the input and output of the modulating cavity which have the dual purpose of electrostatically focusing current from the cathode and reducing space charge in the beam. Reduction in space charge results in a decrease in the diameter of the beam (~10cm to 1cm) due to the influence of the beam's own self generated magnetic field (i.e. the beam pinches). It is the self focusing of the beam which enables the super-reltron to operate with no external magnetic field focusing.

(2) Modulation cavity. A modulated electron beam is generated by periodic virtual cathode formation in a structure which consists of two pillbox cavities coupled to an intermediate cavity by magnetic coupled slots. This structure is basically a three-cavity section of a side coupled, standing wave RF linac. The intermediate cavity is displaced to the side; the beam passes through the two pillbox cavities only with the separation between the grids in these cavities chosen such that a transit-time instability between the beam electrons and the $\pi/2$ mode grows and saturates. The electric field structures of the three resonant modes are illustrated in figure 2.

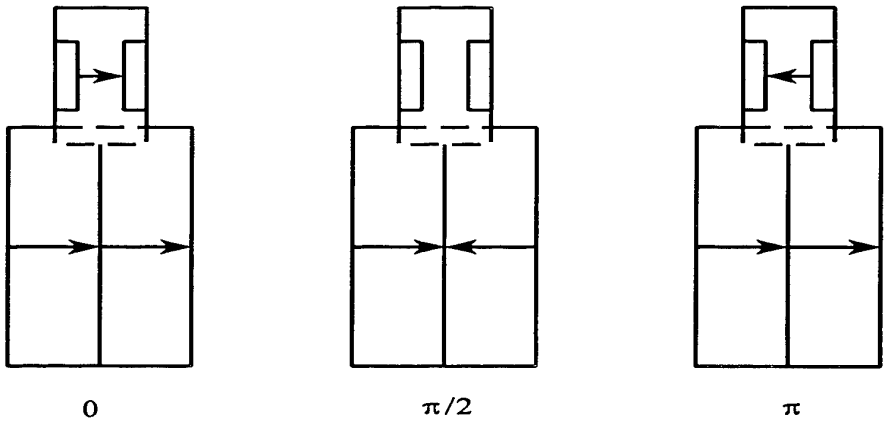

Figure 2. The electric field amplitude of the three resonant modes of the beam modulation structures

By properly adjusting the injector kinetic energy and pillbox cavity width the $\pi/2$ mode can be unstable. Consider an electron which enters the first pillbox at a time when the oscillating field in the pillbox will decelerate the electron. This causes the cavity fields to grow by conservation of energy. Now, suppose that the transit time of the electron through the pillbox is about half the oscillation period; the electron will experience the same retarding field in the second pillbox, and the cavity fields will continue to grow. An electron injected a half-cycle later will be accelerated in both pillboxes. However, because the decelerated electrons spend more time in the cavities, on average, than the accelerated electrons, the net energy transfer is from the beam to the cavity fields. This is a classically unstable situation. Although the 0 and π modes are also excited, only the $\pi/2$ mode grows because it is unstable. If the injected beam current is a significant fraction of the space-charge limited current the instability grows into a non-linear stage characterised by periodic virtual cathode formation. An initial growth phase in the unstable $\pi/2$ resonant mode in the modulation cavity is followed by shock excitation of the structure by the rising self fields of the beam. The resulting RF fields generated become sufficiently large as to act as a gate, alternately stopping, and then accelerating, the beam out of the cavity. It must be noted at saturation there is no net energy transfer from the beam to the system and vice versa and hence a stable operation point is achieved. The operating frequency of the tube is primarily determined by the resonant frequency of the modulating cavity.

(3) Acceleration gap. While the virtual cathode mechanism is quite efficient in modulating the beam, the emerging electron bunches invariably have a large energy spread (~200%). For efficient microwave pulse extraction it is necessary to decrease the relative kinetic energy spread. However, by accelerating the electron bunches immediately after the modulation cavity at velocities approaching the speed of light, the temporal structure of the beam is frozen. The crucial feature which makes the Reltron efficient (~50%) is the large reduction in the **relative** kinetic energy spread of the electrons (to ~30%) as a consequence of this post acceleration mechanism.

(4) Output Cavity. The high energy, high current electron bunches generated enter single or multiple output cavities. The output cavity section couples to the beam without breakdown in a simple rectangular cavity geometry. The rectangular cavities are formed by using a tuning plunger and inductive iris. The modulated beam drives an output cavity in resonance, building a standing wave. Power leaks out of the cavity via the iris opening. At resonance the resulting RF retarding field decelerates the electron bunches, with the net kinetic energy lost by the beam converted into electromagnetic energy, some of which can be usefully extracted.

3. EXPERIMENTAL RESULTS

The high voltage pulser used to drive the super-reltron was a conventional oil-insulated 15 stage Marx bank generator shown in figure 3. Each stage comprised of a (0.08μF) 100kV capacitor resulting in an erected Marx bank capacitance of approximately 53nF. The Marx load consisted of a parallel combination of the super-reltron tube, a variable resistance voltage divider and a liquid crowbar switch as shown in figure 3.

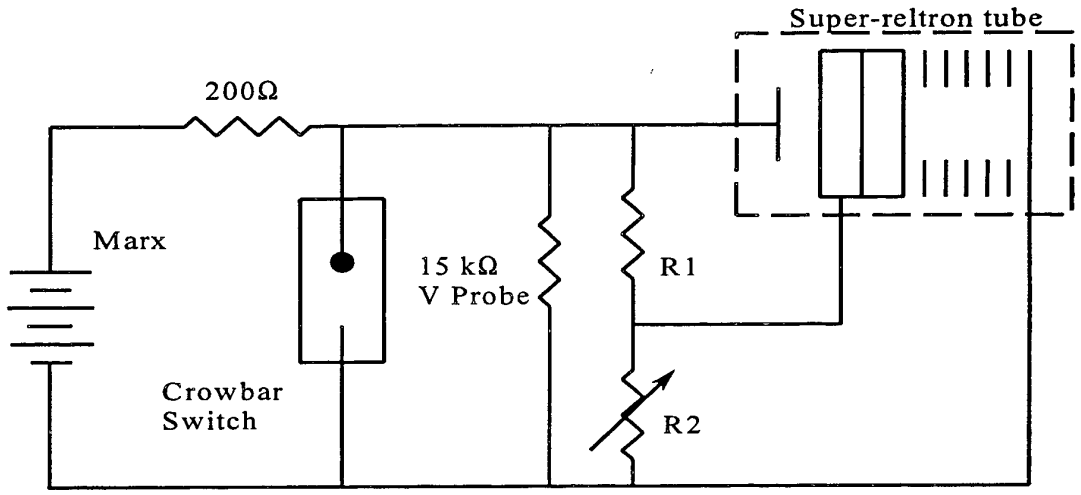

Figure 3. Schematic circuit diagram for the super-reltron.

The 15kΩ resistor represent the voltage monitor. A crowbar switch was used to terminate the voltage pulse, therefore eliminating the possibility of late-time tube arcs. The fixed resistor R1 had a value of ~1kΩ, while the variable resistor R2 could be varied from 3kΩ to 4kΩ but was typically operated at 4kΩ. The high voltage pulse was terminated with a simple liquid crowbar switch consisting of a variable (~4cm) point plane gap immersed in de-ionised water. The duration and magnitude of the accelerating potential applied to the super-reltron was varied between 0.1 to 1μs and 600kV to 900kV respectively by adjusting the distance between electrodes of the liquid crowbar switch.

A crowbar terminated (<1μs) duration super-reltron accelerating potential which could be varied between 600 to 900kV was measured using a 15ns response time high voltage probe (Ref 6). The electron beam current pulse was measured using an in-line 0.1Ω current shunt. A typical voltage and current signal is shown in figure 4.

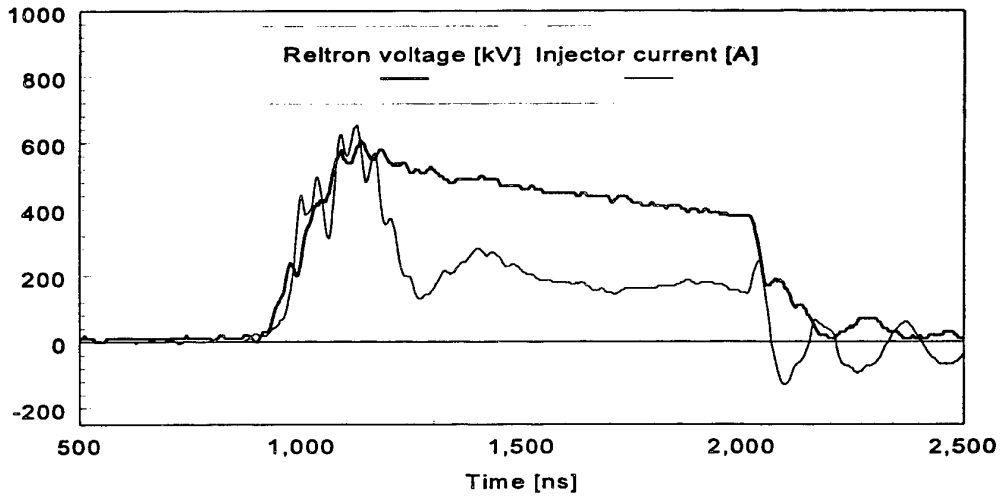

Figure 4. Reltron accelerating potential and injector current

The existence of a multi megawatt electron beam allowed the modulating electron beam bunching input cavity and the microwave output cavities of the super-reltron to be tuned for microwave generation. The operating frequency was selected by adjustment of both the idler and resonant cavities. A B dot probe positioned at the output window of the super-reltron detected a 1.2GHz real time microwave signal recorded on a 7GHz single shot 7250 Tektronix digitising oscilloscope figure 5. The microwave power generated by the super-reltron has been calculated from the size of the signal detected by the B-dot probe and is estimated to be greater than 200MW.

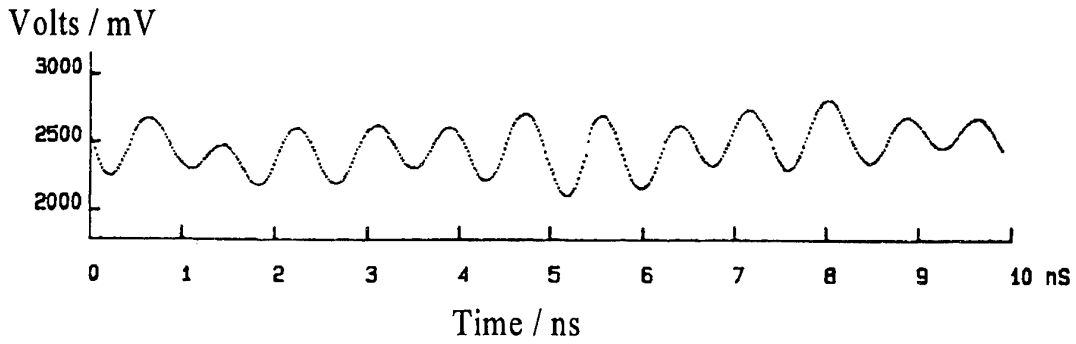

Figure 5. Real time microwave signal from super-reltron HPM source.

Further microwave diagnostics are planned to enable detailed investigation of the super reltron HPM source with respect to energy per pulse, peak power, tuning range, pulse-to-pulse reproducibility, mode purity and pulse repetition frequency.

4. CONCLUSION

The super-reltron tube operating within the laboratory at the University of Strathclyde is a flexible high power microwave source possessing extremely competitive output characteristics which include: peak output power >400MW, baseline RF pulse width >400ns, centre frequency 1.2GHz, a 5% tuning range (with only a 3dB loss in power) and output mode 100% TE_{01}. It is reliable (20,000 pulses), robust, requires no external magnetic field focusing, relatively small (45cm long) and light weight (40kg). We plan to perform a series of experiments to confirm the operational performance of the existing system using various microwave and electron beam diagnostics. We aim in the longer term to investigate the super-reltron with respect to the microwave pulse shape and hence energy content per pulse taking care to match the tube to high energy storage (>1kJ) and hence high energy per pulse modulators such as crowbarred Marx bank generators and PFN Marx Bank generators. At present such modulators are being used to drive the super-reltron at pulse repetition frequencies in the range of 1Hz to 10Hz. Advances in pulsed power technology allowing improved electromagnetic energy storage density, and the switching of higher voltages faster and at higher PRFs, will result in higher voltage, higher peak power, higher energy per pulse modulators (Ref 7). To keep pace with advances in compact Marx Bank design it is important also to optimise the HPM source with respect to diode impedance, electron bunching, microwave output pulse duration and the efficient extraction of electron energy while preventing RF breakdown.

5. ACKNOWLEDGEMENTS

We would like to thank the DRA for support of this work and for the encouragement provided by D.M. Parkes and C.J. Brooker.Helpful discussions with R.B. Miller and K.W. Habiger of Titan Advanced Innovative Technologies are gratefully acknowledged.

6. REFERENCES

1. Miller R.B., McCullough W.F., Lancaster K.T., and Muehlenweg C.A., 1992, "Super-Reltron Theory and Experiments", *IEE Trans. on Plasma Science*, **20,** No3.
2. Miller R.B., McCullough W.F., Muehlenweg C.A. and Lancaster K.T., 1992, "Super-Reltron Analysis and Experiments", *Proc. of Inter. Microwave Symp.*, **MTT-S,** Albuquerque, NM.
3. McCullough W.F., Miller R.B. and Muehlenweg C.A., 1993, "A Tunable S-band Super-Reltron Tube", *Proc. of the Sixth National Conf. On High Power Microwave Tech.*, Lackland ABF, TX.
4. Miller R.B., Muehlenweg C.A. Habiger K.W. and Clifford J.R., 1994, "Super-Reltron Progress", *IEEE Trans. on Plasma Science,* **22,** No 5.
5. Miller R.B., 1994, "Advances in Reltron and Super-reltron Technology", *EUROEM Int. Symposium on Electromagnetic Environments and Consequences.*
6. He W., Cooke S.J., Cross A.W. and Phelps A.D.R., 1996, "Simultaneous axial and rotational electron beam velocity measurement using a phosphor scintillator", *Proc. of 20th Int. Conf. on Infrared and Millimeter Waves*, Orlando, Florida, USA,.
7. Phelps A.D.R., 1991, "Recent Advances in high-power, pulsed microwave and millimeter radiation sources", *New Developments in Pulsed Power Technology*, IEE Digest No: 1991/039, London.

LITTON HIGH-POWER FOLDED-WAVEGUIDE KA-BAND TWTS

A. J. Theiss

Litton Industries, Electron Devices Division
San Carlos, California 94070

Abstract

Litton EDD is developing a new class of small, low-cost, high-power Ka-band traveling-wave tubes (TWTs) that are well suited for lightweight applications. The PPM-focused TWTs use a novel folded-waveguide slow-wave-circuit in which folded-waveguide walls are also polepieces for a unique focusing system. In a baseline design, this circuit is part of a compact, highly reliable, four pound TWT that generates over 250 watts of average power. With minor modifications of that design, a TWT ran CW, producing average powers up to 1500 watts. Other modifications are expected to result in TWTs that operate with lower beam voltages and at W-band.

Introduction

As described in earlier work (e.g., Ref. 1), Litton's new class of small, PPM-focused, Ka-band TWTs utilizes a novel type of folded-waveguide circuit to provide high average power with minimum weight. (Note Ref. 2.) The circuit is machined from a copper-iron laminated block so magnetic flux can pass from small permanent magnets directly into the beam tunnel. The presence of iron at the beam tunnel enhances the PPM focusing parameter λ_p/L, while copper lining on the iron provides thermal robustness.

This circuit, in a baseline Ka-band design, operates with 20 kV beams to produce 40 dB of saturated gain, between 1 percent and 2 percent bandwidth, between 800 and 1400 watts of peak power, and over 250 watts of average power. A single-stage, conduction-cooled, depressed collector provides total efficiencies between 20 percent and 28 percent. Other circuit designs now under development are expected to improve the baseline performance. One such circuit resulted in a TWT that runs at 100 percent duty (Ref.3).

In this paper, the first section describes the laminated folded-waveguide circuit that results in a low-cost, thermally rugged baseline design. The next section discusses the rf performance, the four-pound weight, and the high mechanical reliability of the latest baseline design. The final section comments on developments that result in increased average rf-output power, lower beam voltage, and operation at W-band.

Folded-Waveguide Circuit

Figure 1 illustrates the conceptual development of the folded-waveguide slow-wave circuit. A rectangular waveguide that is bent as in view "A" is shortened by eliminating gaps between adjacent walls as in view "B." Iron walls extending through the vacuum envelope form a unique planar-geometry circuit for both rf and magnetic fields as in view "C."

In practice, plain copper and iron plates that have thicknesses appropriate for the desired rf period are brazed into a low-cost block. Then, electron discharge techniques are used to quickly machine this laminated block into a circuit with the required +/- .0002 inch tolerances. Finally, this circuit subassembly is typically copper plated to minimize rf losses.

Figure 2 shows an uncovered, machined and copper-plated circuit. Horizontal segments, which form the short sides of the folded waveguide channel, eventually become part of the vacuum envelope. Vertical segments, which form the broad sides of the folded waveguide channel, become iron polepieces for a triple PPM-type magnetic circuit. The large polepieces extend through the vacuum wall to contact rectangular-shaped magnets.

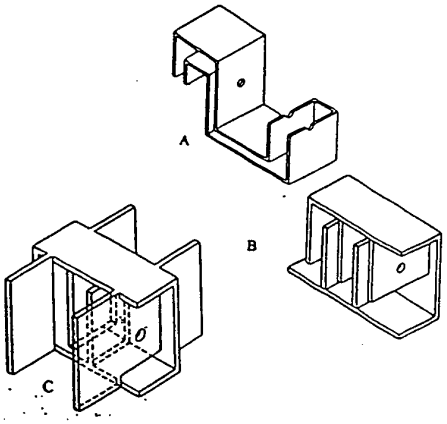

Figure 1. *Schematic development of the integral-polepiece folded-waveguide circuit.*

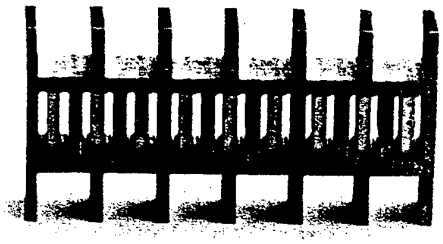

Figure 2. *Copper-plated folded-waveguide circuit without covers.*

For this circuit design, the polepieces extending through the vacuum envelope create a planar magnetic field pattern that allows heat sinks to be placed near the beam tunnel. The resultant short thermal path for both rf losses on the circuit and body current dissipation on the tunnel wall creates a thermally rugged device. For example, a high average power PPM-focused TWT similar to that described below, uses copper block heat sinks, instead of plates as in Figure 1, to cover the circuit. As a demonstration of thermal ruggedness, this TWT dissipated 1000 watts of beam interception on the tunnel wall while generating 1000 watts of average power.

Besides being thermally rugged, the circuit assembly promises to be low cost during production. The planar surfaces simplify electron discharge machine work and the laminar-block approach to fabrication eliminates the high cost of machining many small parts.

Baseline TWT

Figure 3 shows a baseline TWT that has a length under ten inches and a weight under four pounds. In this baseline TWT, the gun, windows, body and collector are optimized for reliable lightweight applications.

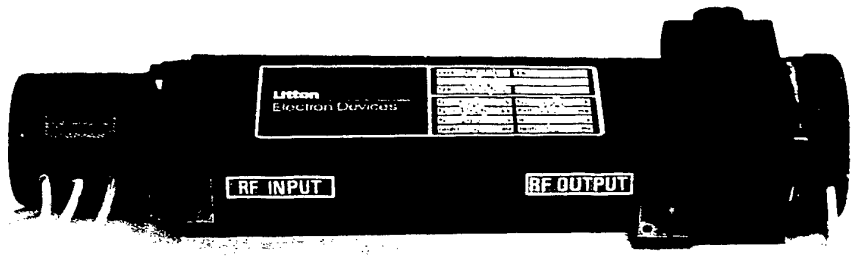

Figure 3. *A baseline folded-waveguide Ka-band TWT.*

The shadow-gridded Pierce-type gun is similar in construction to others used on Litton lightweight TWTs. The present gun uses a 0.25 inch diameter, M-type, barium-impregnated cathode with a 6.3 volt filament to form 0.25 microperveance beams. With cathode current loading levels below 3 A/cm^2, mean cathode depletion lifetimes can exceed 20,000 hours.

A beam area compression of 39 results in low transverse beam temperatures around 20 eV and consequent good focusing. Both grids have Litton-patented "T" shapes to provide small grid-voltage swings that help high-PRF pulse forming. Typically, with respect to the cathode voltage, the cutoff voltage is -200 V and the full-current grid drive is +150 V.

The block window is a Litton-patented design that combines the thermal ruggedness of a half-wavelength-type window with the broadband match of a thin-disk window. Ideal for handling high average powers in stressful environments, the Ka-band window has a typical return loss between -18 dB and -30 dB in the frequency range between 28 GHz and 40 GHz. These window assemblies are attached directly to the TWT body to increase structural rigidity.

The circuit assemblies use perforated block-type circuit covers. This results in a rigid lightweight structure without losing the above-mentioned thermal ruggedness. Also, clearly, the small magnets that fit between polepieces of the circuit in Fig. 2 contribute to lightweight.

The TWT presently uses a conduction-cooled collector with a wrap-around baseplate to eliminate unnecessary thermal gradients. Although this collector handles higher thermal loads with liquid cooling, the present compact design can dissipate 1000 watts per inch of collector length and provide depression levels as high as 75 percent of the cathode voltage.

Figure 4 shows the saturated output power versus frequency for a baseline TWT that operates with a 21 kV beam. Cathode currents vary between 550 mA and 600mA and provide output powers between 1100 watts and 1250 watts. Typically, for a baseline TWT, the beam transmission levels without rf are between 96 percent and 98 percent. With saturated rf output and with -12.5 kV on the collector, body currents are typically between 0.04 A and 0.06 A. Small-signal gains are typically between 45 dB and 55 dB. Average powers are typically above 250 watts.

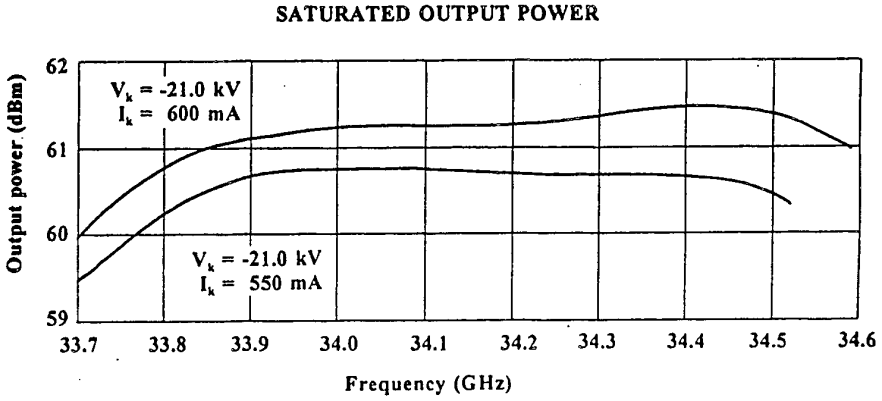

Figure 4. *Saturated output power versus frequency for a four-pound baseline TWT.*

Ongoing Developments

Presently, the folded-waveguide circuit is being modified to develop designs with lower beam voltage, with increased average output power, and with operating frequencies at W-band.

The total weight of an amplifier with power supply is generally low when beam voltages are low. To achieve low-voltage operation with PPM-focused beams, polepieces must be close enough to fulfill the condition $\lambda_p/L > 2.4$, where λ_p is the plasma wavelength of the electron beam and L/2 is the separation between two adjacent polepieces. Unlike the large-diameter widely separated polepieces that lie outside the vacuum envelope of the all-copper types (e.g., coupled-cavity, interdigital-line, folded-waveguide, etc.,) of millimeter-wave circuits, Litton's folded-waveguide polepieces extend to the beam tunnel. This results in λ_p/L values above 9 for a 20 kV 0.25 microperveance beam and suggests that lower voltage designs will be useful. One such Ka-band TWT, designed to operate across one GHz of bandwidth with 16 kV, 0.95 A beams, produced over 200 watts of average rf output. However, further work remains on this design.

In another development, average powers were increased above those of the baseline TWT. A circuit modification resulted in 99% dc transmission and 97% rf transmission. Increased baseplate cooling and a double-size collector resulted in CW operation, during which, the TWT generated average output powers between 1000 watts and 1250 watts. With optimized operating conditions, 1500 watts of average power was demonstrated at a single frequency. This eight-pound TWT, which is shown in Figure 5, is expected to weigh under 5 pounds after weight reduction.

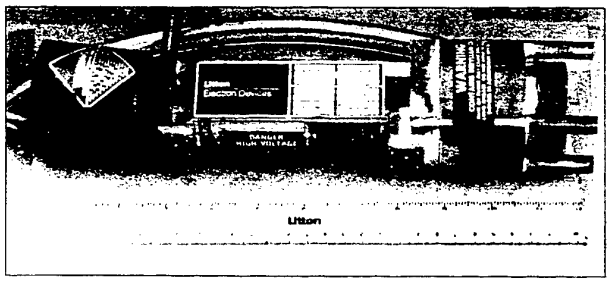

Figure 5. *Folded-waveguide Ka-band* TWT that produced 1500 watts of average power.

Finally, this technology is being extended to W-band by scaling Ka-band parts down by a factor of 2.7. Usually average powers must be reduced with such scaling since additional beam compression increases beam temperatures and results in degraded beam transmission. However, a gridded gun is being developed to produce beams having temperatures of beams from gridless guns. With this gun, 20 kV 0.7 A beams can be focused inside a smaller W-band tunnel. The 250 watts of average output seen at Ka-band can be expected at W-band

Summary

A new type of millimeter-wave TWT which uses a novel folded-waveguide circuit has been developed for high-power lightweight applications. The TWT is low-cost, lightweight and reliable while operating in stressful environments. Capable of high average output powers, a new design ran CW producing over 1500 watts of rf output. The small separation of the polepieces in the magnetic circuit suggests that TWTs can be built to operate at 16 kV. Also, by incorporating a low-temperature gun, this TWT can be scaled to W-band frequencies.

References

(1) A. J. Theiss, D. B. Lyon, and Y. Hiramatsu, "An Integral-Polepiece Folded-Waveguide Slow-Wave Circuit for High-Power Millimeter-Wave TWTs," IEDM, Washington, DC, December 1993, pp. 149-151.

(2) This TWT is covered by pending and issued patents in the U.S. and other countries.

(3) A. J. Theiss and D. B. Lyon, "High-Power Ka-Band TWTs for Airborne Radars," IEEE AES Magazine, November 1995, pp. 33-36.

(4) Y. Hiramatsu, "Thick Waveguide Windows for High-power Wideband Microwave Tubes," Microwave Power Tube Conference, Monterey, CA, May 1984.

PROGRESS IN 94 GHz TWT DEVELOPMENT

P. Malzahn, G. Lippert

AEG Elektronische Röhren GmbH
Ein Unternehmen der THOMSON TUBES ELECTRONIQUES

Abstract:

The development of mm TWT requests new solution for a field of new problem areas, resulting from the dimension related to the frequency. Thermal effects of the electron emmission have a major effect on the gun optics and the magnetic focusing design. The design of the TWT is done for the following data's:

Frequency	94 GHz range
Peak output power	>100W
Bandwidth	> 500 MHz
Duty cycle	above 5 %
Beam voltage	< 22 kV

At 94 GHz 1 mm is a large dimension, 0.01 mm an uncertain tolerance.
The usual surface roughness is allready much more than the skin depth of 0.5 microns.
To overcome the problem new most simple solutions were searched and found.
The delayline will be like two combs. The matching network and the internal sever loads are mainly part of the delayline. The gridded gun is thermally optimised for a beam diameter of 0.3 mm and 0.15 A current.
Interim hardware results of the beam tester, the delayline and the matching network are presented.
A power supply will be developed in parallel. In 1998 a complete amplifier will exist to be used for flight carrier experiments.

HIGH POWER MILLIMETRE WAVES FROM EXTENDED INTERACTION KLYSTRONS.

Chris Nilsen, Brian Steer
Communications & Power Industries Canada Inc.
(formerly Varian)

Abstract

The Klystron amplifier is recognised throughout the world as a rugged and reliable RF power source. They are used in very large numbers for Communications and Radar applications. The microwave spectrum is becoming fully utilised, thus intensifying the need to occupy the millimetre wave spectrum.

Extrapolating microwave vacuum electron devices into the MMW range presents the designer with the challenges of fabricating miniature precision parts, operation at increased voltages, and control of high current density electron beams. These problems are common to Magnetrons, TWTs, and Klystrons.

In the case of the MMW Klystron, CPI Canada has developed an efficient design using a high impedance "ladder" RF circuit. The "ladder" is a section of resonated slow wave structure, giving rise to the acronym "EIK" for "Extended Interaction Klystron." In combination with a permanent magnet, this provides high RF interaction efficiency at a low operating voltage. The small "ladder" circuit is manufactured in one piece very reproducibly using electron discharge machining.

CPI's Klystron technology produces high power at millimetre wave frequencies: 2kW to 40 W from 25 GHz to 220GHz. They are reliable, mature devices that have been manufactured since 1970.

The presentation will describe the operating and construction principles of the EIK, and the resulting performance characteristics, and design trade-off for size, weight, power and life. Particular attention will be paid to the performance at Ka-band and W-band where proposals for communications and for space borne (Cloud) radar are being considered.

CPI has been manufacturing millimetre wave klystrons for over 25 years. It was quickly recognised that if a reliable high power source was to be developed it should combine the attributes of the highly successful klystrons with the efficiency of the extended interaction circuit.
Extended interaction circuits have often been used to increase power and bandwidth[1].

Why use Extended Interaction ?

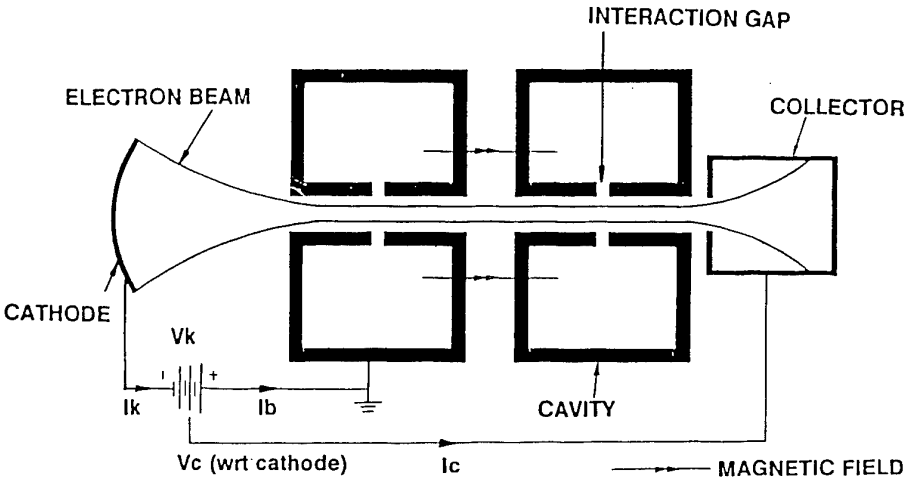

Fig.1. Conventional re-entrant cavity Klystron Schematic

Suppose that a conventional 9.5 GHz Klystron capable of producing 1kW with 45dB of gain were scaled to 1/10 using conventional vacuum device materials. The frequency would scale to 95GHz however the designer would be presented with some impractical problems.
For example
Gain Scaling
* RF gain is proportional to frequency$^{-n/2}$ and cavity Q decreases as a result of increased skin effect losses at higher frequencies.
i.e.

$\therefore$ for a 4 cavity Klystron gain is reduced by 20dB

Magnetic Field Scaling
* The magnetic field strenght is inversely proportional to the beam radius for a given beam current. The calculated field is generally increased by 2.5X, this is called the Brillouin field. Beam radius is usually proportional to frequency.
i.e.

$\therefore$ for a 9.5 GHz Klystron with 2,000 gauss Brillouin field

The magnetic field requirement at 95GHz would increase to 20,000 gauss

A practical maximum using iron pole-pieces and permanent magnets is 10,000 gauss.

Electron Gun Scaling
* Using a constant beam convergence in the electron gun design, the cathode radius scales directly with beam radius and thus with frequency. Current density at the cathode surface (cathode loading) is increased by a power 2.
i.e.
a 9.5 GHz Klystron with cathode loading of 1 amp/ sq.cm. would become
100 amps/sq.cm, at 95 GHz. This is 10X above the accepted values for useful life.

Conclusion

As a result of the above limitations, millimetre wave vacuum devices are usually characterised by higher beam voltage and lower beam current compared to their lower frequency counterpart. Finally these limitations maybe alleviated by considering the following relationship:
i.e.

$$P_{rf} \alpha \text{ (beam conductance).(cavity impedance)}$$

Since we are forced to reduce beam conductance , we compensate by increasing R/Q by using the extended interaction (ladder) circuit.

Typically a single gap Klystron cavity $R/Q = 100$

Whereas a 95 GHz EIA ladder $R/Q = 300$

The EIA concept.

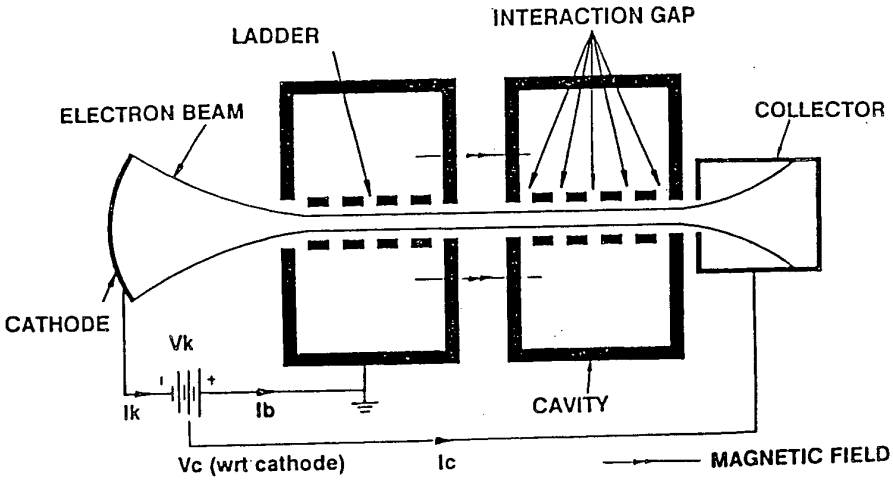

Fig.2. EIA Schematic

The single gap in each cavity of a Klystron is replaced in the EIA by a resonated slow wave circuit. The rf circuit now is comprised of a number of long and short slots in an enclosing tunable cavity. The sketch shows only 2 cavities but there are typically 5 or 6 cavities in an EIA.

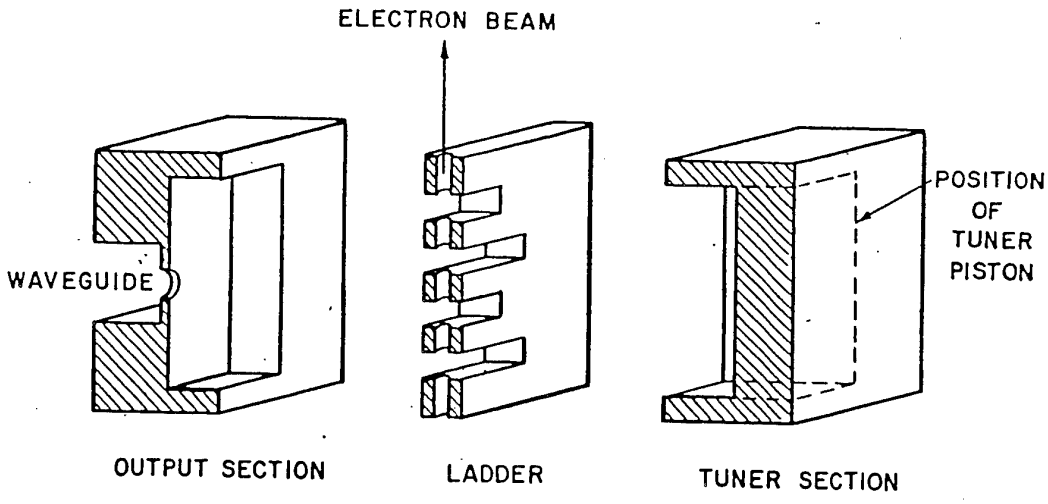

Fig. 3. RF Circuit (ladder) in a single cavity

The slot width is determined by the desired operating frequency and slot height by the desired or necessary operating voltage. An electron beam is focused down a tunnel cut through the centre of the slots and ladder.

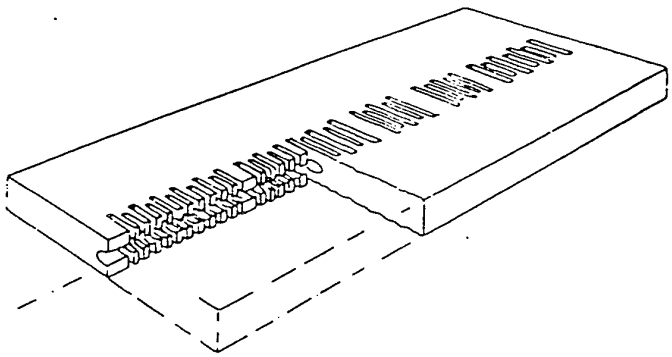

Fig 4. EIA RF Circuit (ladder)

The beam velocity is adjusted by the applied beam voltage, so that a particular electron experiences the rf field in the same phase as it passes each gap in the circuit. Thus, the total impedance experienced by the electron beam is the product of gap impedance and the number of gaps. The resulting high interaction impedance provides high power and gain using conventional electron optics. The EIA cavities may be stagger tuned in a similar fashion to single gap Klystron cavities to maximise gain . bandwidth performance.
The penalty of the extended interaction circuit is increased circuit length. This becomes physically insignificant at millimetre wavelengths when compared to the dimensions of other components such as the magnets and collector assembly of the Klystron.
The type of rf circuit described above is commonly called a ladder circuit.

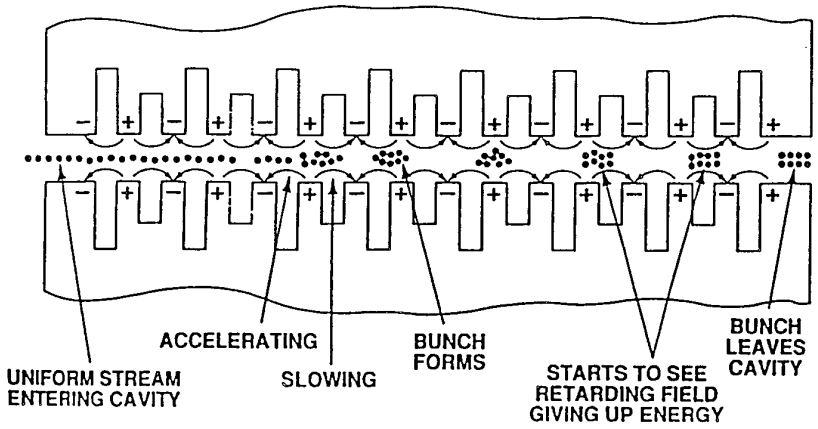

Fig. 5. Electron bunching in the ladder

Like other linear beam vacuum electron devices this Klystron relies on a velocity modulated electron beam converting to density modulation and subsequent conversion into rf in an extended interaction output cavity. The output cavity is coupled to a waveguide to extract the power.

A particular challenge in the design of a millimetre wave Klystron is a well focused and confined electron beam. This is achieved by use of highly refined computer modeling, precision assembly techniques, and high performance cathodes and magnetics. The goal is to produce an electron beam diameter of approximately 0.25 mm. with minimal ripple and cause the beam to pass as close as possible to the beam tunnel without collision. Thus allowing the circuit to be heated mainly by rf losses, enabling the thermal capability of the copper circuit to be utilised for maximum rf power.

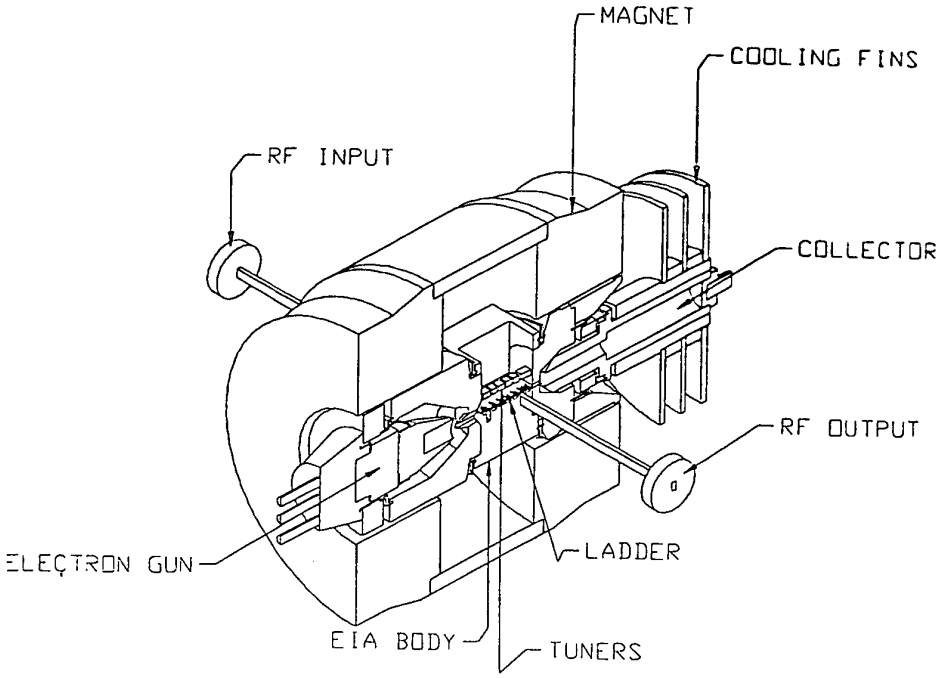

Fig.6. EIA assembly in 3D

The EIK is fabricated using materials and joining techniques proven by many years of experience in vacuum electronics whilst implementing novel techniques for precision machining and alignment. The CPI EIK has been used in varied environments, demonstrating it is a rugged and reliable component for radar and communications applications.

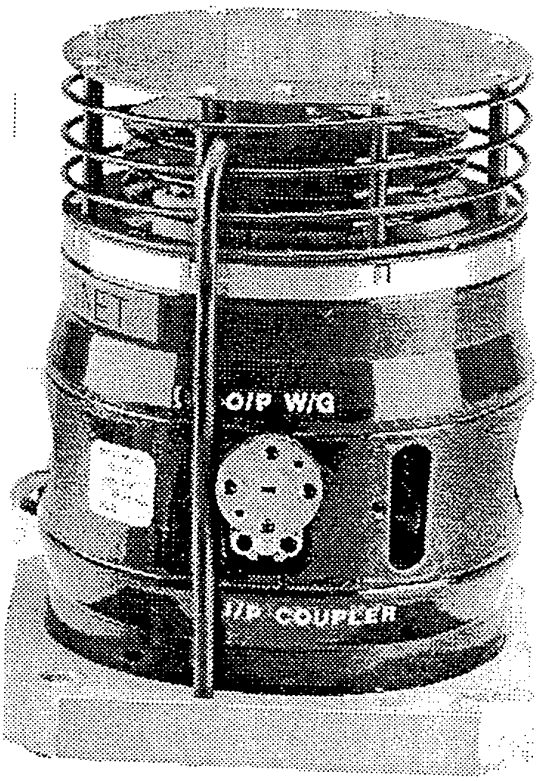

Fig. 7. 95GHz EIA Model VKB2461

Performance

CPI has EIKs available over a frequency range of 25 to 220 GHz to capable of matching an extensive range of performance requirements. We use a standard line of electron guns, magnets and other components where we have gained considerable experience in their use and performance capability. This typically results in CW EIKs operating up to 10,000 volts and pulse Klystrons operating up to 21,000 volts. A plot indicating rf power capability across the frequency range is shown.

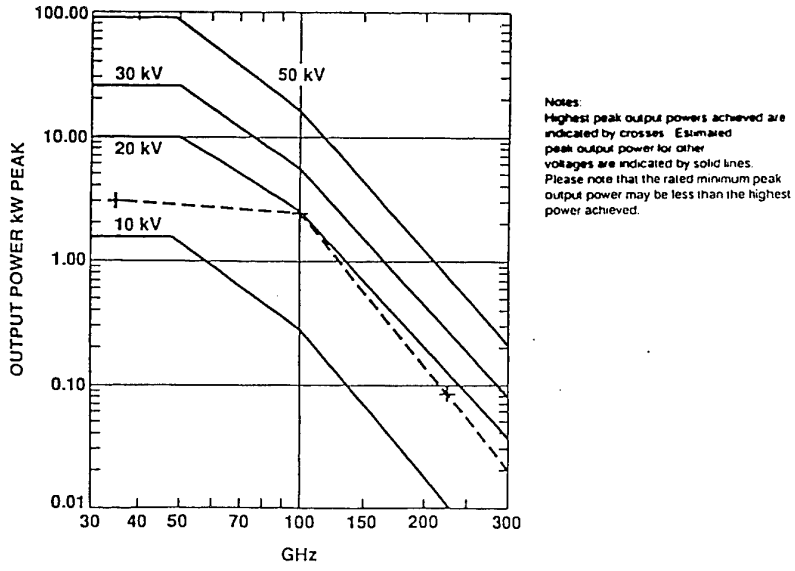

Fig. 8. Power vs frequency for various beam voltages

Typical performance.

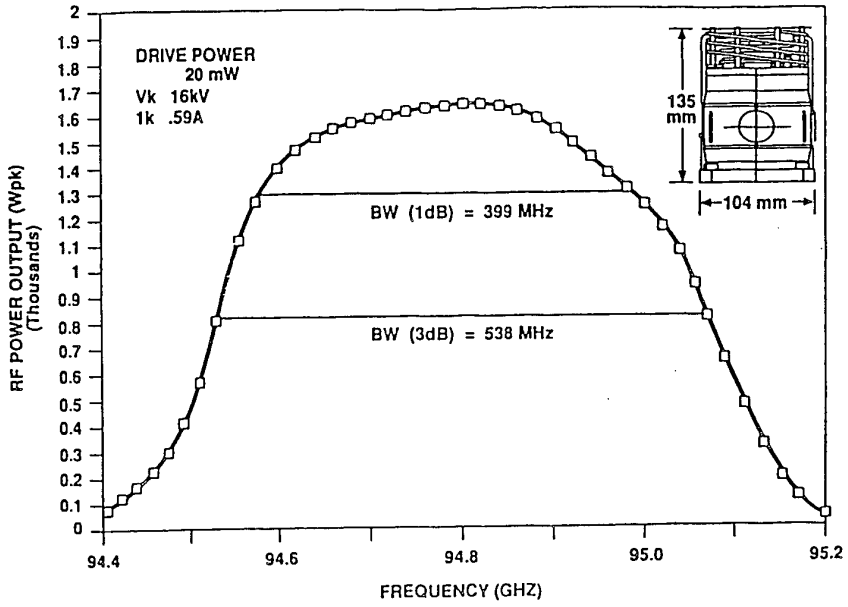

Fig. 9. 95 GHz Pulsed EIA bandpass plot

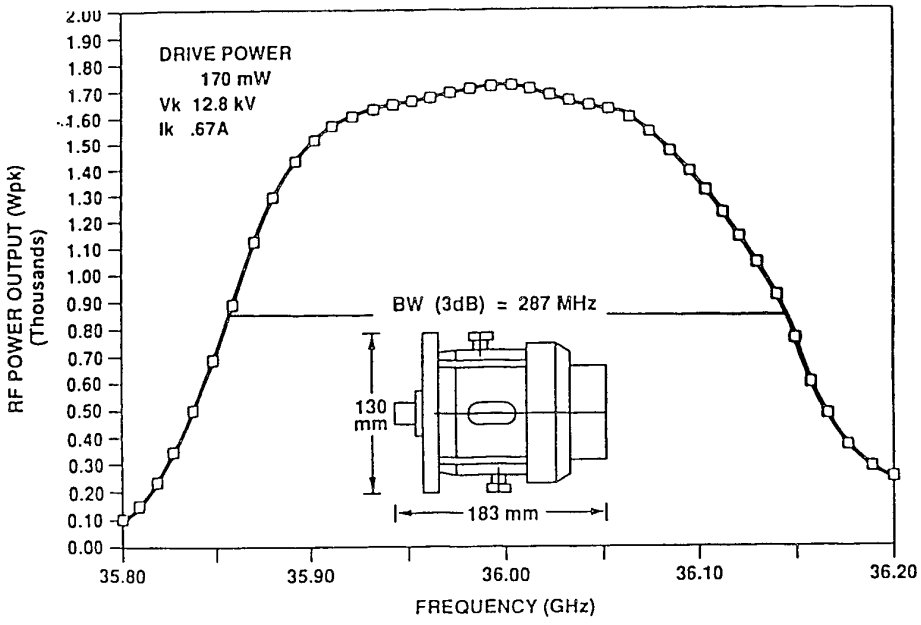

Fig. 1. , 35GHz Pulsed EIA bandpass plot

[1] M. Chodorow and B. Kulke. An Extended Interaction Klystron: Efficiency and Bandwidth. IEEE Transactions on Electron Devices 1966 Vol. ED-13, No. 4. page 440

MAGNETRON FREQUENCY TWINNING

R.G. Carter
Engineering Department, Lancaster University, Lancaster LA1 4YR, U.K.

E.M. Ball and M.B. Brady
EEV Ltd, Waterhouse Lane, Chelmsford CM1 2QU, U.K.

Abstract

Pulsed magnetron oscillators sometimes show an instability known as 'twinning' in which the spectrum shows two, or more, closely spaced peaks. This phenomenon is undesirable and can lead to problems when it occurs in magnetrons used in radars. An experimental investigation of twinning is described from which conclusions are drawn about the design parameters which affect it. It has been shown that changes in factors such as the magnetic field strength, the external match, the cathode coating and the cathode temperature can be used to reduce the probability of twinning or to move the point at which it occurs outside the normal operating range of the tube. A possible theoretical explanation is discussed.

1. Introduction

An instability, known as twinning (Ref.1), is exhibited by some magnetrons under certain operating conditions. This instability causes the magnetron to oscillate at two (or sometimes more) frequencies. Figures 1 and 2 show examples of the frequency spectrum of a low power X-band magnetron. Both spectra were produced by the same tube but at different anode voltages. Figure 1 shows the desired spectrum when the tube is not twinning. When the tube is twinning (Fig. 2) the spectrum shows two peaks separated by only a few MegaHertz. Although this phenomenon has been known for many years it has received surprisingly little attention in the literature. Not all magnetrons suffer from twinning and, in many cases, it does not occur within the normal operating range of the tube. When it does occur, however, it can cause a significant number of tubes to be rejected during manufacture. It may also develop during the life of a tube as a result of aging processes with the consequence that the system in which it is installed does not perform as expected. This paper describes the results of an experimental investigation which aimed to gain a greater understanding of twinning and of the factors affecting it.

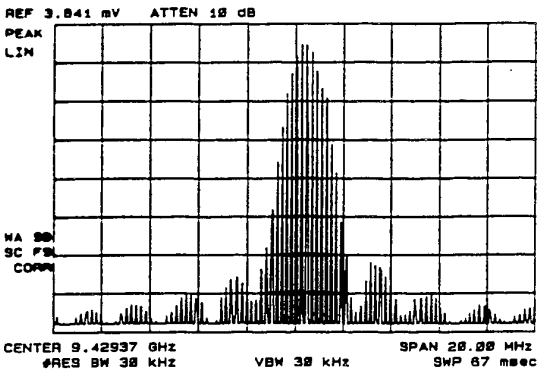

Fig.1 Normal magnetron spectrum

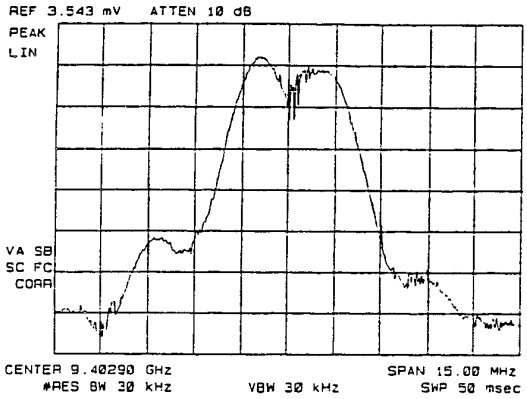

Fig.2 Magnetron spectrum showing twinning

2. Magnetron Performance

A magnetron is a diode which conducts very little current as the anode voltage is increased from zero until the threshold voltage is reached at which oscillations begin. The oscillations then build up rapidly until the output power saturates. Once the tube is oscillating the anode voltage is not found to vary very much over quite a wide range of anode currents. Figure 3 shows the relationship between the anode voltage and current for a typical tube. It can be seen that the current/voltage relationship also depends on the strength of the axial magnetic field in the interaction region. The lines in the current/voltage plot commonly exhibit discontinuities which are known as 'Gauss line discontinuities' (Ref. 1).

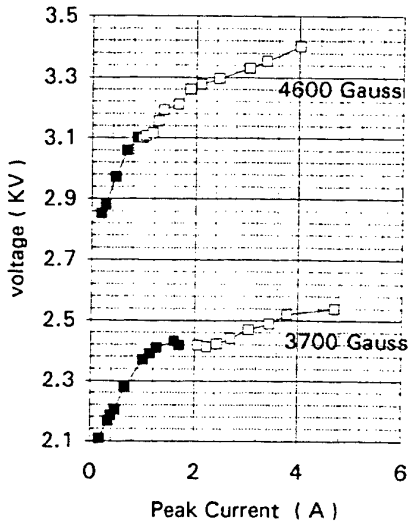

Fig. 3 Typical current/voltage curves

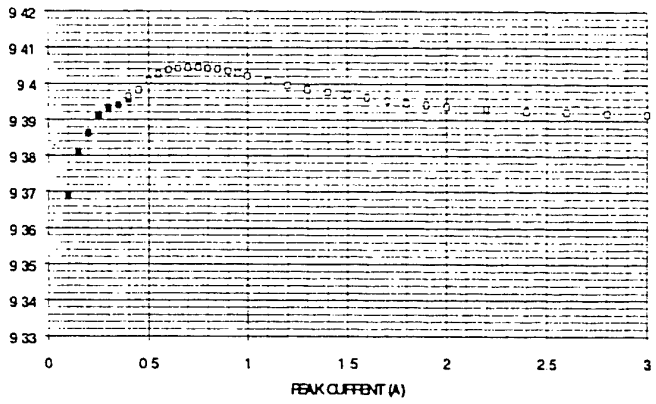

Fig.4 Typical frequency pushing curve

The frequency of oscillation of a magnetron is determined by the resonant frequency of the anode in its π-mode modified by the effects of electron loading. These cause the frequency to change as the anode current changes, a phenomenon known as Frequency Pushing. Figure 4 shows a typical frequency pushing curve for a modern magnetron. The tube is designed to be operated in the region to the right of the peak of the curve so that the frequency is not strongly dependent on the current. The kink in the curve just to the left of the peak is seen in some tubes and twinning commonly occurs close to this point. Twinning may also occur at higher currents within the normal operating range of the tube. It is observed that, even in tubes which do not twin, there is a marked change in the spectrum in the vicinity of the kink in the pushing curve. This is generally attributed to the rapid change in the slope of the pushing curve in this region. The frequency of oscillation is also affected by the amplitude and phase of any external mismatch. This changes the reactive loading on the anode resulting in Frequency Pulling.

3. Observations of Twinning

An extensive series of experimental observations was carried out on standard and modified low-power X-band pulsed magnetrons. The permanent magnets were removed from the tubes to allow them to be operated in an electromagnet so that the magnetic field strength could be varied. It was also necessary to modify the modulator so that fine adjustments could be made to the anode voltage because twinning commonly occurs over a very narrow range of operating conditions. Observations were made of the current, voltage and r.f pulse waveforms and of the frequency spectrum. The onset of twinning was observed in the spectrum and also in the splitting of the R.F. output pulse as shown in figure 5. When a sequence of r.f output pulses was recorded it was found that there were two pulse shapes which occurred randomly with, occasionally, some intermediate shape as shown in fig. 6. From this it appears that the magnetron may switch during a pulse between two states which have different anode currents and frequencies of oscillation. It is important to distinguish between these states and the modes of oscillation associated with different resonances of the anode. When a change of the anode mode takes place the magnetron is said to be 'moding' or having 'missing pulses' and the effects are much larger than those associated with twinning.

Additional studies were carried out using a much wider range of magnetron types to find out which design parameters might be relevant to controlling the occurrence of twinning. This study showed no clear correlations except that twinning was much more likely to be observed in tubes for which the ratio of the cyclotron frequency to the frequency of oscillation lay in the range 0.75 to 1.25.

3.1 Dependence of Twinning on the Voltage Pulse

When a tube twins it does so over one or more quite narrow ranges of the anode voltage and some care is needed to make sure that an occurrence of twinning is not missed. Twinning may coincide with a Gauss Line

discontinuity, but this is not necessarily the case. Not all discontinuities are associated with twinning, and twinning may occur where there is no observable discontinuity. In the latter case it may be that there is a discontinuity which is too small to observe. The frequency difference between the two states of the twin was found to be related to the change in the anode current, and to the slope of the frequency pushing curve at that point, so that large current changes tended to be associated with relatively larger frequency jumps. As the anode voltage was increased through a region of twinning it was observed that there was a steady change in the proportions of the pulses at the two frequencies.

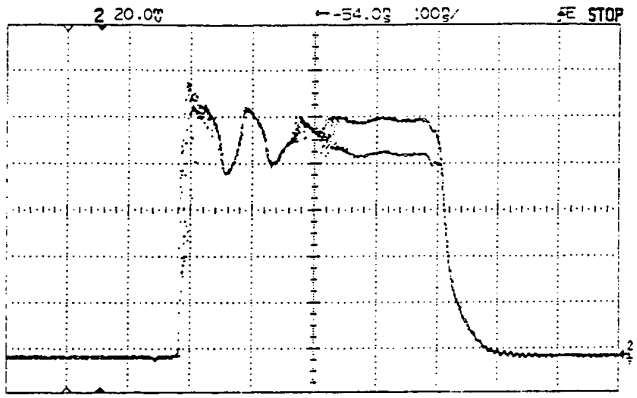

Fig. 5 Typical R.F. pulse when the tube is twinning

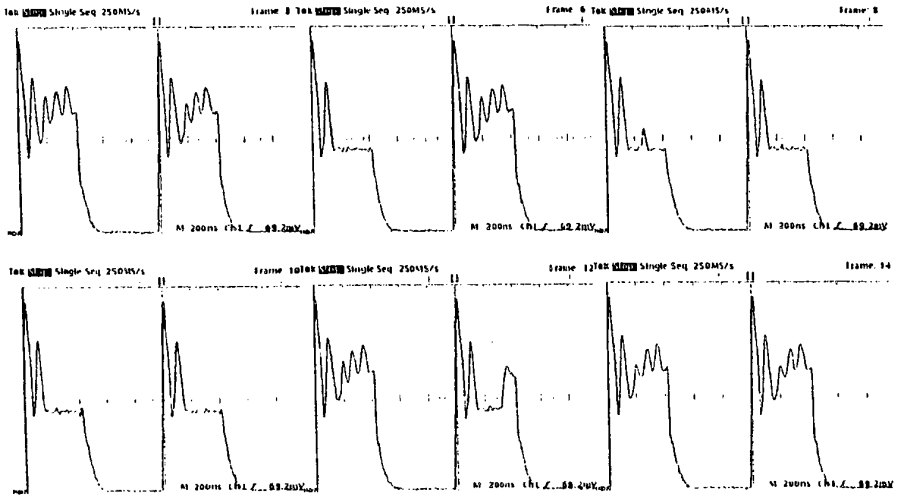

Fig. 6 Example of a sequence of R.F. output pulses when the tube is twinning

For the high current twin it was found that the split in the current pulse occurred somewhere close to the centre of the pulse. When the pulse was then shortened the twinning disappeared. This is consistent with the view that the tube is switching from one state to another during the pulse. For the low current twin, on the other hand, the split in the current pulse appeared to occur at, or near, the beginning of the pulse. The change of state must therefore be happening very rapidly early in the pulse or else, for this type of twinning, the frequency must be changing from pulse to pulse.

If twinning is associated with changes between different states of the electron cloud within the tube then it might be expected that it would be influenced by changes in the impedance of the modulator. We did observe changes in the frequency jump associated with the twin as a result of changes in the modulator impedance, but we were not able to eliminate twining by this means.

3.2 Dependence of Twinning on the Magnetic Field

An investigation was carried out into the effect on twinning of changes in the magnetic field in the interaction region. The range of field strengths which could be used was limited to those for which the magnetron would operate stably. Figure 7 shows the frequency pushing curves at three different magnetic fields for a tube which twinned at both low and high currents. The lower current at which twinning occurs did not change much with magnetic field, whereas the higher current varied widely with changes in the field. This suggests that there may be at least two different types of twinning with different underlying physical mechanisms. In this tube it would be possible to keep the normal operating range free from twinning by a suitable choice of the magnetic field.

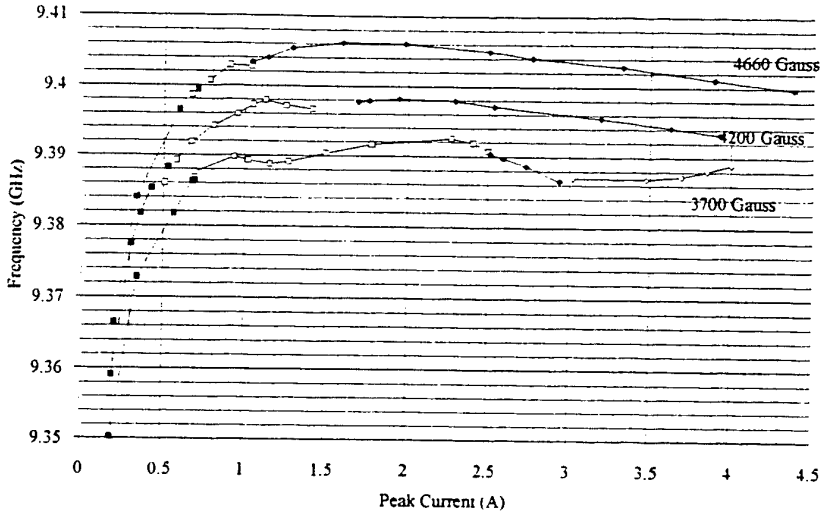

Fig. 7 Frequency pushing curves showing the dependence of twinning on magnetic field

3.3 Dependence of Twinning on the Cathode

It was known from earlier studies that twinning could be affected by changes in the composition of the cathode coating. Experiments were carried out in which the heater power was changed. This was also found to have a marked effect on the twinning but in ways which differed appreciably between nominally identical tubes. In some cases a change in the heater power caused additional twinning frequencies to appear. There was also a change in the frequency jump but the change was an increase in some tubes and a decrease in others. The change in the heater power generally moved the twin to a different operating point and it also affected the frequency through changes in the temperature of the anode.

The concentricity of the cathode is also known to have an effect on twinning. On occasion it is possible to improve the performance of a tube by moving the cathode sideways. Unfortunately it is not easy to tell in any individual case whether the performance has been improved by increasing or decreasing the concentricity. Experimental tubes were manufactured in which the cathode was deformed so that its cross-section was no longer circular but this was found to make little difference to the twinning.

3.4 Dependence of Twinning on the External Match

A variable mismatch whose amplitude and phase could be varied independently was inserted in the output waveguide. The tube was first adjusted to be twinning without any mismatch and the mismatch was then introduced and the behaviour of the tube noted as the amplitude and phase were varied. Figure 8 shows a typical set of results in which the reference plane was chosen so that the points at which twinning was observed lay on the circle corresponding to a mismatch having a real part equal to unity. The twinning could therefore be stopped by changing the mismatch though this presumably moved it to a different operating point rather than eliminating it completely. This was confirmed by setting the anode current to values above and below the twinning point when it was found that the tube could be induced to twin by adjusting the external match. In each case the twinning region divided the chart into two regions in which the shapes of the spectra were different and corresponded to those observed at anode currents above and below the twinning point.

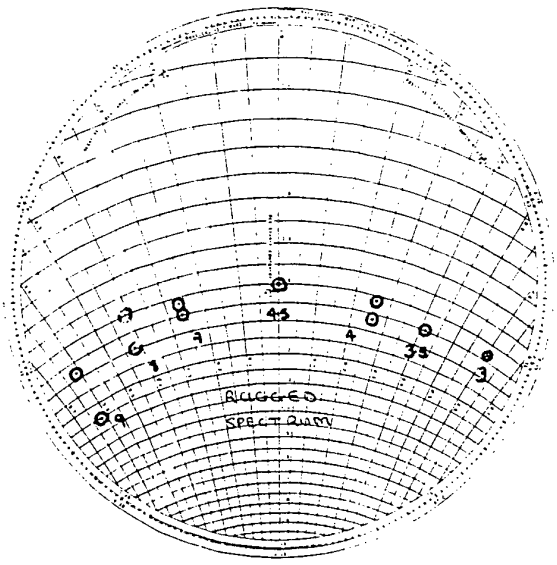

Fig. 8 Rieke diagram showing the effect of external mismatch on twinning

4. Discussion

There seems to be little doubt that twinning is caused by changes in the state of the electron cloud within the magnetron. The existence of twinning and of Gauss Line discontinuities at more than one operating point suggests that there are a number of possible states each of which:

i. is stable over a certain range of operating conditions
ii. has its own Gauss line, and
iii. has its own spectrum

Both twinning and Gauss Line discontinuities would therefore occur under those conditions in which there was a change in the most stable state. Since the oscillation of a magnetron starts up from random noise it would follow that, when two states were equally stable, oscillation might occur in either of them with random occurrence from pulse to pulse. In other cases the starting conditions might be such as to select an unstable state with the possibility of a jump to a more stable state during the pulse. It is not clear, however, whether the twinning observed at different currents is associated with one, or more than one, way in which the state of the electron cloud can change.

Schumacher (Ref. 1) suggested that twinning was caused by axial variations in the electron cloud associated with axial variations in the strength of the magnetic field. His hypothesis was that there could be two, or more, elementary magnetrons each of which would have a slightly different frequency because of the different electron loading of the anode. The frequency would then be determined by whichever of these elementary magnetrons represented the preferred state. We used computer simulation to investigate the uniformity of the magnetic field in the magnetrons used in our experiments. It was concluded that the departures of the field from uniformity were unlikely to be big enough for Schumacher's hypothesis to explain the mechanism of twinning in these tubes.

An alternative, and more attractive, hypothesis is based on the work of Slater (Ref. 2) who showed that the inner electron cloud can have a variety of stable states of which the familiar Brillouin flow is only one. In Brillouin flow the electrons in the inner space-charge follow concentric paths around the cathode and the charge density is uniform. In the other states identified by Slater the electrons follow paths which move from the cathode out to the perimeter of the cloud and back to the cathode again. The inner space charge is then found to have a number of concentric layers of alternately high and low density. The number of layers in the state which had the greatest stability might be expected to vary with the anode voltage and current, the magnetic field and the balance between primary and secondary electron emission from the cathode. Since the anode current, drawn from the inner space-charge cloud, is dependent on the r.f. interaction with the fields of the anode it might also be expected that the stability of each state would be affected by changes in the anode fields produced by an external

mismatch. It seems to us that this hypothesis is broadly consistent with our experimental observations and worthy of closer study.

5. Conclusion

The experimental study carried out has added considerably to our knowledge of the phenomenon of twinning. Design parameters having a critical effect on the occurrence of twinning include the choice of magnetic field, of cathode coating and of cathode temperature. By careful choice of these it is possible, in many cases to eliminate twinning or to move the points at which it occurs outside the normal operating range of the tube. A hypothesis has been advanced which is broadly consistent with our experimental observations. Further research is needed to investigate this hypothesis in detail.

6. Acknowledgements

The support of this work by EEV Ltd and by a Co-operative Research Grant from the Engineering and Physical Sciences Research Council is gratefully acknowledged. The authors wish to thank Mr N.S. Nicholls for helpful discussions and EEV Ltd for permission to publish this paper.

7. References

1. Schumacher, C R, Spectrum Shape, in: Okress, E (Ed.), *Crossed-Field Microwave Devices*, Vol.2., Academic Press, New York, 1961

2. Slater, J C, Microwave Electronics, Dover, New York, 1969

SESSION 6
TWTAs Technologies & Reliability

Chairman: G. Kornfeld (AERG-ULM, Germany)

VACUUM INSULATOR FLASHOVER

MECHANISMS, DIAGNOSTICS AND DESIGN IMPLICATIONS

Jos M. Wetzer

High-Voltage and EMC Group, Eindhoven University of Technology
PO Box 513, 5600 MB Eindhoven, The Netherlands
phone +31.40.247.4492 fax +31.40.245.0735 email J.M.Wetzer@ele.tue.nl

ABSTRACT

This paper presents an approach for obtaining science-based answers to practical vacuum device problems. Recent research on insulator flashover mechanisms, diagnostics and geometry considerations is reviewed, with emphasis on the implications for device performance and design. Secondly, an overview is given of recent research activities, performed at the Eindhoven University of Technology, which aim at improved device performance, design guidelines and device diagnostics, for DC and AC vacuum devices.

1. INTRODUCTION

Scientific literature provides a wealth of information on fundamental processes and mechanisms important for breakdown or surface flashover in vacuum. Usually this information deals with simple geometries (vacuum gap, insulator between parallel electrodes). Industrial engineers, however, deal with complex devices, and with practical questions such as how to design, condition and operate a vacuum device. The question raised by scientists and engineers is how to translate scientific knowledge to design and operation practice.

In many cases the gap between scientific knowledge and engineering practice is too large for a direct translation. Laboratory studies may explain, but not predict, complex devices performance. The device complexity, on the other hand, does not allow to study fundamental processes in realistic designs. In order to bridge this gap we need to aim our research activities at providing science-based answers to practical problems. Such activities have to involve operational mechanisms (1) in simplified insulating structures (2) and should use appropriate diagnostics (3).

In contrast to **fundamental processes**, which describe a single type of event often active on a microscopic scale, **operational mechanisms** are the result of several fundamental processes, and are active on a macroscopic- or device-scale. In general, operational mechanisms modify device conditions or properties. An example is insulator surface charging which 1) is the result of fundamental processes (cathode electron emission, secondary electron emission from insulator surface), and 2) has a direct impact on the device performance. Research can establish how operational mechanisms affect the device performance, and what design rules can be deduced.

Although devices are too complex to study the impact of different mechanisms on the device performance, we can recognize **distinct problem areas**, such as vacuum gaps, insulating spacers and feedthroughs. With separate experiments we can simulate problem areas and study the impact of operational mechanisms on device performance in a realistic environment.

Appropriate **diagnostics** for the study of operational mechanisms in insulating structures should reveal how a mechanism (e.g. insulator charging) takes place, but also how it affects the overall performance.

Device applications, such as design modifications and design rules, can only be achieved in an interaction between science and industry. This interaction should involve the study of **mechanism**, the formulation and verification of **guidelines**, and the formulation and verification of **device modifications**.

In this paper present a review of recent literature, and we discuss recent research activities at the Eindhoven University of Technology aiming at improved device performance and at formulation of design rules for DC and AC insulating structures.

2. REVIEW OF RECENT LITERATURE

In this section we summarize the results of two literature reviews, one reported by Miller in 1993 [1], and an update by Wetzer reported in 1996 [2]. For the original sources the reader is referred two both reviews.

2.1 Mechanisms

Surface Flashover

We can distinguish three insulator flashover stages: 1) initiation, 2) flashover development and 3) final gas breakdown. Cathode triple junction field emission is usually regarded the primary initiating mechanism. In the two leading theories the flashover developes either through a secondary electron emission avalanche (SEEA), or through electron triggered polarization relaxation (ETPR). Other theories are reported as well,

and it seems that no single theory is capable of explaining the surface flashover development under all circumstances. In the final phase a gas breakdown takes place in desorbed surface gas or vaporized insulator material, although in some materials (silicon) breakdown is reported to occur in a highly conductive surface layer.

In recent years many authors report on light emission studies of (pre)flashover surface processes, surface (micro)structure and possible defects.

Surface charging

Many investigators recognize surface charging as an important mechanism in the surface flashover process, and report on the amount and distribution of charge, and on the charging speed. Recent studies show how the cathode geometry affects the charging process, and study the temporal evolution of the charging process with a 2D Monte Carlo simulation technique. Investigations at the Eindhoven University of Technology with many insulator shapes show how surface charging influences the flashover voltage and the conditioning process. The effect of surface charging is determined from flashover and conditioning studies in combination with a non-invasive charge removal technique.

Conditioning

The mechanisms commonly considered relevant for conditioning are removal of emission sites, removal of surface gas, or removal of surface contaminants. Recent studies show that also surface charging plays an important role. The conditioning speed, the conditioning stability, and the conditioning effectiveness depend drastically on the presence or absence of surface charge, and may be optimized by the choice of a proper geometry. With "silent" conditioning, charge traps (or collectors) are used to reduce the triple junction field and make conditioning unnecessary.

2.2 Diagnostics

Electrical diagnostics

Standard electrical diagnostics involve measurement of the dc- and time-resolved current, the voltage waveform and the flashover voltage. Recent studies report on partial discharge (PD) measurement for DC (providing information on charging processes) and for AC, where the analysis of phase resolved PD patterns provides information on the presence of defects.

Optical diagnostics

A variety of optical diagnostics is used in flashover studies: streak camera's, photomultiplier tubes, often with monochromators or filters for spectral resolution, CCD-camera's, often with image intensifiers, laser deflection techniques, X-ray detection, and Scanning Electron Microscopes.

Surface charge measurement

Surface charge distributions may be measured after voltage application (with one of the electrodes removed) with an electrostatic probe. This requires the probe or the insulator to move. Surface charge distributions are also determined with electron beam deflection. With the SEM-mirror-technique a surface is first charged with the SEM electron beam and subsequently observed with the same beam at lower energy. An electrical method which gives indicative information on charge accumulation makes use of the DC-current and PD behaviour of a stressed insulator upon stepwise voltage changes. A helpful tool in surface charge studies is the possibility of removing surface charge, without modifying the insulating structure, by admitting low pressure N_2-gas. This allows a study of the impact of surface charge on the insulator performance.

Other diagnostic techniques

Several studies report on chemical analysis such as desorbed gas analysis.

2.3 Insulating structures

Experimental insulating structures may be chosen to facilitate observation. Examples are a planar radial field system, or geometries with a transparent anode.

In other cases experimental geometries are chosen to resemble a device problem area. A number of authors report on the relation between insulator shape and flashover voltage, which is usually ascribed to the cathode triple junction field in combination with electron propagation processes along the interface. Methods reported for triple junction field control include the use of metal inserts in the insulator or insulators placed in recessed electrodes. Electron propagation is influenced by surface-area, material and treatment, and may be controlled by modifying insulator shape and surface properties. Recently the Eindhoven University of Technology used DC-insulator flashover studies to generate design rules which are applied to specific design problems. Design rules were derived by studying the relation between mechanisms and performance, and the relation between performance and design.

Occasionally, literature reports on specific designs, e.g. for accelerator tubes and spacecraft components.

2.4 Discussion

In recent years considerable progress is made in the study of fundamental processes and surface properties with new, in particular optical, diagnostic techniques. A satisfactory theory on vacuum insulator flashover is not available yet. Vacuum components are often designed by "trial and error" rather than on a scientific basis. Next to flashover theories, a systematic and scientific approach to design is required which aims at

the generation and verification of guidelines

3. DC INSULATING STRUCTURES

In this section we present recent work performed at the Eindhoven University of Technology and aimed at high-voltage design concepts for DC vacuum components. The experiments are described elsewhere [3,4]. We will present the key mechanisms for DC-flashover as derived from experimental results, and focus on the derivation of guidelines by relating mechanisms to performance, and performance to design.

3.2 Key mechanisms

Of the many processes occurring in a flashover event, a dominant role is played by (1) cathode electron emission, (2) insulator surface charging, and (3) high-energy electron impact.

Primary electron emission
Literature shows that the flashover voltage strongly depends on the insulator shape. To some extent this geometry effect can be ascribed to the effect of the cathode triple junction field on electron emission. Experiments show that this process is essential but insufficient to explain flashover behaviour. Therefore other mechanisms must be considered as well.

Surface charging
Experiments performed by the Eindhoven University of Technology and others have shown that insulator surfaces are charged during voltage application [2]. These experiments involve the DC current and partial discharge activity of insulators during stepwise or rampwise voltage changes. Conclusive evidence of surface charging processes was provided by an experiment, in which an insulator is first subjected to a DC voltage ór to a number of flashovers. After the power is switched off and the electrodes are grounded, a small amount of nitrogen is admitted to the vessel. As the pressure approaches the Paschen-mimimum a discharge is observed both optically and electrically. Without an external source present, the discharge is driven by the surface charge built up during the earlier voltage application. Experiments with different geometries show that this behaviour can not be explained by polarization relaxation. Also probe-experiments give clear evidence of surface charge [1,5].

Surface charging is a key mechanism in both the flashover ánd the conditioning process. This is demonstrated with the measurements shown in Fig.1. When subjecting an insulator to a number of successive flashovers, the flashover voltage increases. After a flashover voltage of 60 kV is reached, charge is removed from the insulator surface with a low pressure nitrogen discharge with no voltage applied. Subsequently the series of flashovers is repeated. These experiments show that:

1. the insulator surface collects charge during repeated flashovers;
2. the flashover voltage gain obtained during conditioning is partly, but not solely, due to surface charging: the faster rise in flashover voltage in the second series shows that also a more permanent conditioning has taken place, ascribed to the removal of emission sites;
3. the gain in flashover voltage may be lost when the surface charge is lost.

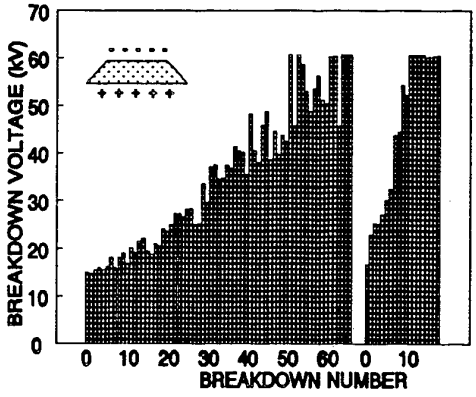

Fig.1 Measured flashover voltage evolution. After reaching a flashover voltage of 60 kV, the surface charge is removed with a low pressure nitrogen discharge (no voltage applied).

High-energy electron impact
Electrons impinging on the insulator surface contribute to surface charging or gas desorption. Unless electrons are safely trapped, a field distribution which forces electrons to move towards the surface, either by shape or by positive surface charge, causes a reduction of the flashover voltage, especially at high electron energy [6].

3.3 Relating mechanisms to performance

Experiments as in Fig.1 have been performed for many insulator geometries. The results are shown in Table 1. The insulator performance is characterized by so-called "performance parameters":

1. the initial or unconditioned flashover voltage
2. the conditioned flashover voltage
3. the conditioning speed
4. the conditioning stability

The number of flashovers required to reach a flashover field of 10 kV/mm is used as a measure for the conditioning speed, the drop in flashover voltage after removing the surface charge is a measure for the conditioning stability. In Table 1 the insulators are divided in four groups based on their performance.

Table 1

Results of flashover evolution experiments. The averaged flashover field is defined as the flashover voltage over electrode distance (5 mm). All values are averaged over two samples. Before charge removal samples are conditioned up to 12 kV/mm. Maximum flashover field is an average over 5 consecutive flashovers.

Sample	Averaged flashover field (kV/mm) MINIMUM	Averaged flashover field (kV/mm) CHARGE REMOVED	Number of flashovers to reach 10 kV/mm	Averaged flashover field (kV/mm) MAXIMUM
I	10.2	11.3	0	19.5
	9.0	12.0	1	16.0
	8.1	10.7	8	18.3
	7.4	12.0	5	20.0
II	7.1	9.3	36	16.1
	7.0	11.8	24	14.3
	6.7	11.3	45	11.4
	6.2	7.0	40	12.2
III	5.3	12.0	78	16.1
	5.1	9.3	61	13.4
	5.0	9.0	188	12.9
IV	4.0	5.4	25	14.1
	3.8	5.2	109	13.0
	2.7	3.5	71	15.4

Table 2

Comparison of performance parameters and design parameters for the groups of insulators in Table 1. E_{ctj} is the cathode triple junction field, V^{bd}_{ini} and V^{bd}_{con} stand for the initial and conditioned flashover voltage. The terms 'impact' and 'traps' refer to the emitted electrons, the terms 'speed' and 'stability' refer to the conditioning process (as explained in the text).

	DESIGN PARAMETERS			CONDITIONING PERFORMANCE			
GROUP	E_{ctj}	Impact	Traps	V^{bd}_{ini}	V^{bd}_{con}	Speed	Stability
I	low	no	-	+	+	+	+
II	med-high	yes	yes	+/-	+/-	+/-	+/-
III	low-high	yes	no	-	+/-	-	+/-
IV	high	yes	no	--	+/-	-	-

3.4 Relating performance to design

For relating performance to design, we formulate **"design parameters"** which are correlated with insulator performance. From the key mechanisms three design parameters are defined, each one characterised by a question:

1. is the cathode triple junction field high or low ?
2. do electrons interact with the insulator surface ?
3. are electrons trapped upon hitting the surface ?

Table 2 combines design and performance parameters for all groups of Table 1. The performance parameters are simplified to a relative scaling. We conclude that:

1. an insulator with a low cathode triple junction field and no electron-surface interaction (group I) performs excellently;
2. an insulator with electron-surface interaction where electrons are trapped (group II) performs well, though inferior to group I;
3. an insulator with electron-surface interaction and no charge traps (groups III and IV) performs badly in particular with respect to unconditioned

flashover voltage and conditioning speed.

3.5 Design rules

The following design rules are derived for DC-insulators:

1: Minimize the cathode triple junction field.
2: Keep electrons away from the insulator surface.
3: If electrons hit the insulator surface, make sure they are trapped.
4: Tailor the design of an insulator shape to the way it is conditioned or operated.
5. Avoid designs sensitive to small defects.

The first three rules are discussed above. Rule 4 is based on the observation that each geometry has its specific conditioning speed and stability. An optimum design of an insulator thus depends on the way it is conditioned and operated. If conditioning flashovers are used a high conditioning speed and a stable performance are required. Conditioning without flashovers requires a high unconditioned flashover voltage. For components which are switched off for a long time stability is important. The flashover voltage of such designs should not rely on surface charging. With the above rules several design were optimized [2,7].

3.6 Conditioning

A step-conditioning procedure, combining flashover conditioning with controlled energy and DC conditioning close to the breakdown voltage, is an efficient way of removing emission sites [4].

For DC voltage "silent" conditioning may be used [6] by which emission sites are not removed but rendered harmless by carefully designed charge traps that collect electrons released near the cathode triple junction. This increases the initial breakdown voltage.

4. AC INSULATING STRUCTURES

4.1 Key mechanisms

The processes important for AC vacuum insulators are the same as those for DC, but their impact on the insulation performance is different for two reasons [8]:

1. At DC voltage one electrode is a cathode; triple junction field control is restricted to that electrode and can be achieved by allowing a high anode field. For AC the field at both electrodes should be controlled.
2. At DC voltage a stable surface charge distribution is attained, which may increase or reduce the flashover voltage. The charge distribution may be used to achieve "silent" conditioning by which emission sites are rendered harmless without being removed. At AC no stable charge distribution is established. The charge deposited during one half cycle is discharged during the next, which results in an increased partial discharge rate, insulator damage and in a reduced flashover voltage by the release of adsorbed gases.

4.2 Flashover Performance

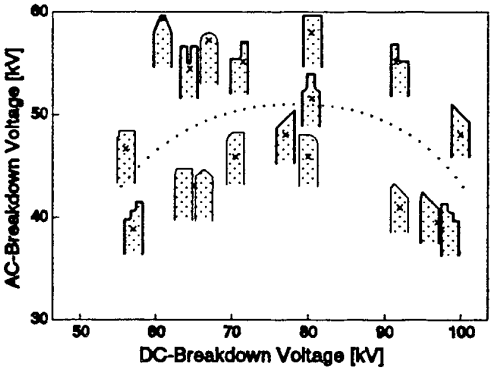

Fig.2 Conditioned AC flashover voltage (peak) versus conditioned DC flashover voltage for different geometries. Left side is negative (in case of DC-stress).

Figure 2 shows the conditioned flashover voltages for different insulator shapes under AC and DC stress. For AC the influence of the shape on flashover voltage is less pronounced as for DC. For each insulator the AC flashover voltage is lower than the DC flashover voltage. Insulators with poor DC performance also have a poor AC behaviour. Insulators with a good DC performance also have a low AC flashover voltage because the DC-strategy of reducing the cathode field and stabilizing the charge distribution does not work for AC.

4.3 PD-patterns

AC PD-measurement is a well developed diagnostic tool for power engineering components, and is a helpful diagnostic for research. Recently this technique was applied to AC vacuum insulators. Some examples are shown, for more details the reader is referred to [8]. PD-measurements may be represented in several ways. Figure 3 shows the PD-rate versus time for two insulators at an AC voltage amplitude which is increased at regular intervals. Figure 4 gives a plot of the number of PD's versus discharge magnitude, and a polar plot of the PD-rate. Two measurements with the same insulator and voltage are shown, but in between the two recordings a flashover has occurred. The difference is an indication of discharge induced damage. This is supported by the results in Fig.5, which gives polar plots for different of insulators shapes, where all insulators show a similar pattern. Deviating polar plots as in Fig.4 can be ascribed to insulator defects. Additional experiments with damaged insulators support this hypothesis. The PD patterns are related to a continuous process of charge redistribution during the voltage

cycles. Further work is needed to investigate the relation between PD patterns and insulator performance.

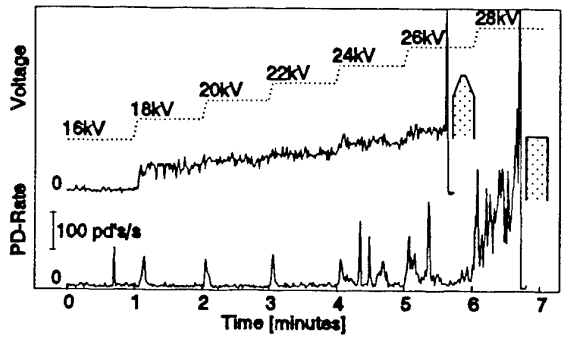

Fig.3 PD-rate (1/s) versus time for two insulators, rms voltage increased by 2 kV every minute.

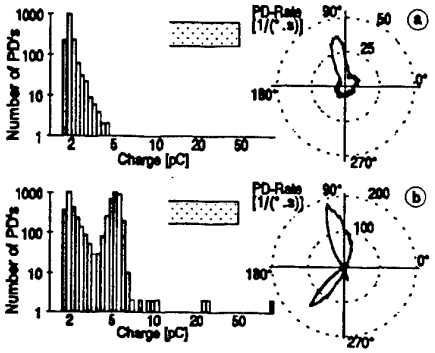

Fig.4 Different PD representations: counts versus magnitude (left) and polar plot (right) for a cylindrical insulator at 28 kV rms. Dotted circles indicate PD-rate in 1/(° s), plotted as a function of phase angle. Between a and b the voltage is increased until breakdown.

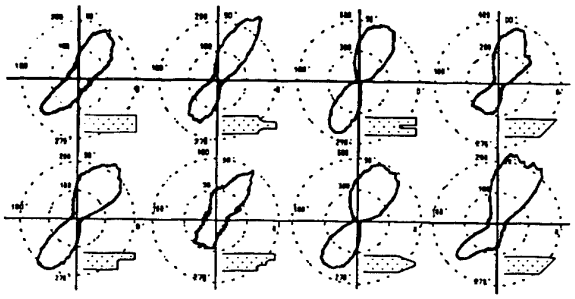

Fig.5 "Standard pattern" of discharge activity in the form of a polar plot.

5. CONCLUSIONS

In recent years considerable progress is made in the study of flashover processes ans surface properties with new, in particular optical, diagnostic techniques. A satisfactory theoretical description is not available yet. Next to flashover theories, the application to devices requires a systematic and scientific approach to design.

An approach is presented for obtaining science-based answers to practical vacuum device problems. With appropriate diagnostics operational mechanisms in simplified structures are studied, with the aim to find design guidelines. This approach is succesfully applied to insulators for DC vacuum devices. Key mechanisms are recognized, and their impact on performance is studied. By relating performance to design, design rules are formulated.

Similar investigations are being carried out for AC vacuum devices, where the impact of flashover mechanisms on flashover behaviour is different. PD measurements are a promising tool for AC device diagnostics.

ACKNOWLEDGEMENT

The research presented in this paper has been carried out by the Vacuum Insulation Project Team of the EUT High-Voltage and EMC Groupy. The author gratefully acknowledges the efforts of all people involved, in particular the invaluable contributions of dr. Peter Wouters and prof. Piet van der Laan, and the technical assistence of Toon Aldenhoven. Further, I am grateful to all our partners from industry who have contributed by supporting our work and confusing us with real life problems.

REFERENCES

[1] H.C. Miller, IEEE Trans. EI, vol.28, no.4, august 1993, pp.512-527.

[2] J.M. Wetzer, Invited paper XVIIth. Int. Symp. on Discharges and Electrical Insulation in Vacuum, Berkeley 1996, pp.449-458.

[3] J.M. Wetzer, P.A.A.F. Wouters, A.J.M. Pemen, M.G. Danikas, P.C.T. van der Laan, A.J. Aldenhoven, "Final Report of the Study on HV-design Aspects of Microwave Tubes", ESA contract no.7186/87/NL/JG(SC), 1991.

[4] J.M. Wetzer, P.A.A.F. Wouters, 1992 IEEE Symposium on Electrical Insulation, Baltimore, 1992, pp.31-35.

[5] I.D. Chalmers, J.H. Lei, B. Yang, W.H. Siew, IEEE Trans. DEI, vol.2, no.2, april 1995, pp.225-230.

[6] P.A.A.F. Wouters, J.M. Wetzer, P.C.T. van der Laan, 8th. Int.Symp.on High-Voltage Engineering, Yokohama, 1993, pp.299-302.

[7] J.M. Wetzer, P.A.A.F. Wouters, IEEE Trans. DEI, vol.2, no.2, april 1995, pp. 202-209.

[8] P.A.A.F. Wouters, H.W.M. Smulders, J.M. Wetzer, 9th.Int.Symp.on High Voltage Engineering, August 28 - September 1, 1995, Graz, Austria, pp. 2287/1-2287/4.

OVERVIEW OF NASA LeRC CATHODE TECHNOLOGY DEVELOPMENT PROGRAM

James A. Dayton, Jr., Edwin G. Wintucky and Isay L. Krainsky
NASA Lewis Research Center
21000 Brookpark Rd.
Cleveland, OH 44135
(216) 433-3515; jdayton@lerc.nasa.gov

Abstract

The NASA Lewis Research Center (LeRC) presently has a broad and active cathode technology development program that includes both thermionic and nonthermionic electron emission and Secondary Electron Emission (SEE). The cathode program, historically an integral part of the LeRC program for the development of microwave tubes for space communication and sensor applications, consists of basic experimental and theoretical studies, the development of specific cathodes types, life testing and the evaluation of novel types of cathodes, through a combination of in-house research, contracts, university grants and collaboration with other US government agencies (DoD, DoE).

Introduction

Present work on thermionic cathodes includes barium impregnated and reservoir dispenser types and oxide coated cathodes. Scandate cathodes are also under development with the emphasis on investigating the thermochemistry and emission properties of various scandia compounds. The barium reservoir cathode, developed under a NASA contract with Varian Associates, is now on life test at NSWC/Crane at 2 and 4 A/cm^2 and has shown no degradation in performance after more than 50,000 hours of operation. A version designed for 10 A/cm^2 and >100,000 hours life is also on life test. Recent work on oxide coated cathodes, involving modifications in coating chemistry and morphology, resulted in a significant improvement in performance. Nonthermionic cathodes include field emitter arrays (FEAs), NEA materials such as diamond, and novel types such as carbon nanotubes. Two of the FEA programs are DARPA funded and application oriented, one for a gate modulated FEA in a 10GHz, 50W klystrode and the other for field emission displays. The SEE program includes basic studies of the SEE properties of clean and treated CVD diamond films and potential applications of treated CVD diamond films as secondary electron emitters in high power, crossed-field devices.

The Improved Reservoir Cathode

The principal features of the improved barium reservoir cathode (Ref. 1) are shown in Figure 1. This cathode was first reported to this conference in 1989 (Ref. 2). These cathodes are now on life test at 2 and 4A/cm^2 (3 each) at the NSWC Crane Division (Ref. 3) and on the average are showing no signs of degradation in emission after more than 50,000 hours of CW operation. NASA is also life testing at Crane barium reservoir cathodes purchased from Siemens (designated by MK) at 2 and 4A/cm^2 (2 each). The MK cathodes have over 80,000 hours of operation and, unlike the improved reservoir cathode (designated as RV) that operate at an average of 100C lower temperature, did show some degradation after the same period of performance. The long-term life test results for the cathodes operating at 2A/cm^2 and 4A/cm^2 are shown in Figures 2 and 3, respectively. Future plans include testing RV cathodes at 10A/cm^2.

Figure 1

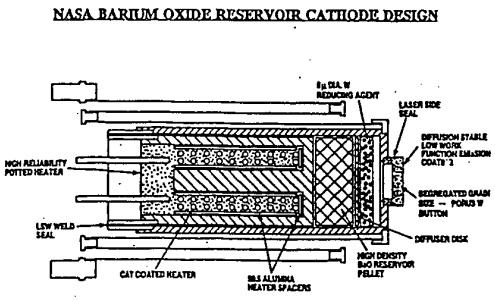

Figure 2

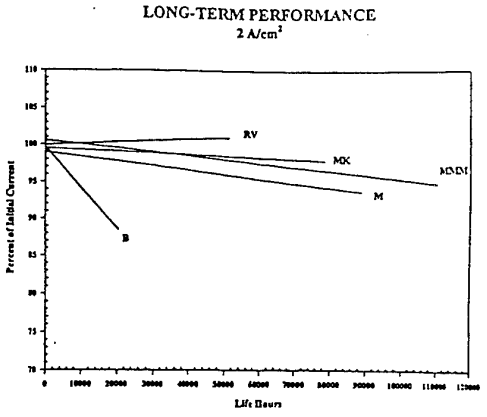

Figure 3

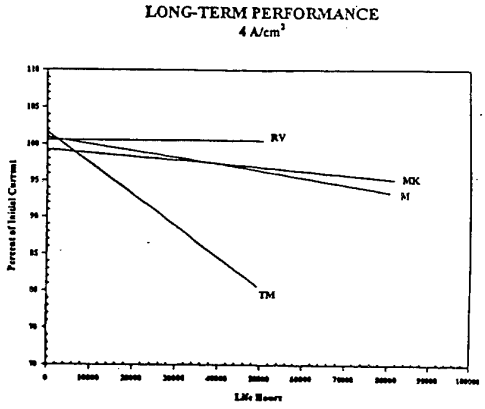

Fundamental Research on Thermionic Cathodes

An important part of the work on cathode technology at NASA LeRC seeks to improve the fundamental understanding of the underlying science of the thermionic cathode. Two long term efforts, one experimental and the other computational, have been drawn together in a recent publication that identifies the geometrical structure of the Ba/O/W surface that is the basic building block of the barium dispenser thermionic cathode (Ref. 4). By employing computational quantum chemistry, the density of electronic states has been computed for two potential geometrical configurations of the Ba/O/W surface as shown in Figure 4. By comparing the computed density of states with the values measured by means of inverse photoemission, as seen in Figure 5, it is concluded that only the "tilted" configuration is consistent with the experimental results.

Figure 4 *Top and side view of cluster models for a c(2x2) ML of Ba and O on W(001) in the (a) tilted, (b) upright configurations. (c) Illustrates the SBZ of the clean W(001) surface (solid square) and that of the c(2x2) BaO/W(001) system (dashed square).*

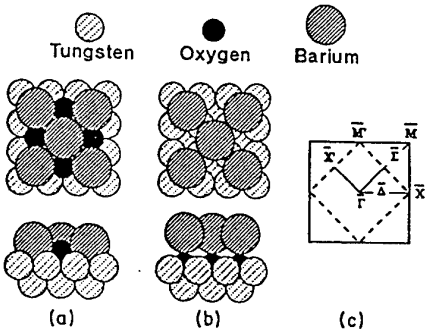

Figure 5 *Left panel: Experimental two-dimensional band structure for a c(2x2) BaO overlayer on W(001) along the ΓΔX and ΓΣM symmetry line of the unreconstructed W(001) surface. Right panel: Fully relativistically calculated DOS for BaO on W(001) in the tilted configuration. The solid line represents the total DOS; the dashed and dotted lines represent the oxygen and barium contributions, respectively.*

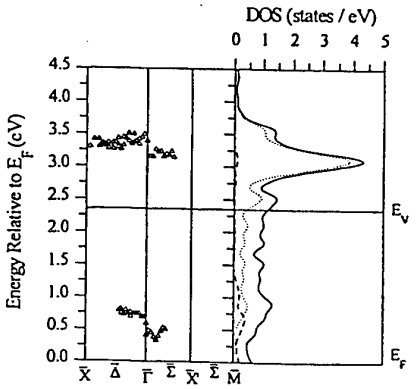

In addition to atomic and electronic structures, the methods of computational quantum chemistry have been successfully applied to the calculation of the surface dipole properties and work functions of a large variety of 5d transition metal cathode surfaces. One of the major accomplishments was a microscopic explanation of the emission enhancement that is observed in

M-type relative to B-type cathode surfaces. Excellent results have been obtained for BaO adsorbed on W, Re-W, Os-W, and Ir-W surfaces (Ref. 5). The reduction of the work function from about 2 eV for BaO/W to a minimum of 1.75 eV for BaO/Os-W is explained by the smaller depolarization of the surface dipoles on the hexagonal M-type alloy surface relative to the cubic B-type tungsten surface. The calculated work function increases with increasing W surface concentration in the alloy, as is observed when the cathode ages.

Scandate cathodes have also been the subject of both experimental and theoretical studies. Experimental studies at NASA LeRC included the investigation of synthesized Ba/Sc/O on W surfaces intended to replicate the emission and chemical properties of scandate cathode surfaces. The results indicated that the low work function areas consisted of BaO adsorbed on Sc_2O_3 (Ref. 6). Sc adsorbed on W(100) was also investigated experimentally by LEED, inverse photoemission and retarding potential work function (WF) measurements, the results showing a minimum room temperature WF at ½ monolayer coverage (Ref. 7). A complementary study of the electronic structure using solid state computational methods for extended surfaces showed good agreement with the experimental inverse photoemission results. Computational quantum chemistry studies of scandate cathode surfaces are also being conducted. Several different models have been investigated (Ref. 8). The calculated work function for a monolayer of Ba and ScO on W(100) of 1.5-1.7 eV is in good agreement with experiment, but more complex surfaces are also likely candidates for actual scandate surfaces. The bulk thermochemistry of the $BaO\text{-}Sc_2O_3\text{-}WO_3$ ternary system, consisting of compounds associated with scandate cathodes, was characterized for the first time under a grant to Georgia Tech (Ref. 9), where emission properties of a number of compounds in this system were also investigated (Ref. 10). A collaborative NASA LeRC-Georgia Tech effort is planned for thin film studies of a number of promising scandate compounds.

Oxide-Coated Cathodes

The significant improvement in brightness of oxide-coated cathodes demonstrated by the CRT industry, reportedly achieved by modifying the coating chemistry, suggests that the same enhancements in electron emission could be beneficial for microwave tube applications. Consequently, NASA LeRC has undertaken an investigation of improvements in electron emission associated with modifications in coating chemistry and morphology. The earliest effort was the successful development under a contract with FDE Assoc. of an improved oxide cathode coating obtained by adding both In and Sc. The main result was a significantly lower knee temperature, higher current density and longer lifetime compared to a standard oxide coating tested under the same conditions. In subsequent emission testing at NASA LeRC (Ref. 11) of cathodes prepared by FDE Assoc. with four different oxide coatings, one coating a standard oxide and the other three coatings modified by the addition of either In, Sc or In+Sc, it was shown that the modified coatings consistently demonstrated superior performance. Figure 6 shows normalized emission current density vs temperature curves for the "best" of each of the four coatings. The emission from the In only coatings was the most reproducible, as shown in Figure 7. It was determined that In does not contribute directly to emission enhancement. Full activation of the cathode was not achieved until In was no longer present on the emitting surface as observed by Auger surface analysis. In situ SEM observations indicated a finer and more uniform distribution of alkaline-earth oxide particles, implying the probability of a more uniform work function distribution. Present and future efforts include the use of x-ray diffraction to study the thermochemistry and crystal structure of the chemically modified coatings and to investigate the effects on electron emission of adding other promising materials to the coatings.

Figure 6

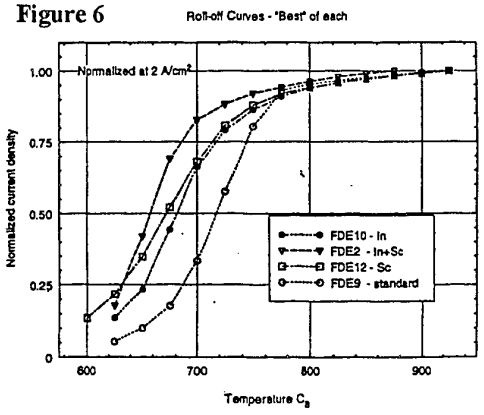

Figure 7

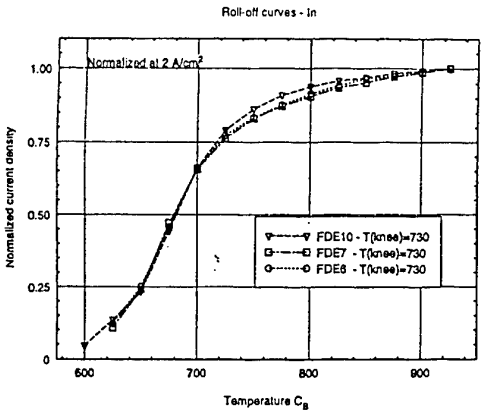

Secondary Electron Emission from Diamond Films

Copious secondary electron emission (SEE) has been observed from chemically vapor deposited (CVD) diamond films produced by a variety of methods (Refs. 12, 13). Typically, CVD diamond films, as deposited, exhibited secondary emission yields of, approximately, 14, but this yield was reduced to a stable value near 3 when subjected to electron bombardment. An example of this effect is presented in Figure 8. Exposure of the electron-bombarded diamond surface to molecular hydrogen restored the secondary yield to its former value as shown in Figure 9. However, the diamond films suffered irreversible deterioration of secondary yield when subjected to ion bombardment. Annealing of the CVD diamond films in vacuum enhanced their secondary yield, but annealing them in a nitrogen atmosphere reduced the yield significantly. Secondary yield as a function of primary energy for as-deposited films and those that have been ion sputtered or annealed in nitrogen are shown in Figure 10. Diamond-like carbon films did not exhibit interesting properties as secondary emitters.

The reduction of secondary yield as a result of electron bombardment would restrict the usefulness of diamond films as secondary electron sources to only very low current applications such as electron multipliers (Ref. 14). However, stable secondary emission could be obtained from diamond films in the presence of a tenuous hydrogen atmosphere as can be seen in Figure 11.

Figure 8

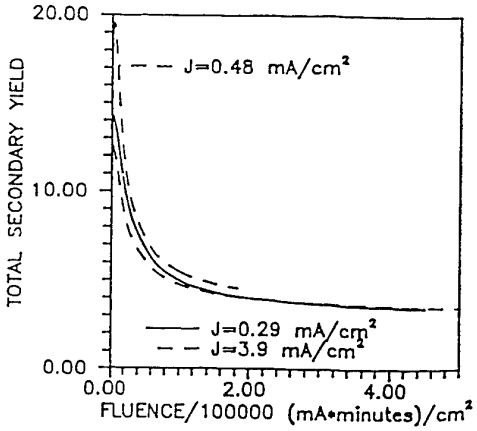

TOTAL YIELD VS FLUENCE OF DIAMOND/Mo SAMPLES AT DIFFERENT CURRENT DENSITIES. HIGH YIELD DUE TO HEATING AT 420°C FOR 20 HRS.

Figure 9

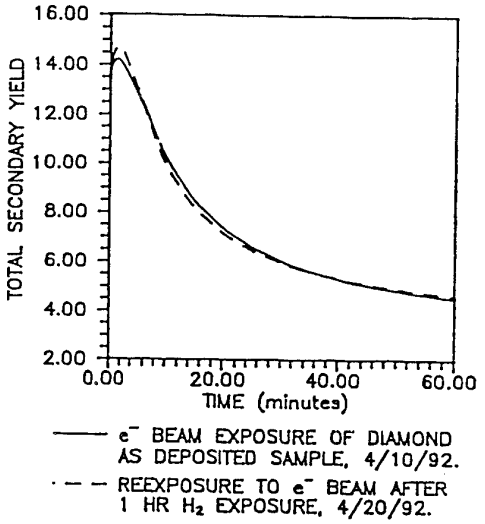

Figure 10 *Summary of total secondary yield vs. Primary beam energy. As deposited samples commonly showed maximum yields of 14 at ~1 keV.*

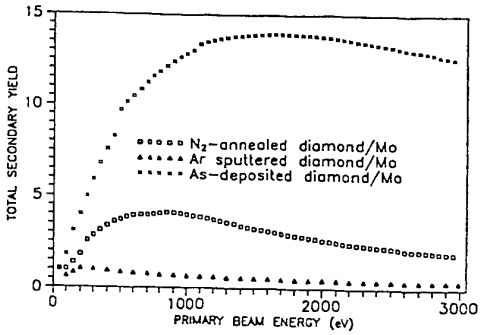

Figure 11

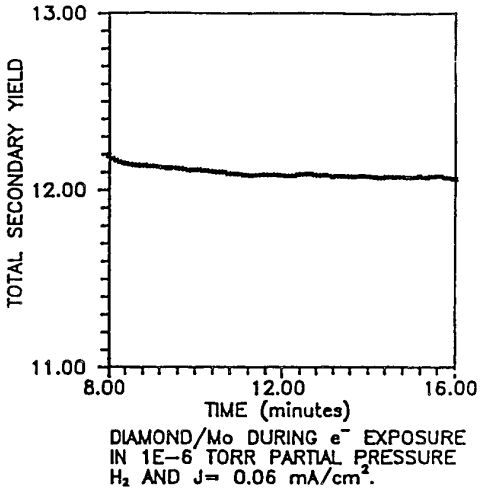

A much more promising method for enhancing and stabilizing the SEE from diamond films was found by coating them with an alkali-halide film (Ref. 15). Under electron bombardment, the halogen element disappeared from the surface leaving a alkali-coated diamond surface that not only exhibited superior secondary emission characteristics, but was also stable in air. The secondary yield as a function of primary energy for a diamond surface before and after being coated with CsI is shown in Figure 12. The stability of this surface under electron bombardment is shown in Figure 13.

Figure 12 *Secondary yield from diamond film as a function of primary energy, lower curve before and upper curve after coating with C_sI.*

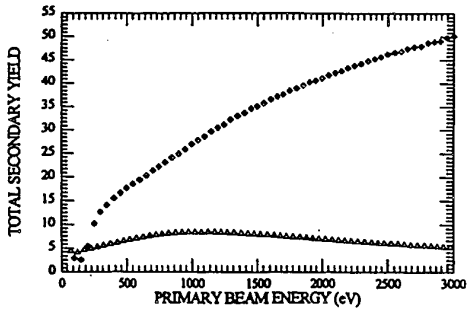

Fundamental studies of the electronic properties of diamond films have demonstrated that the electron emission from diamond surfaces is due to the effect of negative electron affinity (Ref. 16). It has also been demonstrated experimentally that the energy of the carbon Auger peak is shifted 1.2 V when the surface is covered by hydrogen and that this is explained theoretically by the influence of hydrogen on the upper-valence band density of electronic energy states (Ref. 17). Diamond films have been considered for application as cathodes in crossed field devices.

Figure 13 *Secondary yield from diamond film as a function of electron fluence, lower curve before and upper curve after coating with C_sI.*

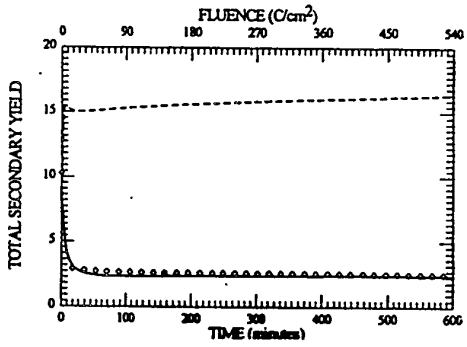

Field Emission

NASA LeRC serves as the agent for DARPA in two projects related to field emission. One is a program to improve the performance of thin film field emitters for use in thin panel displays. This program with SRI International has only been underway for only a few months, and a report of progress would be premature. A more significant program nearing its completion is the development of a 50 Watt, 10 GHz Klystrode which uses field emitters to produce a modulated electron beam that excites a resonant cavity.

This project involves four cathode manufacturers, SRI and Varian Ginzton Lab funded by DARPA and Litton, MCNC and MIT Lincoln Labs funded by NRL (Lincoln was funded by DARPA originally). The cathodes provided by SRI and Lincoln Labs are molybdenum emitters, while the MCNC emitters are silicon and the Varian emitters are GaAs. The Klystrode has been designed and fabricated by CPI which is also testing the cathodes. So far the program has resulted in new records for

emission current density (2000 A/cm2) (Ref. 18) and for modulated electron emission from a field emitter array (10 GHz). However, the actual testing of cathodes in the Klystrode is only beginning and significant results have not been obtained as of this writing.

REFERENCES

1. E. G. Wintucky, D. Windes, J. Dutkowski, and G. Miram, *"Life Test Performance of Reservoir-Type Barium Dispenser Cathodes,"* International Vacuum Electron Sources Conference 1996, Eindhoven, The Netherlands, July 1-4, 1996.
2. J. A. Dayton, Jr., *"NASA Cathode Technology Program,"* Proceedings of an International Workshop on Requirements for Space TWTAs in the 1990's, pp. 261-263.
3. TriService/NASA Cathode Life Test Facility Annual Report, January 1996-January 1997.
4. A. Lamouri, W. Müller, and I. L. Krainsky, *"Geometry and Unoccupied Electronic States of Ba and BaO on W(001),"* Physical Review B, Volume 50-No. 7, pp. 4764-4770.
5. W. Müller, *"Mechanism of Emission Enhancement in Barium Dispense Cathodes,"* Proc. Tri-Service/NASA Cathode Workshop, pp. 96-100, 1992.
6. G. Lesny and R. Forman, *"Surface Studies on Scandate Cathodes and Synthesized Scandates,"* IEEE Transactions on Electron Devices, 37, p 2595-1990.
7. A. Lamouri and I. L. Krainsky, *"Unoccupied Electronic Resonances of Sc Adsorbed on W(001) by k-resolved Inverse Photoemission,"* Physical Review B, Volume 51, Number 3, pp. 1803-1808, January 15, 1995.
8. W. Müller, *"Work Functions for Models of Scandate Surfaces,"* International Vacuum Electron Sources Conference (IVESC'96), Eindhoven, The Netherlands, July 1996, accepted for publication in Applied Surface Science.
9. S. H. Magnus, D.N. Hill, and W.L. Ohlinger, *"Thermochemistry in the BaO-Sc_2O_3-WO_3 Ternary System,"* International Vacuum Electron Sources Conference (IVESC'96), Eindhoven, The Netherlands, July 1996, accepted for publication in Applied Surface Science.
10. S. H. Magnus, D.N. Hill, and W.L. Ohlinger, *"Emission Properties of Compounds in the BaO-Sc_2O_3-WO_3 Ternary System,"* International Vacuum Electron Sources Conference (IVESC'96), Eindhoven, The Netherlands, July 1996, accepted for publication in Applied Surface Science.
11. E. G. Wintucky, G. Lesny, and B. Vancil, *"Emission Characterization of Chemically Modified Oxide-Coated Cathodes,"* International Vacuum Electron Sources Conference 1996, Eindhoven, The Netherlands, July 1-4, 1996.
12. T. L. Bekker, J. A. Dayton, Jr., A. S. Gilmour, Jr., I. L. Krainsky, M. F. Rose, R. Rameshan, D. File, and G. Mearini, *"Observations of Secondary Electron Emission from Diamond Films,"* IEDM Technical digest 1992, pp. 949-952.
13. G. T. Mearini, I. L. Krainsky and J. A. Dayton, Jr., *"Investigation of Diamond Films for Electronic Devices,"* Surface and Interface Analysis, Volume 21, pp. 138-143.
14. G. T. Mearini, I. L. Krainsky, Y. X. Wang, J. A. Dayton, Jr., R. Ramesham, M. F. Rose, *"Fabrication of an Electron Multiplier Utilizing Diamond Films,"* Thin Solid Films 253 (1994), pp. 151-156.
15. G. T. Mearini, I. L. Krainsky, and J. A. Dayton, Jr., *"Stable Secondary Electron Emission from Chemical Vapor Deposited Diamond Films Coated with Alkali-halides,"* Applied Physics Letters, Volume 66-No. 2, pp. 242-244.
16. G. T. Mearini, I. L. Krainsky, and J. A. Dayton, Jr., Surface Interface Anal. 21, pp. 138 (1994).
17. I. L. Krainsky, G. T. Mearini, and V. M. Asnin, *"Auger Electron Spectroscopy of the Hydrogen Terminated Chemical Vapor Deposited Diamond Surface,"* Applied Physics Letters, Volume 68-No. 14, pp. 2017-2019.
18. C. A. Spindt and I. Brodie, *"Molybdenum Field-Emitter Arrays,"* IEDM Technical Digest 1996, pp. 289-292.

THE MEASURED ANGULAR DISTRIBUTION OF ELASTICALLY SCATTERED ELECTRONS AND COMPUTATIONS OF ITS EFFECT ON COLLECTOR PERFORMANCE

J. A. Dayton, Jr., I. L. Krainsky, K. R. Vaden,
NASA Lewis Research Center
Cleveland, Ohio
USA
(216) 433-3515; jdayton@lerc.nasa.gov
G. T. Mearini
General Vacuum

ABSTRACT

Measurements are reported of the angular distribution of energetic secondary electrons emitted from surfaces of isotropic graphite (POCO graphite), polished copper and ion textured copper. The incident electron beam varies from normal to near grazing incidence, while the secondary electrons within 20% of the incident energy are measured throughout the half sphere above the target. It is observed that the character of the surface has a profound influence on the magnitude and angular distribution of the energetic secondary electrons. Computations of the effect of energetic secondary electrons on traveling wave tube (TWT) collector performance are presented.

INTRODUCTION

The secondary emission of materials for use in collectors has been investigated extensively as part of NASA's effort to improve the efficiency of TWT's for space applications. Secondary electrons reduce the efficiency of collectors when the resulting currents impact on less depressed collector electrodes and can also cause oscillations to develop when backstreaming secondary electrons reenter the slow wave circuit of a TWT. Secondary emission in collectors can be substantially reduced by appropriate choice of collector electrode materials and surface treatments and by designing the collector geometry so that secondary emission is suppressed or trapped by electric and magnetic fields.

Earlier work in this area, principally by Forman, Curren, Ebihara and their coworkers (Ref. 1,2,3,4) has measured the absolute yield of true secondary electrons, but only the relative yield of energetic secondary electrons referenced to a standard surface of soot. The data on true secondary yield were incorporated for the first time in a collector design by Force in 1986 (Ref. 5). For each ray of primary electrons, a ray of low energy secondary electrons with a current equal to the product of the primary current and the secondary yield is launched back on the same trajectory as the incident ray.

Actually, low energy secondary electrons are emitted in a cos θ distribution, but it can be demonstrated that the angle of emission for these low energy electrons in not greatly significant in determining their trajectories within the collector. This computational approach is valuable for use in minimizing the influence of low energy secondary electrons on collector designs, but cannot be employed in the analysis of the effect of energetic secondary electrons without a knowledge of their angular distribution. For the purposes of this study, the energetic secondary electrons or scattered electrons are arbitrarily defined as those with energy within 20% of the incident energy. Secondary emission data will be reported on polished copper, textured copper and istropic graphite (POCO graphite).

EXPERIMENTAL APPARATUS

The present work was undertaken to obtain detailed secondary electron emission data for selected materials that have significant engineering interest for collector applications. The angle of incidence of the primary electron beam can be adjusted from normal to near grazing incidence, while the electrons emitted into the half sphere above the target are collected. The electron source is a modified Varian off-axis Auger spectroscopy electron gun that produces an electron beam with energy between 100 and 3000 eV and a spot size less than one mm.

Data were collected for sample orientations at 2 degree increments from normal to near grazing incidence. At each sample orientation the detector was rotated through 200 degrees, and data were recorded at one degree increments.

SECONDARY EMISSION MEASUREMENTS

Copper is the material most frequently used for the electrodes of depressed collectors. Copper has good vacuum properties, excellent thermal conductivity, and the technology for fabrication and brazing is well established in the tube industry. However, copper is not the ideal material for collector electrodes because of its relatively high secondary electron yield.

A sampling of the data for the angular distribution of energetic secondary electrons from polished polycrystaline copper is shown in Figure 1 for angles of incidence of 0, 50 and 80 degrees from normal. It can be seen in Figure 1a and in those that follow that the secondary electrons emitted within +/- 10 degrees of the incident beam cannot be collected. In most cases the plot for each energy level has been normalized to the value at +20 degrees from vertical, that is, from the axis of the incident electron beam. In Figure 1a it can be seen that at normal incidence the angular distribution broadens significantly as the primary voltage is increased.

A much more complex distribution is produced when the incident electron beam is 50 degrees from normal as seen in Figure 1b. For low primary energies almost all the energetic secondaries are back scattered. However, as the primary energy is raised, the magnitude of the forward scattering increases until at 2 kV the forward and backward scattering are approximately equal. The angle of the forward scattered energetic electrons also increases as primary energy is increased.

The prominence of back scattering continues even near grazing incidence at 80 degrees as can be seen in Figure 1c. The back scattering exceeds the forward scattering for primary energies up to 1 kV, but for higher primary energies the forward scattering is predominant.

The surface morphology of the ion textured copper surface is shown in Figure 2. This surface exhibits significantly reduced secondary electron yield, while retaining the advantages of thermal conductivity and ease of manufacture associated with copper. The angular distribution of energetic secondary electrons for textured copper as shown in Figure 3 is radically different from that of polished copper. For normal incidence (Figure 3a), the angular distribution is much more narrow, and at 50

Figure 1a *Normal Incidence*

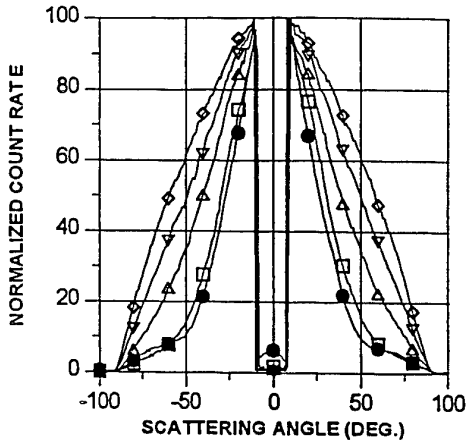

Figure 1b *50° from Normal*

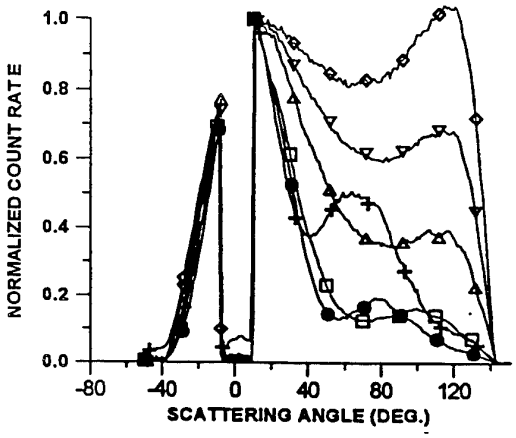

Figure 1c *80° from Normal*

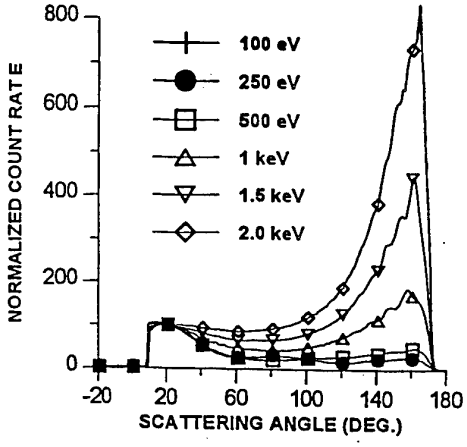

Figure 1 *Normalized angular distribution as a function of incident energy of elastically scattered electrons from a polished copper surface.*

degrees (Figure 3b) and near grazing incidence at 80 degrees (Figure 3c), there is virtually no forward scattering. Compared to polished copper, the yield of scattered electrons is substantially smaller as can be see from Figure 4 which provides a detailed comparison of the two surfaces for normal primary incidence.

Finally, a representation of the angular distribution of energetic secondary electrons from an isotropic graphite surface (POCO graphite) is shown in Figure 5. The shapes of the curves are similar to those for polished copper, but the secondary yield for POCO graphite is significantly lower than for copper.

COLLECTOR COMPUTATIONS

The classic method employed for more than 20 years at NASA Lewis for the analysis and design of collectors uses the Detweiler Helical TWT Code (Ref. 6) or the NASA Coupled Cavity Code (Ref. 7) to compute the distribution in energy, position and direction of the spent electron beam at the entrance to the collector. Typically, the spent electron beam is represented by 80 rays of steady state current. Computation of the collector performance is obtained using the Herrmannsfeldt Code (Ref. 8). Representative examples of this computation can be found in Refs. 9, 10, and 11.

The four stage collector designed for the 32 GHz TWT for the Cassini Mission (Ref. 12) served for computational demonstrations of the application of the data on scattered electrons. This collector is a modern design that has been characterized in detail both experimentally and computationally, and it is the only collector which has been fabricated and tested with identical electrodes of the three materials presented in this paper.

Figure 2 *Photo micrograph of ion-textured copper surface.*

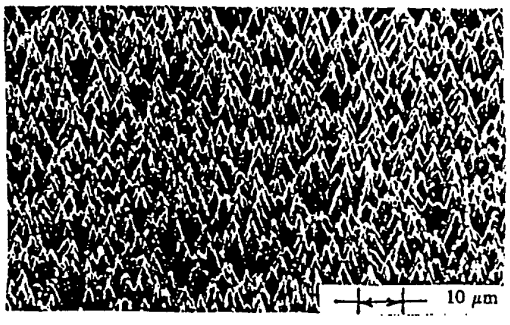

Figure 3a *Normal Incidence*

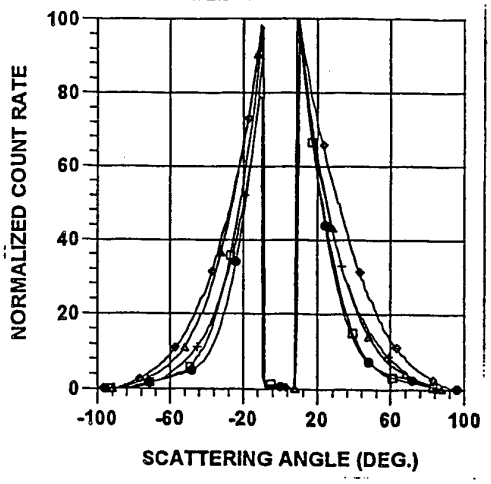

Figure 3b *50° from Normal*

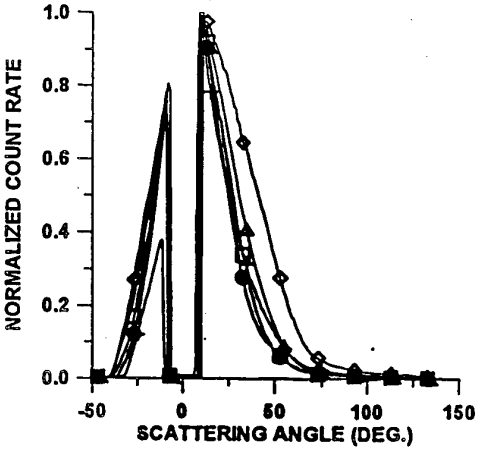

Figure 3c *80° from Normal*

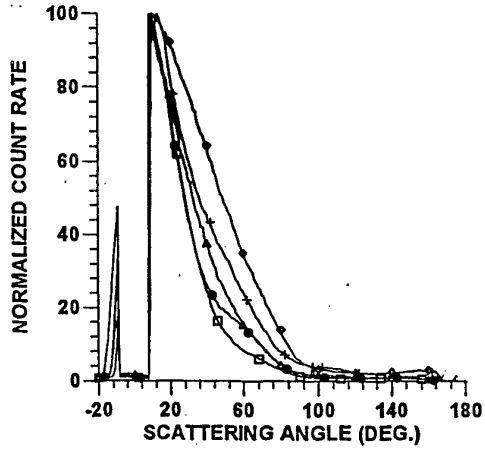

Figure 3 *Normalized angular distribution as a function of incident energy of elastically scattered electrons from an ion-textured copper surface. Figures 3a, 3b, and 3c are for normal incidence, 50° from normal and 80° from normal, respectively. The incident energies are designated as in Figure 1.*

Figure 4 *Total secondary yield and fraction of yield that is elastically scattered at normal incidence into the detector at 20° from normal for polished and textured copper.*

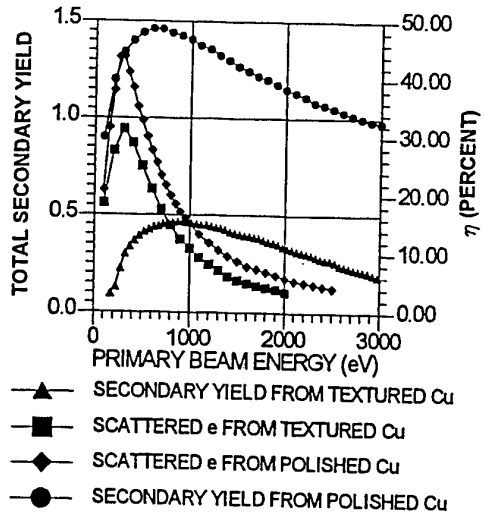

Attempts to incorporate the data on scattered electrons into this classical computational scheme have not been entirely satisfactory. At first the data were curve fit into a linear series of Gaussian and Lorentzian functions which were then organized into a look up table and used in conjunction with an interpolation routine to obtain the approximate distribution of scattered electrons for any arbitrary primary energy or angle of incidence. However, even with the elimination of very low current components, this scheme resulted in a representation of the scattered electrons that consisted of several hundred rays.

This level of complexity created the apparent contradiction of being computationally unwieldy, while at the same time insufficiently detailed to produce meaningful results. Once computations of the trajectories of scattered electrons were begun, it became apparent that forward scattered electrons had very little impact on collector performance; they tended frequently to be recaptured on the same electrode and were never observed to return to the slow wave circuit. In contrast, back scattered electrons frequently were collected on less depressed collector stages and, when emitted at approximately the angle of incidence, could reenter the slow wave circuit. The result of organizing the scattered electron data in this way was to significantly overestimate the current backstreaming from the collector to the slow wave circuit because the curve fitting routine used to characterize the scattered current would in many cases represent all of the back scattered electrons by a single ray at the angle of incidence. This method gave far more information than needed for the forward scattered electrons and not nearly enough to treat the back scattered electrons accurately.

A more accurate computation of the current scattered back into the slow wave circuit was obtained by representing the back scattered electrons with a fan of 50 rays equally distributed over a range of 10 degrees centered at the angle of incidence with currents proportional to the measured distribution. A sample of one of these models of the back scattered electrons is shown in Figure 6. Only electrons emitted into a narrow cone near the angle of incidence can reach the slow wave circuit; most of the backscattered electrons are collected again on the same electrode. At each primary beam impact site the back scattered electrons were modeled as shown in Figure 6 and the fraction of the primary beam reaching the slow wave circuit tabulated. Adding the contributions from each primary impact site, approximately 1% of the primary beam current was found to return to the slow wave circuit, in approximate agreement with experimental observations.

CONCLUSIONS

The data on the angular distribution of energetic secondary electron emission demonstrates that it is not easily characterized. While the textured copper surface produces mostly back scattering, the yield is substantially reduced by the surface morphology. The smooth copper surface produces mostly forward scattering at high primary voltages, but the opposite is true at low voltages, and the secondary yield is high. From the standpoint of secondary emission, POCO graphite is the most attractive material for collector electrodes because it exhibits low yield and very little back scattering.

Computer modeling indicates that back scattering reduces collector efficiency and causes some current to return to the slow wave circuit. Unfortunately, with the experimental method used, back scattered emission must be obtained by extrapolation. This computed result was obtained for a typical NASA style collector and may not be applicable to the bucket collectors used by some manufacturers. In general, computational resources are not adequate to conveniently make use of the volume of data

generated here on secondary emission, nor may it be needed to produce credible designs.

REFERENCES

1. R. Forman, *"Secondary-Electron-Emission Properties of Conducting surfaces with Application to Multistage Depressed Collectors for Microwave Amplifiers,"* NASA TP-1097, 1977.
2. A. N. Curren, *"Carbon and Carbon-Coated Electrodes for Multistage Depressed Collectors for Electron Beam Devices—A Technology Review,"* IEEE Trans. Electron Devices, vol. ED-33, no. 11, Nov. 1986, pp. 1902-1914.
3. B. T. Ebihara, P. Ramins, and S. Peet, *"Traveling-Wave-Tube Efficiency Improvement by a Low-Cost Technique for Deposition of Carbon on Multistage Depressed Collector,"* NASA TP-2919, 1987.
4. A. N. Curren, K. L. Long, K. A. Jensen, and R. F. Roman, *"An Effective Secondary Electron Emission Suppression Treatment for Copper MDC Electrodes,"* IEDM Technical Digest 93, pp. 777-780
5. D. A. Force, *"Calculation of Secondary Electron Trajectories in Multistage Depressed Collectors for Microwave Amplifiers,"* NASA TP-2664, 1986.
6. H. K. Detweiler, *"Ph. D. Dissertation,"* Rep. 01094-108, University of Michigan (1986).
7. J. D. Wilson, *"Revised NASA Axially Symmetric Ring Model for Coupled-Cavity Traveling-Wave Tubes,"* NASA TN-2675, 1987.
8. W. B. Herrmannsfeldt, SLAC-166, Stanford Liniar Accerelator Center, 1973.
9. J. A. Dayton, Jr., H. G. Kosmahl, P. Ramins and N. Stankiewicz, IEEE Transactions on Electron Devices, ED-26, (1979) 1589.
10. J. A. Dayton, Jr., H. G. Kosmahl, P. Ramins and N. Stankiewicz, IEEE Transaction ED, ED-28, (1981) 1480
11. J. D.Wilson P. Ramins, and D. A. Force, *"A High-Efficiency 59- to 64- GHz TWT for Intersatellite Communications,"* IEDM Technical Digest 91, pp. 585-588.
12. A. N. Curren, K. J. Long, J. A. Dayton, Jr., R. W. Palmer, D. A. Force, and R. P. Gruber, *"A High Efficiency, Low Power Ka-Band TWTA for Cassini,"* Proceedings of the Space TWTAs 1994 Workshop, ESA WPP-072, May 1994,

Figure 5a *Normal Incidence*

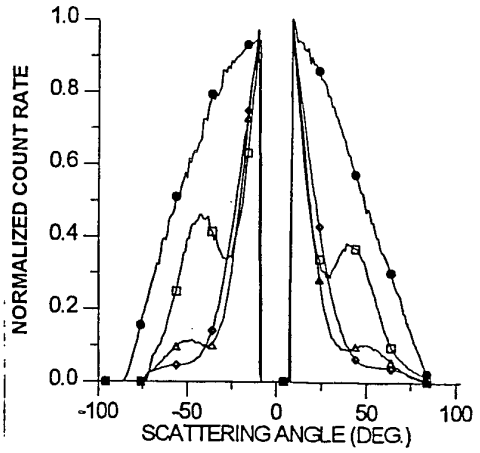

Figure 5b *50° from Normal*

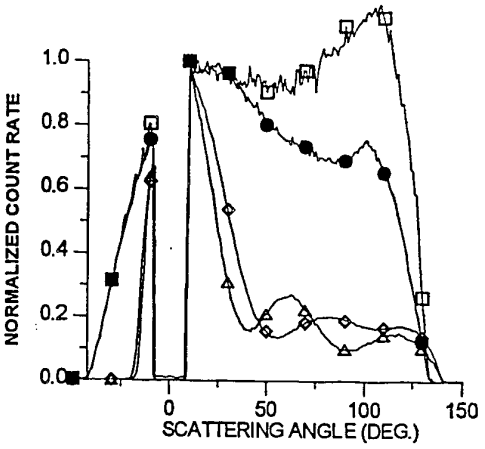

Figure 5c *80° from Normal*

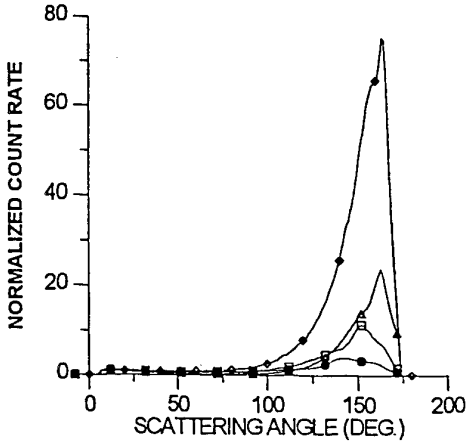

Figure 5 *Normalized distribution as a function of incident energy of elastically scattered electrons from a POCO graphite surface. The incident energies are as designated in Figure 1.*

Figure 6 *Computer model of backscattered electrons from a representative impact site in the collector designed for the 32 GHz TWT for the Cassini Mission.*

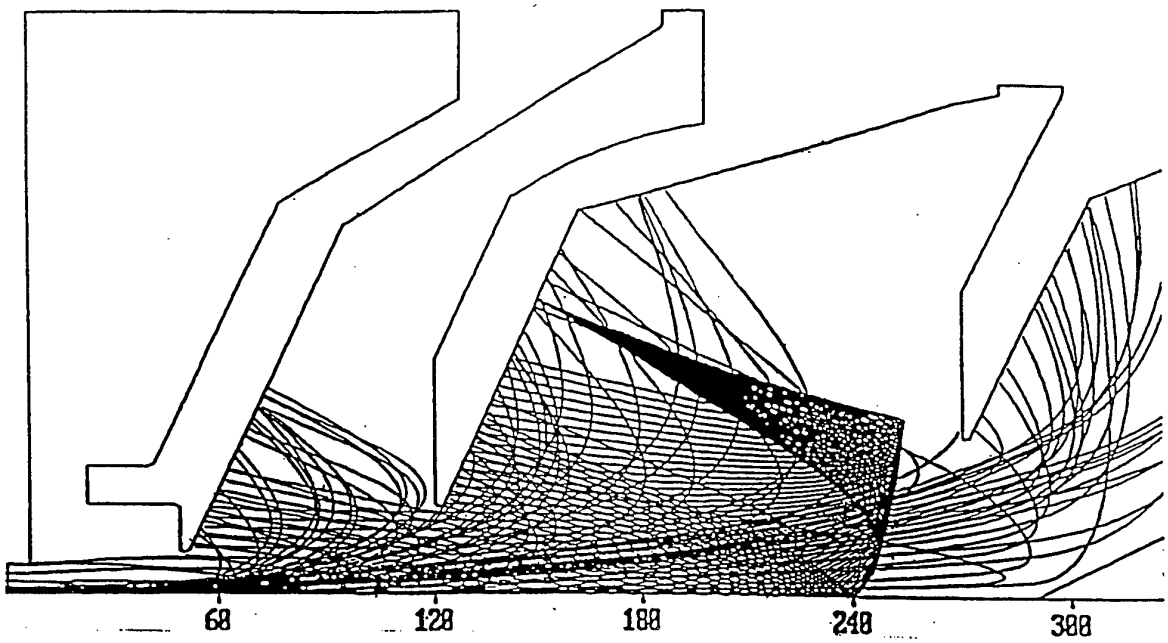

THE EFFECT OF TOLERANCES ON TWT PERFORMANCE

Carol L. Kory
Analex Corporation/NASA Lewis Research Center
21000 Brookpark Rd., MS 54-5
Cleveland, Ohio 44135 USA
phone: (216)-433-3512 email: Carol.L.Kory@lerc.nasa.gov

James A. Dayton, Jr.
NASA Lewis Research Center
21000 Brookpark Rd., MS 54-5
Cleveland, Ohio 44135 USA
phone: (216)-433-3515 email: jdayton@lerc.nasa.gov

ABSTRACT

Recent advances in the state of the art of computer modeling offer the possibility for the first time to evaluate the effect of slow-wave structure parameter variations, such as manufacturing tolerances, on the performance of helical traveling wave tubes (TWT's). This will enable manufacturers to determine the cost effectiveness of controlling the dimensions of the component parts of the TWT, which is almost impossible to do experimentally without building a large number of tubes and controlling several parameters simultaneously.

The computer code MAFIA, is used in this analysis to determine the effect on tube performance (dispersion and on-axis interaction impedance) of several helical slow-wave circuit parameter variations, including thickness and relative dielectric constant of the support rods, tape width, and height of the metallized films deposited on the dielectric rods. Previous computer analyses required so many approximations that accurate determination of the effect of many relevant dimensions on tube performance were practically impossible.

INTRODUCTION

Unfortunately, it is not an uncommon experience that TWT's of the same model, presumably fabricated within manufacturing tolerances, exhibit significant variations in performance. These variations represent a considerable cost to the industry, particularly when they are large enough that completed TWT's do not meet specifications. It would seem likely that these variations are the result of inadequately controlled manufacturing processes, but an accurate investigation of this hypothesis has been impossible until recently. This paper demonstrates the variations that can occur in TWT performance, in terms of dispersion and on-axis interaction impedance, when key parameters of the slow-wave structure vary within and beyond, the tolerances typically employed within the industry.

The most common type of TWT slow-wave structure comprises a helical metal wire or tape supported by three or more dielectric rods in a conducting barrel. This commonly manufactured structure cannot be analyzed by conventional mathematical methods because it cannot be described conveniently in any coordinate system. An accurate simulation of this structure has been recently achieved (Refs. 1, 2, 3) using the computer code MAFIA, allowing for the first time, the analysis of the effect of dimensional variations on TWT performance.

MAFIA (Solution of **MA**xwell's equations by the **F**inite-**I**ntegration-**A**lgorithm) is a powerful, electrodynamic code written in FORTRAN 77 that is used for computer-aided design of two-dimensional and fully three-dimensional electromagnetic devices such as magnets, RF cavities, waveguides, antennas, etc. The Finite Integration Technique (FIT) algorithm produces a set of finite-difference matrix equations for electric and magnetic field vectors in the structure under study. The solution of these equations yields static, frequency-domain or time-domain solutions of Maxwell's equations (Refs. 4, 5). MAFIA accepts data directly from standard engineering design software making analyses using the code convenient and efficient.

The particular device analyzed here is the helical slow-wave structure of the Northrop Grumman microwave power module (MPM) TWT (Ref. 6) shown in Figure 1. The TWT nominally produces 100 Watts of output power at midband and operates over a range of frequencies from 6 to 18 GHz. The MPM circuit was chosen for this analysis because it represents most of the elements of a modern slow-wave structure design including a tape helix supported by partially metallized rectangular support rods, and because a complete set of dimensions and experimental data were available from the manufacturer (Ref. 6). Several Northrop broadband circuit parameters were varied including the tape width, tapew, width and relative dielectric constant of the support rods, rodw and ε_r, respectively, and the distance from the helix axis to the metallized films deposited on the dielectric rods, metalr (See Figure 1). The dispersion and impedance are compared for each set of variations.

The specific results presented here apply only to the mentioned circuit, however, these results can serve as a general guide for similar devices, and the computational techniques are readily applicable to

other TWT's. Based on this kind of information, manufacturers can conduct cost-benefit analyses of their manufacturing tolerances and design optimization for a wide variety of devices, before fabrication.

SIMULATION AND ANALYSIS

Helical Model

The helical tape is generated with the actual width and thickness of the experimental circuit in the cylindrical coordinate system by varying axial and azimuthal coordinates consistent with the formula of a circular helix. Initially, the support rods were modeled using the quasi-rectangular configuration discussed in Refs. 2 and 3, where rectangles are approximated by generating radial increments with decreasing rod angles with increasing radius. With this configuration, it is necessary to use ten radial increments for the dielectric support rods to prevent the protrusion of the dielectric material through the metal coating. This increased number of radial increments, compared to six for the typical circuit, complicates the boundary conditions of the problem, increasing the time for the computation to converge. Because of this added complexity and computational time, the rectangular support rods were generated as wedges divided into p sections with graded dielectric constants consistent with the relationship

$$\varepsilon_{rp}' = 1 + (\varepsilon_{rp} - 1)\frac{A_p}{A_p'} \qquad (1)$$

where ε_{rp}' and A_p' are the effective dielectric constant and cross-sectional surface area, respectively, of the pth section of the wedges in the MAFIA model, and ε_{rp} and A_p are the actual dielectric constant and cross-sectional surface area, respectively, of the pth section of the actual rectangular rods. It was shown in Ref. 2 that there was a significant savings in computational time with negligible change in dispersion and on-axis interaction impedance when using this modeling configuration compared to the quasi-rectangular configuration.

Figure 2 shows the cross-sectional view of the Northrop broadband circuit graded wedge model with p = 4. Figure 3 shows a MAFIA electric field plot of the cross-sectional view of the circuit, the size of the arrows proportional to the magnitude of the field. It is apparent that the electric fields are concentrated more between the helix and the beginning of the metal film than in the region extending from the film to the barrel. Thus, the section of the support rods extending radially from the helix to the metal radius, was divided into three regions, and the section from the metal radius to the barrel was treated as one region. A three-dimensional MAFIA plot of several turns of the Northrop broadband helical slow-wave structure is shown in Figure 4.

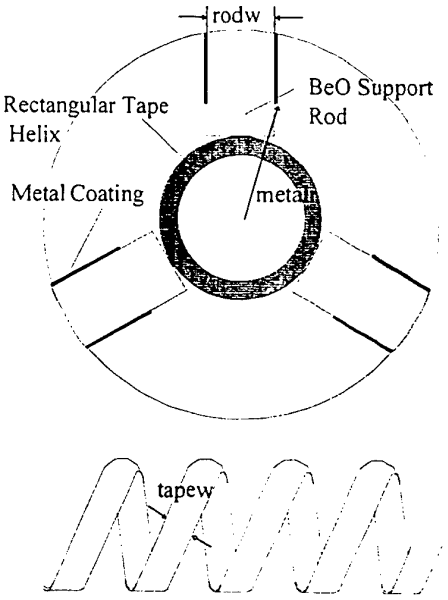

Figure 1 Northrop Grumman broadband MPM TWT helical slow-wave circuit

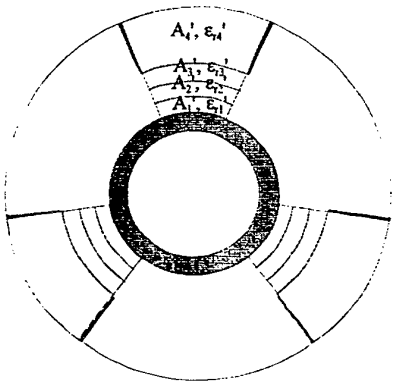

Figure 2 Northrop broadband helical slow-wave circuit model with graded wedge support rods

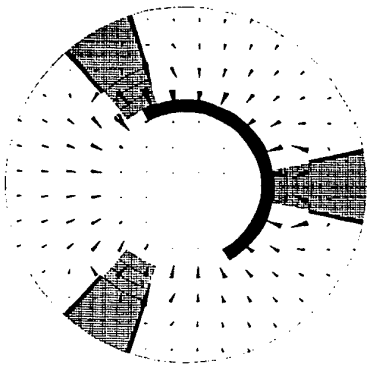

Figure 3 MAFIA electric field plot of cross-section of Northrop broadband helical circuit (βL = 9 degrees)

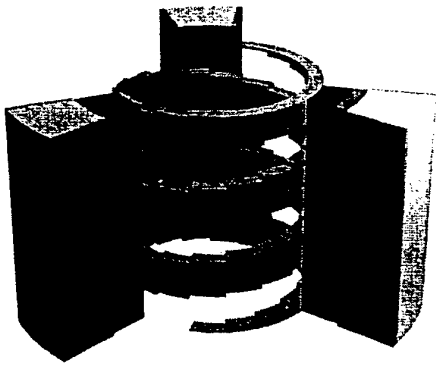

Figure 4 MAFIA three-dimensional plot of several turns of the Northrop broadband helical circuit

Dispersion

The method for calculating the dispersion is similar to experimental methods where frequency-phase characteristics are determined by measuring the resonant frequencies in a section of circuit shorted at both ends. Truncating an infinite circuit at two points with either an electric or magnetic wall with MAFIA corresponds to simulating standing waves with an integral number of half-wavelengths (phase shifts of π) within the isolated circuit section. Although the helix has no symmetry planes at which these boundary conditions are exact, if enough turns are modeled the effects of the fields at the boundaries become small. The results presented here are based on ten helical turns for which the CPU time, using an IBM RISC/6000 Model 590 workstation, was approximately eight hours.

On-axis Interaction Impedance

The same truncation method is also used in the calculation of the on-axis interaction impedance. The on-axis interaction impedance is a measure of the strength of interaction between an RF wave harmonic and the electron beam. In the helix slow-wave circuit, the beam is synchronous with only the fundamental RF space harmonic. For this space harmonic, the interaction impedance on the axis is defined as

$$K_0 = \frac{|E_0|^2}{2\beta_0^2 P_{RF}} \qquad (2)$$

where $|E_0|$ is the magnitude of the fundamental space harmonic of the on-axis electric field, β_0 is the axial phase constant, and P_{RF} is the RF power flow defined by

$$P_{RF} = W v_g \qquad (3)$$

where v_g is the group velocity, and W is the stored electromagnetic energy per unit length (Ref. 7).

SIMULATION RESULTS

The accuracy of the MAFIA model has been validated in Refs. 2 and 3, where the dispersion and on-axis interaction impedance calculated using MAFIA were compared to experiment. The absolute average differences across the bandwidth were 1.5% and ten Ohms, for the dispersion and impedance, respectively.

Various circuit parameters were varied including tape width, support rod width and effective dielectric constant, and metal film radius, and are compared in terms of the cold-test dispersion and on-axis interaction impedance. First the dispersion and on-axis interaction impedance were calculated for several variations on the metal film radius (metalr of Figure 1). The dimension was varied within and beyond its manufacturing tolerance of 0.0005 inches. The results are plotted for the dispersion in Figure 5. From this plot we see that as the film approaches the helix, or the loading is increased, the bandwidth is increased. Figure 6 which plots the on-axis interaction impedance for the same variations, shows that this increase in bandwidth is achieved at the expense of a decreased impedance.

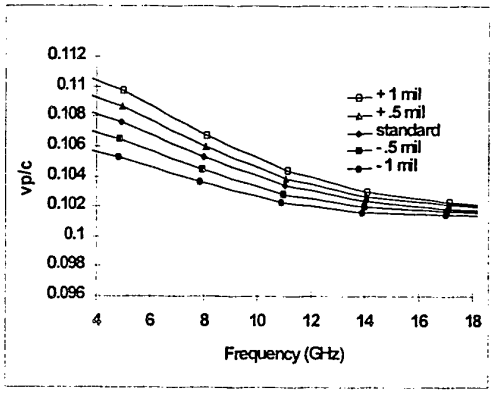

Figure 5 Simulated dispersion for variations on metal film radius, metalr

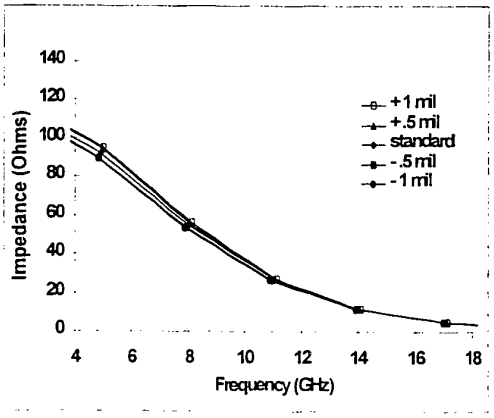

Figure 6 Simulated on-axis interaction impedance for variations on metal film radius, metalr

Next, the dispersion and on-axis interaction impedance were calculated for several variations on

the support rod width, rodw of Figure 1. Figure 7 and Figure 8 show the dispersion and on-axis interaction impedance, respectively, for variations within and beyond its manufacturing tolerance of 0.0005 inches. From these plots we see that these variations will not affect bandwidth, but will increase or decrease the phase velocity, and thus the operating voltage, uniformly across the bandwidth. The impedance is also uniformly increased or decreased across the bandwidth, increasing slightly when the rod is made thinner.

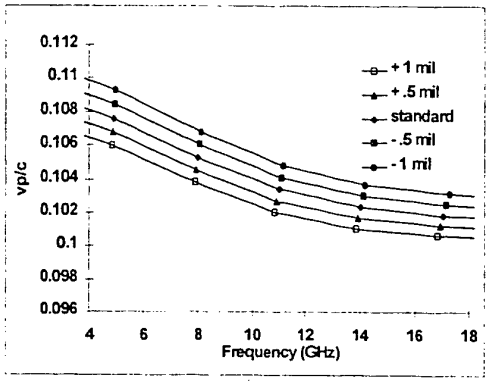

Figure 7 Simulated dispersion for variations on support rod width, rodw

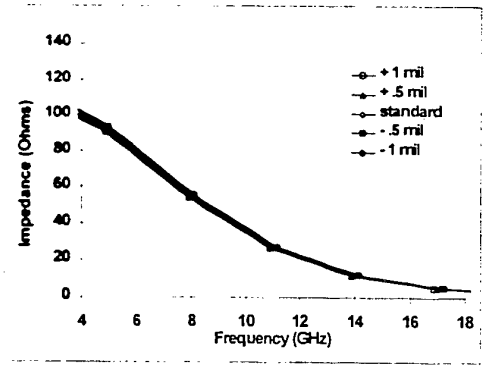

Figure 8 Simulated on-axis interaction impedance for variations on support rod width, rodw

The axial width of the helical tape, tapew, was varied within and beyond its dimensional tolerance of .0005 inches. Figure 9 and Figure 10 show the dispersion and on-axis interaction impedance, respectively. With increased tape width, only a slight decrease in both phase velocity and impedance occurs uniformly across the bandwidth except for the + 1 mil variation which decreases the phase velocity more significantly. Because a helix fabricated with wider tape width would have improved thermal properties. this result may have valuable engineering significance.

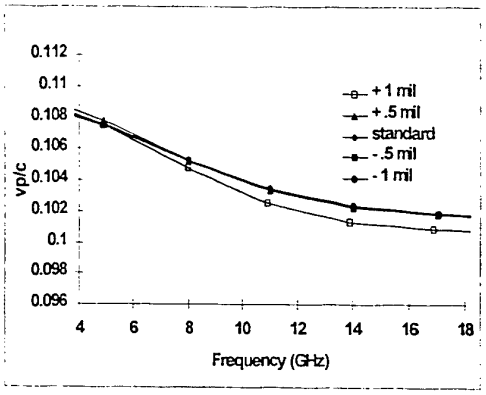

Figure 9 Simulated dispersion for variations on helical tape width, tapew

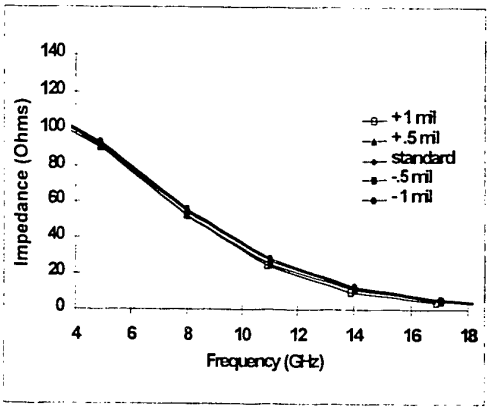

Figure 10 Simulated on-axis interaction impedance for variations on helical tape width, tapew

Lastly, the relative dielectric constant of the support rods was varied. The motivation for this last set of variations was based on citations from various sources that reported the dielectric constant for BeO to be anywhere from 6 to 7.5. As part of another investigation, we have already done some in-house dielectric measurements on anisotropic pyrolytic boron nitride (APBN) where we found variations in the permittivity as high as +/- 10% within the same sample (Ref. 8). We intend to also conduct an experimental study of the permittivity of BeO.

Figure 11 and Figure 12 show the dispersion and on-axis interaction impedance, respectively, for variations on the dielectric constant from 6 to 7.5. The difference in the dispersion and impedance is greater than any of the dimensional variations made, even those beyond the dimensional tolerances. This could be a large contributing factor to why TWT's of the same model, presumably fabricated within manufacturing tolerances, exhibit significant variations in performance. From these results it appears the phase velocity and impedance are uniformly shifted up or down across the bandwidth. With increased permittivity. phase velocity and impedance decrease.

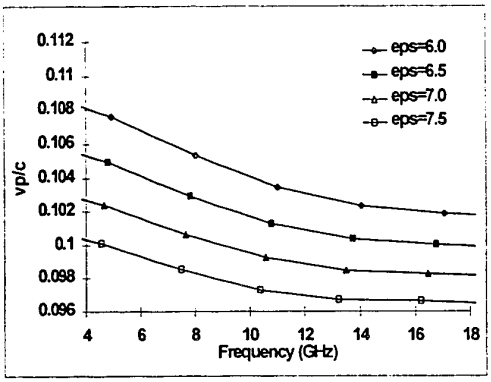

Figure 11 Simulated dispersion for variations on support rod effective dielectric constant, ε_r

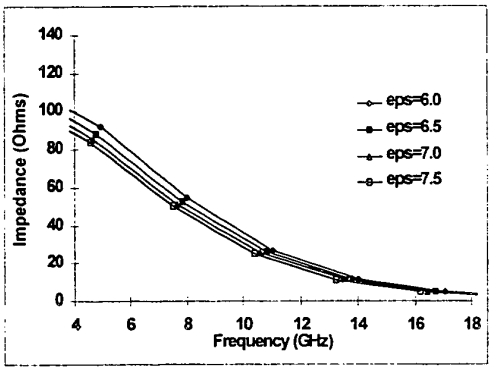

Figure 12 Simulated on-axis interaction impedance for variations on support rod effective dielectric constant, ε_r

CONCLUSIONS

A method has been demonstrated by which the sensitivity of parameter variations can be accurately obtained for helical TWT slow-wave circuits. Several variations were performed with MAFIA on the basic helical circuit parameters. We found the effect on tube performance of the dimensional tolerances on the metal vane radius, tape width and the support rod width. Most importantly we found that the effect on performance due to variations in the dielectric constant was the most prominent, implying that support rod permittivity is the most sensitive parameter of any of the variations made. This demonstrates the need for more complete information about the material being supplied for tube manufacturing.

With this accurate model for helical slow-wave structures, much potential exists to improve reliability and cost effectiveness in TWT manufacturing. A large amount of time and money can be saved by avoiding experimental measurements by optimizing designs and determining tolerance sensitivity with MAFIA previous to fabrication.

REFERENCES

1. Kory, C. L., Three-Dimensional Simulation of Helix Traveling-Wave Tube Cold-Test Characteristics Using MAFIA, *IEEE Trans. on Electron Devices,* vol. 43, no. 8, pp. 1317-1319, August 1996.

2. C. L. Kory, Validation Of An Accurate Three-Dimensional Helical Slow-Wave Circuit Model, NASA Contractor Report, CR-4766, March 1997.

3. C. L. Kory and J. A. Dayton, Jr., Introduction To An Accurate Cold-Test Model Of Helical Slow-Wave Structures, Microwave Tubes for Space, Military and Commercial Applications Workshop, April 7-10, 1997, Noordwijk, The Netherlands.

4. T. Weiland, On the Numerical Solution of Maxwell's Equations and Applications in the Field of Accelerator Physics, Part. Accel., vol 15, pp. 245-292, 1984.

5. T. Weiland, On the Unique Numerical Solution of Maxwellian Eigenvalue Problems in Three Dimensions, Part. Accel., vol. 17, pp. 227-242, 1985.

6. Personal communication with Gary Groshart of Northrop Grumman, Electronics Systems Division, Rolling Meadows, IL, USA.

7. J. W. Gewartowski, and H. A. Watson: Principles of Electron Tubes. D. Van Nostrand Company, Inc. 1965.

8. S. Alterovitz et al., Characterization of Commercial APBN, NASA Technical Paper in preparation, 1997.

Life Test Performance of Impregnated Cathode for High Reliable Satellite TWTs

Akira CHIBA, Yasuhiro AKIYAMA

Microwave Tube Division, NEC Corporation
1753,Shimonumabe,Nakahara-ku,Kawasaki,
Kanagawa,211 JAPAN
Tel. +81-44-435-1696 Fax +81-44-435-1923

ABSTRACT

M-type cathodes are commonly used for Traveling Wave Tubes (TWTs). It is very important to verify the lifetime of cathode used for high reliable satellite TWT which requires long life and high quality. In the M-type cathodes, the work function of 411M-type cathode (impregnant materials are 4BaO, 1CaO and 1Al_2O_3 in mole ratio) is lower than 532M-type cathode (impregnant materials are 5BaO, 3CaO and 2Al_2O_3 in mole ratio). Therefore, 411M-type cathode has the advantage of a reduction in operating temperature or an increase in emission. NEC has evaluated 195 pieces of 411M-type cathodes in Cathode Test Tube (CTT) by continuous operation. These cathodes have been evaluated at four operating temperatures between 910℃b and 1,100℃b, and five kinds of current densities ranging from 0.6 to 4.0 A/cm^2 for 90,000 hours or more. Up to the present, a total accumulate time of the life test is 5,362,800 hours. The results of evaluations verified the life prediction models depending on optimum operating temperature and current density of cathode. According to the life prediction model, 411M-type cathode has a life of more than 200,000 hours (22.8 years) at current density of less than 2.0A/cm^2.

1.INTRODUCTION

As an amplifier for this satellite communication system, TWTs (Traveling Wave Tubes) are in widespread use because of their high power and high efficiency compared with solid-state amplifiers. The space satellite TWTs are required to have high reliability, high power and a long life for 12 to 15 years.

The lifetime of a TWT is mainly determined by the lifetime of its cathode, and obtained by the performance of the cathode which is operated at high current density in its long lifetime.

Feltham, et al.(Ref.1) studied the life test on MM-cathodes, and Akiyama (Ref.2) and Mita (Ref.3) studied the degradation factors of M-type cathode and evaluated them. These papers reported that the optimum operating temperature related to the cathode current density and the prediction of cathode lifetime are very important factors to assure the lifetime of a TWT. Therefore, verification of cathode lifetime is indispensable for a high reliable satellite TWT.

This report describes the evaluation results of the cathode life test for 90,000 hours or more, to verify the optimum operating conditions and the expected cathode lifetime.

NEC's 87 units of space satellite TWTs installed on 13 satellites now have experience of traveling in space and have had no failures. This high reliability is supported by the results of cathode life test.

2. CATHODE FOR HIGH RELIABLE SPACE TWT

The various types of impregnated cathodes is shown in Table I .

The M-type cathode was developed by Zalm and Stratum (Ref.4), in Eindhoven at the Philips Research Laboratories.

The M-type cathodes are the most commonly used for microwave tubes, because M-type cathodes have long life, lower operating temperature, lower barium evaporation, high current density and high reliability.

The M-type cathode is a B or S-type with a several hundred nano-meters thickness thin film of osmium, iridium, or ruthenium applied to the surface. Emission current of cathode at a specified temperature depends upon the work function of the cathode: the lower the work function, the higher the emission level. Thus, the effect of the thin film is to reduce the cathode operating temperature for the same emission density as that obtained from a B or S-type cathode (Ref.5).

In the M-type cathode, the impregnant is 5BaO, 3CaO and 2Al_2O_3 in mole ratio (B-type) which is sometimes referred to simply 532M-type, and another impregnant variation (4BaO, 1CaO and 1Al_2O_3; S-type) referred to as 411M-type. The work function of the 411M-type cathode is 0.05 eV lower than that of the 532M-type at the brightness temperature of 1,000℃b as shown in Table I (Ref.6). The results of this efficiency, as shown

Miram plot (Ref.7) in Fig.1, are very impressive, from the viewpoint that a 411M-type cathode gives a choice of either a reduction in operating temperature for the same emission density or an increase in emission for the same operating temperature as a 532M-type. An operating temperature reduction of a 411M-type to a 532M-type cathode was up to 35°Cb.

NEC adopts the 411M-type cathode for high reliable satellite TWTs, because 411M-type cathodes are used as they are capable of meeting the long life and the high current density requirements.

3.LIFETIME OF CATHODE

3.1 Cathode Structure

The 411M-type cathode structure is shown in Fig. 2. The emissive material, which consists of 4BaO, 1CaO and $1Al_2O_3$ in mole ratio, is impregnated into the porous tungsten cathode pellet. The porosity of their tungsten base metal is 18%. After the impregnation, the surface of the cathode pellet is covered with the osmium/ruthenium film.

NEC has designed the 411M-type cathodes and purchased from SEMICON associates in U. S. A.

Table I Various cathode types.

Cathode type	Emitter $BaO : CaO : Al_2O_3$ (mol)	Matrix	Coating material	Characteristics/ work function ϕ at 1,000°Cb (eV)
S-type	4 : 1 : 1	W	Non	Standard impregnant type ($\phi = 2.04$)
B-type	5 : 3 : 2	W	Non	Low evaporation type ($\phi = 2.09$)
411M-type (Os/Ru)	4 : 1 : 1	W	Os/Ru	Long life and low T_k ($\phi = 1.96$)
532M-type (Os/Ru)	5 : 3 : 2	W	Os/Ru	Long life and low T_k ($\phi = 2.01$)

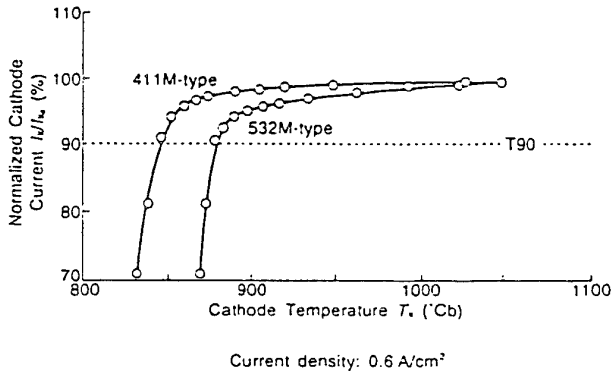

Fig. 1 Miram plot of impregnated cathode.

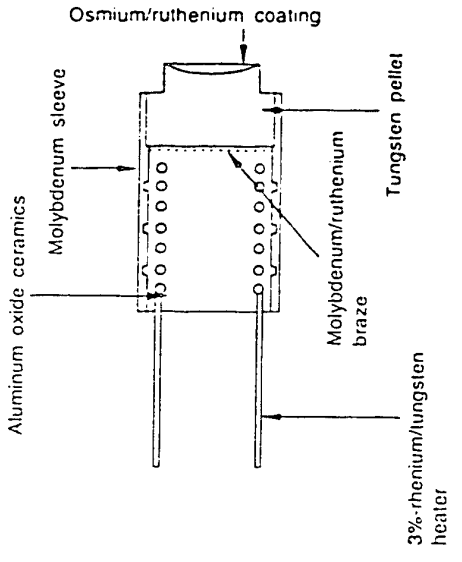

Fig. 2 411M-type impregnated cathode.

3.2 Cathode Life Test Condition

The cathode is the only component subject to wearout in a TWT. Therefore, the lifetime of TWT is strongly determined by the life of its cathode.

Life testing is being performed at this moment at four operating temperatures between from 910℃b to 1,100℃b, and five kinds of current densities ranging from 0.6 to 4.0 A/cm^2 as shown in Table Ⅱ. In this test, 195 pieces of M-type cathodes are evaluated in Cathode Test Tubes by continuous operation. Up to the present, the total accumulated time of the life test amounts to 5,362,800 hours and it will continue to operate stably.

The Cathode Test Tube (CTT) is shown in Photo1. The structure of the CTT is triode, consisting of cathode, anode and collector as shown in Fig. 3. The CTT has the same product process and cathode activation procedure as the existing highly reliable satellite TWT.

Photo 2 shows automatic evaluation equipment for cathode.

Table II Condition for the cathode life test.

Current density (A/cm^2)	Cathode temperature (°Cb)	Quantity (pcs.)	Accumulated life test time as of Oct. 1996 (hours)
0.6	910	9	300,100
	930/940	34	1,725,100
	970	8	361,600
	1,030	8	342,800
	1,100	6	159,300
1.2	910	7	187,700
	970	9	288,000
	1,030	9	225,300
	1,100	7	164,700
2.0	910	6	123,000
	970	12	255,600
	1,030	12	273,300
	1,100	12	228,900
3.0	970	12	229,900
	1,030	12	249,400
	1,100	12	186,000
4.0	1,030	10	28,200
	1,100	10	28,900
Total		195	5,362,800

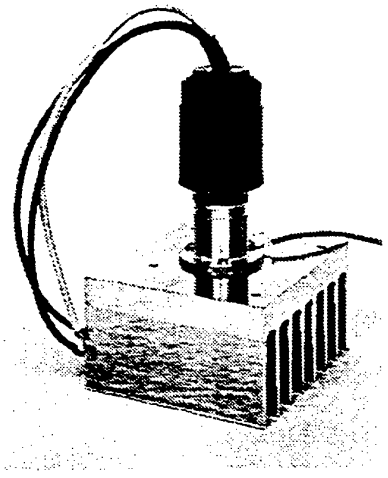

Photo 1 Cathode test tube.

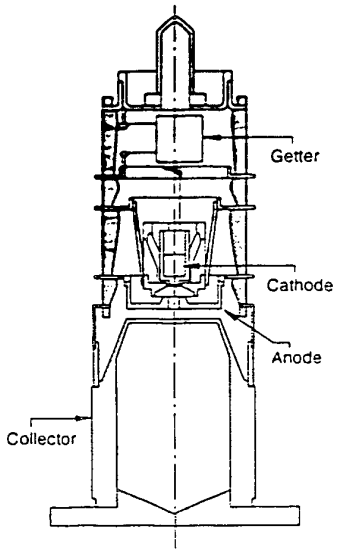

Fig. 3 Structure of cathode test tube.

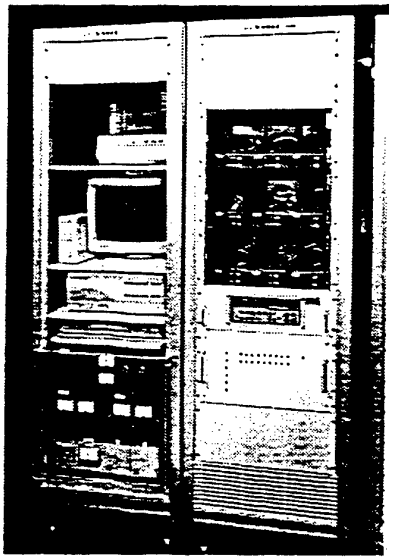

Photo 2 Evaluation equipment for cathode.

3.3 Life prediction Method

To find out the degradation state of the cathode, the following two methods are available:

- Monitoring the amount of degradation in the cathode current(I_k) at the operating temperature.
- Examining the degradation characteristics of I_k, or knee characteristics, obtained by lowering the cathode temperature(Fig. 4).

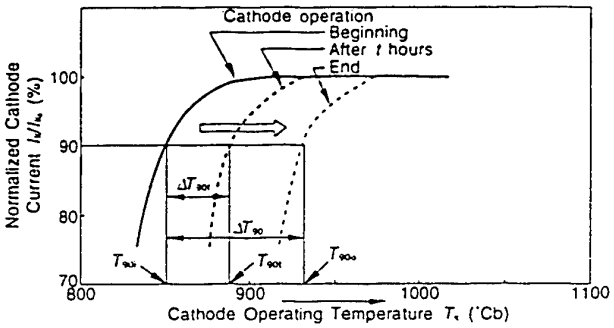

T_{90}: Operating temperature (knee point) when the cathode current had dropped to 90% of full emission
T_{90i}: Initial value of T_{90} before operation
T_{90t}: Knee point after t hour operation
T_{90t}: $T_{90i} - T_{90t}$
T_{90e}: Final value of T_{90} at end operation
T_{90}: $T_{90e} - T_{90i}$

Fig. 4 Times dependence of knee characteristics.

To predict cathode lifetime, it is important to monitor the movement of the knee characteristics with time. Figure 4 shows the knee characteristics.

The knee point (T_{90}) is defined as the operating temperature when the cathode current had dropped to 90% of full emission. The knee point T_{90} changes during operation. As time goes by, T_{90} shows a comparatively large change while I_k shows a much smaller change. Thus, monitoring of the change in T_{90}, whose maximum value is ΔT_{90}, is more suitable for cathode life prediction (Ref.8-9).

4.RESULT OF CATHODE LIFE TEST

Figures 5 and 6 show the monitoring data of the cathode current (I_k) with time.

Figure 5 shows that in case of different cathode temperatures T_k=910, 970, 1,030 and 1,100°Cb at the same cathode current density J=0.6 A/cm^2, the cathode current decreases faster at high operating temperature of the cathode than at a low one.

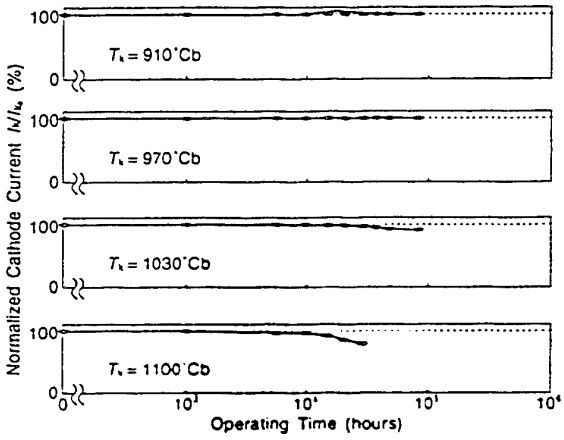

Fig. 5 Trend of cathode current.

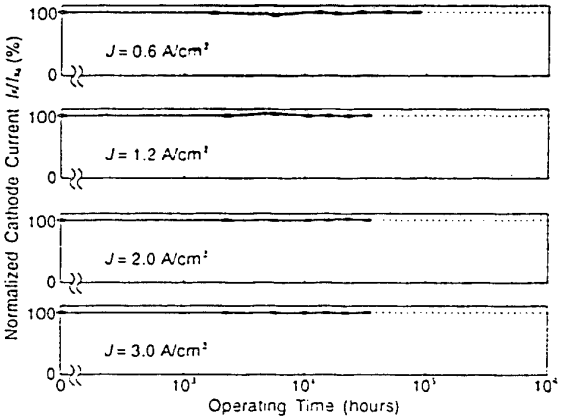

Fig. 6 Trend of cathode current.

On the other hand, Fig. 6 shows the movements of the cathode current in different current densities J=0.6, 1.2, 2.0 and 3.0 A/cm^2 at the same cathode operating temperature T_k=970°Cb. These cathode currents show almost no decrease in several tens of thousands of hours.

Thus, the amount of cathode current change is too small to predict the life of the cathode.

However, as shown in Fig.7, the ΔT_{90} monitored along with the operating time does not depend on the current density even though it changes from 0.6 to 3.0 A/cm^2, but depends on the operating temperature T_k. It also depends on ΔT_{90t} because ΔT_{90} shows the same behavior as ΔT_{90t} (Fig.4). On the other hand, Fig.8 shows that the temperature function $F(T_k)$ depends on cathode temperature T_k, which is derived from ALENIUTH plot.

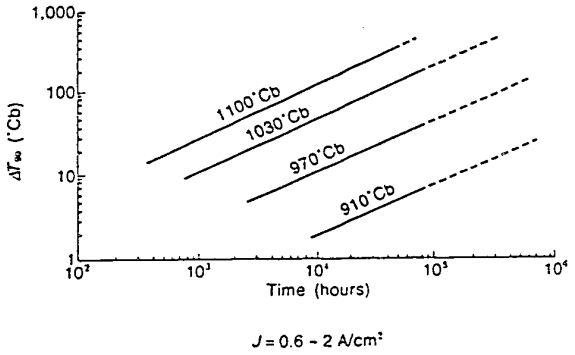

Fig. 7 Time dependence of ΔT_{90}.

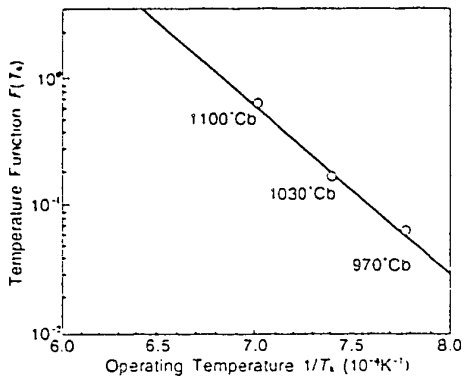

Fig. 8 $F(T_k)$ versus cathode temperature.

Here we introduce an approach to predicting the cathode life using from ΔT_{90t} and $F(T_k)$.

The behavior of ΔT_{90t} with the operating time shows the following:

- ΔT_{90t} and operating time, which are formed in logarithmic functions, can be described as a linearly proportional relation.
- ΔT_{90} increases exponentially along with the operating time ($\Delta T_{90} \propto t^{0.6}$).
- ΔT_{90t} is larger at higher temperature than at lower temperature. It is not dependent on the cathode current density J, but is dependent on the cathode temperature T_k.

The relation of ΔT_{90t}, cathode temperature T_k and operating time t is described as the following equations.

$$\ln(\Delta T_{90t}) = B \times \ln(t) + \ln F(T_k) \quad \text{--- (1)}$$

$$\ln F(T_k) = C_1 / T_k + C_2 \quad \text{--- (2)}$$

Where

ΔT_{90t} :	Deferent of temperature between the beginning and after t hours (Kelvin),
T_k :	Operating temperature (Kelvin),
t :	Operating time (hours),
$F(T_k)$:	Temperature function,
B, C_1, C_2:	Constants.

According to the life test results, constants B=0.6, $C_1 = -2.926 \times 10^4$, and C_2=19.83 are obtained by NEC.

The end of cathode life is defined as the time when the cathode emission has dropped by 10% from the initial current. Thus, cathode lifetime means the shifting time of T_{90} from initial value T_{90i} to the operating temperature T_k.

A temperature margin T_m between the initial value T_{90i} and the operating temperature T_k (Ref.8) is shown as:

$$T_m = T_k - T_{90i} \quad \text{--- (3)}$$

Thus, from Eqs. (1), (2) and (3) the cathode life is predicted by the following equation:

$$\ln(L) = (1/B) \times \{\ln(T_m) - C_1/T_k - C_2\} \quad \text{--- (4)}$$

Where

L : Predicted cathode lifetime (hours),
T_m : Temperature margin (Kelvin),
T_k : Operating temperature (Kelvin)

From the results of our life test, it comes to be clear that the expected cathode lifetime at various current densities can be calculated and the expected value shown by using Eq.(4).

5. DETERMINATION OF CATHODE OPERATING TEMPERATURE

As described in the preceding sections, the cathode lifetime can be obtained from the degradation speed of T_{90} and the temperature margin determined by the operating conditions of the cathode.

The cathode at higher operating temperature has a larger temperature margin but the cathode current degrades at a faster speed.

On the other hand, if the cathode is operated at too low an operating temperature, the temperature margin is small and requires that consideration be given to the possibility of gas poisoning caused by residual gas in a TWT. However, there was no phenomena of contamination by gas poisoning in life test data. Therefore, when the cathode operating temperature is selected at 910℃b or more, it is verified that M-type cathode is not contaminated by gas poisoning.

Consequently, the lifetime depends on the operating temperature. The optimum cathode operating temperature at each current density has the maximum lifetime, as shown in Fig.9.

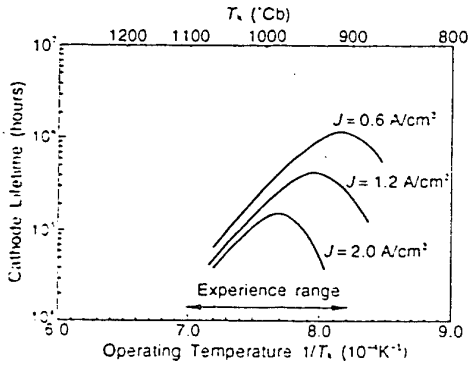

Fig. 9 Expected cathode lifetime.

6. EXPECTED CATHODE LIFETIME

Figure 10 shows the relation of expected cathode lifetime and current density at optimum temperature.

Cathode current density is usually designed to be less than 2.0A/cm^2. Figure 10 shows that the cathode with current density of less than 2.0A/cm^2 has a lifetime of more than 200,000 hours (22.8 years). This value meets the most current requirements.

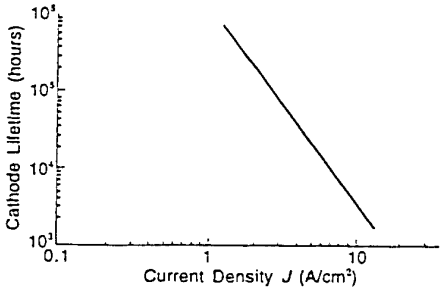

Fig. 10 Life expectancy versus current density.

7. CONCLUSION

The constants for life prediction formula of 411M-type cathode were also obtained. The life prediction formula can give the optimum cathode operation and lifetime.

According to the formula, 411M-type cathode has a life of more than 200,000 hours (22.8 years) with a cathode current density of less than 2.0A/cm^2. This value meets most current requirements.

ACKNOWLEDGMENTS

The authors wish to thank Mr. Louis R. Falce of CERADYNE, Inc. and Mr. James O. Tarter of SEMICON associates in U.S.A for their valuable advice on cathodes.

*** References**

1. S.J.Feltham, et al., "Life Test Studies on MM-Cathodes", IEEE, Vol.37, No.12, Dec. 1990.
2. Yasuhiro Akiyama, et al., "Evaluation of Reliability Impregnated Cathode", NEC Technical Report, Vol.44, No.7,1991. (in Japanese)
3. Nagahisa Mita, "Degradation Factors of a Coated Impregnated Cathode", IEEE, Vol.39, No.9, Sep. 1992.
4. P.Zalm and A.J.A.van Stratum, "Osmium dispenser cathodes", Philips Tech. Rev. , Vol.27, 1966.
5. A. S. Gilmour, Jr., "MICROWAVE TUBES", Artech House, pp. 126.
6. J. L. Cronin, "Modern dispenser cathodes", IEE, PROC., Vol.128, Pt.1, No.1, Feb., 1981.
7. M.C.Green, "Modern Thermionic Cathodes", IEDM,1987.
8. N. Mita and K.Shimokawa, "Reliability Improvement and Evaluation of TWTs for Communications Satellite", Proc. Int. Symp. for Teating & Failure Analysis, pp. 47-52, 1986.
9. S.Miura, et al., "Reliability Assurance of NEC's Space TWTs", NEC Res. & Develop., Vol.37, No.2, pp. 249-259, Apr., 1996.

THE SECRET TO ACHIEVING MICROWAVE TUBE RELIABILITY

Edward J. Jones
US Air Force/Rome Laboratory
ERDS, 525 Brooks Rd.
Rome, NY USA 13441-4505

ABSTRACT

A performance-based acquisition reform reliability and quality process for designing reliability and quality into tubes for military systems was developed. As of June 1994, the US Department of Defense began "A New Way of Doing Business" called "Acquisition Reform" by moving away from using MILSPECs to the use of commercial practices to procure its military systems and parts. The problem is "what is the best commercial practices" for achieving and proving tube reliability under this new system. This paper describes the current "thinking" on how to develop a tailored tube reliability program using commercial best practices to meet the intent of Acquisition Reform.

1.0 INTRODUCTION

There is no "secret" to achieving very high tube reliability. There are many cases of high power tubes that have many thousands of hours of reliability. Throughout many years of investigations Rome Laboratory has discovered that the main causes of poor reliability are due to 1) poor manufacturing quality, 2) poor maintenance techniques, 3) no protection between the system and the tube, 4) poor design techniques, 5) operator misuse, 6) the lack of utilizing derating principles, 7) the acquisition system and going "low bid", and 8) system software faults. These causes of poor reliability do not need to be designed into a tube or system.

Over many years the US Department of Defense (DoD) established a military infrastructure and a documentation system to ensure procurement of high performance and reliable systems. However, as the DoD budget decreases, "A New Way of Doing Business" has become the rallying cry for the procurement of US military systems. The methods for procuring and supporting military systems are changing greatly. The DoD's plan is to leverage best commercial practices by using the commercial/industrial base and emphasizing dual-use practices to the greatest extent possible. The move to commercial products, practices and processes is part of a DoD strategy (called Acquisition Reform) to promote the expansion of a national industrial base, which is capable of meeting DoD needs, while competing effectively in the world marketplace. The culture change of moving away from military specifications and standards (MILSPECs) has raised many questions in the acquisition community. These questions center around determining what constitutes "best" commercial practices and how well suited are they for designing tubes for harsh military environments. To assist tube vendors in this "new way of doing business" Rome Laboratory and the Reliability Analysis Center have evaluated current best practices and developed guidance for a tailored performance-based reliability and quality process plan, called RL 2001, and is intended to provide insight into how to optimize reliability based on continuous and aggressive improvements, with action based on facts, data analysis and value-added practices. This paper will describe the current "thinking" of this process plan.

The result of this paper will provide an example of what should be included in a tube reliability program and is based on the use of the three referenced documents, however, the reader is cautioned that this is only an example and should be used as a starting reference point only.

2.0 DEVELOPING A TAILORED RELIABILITY PROGRAM - RL 2001

Succinctly put, *Reliability* is a performance attribute that is concerned with the probability of success and frequency of failure and is defined as: *The probability that an item will perform its intended function under stated conditions, for either a specified interval or over its useful life.* Reliability is a

measure of a product's performance that affects both product function and operating and repair costs. Too often performance is thought of only in terms of speed, capacity, range, power, bandwidth, gain, and so on. However, if a tube fails so often that it's seldom available for use, its power, bandwidth and gain capacity are not relevant. Reliability is also critical to safety in some systems; e.g., electronic warfare, radar and communication.

The reliability of the power amplifier, in this case a power tube, in the transmitter is the primary factor in determining operating and repair costs, which are partially a function of the number of repairs needed over time, the number of spare tubes required, and the number of maintenance personnel necessary. Other factors such as the repair policy, maintenance concept, affect these costs, but reliability is the significant factor.

Reliability determines whether or not the tube is available to perform its function. A tube with perfect reliability; i.e., no failures during the life of the tube, would always be available for use. But perfect reliability is difficult to achieve. So, even when a high level of reliability is achieved, some failures are to be expected and planned for. The effects of failures on availability (and cost) can be minimized with a proper level of maintainability (a measure of how quickly the system can be repaired). Consequently, tube reliability and system maintainability (R&M) are said to be complementary characteristics, and can be combined to measure the percentage of time that the system is available for use.

From the Customer's perspective he or she needs to know: 1) What measures of reliability are important to them?; 2) What levels of reliability are necessary to meet their need?; and 3) How will they determine if the required levels of reliability have been achieved? From the Supplier's perspective he or she needs to know: 1) What reliability activities are the most effective for the tube or system, such that the reliability program objective is achieved?; 2) What reliability design goals are appropriate to ensure that customer's needs are met?; 3) What design approaches will be most effective in achieving the required reliability in the expected environmental and usage profiles?; 4) What tasks can be effectively used to assess progress towards reliability goals and requirements?; 5) What are the most appropriate means to determine if the reliability objective has been achieved?; and 6) How can the designed-in reliability be retained during manufacturing and operational use, thereby ensuring reliable performance? The answers to these questions must be determined at the start of a new program. The "Science and Engineering of Designing Reliability & Quality" into a part or system is based on Taguchi's "Robust Design" Principles: 1) reduce product sensitivity to the sources of variability through careful selection of design values and 2) minimizes less-than-optimal interactions among a product's parts caused by external factors such as: manufacturing process variations, abusive operation, and the environment. Tube failures are caused by the lack of a "robust design", both hardware and system software. For hardware, failures are caused by deficiencies in design, production, use, and/or maintenance. System software faults are caused by errors made during requirements definition and analysis, design, coding, and/or maintenance. In the commercial world, the average consumer is not usually concerned with the second set of issues - they are left to the supplier to confront. If a supplier does a poor job, the customer will go elsewhere for the product. Thus, competition in the marketplace provides a strong incentive to meet the customer's needs. In the defense tube world, the degree of competition is much less than in the commercial world.

The objective of any set of reliability tasks is to design and manufacture a reliable tube in a cost-effective manner. In order to effectively achieve this result the following "best practices" must be well understood and used, and an example is shown in Table 1.

Table 1: "Best Practices"

• The Customer's Reliability Expectation and Needs Should be Fully Understood. Adequate levels of reliability are essential to the overall performance of the tube. These levels should be expressed by the customer (in which case, they are part of the customer's specification) or determined by the supplier as necessary to compete satisfactorily and to minimize liability. In either case, it is the customer's needs that must be understood at the start of the program and satisfied.

• Supplier Management Should be Actively Committed. The ability to successfully achieve the reliability objective is dependent on the demonstrated level of commitment by management, particularly at the upper levels. This commitment can be reinforced by making sure that this objective is an integral part of the corporate technological and business strategy. Demonstrate and emphatic management commitment will help reinforce any "culture change" that may be necessary to implement those actions necessary to achieve the program objective.

• Reliability Attributes of Design and Manufacturing Should Be an Integral Part of the System Engineering Process. By making the reliability aspects of design and manufacturing an integral part of the system engineering process, reliability requirements will be addressed concurrently with other performance requirements. In this way, reliability activities will be integrated with other engineering and design tasks, thereby avoiding duplicative effort and making the best use of output information and results. In planning a reliability program, the integration of design, analysis, and other tasks to minimize costs and maximize the use of task results should be explicitly addressed.

• Tube Should be Designed for the Intended Use Environment. To be reliable, the tube should be designed for the environment in which it will be used, and the design should be thoroughly understood. Characterizing the environment is a top priority. The use environment includes all the stresses experienced by the tube during manufacturing, packaging, shipping, handling, storage, operation, stand-by mode, and repair/maintenance. Understanding the strengths and weakness of the design requires that critical failures be analyzed to determine their root cause and tube-level effects, and to change the design to eliminate or minimize the effects of the failure modes.

• Reliability of the Design Should be Verified. Verifying that the reliability objective has been met can be accomplished through testing and/or analysis. Through testing, the tube's design (and the tools used to create that design) can be validated. Testing may uncover unexpected design weakness or unsatisfactory performance, and serves as a development tool that provides the feedback needed by engineers to refine their design and revise their analysis. Extensive testing may become prohibitive due to the nature of the product (e.g., too expensive). In such cases, analytical means can be used to determine if requirements have been met. Most of the time, both testing and analysis are used together.

The objective of a sound reliability program should be similar to that for other design characteristics since "reliability is an inherent design characteristic." Attempts to improve the inherent reliability of a tube after the design is "frozen" are expensive and inefficient. In addition, reliability depends on other factors, most notably how the tube is actually used, lack of protection between the system and the tube, operator misuse, poor maintenance techniques, poor manufacturing quality, and system software faults. These factors can easily compromise the performance of a "good" design.

A typical set of Reliability Tasks that have been used are given below in Table 2, note that this is not an all encompassing list but is intended to be the start of a process to develop the technical know-how and provide insights into the development of a tailored performance-based reliability and quality process plan.

Table 2: Reliability Tasks

Design Tasks and Descriptions

• Critical Item Control: Monitoring in-house and tube part supplies' activities to reduce the risk to tube reliability from items identified as critical.

• Critical Item Identification: Cataloging items that have relatively high impact in determining product reliability.

• Derating: Limiting the maximum allowable stresses on a part to a designated value below its rated maximum stress in order to minimize less-than-optimal interactions among a tube's parts caused by external factors.

• Design Reviews: Independent evaluation and critique of a design to identify and correct deficiencies.

• Environmental Characterization: Determination of the operational stresses the tube can be expected to experience.

• Thermal Design: Consideration of heat generation and dissipation in the tube in order to prevent reliability problems.

Analysis Tasks and Descriptions

• Allocations: Translation of tube and system reliability goals into reliability goals for the components making up the tube.

• Design of Experiments (DOE): Systematically determining the impact of process and environmental factors on a desired tube parameter, in order to reduce product variability by controlling the factors.

• Dormancy Analysis: Determination of the effects of expected periods of storage or other non-operating conditions on the reliability of the tube.

• Stand-by Mode Analysis: Determination of the effects of expected periods of stand-by operating conditions on the reliability of the tube.

• Durability Assessment: Determination of whether or not the mechanical strength of the tube will remain adequate for its expected life, including the high voltage cable and connector.

◦ Failure Reporting Analysis & Corrective Action System (FRACAS): A closed-loop system of data collection, analysis and dissemination to identify and correct failures of the tube or process.

• Testing Strategy Analysis: Determination of the most cost-effective mix of tests for the tube.

Testing Tasks and Descriptions

• Accelerated Life Test: Testing at high stress levels over compressed time periods to draw conclusions about the reliability of the tube under expected operating conditions, based on formulated correlation factors.

• Environmental Stress Screening (ESS): Operating the tube under high stress to identify defects in order to eliminate them before a product is shipped to its user.

• Reliability Qualification Test (RQT): Testing the tube to demonstrate whether its reliability requirements has been achieved.

3.0 CONCLUSIONS

The bases of a tailored performance-based reliability and quality process plan to develop the technical know-how and provide insights into developing military tubes in the new era of Acquisition Reform was described above. However, it is important that the tube supplier select only those tasks that are best suited to achieve the desired results given current market conditions, the competitive environment, the phase of system development, and associated technical and strategic risks. An effective reliability program will require the performance of one or more tasks that will add value as a means of satisfying the reliability objective. Remember, "The Customer is the final judge of reliability and quality, quality is driven by and defined by the Customer."

ACKNOWLEDGMENT

The author would like to acknowledge and thank Preston MacDiarmid and Dave Nicholls of the Reliability Analysis Center for their contribution to this paper.

REFERENCES

1. E.J. Jones, et. al., "DRG Handbook: Microwave and Millimeter Wave Tubes and Power Supplies," North Atlantic Treaty Organization (NATO) Defence Research Group AC243, Panel 3, Research Study Group - 19, September 1996, NATO Limited.

2. "Reliability Toolkit: Commercial Practices Edition," a Rome Laboratory and Reliability Analysis Center, Publication, 1995, Unclassified.

3. "Blueprints for Product Reliability," a Reliability Analysis Center, Publication, 1996, Unclassified.

Biography

Edward J. Jones
United States Air Force
Rome Laboratory/ERDS
525 Brooks Road
Rome, NY 13441-4505
Phone: (315) 330-2702

Mr. Jones is Chief of the Design Analysis Branch within the Electronics Reliability Division at Rome Laboratory, Rome, New York. For the past eighteen years, he has been working on developing highly reliable solid-state and vacuum technology, and computer-aided reliability assessment tools for electronic surveillance systems. Mr. Jones has a M.S. in Electrical Engineering from Syracuse University, 25 publications, 3 patents, is a Senior Member of the IEEE and is Chairman of the NATO Research Study Group on "Micro and Millimeter Wave Tubes."

ACHIEVING MICROWAVE TUBE RELIABILITY USING AN ADVANCED COMPUTER SOFTWARE TOOL

Eunice T. Ciskowski, 1Lt, USAF
Rome Laboratory
ERDS, 525 Brooks Road
Rome, NY USA 13441-4505

ABSTRACT

An advanced computer software tool, known as the Microwave Device Analysis System, or MiDAS, was developed by the Royal Netherlands Navy to enable microwave tube designers, manufacturers, and users to calculate reliability figures of merit. Rome Laboratory conducted the first beta test of this new reliability analysis tool and evaluated it in various areas, including its user friendliness and overall accuracy. The research described in this paper shows that MiDAS provides an efficient means of both storing microwave tube failure information and then calculating reliability parameters readily available for analysis. Accurate reliability parameters are essential for identifying potential problems that, if corrected, will lead to increased overall systems reliability and decreased life-cycle costs.

1.0 INTRODUCTION

In 1962, the U.S. Department of Defense developed a military handbook, MIL-HDBK-217, as a standard for predicting the reliability of electronic equipment used by the U.S. military (Ref. 3). Soon after its development, MIL-HDBK-217 was widely used, and today it is still considered an acceptable method for predicting electronic equipment reliability. This success, however, did not come to pass without criticism. Some users of the handbook maintain that it is based on careful analysis of part and system reliability data, and that any problems arising with it are caused by misinterpretation or misuse of it. On the contrary, opponents of the handbook say that it is inaccurate and leads to costly overdesign. Over the years, the handbook has gone through many revisions, the latest version being 217F. The model for microwave tubes in revision 217F is less pessimistic than the 217C model, but in general, it still gives extremely pessimistic predictions of microwave tube reliability (Ref. 2). MIL-HDBK-217 is continually being updated as technology progresses. Unfortunately, it takes much time and funding to produce the revisions. As a result, the empirical and field data collected to be used in the models are no longer current. Thus, there existed a need for an improved reliability tool.

The Microwave Device Analysis System (MiDAS) was developed by the Royal Netherlands Navy to perform reliability analyses on microwave tubes in systems used aboard its ships. Before the development of MiDAS, a 'run to break' strategy was being applied for these microwave tubes since accurate calculations of reliability parameters were lacking (Ref. 1). This particular strategy is far from ideal, and a more preventive maintenance schedule was desired. Such a schedule is possible when one can calculate accurate reliability parameters of microwave tubes. In order to achieve more accurate reliability parameters, MiDAS was developed to offer some advantages over the accepted methodology presented in MIL-HDBK-217. Supposedly, unlike MIL-HDBK-217, MiDAS provided the advantage of using current field data in its tube analyses. The developers also claimed that MiDAS not only provided mean time to failure hours but that it gave information regarding actual tube failure modes. These alleged advantages of MiDAS warranted further research. Thus, Rome Laboratory volunteered to implement and use MiDAS to obtain reliability parameters for a large number of U.S. military microwave tubes.

As with any new product, questions and concerns regarding MiDAS immediately presented themselves. These questions include: 1) How easy is it to implement and utilize MiDAS?; 2) How

user-friendly is it?; 3) What roles, if any, do the sources and methods of microwave tube data collection play in the ability to calculate reliability parameters?; 4) What happens when deficiencies exist?; and 5) How accurate will the output be? This paper discusses the experiences of working with MiDAS. In addition to addressing the above listed questions, the paper also provides insightful comments and information regarding the software's manual, data entry process, reliability calculations, and overall user friendliness.

2.0 SOFTWARE REQUIREMENTS AND MANUAL

The installation of MiDAS is quite easy. The program demands a standard I.B.M. compatible with DOS 2.0 or higher. The graphics run on a standard video card such as CGA, EGA, VGA, SVGA, Hercules, PC 3270 or ATT (Ref. 1). A pentium PC was used for this research study. Installation of the software was completed as described in the manual. Basically, the software was copied onto and run from the hard drive.

The software manual was originally written in Dutch. It was translated to English and used extensively throughout this study. Overall, the manual is easy to read and comprehend. It is divided into three concise and convenient parts. Part I, entitled "Reliability Technique", describes the theory used in the program. Part II, "MiDAS Structure", describes the program set up. Part III, "MiDAS Manuals", describes the program features and output. This layout provides quick reference for the user. If the user is not interested in the theory, then he or she may skip directly to Part III for the features and output.

3.0 ENTERING DATA AND CREATING THE DATABASE

Entering data into the system is rather simple. The most difficult part was figuring out exactly where to input the different field data. At first, it was unclear what information was required and where the information belonged in the database. However, further comprehension of the manual along with some research trial and error soon resolved the initial confusion.

The first step in setting up the database requires the user to input tube setup information. MiDAS has the ability to store up to 96 different tube types and their corresponding information. All information regarding the type (traveling wave tube (TWT), klystron, magnetron) and characteristics (<100kW, helix, pulsed, etc.) of the tube is included in the tube setup. At this point, the user may also enter test information relevant to that particular tube (such as power output at certain frequencies). This test information, however, is not necessary to perform the analyses. The user may also input the installations and platforms for each type of tube. The installations indicate which systems (electronic warfare, communications, etc.) the tubes were used in, and the platforms indicate which vessels (airplane, ship, etc.) the tubes were used on. The installations and platforms are not used in calculating the reliability parameters; however, they could be used for analyzing trend failures.

Once the tube setup is complete, the user is now able to enter failure data. Failure data is entered on livret sheets; (the Royal Netherlands Navy records failure data on livrets, and the name has carried over to MiDAS). The livret sheet contains space for a variety of failure data, but it was discovered that only six of the items are necessary for the reliability calculations; the remainder of the information is used mainly for categorization and recall purposes. The six items necessary include the serial number, installation date, removal date, standby hours, high power operating hours, and the complaint or failure code. Once the user tells the program to add a livret sheet, he or she will be prompted to select the tube type and the appropriate installation and platform. Once selected, these will automatically appear on the livret sheet, and only the above six items need to be inputted. Also, the current date will automatically appear as the removal date, but it could be edited if necessary. Though the process of completing livret sheets is time consuming when hundreds of tubes and corresponding failure data need inputting, it is extremely simple and quick when the data

is inputted on a daily basis as tubes fail (say ten to twenty at a time). The software is even programmed to highlight what necessary information is missing if the user fails to input it.

After the completion of the livret sheets, the user simply creates a database as described in the manual and saves the information. The user now has all the necessary information required to perform reliability analyses saved in the database. Using the information in the database, MiDAS can analyze TWTs, klystrons, and magnetrons. This research focused on TWTs, and thus, the following information pertains only to such tubes.

4.0 ANALYZING THE DATA

When analyzing TWTs, the user has the ability to obtain information in the following three areas: 1) a single tube, 2) mean time to failure (MTTF) vs. Installation, and 3) MTTF vs. Platform. The single tube analysis is described here first. This particular analysis provides output information in three different subsets: 1) Failure Mode Distribution, 2) Weibull Parameters, and 3) Total Failure Distribution.

The first subset observed was the failure mode distribution. This output provides a bar graph that depicts the distribution of the failure modes (or complaint codes) for all livret sheets that were entered. This is extremely useful in getting a representation of which failure (or failures) dominates a particular tube type (see Figure 1).

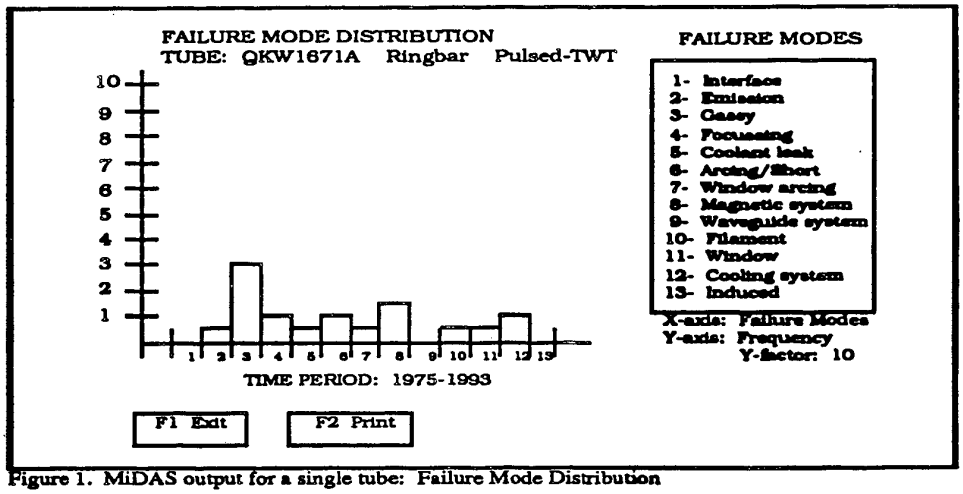

Figure 1. MiDAS output for a single tube: Failure Mode Distribution

The second subset observed was the Weibull parameters. This output allows the user to view the parameters for a single failure mode or as a summary of all failure modes. The output for the single failure mode resulted in a couple of graphical representations of the inputted data. A bar chart in the top half of the screen gave a distribution of the ratios of standby and high power hours. This affords the user an idea of how many tubes are in a particular standby versus actual operating mode ratio. The median, standard deviation, and one-sigma area around the median for the ratios are also indicated in the output. The curve-fitting graph in the bottom half of the screen gave a color representation of the standby and high power hours versus the percentage of tubes that failed. This graph allows the user to see what percentage of tubes had failed at specific standby and high power hours. Additional information contained in this output includes the Weibull parameters. The Weibull shape parameters, location parameters, and the sum of deviations between the estimated curve and field data points for that particular failure mode are conveniently listed for the user (see Figure 2).

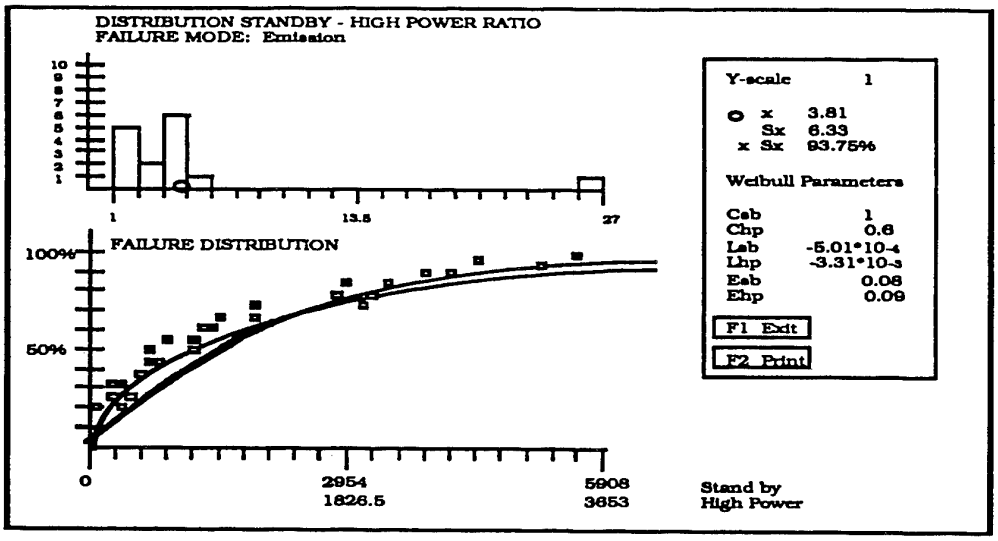

Figure 2. MiDAS output for a single tube: Weibull Parameters

In order to perform the above described single failure mode analysis, it is necessary to have at least eleven tubes within the failure category to be analyzed. Otherwise, the program indicates that there is insufficient data for the software to perform an analysis. Also, the user should review relevant sections of the MiDAS manual before and during the analysis. Figures and text explaining the output are included in the manual. This will afford the user greater understanding of the graphs and tables.

In addition to allowing the user to view the Weibull parameters for just one failure mode, MiDAS has a Weibull Parameter Table for viewing a summary of Weibull parameters for all failure modes. Although the table does not contain all of the information that the single failure mode output contains, it does provide the user with the Weibull shape and location parameters for the standby and high power hours inputted into the system. Again, the output does require at least eleven tubes within each failure category. Otherwise, MiDAS gives the theoretical Weibull parameters calculated by MIL-HDBK-217. This set of Weibull parameters consists then only of two parameters, one shape parameter (C) and one location parameter (L) (see Figure 3).

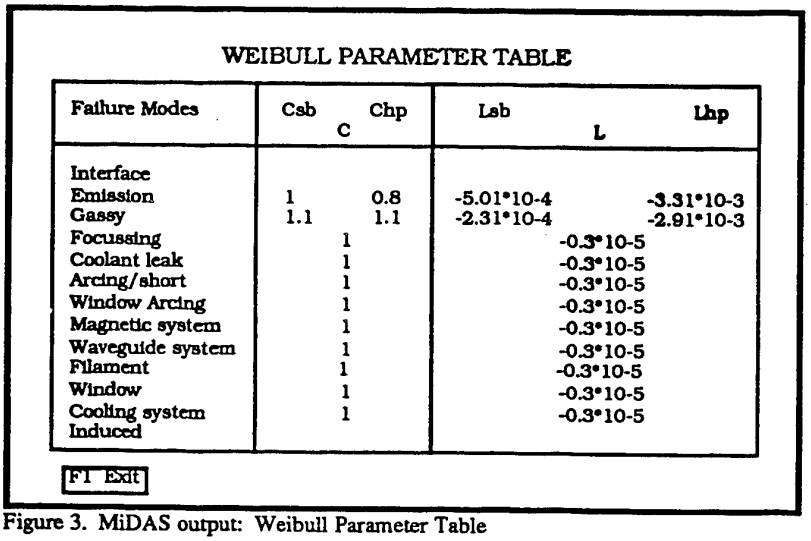

Failure Modes	Csb	Chp	Lsb	Lhp
	C		L	
Interface				
Emission	1	0.8	-5.01*10-4	-3.31*10-3
Gassy	1.1	1.1	-2.31*10-4	-2.91*10-3
Focussing	1		-0.3*10-5	
Coolant leak	1		-0.3*10-5	
Arcing/short	1		-0.3*10-5	
Window Arcing	1		-0.3*10-5	
Magnetic system	1		-0.3*10-5	
Waveguide system	1		-0.3*10-5	
Filament	1		-0.3*10-5	
Window	1		-0.3*10-5	
Cooling system Induced	1		-0.3*10-5	

Figure 3. MiDAS output: Weibull Parameter Table

The final subset available under the single tube analysis is the Total Failure Distribution. Here, the user is able to obtain a graph of the MTTF. The graph depicts hours versus failure percentage. In a quick glance, the user is able to determine the MTTF. MiDAS also gives a graph of the MTTF using reliability methods developed by the Rome Air Development Center, or RADC (now Rome Laboratory) (see Figure 4). MiDAS should always yield a less conservative, i.e., a greater, MTTF value than RADC. The research performed for this paper, however, resulted in a more conservative MTTF from MiDAS. This was probably due to deficiencies in the data that was used (see section 5.0).

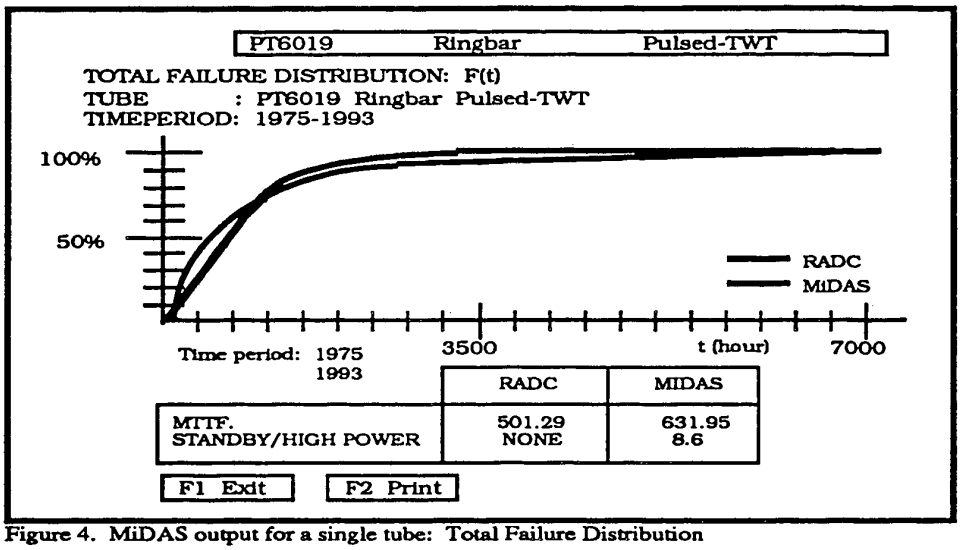

Figure 4. MiDAS output for a single tube: Total Failure Distribution

The final two analyses that can be performed for TWTs is the MTTF vs. Installation, and MTTF vs. Platform. These analyses were not researched in depth because of the data available. First of all, most of the tube failure data corresponded to tubes used mainly in one particular system. Thus, there was not a variety of installations for which to compare MTTFs. Secondly, the data was applicable only to systems used in aircraft, and so there was no need to compare MTTFs for different platforms since there was only one. The importance of such analyses, however, cannot be overlooked. These particular analyses can indicate to the user where his or her next dollar should be spent. Maybe a particular installation is causing most of the failures, or it could be the platforms on which the tubes are used. These analyses could prove very cost effective when it is realized that the tubes themselves may not be the problem.

5.0 THE IMPORTANCE OF DATA COLLECTION

One final area, pertinent to MiDAS, is that of data collection. The importance of data collection cannot be underestimated. "One of the major problems in increasing the reliability of microwave tubes is poor feedback, or the complete lack of feedback from the field concerning tube operating times and conditions of failures" (Ref. 2). Reasons for failure must be specific; such reasons as "not working", "unknown", and "no RF" cannot be correctly categorized and are rendered useless to the analysis. The sources and methods of collecting tube failure data play a vital role in the success of such reliability analysis systems as MiDAS. The sources of data collection, whether it be the front-line technicians or the failure analysis technicians, need to be standardized, and the methods must be thorough and complete. Deficiencies in the data, especially missing installation and removal dates, standy hours, high power hours, etc., cause inaccurate calculation of the reliability parameters. Accuracy directly depends on complete data. MiDAS and other such reliability analysis software are only as good as the data available.

6.0 CONCLUSION

MiDAS is a significant advancement in state-of-the-art computer aided reliability analysis of microwave tubes. Its ability to function as a database and analysis tool provides a convenient and effective method of storing and analyzing tube failure data. Researchers with limited reliability background found the program easy to install and user friendly. The manual provided enough guidance to enable proper data entry and successful retrieval of microwave tube reliability parameters. At the same time, however, it has been noted that the software is not without its limitations. First of all, MiDAS is not a reliability prediction tool. It is a software tool that performs reliability calculations on current field data, providing results for further analysis. Second, because of its use of field data, MiDAS is directly dependent on accurate, thorough, and complete field data. As explained above, the software even requires a minimum number of field data inputs. Regardless, microwave tube designers, manufacturers, and users can benefit from MiDAS. They can apply these results to their own particular microwave tube systems and extract reliability parameters for further analysis. Currently, the manual is being updated to further improve and clarify the translation and to update some figures. Also, the software itself is continually being evaluated for further improvements. Although MiDAS may not be the perfect and all-encompassing microwave tube reliability tool, it has proven that it can be a cost-effective method for analyzing microwave tube field data and providing accurate reliability figures of merit. Overall, Rome Laboratory's experiences with MiDAS has verified that it can provide an efficient means of performing failure analyses and increasing overall microwave tube systems reliability.

7.0 ACKNOWLEDGMENTS

The author would like to take this opportunity to thank the following individuals for their contributions to this paper:

Edward J. Jones, Peter J. Rocci, James P. Ryan, Joop H.M. van Huut, and Jan M. Schouten.

8.0 REFERENCES

1. Bosch, J. 1993, MiDAS: An accurate method to calculate reliability parameters of microwave tubes, 1, 50.

2. Gilmour, Jr. A.S. 1994, Principles of Traveling Wave Tubes, 514-515, 535.

3. Reliability Analysis Center 1996, New system reliability assessment methods, 3-4.

Biography

Eunice T. Ciskowski, 1Lt, USAF
Rome Laboratory/ERDS
525 Brooks Road
Rome, NY 13441-4505
Phone: (315) 330-1740

First Lieutenant Eunice Ciskowski is the team chief for electronic warfare failure analysis in the Design Analysis Branch, Electromagnetics and Reliability Directorate at Rome Laboratory, Rome, New York. For the two past years, she has completed numerous research and development projects resulting in improvements for electronic warfare (EW) systems, including the ALQ-131 (F-16) and ALQ-161 (B-1B). The lieutenant has a B.S. in Civil Engineering from the University of Miami and is currently pursuing a M.S. in Mathematics Education at Syracuse University.

A MODELING AND SIMULATION APPROACH FOR ASSESSING HELIX TWT INTERACTION CIRCUIT THERMAL BEHAVIOR

Peter J. Rocci
US Air Force/Rome Laboratory
ERDS, 525 Brooks Rd
Rome, NY USA 13441-4505

ABSTRACT

A technique was developed to assess the thermal performance of a helix TWT interaction circuit accounting for thermal contact resistance between the circuit's components. An iterative method employing finite element analysis and an analytical expression relating contact pressure to thermal contact resistance was used to determine the effects of interfacial pressure on the circuit's operational thermal performance. Thermal drops across the interfaces between the helix and support rods and barrel increases operating temperatures throughout the circuit which can lead to a decline in the TWT's performance. Since the circuit analyzed contained no brazes or epoxy at the component interfaces, these thermal drops become more significant.

Parametric analyses were made using this technique for different assembly loads as well as for both beryllia and APBN support rods. Results showed that the thermal contact resistance effect was more pronounced at lower assembly loads and higher thermal loads. That is, as the thermal loading to the circuit increases, the percent increase of the maximum helix temperature over the helix temperature when the thermal contact resistance is not accounted for, increases. The effect was also more pronounced when APBN support rods were modeled. The helix temperature increased a greater amount when accounting for the thermal contact resistance for APBN support rods than for BeO support rods.

The heat transfer capability of the slow wave structure is one of the most important factors that limit the output power capabilities of helix TWTs. Tube designers must be able to examine thermal behavior of the circuit, especially the dielectric support rods which play a critical role in removing heat from the helix. The method developed in this study will enable tube designers to rapidly and accurately estimate the feasibility of a projected interaction circuit design or upgrade. The influences of various physical and geometrical parameters on helix operating temperatures can be predicted accurately and with large time and cost savings over prototyping and testing. Finite element methods such as this have great potential to aid in future helix TWT development and upgrade efforts.

INTRODUCTION

The thermal characteristics of contacting materials has become increasingly important in a wide range of technologies. When two surfaces are brought into contact, an imperfect junction exists. This holds true whether there is an interstitial medium present (epoxy, solder, thermal grease), or just a bare junction between the two materials. This imperfect junction creates a temperature difference between two contacting surfaces when there is heat flow. Since the contacting surfaces are not perfectly flat, the heat passes through a finite number of contacting spots, thereby decreasing the heat flow through the joint. Greater contact pressures between the materials generally result in an increased number of contact spots, thereby increasing the flow of heat between the materials. If a fluid is present in the gaps, heat is still conducted across the gap. However, since the thermal conductivities of fluids are orders of magnitude lower than those for metals and ceramics, heat flow becomes more restricted across these gaps, thereby increasing the temperature of the heated material and decreasing the temperature of the unheated material.

The Thermal Contact Resistance (TCR), is defined as the resistance to heat flow across a joint because the actual contact area is only a fraction of the apparent area of the joint. The thermal contact resistance is defined as the ratio of the temperature drop at the interface to the average heat flow across the junction [9]. Heat transfer across the joint may take place by conduction through the actual contact spots, conduction and/or convection through the interstitial medium as well as radiation across the gaps when there is no interstitial material. Thermal contact resistance can play a significant role in determining thermal performance of electronic devices.

The objective of this study was to characterize the effects of contact resistance on the thermal performance of the interaction circuit within a high power helix traveling wave tube. This is of critical

importance since failure of the interaction circuit would lead to failure of the entire TWT, of which replacing is essential and costly.

A typical interaction circuit from a helix traveling wave tube (Figure 1) was modeled and used to study the effects of bare contact on thermal performance. The circuit employs a rectangular cross-section helix tape, usually constructed of molybdenum or tungsten. Dielectric support rods equispaced around the helix act to hold the helix in place and also provide a path by which heat is removed from the helix. In some cases, sections of the rods are coated with a lossy material to dissipate any backward waves reflected back through the circuit from the output waveguide. These rods are usually made of ceramic materials since metallic support rods can not be used to support helices because their negative effect on the RF characteristics on the circuit. The most widely used ceramics are beryllia and APBN. These materials have relatively high thermal conductivities and are well suited for high temperature operation under vacuum. The helix and support rods are enclosed in a vacuum environment by a thin-wall barrel, usually constructed of stainless steel.

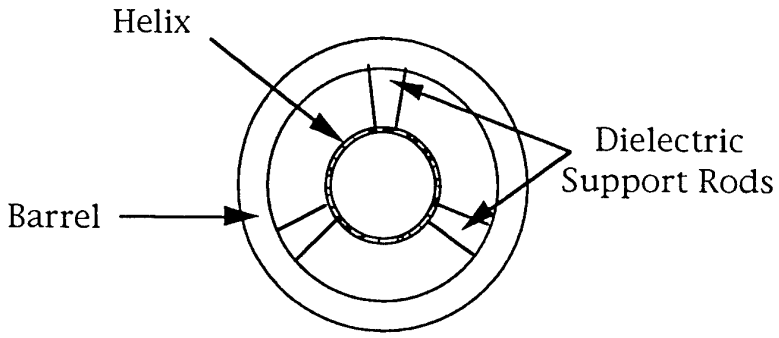

Figure 1: Helix Interaction Circuit Cross-Section

Presently, there are three techniques used for assembling helix/support rod structures. They are [7]:

- Triangulation
- Pressure Insertion
- Brazing

Brazing is the most attractive technique as far as thermal management is concerned. The brazing technique significantly reduces the thermal resistances at the rod interfaces, which reduces the maximum temperature achieved by the helix, thereby allowing the tube engineer a wider choice of helix materials to choose from. Brazing techniques however, are difficult to implement when it comes to helix/support structure assembly. The support rods must be brazed to every turn of the helix and brazing material must be removed from areas between the helix turns. Since this could involve many contact spots (sometimes hundreds), brazing is not always cost effective. Difficulties could also arise from mismatches in thermal expansion coefficient between the brazing material and ceramic. Triangulation and pressure insertion assembly techniques are much easier to implement, but they do not offer the thermal performance characteristics of brazing. The support rod interface resistances are significantly higher since there is only bare contact between the components.

This paper discusses a methodology that was developed employing the finite element method to model thermal contact resistances between contacting components within traveling wave tubes. This method was demonstrated on a model of a helix traveling wave tube's interaction circuit. The circuit components are held together under high pressure, there are no brazes or epoxy present within the interaction circuit assembly. Since the contacting surfaces are not perfectly smooth, temperature drops at the interfaces will be more significant when operational heating takes place. Analyses were performed for both beryllia and APBN support rods. The maximum calculated helix temperature were found to be greater for both materials when interfacial contact resistances are accounted for rather than assuming perfectly smooth contact.

OVERVIEW OF CONTACT CONDUCTANCE HEAT TRANSFER

Heat flow through a homogenous solid is greater than the heat flow through an interface between contacting solids with similar material thermal conductivities. This is caused by the inherent roughness of the contacting surfaces which prevents the solids from making perfect contact. Heat is actually conducted through a finite number of contacting spots within the apparent contact area. The interfacial contact resistance between contacting materials is dependent upon a number of factors. These factors include:

- Direction Of Heat Flow
- Presence Of Surface Films
- Presence Of Interstitial Medium
- Contact Pressure

Because there is an interference (pressure) fit in the interaction circuit assembly, without films or interstitial materials, only pressure dependence was examined for it's effect on interaction circuit thermal contact resistance..

APPROACH

An iterative method employing finite element analysis and an analytic expression relating contact pressure to TCR was used to determine the effects of pressure dependent TCR on the thermal performance of a helix TWT's interaction circuit. The method used is based on a method developed by Simon, et al in Reference 12. It provides for iterative coupling between thermal and mechanical finite element models.

To begin the procedure, an initial thermal finite element model is developed. A one-third model of a typical helix TWT interaction circuit is shown in Figure 2. The support rods are positioned at equal 60 degree intervals around the helix, providing for one-third symmetry. Only a four turn section of the circuit was modeled, representing the circuit's output section. Heat dissipation was simulated on the inside diameter of the helix elements and a boundary temperature of 100 degrees C was assigned to all nodes on the outer surface of the barrel. Relatively thin heat conduction elements were introduced at the helix-rod and rod-barrel interfaces of the model to simulate the interfacial TCR. The TCR is accounted for by assigning thermal conductivity values to these conduction elements. In the initial heat transfer run, these interface elements were assigned artificially high thermal conductivity values. The reason for doing this was to simulate zero thermal resistance at the interface. In subsequent iterations, these conductivities would be adjusted to account for the thermal resistance.

The temperatures calculated in the thermal analysis were then used as a loading condition into a mechanical finite element model. This mechanical finite element model is identical to the thermal finite element model except that there are no thin conduction elements at the material interfaces. The mechanical analysis yields stresses and deflections for combined assembly and thermal loading. A FORTRAN 77 program was written to sort through the resulting output file and calculate the local contact pressures at the material interfaces. The contact pressures, along with the heat flow at the interfaces (calculated in the heat transfer analysis) and material properties were used in an equation relating these parameters to TCR to determine the conductance at each interface. These local conductances were then fed back into the thermal input file and another temperature solution was determined using updated thermal conductivities for the heat conduction elements. The entire process was repeated until convergence in the temperature field was achieved.

CONTACT RESISTANCE MODELING APPROACH

Experiments have shown [3] that thermal contact resistance is directly dependent on contact pressure at the material interface. When two surfaces are pressed together, contact is made at a finite number of discrete points. Increases in contact pressure increase the local deformation at the interface between the two materials, thus increasing the size and number of contact points. This, in turn would cause a lower the TCR between the contacting materials, thus increasing heat flow. Conversely, lower contact pressures tend to increase the TCR at the material interface, thus decreasing heat flow.

This equation is given by Barber in Reference 3. It was assumed that all deformation is elastic and that the solids are in perfect contact throughout the elastic contact area.

The heat flow per unit area through single circular areas of two contacting solids is given by:

$$q = \frac{K_o(T_1 - T_2)}{\pi\sqrt{a^2 - r^2}} \qquad (1)$$

Where: K_0 ~ Equivalent Thermal Conductivity of Contacting Solids

$$K_o = \frac{2K_1K_2}{(K_1 + K_2)}$$

T_1,T_2 ~ Temperature of Solids 1 & 2, Respectively

a ~ Radius of Contact Area

r ~ Distance From Axis of Symmetry

The total heat flow rate (Q) through the contact area is obtained by integrating Eq (1).

$$Q = 2K_o(T_1 - T_2)a \quad (2)$$

Next, a pressure distribution necessary to make the thermally distorted solids conform throughout the contact area must be found. By approximating the equation of a distorted surface as a paraboloid, this pressure distribution (p) is given by:

$$p = \frac{4}{\pi c_o}\left[\frac{1}{2R_o} + \frac{(c_2 - c_1)(T_1 - T_2)K_o(1 - \log 2)}{\pi a}\right]\sqrt{a^2 - s^2} \quad (3)$$

Where: $c_{1,2} = \dfrac{(1 - \upsilon_{1,2}^2)}{E_{1,2}}$

$\upsilon_{1,2}$ ~ Poisson's Ratio of Solids 1 &2, Respectively

$E_{1,2}$ ~ Elastic Modulus of Solids 1 & 2, Respectively

$$c_o = \frac{(1 - \upsilon_1^2)}{E_1} + \frac{(1 - \upsilon_2^2)}{E_2}$$

$$R_o = \frac{R_1 R_2}{(R_1 + R_2)}$$

$R_{1,2}$ ~ Radii of Curvature of the Contacting Surfaces When Unheated

s ~ Distance From Axis of Symmetry

The total load is obtained by integrating equation (3) over the contact area.

$$W = \frac{4a^3}{3R_oC_o} + \frac{8(c_2 - c_1)(T_1 - T_2)K_o(1 - \log 2)a^2}{3\pi c_o} \quad (4)$$

The Thermal Contact Resistance (ρ) is defined as the temperature difference (T_1-T_2) per unit heat flow (Q).

$$\rho = \frac{(T_1 - T_2)}{Q} \quad (5)$$

Substituting Equation (2) for Q gives:

$$\rho = \frac{1}{2}K_o a \quad (6)$$

Finally, combining Equations (2), (4) and (6):

$$\frac{2(1 - \log 2)(c_2 - c_1)Q}{\pi} + \frac{1}{2R_oK_o^2\rho^2} = 3c_oWK_o\rho \quad (7)$$

Equation (7) is the thermal contact resistance equation. It is solved iteratively for ρ. K_o, $c_{1,2}$ and R_o are known quantities while Q and W are determined from the thermal and mechanical finite element analyses.

RESULTS

Temperature contours through the interaction circuit are shown in Figure 3. Convergence in the temperature solution took four iterations. The solution is given for 10 Watts per turn heat dissipation, beryllia support rods, and 200 ksi assembly pressure. Parametric analyses were made for both beryllia and APBN support rods with varying assembly pressures.

The results showed that the effect of TCR on the thermal performance of this structure becomes more pronounced with lower assembly loads. This is no surprise since lower contact pressures effectively decrease the number of contact spots at the material interfaces, thus decreasing heat flow between the materials and, in this case, increasing the maximum helix temperature. The TCR also becomes more significant at higher thermal loads. The results show that the percent difference in the maximum helix temperature increases when the heat input to the system increases, regardless of assembly load. The reason for this is that the equation used to calculate the TCR indicates that thermal loading is directly proportional to the TCR at the material interfaces (see Appendix A). Therefore, an increase in the interfacial TCR brings with it an increase in the helix temperature.

The support rod material also was found to have an effect on the thermal performance of this interaction circuit when thermal contact resistance is accounted for. For the same assembly load, the maximum helix temperature ranged from 6-13 % higher for APBN support rods than for BeO support rods. This demonstrates that this method can play an important role in the material selection process when designing microwave tube components. It allows similar types of materials as well as materials of different classes to be analyzed and evaluated for proposed helix interaction circuit designs.

CONCLUSIONS

Use of the finite element based TCR accounting methodology developed in this study provides the means for helix TWT designers and engineers to more accurately predict thermal instabilities within helix interaction circuits. The phenomena of interfacial thermal contact resistance should not be neglected when characterizing the thermal behavior of helix interaction circuit designs. This especially holds true when the pressure insertion technique is used to assemble the circuit. When brazing or epoxy is used, the TCR effect is less pronounced but still present. The following conclusions were made in demonstrating the TCR accounting method on a typical helix TWT interaction circuit model:

- Lower assembly loads increase the TCR effect thus increasing the maximum temperature attained by the helix for a given heat dissipation.
- Higher thermal loading tends to increase the TCR effect. The increase in helix temperature over the temperature when the TCR is not accounted for was found to increase when the heat load applied to the circuit was increased.
- Although support rod materials are generally limited to ceramics, the choice of support rod material can significantly affect the thermal performance of interaction circuit designs. The circuit temperatures when APBN rods were modeled were found to be greater than the temperatures when BeO rods were modeled.

The TCR accounting method was demonstrated on an interaction circuit model that contained commonly used materials, typical dimensions and an arbitrary geometry for the support rods. Similar types of materials as well as materials of different classes can be analyzed and evaluated for proposed helix interaction circuit designs using this method. This method could also be applied to different component geometries provided the proper geometric properties are known. Finite element based methods such as this have great potential to aid in future helix TWT development and upgrade efforts.

REFERENCES

1. Antonetti, V.W., and Yovanovich, M.M., *Enhancement Of Thermal Contact Conductance By Metallic Coatings: Theory And Experiment*, Journal Of Heat Transfer, Vol. 107, Aug 1985, pp. 513-519.

2. Antonetti, V.W., and Yovanovich, M.M., *Thermal Contact Resistance In Microelectronic Equipment*, The International Society For Hybrid Microelectronics, Vol. 7, No 3, Sep 1984, pp 44-50.

3. Barber, J.R., *The Effect of Thermal Distortion on Constriction Resistance*, International Journal of Heat and Mass Transfer, Vol. 14 1970, pp 751-756.

4. Bartos, K.A., Fite, E.B., Shalkhauser, K.A., and Sharp, G.R., *A Three-Dimensional Finite-Element Thermal/Mechanical Analytical Technique For High Performance Traveling Wave Tubes*, NASA Technical Paper 3081, 1991.

5. Clausing, A.M., *Heat Transfer At The Interface Of Dissimilar Metals - The Influence Of Thermal Strain*, Journal Of Heat And Mass Transfer, Vol. 9, 1966, pp 791-801.

6. Fletcher, L.S., *Recent Developments In Contact Conductance Heat Transfer*, Journal of Heat Transfer, Vol. 110, Nov. 1988, pp 1059-1070.

7. Gilmour, A.S. Jr., *Microwave Tubes*, Artech House, Dedham, MA, 1986, pp 241-261.

8. Godet, M., Berthier, Y., Dubourg, M.C., and Vincent, L., *Contact Mechanics: Needs For Broader Applications*, Journal Of Physics D: Applied Physics, Vol. 25, 1992, pp A273-A278.

9. Madhusudana, C.V. and Fletcher, L.S., *Contact Heat Transfer - The Last Decade*, AIAA Journal, Vol. 24, No 3, 1985, pp 510-523.

10. Rocci, P.J., *Dynamic Behavior Of Helix Interaction Circuits*, Rome Laboratory Technical Report RL-TR-92-298, Dec 1992.

11. Rozon, B.J., Galpin, P.F., Schneider, G.E., and Yovanovich, M.M., *The Effect of Geometry On Contact Conductance Of Contiguous Interfaces*, Journal Of Spacecraft, Vol. 23, No 3, 1986, pp 225-230.

12. Simon, BR., Ortega, A., Kaufmann, M., and Hnat, K., *Finite Element And Experimental Procedures For Determining Thermal Contact Resistance*, ASME Winter Annual Meeting 92-WA/EEP-11, Nov 1992.

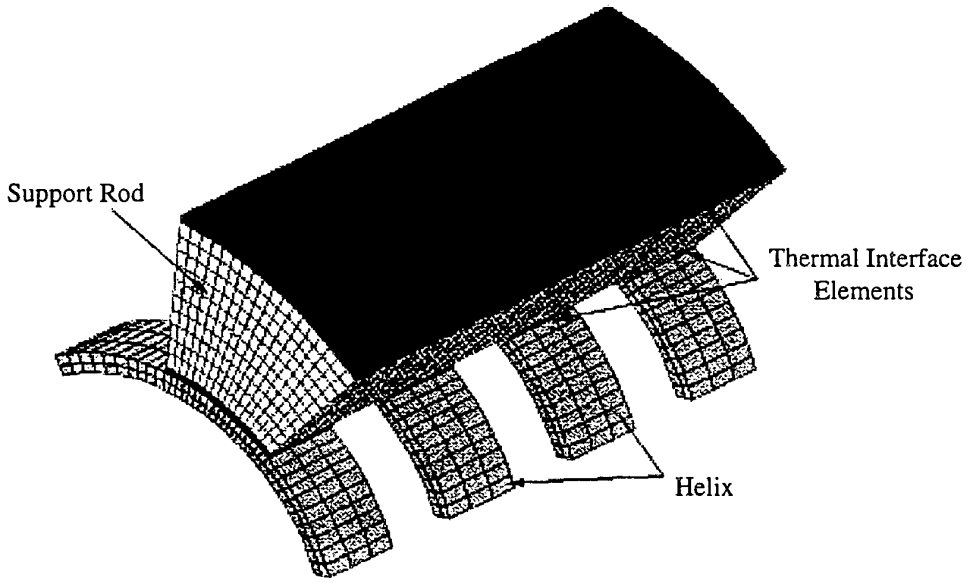

Figure 2: Four Turn, 1/3 Finite Element Model of Helix TWT Interaction Circuit

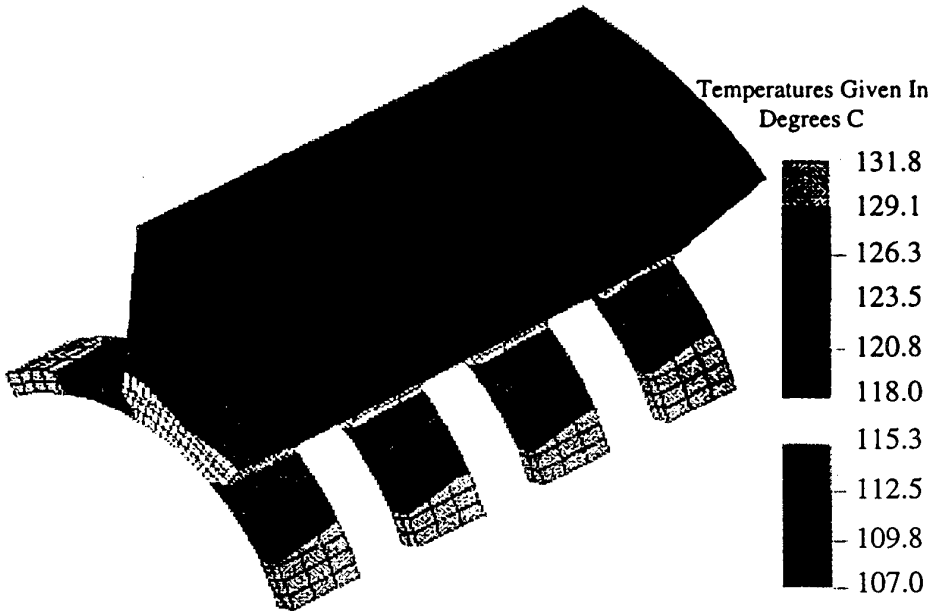

Figure 3: Calculated Temperature Distribution

RF DESIGN FOR LOW COST

James P. Ryan
Rome Laboratory/ERDS
525 Brooks Road
Rome, NY USA 13441-4505

Abstract

Rome Laboratory (RL) in conjunction with Warner Robins Air Logistics Center (WR-ALC) conducted a program to investigate a high power, wideband, Electronic CounterMeasure (ECM) Traveling Wave Tube (TWT). The objective of this program was to investigate and evaluate the cause and effect relationships that each of the design, manufacturing and usage environments have on the TWT such that, the overall cost of ownership of the systems these devices are used in can be reduced. The TWT is operated in the ALQ-131, Block II, ECM, POD system, which was the identified demonstration vehicle. The ALQ-131 is actively flown on a variety of aircraft (F-16, A-10, AC-130) in the USA & NATO countries. There were several principal results of the program. The TWT vendor measured, a 22% first-time delivery yield improvement in this tube's production. Also, based on the program tasks accomplished, the estimated TWT reliability increased by 23% and the acquisition cost was reduced by 10% per tube.

Introduction

In the past, the current method of acquiring tube technology was based on technical goals such as performance, size and weight. There was very little consideration given to cost, reliability and repairability. As the US DoD enter a new era of reduced budgets, the norm will be the acquisition of a smaller number of wide variety power tubes, where cost, reliability, and repairability become increasingly important and require up-front attention. Therefore, this program was funded to investigate a technical approach for developing technologies and techniques to reduce cost of ownership of TWTs early in the Research & Development (R&D) cycle which will impact cost. Specifically, this program was designed to investigate and evaluate the cause and effect relationships that each of the design, manufacturing and usage environments have on the TWT during the life cycle of the device. The program was broken down into several elements, see Figure 1, to accomplish its objective. First, a review of existing TWT failure data, including several new TWT design considerations; second, a review of the TWT specification; third, a measurement of the TWT operational environment and fourth, a review of the TWT manufacturer design and manufacturing process. Qualification Testing of two prototypes was successfully completed. The culmination of the program is the delivery of four improved prototype TWTs. This R&D program was funded through the Tri-Service Vacuum Electronics Initiative, the Naval Research Laboratory (NRL) was the lead organization. The prime contractor was Northrop Grumman (Westinghouse) the Original Equipment Manufacturer (OEM) for the ALQ-131, with Teledyne Electronic Technology (TET), the TWT vendor, as the sub-contractor.

DESIGN FOR LOW COST - PROGRAM PLAN

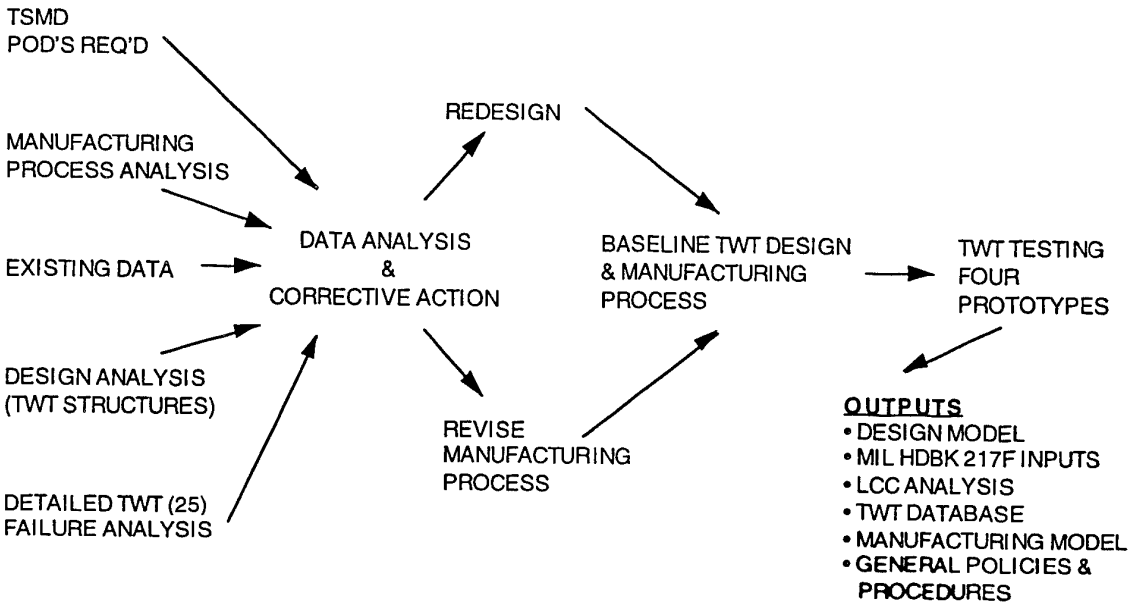

Proper integration of program elements
yields a cost-effective effort

Figure 1

Discussion

The following is a synopsis of the program tasks. First, existing data from the TWT vendor, the system designer/manufacturer and field data were integrated into a single database for identifying operating cost drivers. The field data was information that Northrop Grumman had collected at a variety of US and NATO airbases. Using this database, five design issues were identified initially, of which four, an adjustable and/or mechanical electron gun, a TWT Pre-Matched waveguide output coupler, and a new equalizer were incorporated into the prototype TWT design. The new gun demonstrated an increase in TWT yield, reduced current manufacturing scrap rate, allowed optimization of performance of the gun, and reduced known high voltage breakdown problems. The new pre-matched waveguide design reduced the manufacturing complexity, improved the Voltage Standing Wave Ratio (VSWR), and reduced the occurrence of known arcing problems. The new equalizer design reduced the material cost, manufacturing complexity, and reduced labor. All of these tasks required many hours of design by TET. Also, in the case of the equalizer, TET spent many hours of testing to adequately characterize the standard performance of the old design. A similar project for this TWT was to investigate the redesign of the phase

shifter. However, when the subvendor to TET was approached for a new design, the subvendor declined, due to lack of adequate market capability, in other words, too small return on investment (ROI).

Secondly, the program was to identify cost sensitivity of the TWT specification requirements. A detailed review of the TWT specification requirements was performed. For example, the TWT Acceptance Test Procedure (ATP) delineates the tests needed to demonstrate the tube's compliance with its specification. In addition to verifying the technical content of the ATP, the processes and procedures directly preceding and following the ATP were examined. Is there a benefit to testing the TWT in the factory in a way that is similar to how it is operationally used or tested in the field? Is the ATP deficient in not detecting a fault? As a result of this, the ATP had minimal changes recommended per the detailed review.

Third, the TWT operational environment was measured and recorded. TWTs were modified to accommodate the use of Time-Stress-Measurement-Devices (TSMDs) and a control board was imbedded in the ALQ-131 Block II ECM POD. The most important feature of the TSMDs was to be nonintrusive to the system. This meant that if the TSMD or any other component failed, the system would not be affected. No induced failures. Subsequently, Northrop Grumman, fully tested the TSMD and instrumented TWTs in their Automated Multiple Emitter Simulation (AMES) facility prior to installation in The Netherlands. Three PODs were modified and flown on F-16 aircraft by the Royal Netherlands Air Force. The TSMD allows the measurement, in the same time interval, of shock, temperature and several electrical parameters around the TWT. Such things as ground current, cathode voltage, grid voltage, TWT base plate temperature and shock are accessed and monitored. When the predetermined threshold is crossed a snap shot in time is taken, stored and saved, of all the measured parameters for later analysis. TET instrumented four TWTs with sensors and small printed circuits to allow for several of the measurements. The Dutch used the modified PODs in normal operations. Several hundred hours of POD operation were logged.

The Fourth area involves design and manufacturing process modeling and analysis. The purpose of this activity was to produce a model of the TWT design process that can be used as a vehicle for analyzing the efficiency and capability of the process for the purpose of improving its effectiveness, reducing the overall cost of the manufactured TWT, and reducing time-to-market from design start to delivery of the first production units. The process is modeled by flowcharts showing the steps for each of the major activities of the design phase of a project. Each design activity is assigned a realistic labor time and cycle time chosen on the basis of experience. Several examples are shown. The labor time and cycle time are combined on the example flowchart to show the resulting total labor and cycle time. The total labor and cycle time required for any given project's design phase depends on the complexity of the project and can vary by orders of magnitude from one to another. As a result, there can be no meaningful generic model representing "design." The examples are intended to be realistic representations of actual project design phases experienced by TWT engineers in recent years. These examples will be used as a vehicle for analyzing the design process with a view toward improving efficiency and also toward making manufacturability as important a design goal as functional performance.

A Fifth objective was to identify additional opportunities for improvement during the course of the program. Thus far, one potentially significant project has been identified based on a design for manufacturability. A thin film material called polyimide might possibly be used to coat the collector of the TWT. The benefits of polyimide

versus the current hazardous material Berrylia Oxide are the following: reduce the use of hazardous material, reduce collector complexity (parts count goes down from 38 to 8), reduce cost, and increase reliability. Funding for this experiment was not found, therefore, further work in this area was not performed. However, the concept is still a viable option.

In addition to the universal design and process changes identified as a result of this program. Two of the four prototype TWTs with the identified improvements, were Qualification Tested by TET. The QTP and other documents were reviewed and approved by WR-ALC engineering. WR-ALC provided the funding to perform this testing.

Conclusion

The pay-off for this program was first, the gathering of existing data on the failure modes of this TWT into a database. Secondly, this improved TWT now incorporates a new gun design, a pre-matched waveguide output coupler and a new equalizer. Based on the known failure modes and the impact of the design changes incorporated by this program, the reliability of this TWT is expected to increase by 23%. This is calculated from using the known failure modes and the improvement factor reducing those modes from the design projects and the manufacturing process work in the program. Thirdly, the improved understanding of the TWT design environment. The TSMD provided a detailed insight to the operational environment surrounding this TWT, this information provided the designer with a more complete definition of performance for their design. Fourth, the design and manufacturing process task identified the key design, parts and cost drivers in the various flow diagrams. All of which resulted in a 22% measured, first-time delivery yield improvement for this particular TWT by TET. With all of the above design, component and manufacturing changes incorporated, the acquisition cost per TWT will be reduced by a minimum of 10%. This project itself, has demonstrated significant cost and reliability improvement on this TWT. And finally, as a result of the Qualification Testing, new part numbers have been assigned to these prototypes, and the documentation changes required have been made.

The concept of using polyimide material on the collector is a viable alternative for a tube in this power range, and is worth investigating. The concept and tasks associated with this program are applicable to any EW, Communication or Radar system. The results show that an effort of this nature can provide reasonable increases in reliability and a reduction in cost to the user.

MILITARY SPECIFICATIONS AND STANDARDS REFORM

Mark Gorniak
Rome Laboratory
525 Brooks Rd
Rome, New York 13441-4505

ABSTRACT

Due to the global marketplace demand, technological advances are being driven by the commercial industrial base and not by the Department of Defense (DoD) as in past decades. The DoD has concluded that to maintain technological superiority and to assure itself of a source of suppliers for the future, it must be able to rapidly incorporate state-of-the-art commercial technology into DoD systems in an affordable way. The traditional DoD acquisition process, however, relies heavily on military specifications and standards (MilSpecs), which pose many barriers to the use of commercial technologies. U.S. Secretary of Defense Dr. William Perry's memorandum entitled "Specifications and Standards - A New Way of Doing Business" directed the DoD to reinvent the requirements generation process for defense acquisitions and reform all MilSpec documents. These reforms which allow defense contractors to determine how best to meet DoD system performance requirements and give preference to commercial technology will be discussed.

1. INTRODUCTION

The creation of a dual-use industrial base for producing defense systems has become a priority for meeting U.S. economic and security objectives. The global marketplace has made the latest commercial technologies available to every nation, and the military advantage will reside in the nation which has the quickest insertion time for integrating commercial technologies into its defense systems. Although MilSpecs provide standardization among the military services of reprocurable items and ensure that these items are able to perform in military applications, they are considered to be one of the major impediments to the realization of the dual-use industrial base. The term "MilSpecs" is used to refer to military specifications and military standards which, in general, are faulted for being too rigid and preoccupied with design and process, rather than function and performance. A *military specification* is a type of specification which usually describes a product and may create a barrier to dual-use production when it describes that product in design terms rather than the more generic form, fit, function and performance terms (Ref. 1). "*Military standards* represent a diverse set of instructions to the contractor. Some simply encourage the contractor to pursue commercial alternatives. Others, in particular the management and manufacturing milstandards, tell the contractor in detail how to organize the work, assure reliability or quality, and document it for the Department of Defense. These standards often emphasize how to organize the production process rather than describe the level of performance required" (Ref. 1).

In the past, MilSpecs for electronics - such as MIL-E-1 "General Specification for Electron Tubes" which originated in the early 1950's - benefited the electronics industry by serving as de facto industry standards, capturing lessons learned in electronics manufacturing, and often providing detailed "how to" requirements for ensuring robust combat-ready product. The proven military-unique design solutions of MilSpecs were placed on contract by program managers to avoid risk. However, rather than tailoring a MilSpec for new system applications, program managers invoked the entire MilSpec, often without understanding the requirements. Since the MilSpecs were not always updated to keep pace with technology improvements, obsolete technologies had to be sustained by contractors for military programs. Furthermore, this lack of tailoring resulted in nonvalue-added requirements being placed on contractors which increased system costs.

In 1994, the Coopers & Lybrand/TASC Project Team Report listed 105 of the most costly and troublesome MilSpecs known as the "Heartburn 105." The report indicated that one of the costliest compliance requirements for contractors was MIL-Q-9858 "Quality Program Requirements" which increased the cost of defense systems by 18 percent. The DoD can no longer afford to pay for such overhead costs since in the past 10 years, the DoD procurement budget has fallen from $100 billion to $45 billion. The combination of the decreasing defense budget and the increasing profitability of supplying to the commercial sector has also forced defense companies to drastically downsize, consolidate, restructure, or entirely leave the DoD business. In the past decade, the number of major

U.S. microwave tube manufacturers has decreased from 11 manufacturers to 6, with roughly a 50 percent decrease in the tube industry work force.

Today commercial industry is outpacing military technology particularly in the areas of telecommunications, information systems, and microelectronics. The military research and development (R&D) spending has not kept pace with commercial industry, and by 1990, the ratio of commercial R&D spending compared to military spending was two-to-one. The DoD can no longer subsidize a purely defense-unique industry, but instead must rely on a dual-use industry which is sustained by the commercial marketplace. However, the traditional DoD acquisition system's reliance on MilSpecs, which often specify military-unique manufacturing and management processes, discourages commercial companies from participating in meeting the needs of the military systems. This led the DoD to conclude that the MilSpec culture must be changed if it had any hopes of accessing world-class commercial operations for developing DoD systems.

2. "A NEW WAY OF DOING BUSINESS"

Although the DoD has been studying and attempting to improve the MilSpec system for over 20 years, each past attempt was unsuccessful due to lack of high level management commitment. Since the MilSpec issue is not only a technical issue but also a cultural one, the intervention of top management is required. This leadership was provided on 29 June 1994 when Dr. William Perry, U.S. Secretary of Defense, issued a memorandum entitled "Specifications and Standards - A New Way of Doing Business" (Ref. 2). The memorandum provided an implementation strategy for MilSpec Reform and directed the DoD agencies to commit resources to carrying out the Reform. This commitment of funds in the face of decreasing Defense budgets clearly indicated the serious intention of the DoD to reinvent the acquisition process. This "New Way of Doing Business" set out to accomplish three objectives: 1) to establish a performance-oriented solicitation process, 2) to implement standardization document improvements, and 3) to create irreversible cultural change in the way DoD does business. The progress made in accomplishing each of these objectives will be presented next.

2.1 Performance Oriented Solicitation Process

The first objective of the MilSpec Reform was to addresses the requirements generation process. Secretary Perry's memorandum directed that wherever possible the DoD requirements be defined by performance specifications only. Performance specifications provide form, fit, function, and interface requirements - but do not dictate a predetermined design solution. The memorandum prohibits MilSpecs from being used in a DoD solicitations unless a justification is provided by the program manager to the buying command senior official. The senior official may grant a waiver as a last resort only if no commercial alternative to the MilSpec exists, and provided that the MilSpec is value-added. This reform strikes at the root of the problem by eliminating nonvalue-added requirements. Furthermore, by not prescribing design solutions or "how to" process requirements, it allows contractors the freedom to propose the latest technologies for meeting system requirements.

Although it is not yet possible to calculate the total savings resulting from this performance-based approach, several programs which are implementing the new way of business are showing considerable savings. One such program is the Joint Direct Attack Munitions (JDAM) Program which eliminated all MilSpecs from the solicitation. The estimated unit cost was reduced from $42,000 to $14,000 and production costs were reduced by an estimated $1.5 billion. The JDAM Program had a 34 percent reduction in development time, required less plant oversight, and reduced data requirements from 243 down to 29 data requirements. Similarly, the C-17 aircraft program showed cost savings by replacing MIL-Q-9858 with ISO 9000. Other MilSpecs were also eliminated from the program and replaced with best commercial practices. The end result was advanced schedule deliveries, cost savings of approximately $100,000 per aircraft, and a 40 percent reduction in the Government quality inspection work force (Ref. 3).

2.2 Document Review

While the downsizing DoD does not have the funding, manpower, or expertise to continue maintaining a large technical document infrastructure of detailed MilSpecs, some military-unique documents are necessary for specifying such things as safety, interconnection, and unique design requirements for combat environments. The second objective of MilSpec Reform is to review and improve over 30,000 MilSpec documents. Those documents that are deemed necessary for weapon systems and military-unique

items of supply for future, newly-designed systems are to be converted to performance specifications and interface standards. Those that describe commercial items and processes are to be converted to commercial item descriptions and nongovernment standards. All other MilSpecs are to be canceled, inactivated, or converted to "guidance only" handbooks to preserve lessons learned and offer known technical solutions.

Each preparing activity has been tasked to review the documents for which it is responsible and to convert them to performance specifications if appropriate. The conversions are being monitored by a Defense Standards Improvement Council (DSIC), which is chaired by the Office of the Assistant Secretary of Defense and consists of top ranking officials from each Service and the Defense Logistics Agency. All MilSpec conversions are expected to be completed by December 1997.

Among the canceled documents are MIL-Q-9858 "Quality Program Requirements" and MIL-I-45208 "Inspection System Requirements." These documents, which were canceled on 1 October 1996, specified the quality assurance program requirements for manufacturers. Since many commercially available quality standards also exist such as the ISO 9000 series documents, the DoD now allows contractors to select specifications and standards to establish their quality processes. MIL-E-1 was converted to a performance specification on 29 March 1996 and was renamed MIL-PRF-1L. As a performance specification, it does not require a waiver for use in a DoD solicitation. Over half of the MIL-E-1 detail slash sheets have been canceled or have become inactive for new design. Details on the status of these slash sheets can be found in the DoD Index of Specifications and Standards (DODISS) (Ref. 4). Table 1 provides the status of completed document reform as of November 1996. With an estimate average cost of $3,000 per year for maintaining a specification, the cancellations of the 4,400 MilSpecs have resulted in an $13.2 million per year savings.

4,400	MILSPECS CANCELED
400	PERFORMANCE SPECIFICATIONS REPLACE DETAIL SPECIFICATIONS
1,700	ADDITIONAL NONGOVERNMENT STANDARDS ADOPTED (7,500 TOTAL)
360	COMMERCIAL ITEM DESCRIPTIONS DEVELOPED (TOTAL 5,900)
394	DATA ITEM DESCRIPTIONS CANCELED

Table 1 MilSpec Reform Status

2.3 Irreversible Culture Change

The third objective of the memorandum was to create irreversible cultural change in the way DoD does business. There are a number of initiatives to ensure that the changes of MilSpec Reform will be sustained.

The paradigm shift away from routinely applying MilSpecs during the requirements generation has been reinforced in the revisions to the guidance documents for defense system program managers; namely, DoD Directive 5000.1 "Defense Acquisition" and DoD Instruction 5000.2 "Mandatory Procedures for Major Defense Acquisition Programs (MDAPs) and Major Automated Information System (MAIS) Acquisition Programs." These documents now require Integrated Product Teams to be institutionalized which are *cross-functional* and include industry participants to resolve program issues. Each acquisition program is to be tailored based on the program needs. Contractors are given the flexibility to define and use their preferred quality management process. Also, commercial practices and products are given first preference in meeting requirements. The program managers are to require prime contractors and subcontractors to incorporate commercial and nondevelopmental items as components of items supplied, and even modify requirements to the maximum extent practicable to ensure the requirements can be met by commercial and nondevelopmental items. Training courses and conferences are being offered to help program managers implement these changes.

While DoD Directive 5000.1 and DoD Instruction 5000.2 insure that new systems are developed using commercial technologies and practices, there are many existing contracts which still contain MilSpecs. These contracts continue to impose overhead burdens such as compliance with military-unique administrative and technical requirements, which prevent defense contractors from competing

competitively in the commercial marketplace. Many contractor facilities must maintain separate processes for accomplishing identical manufacturing steps to comply with unique contractual requirements which call out different MilSpecs. The prime defense contractors still have a culture accustomed to MilSpec imposition, and in turn flow down MilSpec requirements to lower tier suppliers, who at the component levels may be able to offer commercial alternatives.

To help industry address these MilSpec culture barriers, Dr. Perry announced the Single Process Initiative on 6 December 1995. The objective of this initiative is to unify manufacturing and management requirements on existing contracts within a facility, without rewriting each contract. Contractors are to propose the elimination of MilSpecs which are nonvalue added or can be replaced by industry or company standards. The contractor's options include standard cancellation without replacement; replacement with either a performance-based requirement, nongovernment standard, or contractor process; or simply to delete the requirement. The DoD reviews the company's process maturation metrics and the cost savings to the government when evaluating such proposals.

The Texas Instruments (TI) Defense Systems and Electronics Group was the first contractor to take advantage of this initiative. It impacted 770 contracts and deleted 19 military or service-specific specifications and replaced them with the standard TI procedure. The areas addressed by the modification included the quality system, soldering, inspection, calibration, and workmanship within the facility.

As of 13 November 1996, over 100 contractors have proposed over 500 process changes. By making these changes now, future savings should be realized by shedding overhead costs and eliminating military-unique requirements.

3. CONCLUSION

Programs such as the JDAM and C-17 are demonstrating that DoD systems do cost less when performance specifications are used. The change of culture introduced by Dr. Perry's Memorandum and subsequent revisions to the MilSpecs and program management guidance documents have allowed commercial technologies to be given first preference in meeting DoD system needs. By replacing multiple military-unique process variations with the single best process of contractor's facility, the Single Process Initiative is helping to make defense industry cost competitive with the commercial industry and therefore helping to realize a dual-use production base.

While many barriers have been removed by MilSpec Reform, some challenges for incorporating commercial technologies into defense systems still exist. Two of the most pressing concerns are how parts designed for commercial applications will perform in military applications, and also how system maintenance will be affected by the short commercial product life cycle (typically 2-3 years) when compared to the life cycle of military systems. While solutions to these barriers are still being addressed, the goals of MilSpec Reform are being realized; namely, saving money, removing impediments to getting state-of-the-art technology into the weapon systems, and facilitating the diversification into commercial markets of firms that have traditionally produced goods primarily, if not solely for the DoD. The ultimate success of MilSpec Reform will be realized when defense systems designed using the reformed acquisition process become fielded.

4. REFERENCES

1. "ROAD MAP FOR MILSPEC REFORM - Integrating Commercial and Military Manufacturing," The Center for Strategic and International Studies (CSIS), Washington, D.C. 1993, pp. 54-55

2. "Specifications & Standards - A New Way of Doing Business," Memorandum issued by Secretary of Defense William Perry, 29 June 1994

3. "MILSPEC REFORM - Results Of The First Two Years," Office of the Under Secretary of Defense for Acquisition & Technology, Acquisition Practices, June 1996

4. DODISS, Superintendent of Documents, US Government Printing Office, Washington, D.C. 20402

SESSION 7
RSG-19 Day

Chairman: R.M.E.M. van Heijster (TNO-FEL, NL)

RSG-19 workshop introduction

Rob M.E.M. van Heijster
TNO-Physics and Electronics Laboratory
The Hague, The Netherlands

Summary

RSG-19 "on micro and millimeter wave tubes" will enhance the Nato-wide R&D on micro and millimeterwave tubes, High Voltage Power Supplies (HVPS). This will improve overall knowledge on this subject and will have a significant impact on the compatibility, maintainability, and reliability of tubes and HVPS. RSG-19 started its work December 1991 and will complete it in 1998.

Introduction

This paper will describe the objectives of RSG-19 on "micro- and millimeterwave tubes". Thereafter the constitution of this NATO RSG-19 will be briefly addressed. The specific tasks and the military benefits are given in order to underline the relevance of RSG-19.

Objectives

The RSG-19 will enhance the Nato-wide R&D on micro and millimeterwave tubes, high voltage power supplies (HVPS), and their shipping, handling, and storage. This will not only improve overall knowledge on this subject, it will have a significant impact on the compatibility, maintainability, and reliability of tubes and HVPS.

The first task is to accumulate a robust data base of tube quality in its operational environment, and specify reliability and applicable standards to measure and verify this. Factors that effect quality and reliability should be clearly recognized. By thorough analysis of now-available systems this data base can be established.

The strong interdependence of the HVPS and tube reliability and applicability leads to the inclusion of the HVPS to the study.

Reliability engineering tools, such as forensic analysis, finite element analysis (FEA), use of time stress measurement devices (TSMD), and lifetime prediction techniques will be employed on existing systems to investigate how the quality and reliability can be increased in new product designs. This information will also serve to provide guide-lines for future system designs.

Constitution of RSG-19

RSG-19 and its constitution are strongly embedded in the NATO organization, as is shown in figure 1. The line NATO - CNAD - is clearly shown. The DRG and Panel 3 play an important role in the constitution of RSG-19.

The subject of "micro- and millimeterwave tubes" has been proposed at the meeting of the Panel 3 on Physics and Electronics in February 1988. The DRG reviewed this proposal and recommended an Exploratory Group (EG) meeting. This EG was constituted and a draft of the Terms of Reference and Program of Work have been formatted at the third meeting in December 1991.

The Terms of Reference give information with respect to background, objectives and military benefit of RSG-19. The Program of Work addresses the specific tasks, the effort involved and the planning of activities.

The Terms of Reference and Program of Work have been approved by Panel 3 and the DRG in 1992 and RSG-19 started November 1992.

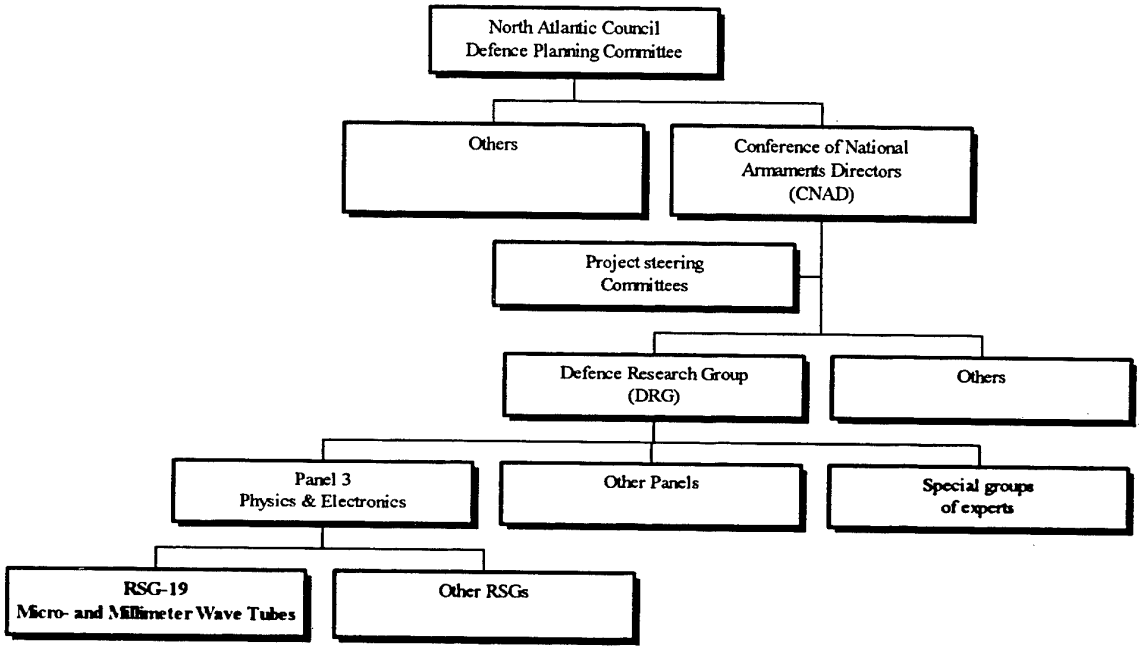

Figure 1 Part of the NATO organization as related to RSG-19

Background

The constitution of RSG-19 in 1988 was based on the proposal of Horst Wittmann 1988 for panel 3. This proposal was based on the following key elements:

- All military radar, EW and communication systems require microwave tubes (US House of rep. 1987) This underlines the importance of microwave tubes and the need for the full availability of the underlying technologies.
- The level of tube R&D is too low to ensure full availability of the technology.
- Tube R&D is not popular, so the technology lacks the necessary improvement.
- The following areas are identified for technology improvement:
    - Interaction circuits
    - Cathodes and guns

- Beam control
- Collector design

- The co-ordination of R&D should be emphasized to avoid duplication of effort and to enhance R&D efficiency.
- A broad academic base should be formed in order to facilitate the necessary R&D enhancement.
- The technology improvement should focus on high efficiency, long lifetime and low cost of ownership.

Specific tasks

The main tasks of RSG-19 will be the creation of a framework to enhance tube and high voltage power supply (HVPS) system compatibility and reliability. This goal will be accomplished in a number of successive steps:

1. Set-up of failure data base

   Based on this data, the most common sources for failure of tubes and HVPS will be identified. The failure cause will be classified. For these classes the predecessors of the cause will be determined by a common forensic analysis of a representative number of the failing HVPS/tubes. The database will not contain any system specific data, it only serves to identify the cause of failure.
2. Specification of tube and HVPS

   The database under 1.1 will be used for the development of a generic "operational envelope" for tubes and HVPS. The generic "operational envelope" will give the relation between all (known) failure causes and the associated operational limit (shock, vibration, temperature, currents, voltages, etc...).
3. Specification of Tube - HVPS interaction

   Failure causes that limit the use of the tube to impractical values have to be avoided using their predecessors. The HVPS "operational envelope" must be adapted to ensure effective protection of the tube against the failure cause. The operational envelope of the tube can be enlarged by choosing the proper operational envelope of the HVPS. This leads to the inter-relation of the operational envelopes and their related failure causes which must be emphasized in the generic operational envelopes.
4. Set-up of acceptance test procedures and standards

   A procedure will be developed to prescribe the testing of this generic tube-HVPS "operational envelope". It will be investigated whether the predecessors are usable to predict future tube and/or HVPS failure and whether they can serve as life-time predictors.
5. Development

   The possibility will be investigated to use the desired operational envelope as a design rule for tube and/or HVPS improvement and/or future development.
6. Update MIL-HDBK 217

   The database will provide the factual information needed to update MIL HDBK 217 for tubes and HVPS.

Members

The proliferation of all the knowledge that is accumulated by RSG-19 will be assured best by involving the people that will use this information. This implicates that RSG-19 has an unusual large membership list that

includes the armed forces as users, all main manufacturers of tubes and HVPS and the involved defense research institutes of the participating countries.

Military benefits

The armed forces uses many systems that rely on microwave power. The reliability of the microwave power source is extremely important, failure of the microwave source can result in the loss of equipment and life. For example, failure of the microwave source in EW equipment can result in the loss of an aircraft, failure of the microwave source in a close-in weapon system can result in the loss of a ship. Reliability is a crucial issue for microwave sources.

The R&D activities of RSG-19 are ultimately guided towards all aspects of reliability enhancement of microwave sources (power tubes and associated HVPS). A secondary target of RSG-19 is the cost reduction of microwave power (The total price that is paid per watt and per hour of RF power). The increase in reliability will lead to a higher Mean Time Between Failure and hence result in cost reduction (more hours of RF for the same price).

The concept of operational envelop will be used to evaluate the reliability of tube and HVPS. A good knowledge of the behavior of the operational envelop will lead to the development of construction guide-lines for reliable tubes and HVPS. The strong and required involvement of the industry in RSG-19 guarantees that new tubes and HVPS are constructed following these guide-lines and that, when necessary, current designs can be upgraded.

The activities of RSG-19 will result in the availability of highly reliable and cost-effective RF-sources. Both reliability and cost-effectiveness are crucial to the military. This results in a major increase in survivability of NATO forces and a decrease in deployability requirements. It is estimated that there will be a 100 to one pay-back from RSG-19 to NATO.

Conclusive remark

RSG-19 now works for 4.5 years and has had major achievements, that are addressed in another paper. The results of its work are presented in the next papers.

RELIABILITY ENHANCEMENT FOR MICROWAVE TUBES AND HIGH VOLTAGE POWER SUPPLIES

Peter J. Rocci
US Air Force/Rome Laboratory
ERDS, 525 Brooks Rd
Rome, NY USA 13441-4505

ABSTRACT

A brief summary of the lessons learned by the NATO Research Study Group on Microwave and Millimeter Wave Tubes and Power Supplies (RSG.19) on aspects relating to reliability enhancement of microwave tubes and high-voltage power supplies is presented in this paper. The reliability of TWTs and high-voltage power supplies is of major importance in NATO systems. These are very complex devices and in the early years of their development, failure rates were high in some applications. Over the years, design and manufacturing technology for tubes and power supplies has steadily improved, and as a result, the industries have developed a good knowledge base on how to provide reliable devices. This knowledge base will help to enhance NATO micro and millimeter wave tube reliability, increase system performance, increase standardization, and decrease system life-cycle-cost across NATO.

1.0 INTRODUCTION

NATO employs many systems that rely on microwave power. The reliability of the microwave power source is extremely important since failure of the microwave source can result in the loss of military hardware and/or human life.

In order to address microwave tube and high voltage power supply reliability issues, NATO AC/243 Panel 3 formed NATO RSG-19, The NATO Research Study Group on Microwave and Millimeter Wave Tubes and Power Supplies. NATO RSG-19, established in 1992, includes government and industry representatives from the United States, The Netherlands, Germany, France, Luxembourg, Belgium and Great Britain. Over the past several years, RSG.19 has discovered that the main causes of poor reliability in tubes and power supplies are due to: 1) poor manufacturing quality, 2) poor maintenance techniques, 3) lack of adequate protection between system components, 4) poor design techniques, 5) operator misuse, 6) lack of utilization of derating principles, 7) inadequacies in the acquisition system ("low bid"), and 8) system software faults. All of these factors, with the exception of #2 apply to both military and space systems. Factors associated with maintenance that contribute to premature failures of military systems include improper handling and wear and tear between high voltage connections which can cause arcing within the tube.

This paper will focus on lessons learned by RSG.19 on the subject of reliability enhancement of microwave tubes and high voltage power supplies. Most of the discussion is associated with design and derating techniques. Brief mention is made of application, testing and standardization issues.

2.0 RELIABILITY ENHANCEMENT FOR MICROWAVE TUBES

Over the past several years, there have been significant improvements made in the design, manufacture, application and screening procedures associated with TWTs which have led to increased field reliability and decreased life cycle cost. The nature of some of these enhancements will be discussed in this section.

2.1 MICROWAVE TUBE DESIGN CONSIDERATIONS

2.1.1 IMPROVED CATHODES

Improvements have been made in recent years in the design of cathodes. Virtually all newer tube designs use cathodes based on M-type construction. M-type cathodes contain a very thin film (several thousand Angstroms thick) of osmium, iridium or rhenium on the surface. The presence of the thin film reduces the operating temperature of the cathode by about 90 degrees C (dependent on film material) without any loss in emission density.

2.1.2 IMPROVED BEAM FOCUSING

Periodic permanent magnets (PPM) are used for focusing electron beams when minimum size and weight are essential. The weight of a PPM system can be one to two orders of magnitude less than a solenoid focusing system. Modern PPM focused tube designs use samarium cobalt magnets. The enhanced magnetic characteristics associated with samarium cobalt magnets permit improved beam focusing which acts to reduce the thermal load and resulting thermal stresses on the RF circuit. Samarium cobalt magnets are also extremely stable. The magnetic characteristics of the PPM structure will not change if the tube is subject to extreme temperature variations.

2.1.3 GETTERS

Getters have been used for decades to help maintain vacuum levels in simple vacuum tubes and cathode ray tubes. Conventional getters use a chemically active metal which is evaporated to form a metallic film on the inside surface of the vacuum envelope. Small amounts of gases that may be present in the vacuum envelope are chemically eliminated by the evaporated film. Conventional getters are not used in high power microwave tubes because the presence of the evaporated film may cause electrical leakage or breakdown.

Nonevaporable getters, which are now commonly used in microwave tubes, employ a combination of materials which do not need to evaporate to eliminate residual gases. Use of nonevaporable getters help ensure a clean vacuum so that a microwave tube will operate properly after extended periods of storage. The probability of arcing after voltage is applied is greatly reduced.

2.1.4 DERATING

Derating is the practice of limiting electrical, thermal and mechanical stresses on parts to levels below their specified ratings. A conservative design approach incorporating realistic derating of parts is a major contributing factor to a product operating reliably. Microwave tubes can benefit enormously from appropriate derating. Derating can provide a buffer between deficient specifications and the real environment. Tube life can be extended in the event that time dependent changes push the tube beyond its capabilities.

Some major parameters for microwave tubes that can be derated include average power, peak power, reflected power and voltage standoff. Depending on the application and

environment, these parameters can be derated between 50%-100% from design capability. In order to ensure that adequate derating is achieved, the following steps are recommended:

- Establish key or critical operating parameters.
- Determine maximum design capability of critical parameters by stress screening preferably more than one tube.
- Perform theoretical analysis and/or computer simulation and verify model by appropriate monitoring during stress testing.
- Limit application or modify design to achieve desired margin.

Derating is straightforward but does come at a monetary cost. However, these costs can be small compared to the expense of replacing unreliable tubes.

2.2 ENVIRONMENTAL STRESS SCREENING

Environmental Stress Screening (ESS) subjects tubes to random vibration and temperature cycling during production. Every tube is screened for defects that have occurred during production. Manufacturing defects are identified and corrected so that the number of flaws remaining in delivered units is reduced. The reduction in flaws is even greater when ESS results are used to modify designs. The cost associated with ESS can be significant but can be far surpassed by the benefits realized.

2.3 APPLICATION

While some tube failures can be attributed to design and manufacturing defects, many result from inadequate system design, poor protection, mishandling and lack of quality feedback from the field. Improvements in tube performance are best implemented as part of a closed loop system in which feedback from field operations provides insight into field problems. The user can improve tube performance by improving the quality of that feedback. This can be done by instituting a formal documentation system which must generate a report prior to the return of the suspect hardware to the manufacturer.

3.0 RELIABILITY ENHANCEMENT FOR HVPS

High Voltage Power Supply (HVPS) reliability is subject to general reliability aspects that apply to all electronic devices. Due to its high power and voltage handling, several aspects are noteworthy:

3.1 HVPS DESIGN CONSIDERATIONS

3.1.1 CORONA SUPPRESSION

Corona discharge is a predominant failure driver in high voltage equipment since it causes degradation in the insulation system. Unlike TWTs, which can tolerate a number of internal arcs without failure, corona in solid dielectric, which usually occurs at dielectric interfaces or voids, is cumulative and eventually results in destructive and catastrophic failure. In short, Corona occurs when materials having dissimilar dielectric constant or bulk resistivity are used in an insulation system or when conductor shapes can generate localized high electric field in an apparently benign environment. They appear to the novice as a paradox where an insulation system fails in spite of considerable derating when only dielectric strength of materials are considered.

The integrity of a high voltage insulation system can be evaluated by performing Corona measurement. The advantage of Corona measurement over hi-pot testing is due to the fact

that Corona measurement is usually performed at nominal operating voltage and does not stress the equipment being tested. Hi-pot, on the other hand, is performed at a much higher voltage and should not be repeated too many times or else the equipment being tested might be overly stressed by the testing itself.

Corona reduction commences at the initial design phase and continues through manufacturing. A key element involves controlling the internal geometry to maintain an acceptable field strength throughout the assembly. Degradation caused by corona can be reduced if materials are chosen carefully. A self-heating dielectric would be desirable but difficult to achieve. Oil systems are somewhat tolerant to arcs as the degradation products become dispersed. However, the degradation is still cumulative.

3.1.2 CREEPAGE

Creepage is a phenomena where electrical discharges occur along the surface of a conductor exposed to air (or gas). It also occurs in potted assemblies when the potting process does not provide near perfect adhesion of the potting material on the insulator. Because of the difference of thermal expansion between substrate and potting material, thermal cycling will eventually stress most potted assemblies to the point where some separation might occur. For this reason, it is essential to considerably derate the voltage stress along an interface to allow for some imperfections in the process. In addition, it is best to also provide for mechanical anchors for the potting material along such surfaces. This can be achieved by machining grooves in the surface which has the added benefit of increasing the creepage distance for a given geometry.

3.1.3 COOLING

Cooling high voltage rectifiers is an art by itself which can drive an otherwise good design to failure if not given proper attention. There are at least as many solutions to the dilemma of providing low thermal resistance and high electrical insulation as there are engineers. Because of the high thermal stress, the distance between rectifiers and the cold plate must be short. The optimum solution will use homogeneous, corona free materials with high thermal conductivity and avoid sharp electrode shapes. The rectifiers will often be fitted with heat dissipaters very near the body to reduce the thermal gradient through the leads.

3.1.4 HIGH-VOLTAGE FIELD CONTROL

Corona is generated by high concentrations of the voltage field. Usually the result of sharp points, small geometries and their associated spacings. Corona inception and associated problems can be avoided by the following:

- A high-voltage "E" field gradient analysis should be performed to ensure that appropriate utilization factors (multipliers) were used with the specific geometries.
- Component edges, corners and fasteners should have a radius or fillet.
- Conductors exiting from high-voltage planes should not create concentrated voltage fields at the exit point.
- Where soldering is used to make connections, a minimum solder ball diameter should be specified and controlled.
- Avoid the use of multiple insulating materials.
- Minimize interfaces.
- Use vacuum impregnation and pressure curing techniques to minimize voids in encapsulation materials.
- Prepare all surfaces for bonding using wet, dry plasma, or etching techniques and cleaning.

- Derate insulating materials based on maximum, not average stress.
- Where printed circuit boards are unavoidably used in high voltage fields, they should be shielded or have barriers added. Corona testing is mandatory to demonstrate the level of design margin.

3.1.5 MAGNETICS

Magnetics represent a major design effort for any HVPS. Guidelines for reliable magnetic design include:

- The voltage gradient between any two adjacent wires in a winding should be minimized.
- A core which is electrically isolated should have an auxiliary lead brought out to facilitate hi-pot test.
- Windings should be impregnated then encapsulated so that no pockets or voids occur.
- Windings that are terminated with insulated lead wires should form a strong mechanical joint.

3.1.6 ADDITIONAL DESIGN RULES

- Consider a slow turn-on scheme that ramps up the HVPS loop reference voltage, rather that shaping the turn-on by the feedback loop. This allows the feedback loop to lock up early during the turn-on and minimizes output overshoot.

- Make sure that the HV dividers are reliably grounded at all times within the unit in which they are located to avoid raising the low voltage end of the divider to a high voltage during any form of testing.

- Simulate the ripple rejection characteristics from the input power bus to the cathode and collector voltages to insure adequate performance.

- If a high performance, high frequency HV divider is used, be sure that partial discharges will not interfere with proper operation.

- If two or more converters are used to generate the HV, insure proper load sharing.

- Obtain and review diagrams of all wiring internal to high voltage capacitors to avoid excessive insulation stresses and potential corona problems. Specify ground planes and shielding where required.

- Design collector and/or cathode current monitors (if used) for proper operation in the noisy environment of the transmitter.

- After the first integration of the HVPS with the tube, allow for the time and resources to iterate the design (especially of the magnetics) to optimize operation.

3.2 STANDARDIZATION

HVPS standardization is an approach to achieving high reliability with affordable costs. Standardization can make available a family of high reliability power supply designs that would, in addition, lead to reduced cost. By limiting the proliferation of unique power supplies, logistic support could also be improved. Power supplies would be partitioned in a manner which would allow for commonality among a majority of equipment applications. Standardization would provide for a quality program to insure interchangeability and reliability. Commonality of a limited number of power supplies would reduce recurring

development costs and ease the logistical support burden. Finally, functional specifications would be developed to avoid dependence on specific technology.

3.3 BUILT IN SELF TEST (BIST)

BIST equipment does not increase reliability in statistical terms. A failure cannot be avoided by BIST. The certainty that both tube and HVPS will run upon switch-on however, can greatly be increased by proper BIST procedures. This reliability aspect is especially important for missile systems, fire control and EW systems, since they are switched on when life-threatening situation occurs.

3.4 RELIABILITY GROWTH

A typical Reliability Demonstration will require to run a number of hours failure free. To shorten the test time, many units are operated simultaneously in a shake-and-bake test fashion. Such demonstration usually fails because the test is performed on early production models and all the bugs have not been worked out. The best way to ensure a reliable product is by performing a Reliability Growth test. A Reliability Growth test is similar to a Reliability Demonstration except that failures are allowed. Failures are analyzed and fixed and all fixes are implemented in all units. The test is completed when enough consecutive failure free hours have been achieved. While expensive and time consuming, the life cycle cost of a program where a well designed Reliability Growth test is conducted will be much lower than the life cycle cost of the program without such test.

4.0 SUMMARY

To date, the work performed by NATO RSG.19 has received very positive feedback from NATO Panel 3 as well as United States and European military and industry communities. This knowledge base developed and shared between the members of NATO RSG.19 will help to enhance micro and millimeter wave tube and HVPS reliability and ensure that systems dependent on microwave power will meet NATO's needs over the life of the system.

5.0 REFERENCES

1. Gilmour, A.S. Jr., *Principals of Traveling Wave Tubes*, Artech House, Dedham, MA, 1994.
2. *Navy Power Supply Reliability, Design and Manufacturing Guidelines*, NAVMAT P-4855-1A, 1989.
3. *Reliability Toolkit: Commercial Practices Edition*, Reliability Analysis Center, Rome, NY, 1995.
4. E.J. Jones, et. al., *DRG Handbook: Microwave and Millimeter Wave Tubes and Power Supplies*, North Atlantic Treaty Organization (NATO) Defence Research Group AC243, Panel 3, Research Study Group - 19, September 1996, NATO Limited.
5. Collins, J.A., Eallonardo, C.M., Hansen, J.W., and Lym, V.W., *Reliability Design Criteria for High Power Tubes*, RADC-TR-88-304, 1989.

ACKNOWLEDGMENTS

The author would like to acknowledge and thank Edward Jones, James Ryan, Jeff Lynch, Rob van Heijster, Jan Schouten, Ernst Mey, Andreas Peters, Graham Phillips, Christian Bonnet, Tom Porter, Patsy Greenman, Ed Fly, Derek Hooker, David Nicholls, Pascal Morin, George Kreager, Stephan Schwarz, Didier Juges, Tom Webb, Al Biddings, Kenneth Craig, David Blough, John Jensen, Lou D'Angelo, and Scott Gilmour for their contributions to this paper.

Generic System Description

Graham Phillips

TMD

England

1.0 Introduction

The component units of a system containing a microwave tube are dictated by the characteristics of the tube as well as by the system performance.

The tube, despite its complexity, is a component which has no feedback mechanisms to maintain a constant output signal if the parameters of the system vary. Thus the characteristics of the system units, which support the tube, have to be defined and controlled to ensure that the overall system specification is achieved.

It has to be mentioned that RSG-19 is focusing on tubes, however the generic system description is also valid when solid state devices are used in the output stage.

In general the system components can be broken down into two groups:-

I) The components necessary to operate the tube or the solid state output stage. These are common to all systems. They include the Electronic Power Conditioner (EPC), RF output circuit and cooling systems.

II) The optional components, which are specific to a particular type of tube or system application. These components include the focusing power supply, which is not required, for example, with a Periodic Permanent Magnet (PPM) focused traveling-wave tube (TWT). The RF input circuit is required with tubes which are amplifiers, such as the TWT or klystron, but not required for oscillators such as the magnetron. The RF input circuit includes the input signal conditioner.

Figure 1 shows a fairly comprehensive block diagram of the generic amplifier system configuration. The components of the first group are shown in heavy outline; the items in the second group are indicated by the outline of normal thickness and the logic and control lines are shown dotted.

The necessary components are required by the physics of system design. The microwave tube converts prime electrical energy to microwave signal and so an EPC unit is needed to supply this energy. Since this conversion cannot be perfectly efficient (and in almost all systems is less than 50%), a cooling system is required to vent the resulting heat into the environment. The microwave signal, being of a high frequency, would disperse immediately by radiation if it were not constrained by an output circuit.

The optional components, which are also dependent upon physical constraints, are principally determined by the specific parameters of the system. The main determining factors are the output power level, the kind of signal modulation used and the type of beam focusing which the tube requires.

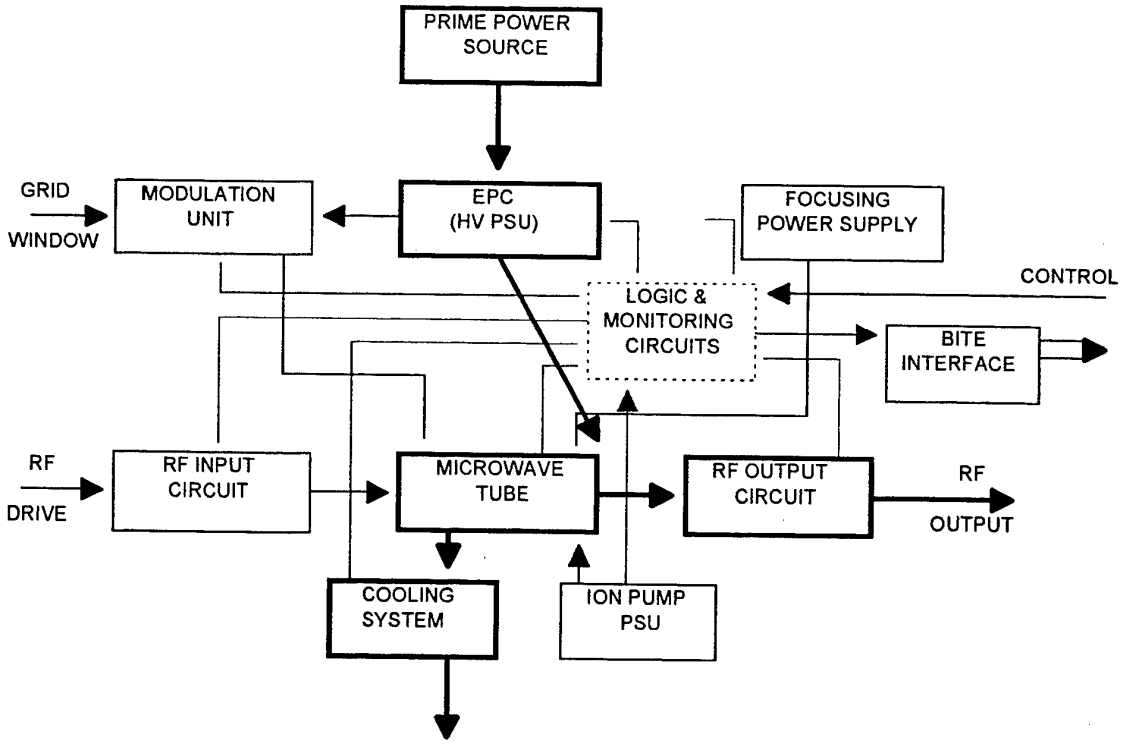

Figure 1 Generic amplifier system configuration

The characteristics of the various system components are described below.

2.0 Component Description

2.1 Prime Power Source

The source of prime power used depends upon the application of the tube system. The most common types of source are:-

I) The public electricity supply.

This option would apply to commercial systems. Even then, this supply would probably be backed-up with a dedicated generator to ensure continuity of operation.

II) AC Generator.

Most military microwave tube systems, ground, naval or airborne, use the electrical generator of the platform upon which they are mounted. There are a number of different standards of voltage, frequency and number of phases.

III) Batteries.

Some short duration tube applications, such as missile guidance, use battery power. For most applications the relatively high average power needed for microwave tubes makes battery power impractical.

IV) Solar Power.

For some specialized uses, such as in spacecraft, solar cells may be used as the prime source of power.

2.2 Electronic Power Conditioner

As indicated above, the EPC is a necessary component of all tube systems. However the particular design employed depends upon the specific requirements of the system.

The physics of microwave tube operation requires that a certain DC EHT voltage is applied to the tube and a particular beam current is used in order to achieve the specified tube performance. The EPC takes the prime supply power, which is normally a low voltage AC, sometimes multi phase, and converts it to the correct voltage; this is typically in the range 5000 to several hundred thousand volts. The EHT voltage must be smooth to ensure that low amplitude and phase noise performance is achieved.

The major types of supply required for different tube types are as follows:-

I) The Unmodulated Supply for Continuous Signal Operation.

In some applications, such as the analogue signal amplification used in communications systems, a CW signal is required. In this case a simple supply, consisting of a step-up transformer, rectification and smoothing, may be adequate.

II) The Unmodulated Supply for Pulsed Operation.

For radar systems, pulsed operation is required. Although this could be achieved, when using an amplifying tube like a TWT, by having a continuous electron beam and a pulsed rf drive signal, this would be highly inefficient in power terms; the proportion of time when the signal is 'on' to the time when the signal is 'off' is less than 10% in most systems. Thus, in pulsed rf operation, the electron beam is also pulsed in time with the rf signal. With many modern microwave tubes the pulses of beam current can be produced by a modulating element in the electron gun of the tube. The most common system uses a grid in front of the cathode to switch the beam current on and off. In this case the EPC supplies a DC voltage to the tube and the pulses are generated by a modulation unit driving the modulating element in the tube.

This power supply design can once again contain the transformer, rectifier and smoothing system. However, the average power required by the tube is normally much lower than the peak power. This gives some added problems for EPC design. When the beam is switched on, the supply is under load and the voltage supplied to the tube tends to drop during the pulse; when the beam is shut off the supply is off load and the voltage rises once again. Although this voltage drop or 'pulse droop', which is small, may not change the output power of the tube by very much, it does change the signal delay time through the tube, which degrades the phase performance of the system. In many sophisticated radar systems the phase information is very important and phase distortions must be avoided. Several methods are used to reduce this voltage drop or to make it linear so that a phase correction can be applied. The simplest method is the use of large capacitors in parallel with the tube. Several configurations of EPC are available to give better control over the voltage between cathode and tube body which controls the electron transit time down the tube and consequently the phase shift of the signal:-

a) Isolated Body and Collector Supplies.

This system takes advantage of the fact that most of the beam current goes to the collector. A very small proportion is intercepted by the tube body. With two separate supplies for body and collector the design can concentrate upon keeping the smaller body supply at a stable voltage with very small voltage droop. This is achieved by using feedback to level the cathode to body voltage. The larger collector supply does not need to be so controlled and is allowed to droop during the pulse. This generally means that the collector at the end of the pulse is negative with respect to the body. In many TWT systems the collector may be depressed to increase efficiency so the collector supply may be providing a considerably lower voltage than the body supply. Indeed, with a supply for multistage depressed collectors several separate supplies may be used to operate each of the collector electrodes at the appropriate voltage. The only problem with allowing the collector supplies to droop is that electrons might back stream down the tube due to the increased negative collector voltage.

b) Tapped Collector Supply.

In this configuration one supply is used for body and collector. The supply is tapped to provide the voltage for the collector. In TWTs where depressed collector operation is common to increase efficiency, the collector voltage can be considerably lower than the body voltage. With this system a triode or solid-state post regulator can be used to keep the body voltage very stable during the pulse while allowing the collector voltage to vary.

It is also important that the supply can operated under open circuit conditions, when no pulse is present; short circuited conditions, if the gun arcs as described below, and under matched conditions during normal pulse operation.

A major problem with this type of system in general, is the possibility of voltage breakdown or arcing occurring inside the electron gun of the tube. This effectively shorts the power supply through the gun which can cause major damage to the tube. This can be reduced by putting a high power, low resistance in series with the tube which will drop most of the EHT voltage when in series with the virtual short circuit presented by the arc in the gun. A more sophisticated method uses a triggered vacuum device called a crowbar tube in parallel with the microwave tube. When the monitoring circuitry detects the beginnings of an arc, the crowbar tube is triggered and the power is dumped through it into a resistor, protecting the microwave tube.

III) The Pulsed Supply.

Before the introduction of grids or modulating anodes, the pulsed beam was produced by switching the power supply on and off. This technique is still used where modulating electrodes are impractical, such as in power supplies for magnetrons.

The most common methods of switch the supply are:-

a) The resonant line method where a line made up of inductors and capacitors is charged up between pulses then discharged through an electrical switch into a step-up transformer or pulse transformer to form the pulse which is applied between cathode and anode of the tube. This method has the advantage that the power applied to the tube is limited to that stored in the line so that, in the event of electrical breakdown in the tube, the next pulse can be inhibited by the electrical switch. The disadvantages of this method are that the pulse length and duty cycle can not be varied easily without altering the construction of the resonant line and the pulse shape produced is poor and susceptible to the match presented by the tube to the system.

b) The directly-switched power supply. In this system a vacuum tube or solid state switching stack switches the EHT to the tube. This method is more flexible in terms of pulse width and duty cycle changing but tends to applied only to low voltage applications. It is however possible to combine this technique with a pulse transformer to produce a higher voltage pulse.

IV) The Heater Supply

Practically all microwave tubes produce an electron beam from a heated cathode. As the body of the tube is normally at earth potential for practical reasons, the cathode is set at a the negative EHT voltage. The cathode heater is normally at the same potential as the cathode so the heater power supply is also operating at the EHT voltage. Thus the heater power supply is normally part of the maim tube power supply taking advantage of the insulation between EHT and earth potential.

Heaters can be AC or DC depending upon application. The AC heater has the disadvantage that, unless care is taken in the design of the heater element, unwanted modulation of the beam can occur because of the varying magnetic field produced by the AC. This can be prevented in the tube design by configuring the heater winding so that any residual magnetic fields are canceled out or, in a pulsed system design, by inhibiting the heater supply during the pulse.

DC supplies can cause problems with potted heater designs. In the potted heater design the fragile heater filament is supported by potting it in a ceramic packing material. Under the very high temperature conditions of heater operation an electrochemical reaction can take place which corrodes the heater filament and causes an open circuit. With an AC supply the change of polarity cancels out the electrochemical effect. Heaters which are self supporting or held by ceramic supports are not affected by this electrochemical effect under DC operation and, of course, the beam modulation problem is eliminated.

2.3 Cooling System

The heat produced by the limited efficiency of the tube, its focusing system and the power supply, is removed from the equipment by means of a cooling system. Several different cooling methods are employed depending upon the constraints of the system:-

I) Liquid Cooling.

Liquid cooling enables large quantities of heat to be removed from the equipment in relatively small space. The hot liquid can easily be piped large distances to a heat exchanger which can vent the heat into the environment. Problems can be encountered due to changes of state of the fluid; freezing of water based coolants can damage the tube or equipment and when boiling occurs the sudden reduction in cooling effect can allow the tube to seriously overheat. Water is often used as it is a very good coolant having high specific heat, low viscosity and it is cheap and easily available without environmental draw backs. Its only major disadvantage, a high freezing point, can be overcome by the use of monoethylene gylcol antifreeze. Different kinds of liquid cooling systems are used :-

a) Natural Convection is used to cool components in power supplies. The cooling fluid is also, generally, an insulator and has a dual function of insulating the components.

b) Forced Convection is commonly used in tubes to give the maximum cooling with the smallest components.

c) Nucleate Boiling. The change of state due to boiling of a fluid, especially water, can give a very high removal rate for unwanted heat. The resultant steam is condensed in a heat exchanger, either to air or to a lower temperature fluid.

II) Conduction Cooling.

In some applications, especially in aerospace systems, it is not convenient to use fluids for cooling. Conduction cooling can be used in these cases. A disadvantage is that a good conducting path must be provided from all the component parts of the tube and system to the heat sink.

III) Air Cooling.

In many systems where the heat density is low, the heat may be removed by providing cooling fins and using forced air cooling. This has the advantage that the air represents the output of the heat into the environment and no further heat exchange system is required. A disadvantage is that the air normally requires filtering because the cooling system is not a closed one. Noise added to the microwave signal by microphony from the cooling system can also be a problem.

IV) Radiation Cooling

In some special systems direct radiation of heat has been used to cool the collectors of microwave tubes. This method is seldom used because, to remove useful amounts of heat from a component of manageable size, the element must be at a very high temperature. The disadvantages of this in terms of outgassing and thermal stresses outweigh any advantages except in exceptional circumstances.

2.4 RF Output Circuit

The output system conducts the output signal from the tube to the point of use, which can be an aerial or other load. The conduit for the signal is typically a waveguide or coaxial line because of the high signal power level.

Once again the exact configuration of the output circuit depends upon the system requirements. Figure 2 shows a typical system used in many high power tube applications. The order of the components may also vary with the specific application.

I) The arc detector.

In all microwave tubes the rf signal must, at some point, pass through the vacuum envelope into the output system. An output window is provided for this purpose. In some cases the electric fields, due to the high level of the output signal, are large enough to cause electrical breakdown in the medium filling the waveguide or coaxial line. This arc tends to move towards the source of power and will eventually reach the microwave window in the tube where the heat produced by the arc can break the window. This can be avoided by detecting the arc by a photoelectric cell, looking into the output system, as soon as it forms, which then causes the rf input power to the tube to be inhibited.

The tendency of the output line to arc can be reduced by pressurizing the gas in the system, which increases its voltage hold-off capacity, or by using a gas with higher breakdown voltage properties such as sulfur hexafluride.

The peak voltage on the output line can be increased by a mismatch occurring in the line or in the external system; an arc also appears as a near short circuit on the output line. An alternative to, or supplement for, the arc detector is to monitor the reverse power caused by mismatches and to inhibit the rf drive power if the match goes out of the specified range.

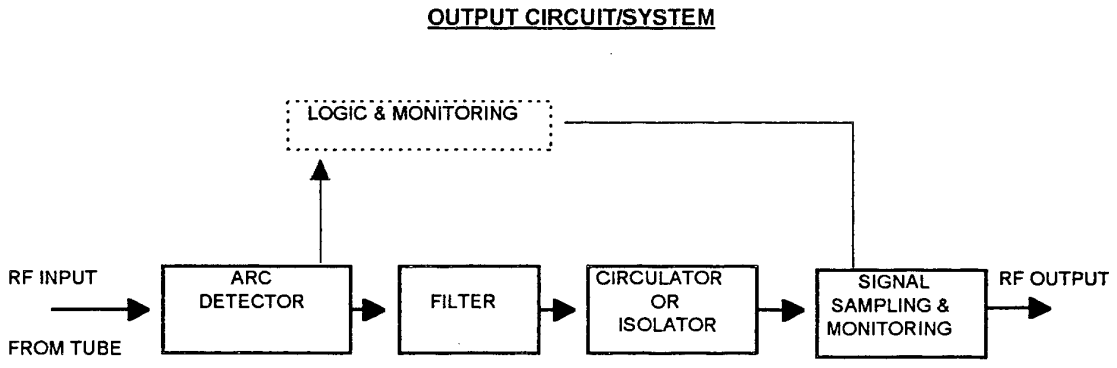

Figure 2 Generic output circuit.

II) The Filter.

The output signal from microwave tubes contains a harmonic power component and, in some cases, spurious output signal produced by the microwave tube or its drive system. In some cases the second

harmonic power level is only 20 dB down on the fundamental signal level, which, in a high power tube, can be a considerable amount of power. The signal purity can be improved by filtering the output signal using an in-line bandpass filter.

III) Circulator or Isolator.

In some systems the external load may have a poor match. The reflected signal from this match can degrade the performance of the microwave tube. The power output levels of magnetrons and klystrons are affected by output match and the severs used in TWTs can be damaged by power reflected back from the load. For this reason some systems use a high power isolator or circulator to provide a matched environment for the tube to operate into. In some radar systems an isolator is in integral part of the system; the returning signal from the aerial is taken from the reflected-signal port of the circulator to the receiver.

IV) Signal Sampling and Monitoring.

In most systems it is necessary to monitor the output signal to ensure correct operation. Typically, some form of microwave coupler is used in the output system so that a low power sample of the signal can be obtained for monitoring purposes. The output power level is generally of interest and can be calculated from the power sample measured and the calibration of the coupler; a microwave power meter is used for this purpose. The form of a pulsed signal can be monitored by means of a crystal detector and oscilloscope rectifying the sampled output. The purity of the signal can be monitored and the presence of unwanted spurious signals can be detected by a spectrum analyzer fed with a sample of the output.

2.5 RF Input Circuit

In some systems, such as those using oscillators, no rf input signal is required. However, in systems using amplifier tubes an rf circuit of some kind is needed. Figure 3 shows a system using components which may be found in a broadband pulsed system. As most microwave tubes have considerable gain, the input circuits are frequently made up of coaxial components and cables. The signals are of generally of such a low level that electrical breakdown in the input system is seldom a problem.

I) Pin Modulator.

In pulsed systems it is usual to pulse the input signal to the tube. The beam pulse is normally slightly longer than the rf pulse requirement and the rf pulse is delayed so that it is 'nested' within the beam pulse. This is to ensure that the beam has stabilized at its full level before the rf signal enters the tube. A pin modulator can provide a very short rise-time for the pulse.

II) Signal Sampling and Monitoring.

As in the case of the output system, it is generally desirable to monitor the input signal to the tube. Often, if the tube is part of a chain of tubes, the input monitoring is part of the output sampling for the previous stage.

As in the output system, power meters, crystal detectors and spectrum analyzers are commonly used to

monitor the signals.

III) Equalizers.

In broadband systems, such as in TWT amplifiers, it is desirable to have a level output power across a wide bandwidth. The natural characteristic of most kinds of TWT is to have lower power at the bandedges and a maximum power 'hump' in the center of the band. This can be improved, to produce an approximation to the desirable flat 'brick-wall' characteristic, by tailoring the rf drive level so that, when a level rf drive is applied across the frequency band, more drive power is delivered to the tube at the bandedges than at the bandcenter. This can be done by using a kind of in-line filter which passes more power at the bandedges. Since the characteristics vary from tube to tube, it is common to customize an equalizer to suit a particular tube.

More complex equalization systems are not only frequency dependent, but also amplitude dependent. These so called linearizers compensate for the non-linearity of the tube thereby creating an amplifier system that can be operated close to saturation without the common drawbacks of non-linear distortion, cross modulation etc.

IV) Isolator.

To ensure that the rf drive system operates into a good match and the input circuit looks like a good match to the tube, an isolator is often fitted to the input circuit immediately before the tube. In systems using klystrons this is particularly important. The input match of a klystron is effectively the match of the input cavity. This is generally well matched at only one frequency and at frequencies away from this frequency it is a virtual short circuit. Reflected power, which is re-reflected from mismatches elsewhere in the system, can badly distort the bandpass of the klystron. An isolator close to the input of the klystron can eliminate this problem.

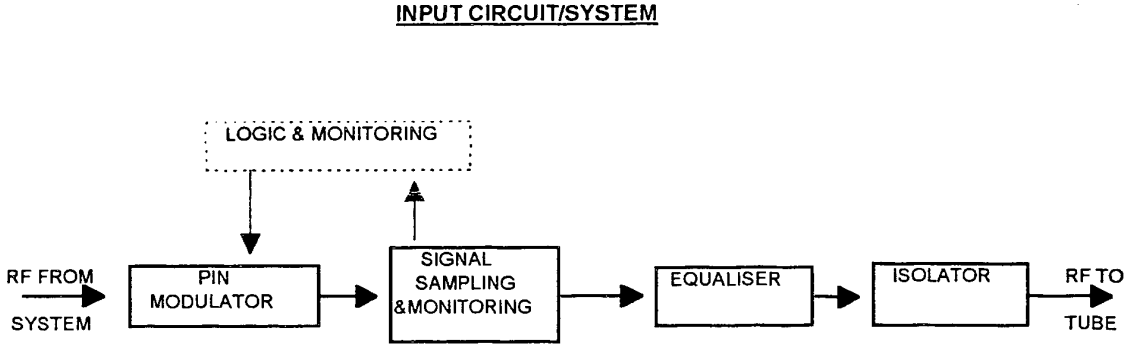

Figure 3 Generic input circuit

2.6 Modulation Unit

In pulsed tubes which use an EPC of the unmodulated type (where the microwave tube has a modulating element built into the electron gun) a modulation unit is required to provide the voltage drive to the modulating element. As the gun of the tube normally operates at high negative EHT voltage relative to earth, the modulation unit must also be

at negative EHT voltage and be well insulated. For this reason it is commonly built into the EPC.

The design of modulation unit used depends upon the type of modulating electrode which the tube has. This governs the voltage and current requirements of the pulse which the unit must deliver. The unit is normally driven from a pulse generator.

The modulator is usually referenced to the cathode potential and a supply holds the voltage at the negative bias voltage with respect to cathode. A positive going pulse drives the modulating electrode positive with respect to cathode during the pulse period. Diodes are used to clip the top of the pulse and produce a level top to the forward drive pulse.

I) Modulating Anode Guns

The modulating anode in a microwave tube requires a relatively high voltage swing to switch the beam on and off but usually draws little current. In some cases the voltage swing can be of the same order as the EHT voltage.

II) Gridded Gun with Intercepting Grid

A grid-switched system has a much smaller voltage swing than a modulating anode to switch the beam; a voltage swing of 6% of the EHT voltage will generally suffice. In the case of an intercepting grid the current which must be supplied by the modulator depends upon the transparency of the grid, i.e. the proportion of the cathode current which is intercepted by the grid. Modern gridded designs have transparencies of the order of 80 to 90%. The modulator supply must be capable of providing the grid voltage with a current which varies from zero at cut-off to a maximum value of 10 to 20% of the peak beam current when the beam is fully on. Another component of current which the modulator unit must be able to supply, is the current into the grid capacitance. Since the grid is physically close to the cathode, this capacitance can be of the order of a few tens of picofarads.

III) Gridded Gun with Non-intercepting Grid.

The non-intercepting gridded gun normally has a shadow grid, between cathode and control grid, which is kept at cathode potential and suppresses electron emission directly to the control grid. This means that the modulator unit is not required to supply the interception current component of grid current. Only the portion of the current required to drive the grid capacitance is required from the supply which means that it can be smaller.

2.7 Focusing Power Supply

In practically all microwave tubes some means of electron beam containment is required and virtually all tubes use magnetic fields to achieve this. In some tubes, such as magnetrons and smaller TWTs, this focusing field is provided by permanent magnets. In other cases the focusing flux is provided by a solenoid. In this case a power supply is required. Since the focusing flux is proportional to the current in the winding and the number of turns wound on the solenoid, this is normally a smoothed DC supply with high current and relatively low voltage. As energy is dissipated

in the solenoid some form of cooling is needed.

In some specialized systems super-conducting solenoids are used. In these cases the solenoid is simply 'charged' with the required current and, as long as the solenoid winding is kept at liquid helium temperature, the solenoid can be treated as a permanent magnet.

2.8 Ion Pump Unit

Microwave tubes are vacuum devices and the quality of the vacuum can have a great affect upon the performance of the tube. Although the tube is processed by pumping on a system capable of achieving an ultra high vacuum while the tube is baked at high temperature, residual gas remains within the vacuum envelope. As time goes by the gas pressure inside the tube can rise due to outgassing of the metal of which the tube is made or by microleaks present in the structure. Some tubes, especially large ones, have a built in ion pump which allows the internal pressure to be measured. This pump has to be supplied with a high impedance voltage supply, typically of 3.5 kV. The current taken by the pump is related to the density of gas molecules present in the tube vacuum and can be calibrated to give an indication of the pressure in the tube.

Ion pump supplies normally have a meter to measure currents of the order of microamps and, in some cases, trip mechanisms which can be set to trip if a set current, corresponding to a particular pressure, is exceeded.

2.9 Logic and Monitoring Circuits

If a microwave tube is to perform correctly it is necessary to control the system operating parameters carefully. Failure of some of the units supporting the tube such as the cooling system or focusing power supply could cause catastrophic tube failure. Even if some of the operating parameters such as beam interception or reflected output power exceed the specified limits, damage can be done to the tube. Thus it is necessary to monitor the important operating parameters continually and take corrective action when the specified conditions are violated. Most tube systems have some electronic system which monitors the parameters and controls the operation of the equipment.

The most common control activities are described below:

I) Cooling Monitoring.

With air or liquid cooling the cooling medium flow is normally monitored and interlocked so that, if the cooling system fails, the power to the tube is switched off. In some cases the temperature of the coolant inlet and the pressure drop through the system are also monitored and interlocked.

With conduction cooled systems the temperature of the heat sink can be monitored and the power to the system switched off if a specified temperature is exceeded.

II) Focusing Supply.

In a solenoid focused system, the failure of the solenoid current will lead immediately to high current interception to the tube body. Thus the focusing current is normally interlocked so that a drop below the specified level causes the tube to be shut down. This could be achieved in a pulsed tube by inhibiting the modulating electrode drive pulse from the modulation unit which would cut off the beam.

III) Current Monitoring

Other faults in the tube may lead to increased interception current which would cause damage to the tube. Thus it is common to monitor the body current where this is possible. In some tubes it is possible to distinguish between beam current which reaches the collector and that which goes to the body by isolating the collector electrically. If this is not possible, then the total beam current can be monitored and the beam inhibited if a safe level is exceeded.

In pulsed systems, both mean and peak monitoring are of interest. The latter can be measured by the use of current transformers on the leads connecting the tube to the EPC. This monitoring will also detect electrical breakdown or arcs from the electron gun to body and a failure of the modulation unit which leads to increased duty cycle operation.

IV) Gas Pressure.

Leaks in the vacuum envelope and faults in tube operation often lead to excessive gas pressure inside the tube. This will eventually lead to tube failure due to cathode poisoning or arcing. The gas pressure can be monitored during operation by measuring the current from an ion pump fitted to the tube. If this current exceeds a specified limit, the rf drive to the tube or the beam switched of by inhibiting the pulse from the modulation unit.

V) RF Power Monitoring

Couplers fitted to the output or input circuits can measure the output and input power. Some tubes are sensitive to excess rf drive signal. Should a failure of the drive circuits occur, the rf system can be shut down. Similarly, excessively high or low rf output power can be detected and the rf input system inhibited. With a bi-directional coupler in the output circuit, reflected power from a faulty output system can be monitored and the rf drive inhibited before damage is caused to the tube.

VI) Arc Detector.

If an arc detector is fitted to the output circuit the rf drive to the tube can be inhibited if an arc occurs in the output system. This can remove the drive before the arc can cause damage to the tube window.

2.10 Built In Test Equipment (BITE) Interface

In many modern systems the system operation is monitored by computer controlled equipment. Data taken during the operational life of the system can be stored for later analysis. To achieve this an interface unit can be fitted to the tube system to take data from the logic and monitoring circuits, digitize it and send it via a standard computer interface system to a system controller.

2.11 Generic system

The topics of RSG-19 are all based on the generic system that has been drawn up here. The lay-out of figure 1 has

been changed and simplified in order to enhance readability and is given in figure 4. Each element in figure 4 is discussed in more detail in the following chapters.

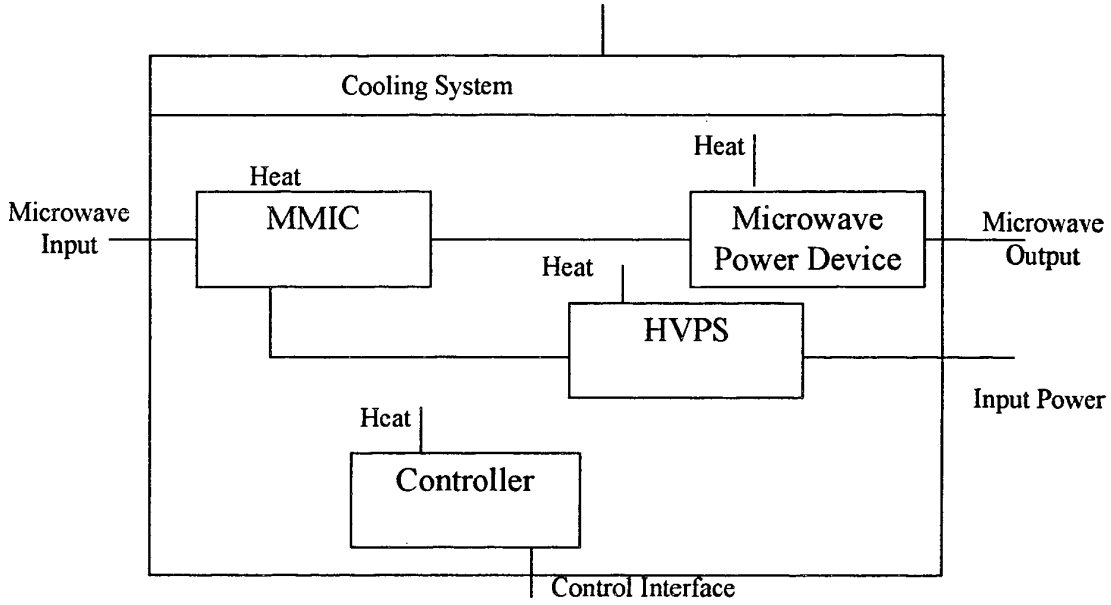

Figure 4 Generic system lay-out

All RSG-19 topics are based on this lay out.

THE OPERATIONAL ENVELOP CONCEPT

Rob M.E.M. van Heijster
TNO - Physics and Electronics Laboratory
The Hague, The Netherlands

Summary: The concept of the operational envelop (OE) will be described. It will be made clear that the operational envelop is a means to describe the way an amplifier should be operated in order to obtain optimum reliability and performance. It also shows how operational envelops influence each other and how the optimum operational envelop can be obtained.

To model all various aspects of tube reliability, RSG-19 introduced the "operational envelop" concept. For the assessment of the various reliability aspects of power amplifiers and their PS the concept of the Operational Envelop is a useful tool. It also helps to adept the feasibility of tube and power conditioner concepts.

The concept of the operational envelop is not limited to microwave power systems but is applicable to almost any system.

What's an operational envelop? To explain the operational envelop it is necessary to use the operation point (OP). An operation point is a combination of parameter values that can occur simultaneously. In microwave power electronics these parameters will in general be voltages and currents. A simple example are the operation points of a light bulb. When we apply 12 V to a 12 V/ 12 W bulb there will run a current of 1 A, so (12 V, 1 A, 12 W) is an operation point. Another operation point will occur when we apply 11 V to the bulb. The current will be again almost 1 A, due to the bulbs current stabilizing properties, so the power will be almost 11 W and hence the operation point will be (12 V, 1 A, 12 W). With the light bulb we can add parameters like for instance, filament temperature or life expectancy to the operation point. In Figure 1 the operation points (power, filament temperature, life expectancy) are given as function of the voltage. The current is left out, since it is almost constant at 1 A.

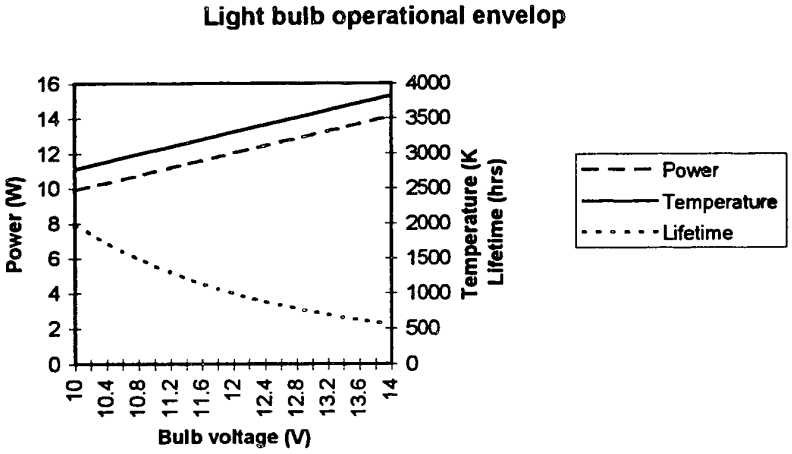

Figure 1 Light bulb operation points.

Back to the operational envelop. When we require a life expectancy of 1000 hr. for the bulb, Figure 1 shows clearly that we need to keep the voltage at or below 12 V, and hence the temperature at or below 3300 K and the power at or below 12 W. So all operation points related to voltages of 12 V or less give a life expectancy of 1000 hr. or more and are called valid operation points. The valid operation points are enclosed by the 12 V boundary. This boundary at 12 V is called the operational envelop.

The above-mentioned example is extremely simple and only showing a part of the story. The operation point is determined by the voltage, there is only one independent parameter[1], the independent parameter space is one dimensional. The operational envelop is a point, 12 V. A two dimensional example is formed by the operation points of a FET. The drain voltage and drain current can be manipulated independently. The resulting operational envelop is shown in Figure 2. The operation points are limited by the maximum current of 10 A, the maximum voltage of 100 V and the maximum dissipation of 100 W.

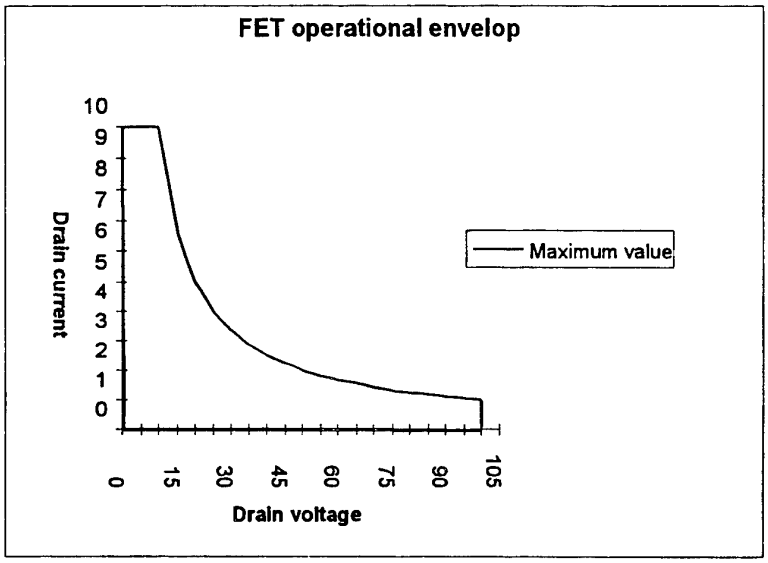

Figure 2 FET operational envelop

A similar picture can be drawn for a microwave tube. Lets take an example where the tube is designed to run at a voltage of 10 kV and a current of 3 A. Due to defocusing, only a limited current may flow for voltages other than 10 kV. The current can be controlled ("independent" of tube voltage) by a grid. The operational envelop for this tube is given in Figure 3. Also shown are two start-up curves, it is clear that the invalid start-up curve will eventually destroy the tube.

[1] an independent parameter is a parameter we can change at will. The dependent parameters will vary according to the independent parameters and cannot be varied independent of them.

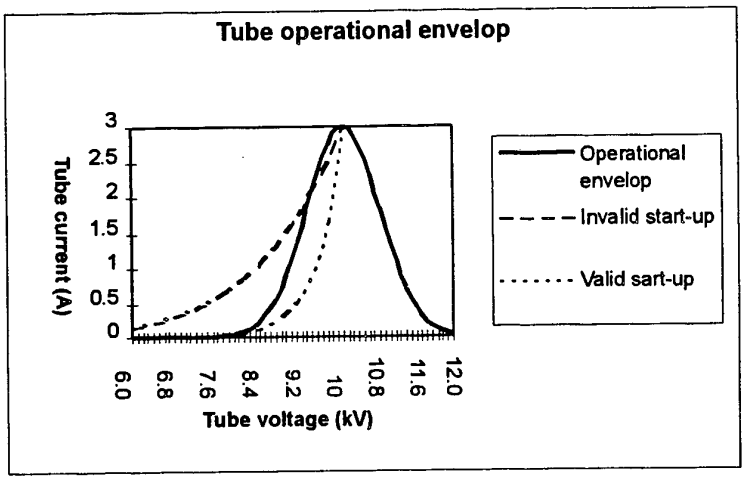

Figure 3 Tube operational envelop (example)

It's obvious that complex systems have often more than two independent parameters. For the ease of understanding (and the fact that two dimensional data is easily captured in graphs) we use two-dimensional examples.

How do we use the operational envelop concept to design new systems and to evaluate existing ones? This will be described by the following example in which we "design" a microwave power system. We will consider two parameters, of course in actual systems there are more parameters. The parameters considered are called "anything", in the actual design they can be cathode voltage, RF-output power, helix current, etc., etc.,...

Any design will start with system requirements. They determine which tube we have to select. To meet all system requirements the tube will have to operate in several operation points, these operation points are determined by the application. The application operation points are within the application operational envelop as shown in Figure 4.

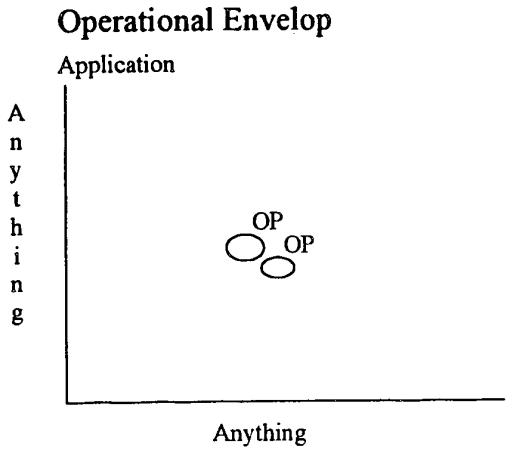

Figure 4 Application operational envelop

The operational envelop of the tube itself should of course be wider than the application operational envelop. When this is not true, we have to consider the selection of another tube. Assuming that we have selected the right tube, its operational envelop in relation to the application will be as shown in Figure 5.

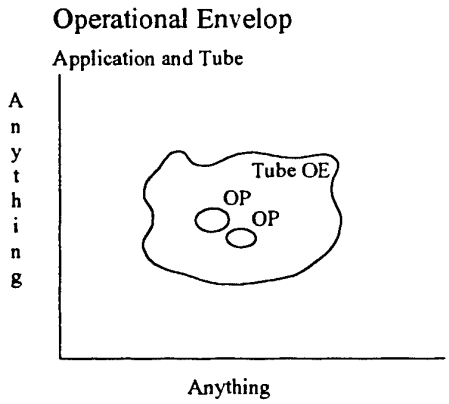

Figure 5 Tube operational envelop

The tube should, in any of its operation point, not be able to destroy the HVPS. The operational envelop of the HVPS should be larger than the tube operational envelop, as shown in Figure 6.

It should be considered that an arc can occur during normal operation and that a low tube impedance is hence a valid operation point. The resulting high currents are only allowable for a short time and hence the operational envelop for energy flow under arc-conditions is set to a maximum of for example 5 J. The HVPS should be able to withstand the arc.

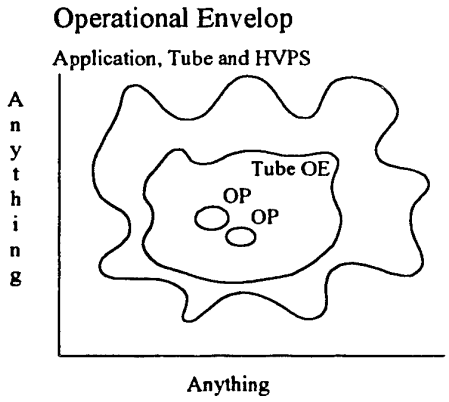

Figure 6 HVPS operational envelop

We want to use both tube and HVPS within their operational envelops. To guarantee this under any operational condition, we use a control systems for the HVPS. This control system should protect both tube and HVPS. This requirement is met by a control system that keeps the operation points within the operational envelops of tube and HVPS.

With respect to an arc keeping the tube and HVPS within their operational envelop this implicitly mean that an arc is handled in a safe way without damaging the tube or the HVPS.

The control limits the operation points to what we call the control operational envelop, as is shown in Figure 6. As long as the tube and the HVPS are operated within this operational envelop, the stress factors are within the limits and the (well designed) tube will exhibit a good reliability.

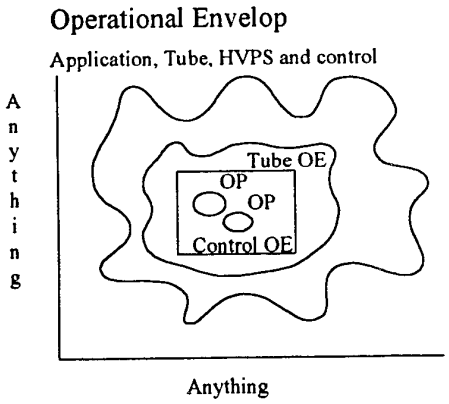

Figure 7 Control operational envelop

As is shown already in the light bulb example, an increase of lifetime and reliability can be obtained by narrowing the operational envelop. Figure 1 shows that a lower maximum bulb voltage increases bulb life expectancy. This principle is more general, as is shown in Figure 8 for the (hypothetical) tube in our design example.

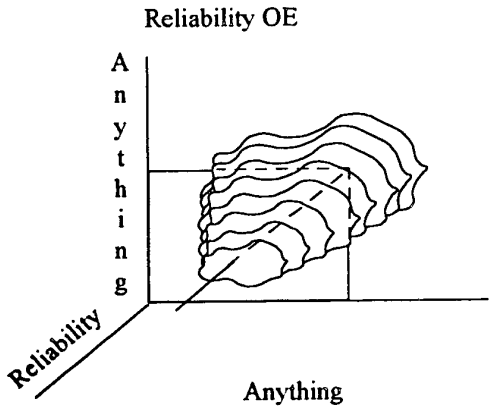

Figure 8 Reliability operational envelop

Summarizing we have three important definitions:

- Operation point (OP):
  Any combination of voltages and currents (temperatures, shock, vibration etc. may also be included) that is applied to the tube or is present on the power conditioner.
- Valid operation point:
  Any operation point that the tube or power conditioner can handle for prolonged time (the specified lifetime).
  Valid Operation points are often subject to time constraints, their validity is restricted to a given pulse width and/or duty cycle.
- Operational envelop :
  The boundary of the set of all valid operation points.

Evaluation of the respective operational envelops of application, tube and HVPS enables us to select the right tube and HVPS components and to specify the required control system. When system evaluation is requested, a comparison of the four operational envelops is sufficient to reveal the major strong and weak points in the design.

The "operational envelop" concept, however, is general applicable. Considering a car we can say that driving is possible when there is a road (independent parameter 1) and enough fuel(independent parameter 2). Combining these two parameters into an operational envelop gives the maximum range (maximum amount of fuel) with respect to the availability of roads. Given a starting point in Amsterdam, the operational envelop will be as shown in Figure 9.

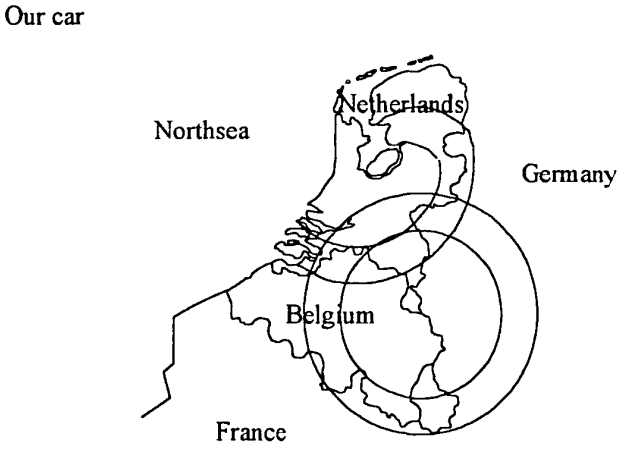

Figure 9 *Car operational envelop example*

ENVIRONMENT

prepared by A. S. Gilmour, Jr. and presented by George Kreager

Naval Surface Warfare Center

Crane, Indiana, USA

Abstract

Applications for microwave tubes vary widely and range from spacecraft systems where, after launch, the environment is benign, to cannon launched systems. In this paper, elements of the physical environment (shock and vibration, temperature, user treatment, etc.) are discussed. Examples of specifications used in some Naval applications for testing to ensure that tubes can survive in actual operation are given. Finally, major improvements made by tube manufacturers in recent years to better fulfill the requirements imposed by various environments are pointed out.

1. Introduction

The environment in which a microwave tube is operated can have a very large impact on performance. Microwave tubes are typically employed in the following environments:

1. Ground based systems
   a. Fixed installations
   b. Mobile installations
2. Seaborne systems
3. Airborne systems
4. Spacecraft systems

The environment to which a microwave tube is subjected may have many facets. As indicated in Figure 1, the overall environment can be divided into two parts. On one hand, the system must interface with the tube and so it contributes to the tube environment. Elements of this environment are the voltages applied to the tube, the RF interfaces, the protection techniques and circuitry used, etc. This aspect of the total tube environment has been discussed elsewhere and will not be covered here.

In addition to the system induced environment, there is the physical environment which consists of:

1. Shock and vibration
2. Temperature extremes and cycling
3. Atmosphere including pressure and humidity
4. Radiation including HPM and EMP
5. Stray electric and magnetic fields
6. User treatment

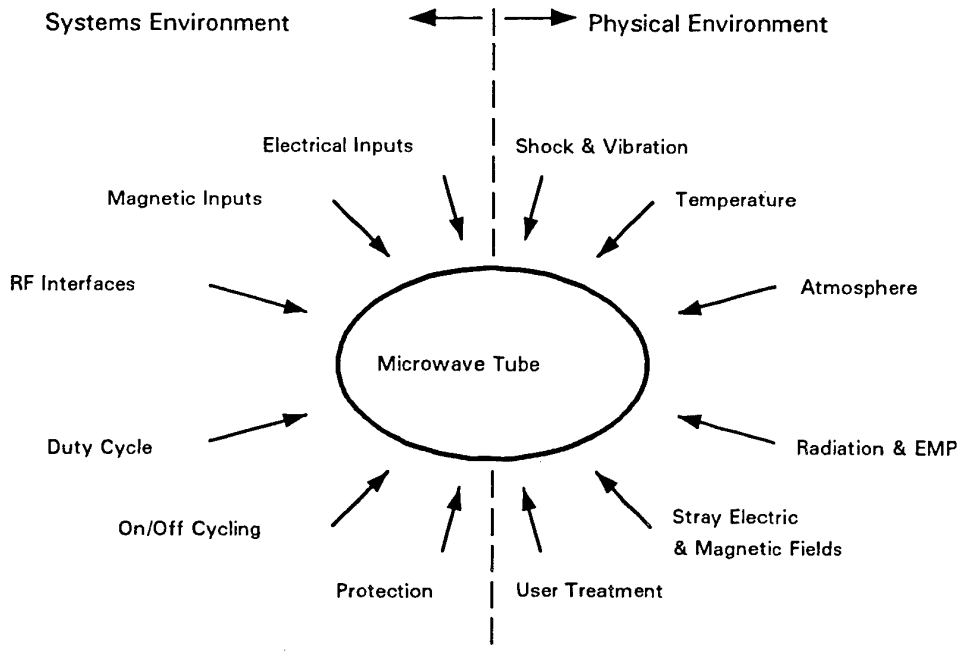

Figure 1 Quantities and phenomena that affect the performance of a microwave tube.

These elements of the environment, along with some techniques and procedures used by the tube industry to enhance reliability, are discussed in this paper.

2. Physical Environment

Whether of not a particular element poses a threat varies a great deal with the system application. For example, radiation is present in satellite systems. Still, while radiation can have a significant deleterious effect on the operation of solid state devices, microwave tubes are immune to radiation effects. Also, electromagnetic pulse (EMP) and high power microwave radiation (HPM) can destroy solid state devices but have no effects on microwave tubes.

Tubes may experience severe shocks in some applications. For example, MIL-STD-202 specifies that a tube shall be able to withstand the impulse shown in Figure 2. Tubes are tested in this manner for some Naval applications.

MIL-STD-202 SHOCK SPECIFICATION

Tubes are Exposed to:

... Half-Sine Impulse

... 3 Blows in Each Direction

... on Each Axis

... Total of 18 Blows

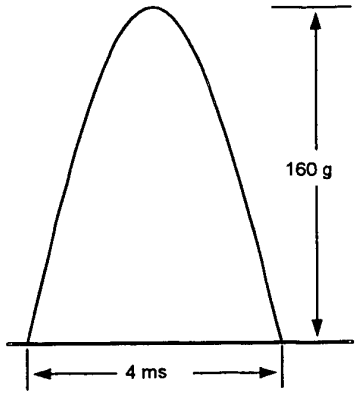

Figure 2 MIL-STD-202 shock specification.

Tubes may also experience severe vibrations in some applications. The vibration tests used for some Naval applications are complex and range from exploratory tests from 5 to 25 Hz at low amplitude to endurance tests from 5 to 25 Hz at high amplitudes for a period of at least two hours. There are variable low frequency and variable high frequency tests during which the tube must be operating. For the variable low frequency test, the vibration amplitude is shown in Figure 3. For the variable high frequency test, the amplitude is as shown in Figure 4.

VARIABLE LOW FREQUENCY VIBRATION TEST

USED IN SOME NAVY APPLICATIONS

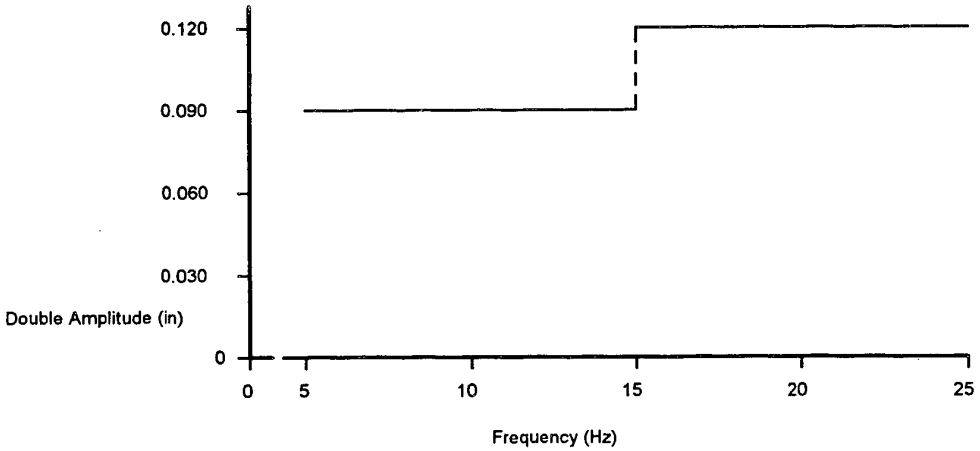

Figure 3 Variable low frequency vibration test.

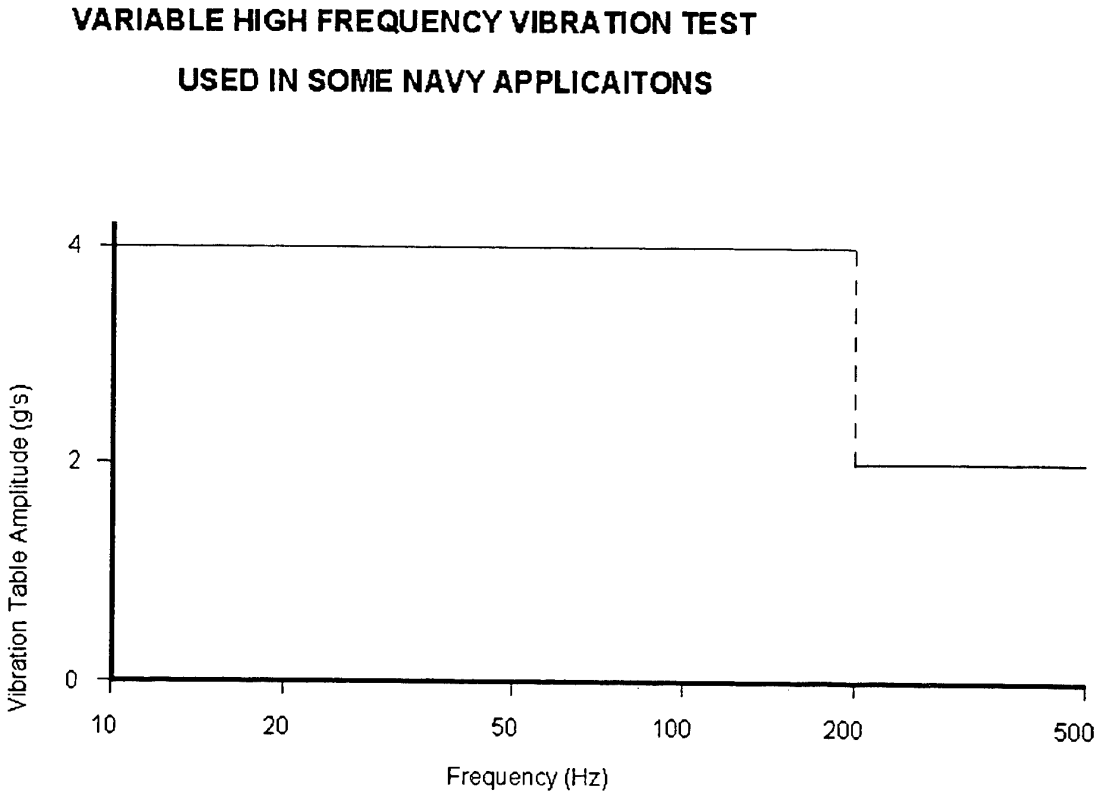

Figure 4 Variable high frequency vibration test.

The temperature to which a tube is exposed can vary over a wide range. In preparing tubes for some Naval applications, tubes must be subjected to three temperature tests. To simulate possible storage conditions, tubes must operate properly after being held at -62°C +0, -5°C for 72 hours, then increased to 75°C -0, +3°C for 4 hours and then reduced to 25°C ±2°C for 4 hours. Also, while operating, a tube must withstand the temperature variations shown in Figure 5. Finally, the tube should be capable of satisfactory operation after being subjected to the temperature shock shown in Figure 6.

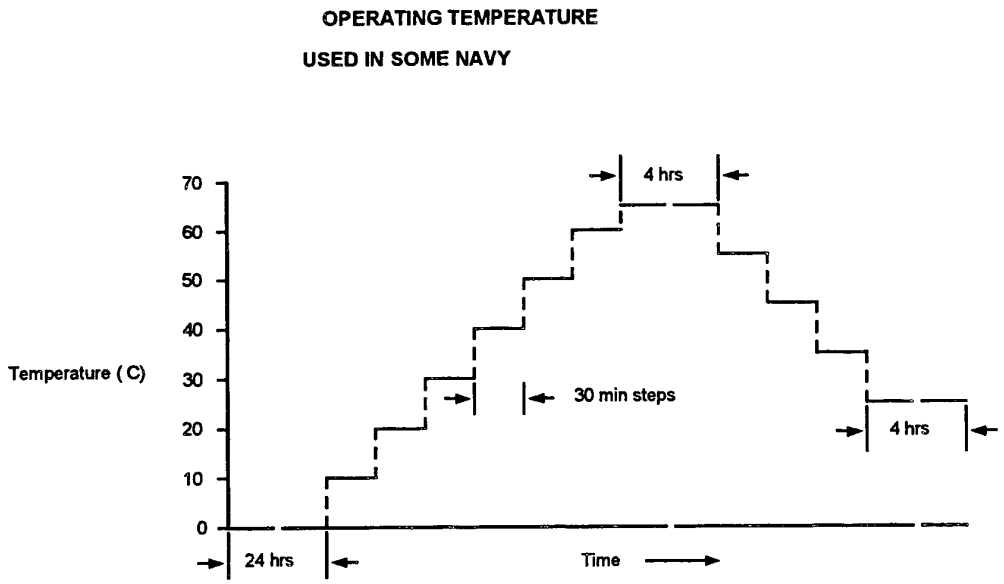

Figure 5 Operating temperature test used in some Navy applications.

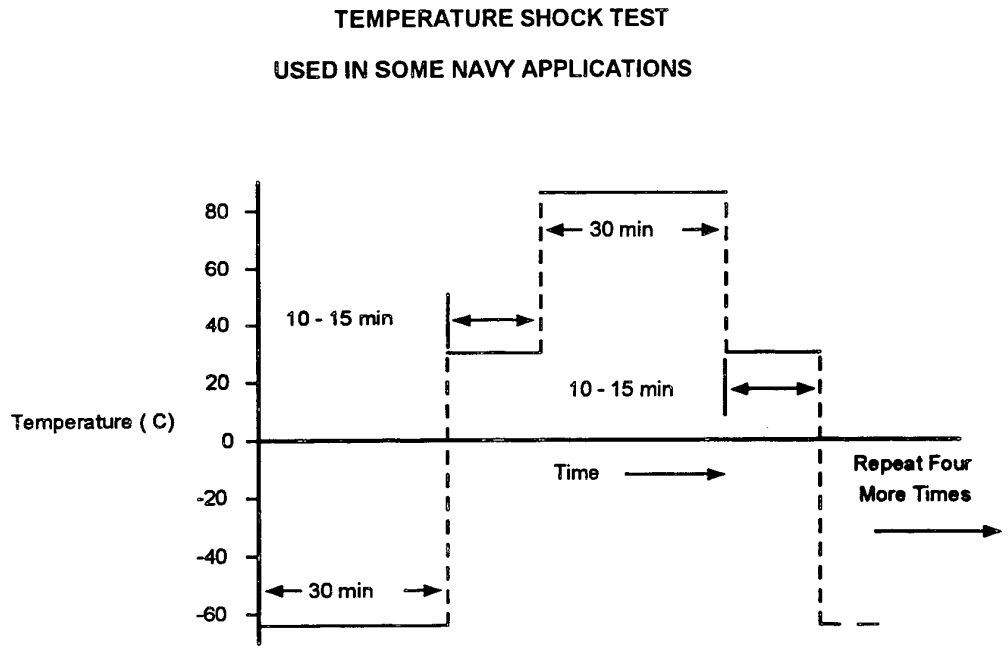

Figure 6 Temperature shock test used in some Navy applications.

The atmosphere surrounding a tube can have an impact on operation. For example, when unpressurized RF components are used in airborne applications, there is the risk of RF breakdown at high altitude and reduced pressure. In space and high altitude applications there can be little or no cooling by the ambient atmosphere. Corrosive atmospheres, including high humidity, can lead to tube problems if proper precautions are not taken in design and manufacturing. For example, exposed ferrous parts may rust in high humidity causing hydrogen to be present. Hydrogen can diffuse through the tube envelope and produce tube gassing and improper

operation. In Naval applications, a salt atmosphere and salt spray are likely to be present and tubes must be designed to operate under these conditions.

The user impact on environment is the treatment that a tube receives during shipment, storage, installation, replacement and system operation and maintenance. In cases where tubes are operated and cared for by knowledgeable, dedicated personnel, outstanding performance can be obtained. An example is ground-based, fixed-installation radar systems for which highly trained dedicated personnel routinely achieve lifetimes in excess of 50,000 hours for klystrons.

On the other hand, user abuse of a tube can be extremely detrimental to tube operation and reliability. Many difficulties with tubes result from inadequate system design and poor tube protection. Then, in addition, there are failures that have resulted from external damage, clearly due to mishandling or abuse. RF connectors and coolant fittings are damaged, coolant lines are clogged, leads are broken, *et cetera*. Furthermore, in many cases, it is estimated that from 25 to 40% of "defective" tubes were not defective after all. Something else in the system failed, but the tube was replaced first, probably because of its reputation as being failure prone. One case has been reported where 1464 "unusable" tubes that had been returned from the field were retested, 655 or 45% were OK.

If the truth were known, it could well be that, in some applications, over 50% of all failures are the fault of the users rather than the tube manufacturers. This is not to say that the manufacturers should not continue their efforts to build more reliable tubes, but it is essential to realize that the "bullet-proof" tube is a virtual impossibility and that intense efforts must be made to better inform the users about the tube characteristics.

One indication of the impact of environment on tubes is the MTBF (mean time between failures) being experienced in various applications. For some satellite TWTs, MTBFs of millions of hours are projected with high confidence. After launch, these TWTs experience no shock and vibration, no changes in pressure, only very small changes in temperature and are never touched by human hands. On the other hand, MTBFs for TWTs used in electronic countermeasures (ECM) applications are in the thousands of hours. These tubes are subjected to wide variations in temperature and pressure, extreme shock and vibration and are used in systems that are often maintained by inexperienced or poorly trained personnel.

One guide to the overall impact of environment on reliability is provided by the military handbook for the reliability prediction of electronic equipment MIL-HDBK-217F, Notice 2. The relation given in that handbook for predicting the failure rate, λ_p, of TWTs is

$$\lambda_p = \lambda_b \pi_E \quad \text{Failures}/10^6 \text{ hrs}$$

where λ_b is called the *base failure rate* and π_E is the *environment factor*. The base failure rate is a function of power and frequency and is given by

$$\lambda_b = .11(1.00001)^P (1.1)^F$$

where P is the rated power in watts (peak, if pulsed), $0.001 \leq P \leq 40{,}000$ and F is the operating frequency in GHz, $0.3 \leq F \leq 18$.

The environment factor depends on the application of the system in which the microwave tube is used. These environments range from those that impose little stress on the equipment, such as space flight, to cannon

launched systems, which produce extreme stress. Values for p_E vary from tube type to tube type and are listed below for TWTs.

Environmental Factor—p_E
(MIL-HDBK-217F, Notice 2)

Environment	p_E	Environment	p_E
Space, Flight	0.05	Ground, Mobile	7
Ground, Benign	0.5	Airborne, Uninhabited, Fighter	9
Ground, Fixed	1.5	Naval, Unsheltered	10
Naval, Sheltered	3	Missile, Flight	11
Airborne, Inhabited	5	Airborne, Rotary Winged	20
Airborne, Uninhabited, Cargo	6	Missile, Launch	33
Airborne, Inhabited, Fighter	7	Cannon, Launch	500

Vibration, shock, thermal conditions and user interface vary in each of the environments. The constraints in weight and size of the tube due to the operational environment is of major importance. In ground based, fixed systems, vibration and shock conditions are of less importance than thermal conditions. However for mobile, ground based systems, adverse shock and vibration environments can be introduced during transportation. In seaborne and airborne systems, operational vibration, shock and thermal conditions are all of major importance. For spaceborne systems, the vibration during launch is of considerable importance but then, as was stated previously, the tubes may experience no significant environmental hazards.

3. Techniques for Achieving High Reliability

To achieve high reliability and to better fulfill the requirements imposed by the various environments that tubes are subjected to, manufacturers have made major improvements and changes in many aspects of tube design and manufacturing in recent years. Some of these are as follows:

3.1 Improved Cathodes

There has been enormous improvement in cathodes in recent years. While B-type cathodes and even oxide-coated cathodes are still used in some old tube designs, virtually all new designs use cathodes based on M-type construction. With their lower operating temperatures, these cathodes have lifetimes an order of magnitude greater than the old B-type cathodes. The lower temperatures also reduce the probability of electrical breakdown and reduce thermal stresses on related elements such as the grid and heater assemblies.

3.2 Improved Magnets

All modern PPM focused tube designs use samarium cobalt magnets. These magnets have an energy product that is over a factor of four above that for the alnico magnets used in older tube designs. These enhanced magnet characteristics permit improved beam focusing, which, in turn, reduces the thermal stress on the RF circuit. Also, these magnets are extremely stable, and this makes it possible for a tube to survive extreme temperature variations without changes in magnet characteristics.

3.3 The Use of Getters

Nonevaporable getters have found use in microwave tubes in recent years. These getters are particularly useful in helping to ensure that a tube will operate properly after standing idle for an extended period. The improved vacuum level produced by the getter helps to prevent arcing and other gas-related problems when a tube is turned on after having been idle for an extended period.

3.4 Improved Test Equipment and Procedures

There have been major improvements in the capabilities of test equipment in recent years. The speed with which data can be obtained has increased significantly, and data analysis capabilities have improved markedly. As a result, errors in tube operation are detected more quickly, and so corrective action can be taken much sooner than was possible a few years ago.

3.5 Environmental Stress Screening

Major improvements in reliability have resulted from the increased use of environmental stress screening (ESS). ESS subjects tubes to random vibration and temperature cycling *during* production. *Every tube* is screened for defects that have occurred during production. This is in contrast to qualification testing, in which prototypes are checked to uncover defects in design *before* being produced in quantity. By testing during production with ESS, manufacturing defects can be identified and corrected so that the number of flaws remaining in delivered units is greatly reduced. When the results of ESS are fed back for use in modifying designs, the reduction in flaws is even greater.

Proper ESS does not cause defects, it brings out latent flaws through thermal cycling and gentle vibration. The cost of equipment necessary for ESS may be significant but can be far outweighed by benefits gained. For example, with warranties now being required with most tube procurements, warranty costs can be reduced by identifying and correcting most defects before the tubes are shipped.

3.6 Robust Design and the Use of Taguchi Loss Functions

Historically, good quality in military procurements has meant that the minimum specification standards have been met. As a result, tube manufacturers had little incentive to do better than meet the minimum specifications. To correct problems resulting from meeting minimum specifications, many procurement agencies now require warranties and also require manufacturers to "meet specs plus margin." As a result, tube

manufactures must do more than just meet specifications. The Taguchi approach to improved reliability is now being used by some procurement agencies. Taguchi loss functions equate higher quality with lower variation of the characteristics of a product about a target. The use of these functions permit an objective and numeric rating of quality to be assigned. For procurement agencies, this permits quality to be used as an award criteria. With quality based on the use of Taguchi loss functions to help determine procurement awards, it is essential for the tube manufacturers to understand and use these same quality determining criteria in manufacturing.

3.7 Total Quality Management

Finally, and this may be the most important item of all, there is a basic change taking place in thinking about how quality can best be improved through better management practices. The overall approach is referred to as *total quality management* (TQM). TQM is occurring in industries throughout the United States including the microwave tube industry. TQM focuses on three critical elements:

1. Customer expectations
2. Full participation
3. Continuous improvement

Item 2, full participation, is based on the premise that nobody understands a process and its shortcomings better than the person working on it. So to make TQM work, organizations must involve everyone in team efforts to investigate ways to improve processes.

TQM is a management style geared toward customer satisfaction. When TQM is coupled with the other factors for improving reliability that are discussed in this section, the result should be a very high level of customer satisfaction with microwave tubes.

4. Reference:

1. A.S. Gilmour, Jr., *Principles of Traveling Wave Tubes*, Boston and London: Artech House, 1994.

INPUT SIGNAL CONDITIONER

Rob M.E.M. van Heijster
TNO - Physics and Electronics Laboratory
The Hague, The Netherlands

Summary: The reason "why its there" is given for the input signal conditioner. How does it increase the performance of the power amplifier and what are the cost implications. In what way is the unit "matched" to the other units and how do they mutually enforce each others benefit?

A microwave power amplifier consists of an and a power amplifier. The input signal conditioner is often implemented in MMIC (Microwave Monolithic Integrated Circuit) technology, where mostly a highly efficient miniaturized vacuum power booster (Short Traveling Wave Tube, STWT) is used for the power amplifier.

The boundary condition for high efficiency operation of the power amplifier is that it will be driven in saturation. A side effect of this operational level is the introduction of non-linearity for drive levels close to saturation. This non-linearity manifests itself as power dependent gain and phase shift. In order to use the amplifier for linear operation, like in multi carrier amplifiers, linearisation is required.

The primary task of the input signal conditioner is the ability to amplify the input signal to the corresponding power amplifier input saturation level.

To improve linearity at saturation level the secondary task of the input signal conditioner is to predistort the input signal of the power amplifier. Predistortion consists of non-linear processing of the input signal in order to obtain an overall linear amplifier signal transfer.

To guarantee optimum signal transfer between input signal conditioner and power amplifier, the output impedance of the input signal conditioner should be matched to the input impedance of the power amplifier. The matching has to cover at least the operational frequency range of the power amplifier to prevent instability due to feedback and Backward Wave Oscillations (BWO).

Apart from the above imperfections, the power amplifier also shows a slope in the gain vs. frequency curve. Also a cascade of MMICs can be afflicted with a considerable gain slope due to process variations. To ensure a flat gain characteristic, the input signal conditioner should compensate for these slopes.

To ensure hardness of the input signal conditioner to excessive signal levels, a limiting function should be implemented at the input of the input signal conditioner.

Temperature variations, aging, power amplifier and MMIC characterization require the ability for adjustment of the input signal conditioner settings. Therefore the amplification, gain-slope equalization and linearization should be adjustable under control of the control module. It can be necessary to provide an ability for readjustment of amplifier settings by external control. Both requirements can be achieved by applying a control module and monitoring of insertion gain and temperature.

Summarizing the functionality of the input signal conditioner, the following sub-functions can be determined:

1. Amplification to power amplifier saturation level.
2. Predistortion to obtain overall linearization

3. Compensating for slope of gain vs. frequency curve.
4. Matching to the input impedance of the power amplifier.
5. Limiting at the input of the input signal conditioner.
6. Temperature and insertion gain monitoring.
7. Controlling of input signal conditioner settings to ensure temperature and age independence.

The combination of input signal conditioner and power amplifier will be a linear amplifier working with high efficiency.

The functionality of the input signal conditioner is determined by the improvements required for linear amplification of the entire amplifier. A functional breakdown of the linear amplifier is shown in Figure 0.1.

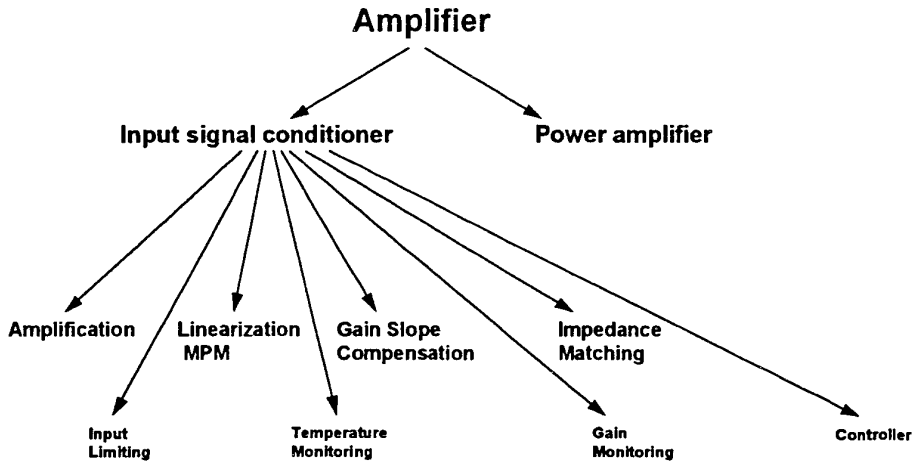

Figure 0.1 Functionality breakdown tree of a linear microwave amplifier.

1.1. Input signal conditioner block description

Close to saturation the power amplifier signal transfer becomes non-linear. This implies that in case of multi carrier applications unwanted in band intermodulation products will be generated by the power amplifier. The unwanted output signals can be canceled by supplying the power amplifier with an inverted replica of the unwanted intermodulation products. This is shown for a hypothetical "input signal conditioner - power amplifier" combination in Figure 0.2.

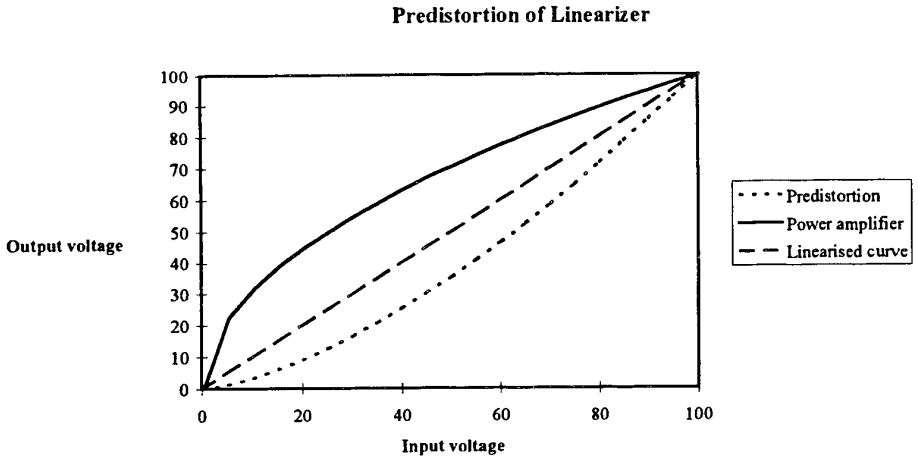

Figure 0.2 Linearisation for hypothetical "input signal conditioner - power amplifier" combination.

In order to generate the appropriate intermodulation products a non-linear circuit is required. The artificially generated non-linear behavior of the linearizer has to be an exact inverted copy of the unwanted non-linearity produced by the power amplifier. The amount of non-linearity must therefore be adjustable in order to compensate for temperature drift and different tube characteristics.

In general can be stated that the linearizer circuitry will include one or more non-linear elements (diode, FET). The non-linearity of the element(s) has to be adjustable, by electrical means. The linearizer topology will be distinguishable by its operating principle, which can be based on transmission, reflection or dissipation of microwave energy in the non-linear element. This can be configured either singular or balanced.

Linear signal transfer between the linearizer and the power amplifier is required, in order to prevent amplitude and phase distortion of the linearizer output signal, which would degrade the effectiveness of the linearizer. Therefore, the linearizer should preferably be "as close to" the power amplifier as possible.

The gain slope equalizer affects the amplitude (and phase) curve vs. frequency. In order to retain the correct replica of unwanted intermodulation products, generated by the linearizer, the gain slope equalizer should be placed in front of the linearizer.

Adequate impedance matching between input signal conditioner and power amplifier is essential, considering the often severe power amplifier properties with respect to input reflection coefficient. Due to the fact that the matching network is located directly in front of the power amplifier and behind the linearizer, it should not degrade the linearization process.

It is expected that the linearizer will not be able to operate properly at the relatively high signal level required at the input of the power amplifier. This implies the linearization to be performed at a lower signal level, requiring amplification afterwards.

The insertion gain of the input signal conditioner has to be adjustable in order to compensate for temperature and aging effects.

The input signal conditioner has to be provided with a set of parameters that describes the working conditions of the input signal conditioner. These parameters contain static and dynamic information. The static information describes the behavior of the power amplifier and the input signal conditioner itself. Dynamic

information describes the effects of temperature and aging. Finally, certain settings (e.g. gain) should be externally controllable.

These functions require the use of a Control Module, which will provide the following functionality:

- Settings for gain
- Settings for slope
- Settings for linearization
- Compensation for temperature
- Compensation for aging
- Interfacing
- Interfacing with EPC
- Monitoring of output power and temperature (telemetry)

The input signal conditioner and power amplifier are characterized and the optimum linearizer setting are determined. These settings are loaded into the Control Module.

The circuit block arrangement process is shown in Figure 0.3.

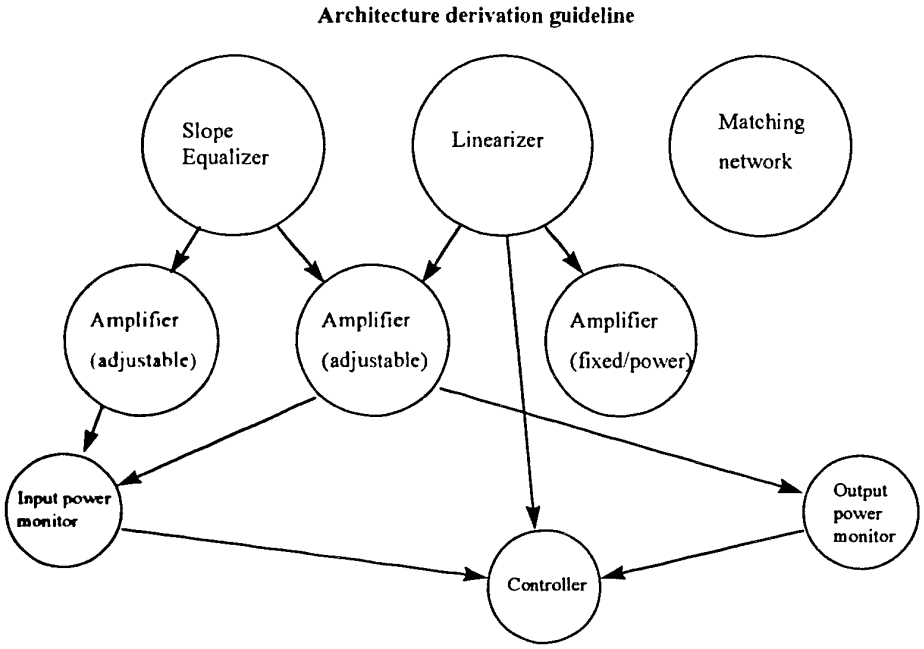

Figure 0.3 Derivation process of architecture of input signal conditioner. The place of the individual circuits is determined by the functionality of the input signal conditioner and individual requirements.

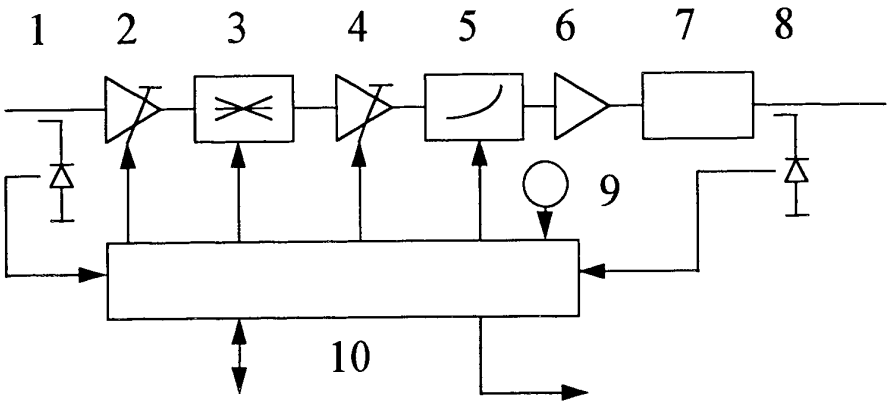

Figure 0.4 Circuit blocks of input signal conditioner. The numbers correspond with the numbers used in the text

Summary of circuit building blocks

1 Input power monitor
Necessary for overdrive detection and gain monitoring.

2 Limiting preamplifier
Part of distributed amplifier. Circuit is equal to adjustable amplifier, but is only adjusted to low gain near overdrive level to ensure optimum noise masking.

3 Slope equalizer
Required to compensate the gain slope vs. frequency of the power amplifier.

4 Adjustable amplifier
Part of distributed amplifier. Circuit is equal to limiting preamplifier. Adjustable in order to compensate for input signal conditioner gain drift due to temperature and aging.

5 Linearizer
Linearization of non-linear power amplifier. Principle must be based on non-linear element. Adjustable to correct for temperature drift. MMIC should be provided with integrated buffering to prevent mismatch gain ripple.

6 Medium power amplifier
Amplification of signal to power amplifier saturation level. Fixed gain to ensure fixed non-linearity.

7 Matching network
Matches medium power amplifier to power amplifier to guarantee optimum signal transfer and prevention of oscillations due to BWO.

8 Output power monitor
Necessary for gain monitoring.

9 Temperature monitor
To monitor temperature.

10 Control module
Acquires information concerning: temperature, input power, and output power. Generates settings for insertion gain, overdrive protection, slope equalization and linearization.

Power Conditioner

Authors: A. Biddings (CPI, USA)

Paper not available

CONTROLLER

A.P. Stegeman
Hollandse Signaal Apparaten
Hengelo, The Netherlands

Abstract

This paper deals with the controller function in high power transmitter systems, with an emphasis on vacuum tube based amplifiers. The controller can be defined as the circuits necessary to keep the amplifier and other sub-systems within their limits for fault-free operation. Especially for high power i.e. tube transmitters, the controller function has a strong effect on reliability and maintainability of the transmitter system. As availability is of prime importance for most systems, military as well as non-military, the controller deserves more attention than might be expected at a first glance. For proper design of a controller, a thorough understanding of the peculiarities of components and sub-system behaviour is necessary.

Introduction

The controller plays a very important role in a transmitter system. It determines reliable operation of the power amplifier and its power supplies by taking the right actions during events, which otherwise might destroy the amplifier or other circuits.
In other words: the transmitter and its sub-systems should be kept within their operational envelope by the controller circuit. An obvious example of this is the occurrence of a vacuum arc in a tube. If in such a case the high voltage power is not switched off properly, the arc will not extinguish and eventually destroy the tube because of local overheating. The controller does not avoid the failure, but prevents the failure from becoming destructive.
It is note-worthy that by using a "parts-count" reliability analysis method (MIL-HDBK-217) the reliability figure of a transmitter system is degraded by the presence of a controller circuit. Actual reliability of course is greatly enhanced by the proper application of -any- protective device!

A second function of the controller is interfacing with the transmitter's environment in two ways:

1. external control of the transmitter / preventing the possibility of operator errors
2. providing status information to the operator for maintenance / diagnostics

Operator errors might occur for instance if the operator attempts to switch on power supplies in the wrong sequence, which, in certain cases, might lead to damage of the tube.
In this paper these items will be addressed in more detail. Also information will be provided regarding realisation technologies as well as (im-)possibilities for diagnostics.

Fault detection

Fault detection is performed by monitoring several parameters. These parameters can be subdivided into three general categories:

1. lf electrical parameters like amplifier operating currents and voltages
2. rf parameters like output power and reflected power
3. environmental parameters like temperature and for instance wave guide air flow or pressure

It is clear that not every possible parameter should always be monitored in every case. The presence of the negative grid bias for a gridded tube for pulse operation can also be checked by monitoring the tube's body current, because improper grid bias will result in excessive body current. For proper diagnostics however, it is a bit more complicated, because excessive body current might also be caused by another fault like a defect modulator switch or a short circuit in the high

voltage power supply. In Table 1. an overview of the most important parameters for a tube transmitter is given. This list should not be regarded as being exhaustive. On the other hand it is also not the absolute minimum required for safe operation.

Parameter	Fault	Possible fault cause	Action
Cathode voltage	Too high / low	HVPS defect / vacuum arc	Switch off HVPS
Cathode current	Too high / low	Improper grid voltage / vacuum arc	Switch off HVPS
Collector voltage	Too high / low	HVPS defect	Switch off HVPS
Body current	Too high	In general defocussing: improper cathode, collector, grid or focus coil voltage / vacuum arc, tube deficiency	Switch off HVPS c.q. filament voltage
Filament voltage / current	Too high / low	Filament short circuit or interrupted / PS defect Note: during warm-up filament current surge is normal due to low resistance in cold state	Switch off filament PS
Focus coil current / voltage	Too high / low	Short circuit or interrupt of focus coil windings	Switch off PS
Negative grid bias	Too low	PS defect / shorted grid	Switch off all PS's
Grid current	Too high	Defocussing / short	Switch off all PS's
Ionpump current	Too high	Vacuum problem	Tube hardening in case of presence of "storage gas"
Forward power	Too low	Cathode exhausted / improper grid voltage	
Reflected power	Too high	Wave guide arc / bad VSWR	Switch off rf
Temperature	Too high	Cooling deficiency	Switch off transmitter
Wave guide air pressure	Too low		In case of wave guide arc: switch off rf

Table 1. Overview of faults & required actions for a tube transmitter

The detection devices and circuits can be of a relative complex nature. Aspects such as required bandwidth, voltage isolation, stability and Electro Magnetic Compatibility and other environmental factors are complicating factors that are not general for the non-complicated nature of the functions. A more detailed discussion however, is not within the scope of this paper.

Controller circuit realisation

A general block diagram (see Figure 1.) of a controller can be divided in two major parts:
1. a detection circuit, converting the mainly analog parameters to be measured into -often one bit- digital information
2. a digital part, interpreting the information and taking the right actions and supplying status information to the operator.

In more sophisticated designs also information can be supplied in the form of the actual values of certain parameters to support proper diagnostics.

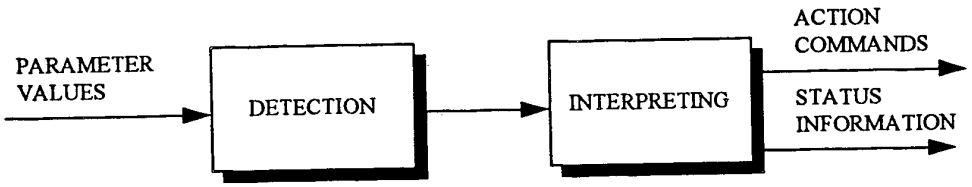

Figure 1. General block diagram of a controller

The detection part can consist of circuits like high voltage dividers, current sensors (transformer, resistor) and for instance diode detectors for rf power measurement. Special attention must be paid if information has to be transferred from the floating hv level to ground potential. Techniques like opto-isolation or transformer coupling have been used for this.
The interpreting part can vary from a simple discrete logic part to a completely microprocessor controlled multi-pcb rack. Higher degrees of integration with less complexity in design can be accomplished by the use of FPGA (Field Programmable Gate Array) or PAL (Programmable Array Logic) technology.
Development of a dedicated analog / digital Integrated Circuit (ASIC) is in many cases a too costly approach. Only with higher production volumes, can the development cost be outweighed by the lower production cost.

Operational Modes

The controller function must be able to handle the operational modes for which the transmitter is designed. Operational modes are characterised by the nature of the amplifier (pulsed / cw), the function of the system (tracking, surveillance, illumination) and the application / user profile (ATC, naval surveillance, airborne radar).
For a short mission fighter aircraft, extensive diagnostics is less important than for a shipborne radar which has to be maintained during a long-time mission. For a tracking radar -operating in stand-by mode for a long time- it is recommended to lower filament voltage during stand-by to prevent cathode wearout, while this is of no importance to an ATC radar which is continuously on for a long period of time.
For each application the different requirements should be considered and implemented for optimum performance.

Status display

For the operator it is essential to know the internal status of the transmitter to be able to give the right commands and to perform maintenance if necessary.
In general the following states can be distinguished:

- "OFF": all the amplifier's power supplies are switched off and no rf is applied
- "WARM-UP": filament voltage is applied, but heater warm-up time is not yet expired
- "STAND-BY": filament voltage applied and warm-up time expired
- "ON": as STAND-BY but also high voltage is applied
- "TRANSMIT": as ON but also rf is applied
- "FAIL": a state that can be reached from any other state in case a failure occurs.

It has to be noted that for gridded tubes, as long as heater voltage is applied the negative grid bias must be present to prevent damage to the tube. Improper grid voltage will lead to excessive grid current and / or body current with the risk of local overheating.

The controller has to generate the internal timing signals to assure the proper sequence of switching on and off the several supply voltages. However the transition from one state to another is normally not initiated automatically by the transmitter itself. The main reason for this is that the user must be able to control the status of the transmitter. The operator decides whether the transmitter must be in the stand-by state for immediate action (tracking radar) or not, while on the other hand, safety reasons prohibit automatic switching on of the high voltage.

This implies that the operator has to know the actual transmitter state to know whether the next status-command can be applied.
Unless the transmitter can be replaced as a complete Line Replacable Unit (LRU), the maintainer has to be provided with more information than a simple fault indication.
The ideal case would be if the controller would provide adequate information to replace a defect unit. In a practical situation this can be very difficult because a single fault symptom can often have many causes. Excessive body current for instance can be caused by improper grid bias or collector voltage, a tube problem, vacuum arcing etc.
Providing not only status display but also information on actual measured values of several parameters can help the maintainer for the right diagnostics. Such an approach however increases cost, while on the other hand the maintainer has to be skilled to an appropriate level to be able to draw the right conclusions.

Protection / Fail Safe

The protection function of a transmitter system, like any high power system, is very essential for reliable operation. This arises from the fact that in case of faults, the consequences are in most cases destructive to the equipment. In general it can be stated that for a high power circuit per definition the internal impedances are low for efficiency reasons, while on the other hand stored energy is often high. So, in case of a failure, large currents will flow, leading to destruction of the equipment if the proper precautions are not taken.
This is especially important for tube transmitters, because high voltage breakdown in the tube or circuits in air can always be expected.
Fail safe means that in case of a failure, this failure may not lead to other damage or unsafe personnel situations.
It is good engineering practice to keep protection functions local, where possible. To give an example for this, in case of a vacuum arc in a tube the power supply must be short circuit protected to prevent damage to the power supply. To protect the tube however the power supply must be switched off, which is a task for the controller.
In case of a very high level of integration, like in a Microwave Power Module (MPM), this general approach does of course not necessarily apply.
Human safety is of course of primary importance. The hazards of lethal voltage levels, X-rays, high power rf radiation and often toxic materials should never be underestimated. A detailed discussion is far beyond the scope of this paper. Proper interlocks, shielding and procedures should prevent any possible dangerous situation even in cases of equipment or operator errors.

Diagnostics

Diagnostics help the maintainer to enhance the system's availability by shortening down-time in case of a failure. It also helps to prevent unnecessary maintenance, which has often led to additional failures caused by this rework.
Because certain failures in a transmitter do not necessarily require maintenance (arcing for instance), a limited cycle automatic re-try circuit helps to improve the availability of the transmitter system. If the failure is persistent however, maintenance is required. Depending on maintenance philosophy the diagnostics can vary from a single failure tellback to a complete set of data regarding internal status, parameter values etc.
Proper diagnostics is not only a matter of a well designed controller, but has to do with the transmitter design as a whole. The way the transmitter is built and divided into sub-units and the way the functionality is mapped onto physical units, greatly influences the adequacy of the implemented diagnostics.
For the designer(s), the important question should be: what can go wrong and how can this be determined unambiguously. For large, complex systems however, the maintainer should have a minimum of understanding about the system and it's do's and don'ts.

POWER AMPLIFIERS APPLICATIONS AND RELIABILITY

Jan M. Schouten

Directorate of Materials Royal Netherlands Navy

s'Gravenhage, The Netherlands

Summary: The power amplifier in general carries the highest power densities and heat flux and is hence vulnerable to any anomaly in power flux. How can we avoid these anomalies and how do they affect reliability and at what cost. The article gives an overview and underlines the importance of failure data acquisition and analysis.

I Introduction

In a system the amplifier is often seen as the weakest link in the chain, because the amplifier carries high power densities and heat fluxes. Careful design of the amplifier and a correct understanding of the specifications and the 'application' of the amplifier is required. Interaction between the system and amplifier designer is a must. In this paper the influence of the amplifying device, the tube and its cathode, will be discussed. A brief comparison with a solid state amplifier will be made.

II Applications

In the design of the amplifier the application plays a major part. The application can be divided into the following areas:

- Search radar
- Tracking radar
- Illumination radar
- Communication system

The application of the amplifier in one of the areas has a significant impact on the reliability of the tube.
A short description is given on the four examples;

1. Search radar

In general a search radar uses pulsed transmissions. The operation time, this is the time the radar is transmitting, is relatively long. Mechanical stress in the components will occur during switch-on and operation. After switch-on the mechanical stress will occur mainly in the gun section. After warm-up the mechanical stress will be found in the slow-wave structure and the collector. Proper design of the cooling and the focusing have to cover this and should have no effect on the reliability. The standby time of such a system is relative short compared to the operational time. The main defects are due to mechanical or electrical stress in the slow-wave structure and the collector(s). The end of life of the cathode is also common defect mechanism.

2. Track radar

The operational use of a tracking radar in fire control systems is different. It uses in general pulsed transmissions also but the number of active transmissions are limited. The Standby hours are relatively long. The mechanical stress due to the short temperature differences and the effects on the cathode require a different design approach. Arcing of the tube may cause disastrous effects on the operational availability of the system. The design of an amplifier has to take this into account. Common defects in this type are: cathode surface deterioration (arcing, poisoning) and slow wave structure defects.

3. Illumination radar

Illumination of targets occur only during the last part of the flight of a missile. This is normally not more than a few minutes. In this time the mode can be CW or pulsed. The time the radar is transmitting is very limited. The main mode of such a radar is STANDBY. Failure of the transmission will have major impacts, loss of missile or endangering of the object to be protected. The design of the gun requires special attention. The most common defect mode of this type of tube is gun arcing and gun poisoning.

4. Communication system

Communication transmitters, specially for satellite communication, are in an active transmit mode. This may be IA a low or high power mode. The normal transmission mode used is CW modulated with a PSK, Phase Shift Keying. This mode can be compared with that of a search radar. The mean defects for this type of tube is cathode wear out.

5. System comparison

Table 1 shows that for Illumination and tracking radar the cathode encounters the most stressful situation. This will lead to a possible arcing or poisoning of the surface and will be explained hereafter.

		Failure mode		
System	**TX/STNBY**	**Gun**	**SWS**	**Collector**
Search	1 : 2	EOL	N.A.	N.A.
Track	1 : 4	Arcing	Defocusing	Temperature
Illumination	1 : 10	Arcing	Defocusing	N.A.
Communication	1 : 2	EOL	N.A.	N.A.

Table 1

6. Cathode behavior

During the activation of a cathode, Barium Oxide will be evaporated from the cathode surface and condense on the surrounding cooler structure. Ions are produced as well. During operation those effects are eliminated by the electron beam by returning the ions to the cathode surface. The beam will have a cooling effect on the cathode. In case of standby, only filament and bias switched on, the ions will be above the cathode surface and the evaporation of Barium Oxide is increased due to the absence of the beam current. Switching a tube to H,V after a standby period of some weeks, may cause an arc.

7. Gun

The quality of the focusing of the electrons determine the interception of the electronbeam. All tube manufacturers use software programs for simulation. These programs are often proprietary. The Royal Netherlands Navy started a program in 1995 for the development of a software program called "Top Gun" for simulation of electron beams. With this program they are able to test the design of the manufacturer independently. The program is not yet finalized, the electrostatic simulation has been proven, the magnetic part is still under development. The program makes use of the electrical parameters of the tube and the dimensions of the gun.

III Solid State and Tubes

The replacement of tube systems by Solid state technology had its start in the beginning of the 80's. This started with frequencies of 200 - 400 MHz. The next step was the D-band 1000 - 2000 MHz. At this moment high power solid state transmitters are available up to C-band 5 GHz.
Comparing the two technologies is difficult, because the application will play a major part in this. Tube systems can be divided in systems using linear or non-linear tubes, Traveling Wave Tubes, Klystrons and Magnetrons. The characteristics of a linear system are wide bandwidth, high duty cycles and low AM/PM noise, while for non-linear systems this is mainly high peak power. The efficiency of a tube system is in the range of 30 to 50%. The cost driving factor in a tube system is the wear out of the tube. Life expectations of a linear tube are 20.000 hrs and up. For a non linear device between 2000 and 5000 hrs. In general the cost per hour of a linear system (TWT) will be $50/Hr and for a non-linear system (Magnetron) 10$/Hr.

If we look into the solid state, the first thing we observe is the limited amount of power per device. At this moment in D-band transistors with a peak power of 400W, duty 15% are available, in S-band this is 150W, duty 20% and in C-band 50W, duty 20%. Going up in frequencies the power drops rapidly to less then 1W. Building an amplifier with those devices requires special technologies. A well established one is the use of building blocks. This is a circuit containing a number of transistors (2, 4, 8) and a stripline combiner. This to get to a workable power level of 500 to 1000W. With those blocks an intermediate amplifier, book, is build. A number of those books are combined (2,4,8,16) to form the final transmitter. The books are combined with a Radial combiner or a Wilkinson (stripline) combiner. The Wilkinson has the advantage of wide bandwidth and high stability under shock and vibration.
In a pulsed mode, during the rise and fall time most power is dissipated in the junction of the solid state device. For this, the device operates best with high duties or CW. An advantage of the solid state is the graceful degradation of

the amplifier because of the large amount of transistors. A disadvantage is the high loss in the combining network and the low efficiency of the device. Efficiencies are to be expected between 10 and 30%. The high number of devices and combiner makes the amplifier expensive. The cost of a solid state amplifier is in the order of 3 to 4 times higher then that of a tube system. The cost per hour is lower then that of a tube system. A proven figure is not yet available but it is expected to be between 5 and 10 $/Hr.

IV Amplifier characterization

An amplifier is characterized by;

- Input level
- Gain
- Frequency response
- AM/PM noise and Spurious levels
- Linearity
- Control
- Protection
- Diagnostics

These parameters are discussed in the presented papers;

- Input Signal Conditioner, R.M.E.M. van Heijster, TNO-FEL, The Netherlands
- Controller, Albert Stegeman, Hollandse Signaal Apparaten, The Netherlands

V Wear out sensing

The wear out mechanisms of an amplifier are in the tube gun. The cathode has a finite life due to the evaporation of the cathode material. A second effect is the condensation of evaporated material on gun parts. This causes a degradation of the tube and finally its defect. The slow wave structure, collector(s) and focusing elements are not directly susceptible to wear out mechanisms. Proper design of those elements will prevent wear-out. Special attention has to be paid to the severs commonly used in the slow wave structure. Heating of those severs may cause degradation and/or gas production which will influence the reliability of the tube.

VI Power consumption

The importance of the power consumption depends on the application. For use in a landbased or shipborne application this is in general not a hard requirement. On board of an airplane/fighter and satellite applications this requirement will be more stringent.

1 Efficiency

The efficiency of an amplifier depends on the interaction of beam and the R.F. field in the slow wave structure. Saturation, spurious and noise affect the efficiency. Slowing down the electrons in the collectors, depression, effect this figure in a positive way. The use of the lineariser will optimize the efficiency of the tube.

VII Reliability

Reliability of an amplifier is influenced by its application and platform. The requirements for a shipborne or landbased system differ substantial in shock and vibration. On board a ship vibration is a constant factor. Compared to satellites the shock, vibration and acceleration during its launch are extreme, but the amplifier is not operational at that time. During its life in space shock and vibration are no longer a concern. Amplifiers in seeker heads of missiles will see the worst conditions: High velocities, accelerations, shock, vibration and short warm-up times are encountered. A difference in those three examples is the expected life. On board of a ship repair can be done by replacement. In this case reliability is related to maintenance and the operational requirement. For a satellite application reliability means 'It has to work'. Repair is not possible and long life is a must. For the seeker application, it has to perform during a very short period. These examples show that reliability in these three cases have a different definition. The design has to cope with that.

Failure analyses is a subject that is left alone in many cases. It requires a well organized set up for the user and manufacturer. However the importance should not be neglected. The operational information available at the end user could improve the reliability of the amplifiers with a large factor. It is important to know for the manufacturer under which conditions and after what time certain defects occur. Feedback of such information will start the discussion between both parties and will enlarge the mutual understanding. The "its your fault" discussion will disappear. Collecting data is not easy. It requires administrative discipline at different levels in the operational and maintenance organization. Important data to be collected is: operational time, filament and HV hours; failure mode; amplifier mode when the failure occurred; corrective actions; results of those actions. As stated before this is not easy implemented. The Royal Netherlands Navy has experienced those difficulties of collecting data and has designed a special software program, called MIDAS, to overcome these difficulties. This program consist of two parts, a data collection part, which is in use on board ships and in workshops, and secondly a data analysis part. This program will be discussed and demonstrated in one of the following workshop presentations.
The results of this program and the cooperation with the different manufacturers improved the reliability and the life of the tubes with a factor 3. The 'its your fault 'discussion is history. The operational cost of the system has gone down linear with the life of the tube.

VIII Conclusion

The reliability of an amplifier depends on the application, operational mode and platform. If this information is supplied to the designer of the amplifier, the reliability will be significantly improved.

Interfacing the tube to its environment, power supply, modulator and R.F. circuitry will prevent induced failures. The protection circuits for the DC and R.F. circuitry are fulfilling a major part.

The technology of the tube has to be related to the application. A TWT will give a large bandwidth and high duty cycle. A magnetron , high peak power with low duty and a klystron a combination of both.
For the design of the cathode, the choice of materials, cathode mixture and temperature, has to be decided on the type of system such as search, track, illumination or communication.

A short comparison with solid state has been made. Solid state is available up to C-band. Reliability is high due to the graceful degradation. The efficiency of the amplifier is low 20 - 30%. The cost are a factor 3 to 4 times higher then a tube amplifier.

COOLING

prepared by A. S. Gilmour, Jr. and presented by George Kreager

Naval Surface Warfare Center

Crane, Indiana, USA

Abstract

In the conversion of dc power to RF power by an amplifier, heat is generated because the conversion process is never 100% efficient. As a result, two major system problems occur. Not only must the heat be disposed of, but the dc power supply must be made large enough to provide the power that is converted to heat. Fortunately, modern microwave tubes are very efficient and so these two problems are minimized in systems using these tubes. Still, there is heat to be disposed of and so cooling is required. Techniques for removing the heat from microwave tubes are the subject of this paper. The techniques discussed are cooling by conduction, convection, forced air, forced-flow liquids, boiling (vapor phase cooling) and radiation.

1. Introduction

The purpose of an RF amplifier is, of course, to convert dc power to RF power. The conversion process is never 100% efficient and so some of the dc power to the amplifier is converted to heat, that is dc = RF power + heat. This conversion of dc power to heat results in two major system problems:

1) The heat must be removed from the amplifier and must be disposed of,
2) The dc power supply must be large enough to provide the power that is converted to heat.

To illustrate the importance of amplifier efficiency, consider two amplifiers, one that is 25% efficient and one that is 50% efficient. The amount of heat generated by the 25% efficient amplifier will be three times the amount of heat generated by the 50% efficient amplifier. The dc power supply for the 25% efficient amplifier has to be twice as large as the power supply for the 50% efficient amplifier. As a result of these considerations, it is clear that the use of highly efficient RF amplifiers is extremely important in most applications.

Modern microwave tubes are very efficient. Efficiencies on the order of 50% are becoming common and 60 - 70% is being accomplished for TWTs for satellite applications. Over 74% has been demonstrated in a klystron and 85 - 90% is predicted to be achievable. Crossed-field tubes routinely operate at efficiencies in the 50 - 80% range. For TWTs and some klystrons, the use of multistage depressed collectors has made these high efficiencies possible. These collectors recover much of the energy remaining in the electron beam after RF interaction has occurred.

In addition to high efficiency, another factor of importance to the cooling process is the ease with which heat can be removed from the RF amplifier. For microwave tubes, two factors alleviate the heat removal process:

1) Most of the heat is generated on large surfaces and so the power density of heat dissipation is low.
2) The materials of which microwave tubes are fabricated can operate at very high temperatures. Most tubes are processed at temperatures above 500°C. They can operate with collectors (the part of the tube from which most of the heat must be removed) at 300°C or higher. This high temperature makes

heat transfer to the cooling medium very effective.

There are several sources of heat in a microwave tube. The most important of these are:

1) electron bombardment of the collector,
2) electron bombardment of the RF circuit,
3) electron bombardment of the cathode in crossed-field tubes,
4) RF heating by ohmic and dielectric losses of the RF circuit and its support structure.

In most cases, the most important problems in the thermal design of a tube are associated with items 2 and 4 of this list. Electron bombardment of the RF circuit usually results from limitations of the effectiveness of the magnetic focusing system for the electron beam. Two focusing techniques are used for most TWTs and klystrons. These are solenoid focusing and periodic permanent magnet (PPM) focusing.

Solenoid focusing provides excellent beam control and low heat loss to beam interception by the circuit. The advantage of excellent beam control must be weighed against the weight, power usage and heat generated by the solenoid. PPM focusing structures consume no power, generate no heat and are very light weight. In general, however, beam control with PPM focusing is not as good as with solenoid focusing. As a result, beam interception is higher and the heat removal problem is more difficult in PPM focused tubes that in solenoid focused tubes. It must be pointed out that significant improvements in PPM focusing systems have been made in recent years with the use of samarium cobalt magnets. These magnets are continuing to be improved and still better magnet materials are being developed and so beam control with PPM focusing will continue to improve.

RF heating by ohmic and dielectric losses is usually most severe near the output end of the RF circuit in a microwave tube because this is where the RF power, the RF currents and the RF fields are maximum. Ohmic heating results from the flow of RF currents in the circuit. Ohmic heating is minimized by using circuit materials that have low resistivity. Surface finish of these materials is important to minimize skin effect losses which occur because, at microwave frequencies, currents flow only near the surface (within ~ 0.0001 cm or less) of the circuit conductors.

When dielectric materials are used near the output end of the RF circuit (for example, as the support rods for the helix in a TWT), dielectric losses occur because of the large RF electric fields that are present. These losses are minimized by using low-loss dielectric materials. Usually (as is the case with helix support rods) these materials also have to be good thermal conductors and there is sometimes a tradeoff between obtaining high thermal conductivity and low dielectric loss. The dielectric materials that are usually used in high power devices are beryllium oxide or boron nitride. Diamond is being considered for use in some cases.

Within a tube, the only technique available for transfer of heat from the heat sources is by conduction. For maximum heat transfer, thermal resistances must be minimized. The most severe impediments to heat transfer are usually the interface resistances between dielectric materials and metals. These are minimized by using high pressure or by brazing. Once the heat has been transferred away from the generation region, several techniques are available for removing the heat from the tube.

For low power tubes, cooling can occur by conduction to a heat sink through the attached waveguides or the tube mounting flanges. Cooling can also be achieved by the normal convection of air flowing around the tube.

For intermediate power levels, air is often forced to flow across the tube. In this method, heat is first conducted from the tube by cooling fins with a large surface area. Air is then blown along the surface of these fins, carrying away the heat by forced air convection. For high power tubes, liquid cooling is required. Several methods of liquid cooling are employed in field applications. Proper maintenance of cooling systems is necessary for microwave tubes. Lack of regularly scheduled maintenance of cooling systems can lead to substantial reduction in the useful operating life of a tube.

2. Cooling Methods

2.1 Conduction Cooling

Heat transfer by conduction to a heat sink is the simplest form of cooling where the power level of the tube is low enough to permit it. Little maintenance is normally required. However, it is necessary to make sure that tubes are tightly bolted to the heat sink and that no gaps exist between surfaces. Mating surfaces should be kept clear of any dust or obstructions, so that normal air flow can provide additional cooling through convection. All air filters and vents should be kept clean and free of obstructions.

2.2 Convection Cooling

Devices which generate only up to a few watts of average power may require no specific cooling other than natural air convection. To take best advantage of this type of cooling, the surface exposed to the surrounding air is often many times larger than the actual collector inside area. About 1 watt/cm^2 of surface exposed to open air can be handled by this approach.

2.3 Forced-Air Cooling

Forced-air cooling systems usually employ some form of motor-driven fan to produce air movement for removing heat. (In some airborne applications, instead of a fan, outside air is vented through the system.) The amount of circulating air is not critical as long as it is adequate. Excess cooling will have only beneficial effects, while inadequate cooling is almost certain to invite premature failure of a microwave tube. Forced-air cooling systems are usually the simplest cooling systems and they are also one of the easiest to maintain. Although forced-air cooling is capable of dissipating power densities nearly as large as water cooling can, it has experienced only limited application because of certain practical considerations. A typical air-cooled collector which has been used to dissipate a power density of 200 watts/cm^2 is shown in Figure 1. The cooling fins are brazed to the cylindrical body of the collector to provide a large area multiplication factor (larger than 10) from the power-intercepting area to the air-exposed surface. One of the limitations of air cooling is that of blower power. In order to minimize the input to the air pump it is necessary to have a large number of short air passages in parallel. An optimum cooling fin arrangement, shown in Figure 1, requires a blower power of from 5 to 10% of the average collector power, a much higher level than for water cooling. Another limitation of air cooling is that it is not easily applicable to other portions of the tube such as the interaction structure. Because of the above disadvantages, forced-air cooling is generally used only for tubes up to the few kilowatt level of RF output. At higher power levels the circulating water system is preferred to the bulky collector and air pump system and the pump power required for air cooling.

FLOW PATTERNS IN AN AIR-COOLED COLLECTOR

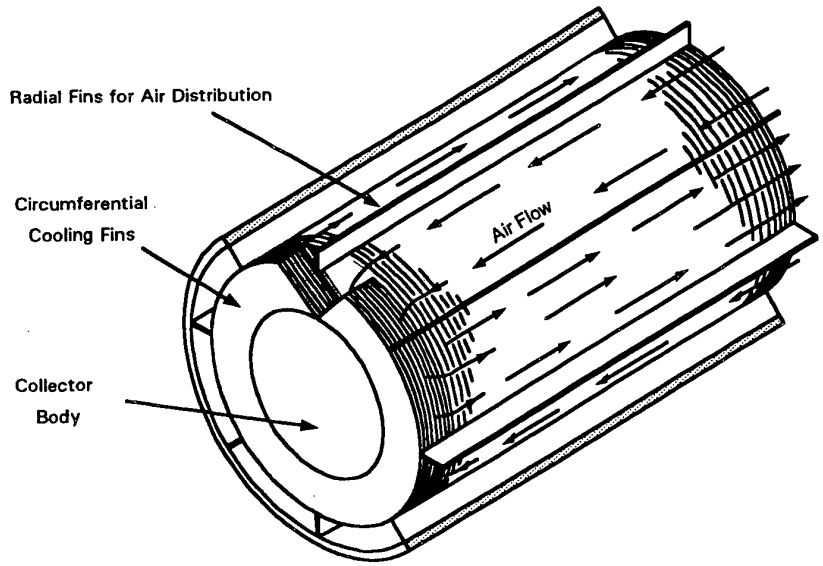

Figure 1 Flow patterns in an air-cooled collector.

2.4 Forced-Flow Liquid Cooling

Forced-flow liquid cooling is by far the most often used means of cooling collectors for medium- and high-power microwave tubes. The very highest power tubes are all water cooled. An effective method is simply to water-jacket the collector and remove heat by conduction from the collector body to the water. The amount of heat which can be transferred to the water is directly proportional to the wetted surface area and the heat transfer coefficient. Both are optimized when many narrow channels with large perimeters but small cross-sectional areas are used together with high velocity flow. In order to avoid excessively high temperature rises in the collector walls, water channels must be located near the intercepting surface; thus the wetted surface area multiplication factor is generally limited to about 3 or 4. Higher factors could be achieved, but this generally requires machining of channels of more complicated cross-section than is convenient with ordinary techniques. Some typical collector wall sections showing water channel shapes are illustrated in Figure 2.

TYPICAL WATER COOLING CHANNELS

(Area Multiplication Factors Increasing from a to c)

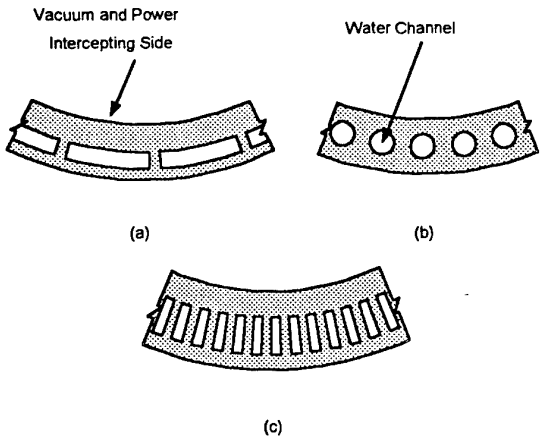

Figure 2 Typical water cooling channels with area multiplication factors increasing from (a) to (c).

The heat transfer coefficient used is usually computed on the basis of allowing no boiling of water at the surface. The heat transfer coefficient will characteristically be on the order of 1 cal/cm^2/sec/°C temperature rise in the surface film of water. Much higher heat transfer coefficients can be achieved if the water is allowed to boil, as is frequently the case with high-power collectors. Care must be taken to insure that operation occurs in the nucleate boiling region which has a high heat transfer capability and does not enter into the film boiling region, for which the surface temperature must be very high and might cause melting of the collector material. It is customary to design water cooling to be operable at pressure drops of less than 100 lb/in^2 and flow rates commensurate with average temperature rises of from 30 to 50°C. If a specific design has been made for water, cooling will generally suffer when other fluids are used because of differences in thermal conductivity, heat capacity, viscosity, and other characteristics. Ethylene glycol is used for low temperature applications, principally to avoid the problem of freezing during storage. It is inferior to water as a coolant. Other fluids have been considered but are seldom used in practice, even though some have advantages with respect to water. Cost and availability are the most frequent deterrents to the use of most of the special fluids.

2.5 Vapor Phase Cooling

Vapor phase cooling, which is sometimes called "boiler cooling", has become widely used for some microwave tube applications.This method takes advantage of the latent heat of evaporation of water by allowing the water to boil at the collector surface. The steam is then condensed in a heat exchanger and returned to the collector, forming a closed system.

Figure 3 illustrates schematically the elements of a boiler cooler. In its simplest form, it consists of a container of liquid (such as water) thermally attached to the tube, the whole combination being surrounded by insulation except for passages for electrical leads to the tube, RF input/output from the tube and a steam outlet. As the tube heats up, no heat can escape until the temperature of the liquid reaches the boiling point. At this time, the

temperature stabilizes, since the steam carries away the additional heat and the temperature cannot rise further until the liquid is boiled away. To prevent the latter from happening, it is necessary to have a continuous supply of liquid or to condense the steam and return it to the boiler. The total heat input to the system must be removed from the condenser by natural convection of the ambient air, by forced air cooling or by any other convenient means.

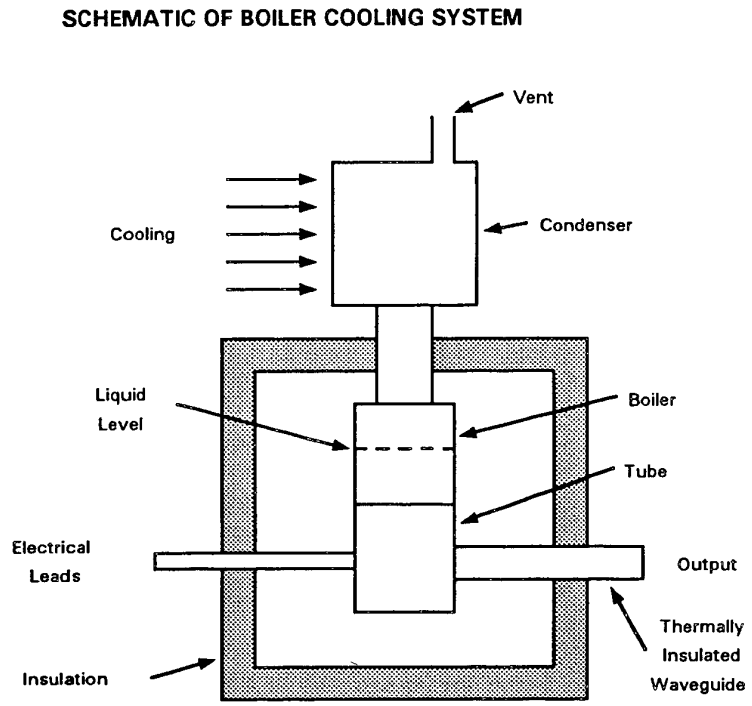

Figure 3 Schematic of boiler cooling system.

In order to achieve reasonable dissipation densities, one must operate either in or near the transition region between film boiling and nucleate boiling. Since this would ordinarily represent a runaway region, it is possible only when means are devised to maintain equilibrium of the boiling. Beurtheret pioneered this type of cooling for vacuum tubes in the "Vapotron®" type collectors. To understand the principle, the curve shown in Figure 4 is required. Heat transfer increases very rapidly with temperature of the surface until the discontinuous region is reached where heat transfer actually drops as nucleate boiling changes into film boiling. At this point the surface temperature will undergo a temperature increase of about 1000°C for the same heat flux, which is prohibitive from the standpoint of burnout.

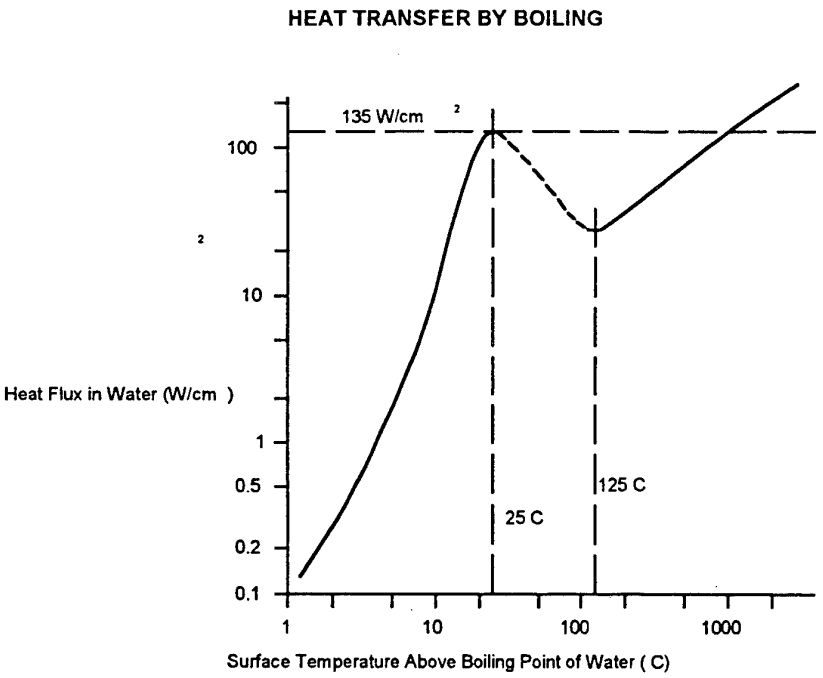

Figure 4 Heat transfer by boiling.

The vapor-phase-cooled collector (section shown in Figure 5) has an array of protruding bars which, during operation, develop a thermal gradient along them such that the outer end does not boil at all, the base of the protrusions is always low in the film boiling region, and all other regions of boiling exist continuously between the two extremes. Maximum heat transfer occurs near the middle of the bar. Any small change of heat transfer in the system will shift the point of maximum heat transfer along the bar, thus readily absorbing the fluctuation without a discontinuous jump in the temperature. The shape of the collector protrusions is crucial in the proper functioning of the system.

Figure 5 Partial cross section of a vapor-phase cooled collector.Vapor-phase-cooled collectors have found much application in high-power tubes where dissipation densities are on the order of 1 to 200 watts/cm^2 and where it is preferable to avoid a forced-flow system with water pumps. Certain cw klystrons designed for UHF television transmitters in the 30 to 50 kW range are typical examples.

Whatever the form of the boiler, an insulating section must be provided in the output waveguide of the tube to prevent variable heat loss to the system waveguide. A convenient form of insulation is a short length of guide made of thin wall stainless steel or other material of low conductivity. For example, the heat loss through a 1 in (2.54 cm) length of 0.020 in (0.51 cm) wall stainless guide in the 0.622 x 1.372 in (1.58 x 3.48 cm) size amounts to about 1.3 watts when the ends of the guide are at 100°C and 60°C and to about 4.1 watts when the ends are at 100°C and -30°C.

Thin wall stainless steel also makes a good thermal dam in the duct to the condenser. A flexible plastic or rubber hose of suitable cross section is sometimes used, but it must be chosen to withstand the hot vapor. Convection cooling of the tube and boiler is sometimes reduced by enclosing them in an insulating box. All the hot portions are enclosed, including the hot portion of the insulating waveguide. The heat loss through the

walls of such a box can be limited to a small fraction of the total heat generated. Heat lost from the hotter parts of the tube by convection to the inside walls of the box will now go to the more nearly constant temperature of the liner, reducing the variation of heat flow through the resistance between the tube and the boiler. Such a sophisticated liner is generally not needed unless space for sufficient insulation is at a great premium.

2.6 Radiation Cooling

Radiation cooling is commonly used in satellite applications of microwave tubes. One approach to radiation cooling is to allow the collector to run at a sufficiently high temperature so that heat is lost by radiation directly into space. This approach, although attractive because of its simplicity, poses certain problems. The collector temperature must be in the neighborhood of 1000°C to provide a reasonable dissipation capability. In order to minimize temperature rise on the inside as well as to suppress lateral flow of heat to the tube body, a thin membrane type collector is necessary. This raises problems with mechanical strength as well as gas diffusion through the collector. The latter, at least in principle, may be avoided if the tube is intended for use in a space environment. However, some tube testing at atmospheric pressure is always necessary. Thus, it is preferable to enclose the collector in a vacuum envelope essentially transparent to radiated heat. Some of the possible collector materials are the common refractory metals, such as tungsten, molybdenum, and tantalum.

Black-body radiation at 1000°C is approximately 12 watts/cm^2. A reasonable value of emissivity with proper carbonization is about 80%, reducing the above value to about 10 watts/cm^2. So, according to the fourth power-of-temperature law for radiated power, operation between 1000°C and 2000°C yields a cooling capability on the order of 100 watts/cm^2. One of the largest problems is back radiation to the tube, which dictates the use of a fairly large collector with a small beam entrance aperture. Also, problems may arise from collector evaporation deposition inside the tube as well as on the radiation window.

A radiation-cooled collector used by Lien et al. in a lightweight space communications tube is shown schematically in Figure 6. A reflector was used inside as well as outside the vacuum envelope to protect the tube from back radiation. A sapphire radiation window was chosen because of its high transparency to infrared. This collector was operated at a power level of about 300 watts at a temperature of 1500°C. The collector material was tungsten. The measured radiation-cooling efficiency was approximately 75%, indicating that 25% of beam power striking the collector was returned to the tube body.

SCHEMATIC LAYOUT OF RADIATION-COOLED COLLECTOR

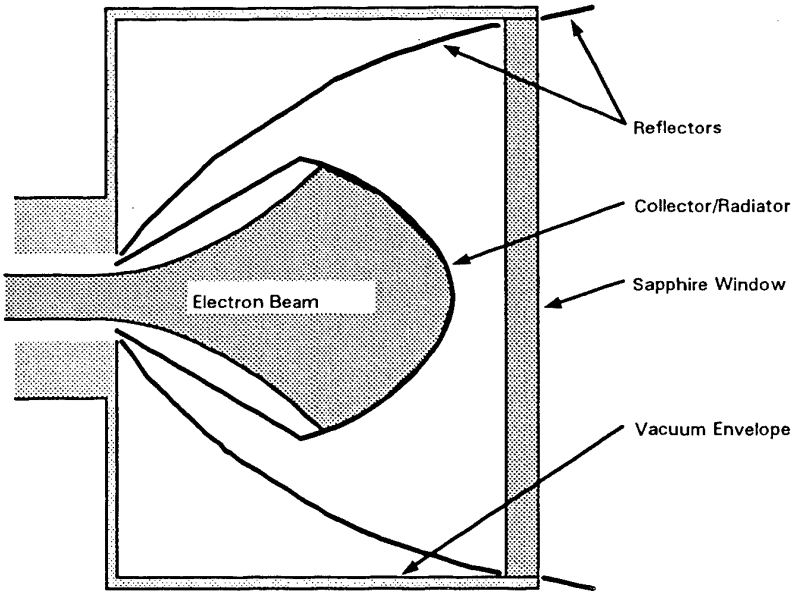

Figure 6 Schematic layout of radiation-cooled collector.

3. References:

1. A.S. Gilmour, Jr., *Principles of Traveling Wave Tubes*, Boston and London: Artech House, 1994.
2. Varian Associates, *Microwave Tube Manual*, Air Force Publication No. T.O. 00-25-251, 1979.
3. A. Staprans, "Linear beam tubes," Internal Varian Report, September 1968.
4. C. Beurtheret, "The Vapotron technique," *Revue Technique C.F.T.H.*, no. 24, December 1956, pp. 53-82.
5. E.L. Lien, A. Mizuhara and D.I. Boilard, "Electrostatically-focused extended-interaction S-band klystron amplifier," *Proc. 6th International Conference on Microwave and Optical Generation and Amplification*, Cambridge, England, September 1966.

Reliability and Measurement Tools

James P. Ryan
Rome Laboratory/ERDS
525 Brooks Road
Rome, NY USA 13441-4505

Abstract

This paper discusses the need for reliability and the analysis or "tools" used to measure or calculate performance. Reliability is defined as the probability that an item will perform its intended function for a specified interval under stated conditions. Regardless of what product/service is being offered, or who the intended customer may be, it should be a reasonable assumption to state that the degree of product success is directly related to the ability of that product to meet or exceed customer expectations. Therefore, customer expectations, positioning in the market place, product availability, life cycle cost (LCC), liability and needs, be it commercial or military, are important factors that must be addressed by the manufacturer. The vacuum electronics market has a small, divested number of companies, each company attempting to control its own market niche. As the military market becomes smaller, due to the general reduction in each country's defense budget, market positioning, LCC, and availability become increasingly important. The information presented is an accumulation of corporate knowledge from the members of NATO AC243 Panel 3, Research Study Group (RSG)19. The information presented demonstrates the importance of reliability, of collecting and transforming the data into a useable medium and that reliability growth is an ever-evolving measurable process.

Introduction

Reliability & Measurement Tools (R & M) as the title states, but in reality, there are no defined reliability tools. There are standard measurements, standard test procedures, and models, handbooks and reliability databases that can be used to quantify and estimate reliability factors. Tools can enable a process, they don't drive the process. Metrics are the drivers.

The Reliability analysis tools, measurement techniques or tools, databases and strategies have been developed over the past years. However, putting these tools and techniques to practice in the vacuum electronics arena is still an evolving process. The vacuum electronics industry is a mature group of scientists and engineers (S&E), new talent is slow to emerge, this is true as well in the government organizations. Therefore, the established scientist and engineer has been through the early stages of the learning curve. This paper as part of the NATO Defence Research Group (DRG) Handbook on "Microwave

and Millimeter Wave Tubes and Power Supplies," provides an accumulation of knowledge on Reliability that the new scientist and engineer must know. Even the mature S&E can benefit by learning about newer analysis techniques that can be used for evaluation of the product.

Discussion

The discussion on Reliability & Measurement Tools is organized in the following order, Product Source Selection, the three phases of a typical Research & Development (R&D) program, Phase 1 - Conceptual, Phase 2 - Experimental, Phase 3 - Delivery and finally, some comments about the US DoD acquisition changes. The following criteria should be considered when evaluating a manufacturer's product in response to your Request For Proposal: Understanding Needs, Approach to Design, Approach to Quality, Approach to Product Verification, and some form of Rating Methodology. First, Understanding Needs, this details how the manufacturer's component will meet the requirements for operating, storage and environmental conditions of the system. Questions that need to be addressed are: What is the manufacturer's process for translating customer needs into qualified technical objectives? What is the manufacturer's process for including RELIABILITY & MAINTAINABILITY techniques, methodology and concepts into the design and manufacturing procedures? Has the manufacturer performed any Finite Element Analysis (FEA) to verify the design? Has the manufacturer performed any Life Cycle Cost (LCC) analysis to demonstrate the benefits of the design? 2) Approach to Design: Does the supplier provide sufficient information to indicate that the performance-based requirements can be met? Does the manufacturer's' management demonstrate suitable control over subcontractors and vendors to ensure proper attention is paid to reliability and quality? 3) Approach to Quality: Does the supplier work with their vendors to improve the quality of the products or services? Are customer needs/requirements being met? 4) Approach to Product Verification: Does the manufacturer collect and analyze failure data from previous and current products for reliability and quality improvement? Does the manufacturer propose to verify product performance requirements? Is there a process for identifying and resolving product problems? 5) Rating Methodology: Defines a list of factors to be considered, an indication of their relative importance and a scheme for rating each factor. This methodology can be simple or complex.

In general, the initial reliability requirements for a product are generated by thoroughly understanding the customer's needs, Reliability & Maintainability requirements, and the application/environment that the product will operate in. Once this is understood, analysis can be performed based on comparisons of this product to a similar product. This provides the manufacturer with a quantitative analysis of estimated reliability. The information used is generally some form of calculated failure rate versus time. Handbooks or models can be used to calculate and estimate the expected product reliability. Models such as Audette, Lalli & Speck, MIDAS (Microwave Device Analyze System) - Markoff,

and Mil HDBK 217F. Finite Element Analysis (FEA), thermal analysis or electromagnetic analysis can be performed on the initial product design to determine weak points, material choices, cooling requirements, shielding or packaging requirements and environmental considerations. Tasks can be added to the program to report on hazard analysis, configuration audits, design specifications, test plan and procedures, or acceptance and qualification tests. The use of an integrated program management system utilizing a Contract Work Breakdown Structure (CWBS), program milestones and cost/schedule status reports as the framework for management control is suggested. This system would provide an auditable or otherwise traceable summarization of internal data generated by performance measurement procedures.

In designing a vacuum electronic device, the manufacturer should provide information on cathode emission such as a plot of long term degradation, cathode emission, recorded at its operating temperature versus time. The manufacturer should be performing life tests on their cathode materials and designs to substantiate this data. The manufacturer should provide the theory behind the solution proposed, as well as the rationale for the technology, design and implementation. The manufacturer should provide sufficient background information as to compliance with customer needs and/or requirements and the techniques used to measure them. Exceptions, variations or deviations to a customer specification or requirement must be stated with a detailed explanation of cause and effect. The manufacturer should provide a detailed listing of products produced and how and when the product was used or implemented. The manufacturer should detail up front, any portion of the program of work that will be performed by a subcontractor, i.e. special equipment, testing, manufacturing etc. The manufacturer should produce a list of key personnel working on the program and their availability to the program versus the experience required to perform the job. Finally, the suggested number of deliverable devices/components is four. This will verify quality of design, manufacturing, repeatability and provide components for specific testing.

Phase 2, the initial hardware is developed, fabricated and tested. Reliability can be calculated based on two kinds of testing. First, there is Dedicated Reliability testing such as reliability growth tests, accelerated life tests, environmental stress screening (ESS), electromagnetic testing etc. For example, Accelerated Life Testing employs a variety of high stress test methods that shorten the life of a product or quicken the degradation of the product's performance. The goal of such testing is to efficiently obtain performance data that, when properly analyzed, yields reasonable estimates of the product's life or performance under normal conditions. Note well, under normal conditions, the testing should not damage the component above and beyond the normal field use failures. Otherwise, over stressing the component, provides test data that is not relevant to the required performance specification. Some types of analysis that can be performed are fault tree analysis, worst case circuit analysis, durability, maintainability, and testability. For example, Fault Tree Analysis, is a systematic, deductive methodology for defining a single specific

undesirable event and determining all possible failures that could cause that event to occur. Remember, the estimates made in Phase 1 of the program are subject to change. The calculated and estimated numbers are not set in concrete. Failure reporting and corrective action provides for reliability growth. The second type of testing is called Non-Dedicated Reliability tests, this type of testing which is not dedicated to reliability such as Acceptance Tests, Qualification tests, Developmental testing, Integration testing, etc. For example, Acceptance Testing is a very long and tedious test which specifically details what is to be tested, RF test, Turn-on procedures, measurements of: small signal gain and variation, second harmonic, RF output power, DC power input and many more. Also, block diagrams and an equipment list are provided for each procedure. The order of the testing may be specified. The calibration of the test equipment must be documented. These types of tests are verifying the measured component performance versus the required customer specification.

Phase 3, the hardware is delivered, installed, and the system is field operational. Data must be collected from the field. This data is used to calculate the actual measured component reliability such as Failure rate, Mean Time To Failure (MTTF), Mean Time Between Maintenance (MTBM), Mean Time Between Failure (MTBF) etc. These failure rates can be compared to the original estimates and the revised estimates made during Phase 2. This information allows for trend analysis, corrective action, and reliability growth. The data can be used to verify any of the models or handbooks, MIL-HDBK-217F, analyses that were performed during Phase 1 or 2. Remember, you can achieve better reliability than was previously calculated. The important point here is that the field data must be collected and must be collected properly. Any trend analysis or reliability analysis where a comparison is to be made about how to efficiently budget R&D or Operation & Maintenance (O&M) funds cannot be properly performed unless the categorized data is collected. For example, the US Navy has demonstrated this point on the their Aegis AN/SPY-1A & 1B/D radars. The program started in 1983, at a cost of $4.55 per operating hour per tube socket. The US Navy spent approximately $10 million dollars not only collecting the data, but setting up an efficient O&M facility at Crane, Indiana, to use the data for failure analysis and corrective actions. The latest calculation shows that in 1996, the same cost was reduced to $0.39.

The US DoD acquisition procedures have been changed to meet future needs, in an attempt to access the latest commercial state-of-the-art technology. This was accomplished by removing the requirement for military specification and relying on best commercial parts and processes as performed in the industry. Also, the US DoD has recently directed the use of concurrent engineering principles in the DoD acquisition process. Also, under the new DoD acquisition procedures, the preferred means for managing risk are integrated process/product development (IPPD) teams, and integrated product teams (IPTs). These teams are to infuse a spirit of teamwork, and empower the participants, giving them authority to make commitments for the organization or the functional area they represent. For example, the Integrated Product & Process Development (IPPD) Process Model can provide an improved process

and metrics for evaluating a component/system. It can provide an improved method to quantify during technology development the potential risks associated with new technologies. The model can also provide better ways to address cost and risk drivers. The goal of the Process Model is "Best Value" not "Cheapest."

Conclusion

While there are numerous differences between the needs of the military customer and those of the commercial customer, the reliability needs of the military focus primarily on operational readiness (product performance on demand), operational longevity (long useful life versus short life cycles), operational supportability (repair/replace versus throwaway components), and operational robustness (satisfactory performance over environmental extremes). Reliability can be measured and must be measured for the purposes of meeting the military reliability needs. The military and the manufacturer must understand the importance of collecting this data and transforming this data into a useable medium for analysis.

The Reliability world is changing; no longer are the commercial and military industrial approaches distinct. For years the military has had its advocates for the use of commercial off-the-shelf (COTS) equipment and nondevelopmental items (NDI), but now the military use of commercial designs is required. The future of obtaining a RELIABLE product is everyone's business. As the RELIABILITY world changes so will the means to obtain the best product. Therefore, the future is meeting the customer's required product needs, with the best reliability and value for the customer.

References

1. "Reliability Toolkit: Commercial Practices Edition," Reliability Analysis Center/Rome Laboratory, 1995

2. "Commercial Parts and Processed for Military Applications," Reliability Analysis Center/Rome Laboratory, 1996

AEG ELEKTRONISCHE RÖHREN GmbH
Ein Unternehmen der THOMSON TUBES ELECTRONIQUES

Shelflife Study of Missile TWTs - Results and Conclusions

Authors: H. Vetter, A. Peters

Abstract

Missile TWTïs in present and future systems provide a special challenge to designers, manufacturers and users: immediate 100% performance is required after a snapstart following a dormant storage life of typically more than a decade, under possibly adverse conditions and without any intermediate recertification or operation.

Only in recent years has the justification of such a requirement been validated by a number of quantitative investigations. Under German MoD contract, AERG has performed an early design optimization to build fast-startup radar TWTs with a maximum potential life expectancy, followed by a shelflife test study to validate this approach by predicting the "natural", design determined TWT shelflife limits under normally occurring environmental conditions.

Operating data obtained from life tests on the mixed metal dispenser cathodes generally used in AERG TWTs, and from space and ground TWTs in service, exclude cathode degradation as a dominant life-limiting mechanism. However, while TWTs constantly in operation are stabilized by the excellent gettering properties of the electron beam, non-operating TWTïs will exhibit a steady increase of gas present inside the vacuum envelope, resulting from diffusion and desorption processes. This can be minimized by material selection, surface treatment, optimization of critical processes and careful outgassing during manufacturing, but still seems to remain the ultimate reason for the limitation of TWT storage life, much more than any material degradation process.

To monitor the gas pressure progress over very long observation periods, suitable ion-current test methods have been determined that can use TWT inherent electrodes as electron and ion collectors. The selected method has been calibrated under varying gas pressure with the TWT on the pump, and the deviation of the most gas-sensitive parameters has been recorded in order to define the life-limiting critical pressure.

Life tests on different TWT lots in Ku- and Ka- band have now been running for up to seven years, and will be continued as long as possible. Although individual test data exhibit a considerable variation, due to the very low observed changes in ion current, a worst case interpolation seems to provide a safe prediction of 15 years of storage life and more for TWTs with no extraordinary faults. Next tests to be performed shortly should support confidence in these extrapolations. If soft degradation of system performance could allow some relief of TWT specification over life, the useful TWT life could be extended considerably, possibly by a factor of two or more.

While screening methods can easily be applied to remove TWTïs with major faults or leaks within a normal production period, screening of potential faults to be expected after several years, caused by gas influx only slightly above the admissible limit ("microleaks"), cannot be detected by normal storage periods. An acceleration method can be applied within the screening storage period, but a life reduction of good tubes has to be minimized by careful application of any such method.

Testing

Authors: E. Fly (TASC,USA)

Paper not available

SYSTEMS EXAMPLES

Jan M. Schouten

DIRECTORATE OF MATERIAL ROYAL NETHERLANDS NAVY

s'Gravenhage, The Netherlands

I Introduction

This paper will discuss the evolution of transmitter design starting from the mid '70s onwards. In this period the design evaluated from the use of TWTs in the design of amplifiers to solid state devices. The electrical and mechanical requirements were based on the available technology used in amplifiers, tubes, power supplies and the control/protection circuitry. The microprocessor has been introduced in the amplifier designs in the mid '80s for control, protection and power management. The amplifiers discussed in this paper are in use by the Royal Netherlands Navy and other NATO countries whereas the L-band system is in use as the main surveillance radar for airports in different countries. The evolution of transmitter design will be given based on system examples. All discussed systems are designed and manufactured by Hollandse Signaalapparaten, Hengelo, The Netherlands.

II Applications

Systems can be categorized as Landbased, Shipborne, Airborne, Spaceborne and Mobile. Of course this is not a complete list. Depending on the application special attention has to be paid to the construction of the amplifier on both electrical as well as mechanical aspects. The cooling also differs per application. As an example, the cooling of a space tube might be accomplished by radiation of the collector heat directly into space while for the same tube in a mobile application air or water cooling has to be used. In the following discussion the focus will be on systems in use on ships. The landbased L-band radar used for air traffic control is derived from the shipborne radar. Mechanically and electrically no changes have been made to the amplifier. The other way around, using a landbased system for a ship application is not possible without major modifications. Those modifications are mainly mechanical and will be concentrated on the shock and vibration. An electrical modification may required due to the difference in operational modes between the two applications. One difference in operational use between the Navy Radar and Air Control Radar (ACR) is the standby time The ACR will be operational 24 hr./day, while in the navy application the radar will be in a standby mode depending on the operational need.

III Systems

1. L-band TWT.

The design of this amplifier was the start of a new generation TWT amplifiers for radar systems. It became operational in 1977 and has been the basis for the later designs of radar amplifiers. The amplifier can be divided into groups:

- The HV transformer with a series regulator (triode ML 7001);
- The modulator using a series of transistors as switching element;
- The waveguide section;
- The actual amplifier.

The TWT in this amplifier is cooled with demineralised water. The TWT has a ring bar structure, single collector, a winded solenoid using aluminum foil and the gun uses an oxide coated cathode. There is no vac-ion pump on the TWT. The HV transformer is filled with a mineral oil and contains the HV rectifier diodes. The weight of the tube is about 150 kg. The regulator of the power supply uses a reference voltage and a ladder divider to stabilize the voltage via a triode. (Figure 1)

2 X-band TWT

The amplifier showed in figure 2 belongs to the next generation of amplifiers designed for ship application and became operational in 1985. This amplifier is part of a number of different radar systems. One of the applications is a Close In Weapon System (CIWS) which requires high reliability. As in the amplifier of figure 1, the same components can be identified. In this case a switched power supply has been used. This improves the efficiency remarkably and reduces the size of the power supply with a factor of 2. The modulator uses FETs in stead of bipolar transistors. The cooling of the TWT is performed by using a mineral oil, called SHELL DIALA DX. The gun of the TWT is placed in an oil tank for isolation (-56kV) and cooling. Use is made of a microprocessor in the control and protection circuits. The tube parameters such as power and gain are watched and the microprocessor takes the required actions based on these signals. The TWT is a coupled cavity tube with an integral copper tape solenoid, M-type cathode and depressed collector. The applied cathode voltage is -56kV and the cathode current about 20A peak. The efficiency is about 40%.

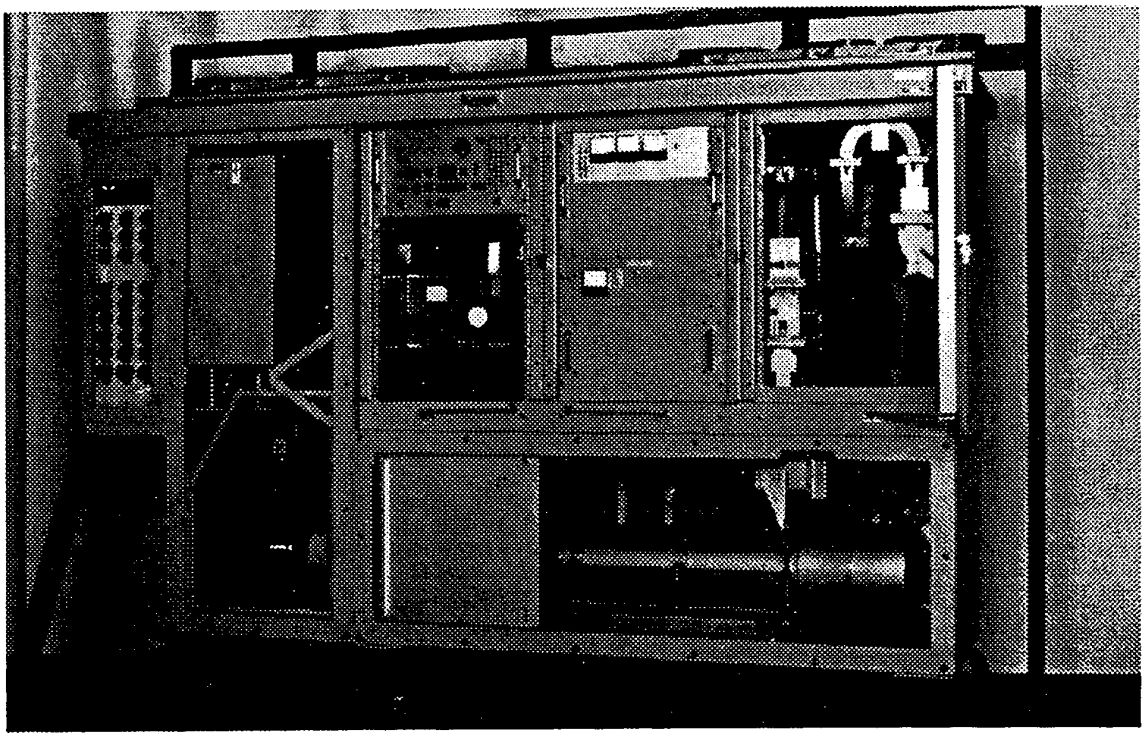

Figure 1 Power amplifier with triode stabilization.

Photo courtesy Hollandse Signaalapparaten, Hengelo, The Netherlands

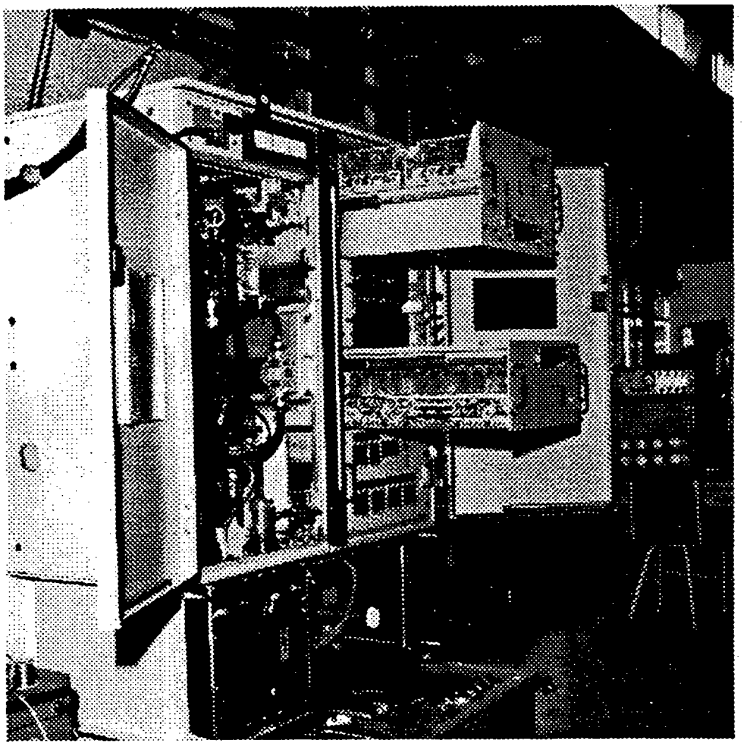

Figure 2 Power amplifier with switched mode power supply drawer and RF-section opened.

Photo courtesy Hollandse Signaalapparaten, Hengelo, The Netherlands

3 Solid State L-band

The solid state transmitter has been introduced as a next step in the development of radar transmitters (Figure 3). The amplifier has been designed in 1994 and will be used in the next generation of L-band search and track 3D radars. The systems consist of the following major components; DC power supply (Transformer with diode rectifiers, not stabilized), power books (as a driver and as part of the power stage), microprocessor control, protection and sensing system, and microstrip combiner divider networks. The power books consist of the R.F. circuitry, power transistors, and DC conditioner. The books R.F. circuitry is divided into the combining and dividing networks and the power blocks. The power blocks 450W L-band silicon transistors are used to amplify the R.F. input signal to more than 1kW. Four of those blocks are used in the output stage of a book, one is used as the driver for the output stage. The power blocks are cooled via the back plate of the book. Cooling channels for the water/glycol coolant mixture are machined in the backplate. The microprocessor watches the performance of the power books and the other electronics and will report this to a central monitor panel in the amplifier. It is also possible to interface this data to an external system Depending the type of failure and the effect of this failure on the performance of the system the microprocessor will propose a possible reconfiguration of the power components in the amplifier.

One of the features of the solid state amplifier is its flexible power level without the decrease of efficiency. This can be obtained by lowering the drive level or reconfiguring the number of power books. However the efficiency of solid state transmitter is about 15-20%. The reliability is much improved over that of the TWT amplifier. The TWT amplifier has a single failure mechanism while the SSA has graceful degradation. The MTBF of a SSA is at least a factor 5 higher then that of a TWT amplifier.

The SSA is now under test and evaluation for a period of three years. So far no major defects have been observed. The reliability of the silicon transistors is greater than expected and the new generation of transistors have more gain.

Up to C-band, power transistors are giving, depending on the application, a good alternative for power generation. Above C-band, power output and gain decrease rapidly and more power transistors are required the amplifier for the required output powers. The efficiency decreases as well. The use of TWTs or other tube devices becomes more attractive in those frequencies. The introduction of MPMs will be seen more and more for applications above C-band. A general idea about the application area of Tube and Solid State Amplifier is given in figure 4.

The systems discussed in this paper are designed and manufactured by Hollandse Signaal Apparaten, Hengelo, Netherlands.

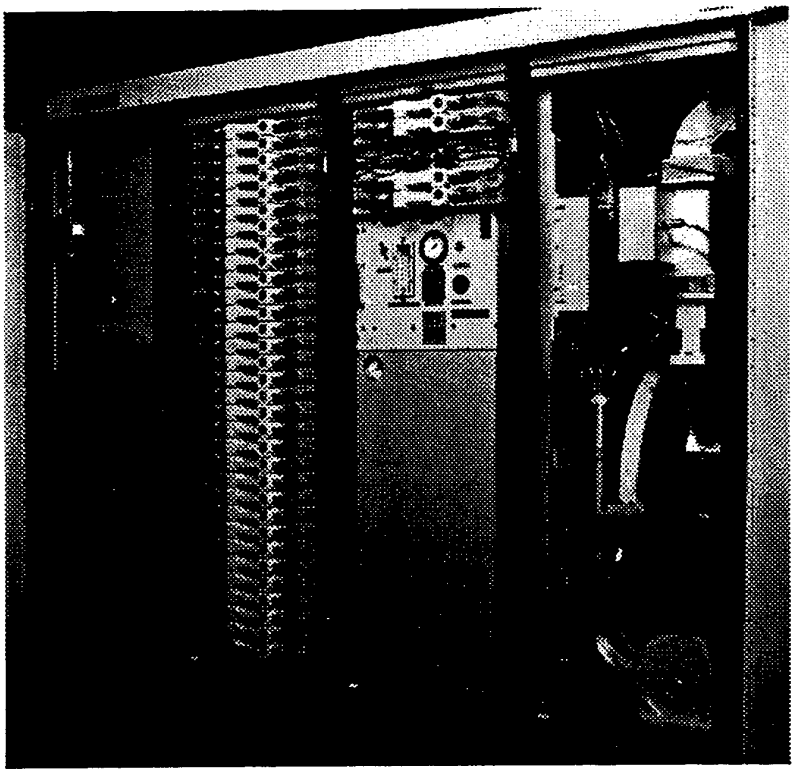

Figure 3 Solid state D-band amplifier

Photo courtesy Hollandse Signaalapparaten, Hengelo, The Netherlands

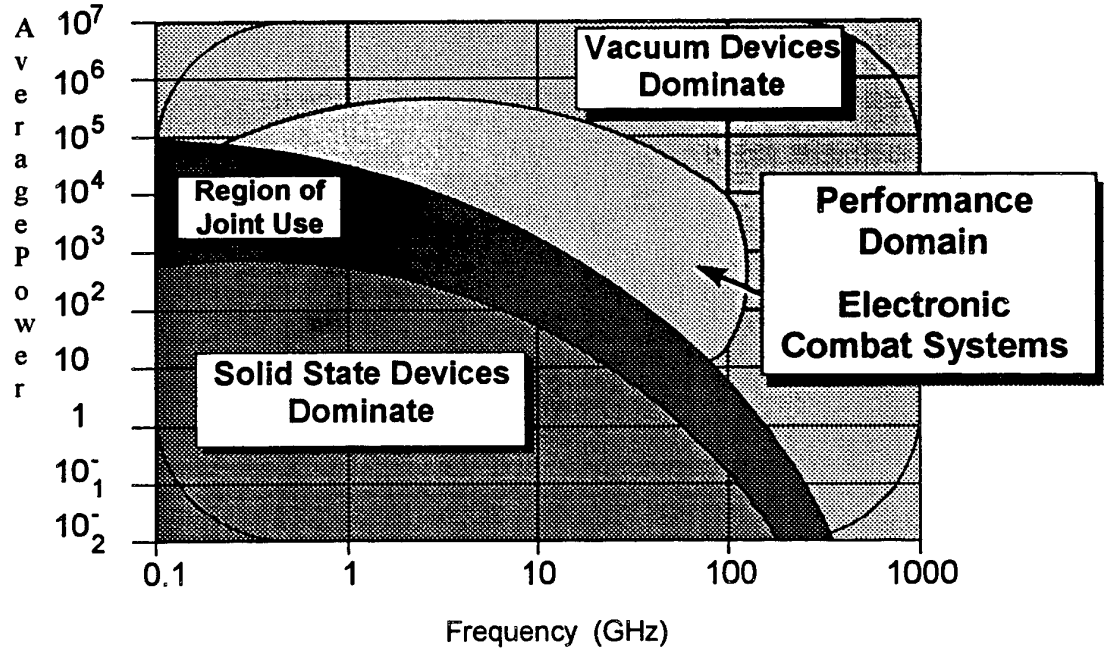

Figure 4 Application area for Solid state and Vacuum devices.

IV Conclusion

The development of new technologies in microwave tubes and amplifiers is still in progress. In tubes the introduction of new materials, better controlled manufacturing technologies and software simulation programs are improving the reliability of the microwave tubes. A better understanding of the operational application of the amplifier (system) by the micro wave tube and amplifier designer and the application of microprocessors in the control and protection circuits have an other positive influence on the reliability.

Solid state technology has entered the high power area. Power transistors and FETs (400 - 100W) are available up to C-band and a further development to higher frequencies is going on. The efficiency of multi-transistor amplifiers is low due to the combining losses and the device efficiency.

The combination of tube technology and solid state has entered the market with the introduction of the MPM, and will play a major role in the future design of Phase Array type of systems.

RSG-19 ACCOMPLISHMENTS

Rob M.E.M. van Heijster
TNO-Physics and Electronics Laboratory
The Hague, The Netherlands

ABSTRACT

The accomplishments of the North Atlantic Treaty Organization's Research Study Group on Microwave and Millimeter Wave Tubes (RSG-19) are summarized in this paper. The scientific work of RSG-19 is described in more detail in other papers in this workshop. The relevance of RSG-19 for NATO and its financial and technical impact is clearly shown.

1.0 INTRODUCTION

The background, origin and specific tasks of RSG-19 on micro- and millimeter wave tubes are described in the paper RSG-19 introduction. This paper will focus on the results that are accomplished or will be accomplished in the near future. RSG-19 will finish its activities during the spring of 1998.

RSG-19 has followed a well structured methodology:

1. Failures in traveling wave tubes (TWTs) and high voltage power supplies (HVPSs) were analyzed.
2. The failure causes were determined.
3. Operational envelopes to avoid these failure causes were defined.
4. Design guidelines and procedures were developed to keep systems within their operational envelop and hence to improve reliability and to enhance the availability of high power microwave systems.

The first part of this paper will summarize the scientific work with respect to database development, data analysis, operational envelop and design rules. The second part of the paper shows how the results of our work are made profitable to the NATO partners. The distribution of knowledge, guidelines and recommendations is performed in three ways:

1. the RSG-19 handbook.
2. the RSG-19 workshop.
3. the RSG-19 network.

The paper will end with a summary of the military benefits of the RSG-19 work.

2.0 FAILURE DATABASE

Microwave Device Analysis System (MIDAS) was developed by the Royal Netherlands Navy. It's a database and a data analysis tool combined in one program. RSG-19 has set-up a failure database, based on MIDAS. This database is used to identify the most common sources for failure within tubes. The Royal Netherlands Navy has released their MIDAS data collection and analysis program for free use by RSG-19. MIDAS can

calculate all necessary statistical data and will compare this data with the values that are predicted by the Rome Lab Reliability Toolkit. The program was thoroughly tested by mathematical and logistic experts of Rome Laboratory and Naval Surface Warfare Center at Crane. To date, thousands of failing items have been stored in the database and this process will continue over the lifetime of RSG-19. Provisions will be made to keep the database updated when RSG-19 has finished its activities.

The results of the data-analysis has directed the work of RSG-19 on specification of tubes, HVPS and their interaction.

MIDAS is described in more detail in another paper in this workshop session. An example of MIDAS analysis output is given in Figure 1.

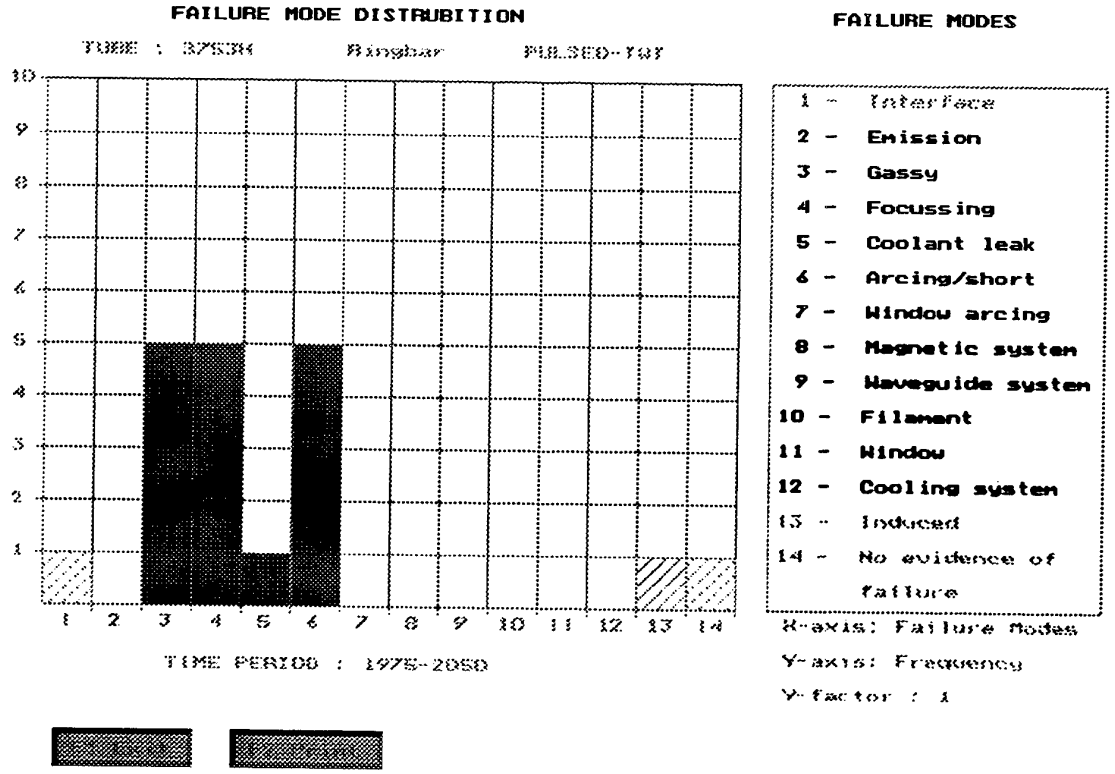

Figure 1 Screen of MIDAS program showing analysis output:
Failure mode distribution of a ring-bar TWT (Courtesy Royal Netherlands Navy)

3.0 OPERATIONAL ENVELOP

To model all various aspects of tube reliability, RSG-19 introduced the "operational envelop" concept. Three definitions will clarify this concept:

- Operation Point (OP):
  Any combination of voltages and currents (temperatures, shock, vibration etc. may also be included) that is applied to the tube or is present on the HVPS.
- Valid Operation Point (VOP):
  Any OP that the tube or HVPS can handle for a prolonged time (the specified lifetime).
  Valid OPs are often subject to time constraints, their validity is restricted to a given pulse width and/or duty cycle.
- Operational Envelop (OE):
  The boundary of the set of all valid OPs.

As long as the tube is operated within the OE, the stress factors are within the limits and the (well designed) tube will exhibit a good reliability. A more comprehensive description of the operational envelop concept is given in another paper presented at this workshop. In Figure 2 an example of the operational envelop of a FET is given.

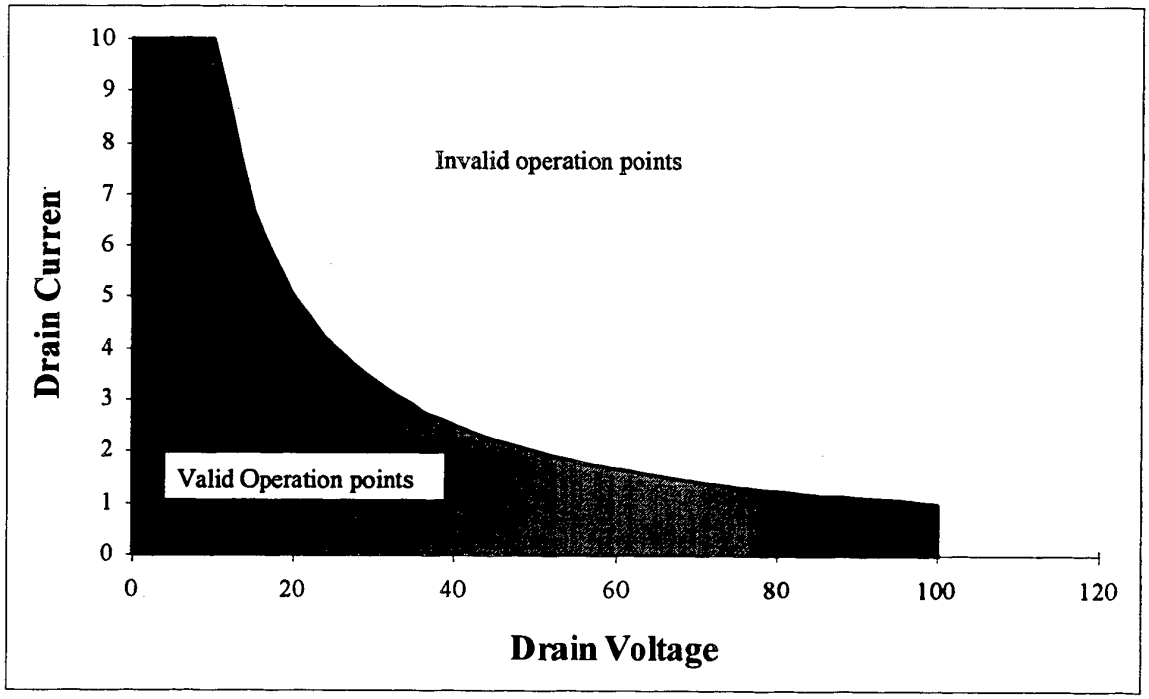

Figure 2 Operational envelop example.
All valid operation points for the drain voltage and current are given (under DC conditions).The boundary of all valid operation points is the operational envelop.

The operational envelop concept is used to define generic envelopes for tubes and HVPSs. The specification guidelines, given in the RSG-19 handbook are developed using these generic operational envelopes.

4.0 UPDATE MIL-HDBK-217

The database provides the factual information needed to update MIL HDBK 217 for tubes and HVPS. The first update, based on information of RSG-19, is already effectuated in version F-Notice-2.

5.0 OTHER ACHIEVEMENTS

Apart from the already mentioned results RSG-19 has additional achievements:

1. Efficiency: The available information and cooperation helps the participants to redirect their R&D effort. This results in reduction of the duplication of efforts on tube and HVPS R&D within NATO. This increase in efficiency means a multiplying factor on the present R&D budgets.
2. Multidisciplinary Approach: The different disciplines available within RSG-19 (mathematics, logistics, power electronics, microwave etc.) leads to a strong multidisciplinary approach of all subjects that RSG-19 deals with according to its Program Of Work. Via the network, all disciplines are mutually available for advice and recommendation.
3. The provision of guidance to each nation on where and when to expend their limited R&D budgets.
4. Robust design techniques for tube and power supply design were developed.
5. The development of an acquisition engineering program.
6. Guidelines to translate NATO user needs into performance specifications.
7. The determination of the interaction between cost and performance.
8. The development of a NATO quality assurance program.

6.0 RSG-19 HANDBOOK

The handbook is of great importance to RSG-19, it summarizes all achievements and it will be a useful guideline to designers, development engineers as well as maintenance personnel. This book is to date over 400 pages. The handbook is available via RSG-19 members.

The handbook covers all topics of RSG-19 including all the results of our specific tasks. The handbook covers:

- The operational envelop; the failure database is used for the development of a generic "operational envelope" for tubes and HVPS. The generic "operational envelope" gives the relation between all (known) failure causes and the associated operational limit (shock, vibration, temperature, currents, voltages, etc.).
- The generic specification of tube, HVPS and of Tube - HVPS interaction; the HVPS "operational envelope" must be adapted to ensure effective protection of the tube against the failure cause. The operational envelope of the tube can be enlarged by choosing the proper operational envelope of the HVPS. This leads to the inter-relation of the operational envelopes and their related failure causes which must be emphasized in the generic operational envelopes.
- The description of test procedures and standards; a procedure was developed to prescribe the testing of the generic tube-HVPS "operational envelope."
- The development guidelines; the desired operational envelope is used to develop design rules for tube and HVPS development. These design rules can also be used for improvement of existing systems.

The RSG-19 handbook is discussed more in detail in another paper within this workshop.

7.0 WORKSHOP

RSG-19 has developed a workshop that has a dual purpose:

1. The distribution of knowledge, guidelines and recommendations. The workshop will give a good understanding of the relevant topics covered by RSG-19.
2. The acquisition of additional information with respect to reliability, failure mechanisms, tube-HVPS interaction and the operational envelop of tube and HVPS.

To reach all relevant people, including design engineers, system designers, maintenance employees, logistic controllers, mathematicians etc., the workshop will be held both in Europe and in the US. The European workshop will be held in cooperation with ESA.

8.0 NETWORK

The RSG-19 members and those that have shown their interest, form a tube-HVPS network that has already proven its effectiveness. Provisions have been made to maintain and enlarge this network.

RSG-19 holds representatives of all relevant users and manufacturers of microwave power tubes and high voltage power supplies. Also, the representatives cover most related disciplines (mathematics, electronics, physics etc.). Various industrial parties have visited, partially on our invitation, one or more meetings.

In RSG-19 four countries are represented: France, Germany, the Netherlands and the United States of America.

The RSG-19 attendees and representatives are:

- US
  - US AIR FORCE - Nation Representative Armed Forces
    - Warner Robins Armed Forces
  - US NAVY - NWSC Crane Armed Forces
  - US manufacturers - ST Keltec HVPS
    - CPI HVPS & Tubes
    - Teledyne HVPS & Tubes
    - Northrop Grumman HVPS, System House
    - Lockheed Martin System House
    - Litton HVPS & Tubes
    - TASC Test Systems

- Europe		
- Netherlands	- Nation Representative	Defense Research
	- RNlN	Armed Forces
- France	- Nation Representative	Armed Forces
- Germany	- Nation Representative	HVPS & Tubes
- European Man.	- Thomson (FR)	HVPS & Tubes, System House
	- TMD (UK)	HVPS & Tubes
	- AEG (D)	HVPS & Tubes, System House
	- Signaal (NL)	System House, HVPS
- NATO	- NAMSA	Armed Forces
- EC	- ESA	Space

9.0 MILITARY BENEFITS

The NATO armed forces uses many systems that rely on microwave power. The reliability of the microwave power source is extremely important, failure of the microwave source can result in the loss of equipment and life. For example, failure of the microwave source in electronic warfare (EW) equipment can result in the loss of an aircraft, failure of the microwave source in a close-in weapon system can result in the loss of a ship. Reliability is a crucial issue for microwave sources.

The R&D activities of RSG-19 are ultimately guided towards all aspects of reliability enhancement of microwave sources (power tubes and associated HVPS). A secondary target of RSG-19 is the cost reduction of microwave power (the total price that is paid per watt and per hour of RF power). The increase in reliability will lead to a higher Mean-Time-Between-Failure and hence result in cost reduction (more hours of RF for the same price).

The concept of operational envelop will be used to evaluate the reliability of tube and HVPS. A good knowledge of the behavior of the operational envelop will lead to the development of construction guidelines for reliable tubes and HVPS. The strong and required involvement of the industry in RSG-19 guarantees that new tubes and HVPS are constructed following these guidelines and that, when necessary, current designs can be upgraded.

The activities of RSG-19 will result in the availability of highly reliable and cost-effective RF-sources. Both reliability and cost-effectiveness are crucial to the military. This results in a major increase in survivability of NATO forces and a decrease in deployability requirements. It is estimated that there will be a 100 to one payback from RSG-19 to NATO.

The benefits of RSG-19 are best shown by in Figure 3. This figure is originally shown to USAF directors to show the ultimate importance of the RSG-19 work. Other nations have claimed to have comparable savings and achievements.

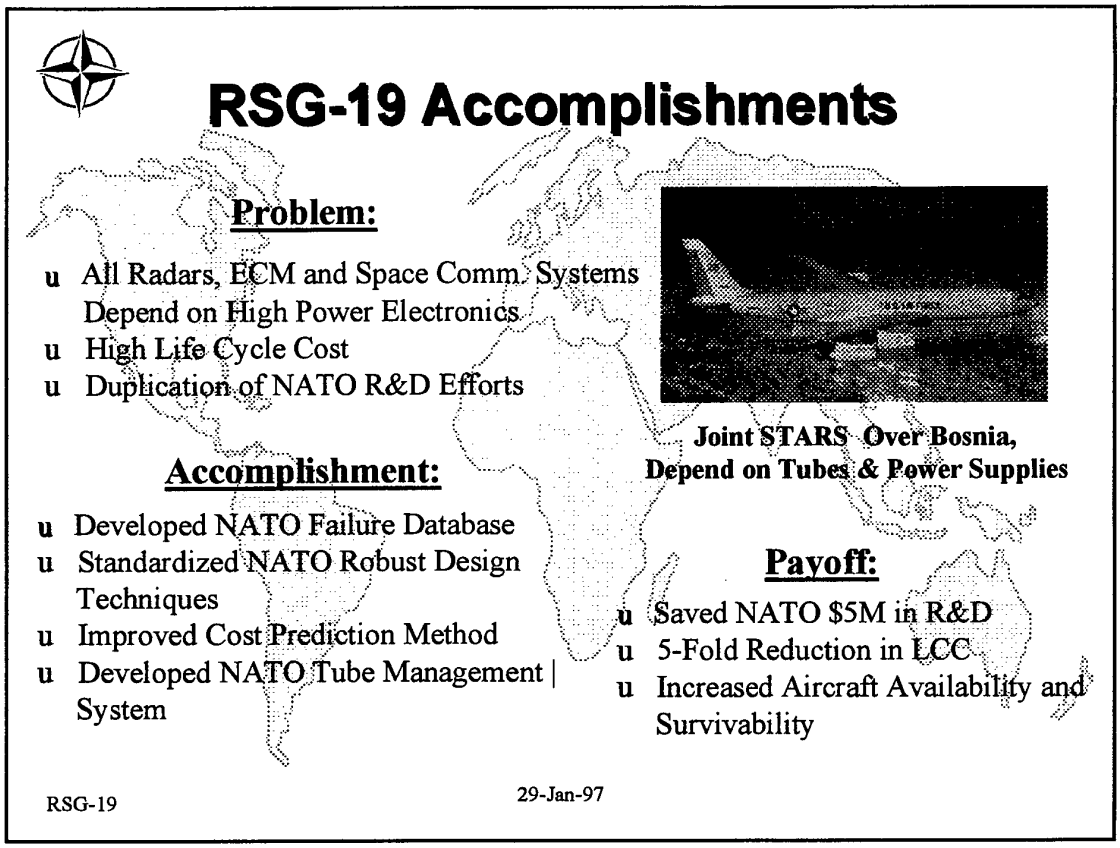

Figure 3 Sheet showing the relevance of RSG-19
This sheet is originally shown to USAF directors to show the ultimate importance of the RSG-19 work (Courtesy USAF/Rome Laboratory)

10.0 CONCLUSION

RSG-19 has, using a well structured methodology, deduced a set of guidelines and procedures based on the analysis of failures. The three way option of "handbook-workshop-network" is chosen to distribute the results.

Microwave power has two interrelated key characteristics:

- It is often of life-importance for military users;
- A significant part of budgets is dedicated procurement and maintenance of systems.

RSG-19 work has led to significant costs savings and to an increase in reliability, availability and survivability.

FURTHER INFORMATION

The latest information on RSG-19 is available on : http://www-er.rl.af.mil/ER-News/23/nato.htm

MiDAS

Microwave Device Analysis System

Joop van Huut

Naval Electronics and Optics Establishment

The Netherlands

Summary

In this paper a short introduction to the MiDAS program is given. MiDAS is used for the acquisition of data both on board of a ship and in the workshop. The program also has powerful data analysis capabilities, which will be shown more in detail.

Introduction

There are enough reasons to design a reliability system for microwave tubes and the RNLN decided to develop the reliability system MiDAS. MiDAS stands for Microwave Device Analysis System.

Within the Navy Electronic and Optics Establishment a need exists to set up a reliability system for all kinds of microwave tubes that are used within the Royal Netherlands Navy.

At the moment a ´run to break´ strategy is being applied to these microwave tubes. Accurate calculations for reliability properties of these tubes are missing. So, there is no optimal logistic and repair strategy possible.

Until recently, one could only base oneself upon the simplified models that are described in Mil. Standards and Mil. Handbooks. Improved models are set up by the Rome laboratories in which models are developed for the failure mode distribution. These models are set up on theoretical grounds because no sufficient practical information is available.

In recent years the reliability technique has been expanding. Mainly for use with micro-electronics, new techniques have been developed to calculate the reliability parameters. These methods can also be applied for reliability calculations of microwave tubes.

The objectives of MiDAS are the following:

* To improve the reliability of microwave tubes by:
    * identifying reliability trends
    * an efficient system application
    * improvements in the design of tubes in collaboration with the manufacturer
    * FRACAS methodology (Failure Reporting And Corrective Action System)
* Achieve adequate reliability models of different types of microwave tubes

The actions of the MiDAS reliability system in order to achieve the above mentioned objectives consists of:

* the collection of field data of microwave tubes by means of data collectors
* the calculation of reliability and statistic parameters
* the analysis of microwave tubes on so-called 'physics of failure'

A preventive maintenance schedule is possible when we can calculate accurate reliability parameters of microwave tubes via MiDAS. We could use a time based maintenance or condition based maintenance schedule. It is also possible to set up an adjusted storage and repair policy, when one has accurate reliability figures.

Reliability Technique

The subject of reliability theory covers a large and very varied area:

* Reliability theory: the mathematical approach of the reliability problem with statistical and stochastical means. For example: life span valuation/confidence theories, the innovation theories, waiting time theory, supply theory.
* Measuring, examining and testing: measuring the achieved reliability of a product on the basis of experiments (test), performed only on product samples, during a relatively short time span (accelerated test).
* Reliability analysis: the collection of failure data, the reduction and processing of these data to use them to improve future designs. The mistakes that appear can be analyzed physically (physics of failure), but also statistically. The data about failure causes, failure mechanisms and failure modes of components are fed back to the designing phase in order to limit the consequences of such failures in future products.
* Design techniques: the inherent reliability of a product can be increased by:
    * special reliable components (hi-rel components)
    * reducing the stress level of the components (derating)
    * reviewing the designs at regular intervals (design reviews)
    * adapting the product to the user and the using environment (human engineering protection)
    * making the product easy to maintain (modular structure, standardization)
    * the use of extra components (hardware redundancy) or of extra calculations or operations (software redundancy).
* Reliability management: the structure and preservation of an operational organization suitable for design, development and maintenance of reliable products. The development of the necessary administrative and logistic support. This includes the inspection, testing and maintenance procedures, as well as the cost-benefit analysis of the applied reliability techniques.

Mi.D.A.S. Structure

The MiDAS program consists of three parts.

The first part is the data collection phase. Here the data about the different microwave tubes, that are relevant for the calculation of the reliability, are being collected. The second part, the storing phase, consists of storing the data into a database. The last and most important part is the reliability analysis phase in which the calculations are being executed.

Information resulting from the reliability analysis is feed back to the system operators and the manufacturers. Manufacturers will use the information to improve, in close co-operation with the customer, their products. The system operators obtain valuable reliability information with respect of handling, operation and use of the tube.

This procedure is given in Figure 1.

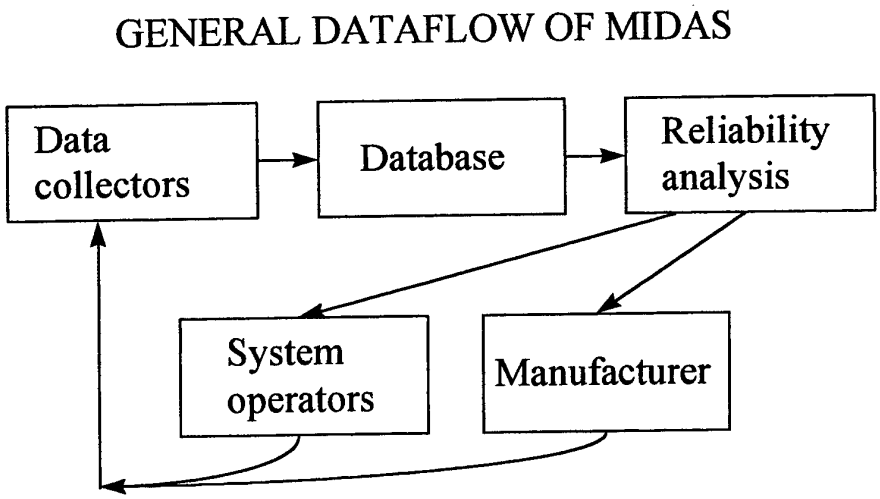

Figure 1 Data flow and feed back using the MIDAS program.

Data Collection

MiDAS uses two standard forms for data collection: the livret sheet and the test sheet . These two are briefly discussed below.

Livret Sheet (shop traveler)

A sheet that serves to record the following data of the microwave tubes:

* installation- and removal dates,
* the number of hours that the tube has run in a high power state and in a stand-by state,
* a description of the failure mode.

This livret sheet is stored into MiDAS data collection system. The used program, MiDAS-livret sheets, the user has his own database that can communicate with the main database in order to be able to do the accounting of the livret sheets independently.
Within this program, the user can add, mutate, remove livret sheets and look up the tube type and serial number within his own database, print all data and all livret sheets. The tubes that can be added in the MiDAS database are not only traveling wave tubes, klystrons and magnetrons, but also other types of tubes such as: t.r.-cells, switch tubes, tetrodes, etc.

Test Sheet

The second form for data collection in MiDAS is the test sheet. This sheet is used in workshops where the defective microwave tubes are being tested in order to get a correct diagnosis of the failure mode.

The following data of a tested microwave tube can be recorded on this test sheet:

* pre-installation
* post-removal
* electric currents and voltages, and resistance values
* input and output power plus body current as function of the frequency
* a failure mode identification and other details

A program, MiDAS test sheet, is available to enter the collected data. In this program the user has, just as with the livret sheet, his/her own database that can communicate with the main database. The livret- and testsheet data of the microwave tubes are stored in the database.

Database

The livret and test sheet data of the microwave tubes are stored in the database.

The database tree is built up as drawn in Figure 2. There is one separate branch for each category of microwave tube: traveling wave tube branch (twt-branch), klystron branch and magnetron branch. There is a subdivision given after the type number for each type of microwave tube within these branches.

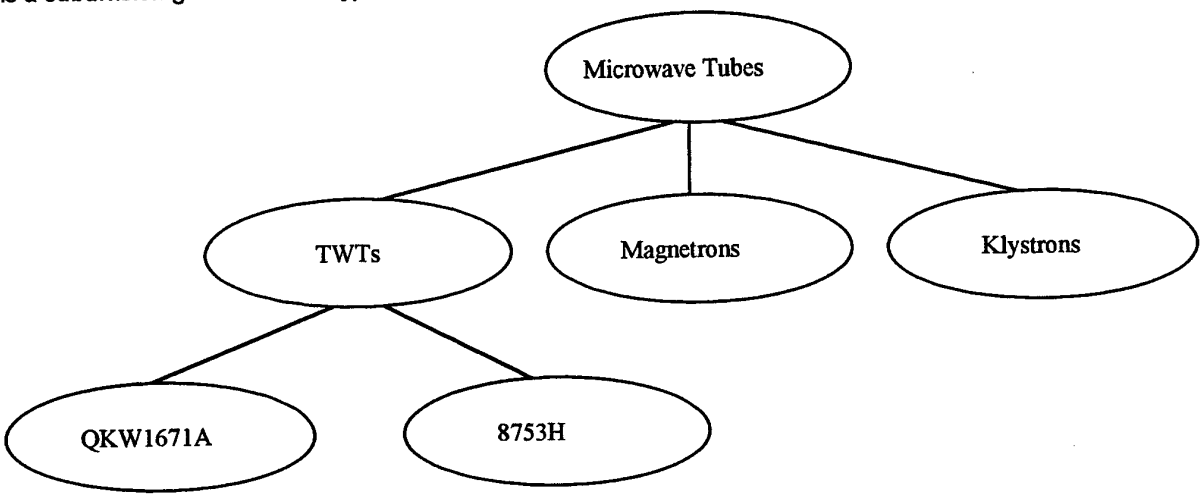

Figure 2 The database tree within MiDAS

The twt branch in the figure for example, is further split up in branches that represent a specific type twt: the twt types QKW1671 and 8753H, for instance.

In order to be able to calculate the reliability of a microwave tube, analysis has to be made of each failure mode, from the failure distribution and the distribution type. The Weibull distribution appeared to be appropriate for analysis, given the general character of this distribution.

This analysis is performed by the MiDAS program, a sample screen is shown in Figure 3.

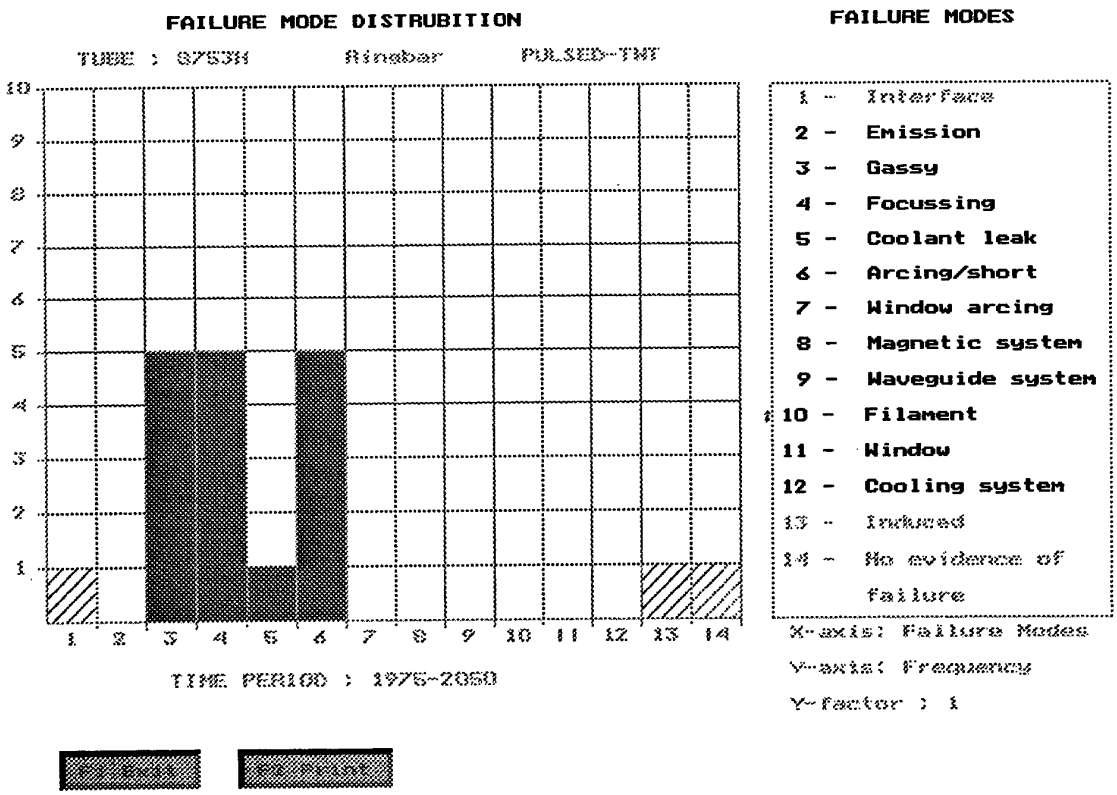

Figure 3 Sample screen of MIDAS program (shown here in black and white).

NATO HANDBOOK ON: *MICROWAVE & MILLIMETER WAVE TUBES*

Edward J. Jones
US Air Force/Rome Laboratory
ERDS, 525 Brooks Rd.
Rome, NY USA 13441-4505

ABSTRACT

A short summary of the Defence Research Group handbook developed by the North Atlantic Treaty Organization's Research Study Group on Microwave and Millimeter Wave Tubes is presented in this paper. This handbook was developed to fill the void that exists between technical papers stressing discouragingly technical tube theory and system design textbooks. Accordingly, this handbook starts from describing tube state-of-the-art and its effect on system design and reliability and builds on how to translate user needs into specifications, provides a set of general design rules to follow, shows how to develop a comprehensive tube acquisition engineering program, and shows how to design reliability into tube based systems. The result is, the creation of a knowledge base to enhance NATO micro and millimeter wave tube reliability, system compatibility, increase system performance, increase standardization, and decrease system life-cycle-cost across NATO.

1.0 INTRODUCTION

In light of the vital influence that tubes and power supplies have on the reliability and life-cycle cost of military systems, a major responsibility of the system engineer and/or manager is ensuring that the system will meet the user's needs over the life of the system. However, many system engineers/managers have little or no knowledge of tube and/or power supply technology, design, or operation. Moreover, textbooks and handbooks published to date have stressed theory and are far too cumbersome to be used by one whose primary responsibility is system performance and reliability.

In order to address microwave tube and high voltage power supply reliability issues, NATO AC/243 Panel 3 formed NATO RSG-19, The NATO Research Study Group on Microwave and Millimeter Wave Tubes and Power Supplies. NATO RSG-19, established in 1992, includes government and industry representatives from the United States, The Netherlands, Germany, France, Luxembourg, Belgium and Great Britain. The main objective that NATO RSG-19 has been working towards is to create a framework to enhance NATO-wide research and development on microwave tube and high voltage power supply (HVPS) reliability, increase system compatibility, increase system performance and decrease cost, as well as, reduce duplication of research and development efforts.

The first task undertaken by RSG-19 was to accumulate and develop a robust database of microwave tube failures. Standards were developed for collecting and specifying reliability data across all platforms, and each member nation representative contributed microwave tube data to the RSG-19 database. The result of this effort has been the revision of the MIL-HDBK-217F reliability prediction model for microwave tubes. This more accurate model (217F -Notice 2) was influenced by the tube reliability data generated by RSG-19. Predicted MTBF values increased on the average by a factor of two over the MIL-HDBK-217F model and more closely resembled actual field data.

NATO RSG-19 then developed The NATO Defense Research Group (DRG) Handbook on Microwave and Millimeter Wave Tubes and Power Supplies to provide system engineers and program managers with comprehensive guidelines and references on microwave tube and HVPS technology. The DRG Handbook, which has been developed from the corporate knowledge of NATO RSG-19 members, is a repository of information on tube and power supply technology, performance specifications, design guidelines and reliability techniques.

2.0 THE HANDBOOK

2.1 TUBE AND POWER SUPPLY STATE-OF-THE-ART

The DRG Handbook (HB) addresses tube state-of-the-art and its effect on system design and reliability. "Snapshots" of tube state-of-the-art are presented in graphical format. The process in which a microwave tube is designed usually involves a process in which a number of baseline designs are reviewed, the candidate design closest to the requirement at hand is examined in detail, experience in constructing and using the assembly or subassembly is considered, and changes are effected as necessary. The handbook describes a process which involves a series of compromises and trade-offs. The tube design that evolves from such a process is not unique, given that another group of engineers or another vendor would probably select a somewhat different set of compromises and trade-offs. The problem of course it that the state-of-the-art is constantly changing as new technology, design and materials become available. A second problem is that a single relationship between peak and average power capabilities, or for absolute power capability, does not exist for all tube types. The HB also provides examples and the difference between the two major families of microwave tubes; i.e., linear beam and crossed field devices.

The HB also addresses linear beam tube power supply state-of-the-art and its effect on system design and reliability. Interactions between the power supply and the tube are discussed and it is shown how to take into account this effort during the power supply design. A section on lessons learned is also included.

2.2 TRANSLATING USER NEEDS INTO SPECIFICATIONS

The HB provides the reader with a process on how to translate the user's needs into specifications. One of the most important tasks in a procurement of a microwave tube or power supply is the preparation of a suitable specification. Careful consideration of both form and content are necessary parts of the process. Specific requirements are largely system-related and must reflect the actual needs to assure adequate performance while permitting the tube design to be optimized through the trade-off process. Sections include: Performance Specifications - The User, Testing and Screening, Cost and Schedule Constraints, Sample Specifications, Specifications Checklist, Reliability/Life Cycle Cost Predication Methods, Operation and Handling Instruction For Microwave Tubes, Qualification Issues, Operating Instructions For Maximum TWT Life, and Ramifications of TWT Set-up in the Field.

2.3 GENERAL DESIGN RULES

Design decisions on interface matters require a great deal of coordination between the tube designers, the power supply designers, the system designers and the procurement agency. It is important that an adequate level of detail be addressed to ensure that the design philosophy, the design trade-offs and all interfaces are properly covered. Decisions made early in the program result in design features that can be incorporated into the equipment with a minimum effect on cost, schedule, and reliability. Adding a feature later in the program usually has undesirable effects on cost and schedule and may have an unfavorable effect on reliability if the change is not considered carefully and thoroughly. This chapter of the HB provides the reader with a set of general design rules to follow, which includes the concept of derating and how to apply it to microwave tubes. Other sections in this chapter are: Microwave Tube Trade-off Parameters, Design Considerations for Tubes, and Design Reviews.

2.4 MANAGEMENT OF TUBE DEVELOPMENT PROGRAMS

At the inception of a comprehensive microwave tube acquisition engineering program the goals must ensure that microwave tubes are designed to meet system technical requirements and exhibit a high degree of reliability, while maintaining reasonable acquisition cost. Components of this program include: a stringent qualification process, tight configuration control of materials and

processes, use of in-plant technical representatives to oversee production problems, a surveillance testing program, maintenance of continuous production at the tube suppliers, administration of a warranty program, and a closed-loop, systematic failure reporting, analysis, and corrective action system directed at evaluating and improving product quality and reliability. The technical knowledge and experience obtained from these efforts will result in concurrent gains in a set of usually mutually exclusive attributes, lower item cost with improved reliability. A measure of the success of this program is the reduction in cost of initial outfitting of the designed system and the reduction in microwave tube operating cost. The intent of this chapter is to share the concepts of this acquisition engineering program and identify the specific benefits of such a program.

2.5 TYPICAL FAILURE MODES AND A DATA COLLECTION FORMAT

A logical assumption might be that failure modes are highly dependent on those specialized applications, and possibly on the unique environments. A review of failure modes encountered in all applications, however, shows that while the symptoms may appear to relate to the application, the root failure causes are common to essentially all of the available device types. Treating the array of failure modes as if they stem from a few basic causes is important because the user will find that he can apply very similar controls for protection in most applications. In analyzing problems, the mistake of assigning the wrong root cause can be avoided. This chapter provides tables that review the relationship between the observable symptom and the most basic reason for the problem, the variable that must be controlled to avoid the described failure mode and describes a data collection to be used in the field.

3.0 SUMMARY

To date, the DRG Handbook has received very positive feedback on its work. United States and European military and industry communities recognize the need for tube and HVPS system development and acquisition guidelines since there is presently no recognized standard guidelines available. It provides the program manager with a comprehensive guide to writing quality specifications. Performance and environmental requirements are defined, as well as quality assurance provisions, performance specifications, design constraints and operational use. Guidance is given to the program manager on how to define qualification and acceptance testing procedures, tube, power supply, material and subassembly screening. Examples of actual tube and power supply specifications are provided. Discussions are also presented on reliability/life cycle cost prediction methods, operation and handling instructions, mechanical installation, environmental control, handling, storage and qualification issues. General design rules and management of tube development programs for microwave tubes are also covered. A discussion is given on electronic part derating concepts and how these concepts are applied to microwave tubes. Trade-off parameters and considerations for TWT, klystron and magnetron designs are defined and discussed in detail. The DRG Handbook also outlines microwave tube failure modes and mechanisms. These failure modes are described in terms of five different root causes: tube design, tube manufacture, tube operation, system related and environmental stress related. The actual failure data collected and characterized by RSG-19 for several different tube types and system application are included.

ACKNOWLEDGMENT

The author would like to acknowledge and thank James Ryan, Peter Rocci, Jeff Lynch, Rob van Heijster, Jan Schouten, Ernst Mey, Andreas Peters, Graham Phillips, Christian Bonnet, Tom Porter, Patsy Greenman, Ed Fly, Derek Hooker, David Nicholls, Pascal Morin, George Kreager, Stephan Schwarz, Didier Juges, Tom Webb, Al Biddings, Kenneth Craig, David Blough, John Jensen and Scott Gilmour for their contribution to the handbook.

REFERENCE

E.J. Jones, et. al., "DRG Handbook: Microwave and Millimeter Wave Tubes and Power Supplies," North Atlantic Treaty Organization (NATO) Defence Research Group AC243, Panel 3, Research Study Group - 19, September 1996, NATO Limited.

SESSION 8
TWT Design/CAD

Chairman: E.J. Jones (US Air Force/Rome Laboratory, USA)

The MMACE Framework: An Integrated Environment for Power Tube Design and Analysis

Authors: B. Hantman*; R. Abrams**; J. Labelle*; K. Siarkiewicz***;
(*Raytheon Company, USA; **Naval Research Lab (NRL), USA;
***US Air Force / Rome Laboratory, USA)

Paper not available

EQUIVALENT CIRCUIT MODELLING OF HELIX SLOW-WAVE STRUCTURES

R.G. Carter and P.Wang
Engineering Department, Lancaster University, Lancaster LA1 4YR, U.K.

Abstract

A simple equivalent circuit has been developed for the helix slow-wave structures used in travelling-wave tubes. The parameters of the model can be determined using numerical methods or from simple closed-form expressions based upon approximate field solutions. The model has been validated by comparison with experimental results and shown useful accuracy. It has the advantage over numerical simulations and previous equivalent circuit models that the ways in which the electrical properties of the slow-wave structure depend on its dimensions are made explicit.

1. Introduction

The helix slow-wave structure used in the first travelling-wave tube (TWT) remains the most widely used configuration today because of its simple construction and excellent bandwidth. A knowledge of the dispersion characteristics and the impedance of the slow-wave structure is essential for the design of a TWT. Although these can be measured (Ref. 1) it would be extremely useful if they could be computed from the dimensions of the structure. Conventional modelling of helix slow-wave structures is based upon electromagnetic field theory (Refs. 2, 3). Despite considerable effort, such models have not yet shown close agreement with experiment and they give little insight in to the factors which determine the behaviour of the structures. By interpreting the results of field theory in terms of the inductance and capacitance of a transmission line Paik (Ref. 4) developed an equivalent circuit model which was subsequently developed by other workers (Ref. 5). This model agreed well with experimental results for the dispersion but the accuracy with which it predicted the interaction impedance was far from satisfactory because it was based on a sheath helix approximation. More recently attempts have been made to model helix slow-wave structures using numerical methods (Ref. 6) but these require large computer resources and have yet to yield good accuracy.

The authors have developed a novel equivalent circuit for helix slow-wave structures whose parameters can be determined from computations or from simple closed-form expressions based on static field theory (Ref. 7). This model has shown useful agreement with experiment and has the advantage over preceding models that the relationship between the dimensions of the structure and its electrical parameters can be readily understood. This paper describes the further development of that model.

2. The Equivalent Circuit Model

A helix slow-wave structure consists essentially of a coaxial transmission line with a helical inner conductor which is held in place by several (usually three) dielectric rods. The phase velocity of the waves on such a structure is usually around one tenth of the velocity of light and the characteristic dimensions are much less than a free-space wavelength. For this reason it is legitimate to model the slow-wave structure by an equivalent circuit whose parameters are determined from quasi-static solutions to Maxwell's equations. The advantages of this approach are that the parameters have fixed values which depend only on the geometry of the slow-wave structure and that the ways in which the electrical properties of the structure are related to its dimensions become easier to understand. If approximate, closed-form, expressions are used to determine the values of the parameters then the model can easily be constructed on a spread-sheet making it particularly simple to use.

For the purposes of constructing the model the helical geometry is ignored, except for the inclusion of the current path from turn to turn, on the grounds that the pitch angle is small (typically 10°). The slow-wave structure is represented by a set of equally spaced wire loops supported by a homogeneous dielectric within a concentric conducting shield as shown in Fig. 1. In order to construct the equivalent circuit it is simplest to consider the capacitances and inductances separately.

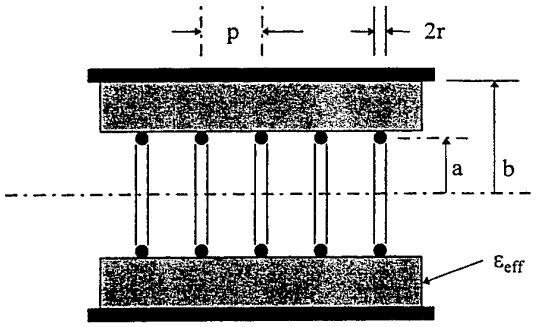

Fig.1 Arrangement of the structure modelled

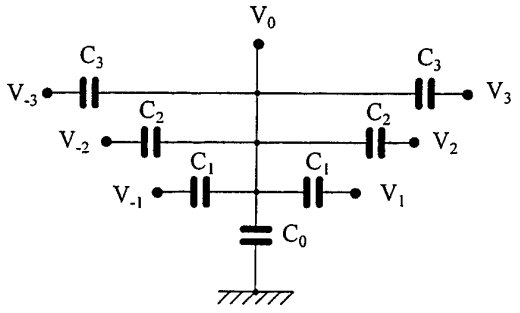

Fig.2 Network of capacitances relating to one turn

Figure 2 shows the network of capacitances relating to one turn. The coefficients of capacitance are the self-capacitance (C_0) between that turn and the shield and the mutual capacitances (C_n) linking it to the other turns. It is assumed that the voltage between each turn and the shield is given by $V_n = V \exp j(\omega t - n\beta p)$ where n is the serial number of the turn. Then the current flowing from the turn through the network of capacitances is given by

$$i = C_0 \frac{\partial V_0}{\partial t} + \sum \left\{ C_n \frac{\partial}{\partial t}(V_0 - V_n) + C_n \frac{\partial}{\partial t}(V_0 - V_{-n}) \right\} \quad (1)$$

Substituting for V_n in (Eq. 1) and rearranging yields

$$i = \left\{ C_0 + 4 C_n \sin^2(n\beta p/2) \right\} \frac{\partial V_0}{\partial t} = C \frac{\partial V_0}{\partial t} \quad (2)$$

so that the effective capacitance to ground (C) from this node is given by the expression in braces in (Eq. 2).

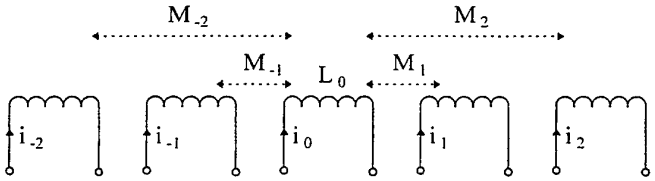

Fig.3 Network of inductances linking adjacent turns

Figure 3 shows the network of inductances linking adjacent turns. If we assume that the current in each turn of the helix is given by $i_n = i \exp j(\omega t - n\beta p)$ then potential difference between the turns is given by

$$V = L_0 \frac{\partial i_0}{\partial t} + \sum \left\{ M_n \frac{\partial i_n}{\partial t} + M_n \frac{\partial i_{-n}}{\partial t} \right\} \quad (3)$$

Substituting for i_n in Eq. (3) and rearranging yields

$$V = \left\{ L_0 + \sum 2M_n \cos(n\beta p) \right\} \frac{\partial i_0}{\partial t} = L \frac{\partial i_0}{\partial t} \quad (4)$$

so that the effective series inductance between turns (L) is given by the expression in braces in (Eq. 4).

The slow-wave structure can therefore be represented by a transmission line whose series inductance and shunt capacitance per unit length are L/p and C/p respectively. This transmission line has phase velocity and characteristic impedance given by $v_p = p/(LC)^{1/2}$ and $Z_0 = (L/C)^{1/2}$. It can be shown (Ref. 7) that the Pierce interaction impedance is given by:

$$K = Z_0 \left[\frac{\sin(\beta p_1/2)}{\beta p_1/2} \right]^2 \left[\frac{\sin(\beta g_1/2)}{\beta g_1/2} \right]^2 \frac{\cos^4 \psi}{I_0^2(\beta a_i)} \quad (5)$$

where p_1 is the axial separation of points on the centre lines of adjacent turns which lie on a line perpendicular to the direction of the wire, g_1 is the gap between turns measured in the axial direction a_i is the inside radius of the helix and I_0 is the modified Bessel Function of the first kind.

3. Determination of the Circuit Parameters

The charges on each capacitor can be expressed by the infinite matrix equation

$$\begin{bmatrix} \cdot \\ q_{-2} \\ q_{-1} \\ q_0 \\ q_1 \\ q_2 \\ \cdot \end{bmatrix} = \begin{vmatrix} \cdot & \cdot & \cdot & \cdot & \cdot & \cdot & \cdot \\ \cdot & C_0 & C_1 & C_2 & C_3 & C_4 & \cdot \\ \cdot & C_1 & C_0 & C_1 & C_2 & C_3 & \cdot \\ \cdot & C_2 & C_1 & C_0 & C_1 & C_2 & \cdot \\ \cdot & C_3 & C_2 & C_1 & C_0 & C_1 & \cdot \\ \cdot & C_4 & C_3 & C_2 & C_1 & C_0 & \cdot \\ \cdot & \cdot & \cdot & \cdot & \cdot & \cdot & \cdot \end{vmatrix} \begin{bmatrix} \cdot \\ V_{-2} \\ V_{-1} \\ V_0 \\ V_1 \\ V_2 \\ \cdot \end{bmatrix} \tag{6}$$

Here C_0 is the capacitance between a ring and the shield and the other coefficients are the mutual capacitances between pairs of rings. Since the magnitudes of C_n decrease as $|n|$ increases it would be possible, in principle, to determine their values from a numerical solution of Laplace's equation in which the central ring of a finite set was held at a known positive voltage and all the other rings and the shield were fixed at zero potential. The coefficients of capacitance would then be given by the ratio of the charge on each earthed electrode to the potential of the central ring. By inverting the capacitance matrix we obtain the matrix of the potential coefficients

$$\begin{bmatrix} \cdot \\ V_{-2} \\ V_{-1} \\ V_0 \\ V_1 \\ V_2 \\ \cdot \end{bmatrix} = \begin{vmatrix} \cdot & \cdot & \cdot & \cdot & \cdot & \cdot & \cdot \\ \cdot & P_0 & P_1 & P_2 & P_3 & P_4 & \cdot \\ \cdot & P_1 & P_0 & P_1 & P_2 & P_3 & \cdot \\ \cdot & P_2 & P_1 & P_0 & P_1 & P_2 & \cdot \\ \cdot & P_3 & P_2 & P_1 & P_0 & P_1 & \cdot \\ \cdot & P_4 & P_3 & P_2 & P_1 & P_0 & \cdot \\ \cdot & \cdot & \cdot & \cdot & \cdot & \cdot & \cdot \end{vmatrix} \begin{bmatrix} \cdot \\ q_{-2} \\ q_{-1} \\ q_0 \\ q_1 \\ q_2 \\ \cdot \end{bmatrix} \tag{7}$$

Thus an alternative way of obtaining the values of C_n is to use a numerical solution to find the P_n from the potentials at each of the rings due to a known charge placed on the central ring and then to invert the matrix of potential coefficients.

In the same way the self and mutual inductances can be determined from numerical solution for the field of a single current loop. The solution, in this case, cannot be a simple quasi-static solution because the eddy currents induced in the shield cause all the flux to be confined within it. To generate a static solution either the region outside the shield must be defined as having zero permeability, or else the region within the shield must have a very high permeability so that the flux outside it is effectively zero. The inductances are assumed to be associated solely with the tangential component of the current. The contribution from the axial component of the current is negligible.

4. Approximate Expressions for the Circuit Parameters

Since the circuit parameters are determined from quasi-static solutions to the field problem it is possible to generate simple approximate expressions for them using elementary methods. The approximate model developed in this way can readily be programmed on a spread-sheet and it is accurate enough to make it a useful tool for exploring the ways in which the properties of the slow-wave structure depend on its dimensions. If the shield radius is very large then the electric field around a charged ring is essentially that of the ring in free space. The potential at a point on the axis of a ring of radius a carrying charge q is given by

$$V = \frac{q}{4\pi\epsilon_0} \frac{1}{\sqrt{a^2 + z^2}} \tag{8}$$

where z is the distance of the point from the plane of the ring and the zero of potential is taken at infinity. The coefficient of potential of the nth ring is then

$$P_n = \left(4\pi\epsilon_0 \sqrt{a^2 + n^2p^2}\right)^{-1} \tag{9}$$

No simple expression for P_0 exists but we note that, if equal charges are placed on all the rings, then the situation is very similar to that of a uniformly charged rod carrying charge q/p per unit length. When the shield radius is large we expect that

$$V = \frac{q}{2\pi\epsilon_0 p} \ln(b/a) = P_0 q + \frac{q}{2\pi\epsilon_0 p} \sum_{n=1}^{\infty} \frac{1}{\sqrt{a^2 + n^2p^2}} \tag{10}$$

whence

$$P_0 = \frac{1}{2\pi\epsilon_0 p} \ln(b/a) - \frac{1}{2\pi\epsilon_0 p} \sum_{n=1}^{\infty} \frac{1}{\sqrt{a^2 + n^2p^2}} \tag{11}$$

If the radius of the shield is reduced then the potential will fall off more rapidly with distance than indicated by (Eq. 8).We have not yet been able to find an appropriate expression for this and have used it as a parameter to fit the computed curves to the experimental results. The effects of dielectric support rods can be included by replacing ϵ_0 by the effective permittivity ϵ_{eff} in the first term of (Eq. 11) and by $(1 + \epsilon_{eff})/2$ in the second term. This assumes that the dielectric support rods only affect the part of the longitudinal electric field lying between the helix and the shield. The coefficients of capacitance required by the model can then be computed by inverting the matrix of coefficients of potential. We found that including terms up to n = 5 gave satisfactory results.

The self-inductance of a loop of wire in free space is given by (Ref. 8)

$$L_0 = \mu_0 a (\ln(8a/r) - 2) \tag{12}$$

For a tape helix we assumed that

$$r = (w + t)/\pi \tag{13}$$

and the mutual inductances are given approximately by

$$M_n = \frac{\mu_0 a}{2} \frac{a^3}{(a^2 + n^2p^2)^{3/2}} \tag{14}$$

The effect of reducing the shield radius is to increase the reluctance of the return path for the flux and so reduce both the self and the mutual inductances. The reduction factor is easily shown to be $(1 - (a/b)^2)$ for the case of a uniform solenoid whose external field is constrained to lie within a concentric boundary of radius b. This factor gave satisfactory results.

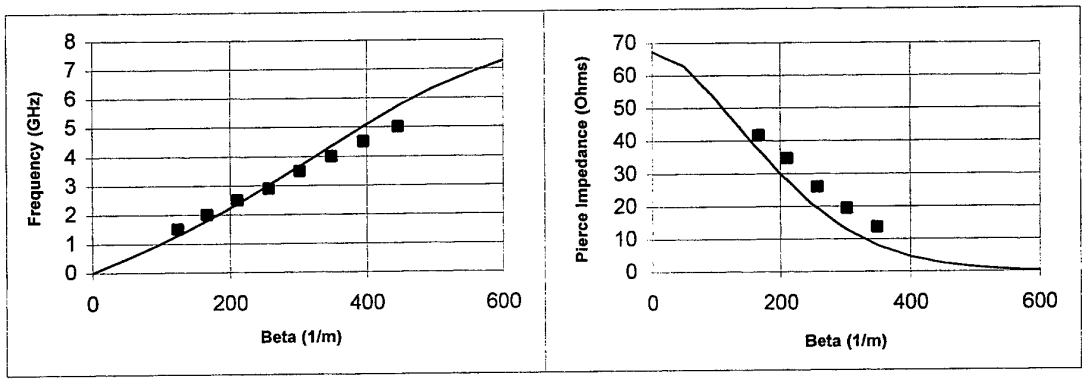

Fig. 4 Experimental and computed results for a helix without dielectric loading
(a = 4.8 mm, b = 7.0 mm, p = 7.0 mm, w = 1.4 mm, t = 1.0 mm)

This approximate theory has been programmed on a spread-sheet. It has been found possible to fit the model to most sets of experimental data by adjusting the parameter representing the effect of the shield on the mutual capacitances. Figures

4 and 5 show typical results obtained with this approximate model. The computed curves are generally close to the experimental results.

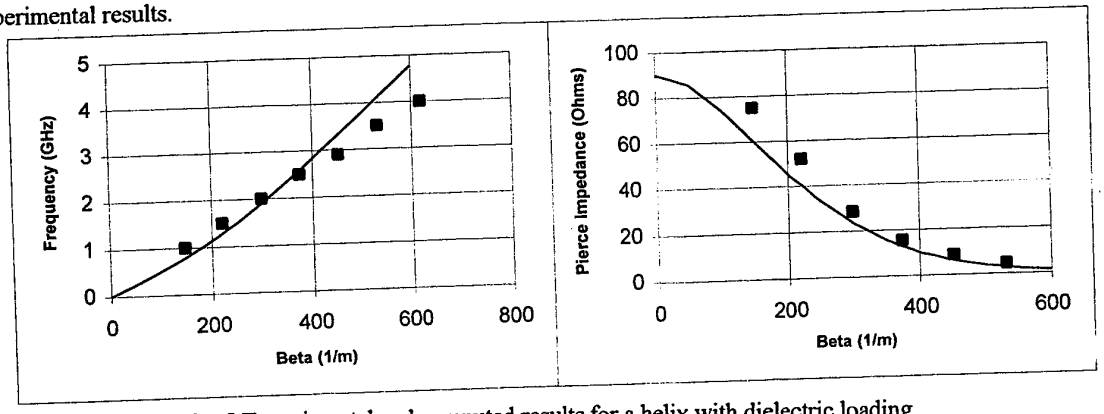

Fig. 5 Experimental and computed results for a helix with dielectric loading
(a = 4.7 mm, b = 9.0 mm, p = 4.9 mm, w = 1.0 mm, t = 1.0 mm, 3 support rods, 30° angles, $\epsilon_r = 9.3$)

5. Conclusion

The model showed an acceptable fit to experimental data when approximate expressions were used for the circuit parameters. This tends to confirm the validity of the model. It is believed that its accuracy could be improved still further by using more accurate values for the circuit parameters.

6. References

1. Wang, P, Carter, RG and Basu, BN, An improved technique for measuring the Pierce impedance of helix slow-wave structures, Proc. 24th European Microwave Conference, Cannes, Sept. 1994,

2. Sensiper, S, Electromagnetic wave propagation on helical conductors, ScD Thesis, Dept. Elec. Engg., MIT, 1951

3. Stark, L, The lower modes of a concentric line having a helical inner conductor, J. App. Phys., Vol.25, pp.1155-62, 1954

4. Paik, SF, Design formulas for helix dispersion, IEEE Trans. Electron Devices, Vol.ED-16, pp.1010-14, 1969

5. Jain, PK, Basu, BN and Sinha, AK, Analytical approaches to the study of helical slow-wave structures for broadband TWTs, IETE Tech. Rev., Vol.10, No.4, pp.369-78, 1993

6. Ward, KD and Wlodarczyk, J, Transmission line modelling of helix slow-wave structures, Proc. Int. Electron Devices Mtg., p.7.5.1-4, 1993

7. Carter, RG and Wang, P, An equivalent circuit model for helix slow-wave structures, Proc. CAE Workshop, Conf. Microwaves 94, London, Oct. 1994

8. Ramo, S, Whinnery, JR and van Duzer, TV, Fields and Waves in Communication Electronics, Wiley, New York, 1965

A Three-Dimensional Finite-Element Simulator for the Design of High Efficiency TWTs Multistage Depressed Collectors

S. Coco*, S. D'Agostino**, F. Emma***
* University of Catania, Faculty of Engineering (I)
** University of Rome "La Sapienza", Faculty of Engineering (I)
*** ESA/ESTEC (NL)

Abstract

During past years, ESTEC has been actively involved in the development of new software tools for Travelling Wave Tubes (TWTs) design. Recently, in the frame of this activity, an integrated software package for TWT's design has been realised. An important part of this integrated environment is a novel, fully three-dimensional, finite element simulation tool for collector's design. The development of this program has been carried out in co-operation with the University "La Sapienza" of Rome and the University of Catania. This paper discusses the basic philosophy of the developed finite-element code, together with its main features. In particular, the attention is focused on the dedicated fully three-dimensional mesh generator and the strategy followed for the solution of the coupled electromagnetic and motion problem within the same finite element discretization context. Some examples of simulations carried out and projections of future improvements are also provided.

Introduction

Traveling Wave Tubes are components used for the generation of high R.F. power levels since early forties till now, for various civil and military applications ranging from telecommunications to radar systems. Although the basic principles of TWTs have remained unchanged, refinements in design methods, improvements in materials and the availaibility of new more powerful Computer Aided Design tools, have led to more efficient, smaller, and more reliable Traveling Wave Tubes.
One of the key elements to achieve high efficiency (especially in space applications), linear performance and several other advantages, is the effective design of multistage depressed collectors (up to five/six stages for advanced applications). In fact, when the spent beam enters the collector region after the interaction with the R.F. signal, it carries useful power that is lost in the collector region, where a relatively large fraction of the input power is dissipated. With multistage depressed collectors, the slower electrons are addressed towards low voltage electrodes, while the faster ones are addressed towards high voltage electrodes. As a consequence of this electron sorting, the collector can recover a significant percentage of the spent beam energy, thus increasing the TWT overall efficiency.
In order to recover the maximum fraction of the power from the spent beam and avoid the reflection of electrons back to the delay line, the electric field in the collector region must be properly shaped. This means that the collector's electrodes shall be designed and optimized to sort the electrons of the beam into different energy classes. In the ideal case, when the beam enters the collector, if the electron velocity goes down to zero, no heat is generated and no power is dissipated. The possibility of simulating arbitrarily shaped, non-symmetrical collector's electrodes is of paramount importance to achieve high level of efficiency, thus a three-dimensional simulation code is needed to carry out the design process. The tools currently available to perform a collector design are normally, either 2D codes, or 3D programs based on the finite difference method (FDM). Both these kind of tools may be inadequate to carry out accurate simulations of new collector's geometries.
In fact, the current non axi-symmetrical collectors very often utilised for highly efficient, space TWTs, cannot be simulated by using 2D tools, while the 3D FDM programs do not allow a very flexible meshing and therefore do not lend themselves to accurately simulate complex geometries. To overcome these limitations, a finite-element approach can be pursued, this gives the possibility of using irregular meshes to fit properly the collector's geometry, additionally a mesh refinement in critical regions can be easily performed. This flexibility in mesh generation gives furthermore relevant advantages in terms of computational effort, because it makes use of only

the strictly required degrees of freedom in the discretization process.
In this paper we present a fully three-dimensional code, based on the finite element method (FEM), for the simulation of multistage depressed TWT's collectors. The complete tool consists of a dedicated fully three-dimensional mesh generator, a finite-element Poisson solver with an integrated electron trajectory tracer and a post-processing module for result restitution.
The paper is structured as follows: in Section 2 a sintetic description of the features of the code is given; in Section 3 some examples of collector simulations are presented; the authors' conclusions follow in Section 4.

The FE Code for TWT's collector analysis

The code is written in Standard ANSI C language and has been developed on a SPARC 20 Sun Solaris workstation under the UNIX operating system. The code architecture follows the classical scheme of FE codes in which three distinct main programs are devoted to preprocessing, processing and postprocessing phases respectively.
The presentation focuses on the aspects which are relevant to TWTs collector design, neglecting all the standard FEM SW description. More precisely, the dedicated mesh generator, the iterative solution of the Poisson and dynamical equations are described. In the same context the organization of data adopted is illustrated and a brief overview of the postprocessing functions is also offered.

Mesh Generation

The developed preprocessor has been expressely conceived in order to facilitate the definition of geometrical data and boundary conditions. It allows to obtain a fully 3D discretization of collector regions of arbitrary shape by following a dedicated strategy. In this specific strategy the collector geometry is thought as the union of building blocks of simpler shape. The building blocks considered consist of cylinders, cones, slanted apertures, which can be positioned on or off axis and other non axisymmetrical blocks like spikes, etc.
The entire process of mesh generation is thus articulated in two steps: in the first one a rough partition of the whole geometry into simpler domains is actuated by individuating the pertinent costituent blocks from an apposite catalogue. Each block is specified by assigning a suitable set of the 3D discretization process curved boundary surfaces parameters such as lengths, radii, angles, etc. In of building blocks are locally approximated by plane rectangular surfaces (in the same way as circular boundaries in 2D problems are approximated by the union of straight line segments).
In the subsequent step the connected regions so obtained are partitioned into finite elements of tetrahedral shape; tetrahedra are used because of their flexibility in approximating complicated geometries. Presently the definition of the basic collector blocks is carried out by using an interactive / batch modality. The boundary conditions for the electromagnetic problem are imposed during the mesh generation by associating at each electrode the pertaining voltage. The output of the mesh generation program is an ASCII file containing all the geometrical information regarding the collector geometry together with the boundary conditions required for the problem.

Iterative Solution of the Poisson and Dynamical Equations

The fundamental objective of the simulation is the determination of the electrical field inside the collector, which depends on the voltages assigned on the electrode surfaces and on the space charge constituted by the electron beam transitating across the collector region.
The resulting coupled electromagnetic-motional problem is governed by a Poisson equation for the associated with the electron dynamic equations.
Since the space-charge distribution is not known a priori, the numerical solution of the above complete set of equations has been conveniently performed by following a two-step iterative scheme.
In the first step an initial guess (usually zero) for the unknown space-charge density is assumed and the Poisson equation is solved. Starting from the obtained potential values, the electrical field in the collector region is easily derived. This electrical field distribution is used in the subsequent step to determine the electron trajectories by solving the dynamical equations. From the calculated trajectories a more accurate evaluation of the charge distribution is computed and used to perform a new Poisson-solver step and an improved electrical field distribution is obtained. The above two steps are iteratively repeated until convergence is reached. This guarantees that the current solution is congruent with the charge distribution computed in the previous step.
The procedure stops when the "distance" between two consecutive solutions is less than an user-specified end-iteration tolerance.

In Fig. 1 the functional block diagram of the processing program is shown.

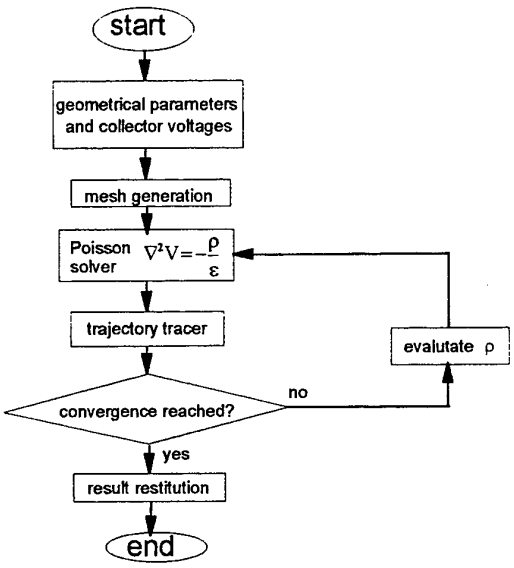

Fig. 1 - Block diagram of the FE simulator

A summary description of its constituent blocks is given hereafter.
In the FE solution of the Poisson equation the potential v(P) within each tetrahedral finite element is approximated in terms of unknown nodal values v_i at N_e tetrahedral nodes and Lagrange interpolation polynomials $\alpha_i(P)$ as:

$$v(P) = \sum_{i=1}^{N_e} v_i \, \alpha_i(P)$$

A classical variational approach is then followed: the solution is obtained by minimizing the approximated energy functional for the Poisson problem. This leads to a global linear algebraic system in all the unknown nodal potential values which is built by ordinately adding all the contributions coming from the finite elements.
The solution of such algebraic system is carried out by using iterative solvers and the associated electrical field distribution is obtained by direct derivation from the calculated potentials.
The computed electrical field distribution within each tetrahedron is used for the determination of the electron trajectories. The trajectory tracer solves the dynamical equations by using a standard fourth-order Runge-Kutta integrator.

The evaluation of the space-charge density is then easily obtained by counting the number of electrons within each tetrahedron.
The adopted data structure is suitable for an easy addition of new procedures to get a more sophisticated modeling of the device, without introducing relevant modifications to the code.

Postprocessing

The implemented postprocessing functions presently allow 3D displaying of geometries, displaying of potential nodal values, 2D restitutions (contour line plotting), 3D axonometric trajectory tracing and evaluation of global quantities (such as charge and current)

Simulation of two collector's geometries

The code operation has been tested by running several examples of collector's geometries. Here below, in order to show some of the present code capabilities two different simulations are reported. The two study-cases presented regard an axisymmetrical two stage collector and an asymmetrical single stage collector respectively.
In figs. 2 and 3 the two collector geometries are shown.

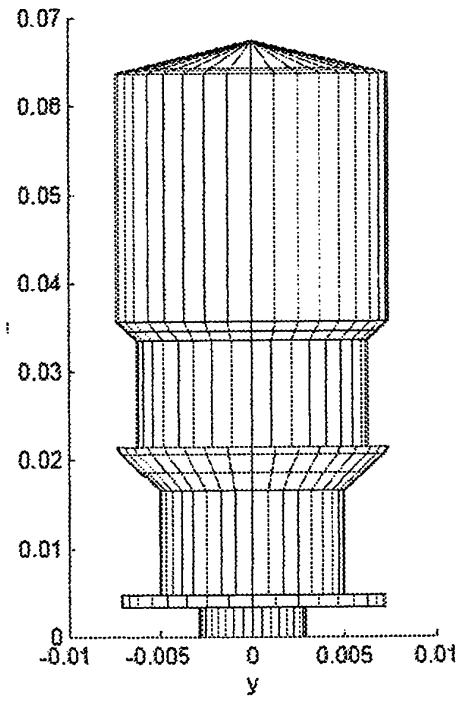

Fig. 2 Axisymmetrical two-stage collector

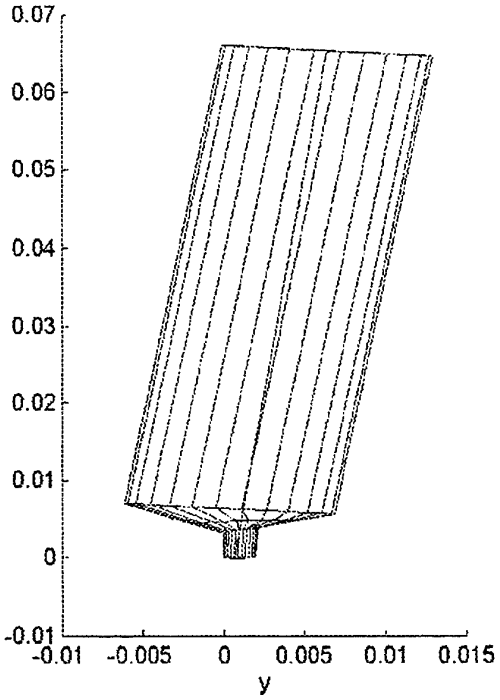

Fig. 3 Asymmetrical single-stage collector

For these collectors two irregular tetrahedral meshes have been used. Two sections of the mesh utilised are illustrated in figs. 4 and 5 (note that the number of employed tetrahedra is greater in the region where the beam is expected to be more concentrated). The single stage mesh consists of 16223 first-order tetrahedral finite elements. The number of unknown potential values in the Poisson solver is 4180.

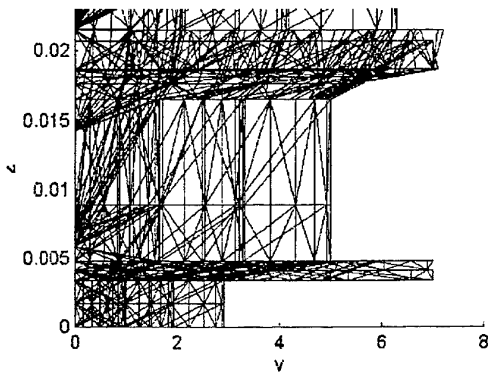

Fig. 4 Mesh at the two stage collector input

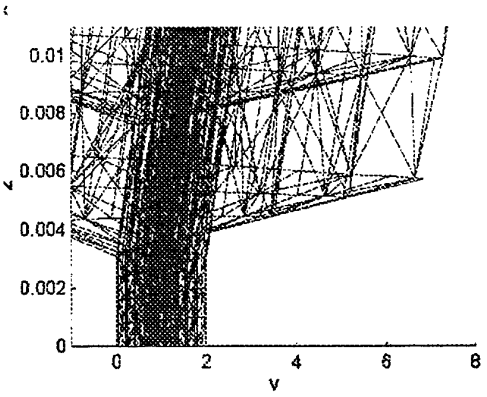

Fig. 5 Mesh at the single stage collector input

The dual stage mesh consists of 25354 first order tetrahedral finite elements. The number of unknown potential values in the Poisson solver is 7590.

The trajectory plots for the two collector are shown in figgs. 6. and 7

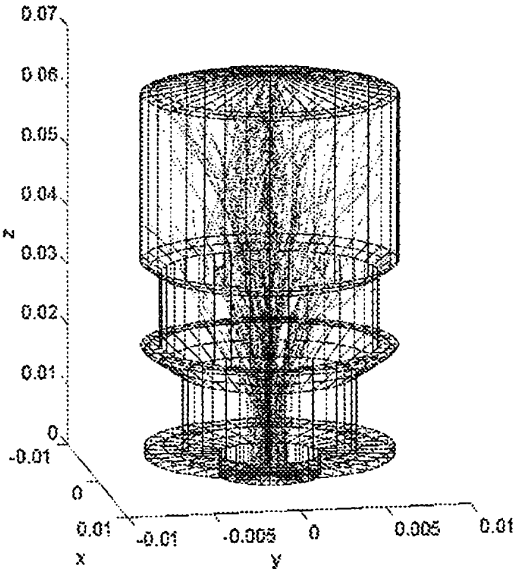

Fig. 6 Dual stage trajectory plot

The results obtained from these simulations, in terms of collector's stages currents and efficiency, are in good agreement with available experimental data.

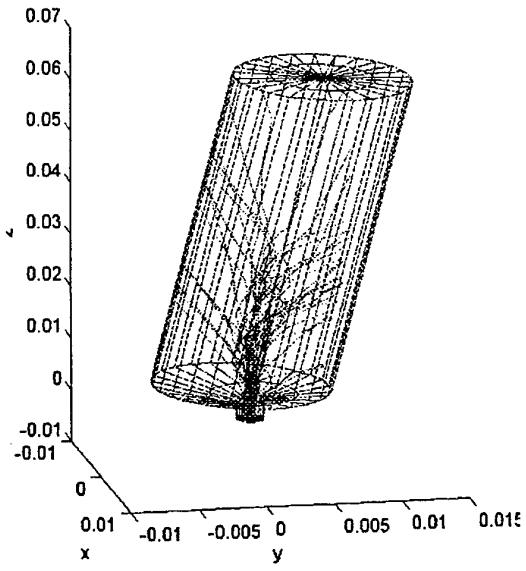

Fig. 7 Single stage trajectory plot

Conclusions

In this paper the first release of a FE code for simulation of TWT's collectors has been presented. The present version of the code has been used to perform the analysis of two sample collectors, and the obtained results are in good agreement with measure, available data. The code capabilities are being expanded in several directions. A more sophisticated and general 2D and 3D mesh generator is currently being developed. Utilization of high-order and/or curved-side elements is foreseen in processing. Other postprocessing function are going to be added to facilitate the designer. The objective of this work is to provide the user with a flexible and effective tool to design, test, optimize and verify new geometries for collectors.

Acknowledgements

The authors gratefully aknowledge the contribution of Dr. P. Galuppi from ALELCO who provided the data utilised for the simulations.

REFERENCES

[1] P. Silvester: "Construction of triangular finite element universal matrices". *Intemational Joumal for Num. Methods in Eng.*, vol.12, pp.237-244, 1978.

[2] J. A. Dayton, H. G. Kosmahl, P. Ramins and N. Stankiewicz: "Analytical prediction and experimental verification of TWT and depressed collector performance using multidimensional computer programs". *IEEE Trans. on Electron Devices*, vol. ED-26, no.10, Oct.1979.

[3] P. Ramins and T. A. Fox: "Efficiency enhancement of octave bandwidth TWT's by the use of multistage depressed collectors". *NASA Tech. Paper* 1416, 1979.

[4] H. G. Kosmahl: " Modern multi-stage depressed collectors- a review" *Proc. IEEE*, vol. 70, no.llpp. 1325-1334, Nov.1982.

[5] D. A. Lindholm: "Automatic Triangular mesh generation on surfaces of polyhedra". *IEEE Trans. on Magnetics*, vol. MAG-19, no.6, pp. 2539-2542, Nov.1983.

[6] Z.J. Cendes, D. Shenton, H. Shahnasser: "Magnetic field computation using Detaunay complementary finite element methods". *IEEE Trans. on Magnetics*, vol. MAG-19, no.6, pp.2551-2557, Nov.1983.

[7] P. P. Silvester and R. L. Ferrari: " Finite elements for Electrical Engineers". Cambridge: *Cambridge Univ.* Press.1983.

[8] P. Ramins, H. G. Kosmahi, D. A. force, R. W. Paimer and J. A.Dayton Jr.: "Verification of computer-aided-design of Travelling Wave Tubes Utilizing Novel Dynamic Refocuser and Graphite Electrodes for the Multistage Depressed Collector" *NASA Tech. Paper* 2524, 1985.

[9] J.C. Cavendish, D.A. Field and W. Frey: 'An approach to automatic three-dimensional finite element mesh generation". *Intemational Joumal for Num. Methods in Eng.*,vol.21, pp. 329-347, 1985.

[10] B.Joe and R.B. Simpson: "Triangular meshes for regions of complicated shapes. *International Joumal for Num. Methods in Eng.*, vol.23, pp.751-778, 1986.

[11] P. Spatke, S. Wipf, "KOBRA3, a code for the calculation of space charge influenced trajectories in 3-dimensions", *GSI, Darmstadt*, June 1989.

[12] L. Kumar, R.G. Carter, and D. Perring: "Three-Dimensional Modelling of Asymmetric Depressed Collectors. *GSI, Darmstadt*, 1990.

[13] L. Kumar and R. G. Carter: "Microwave tube design: 3-D depressed collectors, Final Report" Report No.MRG/91/2, *Lancaster University*, Lancaster, Apr.1991.

[14] K.F. Bartos, E.B. Fite, K.A. Shalkhauser, G.R. Sharp " A Three-Dimensionale Finite-element Thermal/Mechanical analytical technique for High-Performance Travelling Wave Tubes" *NASA Technical Paper* 3081 - June 1991

[15] B. Joe: "Delaunay versus max-min solid angle triangulations for three dimensional mesh generation". *International Joumal for Num. Methods in Eng.*, vol-31, pp. 987-997, 1991.

[16] B. Joe: "Tetrahedral mesh generation in polyhedral regions based on convex polyhedron decompositions". *Intemational Joumal for Num. Methods in Eng.*, vol.37, pp. 693-7139 1994,

[17] L. Kumar, P. Spatke, R.G. Carter, and D. Perring, "Three-Dimensional Simulation of Multistage Depressed Collectors on Micro-Computers". *IEEE Trans. on Electron Devices*, vol.ED-42, no.9, pp.1663-1673, September 1995.

A New Criterion for the Comparison of TWT and Linearized TWT and for the Optimization of Linearizers used in Transmission Systems

Jacques SOMBRIN

CNES, 18 Avenue Edouard BELIN, 31401 TOULOUSE Cedex 4, FRANCE

Abstract

In this paper we present a new criterion that is based on the optimization of the curve giving the carrier to noise plus intermodulation ratio C/(N+I) as a function of the consumed power.

We apply the criterion to the comparison of TWTAs, linearized TWTAs and SSPAs.

It can also be used to optimize a linearizer or the operating point of a given TWTA in a transmission system.

Introduction

Usual characteristic curves such as amplitude conversion (AM/AM), phase conversion (AM/PM), efficiency (η) and carrier to intermodulation ratio (C/I), with respect to input power, output power or compression cannot be used directly to compare and select TWTs or amplifiers, to optimize a given amplifier or linearizer or to optimize the RF operating point of the chosen amplifier in a system.

In this paper we present a new criterion that is based on the optimization of the curve giving the carrier to noise plus intermodulation ratio C/(N+I) as a function of the consumed power.

The C/(N+I) ratio is generally used by system engineers during the computation of link budget for transmission systems. One considers generally that the received signal contains useful carriers or signals, additive noise and intermodulations. When the signal is complex enough the intermodulations can be approximated by a noise defined by its power or power density and added with the true noise in the link budget. This approximation is particularly valid for multicarrier operation (FDMA or CDMA) where the C/I ratio can be replaced by the noise power ratio (NPR).

$$\left(\frac{C}{N+I}\right)^{-1}=\left(\frac{C}{N}\right)^{-1}+\left(\frac{C}{I}\right)^{-1} \text{ or } \left(\frac{C}{N+I}\right)^{-1}=\left(\frac{C}{N}\right)^{-1}+(NPR)^{-1}$$

The consumed power is one of the main constraints in satellite payloads.

The optimization of the C/(N+I) ratio as a function of consumed power permits to obtain the best compromise between linearity and efficiency in an amplifier from the point of view of the system requirements and constraints.

Definition of the new criterion

We will first define the nominal output power of the amplifier, P_{nom}, e.g. the single carrier saturation output power P_{sat} for a TWTA or the single carrier output power at the 1 dB compression point P_{1dB} for a SSPA. Other conventional definitions can be used.

C is the total carrier power and P_{DC} is the power consummed by the amplifier.

We suppose that the amplifier gain is high enough (more than 20 dB). If this is not the case, we will add a reasonable driver power consumption or use the power added efficiency to compute the power consumption of a high gain amplifier obtained by chaining similar amplifiers.

We define the output RF operating point as $\Omega=C/P_{nom}$.

We can suppose that along with the C/I or NPR curve as a function of Ω we have measured (or obtained by simulation) the efficiency $\eta=C/P_{DC}$ as a function of Ω also. The efficiency is measured in the same conditions as the other curve, i.e. two carrier for C/I or multicarrier for NPR.

Generally C/I or NPR and η or PDC are given as a function of input drive or input back-off. Then a curve giving Ω as a function of the same parameter is necessary.

For the sake of clarity, all demonstrations will be made in the case of C/(N+I) ratio but can be applied also to NPR ratio.

As the amplifier will be used to transmit information through a noisy channel, we will define and use as a parameter in our computations the nominal power to noise ratio P_{nom}/N which is the signal to noise ratio that will be obtained in the channel when the amplifier delivers its nominal power. In this definition, N is the equivalent noise power in the channel bandwidth computed at the amplifier output.

For any given nominal power to noise ratio P_{nom}/N, we will draw a curve of C/(N+I) as a function of P_{DC}/N by the following method. Along this curve we have for each value of operating point $\Omega = C/P_{nom}$:

$$\frac{C}{N}\left(\Omega, \frac{P_{nom}}{N}\right) = \frac{C}{P_{nom}} \cdot \frac{P_{nom}}{N} = \Omega \cdot \frac{P_{nom}}{N};$$

$$\left[\frac{C}{N+I}\left(\Omega, \frac{P_{nom}}{N}\right)\right]^{-1} = \left[\frac{C}{I}(\Omega)\right]^{-1} + \left[\Omega \cdot \frac{P_{nom}}{N}\right]^{-1};$$

and:

$$\frac{P_{DC}}{N} = \frac{\frac{C}{N}\left(\Omega, \frac{P_{nom}}{N}\right)}{\eta(\Omega)} = \frac{\Omega}{\eta(\Omega)} \cdot \frac{P_{nom}}{N}.$$

We obtain a set of curves, one for each value of the parameter P_{nom}/N. This set of curves has an envelop that gives the optimum (highest) value of C/(N+I) for a given P_{DC}/N (figure 1).

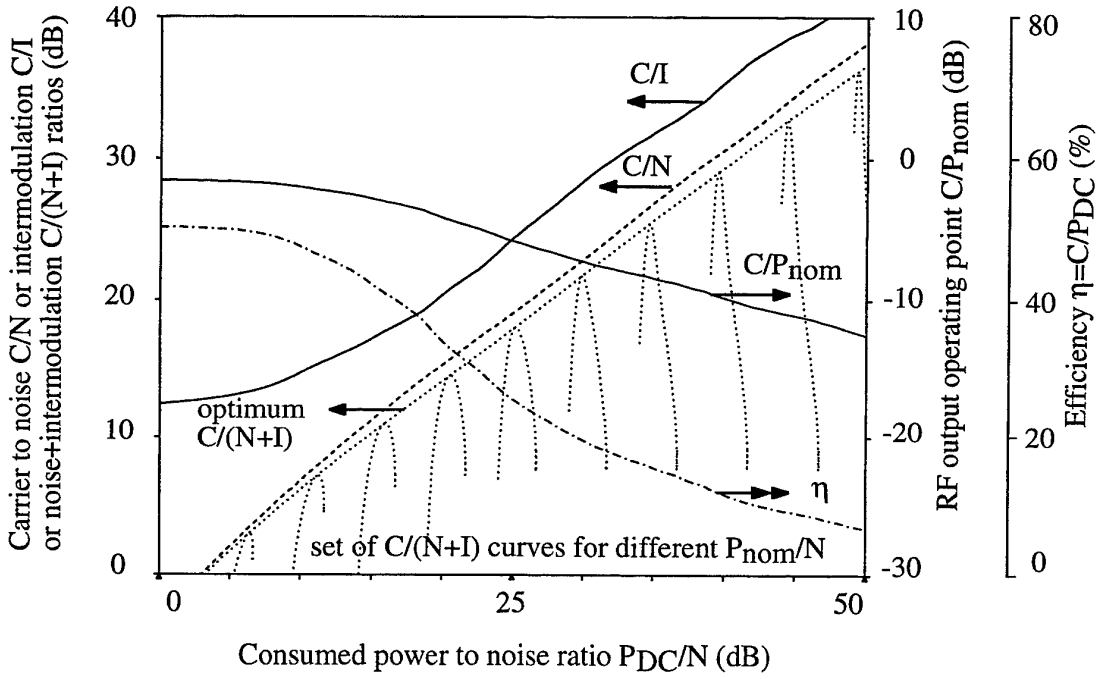

figure 1: TWT optimum C/(N+I) curve as a function of the ratio of consumed power to noise in the channel bandwidth: P_{DC}/N. Other curves give the optimum RF operating point and the C/N, C/I and efficiency corresponding to this point.

The TWT of figure 1 was chosen for good linearity and its maximum efficiency is 63 % at single carrier saturation. This efficiency is reduced to 50 % maximum in 2 carriers operation.

This envelop is the criterion that we need to compare different amplifiers. It is a function of the amplifier performances only and does not depend on N. However for a wanted C/(N+I), the nominal power and the consummed power of an amplifier will be proportional to the noise power N that will be computed from the link budget.

All useful parameters of the amplifier can be derived from this optimization, particularly the optimum nominal power given by the P_{nom}/N parameter of the curve that is tangent to the envelop at P_{DC}/N and the optimum operating point Ω_{opt} that gives the corresponding point on this curve.

Figure 1 shows some additional curves, they are the optimum ouput RF operating point Ω_{opt} and the C/N, C/I and efficiency η corresponding to this operating point for the same value of P_{DC}/N.

It must be stressed that the optimum C/(N+I) curve is different from the locus of all maxima of the set of curves. The optimum operating point obtained by this method is also different, it is generally lower than the one obtained by the classical method giving maximum C/(N+I) as a function of input or output power. These points are the same only for amplifiers having a constant power consumption with respect to the drive like class A amplifiers.

As can be seen the optimum C/(N+I) curve is monotonically increasing and is quite smooth. The same characteristics have been obtained for SSPAs.

Use of NPR or C/I

NPR measurements or simulations are more difficult than C/I measurements or simulations.

True NPR measurement equipment is less current and more specialized for a given frequency bandwidth than C/I measurement equipment: amplified noise sources, bandpass and bandstop filters.

Simulated NPR can be obtained with a finite number of equal amplitude, random phase carriers typically 16 to some thousands. They are equi-spaced in frequency and one or more carriers are missing in the center of the bandwidth where the NPR measurement will be made at the output of the amplifier.

For this type of NPR measurements a waveform synthesizer like the HP8770A can be used (Ref. 1). This measurement or simulation is affected by a systematic error which can be as high as 0.7 dB in small signal for 16 carriers (Ref. 2). This systematic error should be lower at saturation but it can be higher for some values of drive where the intermodulation is very low due to internal compensation of non-linearities in the amplifier. This error becomes negligible (less than 0.1 dB in small signal) for more than 100 carriers.

In addition to the systematic error, this measurement or simulation is affected by a huge random error because the total intermodulation at the frequency of one missing carrier is the sum of a great number of intermodulation products with random phases. Its power has an exponential probability distribution $\lambda e^{-\lambda x}$ and so its standard deviation σ is equal to its average value m: $\sigma = m = 1/\lambda$.

Averaging n independent power measurements will give a ratio of standard deviation over average $\sigma/m = 1/\sqrt{n}$ and about 0.5 dB average error for n=100.

Multicarrier simulations shown in this paper have been made with 10 000 random phase carriers and averaging on the missing central 1000 carriers, which are nearly independent, for a "worst case" $\pm 3\sigma/m$ error of ±0.5 dB.

The simulation time is much longer than the simulation time for two carriers C/I even with envelop transient analysis software (Ref. 3).

However NPR is preferred over two carrier C/I for the comparison of amplifiers because it is less sensitive to local improvements of the third order intermodulation C/I as a function of RF operating point.

It is better suited for the global optimization of an amplifier.

Figure 2 shows the curves obtained with NPR instead of 2 carriers C/I for the same TWT as in figure 1. Maximum efficiency is reduced to 47 % in multicarrier operation.

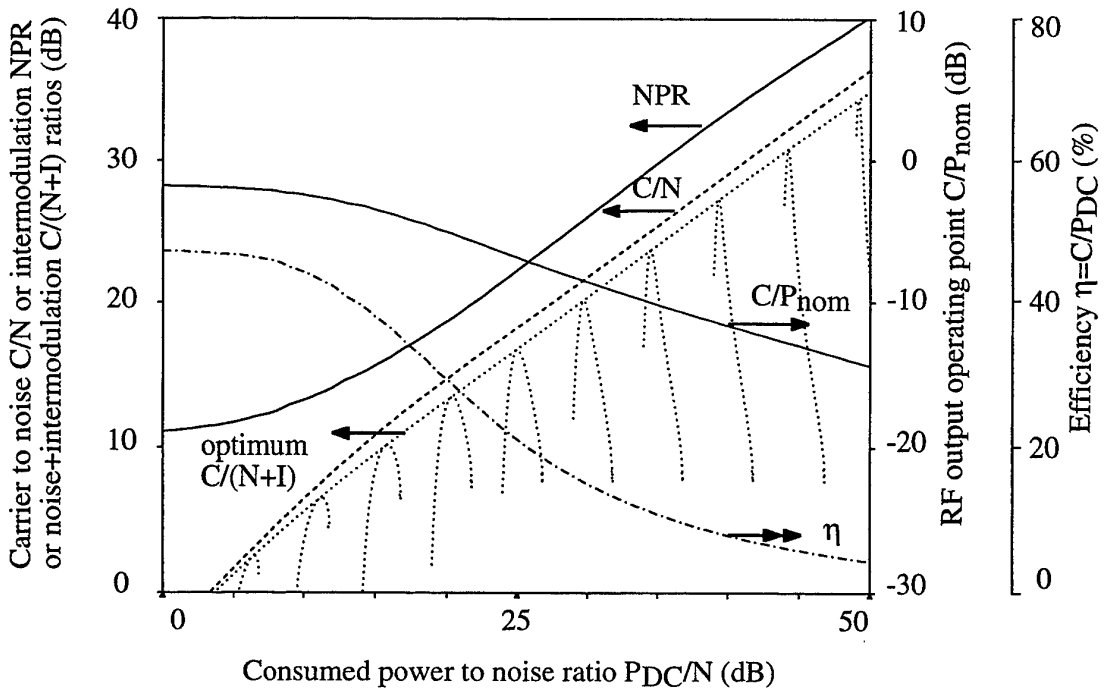

figure 2: same TWT as in figure 1, multicarrier instead of 2 carriers, optimum C/(N+I) curve as a function of the ratio of consumed power to noise in the channel bandwidth: P_{DC}/N. Other curves give the optimum RF operating point and the C/N, NPR and efficiency corresponding to this point.

Comparison of amplifiers or technologies

The comparison of amplifiers of different technologies has been up to now difficult, C/I curves as a function of input power show a better linearity for SSPAs compared to TWTAs while the same curves as a function of efficiency show the contrary and curves as a function of output power are in between. The important change of the AM/AM curve when using a linearizer makes also the comparison of TWTAs and linearized TWTAs difficult.

We now dispose of an objective method to compare two amplifiers even if they are of completely different technologies in the sense that the best one gives the highest C/(N+I) ratio for the lowest use of available DC power.

We only need to plot the optimum C/(N+I) curve as a function of P_{DC}/N for both amplifiers (for both amplifier technologies in fact as the output power of each amplifier is not pre-defined).

The method has been used to compare the TWT of figure 2 and the same TWT with a linearizer (figure 3), showing a possible improvement of between 1 and 2 dB, in agreement with experience at system level and much less than the more than 10 dB local improvement of C/I or NPR that can be obtained at well chosen points of input drive. The multicarrier operation maximum efficiency of the linearized TWTA has been increased to 50 %.

The computer aided design of an S Band AB class PHEMT amplifier (Ref. 4) has been evaluated.

This designed amplifier has a single carrier efficiency of 70 % at 2 dB compression point and an AM/AM curve with gain expansion that gives a local 2 carriers C/I improvement in the C/I range of 20 to 30 dB. However this does not give a much better NPR optimum C/(N+I) curve and introduces a degradation for higher values (figure 3).

The maximum multicarrier operation efficiency is 57 %, higher than the TWT or linearized TWT multicarrier efficiency (47 to 50%) but the optimum C/(N+I) curve is comparable to the TWT curve and it is lower than the linearized TWT curve.

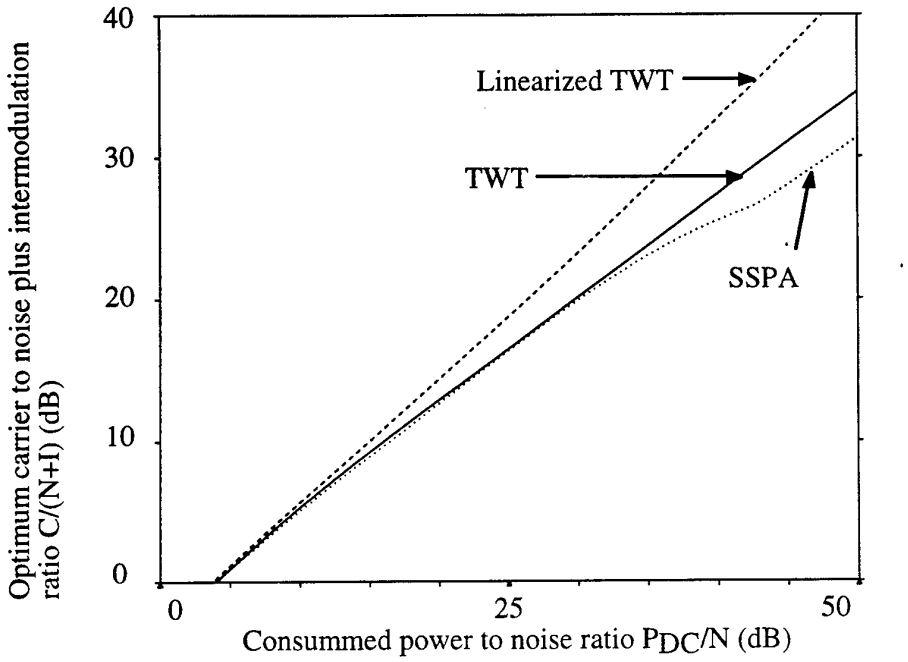

figure 3 : Comparison of TWT, linearized TWT and SSPA

One main result found during the study is that, using this criterion, state of the art linearized TWTs present a better compromise of efficiency and linearity than state of the art microwave SSPAs.

More results are given in (Ref. 5).

Specification and optimization of amplifiers or linearizers

We now dispose of a better method for specifying an amplifier, that is a method that constrains much less the design of the amplifier and its optimization. The method also gives the criterion to be used during the optimization of the amplifier.

A conventional specification of amplifier is based on the following 3 main performances :

- output power;
- C/I or NPR;
- efficiency or consumed power.

We propose to use the following ones :

- N: the noise power in the channel bandwidth at the output of the amplifier. It is fixed by link budget and receiver noise factor so it cannot be optimized at amplifier level. A change in this value will result in a change in nominal output power and consumed power of the amplifier but no change in the other characteristics like C/(N+I), C/I, C/N, drive, efficiency...
- C/(N+I): the carrier to noise plus intermodulation ratio. This defines the quality of the amplifier used in a noisy channel. It can be defined for 2 carriers or in multicarrier operation.
- P_{DC} or P_{DC}/N: the consumed power or its ratio to the noise power. This defines the amount of system resources that is used by the amplifier.

The optimizing process will be two-fold:

1) find an amplifier technology with a curve of C/(N+I) as a function of P_{DC}/N higher than the specified point;

2) choose a point on the part of this curve that verifies both C/(N+I) and P_{DC}/N specifications.

The parameter along the curve can be the amplifier nominal output power and this permits to re-use existing designs or use catalog components more easily.

If no available technology can be found that verifies both specifications, the criterion can be used to optimize the amplifier directly, propose the best feasible specification or design and optimize a linearizer.

The criterion will be used to compare linearizers designs when combining their pre-distorsion curves with that of the TWT, to chose the best design and to optimize the settings of the linearizer during integration tests.

Optimization of the operating point of the amplifier

The measurement of the amplifier will show a margin with respect to the specifications. This margin will be hopefully positive but in all cases it will be interesting to optimize the utilisation of the amplifier in the system. From the measured curves the optimum C/(N+I) as a function of P_{DC}/N curve can be obtained.

On this curve only one point correspond to the as-built amplifier, the point corresponding to the nominal output power. This point will also correspond to an optimum operating point.

If there is a positive margin a change in operating point will permit either to increase the C/(N+I) or to decrease the consumed power but the new operating point will not be optimum and will be under the optimum curve on the graph.

If the margin is negative a change in operating point may permit to satisfy one of the specification but at the cost of an even worse performance on the other.

Conclusion

A criterion has been proposed for the comparison of different amplifiers, amplifiers technologies or transmitter architectures.

This criterion has been applied to measurements or simulations of TWTAs, linearized TWTAs and SSPAs.

Some interesting results have been obtained on the usefulness and extent of the linearization of traveling wave tube amplifiers and the comparison with solid state power amplifiers: a linearized TWTA gives a better compromise between efficiency and linearity than SSPAs.

References

[1] M. M. Begue "Testing new digital RF communication systems with smart stimulus and analysis" in the 1995 advanced test solutions for aerospace and defence seminar.

[2] R. J. Westcott, "Investigation of multiple FM/FDM carriers through a satellite TWT operating near to saturation", Proc IEE, Vol 114, n° 6, pp. 726-740, June 1967.

[3] E. Ngoya, R. Larchevèque, "Envelop transient analysis: a new method for the transient and steady state analysis of microwave communication circuits and systems", 1996 IEEE MTT-S digest, pp 1365-1368

[4] M. Zoyo, "Conception et réalisation d'amplificateurs de puissance micro-ondes à l'état solide et à fort rendement pour des applications spatiales en bande S et en bande X", Thèse de doctorat de l'Université Paul Sabatier de Toulouse, 11 octobre 96

[5] J. Sombrin, "Critère de comparaison, d'optimisation et d'utilisation optimale des amplificateurs de puissance non-linéaires", Note Technique CNES, DT-96-16 CT/AE/TTL/HY du 24 mai 96

OPTIMIZING EFFICIENCY IN A COUPLED-CAVITY TWT WITH A SIMULATED ANNEALING ALGORITHM

Jeffrey D. Wilson

NASA Lewis Research Center
21000 Brookpark Rd., MS 54-5
Cleveland, OH 44135 USA
Phone: 216-433-3513 Fax: 216-433-8705 Email: jdwilson@lerc.nasa.gov

ABSTRACT

Decreasing the radio frequency (RF) phase velocity in the output section of a traveling-wave tube (TWT) is a technique commonly used to increase RF power efficiency. In order to optimize the profile of the phase velocity, a simulated annealing algorithm has been developed and implemented into the NASA multidimensional large-signal coupled-cavity TWT computer model. This algorithm allows the computer to determine the lengths of the individual cavities at the end of the output section necessary to provide the optimized phase velocity profile. The resulting nonlinear computer-generated phase velocity profile provides a design with optimized RF efficiency. In this paper, the optimization algorithm will be described and computational results will be shown. These results indicate an increase in center-frequency RF efficiency from 7.1% to 13.5% for a V-band coupled-cavity TWT.

INTRODUCTION

The mechanism for RF power amplification in a traveling-wave tube (TWT) involves the transfer of kinetic energy from electrons in an electron beam to the electromagnetic field of the traveling radio-frequency (RF) wave. In order to maximize this energy transfer, the majority of electrons in the beam must travel at near synchronous velocities with the phase velocity of the RF wave. This is generally accomplished by decreasing the circuit period in the last part of the TWT circuit, so that the phase velocity decreases in step with the decelerating electrons in what is referred to as a phase velocity taper.

Early phase velocity tapers for coupled-cavity TWT's used linearly decreasing tapers with up to three constant period sections (Refs. 1,2,3) to increase RF power efficiency. More recently, the phase-adjusted taper (PAT) design procedure (Ref. 4) was developed . A PAT was used to more than double the peak RF efficiency of a ferruleless coupled-cavity TWT (Ref. 5). Although successful, the PAT design methodology was limited to producing phase velocity profiles that maintained a constant relationship between the circuit phase velocity and the electron bunch velocity in the taper.

This paper describes an improved and more generalized approach to TWT design optimization based on a simulated annealing algorithm. The major advantage of simulated annealing is that it enables a globally optimized solution to be determined, while other optimization techniques converge on the closest local extremum. The algorithm is described and computational results from its implementation into the NASA multidimensional large-signal coupled-cavity TWT computer model are presented.

BACKGROUND

In conventional optimization procedures, perturbations are made to the input design variables. If the perturbations improve the output parameter to be optimized, more perturbations are made in the same direction. This continues until the output parameter no longer improves. These procedures can cause the solution to be easily trapped in a local extremum, that is one that is optimal with respect to a small neighborhood of input variables, but is not necessarily the global optimum over the entire range of possible input variable values. Simulated annealing avoids this problem by carefully allowing the

configuration of input variables to temporarily make the output parameter worse, enabling the solution to jump out of a local extremum and fall into a more productive path toward the global optimum.

The concept of combinatorial optimization by simulated annealing was introduced in the early 1980's (Ref. 6). The idea is derived from the annealing process in condensed matter physics, a thermal procedure for obtaining the lowest energy (ground) state for a solid. In this procedure, the solid is first heated to just below its melting temperature and is then slowly cooled. This causes the randomly arranged atoms to gradually arrange into the highly structured lattice of the ground state in which the energy of the system is minimized. The essence of the procedure is that the slow transformation from a random to a highly ordered state allows the atoms to escape from meta-stable energy states with localized energy minima. If the initial temperature is not high enough or if the cooling is too rapid, the resulting solid will be at a higher energy than the ground state.

The simulated annealing formulation is based on the Metropolis algorithm (Ref. 7). From the starting configuration of the heated solid, a random atom is moved to a new location. If the resulting energy is reduced, the new configuration is automatically accepted as the starting point for the next move. However, if the energy increases, the new configuration also has a possibility of being accepted. This possibility is high at high temperatures and decreases as the temperature cools. The probability of acceptance $P(\Delta E)$ is modeled with a Boltzmann distribution

$$P(\Delta E) = \exp(-\Delta E/kT) \qquad [1]$$

where ΔE is the change in energy and kT is a base energy with k as Boltzmann's constant and T as temperature. This probability is then compared to a random number between 0 and 1. If the random number selected is less than $P(\Delta E)$, the new configuration is saved; if not, the previous configuration is used to start the next step. This basic step is repeated many times until equilibrium is reached at temperature T. This step continues to be repeated at a succession of lower temperatures until final equilibrium is attained. The beginning temperature is high enough to allow most uphill moves. As the temperature cools, fewer uphill moves are allowed, until at the coldest temperature the solution freezes into its final form with virtually no chance of an uphill move being accepted. In applying simulated annealing to general problems, the energy in the Metropolis algorithm can be replaced by any quantity to be optimized. Simulated annealing has been used to solve optimization problems in a wide variety of areas including operations research, very large-scale integrated (VLSI) circuit design, code design, image processing, and molecular physics (Ref. 8).

ANALYSIS

The NASA multidimensional large-signal TWT model (Refs. 9, 10, 11, 12) determines the interaction between a two-dimensional slow-wave RF circuit field and an electron beam with disks or rings of electrical charge which have axial, radial, and azimuthal velocity components. The amplitude and phase of the RF circuit electromagnetic field and the trajectories of the electron disks or rings are determined from the calculated axial and radial space-charge, circuit and magnetic forces as the disks or rings pass through the individual cavities of the circuit. Independent geometrical and electrical parameters are input for each cavity.

The Hughes Aircraft Company 961HA TWT, a 59-64 GHz, 75-Watt coupled-cavity TWT developed under NASA Contract NAS3-25090 (Ref. 13), was used as a baseline for this study. Previously, this TWT was modeled with very good agreement with experimental results for the output RF power from 60 to 64 GHz (Ref. 14). The end of the output section has a mild two-step phase velocity taper (Fig. 1). This taper was designed to provide 75 Watts of RF power over the 5-GHz bandwidth. In this study, the taper design will be optimized for RF power efficiency at the center frequency of 61.5 GHz, without consideration of the performance over the bandwidth range.

The following simulated annealing algorithm was developed and implemented into the model to determine an optimized phase velocity taper:

Step 1. The initial conditions for the taper are selected. These include the starting and ending cavities of the taper and the initial length of each cavity.

Step 2. A typical taper for this TWT will be on the order of 20 to 40 cavities long. To optimize the length of each of these cavities in a reasonable amount of time would require a faster computer processor than is currently available. Therefore the taper is divided into segments of five equal-length cavities each. At each pass, a segment is selected by a random number generator. The first time that a segment is selected, the length of each cavity in the segment is increased by 1%. On succeeding alternate selections of a segment, the lengths are decreased and increased by 1%. With each change in cavity length, the impedance, phase shift per cavity, and gap length are adjusted. From calculations with the 3-dimensional electromagnetic simulation code MAFIA (Refs. 14, 15), it is a very good approximation for this TWT at the center frequency of 61.5 GHz to assume that the impedance decreases 1.97% and that the phase shift per cavity decreases 0.179% for every 1% decrease in cavity length. The gap/cavity length ratio is kept constant. The attenuation per cavity has a weak dependence on length and is assumed to be constant.

Step 3. With the new taper cavity parameters, the NASA multidimensional large-signal coupled-cavity TWT model is used to evaluate the new RF power efficiency.

Step 4. With a random number generator, a value 'R' is obtained between 0 and 1. This value is compared to the probability of acceptance defined as

$$P = e^{(\eta' - \eta)/kT} \qquad [2]$$

where η' and η are the new and old values of efficiency respectively. The base efficiency is kT which corresponds to Boltzman's constant multiplied by temperature in the physical analogy of simulated annealing. If R < P, the new cavity length of Step 2 is accepted; if R > P, the new length is rejected. Note that if the efficiency increases, acceptance of the new length is insured. If efficiency decreases, acceptance may occur but becomes less probable as kT decreases.

Step 5. Steps 2 through 4 are repeated for a total of 'N' passes. If there is at least one acceptance after 'N' passes, the value of kT is decreased by a reduction factor designated by r_T and Steps 2 through 5 are repeated. Convergence to a final solution is assumed after there are no acceptances with 'N' passes at a value of kT.

RESULTS AND DISCUSSION

The phase velocity tapers calculated with the simulated annealing algorithm described above will be compared to that of the baseline TWT. The output section of this TWT contains 65 cavities, of which 47 are a standard length of 0.09677 cm, 11 are reduced in length by 2%, and 7 are reduced 4%. The cavity lengths at the end of the output section are shown in Fig. 1.

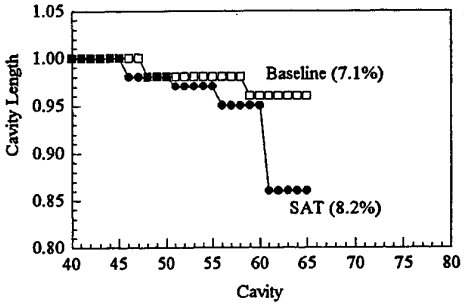

Fig. 1. The cavity length profiles for the phase velocity tapers at the end of the output sections for the baseline Hughes 961HA TWT and a simulated annealing taper (SAT). The baseline TWT, which was designed for wide-bandwidth performance, has a center-frequency (61.5 GHz) RF efficiency of 7.1%, while the SAT has a computed efficiency of 8.2%.

Before beginning the simulated annealing algorithm, the 'cooling schedule' must be selected. This is defined by the values for the following parameters which were described in the previous section: r_T , N, and the initial value of kT (kT_0). In order for a globally optimized solution to be obtained, kT_0 should be large enough so that at the beginning of the optimization, a decided majority of the proposed cavity length changes are accepted. It is also necessary that kT decrease sufficiently slowly.

The algorithm was used with a variety of cooling schedule parameters to calculate simulated annealing tapers (SAT's) from cavity 46 to 65, starting with all cavity lengths equal to that of a standard cavity. It was found that parameter values of $kT_0 = 0.002$,

r_T = 0.5, and N = 10n, where n is the number of cavity segments in the taper, provided a sufficient cooling schedule to obtain an optimized solution. The resulting SAT as shown in Fig. 1 was obtained after 270 passes. Although it is a much stronger taper than that of the baseline TWT, it only increases the RF power efficiency from 7.1% to 8.2%. However, by applying the algorithm to longer output sections, significantly higher values of efficiency were obtained. Fig. 2 shows the resulting efficiencies for SAT's as a function of end cavity. A clear maximum of 13.4% occurs with an end cavity of 80.

The cooling schedule was reexamined with SAT's from cavity 46 to 80 and it was found that increasing r_T from 0.5 to 0.7 resulted in an SAT with a slightly higher efficiency of 13.5%, which is shown in Fig. 3. The progressions of efficiency and acceptance percentage for this taper are shown in Fig. 4. The efficiency increases very rapidly during the first 200 passes while the majority of the proposed length changes are being accepted. As the taper profile converges to its final form, the efficiency increase slows down and the acceptance percentage drops rapidly and reaches zero after 770 passes.

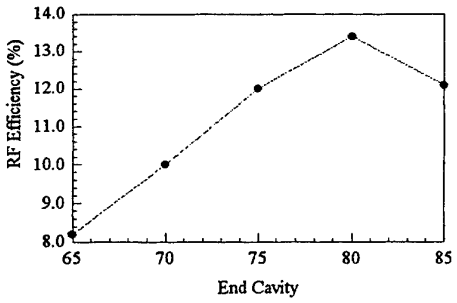

Fig. 2. The computed RF efficiencies for SAT's as a function of length. The maximum occurs with an end cavity of 80, indicating an output circuit 15 cavities longer than that of the baseline TWT.

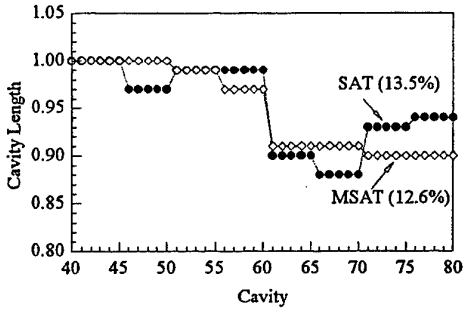

Fig. 3. The best SAT is obtained with an output circuit length of 80 cavities and has a computed RF efficiency of 13.5%. For comparison, a monotonic SAT (MSAT) was determined, in which the generating algorithm was modified to prevent a cavity from being longer than the previous cavity. The MSAT achieves an RF efficiency of only 12.6%.

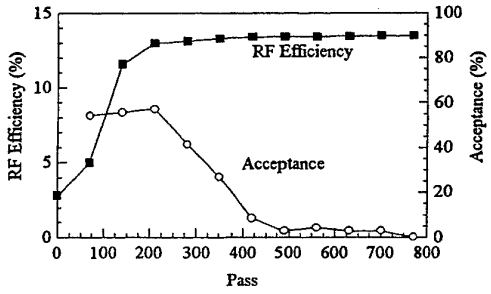

Fig. 4. The progressions of RF efficiency and algorithm acceptance percentage for the determination of the SAT of Fig. 3.

The profile of the SAT in Fig. 3 is interesting in that instead of decreasing smoothly and monotonically, it decreases sharply at first and then reverses to increase cavity lengths and RF phase velocity in the last part of the taper. In order to understand this behavior, a comparison taper was determined with the algorithm modified to force a monotonic decrease in cavity length. The resulting monotonic

simulated annealing taper (MSAT) is also shown in Fig. 3 and achieves an RF power efficiency of only 12.6%. The kinetic energies of the electronic disks in the SAT and MSAT are examined for each taper at every five cavities. The 24 electron disks of the model are divided into two groups: the 12 fast disks and 12 slow disks with kinetic energies respectively greater and lesser than the median. The average normalized kinetic energies for each group are shown in Fig. 5. For both tapers, the kinetic energy of the disk groups decrease as the electrons give up energy to the RF signal. Also for both tapers, the spread between the fast and slow disks increase as the electron bunch deteriorates. The energies are quite similar for the two tapers except at the end. It can be seen that the SAT achieves its superior efficiency by more effectively decreasing the energies of the fast electrons at the end of the taper. (The MSAT is more effective in extracting energy from the slow electrons, but this difference is not as large as that for the fast electrons.) The smaller energy spread between the slow and fast electrons at the end of the circuit for the SAT should also be an advantage in optimizing for overall efficiency, where it is desirable to recover as much energy as possible from the spent electron beam with a multistage-depressed collector.

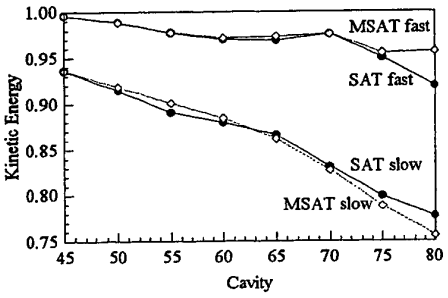

Fig. 5. The average kinetic energies of the slow and fast electron disks of the modeled electron beam for both the SAT and MSAT of Fig. 3. This indicates that the SAT is more effective in decelerating the more energetic electrons at the end of the taper. The kinetic energy is normalized to the initial value at the beginning of the input circuit.

CONCLUSIONS

A simulated annealing optimization algorithm has been developed and implemented into the NASA multidimensional large-signal coupled-cavity TWT computer model. The algorithm was tested by using it to determine the profile of cavity lengths at the end of the output section in order to optimize center-frequency RF efficiency for a V-band coupled-cavity TWT. The resulting taper design showed a computed RF efficiency at center frequency of 13.5% compared to 7.1% for the baseline TWT. The taper provided a sharp decrease in RF phase velocity and then a reversal to increasing phase velocity at the end. This profile allowed the taper to capture more of the energy of the fast electrons than was possible with a monotonic taper. Further work is planned to optimize the efficiency over a wide bandwidth.

A primary advantage of this algorithm is that the simulated annealing allows a global optimum solution to be obtained whereas most optimization algorithms converge on a local optimum. Another major advantage is that the algorithm can be readily adapted to optimize any calculable TWT output characteristic in terms of any combination of the model's cavity, beam, and focusing parameters.

Recently the model and algorithm have been adapted to optimize helical TWT's. Work is underway on a design for a helical space TWT to optimize the overall efficiency, which is dependent on both the RF efficiency and the spent energy distribution of the electron beam.

REFERENCES

[1] J. R. M. Vaughan, "Calculation of coupled-cavity TWT performance," *IEEE Trans. Electron Devices,* vol. ED-22, pp. 880-890, Oct. 1975.

[2] C. L. Jones, "A 200 watt traveling-wave tube for the communications technology satellite," NASA, CR-135029, 1976.

[3] W. R. Ayers and F. R. Walker, "Efficiency improvement in coupled cavity traveling wave tubes," Rome Air Development Center, Griffiss AFB, NY, Tech. Rep. TR-79-264, 1979.

[4] J. D. Wilson, "Computationally generated velocity taper for efficiency enhancement in a coupled-cavity traveling-wave tube," *IEEE Trans. Electron Devices,* vol. 36, pp. 811-816, Apr. 1989.

[5] J. D. Wilson, H. C. Limburg, J. A. Davis, I. Tammaru, and J. P. Vaszari, "A High-Efficiency Ferruleless Coupled-Cavity Traveling-Wave Tube with Phase-Adjusted Taper," *IEEE Trans. Electron Devices,* vol. 37, pp. 2638-2643, Dec. 1990.

[6] S. Kirkpatrick, C. D. Gelatt Jr., and M. P. Vecchi, "Optimization by simulated annealing," *Science,* vol. 220, pp. 671-680, May 1983.

[7] N. Metropolis, A. W. Rosenbluth, M. N. Rosenbluth, A. H. Teller, and E. Teller, "Equation of State Calculations by Fast Computing Machines," *J. Chemical Physics*, vol. 21, pp. 1087-1092, June, 1953.

[8] E. Aarts and J. Korst, *Simulated Annealing and Boltzmann Machines*, pp. 88-91. New York: John Wiley & Sons, 1989.

[9] D. J. Connolly and T. A. O'Malley, "Computer program for analysis of coupled-cavity traveling-wave tubes," NASA, TN D-8492, 1977.

[10] T. A. O'Malley and D. J. Connolly, "Users' manual for computer program for one-dimensional analysis of coupled-cavity traveling-wave tubes," NASA, TM X-3565, 1977.

[11] T. A. O'Malley, "User's manual for computer program for three-dimensional analysis of coupled-cavity traveling-wave tubes," NASA, CR-168269, 1984.

[12] J. D. Wilson, "Revised NASA axially symmetric ring model for coupled-cavity traveling-wave tubes," NASA, TP-2675, 1987.

[13] H. Limburg, D. Zamora, J. Davis, and I. Tammaru, " A 75 watt, 59 to 64 GHz Space TWT," NASA, CR-195450, 1995.

[14] J. D. Wilson and C. L. Kory, " Simulation of Cold-Test Parameters and RF Output Power for a Coupled-Cavity Traveling-Wave Tube," *IEEE Trans. Electron Devices,* vol. 42, pp. 2015-2020, Nov. 1995.

[15] C. L. Kory, Analex Corp., personal communication.

HIGH EFFICIENCY LINEAR TWT IN KU-BAND (HELT)

R. NUNN

AEG Elektronische Röhren GmbH
Ein Unternehmen der THOMSON TUBES ELECTRONIQUES

Abstract
The design and development of a high power, Ku-Band, highly linear TWT for use in a satellite, broad-band, multi-carrier environment is described. Possible application is the use of parallel amplifiers in a Butler matrix configuration.
The TWT efficiency was optimised for operation in the linear (back-off) region with a special helix taper and up to five stages of collector depression using large signal computer simulation.
The linearity of the TWT was defined in terms of the noise power ratio (NPR) to simulate operation with a large number of carriers
The operation point of the TWT, which had a theoretical saturated single signal output power of 200 W, was defined as that RF noise output power at which the NPR equals -21 dBc.
With the TWT alone a total noise output power of 40 watts was achieved corresponding to an efficiency of 34%.
Additional results using a pre-distorting lineariser at the input of the TWT showed an improvement in performance of up to 62 watts of noise power and 42% efficiency.

Summary
The work described in this paper was performed under contract with ESA/ESTEC and was intended to demonstrate the feasibility of using highly efficient depressed collectors in conjunction with backed-off operation to produce a practical, highly efficient, highly linear, broad band TWT(A) suitable for use in Butler Matrix Network applications. A total noise output power, at the backed-off operating point, of 80 W with an efficiency of 50 % over the frequency range 10.7 to 12.7 GHz was aimed at.
The work was divided into several phases :

- A trade-off phase in which the linear performance of various types of helix systems were calculated and optimised using a large signal computer program.
- A construction phase in which three TWTs were built. The TWTs differed in their collector configurations which consisted of 3, 4 and 5 voltage depressed stages respectively. The TWTs were focused for best efficiency at the desired (backed-off) operating point (-21 dBc NPR) and the performance was measured over the full operating band.
- Measurements of the third TWT (5 stage collector) with an additional lineariser connected to its input were performed.

Trade-off Design Phase
Simulation of the single carrier input power to output power and phase characteristics of a number of helix designs were made using the AERG large signal computer programme „TWA3". The results of these simulations were used with the ESA/ESTEC computer programme „IMAL" to calculate the multiple carrier performance of the TWT. Fifteen carriers were used in the calculations to simulate a noise power ratio (NPR) measurement. The helix

system was optimised for the lowest value of output power back-off from saturation and highest value of overall efficiency that could be achieved with a NPR of -21 dBc. Simulation and optimisation of a constant pitch helix, a step taper helix and an AERG „HELOS" taper helix was carried out. The following table shows the best results that were calculated for each helix type.

Helix Type		Constant Pitch	Step Taper	HELOS
Helix Voltage	V	6000	6000	6000
Cathode Current	mA	220	180	180
Saturated output power	W	251	298	270
Beam efficiency at saturation	%	19,0	27,6	24,9
Total efficiency at saturation	%	66,4	59,0	73,9
Back-off with NPR of 21 dBc				
Output power	W	64,6	53,0	81,3
Input power	dBm	-5,0	-4,7	-6,2
Gain	dB	53,1	51,9	55,0
Beam efficiency	%	4,8	4,9	7,5
Total efficiency	%	48,3	38,4	50,2
Input back-off from saturation	dB	12,6	11,1	12,3
Output back-off from saturation	dB	5,3	7,3	4,4

The results were extrapolated to obtain an noise output power of 80 W (at 21 dB NPR), it was found that a beam current of 310, 440 or 270 mA would be required for the three helix types respectively. Such beams could not be focused with the available magnet system for which an estimated 140 mA maximum beam current was calculated.
For this reason further optimisation was concentrated on the HELOS taper, which required the lowest beam current with a maximum of 140 mA. The following results were obtained :

Single carrier calculated at	GHz	11,00	12,00	12,75
Helix Voltage	V	6000	6000	6000
Cathode Current	mA	140	140	140
Saturated output power	W	190	202	199
Beam efficiency at saturation	%	22,7	24,0	23,6
Total efficiency at saturation	%	66,2	73,1	72,5
Multi-carrier calculated				
Back-off with NPR of 21 dBc				
Output power	W	55,2	58,2	55,8
Input power	dBm	-1,9	-3,2	-3,5
Gain	dB	49,3	50,8	50,9
Beam efficiency	%	6,6	6,9	6,6
Total efficiency	%	50,2	49,2	46,7
Input back-off from saturation	dB	11,1	12,2	12,9
Output back-off from saturation	dB	4,4	4,4	4,7

With the chosen design for 200 W of single carrier saturated output power it was calculated that the -21 dBc NPR could be achieved with between 4.4 and 4.7 dB of output power back-off depending on the frequency, corresponding to between 55 and 58 W of noise output

power. The calculated noise power efficiency, assuming a ideal four stage collector, with fourth stage at cathode potential, was between 47 and 50%.
The shape of the collector electrodes was not considered at this stage, only the voltages were freely adjusted, for each frequency, to reduce the energy dissipated in the collector (at the selected operating point) to a minimum. These voltages depend on the energy spectrum of the spent electron beam entering the collector.
Experience shows however that with a real collector the efficiency at saturation lies approximately 10 percentage below the calculated value. hence an efficiency at the -21 dBc NPR operating point of between 42 and 45 % was to be expected.
In general it was found during the optimisation process that the best efficiency configuration of the helix taper for the back-off or linear condition gave also the best results at the saturation point.

Design and construction of TWTs
Based on the results of the design trade-off phase three TWTs was designed an constructed. The tubes were mostly built from standard AERG satellite TWT parts and differed essentially only in the collector configuration.
Electron Gun: The electron gun is a modified Pierce type optics operating at about 6 kV with 140 mA of beam current. The cathode loading is approximately 2 A/cm². The beam current can be controlled with a separate anode voltage. The gun is of a stacked ceramic insulator design and is common to all AERG satellite TWTs at power levels of 100 W or above.
The electrode shapes were determined using the AERG gun program.
Delay line system : The delay line is a two section helix with sever. The molybdenum helix with the BeO helix support rods is inserted into the barrel using thermal shrink technique as is standard practice for AERG satellite TWTs. The helix pitch profile was determined from the large signal program.
Beam Confinement : The electron beam is confined with a PPM magnet system using an integrated pole piece and spacer barrel construction. SmCo high energy magnets are used to provide a peak focusing field of 230 kA/m which has a sufficient safety factor to ensure beam confinement under all operating conditions.
RF Connectors : Input and output connections to the helix are made with coaxial lines including ceramic vacuum windows. The input is fitted with a standard SMA connector. The coaxial output system is connected via an adapter to a waveguide.
Collector : The collectors design chosen for all three TWTs is a conduction cooled magnetically focused multi stage depressed collector as is a standard for all AERG satellite TWTs. For the three TWTs the collector differed in the number of stages.

- For TWT No. 1 the collector had 3 separate stages with an additional „spike" at cathode potential. Because of its delicate nature the spike cannot dissipate any energy but serves to form the electric field inside the collector.
- For TWT No. 2 a full 4 stage collector was installed. The 4th stage can be operated at other potentials and serves to reduce the total dissipation especially in the back-off region.
- For TWT No. 3 a five stage collector was used.

Test Results
The TWTs were measured for the normal single RF signal parameters and also multi-carrier performance. The latter was characterised by the noise power ratio method. This method consists of applying a band of constant amplitude noise with a narrow „notch" or stop band in its middle to the input of the test device. At the output of the device the notch filled in by the intermodulation products produced by the non-linearity of the device. The depth of the

notch is the NPR. It was found that the different test equipment available to AERG gave differing results for NPR depending on the relative noise pedestal and notch bandwidth. For TWT No. 1, using the original AERG equipment with pedestal and notch bandwidths of 200 and 50 MHz respectively, it was found that a NPR of -21 dBc could be achieved with 65 W of noise output power corresponding to an efficiency of 37%. This corresponds to an output power back-off of about 4.7 dB which agreed with the theoretical prediction. However more recent measurements with a commercially available equipment (Noise/Com UBX-NPR) with pedestal and notch bandwidths of 40 MHz and 100 kHz respectively, showed much lower (worse) values of NPR for the same TWT setting. Thus the values of efficiency at the -21 dBc NPR point had to be revised downwards. This trend was later confirmed with measurements using equipment from ESTEC with pedestal and notch bandwidths of 400 MHz and 16 MHz.
A comparison of the noise output power and efficiency achieved for the three TWTs at a NPR of -21 dBc is shown in the following table. For TWT 1 and 2 the values are measured with the Noise/Com equipment, for TWT 1 the values have been extrapolated from the AERG equipment.

TWT		1	2	3
Frequency	GHz	11.90	11.90	11.90
Noise power	W	40	37.5	37.5
Efficiency	%	29.5	33.5	35.5
Efficiency beam	%	--	6.1	6.0

During focusing of the TWTs the collector voltages were adjusted to give the best efficiency compatible without excessive back streaming of electrons to the helix system. The performance of the 3 collectors is shown as follows:

TWT		1		2		3	
Collector		3 Stage + Spike		4 Stage		5 Stage	
		Uh / V	Ic / mA	Uh / V	Ic / mA	Uh / V	Ic / mA
Stage	1	2572	18.2	2500	15.4	2610	15.7
	2	1607	36.1	1791	17.7	1611	13.3
	3	686	79.6	954	33.8	1110	20.4
	4	0	6.0	299	72.6	602	39.8
	5	-	-	-	-	186	54.1
Collector eff.	%	87.3		91.5		92.0	

It was found that the collector voltages could not be set to theoretical best values which lead to an overall reduction in efficiency.
As only a very small increase in efficiency improvement was achieved between 4 and 5 collector stages it was decided not to proceed with the originally planed up to eight collector stages. Instead efficiency improvement using a linearisier would be investigated.

Measurement of TWT with Linearisier
Using a linearisier enables the TWT to be driven to higher output powers for the same level of non-linearity, how far could not be determined before the tests. It was decided that an output power of 120 W, corresponding to about 2 dB OBO and a single carrier efficiency of about 50% would be sufficient to cover all cases. The TWT was then re-focused and the collector voltages adjusted so that it could be operated reliably up to this power level for all

frequencies. As a result of this re-focusing the efficiency at the previously optimised 21 dBc NPR point (about 40 W output power) was slightly reduced by 1 percentage points.
The results obtained for the TWT No. 3 (5 stage collector) with single carrier operation with and without linearisers are summarised in the following table:

Phase change

Frequency GHz	10.75	11.00	11.90	12.75
TWT alone	-8.2°	-10.0	-16.3	-19.0
TWT with Lineariser	0°	-1.0	-2.0	-2.5

Gain compression

Frequency GHz	10.75	11.00	11.90	12.75
TWT alone	-2.4 dB	-2.3	-2.3	-2.2
TWT with Lineariser	-1.0 dB	-0.3	-0.5	-0.4

At the reference NPR level of -21 dBc (measured with Noise/Com equipment) a substantial improvement in both output power and efficiency is achieved at all frequencies by the addition of a linearisers. The improvement is shown in the following tables:

Noise output power at -21 dBc NPR in W

Frequency	10.75	11.00	11.90	12.75
TWT alone	38	41	38	37
TWT with Lineariser	53	60	60	60
Improvement	15	19	22	23

Noise power efficiency at -21 dBc NPR in %

Frequency	10.75	11.00	11.90	12.75
TWT alone	33.0	35.0	33.0	33.0
TWT with Lineariser	38.0	40.5	42.0	41.5
Improvement	5.0	5.5	9.0	8.5

Measurement of TWT with broad band noise

For certain applications considered in this project such as parallel amplifiers in a Butler matrix configuration the 40 MHz bandwidth of the Noise/Com NPR equipment is too narrow. To determine the performance of the TWT with broad band noise a set of microwave filters was supplied by ESTEC. These provided in combination with a wide band noise source a pedestal and notch bandwidth of 400 and 16 MHz respectively. The centre frequency of 11 GHz could not be changed.
Measurements were carried out both with and without an equaliser.

Noise output power at -21 dBc NPR in W

Frequency GHz	11.00
TWT alone Noise/Com 40 MHz	42
TWT alone ESTEC 400 MHz	45
TWT with Lineariser Noise/Com 40 MHz	59
TWT with Lineariser ESTEC 400 MHz	52

Noise power efficiency at -21 dBc NPR in %

Frequency GHz	11.00
TWT alone Noise/Com 40 MHz	34.5
TWT alone ESTEC 400 MHz	35.5

TWT with Lineariser Noise/Com 40 MHz	40.5
TWT with Lineariser ESTEC 400 MHz	38.0

A probable explanation for the lower power and efficiency obtained with the broad band noise power from the ESTEC filters (400 MHz) compared with the narrow band Noise/Com equipment (40 MHz) lies with the large gain variation of the combined TWT and lineariser over the wider bandwidth.

Comparison of high efficiency linear TWT (HELT) with conventional TWT in back-off
The principle of using a lineariser to increase the available output power (and efficiency) at a specific level of non-linearity from conventional TWTs (TWT designed to operate at saturated output power) is well established. It is evident however that even for an ideal lineariser, i.e. one that produces a perfect limiter characteristic of constant gain up to saturation and then constant output power with zero phase change, a degree of output power back-off is still required to achieve a noise power ratio (NPR) of -21 dBc. Calculations show that at a NPR of -21 dBc an output power back-off of 3.8 dB from the saturated output power would be required. For a typical TWT an output power back-off of between 7 and 8 dB is required to achieve this degree of linearity.
What advantage does the concept of a TWT specially designed and optimised for operation in this back-off region offer ? To answer this question a comparison of the non-linear and efficiency performance of the HELT TWT with a conventional satellite TWT has been made. The conventional TWT chosen for the comparison was a 75 W Ku-Band low gain TWT for which extensive measurements of NPR both with and without a lineariser were available. The TWT had a maximum single carrier efficiency of 63 % at saturation and its non-linear performance is typical for this class of TWT

.

Efficiency at NPR of -21 dBc in %

	Without Lineariser	With Lineariser
High Efficiency Linear TWT	33.5	42.0
Conventional TWT	22.0	36.0

It can be seen that without lineariser the HELT TWT has a 50% higher efficiency.
It is to be seen that the efficiency improvement of the HELT TWT at -21 dBc NPR compared with a conventional TWT is less due to an improvement in the linearity performance of the helix system, as they both require about the same degree of output power back-off to achieve this figure, but more to the reduced collector dissipation.
When fitted with a lineariser both TWTs showed an improvement in efficiencies up to 36% and 42% for the conventional and HELT TWTs respectively. The degree of improvement is greater for the conventional TWT, it should be noted however that the lineariser was especially designed to fit this TWT and had a better fit to its gain and phase expansion curves than was the case for the HELT TWT.

Conclusions
A design phase has been performed to determine the optimum helix system to operate in power back-off for best efficiency combined with high linearity. The linearity being defined as the operating point with an noise power ratio of -21 dBc.
Based on the design study three TWTs were constructed and tested, they differed essentially only in the number of collector stages used between 3 and 5 stages. The best

results were achieved with the 3rd TWT with 5 stage collector but it was only marginally better than the 4 stage collector.
It was found that an output power back-off of about 7.5 dB from the saturated output power was required to achieve á NPR of -21 dBc (measured with 40 MHz bandwidth) corresponding to a noise output power of 35 to 40 W depending on the frequency. Although the degree of output back-off required is similar to a conventional TWT the efficiency achieved at this point is much better. A best efficiency of 35.5% was reached compared with about 22% for a conventional TWT.
As the change from four to five collector stages resulted in only a slight improvement in efficiency it was decided not to build any further tubes with more collector stages (up to eight stages was planned). Instead the influence of a pre-distorting lineariser on the non-linear performance of TWT 3 was investigated.
With the lineariser the efficiency at the -21 dBc NPR operating point could be increased from 33% to 42%. This compares with a best value of 36% achieved with the conventional TWT with lineariser.
It is estimated that if a lineariser were available that had a better fit of phase and gain characteristics of the HELT TWT than that available for the present measurements, then a further increase in efficiency up to 46,5% could be expected.
The measurements comparing performance with and without lineariser were carried with a collector voltages that enabled operation up to 120 W of output power. This lead to a slight decrease in efficiency of 1 percentage points over that that could have been achieved at the power level at which a NPR of 21 dBc was measured (about 60 W with lineariser).
Throughout this project various methods were used to measure the noise power ratio and considerable differences were found. The estimated efficiency at the reference value had to be revised downward several times. The final results presented in this report are all measured using an equipment from Noise/Com.

Fig. 1 Performance of HELT TWTs No. 2 and 3

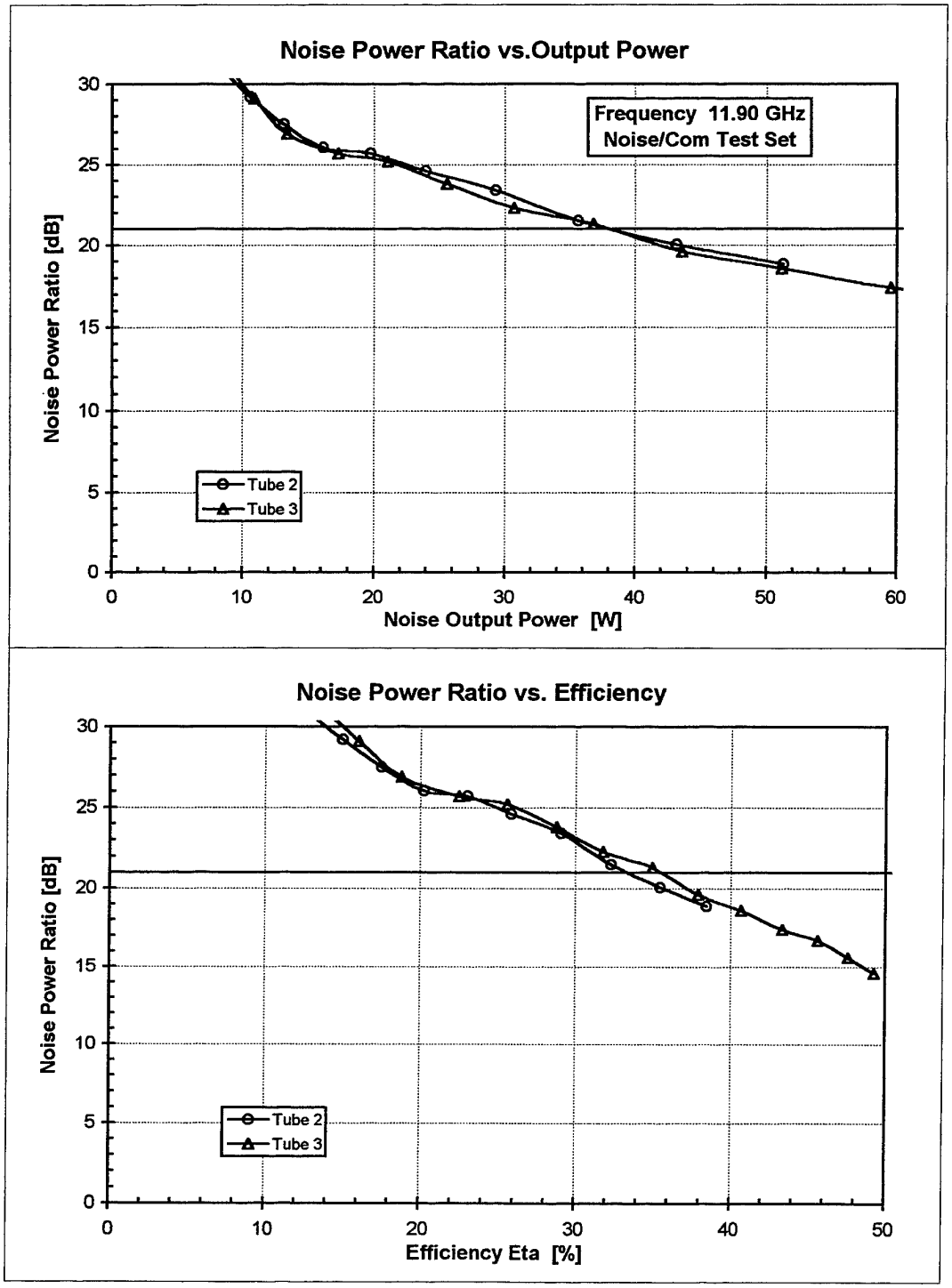

Fig. 2 Performance of HELT TWT3 with lineariser

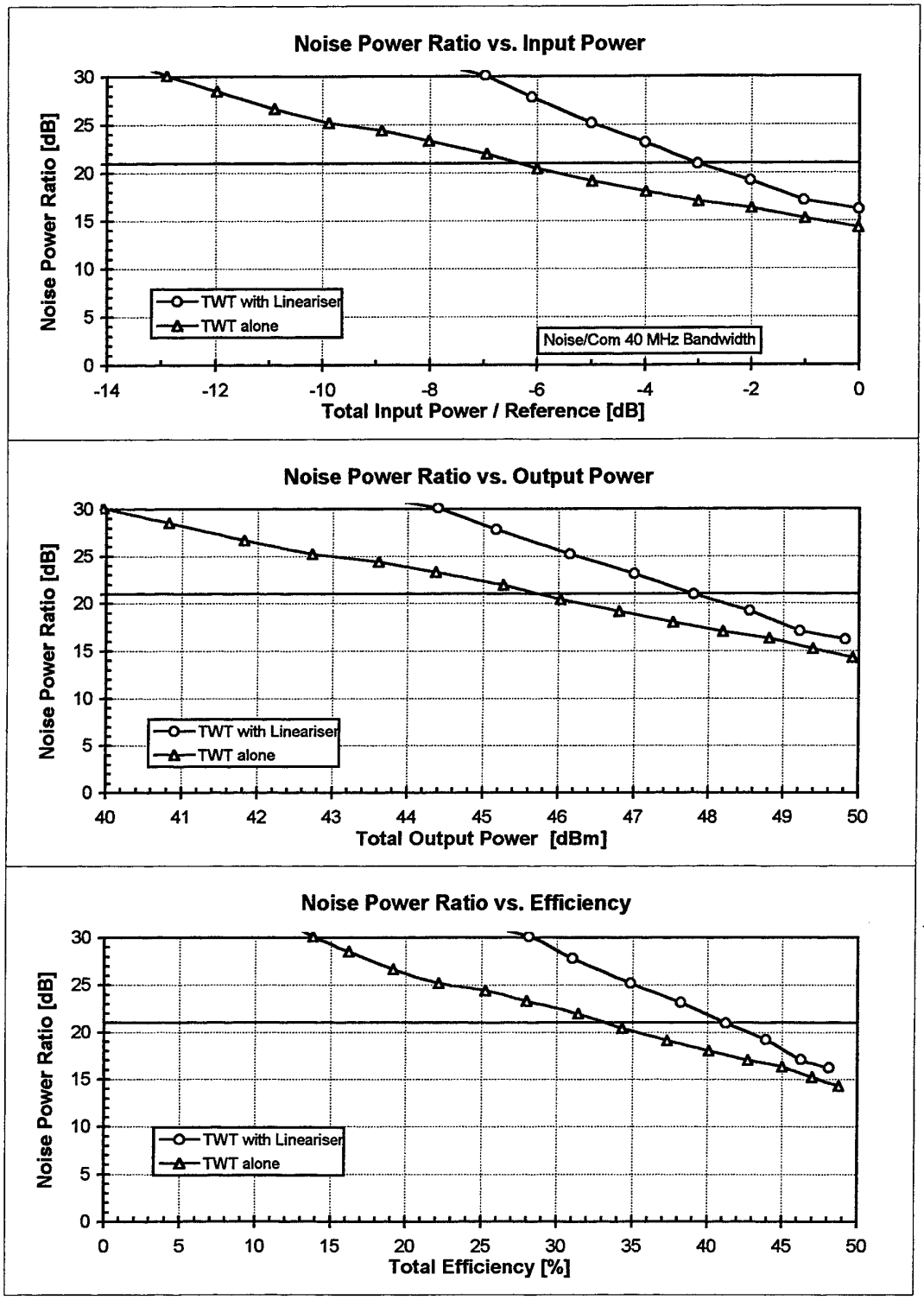

Fig. 3 Comparison of wide and narrow band noise

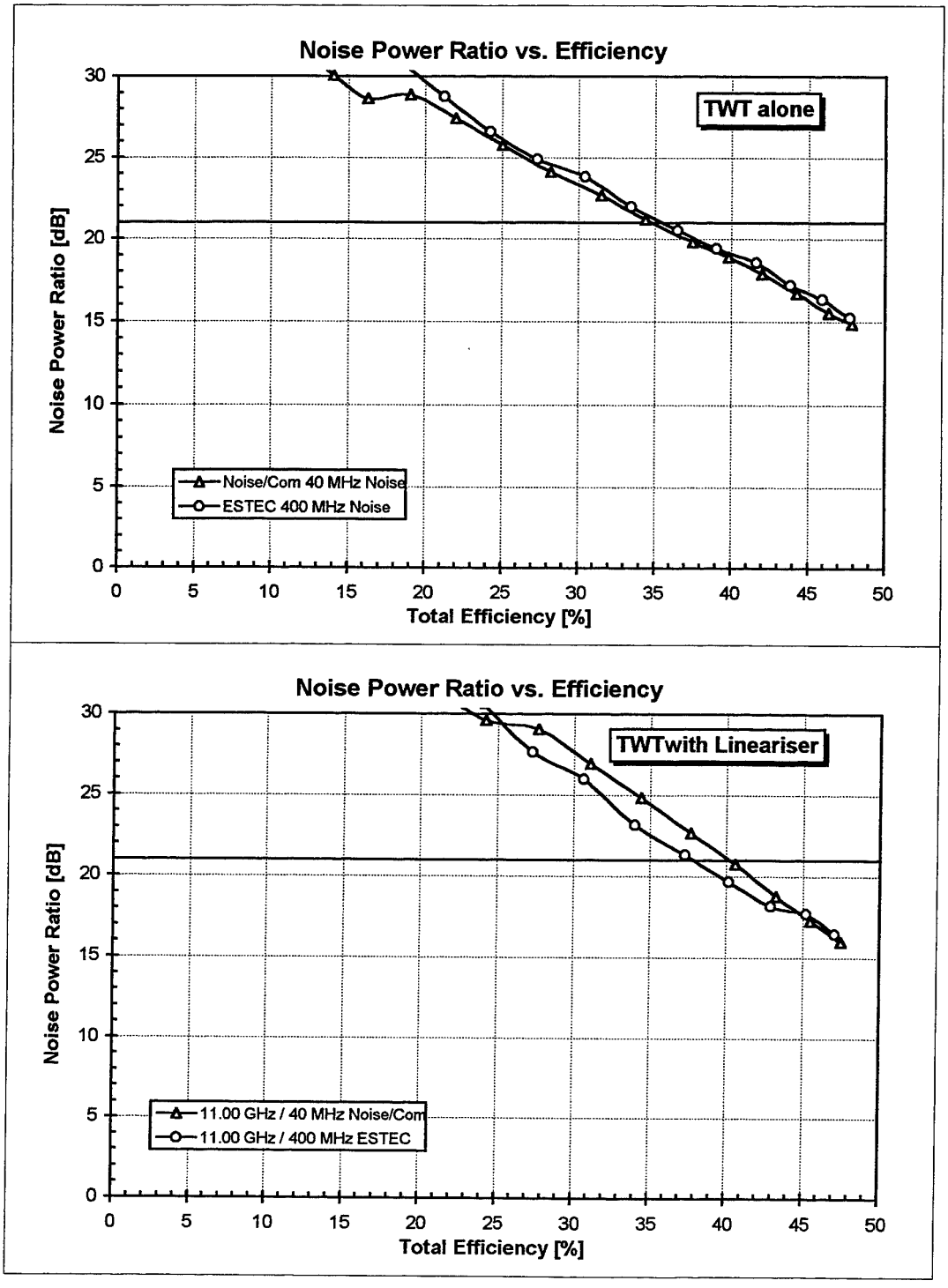

Fig. 4 Comparison of HELT TWT with conventional TWT

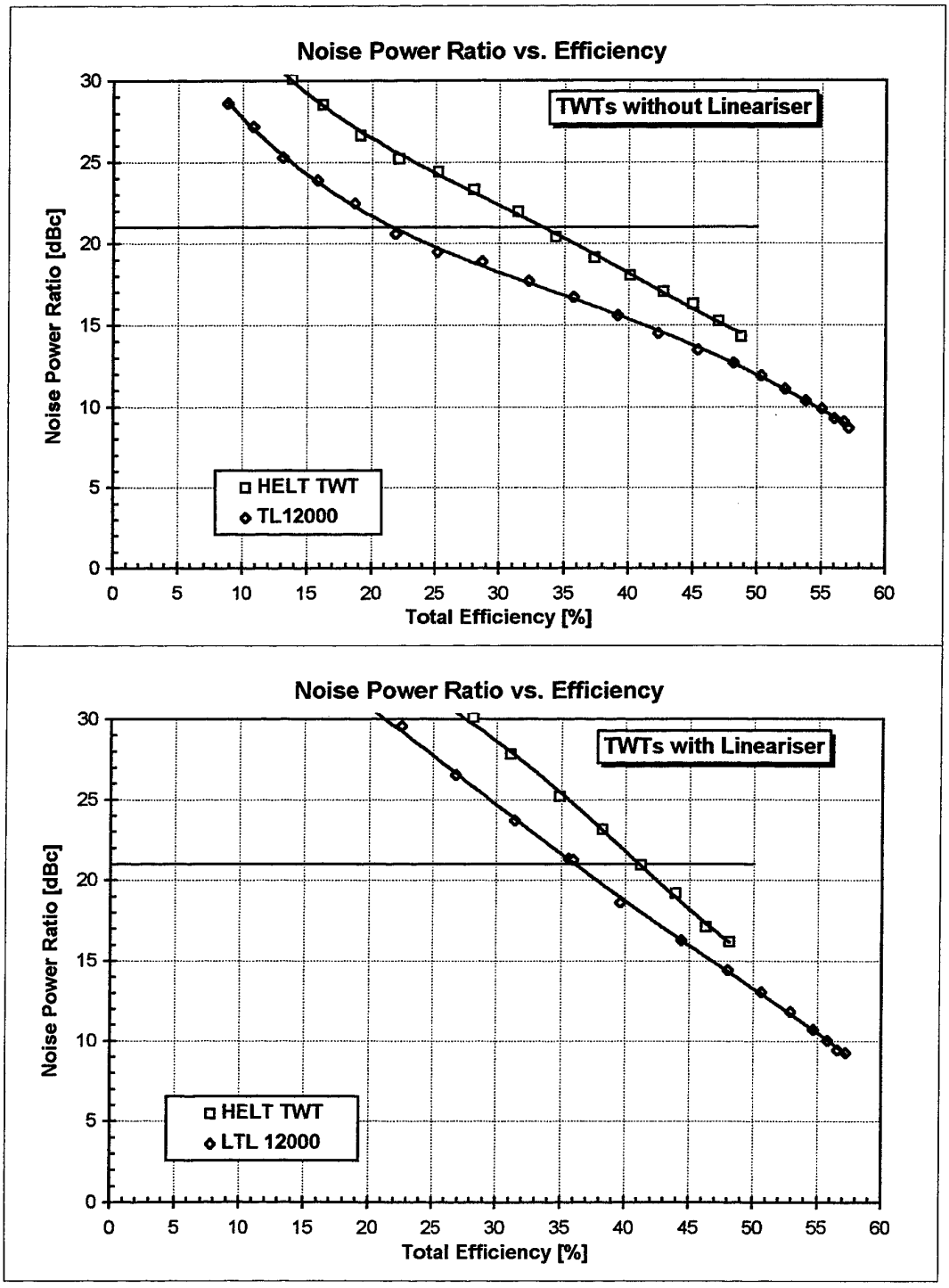

EFFICIENCY IMPROVEMENTS IN KU-BAND SPACE HELIX TRAVELING WAVE TUBES

R.T. Benton, J.T. Burdette, J.A. Davis, J.R. Feicht, D.S. Komm,
W.L. Menninger, N.R. Robbins, C.B. Thorington, X. Zhai, E.A. Adler
Hughes Telecommunications and Space Company
Electron Dynamics Division
Torrance, California, USA

D.A. Force, V.O. Heinen, K.R. Vaden, J.D. Wilson, J.A. Dayton, Jr.
NASA Lewis Research Center
Cleveland, Ohio, USA

ABSTRACT

Hughes Electron Dynamics Division (HEDD) and NASA Lewis Research Center (LeRC) have been using advanced computer simulations, including both in-house simulations and commercial simulations, to improve the performance of space helix traveling-wave tubes (TWT's). At NASA LeRC, efforts have focused on using the well-known electromagnetic simulation, MAFIA, to model time-dependent beam flow in our TWT collectors, and also to accurately predict circuit performance for various cross-sectional geometries. At Hughes EDD, Ansoft's Eminence, combined with a conjugate-gradient parameter searching engine as a front-end, is used to design, in full 3D, helix-to-waveguide matches with minimal loss and reflectivity over a wide bandwidth. Ansoft's static field 3D solver is used to model 3D magnet stacks and collector geometries. In-house simulators to predict 3D collector effects, secondary electron emission, and TWT intermodulation performance have all been developed within the last year. Using results from the aforementioned simulations, we have designed a new line of TWT's that demonstrate improved overall efficiency in test measurements.

I. INTRODUCTION

The competitive world of space communications is constantly setting higher and higher standards for space helix traveling-wave tube (TWT) performance, particularly in the area of overall efficiency. Today's state-of-the-art KU-band space helix TWT's perform at power levels of 100-200 W, overall efficiency levels of 65-70%, and bandwidths up to 2 GHz. Efficiency improvement in particular requires careful examination of all areas in the TWT where power is dissipated. It is critical to have a well-focused electron beam, an efficient interaction circuit with minimal loss, a well-matched vacuum window, and an efficient beam collection system. To improve such a system, computer design tools must be very accurate. Every watt of lost power must be understood before it can be eliminated.

II. HELIX TWT DESIGN

Though we do not yet have a single simulation that predicts TWT performance from the electron gun through the collector, we have developed a consistent method for using our separate gun, circuit, and collector codes to design a single TWT. The gun code, "Thermgun," generates output directly used by the circuit code, "Qhelix," which then generates a spent beam which is passed directly to the collector code, aptly named "Collector." The different parts of the TWT, each with different physical interactions, provide for this clean division of code work.

A. ELECTRON GUN

Efficient TWT performance begins with a well-focused electron beam. The beam size must be as large as possible for good interaction efficiency while being small enough to avoid circuit interception and backward wave oscillations. It is well know that the backward wave on a helix circuit has an E-field profile

that is proportional to $I_1(\gamma r)$, where γ is the perpendicular helix wave number and r is radial distance from

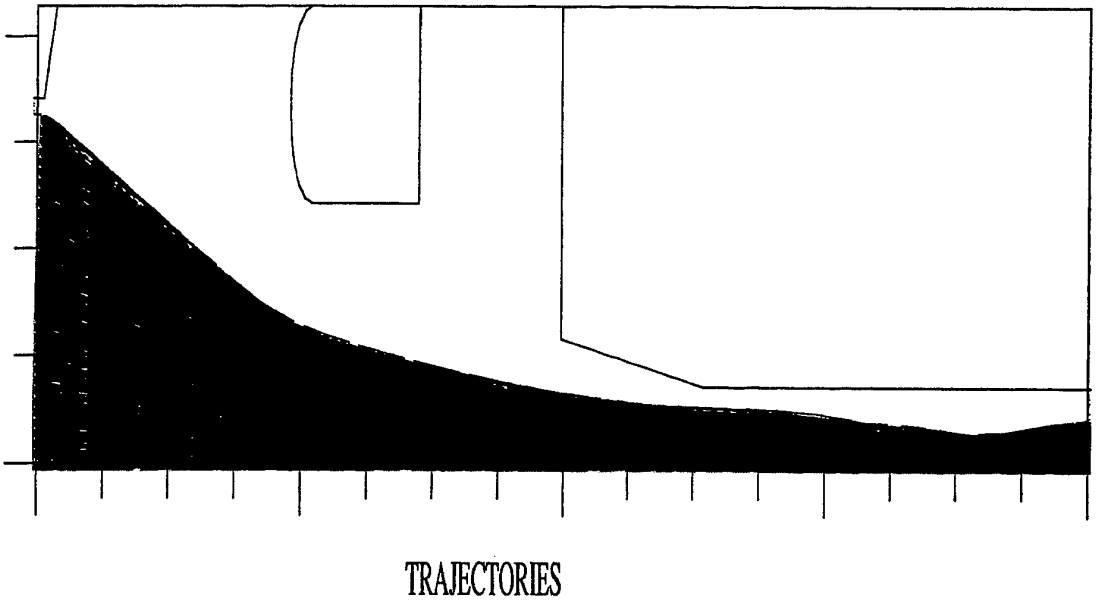

Figure 1. Electron focusing simulation for an HEDD TWT electron gun.

the axis, whereas the forward wave has an E-field proportional to $I_0(\gamma r)$. The sharper rise of $I_1(\gamma r)$ with radius makes BWO especially sensitive to beam radius. At HEDD, we continue to improve both our simulation capability and our design philosophy for electron guns. The HEDD gun code "Thermgun" is a two-dimensional (with three dimensional particle velocity vectors) particle simulation program which uses variable size finite-element meshes and allows a thermal velocity distribution in the electron beam. The simulation is driven by easily formed input from CAD files and has recently been entirely rewritten in C++ for improved extensibility, modularity, and robustness. Example output from Thermgun is shown in Figure 1.

B. HELIX CIRCUIT

A useful helix TWT circuit must combine many important characteristics. It must deliver a given level of rf output power and amplitude gain over a given bandwidth, perhaps also meeting linearity and/or phase shift specifications, while also avoiding regenerative and backward-wave oscillations and providing good matching conditions for the TWT input and output windows. As customers continue to escalate the performance expected from helix-TWT's, the best designs will be forced to make the right trade-offs in all of these areas, and this requires a sophisticated design code that can do exactly that--trade-off different areas of TWT performance depending on the customer requirements. Qhelix, initially developed in 1995 at HEDD and based on TWT physics similar to those in the well-known Detweiler simulation, provides just such a tool, utilizing a conjugate-gradient optimizing algorithm with the flexibility to allow the user to optimize virtually any TWT parameter while arbitrarily constraining any number of other parameters. A common design run, for example, might optimize the phase velocity profile of the helix TWT to deliver maximum rf output power for fixed beam parameters while being constrained by linearity or BWO limits. With the computational power available at HEDD and the speed at which Qhelix operates, the optimizer can attempt many thousands of iterations in a single day. Qhelix has successfully been used to design tubes from S-band to V-band frequency ranges. NASA LeRC has also been exploring circuit optimization techniques with their own code (see J. Wilson's paper in this same publication).

One of the first tests of Qhelix, both as an optimizer and as a TWT simulator, was to design a TWT with a phase velocity profile that would generate maximum basic (rf-interaction) efficiency from a typical HEDD helix circuit geometry. While our standard KU-band space tubes deliver approximately 25% basic, the optimizer results yielded a profile that was predicted to achieve 50% basic efficiency. As an early benchmark of Qhelix, this tube, designated MT-1, was built and tested at HEDD in 1995, and the result was 47.5% basic efficiency. The performance is shown in Figure 2. The discrepancy between predicted and measured efficiency is not surprising given the fact that Qhelix was using a one dimensional model for the design iterations that assumed no beam interception.

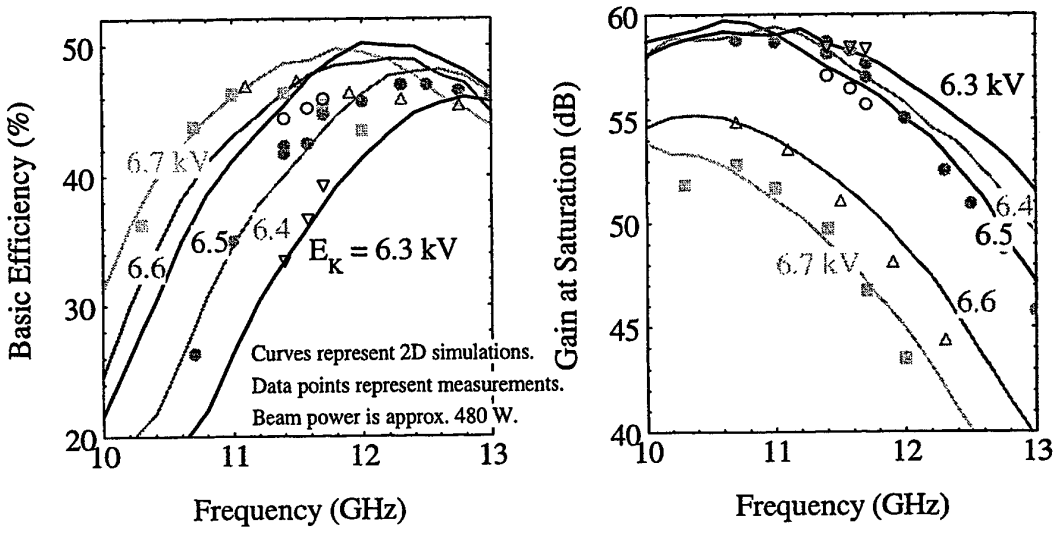

Figure 2. Simulation and test measurements for the HEDD MT-1 TWT, which was designed for maximum basic rf interaction efficiency.

C. Helix-to-Waveguide Coupling

With any vacuum rf device, the coupling of the rf from the vacuum to the outside world is always a significant challenge. With helix TWT's, this is particularly true. Most of the prerequisites for a good coupling match are in direct contention with the prerequisites for an efficient interaction circuit, e.g. low loss and high helix impedance improve circuit performance, but do not improve matching conditions. In addition, the coupler designer must create a design that is easily machineable and manufacturable and that can stand up to the thermal stresses created by today's high power TWT's. Fortunately, many sophisticated EM computer modeling tools are continuing to mature and are resulting in less time spent in the lab and more time spent creating accurate first designs that work very well. A conjugate-gradient optimizer running on top of Ansoft extends the design capability. HEDD's most recent window and coupler design, which has been tested, achieves a broadband match with less than 4% voltage reflection across a bandwidth of 15%. Agreement between the simulation and theory is exceptional. Figure 3 shows example output from an Ansoft Eminence simulation. In addition to HEDD's work in this area, NASA LeRC has been using MAFIA to simulate cold circuits (see C. Kory's paper in this same publication).

D. Collectors

Perhaps the most difficult number to accurately predict for a TWT is the one number that customers care the most about—overall efficiency. The part of the TWT that is most responsible for this difficulty is the

collector. The collector physics are perhaps the most demanding to simulate, because a complex, bunched beam is entering a device which often must be modeled in fully three dimensional manner.

1. MAFIA simulations: 3D Collector Problems

To address the three dimensional nature of the problem we are currently working with the electromagnetic simulation program MAFIA to determine its suitability for this application. MAFIA has already been used extensively at NASA LeRC for collector modeling. Given the early success that NASA has had with their MAFIA license, HEDD purchased a separate license which was partially funded by NASA LeRC. Drawing on their expertise, we have initially conducted analysis on a simple two dimensional symmetric collector configuration to develop the required translations from Qhelix, and to determine the trade-offs between model detail and computer CPU time. An example of a MAFIA simulation is shown in Figure 4. In the figure, a bunched beam from a TWT interaction enters a large collector area with two collector stages set to different potentials. The TWT bunches are clearly shown by the high velocity particles at the right as they pull away from the lower velocity particles, which are shown to be moving radially outward on the left and even reversing direction. A standard steady-state simulation as is commonly used to model electron guns cannot simulate the bunches shown in Figure 4. Thus far we have found that MAFIA CPU time seems to be proportional to N^2; where N is the number of "bunches" introduced into the problem. The number of bunches required is in turn determined by how an RF cycle of the electron beam is resolved, and how many RF cycles are to be replicated for the collector analysis. One

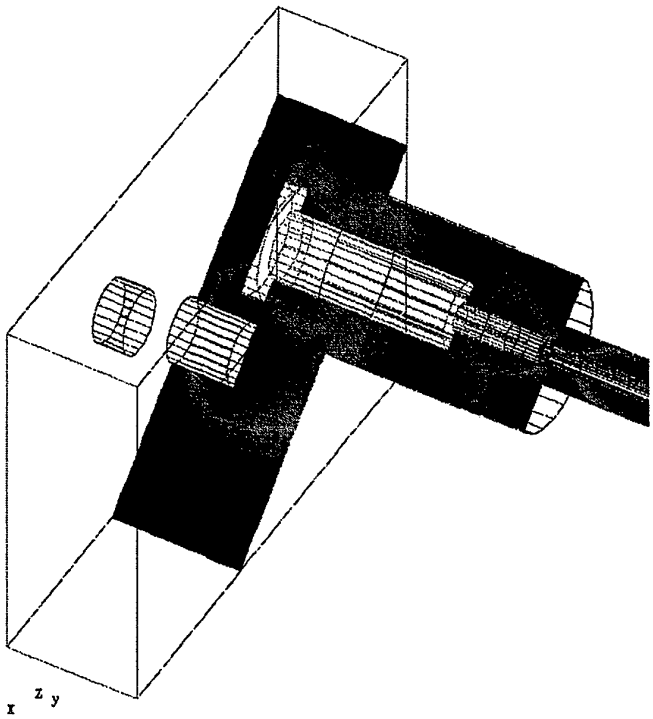

Figure 3. Ansoft Eminence simulation for a coaxial TWT window and waveguide coupler. The colored cut-plane shows E-field strength.

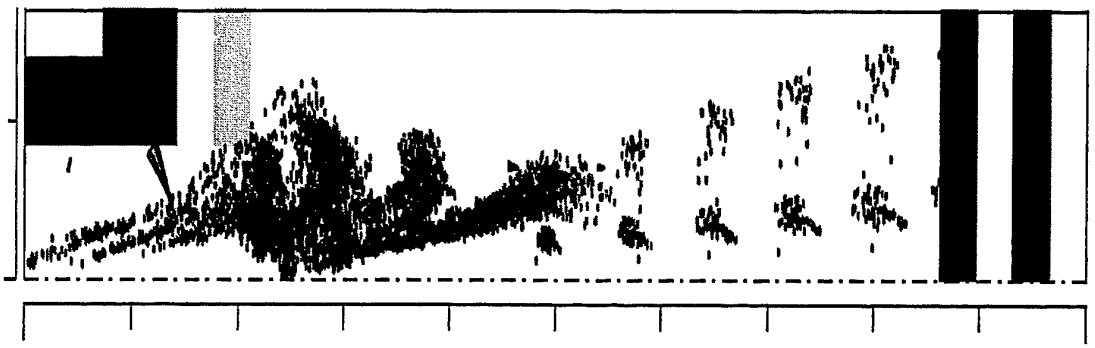

Figure 4. MAFIA simulation of electrons from a TWT interaction entering a collector region. The horizontal axis is the z-direction. The vertical axis is the radial direction.

attractive feature of MAFIA is the fact that there is little difference in the problem set-up and input data required to go from a two dimensional model to a fully three dimensional simulation.

Because MAFIA is CPU intensive, HEDD is also currently developing a partially three dimensional collector code to simulate a collector with asymmetric stages. This code pushes particles in three dimensions using fields interpolated in angle between fields from two dimensional simulations at different angular planes. The program also allows completely three dimensional magnetic fields from arbitrary magnetic dipoles. The advantage over MAFIA is that the partially three dimensional code would use much less CPU time per simulation.

2. Emission of Secondary Electrons

Another factor making collector simulation difficult is the physics involved when the electrons strike the collecting surface. When the beam is collected, secondary electrons are generated at the points of impact. If the local electric fields at the point of impact allow it, the secondaries will go to regions of higher potential, wasting energy. Hence an electron originally collected at, for example, the fourth stage of a collector can generate secondaries that end up on a less depressed stage, or that go back down the beamhole. A two-dimensional code (three dimensional velocity vectors), based on our steady-state gun code, has been developed at HEDD that allows these secondaries to be simulated, thereby allowing appropriate collector design to maximize efficiency. For the purposes of secondary emission simulations, NASA LeRC has provided HEDD with carefully measured data on secondary emission from various surface types at various angles. MAFIA can also model secondaries, but the in-house two-dimensional code uses much less CPU time. Figure 5 shows results from the two-dimensional simulation. As can be seen in the top graph, the secondaries come predominantly from the stage at the highest potential.

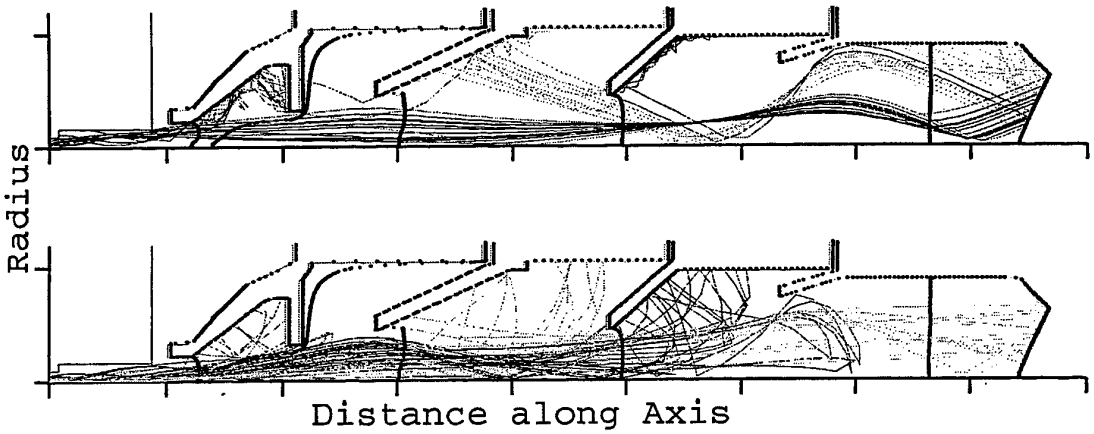

Figure 5. Simulation of collector performance. The bottom graph shows incoming primary electrons. The top graph shows generated secondary electrons. Different colors are used for trajectories that land on different stages.

III. SUMMARY

At HEDD and NASA LeRC, aggressive research and development work continues in all areas of TWT design. We have dramatically improved our design capability with an improved electron gun code, an optimizing helix circuit design code, Ansoft's EM software, MAFIA, and in-house codes for time-dependent and secondary particle modeling in collector simulations. Using the aforementioned simulations, HEDD continues to improve the design of all TWT lines. For Ku-band TWT's in particular, HEDD now can offer TWT's from 40W to 150W, all with overall efficiencies exceeding 65% over bandwidths of 2 GHz. Test results taken in early 1996 show TWT's with recently incorporated improvements yielding over

66% efficiency, and we have continued throughout 1996 and 1997 to improve collector modeling and performance in particular.

IV. ACKNOWLEDGMENTS

Procurement of the MAFIA electromagnetic simulation by HEDD was partially supported by NASA Contract #NAS3-27363.

L-Band TWT for Worldstar

G. Fischer, P. Heumüller, M. Hördler, Dr. M. Schmelzer

AEG Elektronische Röhren GmbH,
Ein Unternehmen der THOMSON TUBES ELECTRONIQUES

Summary
This paper describes a TWT for the Worldspace system. 150W outputpower at 1.5 GHz shall serve the southern countries with high quality radio channels. About 54% efficiency was achieved in a 40 MHz bandwidth.
A challenging schedule for the full qualification was requested in order to meet the duedate of the start of system operation.

Introduction

Worldspace is a digital broadcasting system for portable radios world wide.
The market for the World Space system is estimated to 4 billion peoples that are underserved by radio channels (Fig. 1.)

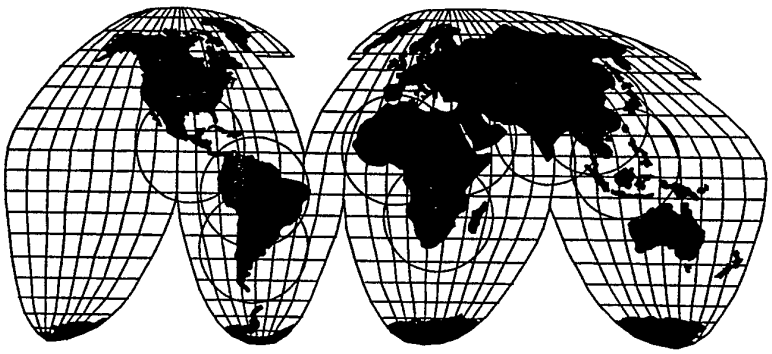

Fig 1: Worldspace System

Driven by this market, World Space started a co-ordinated development in three systems simultaneously, that means in satellite system, radio and multimedia receivers.

Schedule

The tight plan for the payback of the system development cost requested a high sophisticated schedule.
Only a co-ordinated plan for all the system equipment gave a chance to meet the goal of system operation in 1998.
In 1996 the system manufacturers started their projects.

Requirements for the TWT:

The frequency of 1,5 GHz was selected for enabling a hand held radio with a built-in antenna.
150 W output-power for the TWT with a bandwidth of 40 MHz was chosen for sufficient irradiated power.
The power consumption was settled to 282 W max. The mass for a 34 dB gain tube was limited to 2,2 kg. Schedule of the TWT Kick off of the program was January 1996. The requirement was to have the first FM delivery in February 1997. The CDR was held after 10 months time only.
Qualification program
Due to the untypical frequency range and new power class a whole qualification program was required.
The realisation of tube models occurred according to the following list.

First BB	May 1996
First EM	July 1996
First TV Test	October 1996
First Vibration Test	October 1996
TV Test QM	January 1997
Vibration Test on QM	February 1997
First FM Exhaust	November 1996

Technological architecture

In general the architecture is known from Satellite TWT´s in other frequency ranges. Fig.: 2 shows the cross-section of the tube:

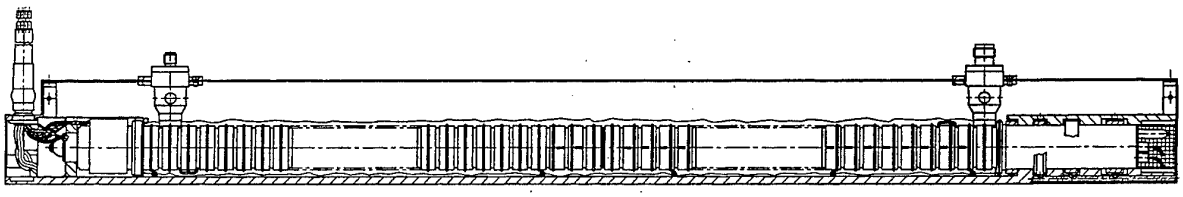

Fig 2: Cross-section of the TWT

It contains:
- Electron gun in a stack design
- Shrink force fitted helix
- Four stage collector with conduction cooling

The uncommon frequency range required a redesign of all tube components. A major challenge was to get the parts from external suppliers in time. That means the extension of the Worldspace schedule to another level of suppliers.

Technological realisation

Electron gun
The optic was adapted to the larger beam size. A major trade off was done for the beam compression and the cathode diameter. High performance cathodes give excellent cathode current densities. But beam compression is needed to suppress thermal effects of the electron emission.
An enhanced cathode surface on the other hand requires more irradiated heat and gives a negative contribution to the efficiency. Therefore a trade off had to be found to get the optimum with respect to beam focusing and power consumption. Fig.:3 shows the cross-section of the electron gun.

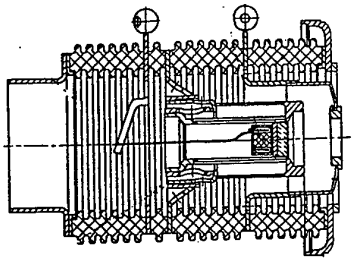

Fig 3: Cross-section of the electron gun

Helix
The helix was designed for its RF features with the standard Helos-taper giving optimum electronic efficiency and low nonlinearities. Fig.: 3 shows the pitch profile of the TWT.

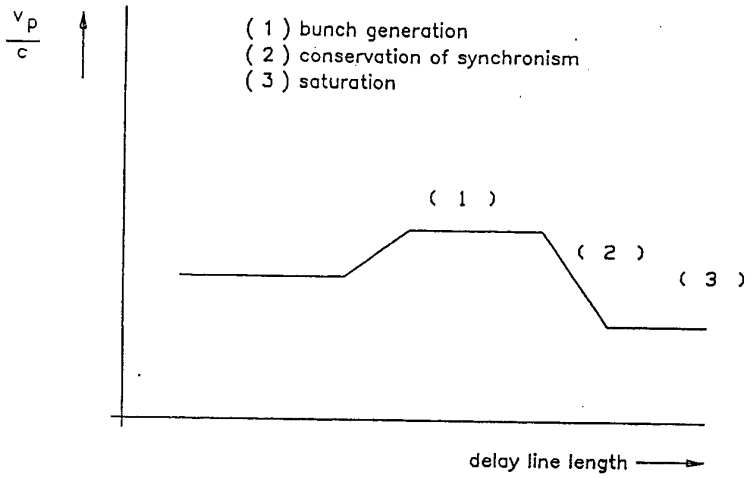

Fig 3: Pitch Profile of the L-Band TWT

The thermo mechanical interface of the helix is a shrink force fitting with BeO ceramic rods into the vacuum envelope. (Fig.: 4 shows the principle).

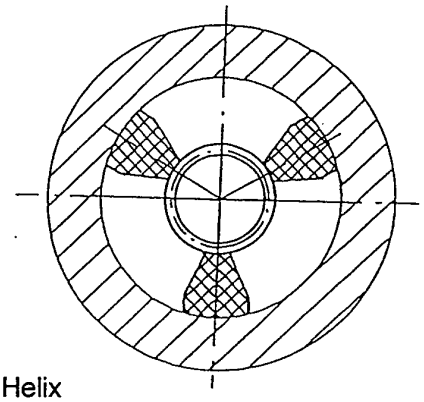

Fig 4 Shrink Force fitted Helix

It is evident that this system relays on a proper selection of materials for the helix system and its vacuum envelope. In order to give sufficient stress to the system under all processing and operation conditions the vacuum envelope was designed from a new spacer material with an adapted thermal expansion.

Collector

The collector-design is a four stage collector with four voltages.
The advantage is a lower power consumption under no drive condition. The design was adapted to a larger beam size and an increased thermal loading. Fig.: 5 shows the collector of the TWT:

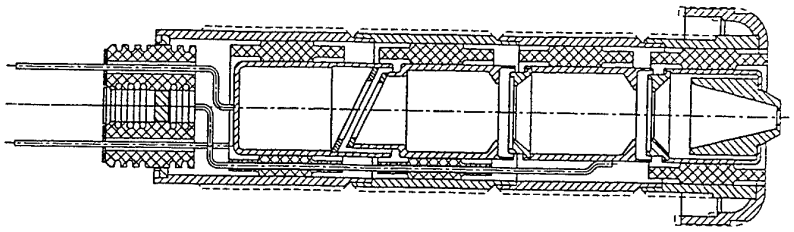

Fig 5: Cross-Section of the Collector

Results of the TWT
The minimum output-power of the TWT is 150 W min in the 40 MHz bandwidth.
(Fig.: 6) The DC-power consumption is below 280 W which calculates to an efficiency of about 53,5 %.

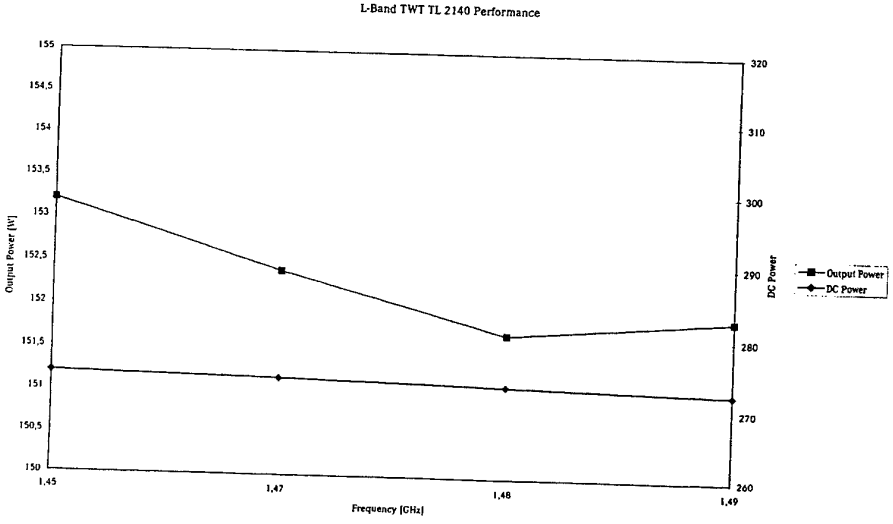

Fig.: 6 Output-power versus Frequency of the TWT
Due to the low frequency the channel amplifier can provide a larger contribution to the system-gain. The 34 dB gain at saturation enable a tube mass of 2,2 kg only. (Fig.: 7) The frequency response of the gain is rather flat.

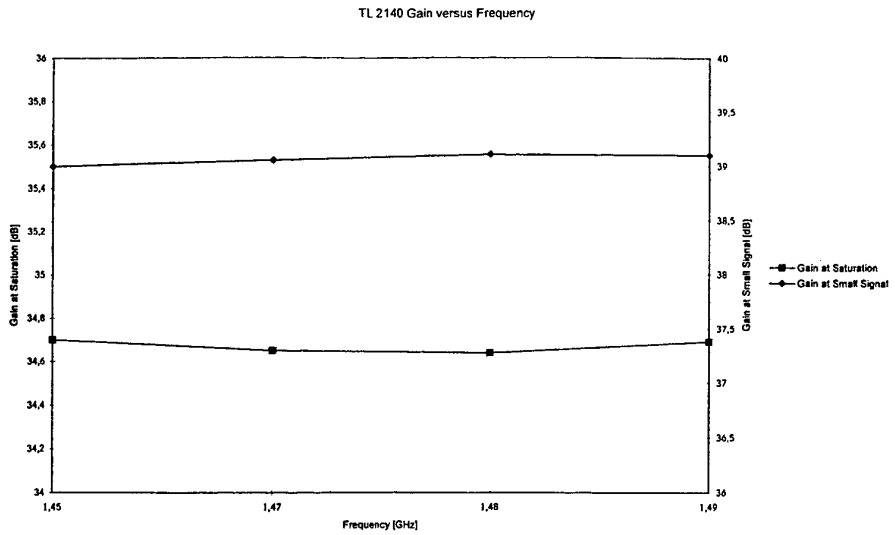

Fig.7: Gain versus Frequency of the TWT

Nonlinearities

The nonlinearities of the TWT are 38° for the non-linear phaseshift and 4°/dB for the AM/PM conversion. These values are rather low coinciding with the high efficiency.
The intermodulation between two carriers is at saturation input power better than 9,5 dBc.

Conclusion

New broadcasting systems are being built by simultaneous engineering of all system components.
Ground stations, satellite and receivers are being developed in a tight co-ordinated schedule.
Close cooperation between customer (in this case Alcatel) and suppliers is a major factor of success.
The benefit for the system owner will be a major advantage in an attractive payback period for the investment.

INTRODUCTION TO AN ACCURATE COLD-TEST MODEL OF HELICAL SLOW-WAVE STRUCTURES

Carol L. Kory
Analex Corporation/NASA Lewis Research Center
21000 Brookpark Rd., MS 54-5
Cleveland, Ohio 44135 USA
phone: (216)-433-3512 email: Carol.L.Kory@lerc.nasa.gov

James A. Dayton, Jr.
NASA Lewis Research Center
21000 Brookpark Rd., MS 54-5
Cleveland, Ohio 44135 USA
phone: (216)-433-3515 email: jdayton@lerc.nasa.gov

ABSTRACT

Recently, a method has been established to accurately calculate cold-test data for helical slow-wave structures using the three-dimensional electromagnetic computer code, MAFIA (Ref. 1). Cold-test parameters have been calculated for several helical traveling-wave tube (TWT) slow-wave circuits possessing various support rod configurations, and results are presented here showing excellent agreement with experiment. The helical models include tape thickness, dielectric support shapes and material properties consistent with the actual circuits.

INTRODUCTION

The analysis, including cold-test calculations, for helical slow-wave structures has been a long standing problem within the traveling-wave tube (TWT) industry. Although the helix slow-wave circuit remains the mainstay of the TWT industry because of its exceptionally wide bandwidth, a full helical circuit, without significant dimensional approximations, has not been successfully modeled until now. Numerous attempts have been made to analyze the helical slow-wave circuit so that the performance could be accurately predicted without actually building it, but because of its complex geometry, many geometrical approximations became necessary rendering the previous models inaccurate. In the course of this research it has been demonstrated that using the simulation code, MAFIA, the helical structure can be modeled with actual tape width and thickness, dielectric support rod geometry and materials. To demonstrate the accuracy of the MAFIA model, the cold-test parameters including dispersion, on-axis interaction impedance and attenuation have been calculated for several helical TWT slow-wave circuits with a variety of support rod geometries including rectangular and T-shaped rods, as well as various support rod materials including isotropic, anisotropic and partially metal coated dielectrics. Compared with experimentally measured results, the agreement is excellent.

This study involves the use of MAFIA (Solution of **MA**xwell's equations by the **F**inite-**I**ntegration-**A**lgorithm), a powerful, electrodynamic code written in FORTRAN 77 that is used for computer-aided design of two-dimensional and fully three-dimensional electromagnetic devices such as magnets, RF cavities, wave-guides, antennas, etc. The Finite Integration Technique (FIT) algorithm produces a matrix of finite-difference equations for electric and magnetic field vectors in the structure under study. The solution of these equations yields static, frequency-domain or time-domain solutions of Maxwell's equations (Refs. 2, 3). The code includes nine modules, the cold-test characteristics of this report were calculated using the M (mesh generator), E (eigenmode solver), and P (postprocessor) modules of MAFIA. The remaining modules are S (static solver), T2/T3 (two-dimensional (2D) and three-dimensional (3D) time domain solvers, respectively), TS2/TS3 (2D and 3D particle-in-cell codes, respectively) and W3 (3D frequency domain solver).

ANALYSIS AND SIMULATION

The dispersion relation was calculated using a method similar to experimental methods in which the frequency-phase dispersion characteristics are calculated by measuring the resonant frequencies in a truncated circuit section. The resonances correspond to standing waves that occur wen the circuit length is an integral number of half wavelengths (phase shifts of π).

The on-axis interaction impedance is a figure of merit proportional to the strength between the RF wave and the electron beam, defined for the n^{th} RF space harmonic (Ref. 4) as

$$K_n = \frac{|E_n^2|}{2\beta_n^2 P_{RF}} \qquad (1)$$

where $|E_n|$ is the axial electric field magnitude of the n^{th} space harmonic, β_n is the axial phase constant of the n^{th} harmonic defined by

$$\beta_n = \frac{\phi + 2\pi n}{L} \qquad (2)$$

where ϕ is the phase shift per turn in radians of the fundamental harmonic, n is the space harmonic order, L is the length of one turn. P_{RF} is the time

averaged RF power flow defined by

$$P_{RF} = w v_g \qquad (3)$$

where v_g is the group velocity and w is the time averaged stored electromagnetic energy per unit length,

$$w = \frac{W_T}{NL} \qquad (4)$$

with W_T the total energy in the N turns. Amplification requires synchronism of the electron beam with the fundamental space harmonic, therefore, the fundamental (n = 0) harmonic term in (1) is calculated to determine the on-axis interaction impedance.

The circuit attenuation is calculated using the same truncation method as with the dispersion and impedance calculations. The attenuation, α, is defined in dB per unit length as

$$\alpha = 8.686 \frac{P_L}{2 P_{RF}} \qquad (5)$$

(Ref. 5) where P_L is the total power loss per unit length

$$P_L = \frac{P_{LT}}{NL} \qquad (6)$$

and P_{LT} is the total power loss for a traveling wave in the N turns.

The current version of MAFIA (3.20) does not posses the capability to generate a helical structure automatically. Thus the helix was generated in the cylindrical coordinate system by varying axial and azimuthal coordinates consistent with the formula of a circular helix.

RESULTS

The first circuit modeled is the helical slow-wave circuit from a Northrop Grumman C-Band TWT for the Microwave Power Module (MPM) (Ref. 6). The experimental circuit includes a rectangular, copper plated tungsten helical tape supported by rectangular BeO rods inside a conducting barrel as shown for the end view in Figure 1. Because the support rods do not conform to the cylindrical coordinate system, "quasi-rectangular" rods were modeled in radial increments by reducing the rod angles with increasing radius. The MAFIA three-dimensional plot of the circuit is shown in Figure 2.

The dispersion, attenuation and on-axis interaction impedance were calculated for this circuit using MAFIA and compared with measured results in Figure 3 and Figure 4. The agreement is excellent with absolute average differences across the bandwidth of 0.7% and six Ohms, for the dispersion and impedance, respectively. The necessary MAFIA input for attenuation calculations includes an effective conductivity value and appropriate dielectric loss tangent. The loss tangent for BeO was taken to be .0001. The effective conductivity value was taken from Gilmour et al. (Ref. 7) where theoretical and experimental TWT helix loss was determined from about 2 to 16 GHz for a copper plated helix. Gilmour et al. found excellent agreement between calculated and measured loss when helix surface roughness was assumed to cause the resistivity to increase by a factor of approximately two. Using a conductivity consistent with these results (1.45×10^7 S/m), the average absolute attenuation difference was about .0005 dB per turn. The CPU time to simulate ten turns of this MAFIA C-band model is about 30 hours using an IBM RISC/6000 Model 590 Workstation.

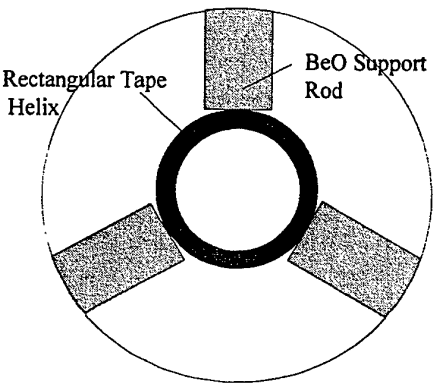

Figure 1 Northrop C-Band helical TWT slow-wave circuit

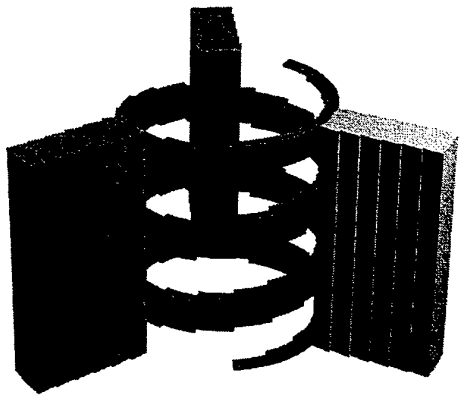

Figure 2 MAFIA three-dimensional plot of Northrop C-Band helical circuit

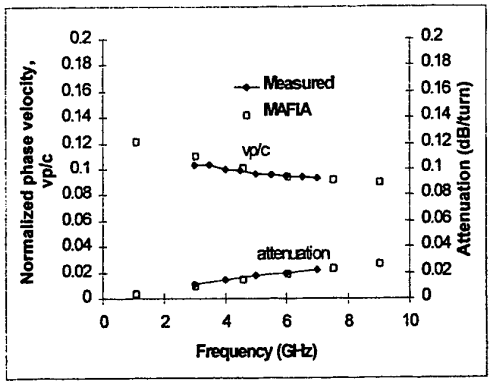

Figure 3 Measured and simulated dispersion and attenuation for Northrop C-Band helical circuit

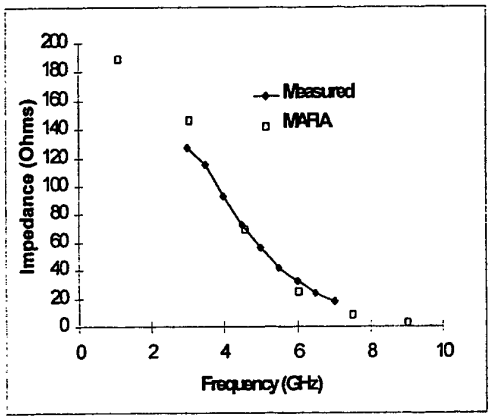

Figure 4 Measured and simulated on-axis interaction impedance for Northrop C-Band helical circuit

A Northrop Grumman broadband helical slow-wave circuit was also modeled using MAFIA and the dispersion, on-axis interaction impedance and attenuation were calculated and compared with measured results (Ref. 6). The circuit, shown in Figure 5, embodies a tungsten/rhenium tape helix supported by rectangular BeO rods, with a copper film partially coating the support rods to broadband the circuit. Initially the support rods were modeled using the quasi-rectangular configuration discussed previously but with this configuration, it is necessary to use ten radial increments for the dielectric support rods to prevent the protrusion of the dielectric material through the metal coating. This increased number of radial increments, compared to six for the C-Band circuit, complicates the boundary conditions of the problem, increasing the time for the computation to converge. Because of this added complexity and computational time, the support rods were generated in wedges using graded effective dielectric constants (Ref. 8). It was shown in Ref. 9 that there was a significant savings in computational time with negligible change in dispersion and on-axis interaction impedance when using this modeling configuration. Figure 6 shows the cross-sectional view of the Northrop broadband circuit graded wedge model.

The dispersion, attenuation and on-axis interaction impedance were calculated for this circuit using MAFIA and compared with measured results in Figure 7 and Figure 8. Compared to measured data the absolute average differences across the bandwidth are 1.5%, .003 dB/turn and ten Ohms, for the dispersion, attenuation and impedance, respectively.

The conductivity of the tape was initially approximated to be consistent with twice the resistivity of the theoretical value for tungsten, in line with Ref. 7 as described previously. The conductivity of the copper loading film was also kept consistent with twice the resistivity of the theoretical value for copper. When these values were used, the attenuation obtained using MAFIA was lower than experimental data. It was found that using a value 2.46 times the theoretical resistivity value of tungsten for the helical tape gave the best agreement with measured attenuation as shown in Figure 7.

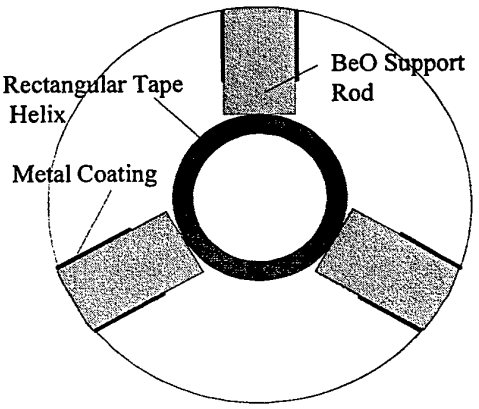

Figure 5 Northrop broadband helical TWT slow-wave circuit

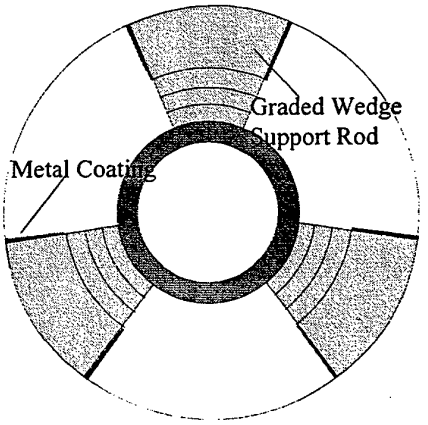

Figure 6 Northrop broadband helical slow-wave circuit model with graded wedge support rods

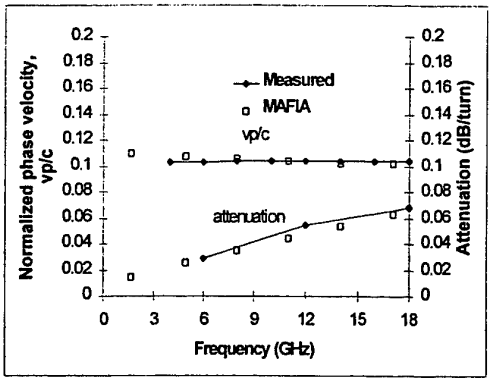

Figure 7 Measured and simulated dispersion and attenuation for Northrop broadband helical circuit

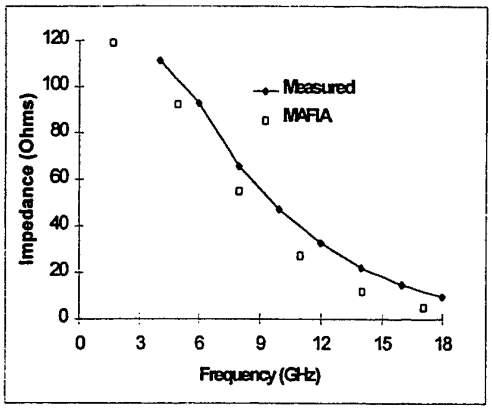

Figure 8 Measured and simulated on-axis interaction impedance for Northrop broadband helical circuit

Next, to demonstrate how MAFIA can be used to study circuits having more complex material characteristics, a circuit with anisotropic pyrolytic boron nitride (APBN) support rods was modeled. The circuit embodies a rectangular, copper plated tungsten/rhenium, helical tape supported by rectangular APBN rods oriented for low RF losses, rather than thermal conductivity. The helical slow-wave circuit is from a 10 Watt, 32 GHz traveling-wave tube amplifier (TWTA) for incorporation into the Ka-Band Transmitter package for the Cassini mission (Ref. 10). It resembles the Northrop Grumman C-Band circuit of Figure 1. Similarly, the support rods were generated in the cylindrical coordinate system by using six radial increments by reducing the rod angle with increasing radius, or the quasi-rectangular configuration. Only the measured dispersion and attenuation were available from the manufacturer for comparison, which are compared to the values obtained using MAFIA in Figure 9.

For this circuit with the APBN support rods, the nominal dielectric constant is 5.1 parallel to the layers and 3.4 perpendicular. Since the rods are oriented for low RF losses, rather than thermal conductivity, this implies an effective dielectric constant of 5.1 in the azimuthal and axial directions, and 3.4 in the radial direction. Using these nominal values, the dispersion obtained using MAFIA was consistently lower than measured values by about one GHz, or an absolute frequency difference of about 3%. By varying the relative dielectric constant of the rods to 4.6 in the azimuthal and axial directions, and 2.3 in the radial direction, the results shown in Figure 9 were obtained. The average absolute difference across the bandwidth between measured dispersion and that obtained using MAFIA, is only 0.6%.

Some in-house measurements of APBN showed that the permittivity can vary within the same plate of material from the same manufacturer by as much as +/- 10% (Ref. 11). With this information, the variations made from the nominal permittivity values for the Cassini support rods are approximately justified. Unfortunately, it is impossible to establish the exact anisotropic permittivity of the dielectric rods used in these already assembled tubes.

The attenuation was calculated for the Cassini circuit using a conductivity value of 2.25×10^7 S/m for the helical tape, nearly the theoretical value of pure copper, and compared with measured values in Figure 9. Much attention was given to polishing the helical tape to a bright, shining finish, therefore explaining this large conductivity value.

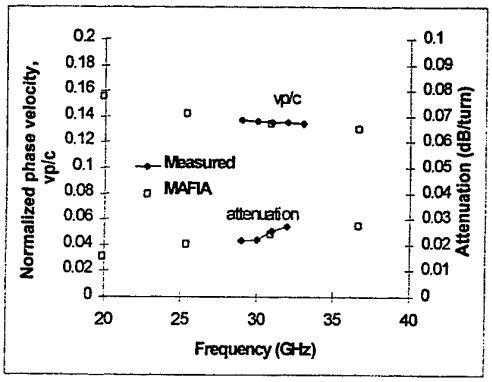

Figure 9 Measured and simulated dispersion and attenuation for Cassini helical circuit

The last circuit modeled was the helical slow-wave circuit from a Hughes TWT for the MPM (Ref. 12). The experimental circuit includes a rectangular, copper plated helical tape supported by T-shaped BeO rods inside a conducting barrel as shown for the end view in Figure 10. Only the measured dispersion values were available from the manufacturer for comparison which are compared with the values obtained using MAFIA in Figure 11. The results using MAFIA agree very well with measured data with an absolute average difference across the bandwidth of 1.8%

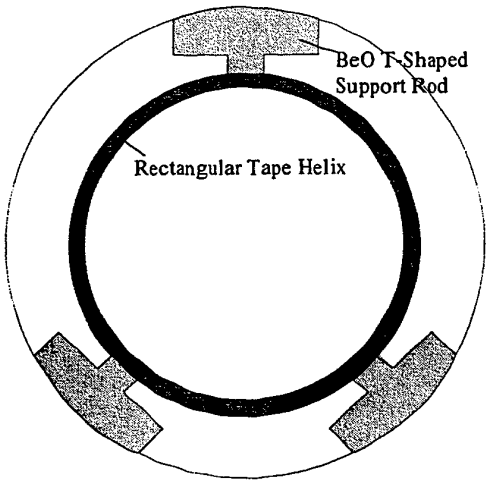

Figure 10 Hughes MPM helical slow-wave circuit

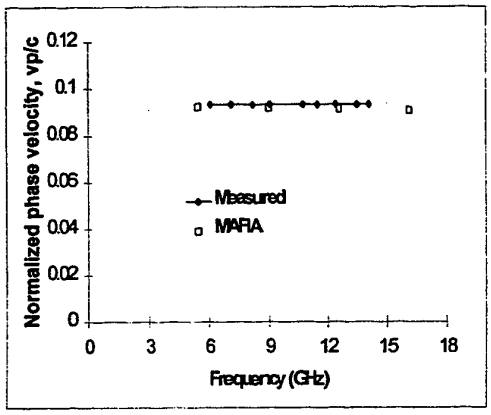

Figure 11 Measured and simulated dispersion for Hughes MPM helical circuit

CONCLUSIONS

An accurate three-dimensional TWT helical slow-wave circuit model has been introduced and the accuracy validated by comparing measured cold-test results with those obtained using MAFIA with excellent agreement. First an in depth analysis was given describing how MAFIA can be used to obtain the cold-test characteristics including dispersion, on-axis interaction impedance and attenuation. Then the simulated results for several TWT helical slow-wave structures were presented.

The Northrop Grumman C-Band helical circuit, representing one of the most basic helical slow-wave structure designs, was modeled first. The cold-test results using MAFIA showed excellent agreement when compared to measured values with absolute average differences across the bandwidth of 0.7%, six Ohms and .0005 dB/turn, for the dispersion, impedance and attenuation, respectively.

Next the cold-test characteristics for the Northrop Grumman broadband helical circuit were presented and compared to measured data with absolute average differences across the bandwidth of 1.5%, ten Ohms and .003 dB/turn, for the dispersion, impedance and attenuation, respectively.

Two additional helical slow-wave circuits were modeled using MAFIA, the Ka-Band circuit from the TWTA for the Cassini mission, and the Hughes MPM circuit embodying T-shaped support rods. The results for the Cassini circuit using MAFIA, compared to measured data, showed an absolute average difference across the operating range of 0.6% for the dispersion. The conductivity value used in the MAFIA simulation for the helical tape was obtained by matching the measured attenuation with experimental data. The conductivity for the helical tape was found to be 2.25x107 S/m, very close to the theoretical value of copper, indicating a very smooth helical surface. An absolute average difference of 1.8% across the operating range was obtained for the dispersion for the Hughes MPM helical circuit.

A discrepancy in the agreement between the on-axis interaction impedance supplied from industry and that calculated using MAFIA is expected, since the methods used to calculate this cold-test parameter differ. To experimentally obtain on-axis interaction impedance, the circuit is perturbed with a small dielectric rod at the center of the helical axis, and the change in phase shift between the perturbed and unperturbed circuit at a constant driving frequency is measured. From Slater's perturbation theory (Ref. 13), the formula for on-axis interaction impedance is derived involving several approximations for the fields within the circuit.

REFERENCES

1. Kory, C. L., Three-Dimensional Simulation of Helix Traveling-Wave Tube Cold-Test Characteristics Using MAFIA, *IEEE Trans. on Electron Devices*, vol. 43, no. 8, pp. 1317-1319, August 1996.

2. T. Weiland, On the Numerical Solution of Maxwell's Equations and Applications in the Field of Accelerator Physics, Part. Accel., vol 15, pp. 245-292, 1984.

3. T. Weiland, On the Unique Numerical Solution of Maxwellian Eigenvalue Problems in Three Dimensions, Part. Accel., vol. 17, pp. 227-242, 1985.

4. J. W. Gewartowski and H. A. Watson, Principles of Electron Tubes. D. Van Nostrand Company, Inc. p. 357, 1965.

5. O. P. Ghandi, Microwave Engineering and Applications. Pergamon Press, Elmsford, New York, 1981.

6. Personal communication with Gary Groshart of Northrop Grumman Corp., Electronics Systems Division, Rolling Meadows, IL, USA.

7. A. S. Gilmour, Jr., M. R. Gillette and J-T. Chen: Theoretical and Experimental TWT Helix

Loss Determination, *IEEE Trans. on Electron Devices,* vol. 26, no. 10, pp. 1581-1588, October 1979.

8. C. L. Kory and J. A. Dayton, Jr., The Effect Of Tolerances On TWT Performance, Microwave Tubes for Space, Military and Commercial Applications Workshop, April 7-10, 1997, Noordwijk, The Netherlands.

9. C. L. Kory, Validation Of An Accurate Three-Dimensional Helical Slow-Wave Circuit Model, NASA Contractor Report, CR-4766, March 1997.

10. A. N. Curren et al., A High Efficiency, Low Power Ka-Band TWTA for Cassini, Prepared for the 1994 IEEE IEDM, San Francisco, CA, pp. 783-786, December 11-14, 1994.

11. S. Alterovitz et al., Characterization of Commercial APBN, NASA Technical Paper in preparation, 1997.

12. Personal communication with Ron LeBorgne of Hughes Aircraft Co., Electron Dynamics Division, Torrance, CA, USA.

13. J. C. Slater, Microwave Electronics. Van Nostrand, New York, 1950.